Studies on the Bacterial Uptake and Biological Evaluation of Nucleoside Antibiotics

DISSERTATION

Zur Erlangung des Grades
des Doktors der Naturwissenschaften
der Naturwissenschaftlich-Technischen Fakultät
der Universität des Saarlandes

von
Stefanie Christine Weck,
Staatlich geprüfte Lebensmittelchemikerin

Saarbrücken
2023

Tag des Kolloquiums:	13. Dezember 2023
Dekan:	Prof. Dr. Ludger Santen
Berichterstatter:	Prof. Dr. Christian Ducho Prof. Dr. Anna K.H. Hirsch
Akad. Mitglied:	Dr. Josef Zapp
Vorsitz:	Prof. Dr. Andriy Luzhetskyy

Die vorliegende Arbeit wurde an der Universität des Saarlandes an der Naturwissenschaftlich - Technischen Fakultät im Fachbereich Pharmazie im Zeitraum von März 2018 bis April 2022 angefertigt.

Erstgutachter: Prof. Dr. Christian Ducho

Zweitgutachter: Prof. Dr. Anna K. H. Hirsch

Für Papa

** 27.10.1958*

† 11.11.2017

Abstract

This PhD thesis was divided into biological and synthetic studies with a focus on muraymycins, a class of nucleoside antibiotics which inhibit the bacterial, membrane-bound enzyme MraY.

The biological projects included the development and validation of assays that were used to determine the structure-activity relationship of drug candidates. Cellular uptake into Gram-positive and Gram-negative bacteria was of special interest in this work. MraY, its different preparations, the corresponding activity assays, resistance development and protein-protein interactions of MraY were studied. Membrane disruption by hemolysis and methods for the determination of esterase activity in biological media were investigated.

The synthetic project focused on muraymycin prodrugs. Muraymycins exhibit low antibacterial activities, which is attributed to limited cellular uptake into bacterial cells. It was therefore envisioned to increase the lipophilicity of known muraymycin analogues to achieve better antibacterial activities using a prodrug approach. These prodrugs will make use of intracellular esterases to release the potent drug after cellular entrance. Synthesis of the muraymycin prodrugs was performed by stereoselective multistep routes.

Zusammenfassung

Diese Dissertation ist in biologische und synthetische Studien gegliedert. Schwerpunkt der Projekte waren Muraymycine, eine Klasse von Nucleosid-Antibiotika, die das bakterielle, membranständige Enzym MraY hemmen.

Zu den biologischen Projekten gehörte die Entwicklung und Validierung verschiedener Assays, mit deren Hilfe Struktur-Aktivitäts-Beziehungen von Wirkstoffkandidaten ermittelt wurden. Von besonderem Interesse war die Zellaufnahme in Gram-positive und Gram-negative Bakterien. MraY, unterschiedliche Präparationen des Proteins und die dazugehörigen Assays zur Bestimmung der Proteinaktivität sowie die Möglichkeit der Resistenzentwicklung und Wechselwirkungen zu anderen Proteinen wurden thematisiert. Membrandisruption in Form von Hämolyse sowie Methoden zur Aktivitätsbestimmung von Esterasen in biologischen Medien wurden untersucht.

Das Syntheseprojekt konzentrierte sich auf Muraymycin-Prodrugs. Muraymycine weisen geringe antibakterielle Aktivitäten auf, was auf eine begrenzte zelluläre Aufnahme in Bakterienzellen zurückgeführt wird. Ziel war es daher, die Lipophilie bereits bekannter Muraymycin-Analoga zu erhöhen, um mit Hilfe eines Prodrug-Ansatzes bessere antibakterielle Wirkungen zu erzielen. Bei diesem Prodrugansatz sollen bakterieneigene Esterasen genutzt werden, um den potenten Wirkstoff nach erfolgter Zellaufnahme freizusetzen. Die Synthese der Muraymycin-Prodrugs erfolgte auf Basis stereoselektiver, mehrstufiger Syntheserouten.

Danksagung

An erster Stelle möchte ich mich bei meinem Doktorvater Prof. Dr. Christian Ducho für die vielfältigen, spannenden Forschungsprojekte und die hieraus resultierenden Themen meiner Dissertation bedanken. Danke für Deine stete Diskussionsbereitschaft sowie der Möglichkeit, meine Ergebnisse im Rahmen einiger Konferenzen vorzustellen. Mein Aufenthalt am DFCI in Boston 2021 war mein persönliches Highlight, an das ich mich immer sehr gerne zurückerinnern werde. Insbesondere möchte ich hier auch Karin Maria Piening danken. Liebe Karin, ohne Deine tatkräftige Unterstützung wäre ich 'lost' gewesen. Danke Christian und Karin, dass Ihr mir diesen USA-Aufenthalt ermöglicht habt.

Im Zuge dessen möchte ich dem gesamten Arthanari Lab vom DFCI in Boston danken, insbesondere Prof. Dr. Haribabu Arthanari und Dr. Patrick Fischer. Danke für die vielfältigen Projekte, in die Ihr mich von Anfang an integriert habt, für Euer Vertrauen und dafür, dass Ihr mir eine unvergessliche Zeit bereitet habt, die ich niemals vergessen werde.

Prof. Dr. Anna K. H. Hirsch danke ich für die Übernahme des Zweitgutachtens und die Betreuung als wissenschaftliche Begleiterin.

Allen ehemaligen und aktuellen Mitgliedern des Arbeitskreises Ducho danke ich für die angenehme Arbeitsatmosphäre und Zusammenarbeit. Bei Dr. Stefan Boettcher möchte ich mich für die zahlreichen Diskussionen rund um meine Orbi-Daten bedanken. Ein großer Dank gilt auch allen Korrekturlesern dieser Arbeit.

Vielen Dank an mein Saarbrücker Bio-Team Martina Jankowski, Jannine Seelbach, Dr. Patrick Fischer, Dr. Reem Fathalla, Nathalie Kagerah und Stefan Koppermann für vielen gemeinsamen, lustigen Labortage und die tolle Zusammenarbeit. Insbesondere Martina danke ich für die unzähligen Resuspensionen meiner Pellets – Du weißt, welche ich meine. Ohne Dich hätte ich vermutlich heute noch wunde Daumen (und schlechte Laune). Jannine, wir haben uns blind verstanden. Ich danke Dir für die tolle Zusammenarbeit und Unterstützung. Danke für die Wochenenden, die Du bereitwillig geopfert hast, Stefan, um all meine Biofragen zu klären. Patrick, Dir möchte ich für Deine nie endende Unterstützung meiner und unserer gemeinsamen Projekte danken. Du hast in der noch so aussichtslosesten Situation immer noch eine Idee parat. Wir haben diskutiert was das Zeug hält, es hat so unfassbar viel Spaß gemacht, mit Dir zusammenzuarbeiten. Selbst kleinere Meinungsverschiedenheiten in Boston („Das ist mein geordnetes Chaos, lass das bitte so stehen, Steffi“) haben unserer hervorragenden Teamarbeit nie im Weg gestanden. Wir haben uns immer gegenseitig unterstützt und das nicht erst in Boston „live“, sondern von Beginn an, obwohl wir lediglich einen Tag Überschneidung hatten. Du bist ein sehr wichtiger Freund für mich geworden, der einen bedeutenden Abschnitt in meinem Leben – meine Dissertation – von Anfang an begleitet hat. Danke für alles, Patrick.

Dem OC-Team Dr. Verena Böttner-Schäfer, Dr. Christian Rohrbacher, Manuel Hawner, Tobias Betzholz und Anna Heib möchte ich für die vielen gemeinsamen, teilweise sehr langen Abende im Labor danken. Wir waren ein super Team.

Bei meinen Studenten Morvarid Ajdari Rad, Hendrik Rolshausen, Pit Ries, Laura Thilmont, Katharina Ringle möchte ich mich für die tatkräftige Unterstützung meiner Projekte und die angenehme Zusammenarbeit bedanken.

Bei der Arbeitsgruppe Kiemer, insbesondere bei Dr. Charlotte Dahlem, Dr. Britta Diesel und Simon Beth, möchte ich mich für die Bereitstellung des plate readers und die großartige Unterstützung beim Western Blotting bedanken.

Dr. Asfandyar Sikandar und Pascal Paul möchte ich für die zahlreichen Ultrazentrifugationen und 'SEC runs' danken. Ohne Euch wären meine Experimente nicht durchführbar gewesen.

Ein großer Dank geht an meine Mädels Giu, Melli, Reemy und Verena. Ihr habt immer hinter mir gestanden und habt mich immer unterstützt, ganz egal was war. Ich bin unfassbar froh, Euch in Saarbrücken kennengelernt zu haben. Ihr seid weit mehr als nur Freunde. Ihr seid die Besten. Ich danke Euch für alles.

Lothar Jager möchte ich danken für sämtliche Unterstützung in Sachen Reparaturen, IT und „Allerlei“. Lothar, ganz egal, bei was ich ein Problem hatte, du warst immer zur Stelle und hattest für alles eine Lösung. Ein „das geht nicht“ gibt es bei Dir nicht. Lediglich in einer Sache bin ich enttäuscht von Dir, Du hast unseren Deal „wir gehen gemeinsam Steffi“ gebrochen, sodass ich gezwungen war, von dort an allein zu schrauben und zu tricksen.

Ein großer Dank geht an meine Freunde. Ihr habt dafür gesorgt, dass ich den perfekten Ausgleich zu meinem 'PhD life' hatte. Ich habe unsere gemeinsame Zeit sehr genossen. Danke für Euer offenes Ohr, Euer Verständnis und vor allem den unfassbaren Rückhalt, den ihr mir immer gegeben habt. Insbesondere Karo möchte ich danken für vielen tollen gemeinsamen Erlebnisse, Urlaube und Treffen.

Der größte Dank gilt meiner Familie, meiner Mutter Friederike, meinem Vater Manfred und meiner Schwester Monika für die bedingungslose Unterstützung und die vielen offenen Ohre (und grauen Haare, sorry Mama). Ihr habt immer an mich geglaubt und mich zu der Person gemacht, die ich heute bin. Papa, ich danke Dir für alles, was Du für mich getan hast. Du bist viel zu früh von uns gegangen, dennoch warst Du auch bei diesem bedeutenden Lebensabschnitt ständig von Deiner Wolke aus an meiner Seite. Ich widme diese Arbeit Dir.

Abbreviations and symbols

°C	degrees Celsius
δ	chemical shift [ppm] (NMR)
Å	Ångström
AB	acetoxybenzyl
ABC	acetoxybenzyloxycarbonyl
ADME	absorption, distribution, metabolism and excretion
Ala	alanine
AM	acetoxymethyl
Amp	ampicillin
Asp	aspartic acid (aspartate)
APS	ammonium persulfate
BB	blocking buffer
BME	β-mercaptoethanol
BOP	(benzotriazol-1-yloxy)tris(dimethylamino)phosphonium hexafluorophosphate
bp	base pair(s)
Bu	butyl
CAM	chloramphenicol
Cbz	benzyloxycarbonyl
CH_2Cl_2	dichloromethane
cND(s)	circularized nanodisc(s)
COSY	correlation spectroscopy (NMR)
CPP	cell-penetrating peptide(s)
d	doublet (NMR) or day(s)
Da	Dalton
DAP	2,6-diaminopimelic acid
DDM	dodecyl-β-D-maltopyranosid

DIPEA	*N*,*N*-diisopropylethylamine
DM	decyl-β- D-maltopyranosid
DMF	*N*,*N*-dimethylformamide
DMPG	1,2-Dimyristoyl-*sn*-glycero-3-phospho-*rac*-(1-glycerol) sodium salt
DMSO	dimethyl sulfoxide
DNA	deoxyribonucleic acid(s)
DOPE	1,2-Dioleoyl-*sn*-glycero-3-phosphoethanolamine
d.r.	distereomeric ratio
DTT	dithiothreitol
E. coli	*Escherichia coli*
EDCI	1-ethyl-3-(3-dimethylaminopropyl)carbodiimide
EDTA	ethylenediaminetetraacetic acid
e.g.	for example (lat. *exempli gratia*)
ESI	electrospray ionization (MS)
et al.	and others (lat. *et alii*)
Et_2O	diethyl ether
EtOAc	ethyl acetate
FRET	Förster resonance energy transfer
fwd	forward
g	gram(s)
Glc*N*Ac	*N*-acetylglucosamine
Glu	glutamic acid (glutamate)
GuCOSS	guanidylated cube-octameric silsesquioxane scaffold
GuHCl	guanidine hydrochloride
h	hour(s)

His	histidine
His-MBP	decahistidine maltose-binding protein
H324	histidine (at position) 324
HIV	human immunodeficiency virus
HMBC	heteronuclear multiple bond coherence (NMR)
HOBt	1-hydroxybenzotriazole
HPLC	high pressure liquid chromatography
HRMS	high resolution mass spectrometry
Hrp	horseradish peroxidase
HSQC	heteronuclear single quantum coherence (NMR)
Hz	Hertz (NMR)
i.e.	that is (lat. *id est*)
IBX	2-iodoxybenzoic acid
IC_{50}	inhibitory concentration (50%)
IPTG	isopropyl-β-D-thiogalactopyranoside
IVA	*in vivo* assembly
J	scalar coupling constant [Hz] (NMR)
KAN	kanamycin
K_D	dissociation constant
kDa	kilodalton
λ	wavelength [nm]
λ_{em}	emission wavelength [nm]
λ_{ex}	excitation wavelength [nm]

L	liter(s)
LB	lysogeny broth
LC	liquid chromatography
m	multiplet (NMR)
M	molar
MeCN	acetonitrile
mg	milligram(s)
MIC	minimal inhibitory concentration
min	minute(s)
mL	milliliter(s)
mM	millimolar
mol	moles
$MraY_{AA}$	MraY from *Aquifex aeolicus*
$MraY_{BS}$	MraY from *Bacillus subtilis*
$MraY_{CB}$	MraY from *Clostridium boltae*
$MraY_{Mtb}$, MurX	MraY from *Mycobacterium tuberculosis*
$MraY_{SA}$	MraY from *Staphylococcus aureus*
$MraY_{SP}$	MraY from *Streptomyces platensis*
MRSA	methicillin-resistant *Staphyloccoccus aureus*
MS	mass spectrometry
MSP(s)	membrane scaffold protein(s)
Mur*N*Ac	*N*-acetylmuramic acid
M. tuberculosis	*Mycobacterium tuberculosis*

m/z	mass-to-charge ratio
n.d.	not detectable
NB7	nanobody 7
ng	nanogram(s)
nM	nanomolar
NMR	nuclear magnetic resonance
OD (OD_{600})	optical density (optical density at 600 nm)
P. aeruginosa	*Pseudomonas aeruginosa*
Pd black	palladium black
PBS	phosphate-buffered saline
PCR	polymerase chain reaction
PEP	phosphoenolpyruvate
PLE	porcine liver esterase
PMSF	phenylmethylsulfonylfluorid
POC	*iso*-propyl-oxycarbonyl-oxymethyl
POM	pivaloyloxymethyl
ppm	parts per million (NMR)
PyBOP	benzotriazol-1-yl-oxytripyrrolidinophosphonium hexafluorophosphate
q	quartet (NMR)
R^2	coefficient of determination
R_f	retardation factor (TLC)
rev	reverse

(*R*,*R*)-Me-DUPHOS-Rh	(-)-1,2-Bis-((2*R*,5*R*)-2,5-dimethylphospholano)-benzene-(1,5-cyclooctadiene)-rhodium(I)-tetrafluoroborate
RNA	ribonucleic acid(s)
rt	room temperature
s	singlet (NMR) or second(s)
S. aureus	*Staphylococcus aureus*
SAR	structure-activity relationship
SDS	sodium dodecyl sulfate
SDS-PAGE	sodium dodecyl sulfate polyacrylamide gel electrophoresis
SEC	size exclusion chromatography
SIM	single ion monitoring
(*S*,*S*)-Me-DUPHOS-Rh	(+)-1,2-Bis-((2*S*,5*S*)-2,5-dimethylphospholano)-benzene-(1,5-cyclooctadiene)-rhodium(I)-tetrafluoroborate
t	triplet (NMR)
TAE	tris-acetate-EDTA
TB	terrific broth
TBDMS	*tert*-butyldimethylsilyl
TEMED	tetramethylethylenediamine
TEV	tabacco etch virus
TFA	trifluoroacetic acid
TLC	thin-layer chromatography
THF	tetrahydrofuran
T_m	melting temperature
t_R	retention time(s)

UDP	uridine diphosphate
UDP-Glc*N*Ac	uridine diphosphate-*N*-acetylglucosamine
UDP-Mur*N*Ac	uridine diphosphate-*N*-acetylmuramic acid
µg	micogram(s)
UHPLC	ultra high pressure liquid chromatography
µL	micoliter(s)
µM	micromolar
UMP	uridine monophosphate
UV	ultraviolet
VSS	vanillin/sulfuric acid solution

Content

1 Introduction

1.1 Antibiotics

The discovery and the application of antibiotics more than 70 years ago represent one of the most important developments in medical history.[1] With the multitude of bacterial infections and the rise of resistant bacteria, infectious diseases are the second major cause of death worldwide, and the need for novel antibiotics in society is steadily increasing.[2] The term 'antibiotic' has its origin in Greek and consists of 'ἀντί' meaning 'against' and 'βίος' meaning 'life'. It is derived from the term 'antibiosis' which was originally introduced by Paul Vuillemin in 1889 as a relationship between organisms that is destroyed by their reciprocal killing, growth or reproduction inhibition.[3] In 1942, Nobel prize winner Selman Abraham Waksman referred to this definition in his introduction of the term 'antibiotic'. He defined it as "a chemical substance, produced by microorganisms, which has the capacity to inhibit bacterial growth and even to destroy bacteria and other microorganisms".[4,5] Nowadays, this definition only applies to a limited extent as a high variety of naturally occurring antibacterial agents as well as semisynthetic and synthetic variations thereof with antimicrobial potential exist.[1] There are basically two modes of action of antibiotics: bacteriostatic and bactericidal. With the application of bacteriostatic antibiotics, bacteria are prevented from multiplying by growth inhibition, whereas bactericidal antibiotics cause the death of bacteria by, e.g., destroying their cell wall.[2] In 1928, antibiotics research was incredibly shaped by Alexander Fleming who observed penicillins from a moldy bacterial culture being antibacterial.[6] This observation and the subsequent isolation and large-scale fermentative production by Howard Walter Florey and Ernst Boris Chain in 1940 marked the beginning of the so-called golden age of antibiotics.[7] During this time, new drugs were more in demand than ever before resulting from the high number of infectious diseases, especially wound infections during the Second World War. With the introduction of the first sulfonamides and penicillins in 1935 and 1940, the once high mortality rate caused by bacterial infections has fallen dramatically, thus saving many lives and preventing patients' suffering.[2] Since the introduction of penicillin, multiple antibiotics such as β-lactams, tetracyclines, aminoglycosides, chloramphenicol (CAM), macrolides, glycopeptides and quinolone antibiotics were discovered (Figure 1.1).[1,2] Between 1940 and 1960, antibiotic research experienced the aforementioned golden age and greatly stalled afterwards. From 1970 onwards, only a few new antibiotics were introduced to the market (Figure 1.1), and the need for new antibacterial agents was questioned, leading to dwindling public interest and declining support for antibiotics research in pharmaceutical industry.[2] In this context, one of the most famous quotes which is said to have been made by United States Surgeon Dr. William H. Stewart (1965-1969) should be mentioned: “It is time to close the book on infectious diseases, and declare the war against pestilence won.”.[8] Although the primary source of this

statement has never been clarified and this quote is more an urban legend, this quote perfectly demonstrates the increasing problems of emerging bacterial infections at this time.[8] After an innovation gap of nearly 20 years, the oxazolidinone linezolid and daptomycin, a cyclic lipopeptide, were approved by the U.S. Food and Drug Administration in 2000 and 2003, respectively (Figure 1.1).[9] Both were the first representatives of structurally new antibacterial agents named "new chemical entities" approved for human therapy.[2,9] A growing population of older people and immune-suppressed patients as well as rising costs for the treatment of resistant bacterial strains illustrate the current situation in global health care and mark today's urgent need for new antibacterial agents.[2]

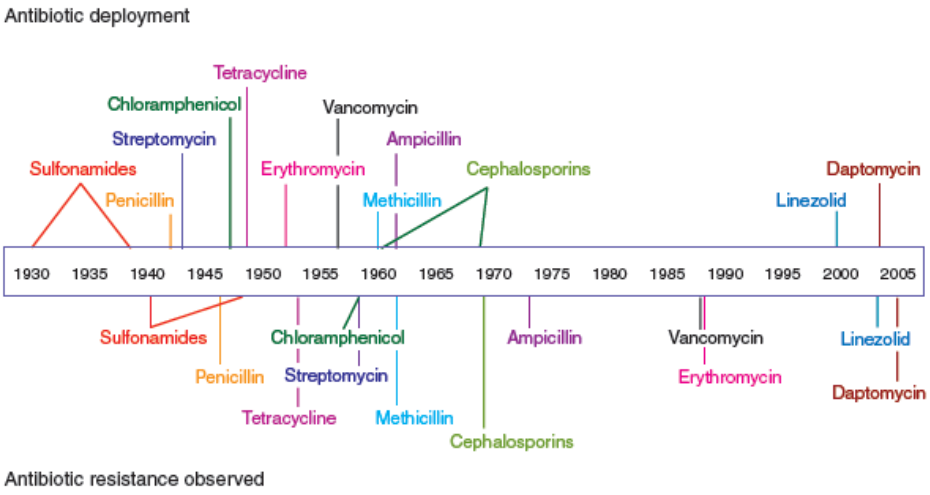

Figure 1.1: Timeline of antibiotic deployment and the evolution of antibiotic resistance (taken from: Clatworthy et al., Nat. Chem. Biol. ***2007****, 3, 541-548).*[10]

1.2 Resistances and their development

Beside the hampered development of novel antibiotics, clinically significant antibiotic resistance formation occurred, limiting the efficacy and lifespan of antibiotics.[2,10] Antibiotic resistance is defined as "the insensitivity of microorganisms to antibiotics, naturally occurring or acquired, through habituation, selection or mutation".[11] There are different forms of resistances depending on their origin: the natural, intrinsic resistance and the acquired form of resistance.[12] The natural form is characterized by a lack of effectivity in a certain bacterial species, such as all species of *Pseudomonas aeruginosa* (*P. aeruginosa*), which carry ampicillin (Amp) resistance.[12] In contrast, acquired resistance arises spontaneously through obtaining any genetic material by bacteria via transformation, transposition, conjugation or transmission and may occur temporarily or permanently.[12] In both cases, bacteria develop ways to circumvent established therapies and spread worldwide. Even the proper use of antibiotics can only slow this process down but cannot ultimately prevent it. This problem is nowadays particularly common in hospitals where carbapenem-resistant *Enterobacteriaceae*, vancomycin-resistant *Enterococci* and the extended spectrum-β-lactamase-producing *Enterobacteriaceae* are the most common resistant pathogens beside better-known species

such as methicillin-resistant *Staphylococcus aureus* (MRSA), *P. aeruginosa* and *Clostridium difficile*.[13,14] With a high rate of mortality due to its resistances against β-lactams, quinolones, macrolides and sulfonamides, MRSA has become the most important *Staphylococcus aureus* (*S. aureus)* strain in hospitals with incidences over 60%.[15] In principle, resistance mechanisms can be manily classified mainly into the following four categories:[12,16,17]

(1) Modification and/or inactivation of antibacterial agents by drug-modifying enzymes

(2) Decreased penetration and limited uptake of drugs via, e.g., the alteration of penetration barriers and/or active drug efflux mediated by efflux pumps

(3) Modification of drug target sites and/or target protection

(4) Adaption and/or defense of cell adaptive processes

The prevalence of resistance mechanisms varies between Gram-positive and Gram-negative bacteria. While Gram-negative bacteria such as *Escherichia coli* (*E. coli*) utilize all types of resistance mechanisms, Gram-positive bacteria such as *S. aureus* primary adopt mechanisms (3) and (4) due to the absence of an outer membrane (the structure of the bacterial cell wall will be described in Chapter 2.1).[12,16] The basic binding of antibtiotics to their targets that cause inhibitory effects is schematically depiced in Figure 1.2.

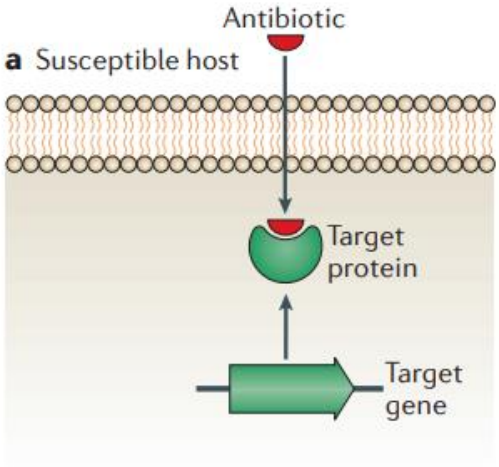

Figure 1.2: Antibacterial resistance mechanisms. Initial situation: Antibiotics binding to their specific target, thus inducing antibacterial effects.

Now, one of the most successful bacterial strategies to develop resistances is the production of enzymes that cause drug inactivation by destroying antibacterial agents ('drug degradation') or by adding chemical moieties to antibiotics (1).[12,16] The group of β-lactamases is the most prominent example of the former. They hydrolyze β-lactam antibiotics leading to their ineffectiveness (Figure 1.3, left top). Representatives of enzymes adding chemical moieties to antibiotics are acetyltransferases, phosphorylases and adenylyltransferases which add acetyl,

phosphoryl and adenylate groups to antimicrobial agents, respectively. This transfer confers a declined interaction between the drug and its target (Figure 1.3, right bottom).[17]

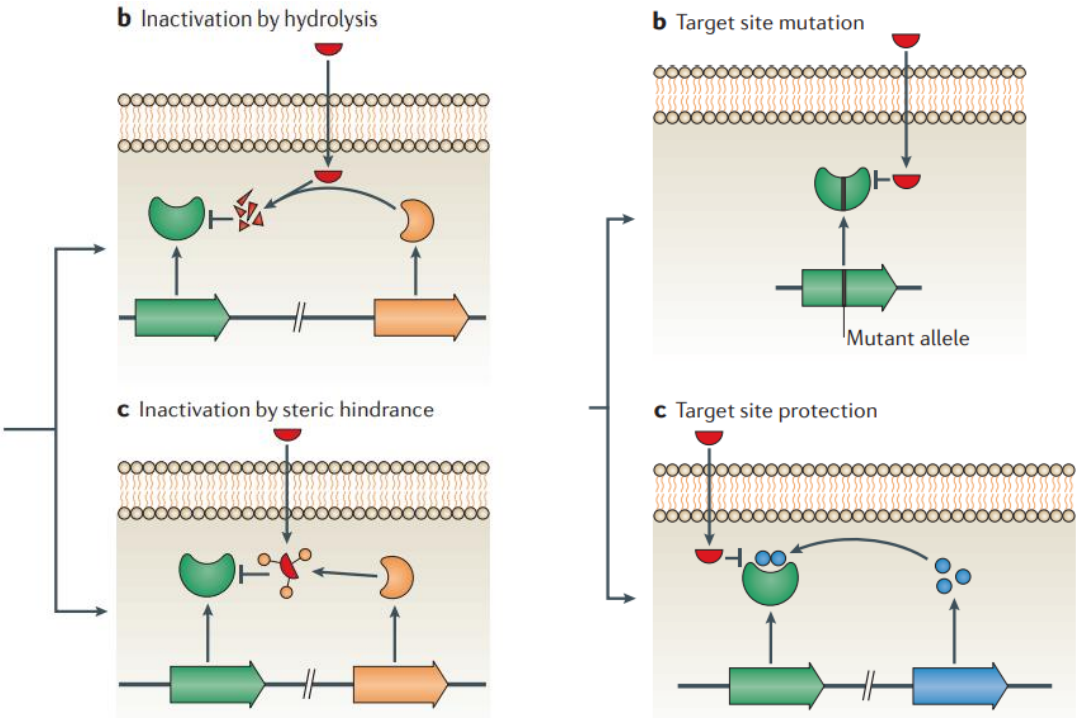

*Figure 1.3: Antibacterial resistance mechanisms. Left: drug-modifying enzymes leading to drug inactivation by hydrolysis (b) or covalent attachment (c). Right: Modification of the drug target site by mutation (b) or protection (c) (taken from: Blair, Nature. **2015**, 13, 42-51).[17]*

In order to prevent drugs from reaching their targets, bacteria have developed another important resistance mechanism by decreasing and limiting cell wall permeation and cellular uptake of antibiotics (2).[12,16] This is particularly important for Gram-negative bacteria which possess an inner and an outer membrane, with the latter functioning as the first barrier for toxic compounds such as drugs (Chapter 2.1). To exhibit antibacterial activity, antibiotics generally need to reach their targets which are often intracellularly.[16] In this context, a general distinction between the passive diffusion of drugs through membranes, the passive diffusion through membrane channels and active transport mechanisms[18] will be drawn in Chapter 2.3. As a second effective bacterial resistance strategy, limited uptake of hydrophilic antibiotics such as β-lactams is achieved by reducing or changing the permeability of the outer membrane,[17] mutations in the corresponding transporter channels[12] or a decrease of their abundance in the membrane[12]. The formation of biofilms by certain bacteria also causes resistance development or at least enforces the use of higher drug concentrations to be effective.[12] However, this phenomenon is not as frequently reported as the other resistance mechanisms. Much more common are drug efflux pump systems, expressed constitutively, induced or overexpressed, which directly extrude antibacterial agents after their entry into bacteria.[12,16,17] They may function as single- or multi-component pumps[12] and are either substrate-specific or

substrate-unspecific and transport a large number of drugs[17]. One of the best studied systems is TolC, an outer-membrane channel found in *E. coli* that pumps drugs out of the cell in an unspecific manner.[16,17] In laboratories, the efflux-deficient strain *E. coli* Δ*tolC* is often used for the investigation of unspecific efflux of candidate compounds by comparing the corresponding data with wild-type-like *E. coli* strains such as DH5α (addressed in Chapter 4). Another common resistance mechanism focusses on the target of drugs (3) via target site modification (Figure 1.3, right top) or target protection (Figure 1.3, right bottom) in order to lower the affinity for the drug.[12,16,17] Target site modifications are realized by mutations in the gene encoding the target, enzymatic modifications of the binding site (e.g., methylation) or the replacement or bypass of the original target site.[16] In comparison, many clinically relevant mechanisms nowadays reveal that mutational changes are not necessarily involved in target protection.[17] The basic strategy of bacteria is to prevent the (efficient) interaction between antimicrobial agents and their targets by interfering with the compound itself. The last resistance mechanism (4), not as frequent as the other three mentioned above, includes the compensation of biosynthetic pathways crucial for bacterial survival, such as cell wall synthesis and membrane homeostasis, which would be blocked by antibiotics.[16] Beside the competition for nutrients, bacteria are forced to defend themselves against various attacks of the surrounding environment in order to survive. Thus, they have developed complex mechanisms to prevent these fundamental processes from being disrupted. This strategy can be summarized as a global adaption of cellular processes by bacteria caused by antibacterial treatments. Clinically relevant drugs affected by this strategy are daptomycin and vancomycin.[16]

1.3 Classification of antibiotics

Generally, antibiotics can be classified by different aspects. Beside a classification based on their targets and modes of action, a distinction according to their chemical properties and their origin can be made. A differentiation between bacteriostatic or bactericidal modes of action has already been mentioned (Chapter 1.1). Additionally, there are basically four classical main targets for antibiotics involving mechanisms in bacterial cells that do not occur in animal or human cells (Figure 1.4).[10]

(1) Bacterial cell wall synthesis

(2) Bacterial protein biosynthesis

(3) Deoxyribonucleic acid (DNA) or ribonucleic acid (RNA) replication

(4) Folate metabolism

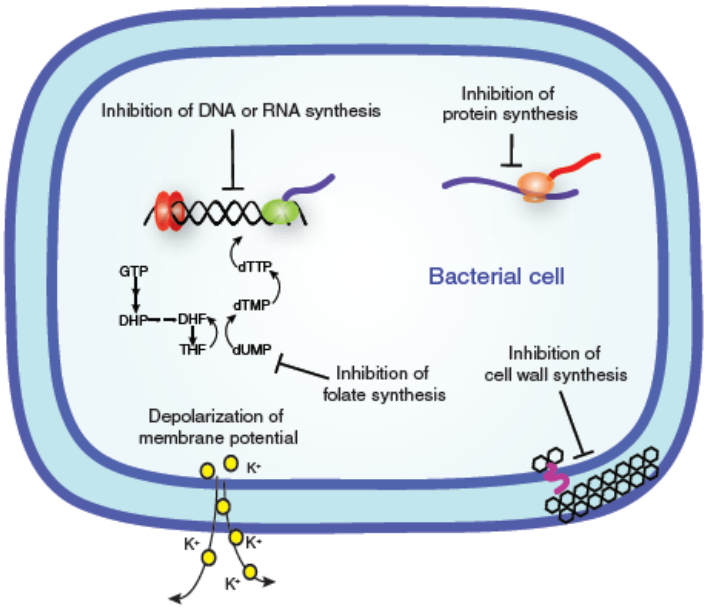

*Figure 1.4: Classical targets of antibacterial compounds (taken from: Clatworthy et al., Nat. Chem. Biol. **2007**, 3, 541-548).*[10]

An essential process for bacterial survival is their cell wall biosynthesis (1). It represents an attractive bacterial target for antibiotics as there is no counterpart in eukaryotic cells, except for plant cells and fungi.[19–21] The intracellular steps of peptidoglycan biosynthesis, a heteropolymer forming bacterial cell walls[22], are mainly catalyzed by the Mur enzymes[23] and will be discussed in Chapter 2.1.2. A second major target for antibacterial agents is bacterial protein biosynthesis (2) performed by ribosomes, rather conserved large bimolecular machines.[23–25] Although bacterial and eukaryotic ribosomes vary significantly[26], enabling the bacterial ribosome to be used as a specific target for drugs, there is the hypothesis that they have evolved from a common ancestor sharing the same core[24]. In this context, the binding of main classes of antibiotics to either the full ribosome or its subunits was elucidated by X-ray crystal structures.[23,25,27] DNA or RNA replication processes (3) represent another important bacterial target for antibiotics. A class of proteins called topoisomerases, also known as gyrases, is important for DNA topology as well as DNA decatenation, repair and replication.[28,29] Thus, drug binding to any of these proteins interferes with bacterial DNA replication. While the formation of supercoils in DNA is restricted by the binding of ciprofloxacin to DNA gyrase, a transcription inhibition occurs, e.g., as a result of rifampin binding to RNA polymerase.[23] The last bacterial target for antibiotics is represented by the folic acid biosynthesis pathway (4). Folate is crucial for DNA synthesis as it is necessary for producing thymidylate. Since folate metabolism is vital for bacterial survival and finds no equivalence in eukaryotic cells of higher organisms, bacteria will die as DNA synthesis is disrupted by antibacterial agents inhibiting this pathway.[23,30]

As already mentioned, antimicrobial agents can also be classified with respect to their chemical structure. Some selected, structurally different classes of antibiotics will be depicted and briefly described. A large group of antibiotics that inhibits bacterial cell wall biosynthesis[12] is represented by β-lactams that all share a four-membered lactam ring. Among others, typical representatives of this family are penicillins[6,7] (e.g., penicillin G, Figure 1.5), cephalosporins[31], monobactams[32–34] (e.g., aztreonam, Figure 1.5) and carbapenems[35]. Glycopeptide antibiotics are complex peptides with at least one glycosylation motif and are another group of drugs, with vancomycin being a classical representative.[36] They yield similar effects like β-lactam antibiotics and inhibit bacterial cell wall biosynthesis at a late step.[36] Another large group of antibiotics is formed by the family of aminoglycosides which inhibit bacterial protein biosynthesis and consist of a basically functionalized glycosylated cyclohexane unit.[37] The first and nowadays best-known aminoglycoside is streptomycin[38,39] (Figure 1.5) that was discovered by Waksman in 1944. Basically, aminoglycosides as well as tetracyclines (that are characterized by their tetracyclic core structure based on four carbon rings[40]) inhibit bacterial protein biosynthesis by binding to the 30S subunit of ribosomes[12]. Binding to the 50S ribosomal subunit by lincosamides (e.g., clindamycin, Figure 1.5), macrolides, oxazolidinones, streptogramins and phenicols (e.g., CAM, Figure 1.5) causes similar effects.[12,41] Lincosamides are structurally derived from pyranoses[41], macrolide antibiotics are macrocyclic lactones[42] and oxazolidinones contain a saturated heterocyclic system[41]. The group of antibiotics belonging to streptogramins is more complex and can be divided into the two sub-groups A and B with poly-unsaturated lactones being part of group A and branched cyclic peptides included in group B.[41] An example of an antibiotic class that address DNA and RNA processing in bacteria is the group of quinolones.[43] The family of sulfonamides, a large group of sulfonic acid amide derivatives (e.g., sulfamethoxazole, Figure 1.5), prevents bacteria from producing folic acid.[44,45]

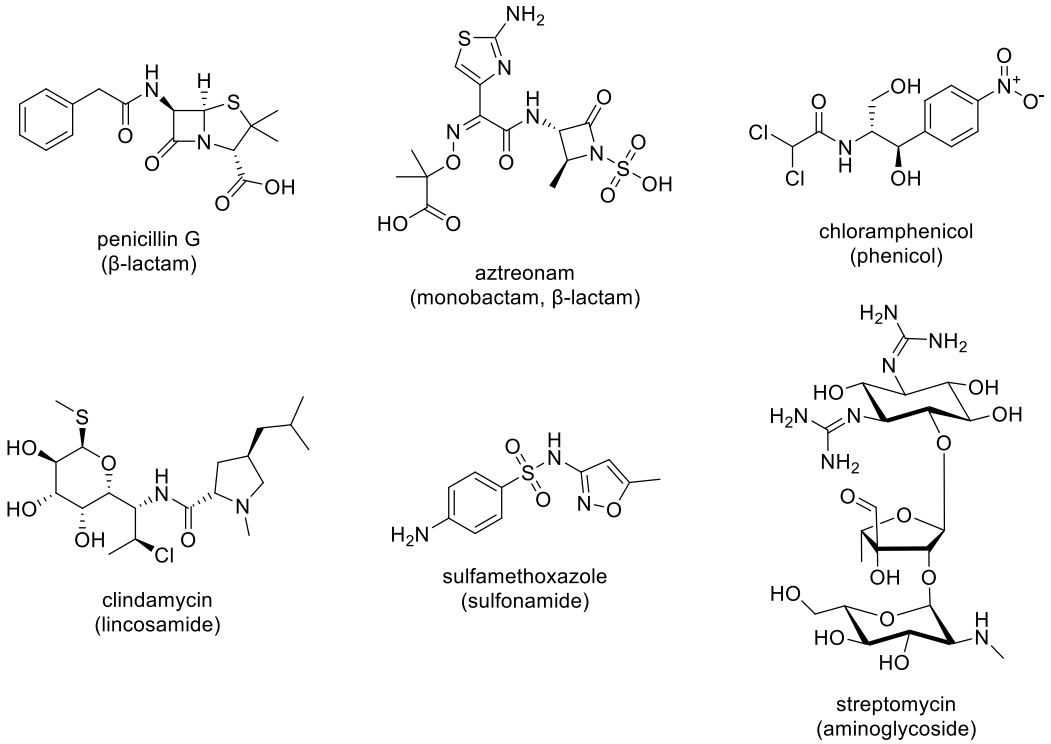

Figure 1.5: Selected examples of different antibiotics classified by their chemical structure.

Besides the classification of antibiotics in terms of their modes of action and their chemical properties, it is also possible to classify them based on their origin, i.e., whether they occur naturally or have been obtained (semi-) synthetically. This subject will be examined in more detail in the following chapter.

2 Literature review

In the following chapter, an overview of the structure and function of bacterial cell walls in general, a distinction between those of Gram-positive and Gram-negative bacteria and the biosynthesis of peptidoglycan, a crucial component of cell walls,[22] will be given. The bacterial membrane protein MraY and its interactions with other proteins as well as cellular uptake of antibiotics will be discussed. Furthermore, nucleoside antibiotics, in particular muraymycins and their semisynthetic and synthetic access, will be introduced with a focus on synthetic pathways and structure-activity relationship (SAR) studies relevant for this work. The concept of prodrugs and the self-resistance theory of muraymycins complete this chapter.

2.1 Bacterial cell wall

Irrespective of the type of bacteria (Chapter 2.1.1), bacterial cell walls are essential in bacterial growth and survival and capture versatile important functions:[46] Besides their role as penetration barrier for toxic molecules like antibiotics, bacterial cell walls control cell shape and support the cytoplasmic membrane against the high internal osmotic pressure. Additionally, bacterial cell walls are involved in the export of cellular products and mediate the adhesion to surfaces and other cells.[46] Bacteria are classified into Gram-positive bacteria, Gram-negative bacteria and mycobacteria due to their cell wall.[46] In this context, the so-called Gram stain named after its developer Hans Christian Gram should be mentioned.[47] This staining method enables the distinction between Gram-positive and Gram-negative bacteria based on the different staining behavior of their cell walls. Cell walls of Gram-negative bacteria decolorize quickly after treatment with ethanol, whereas cell walls of Gram-positive bacteria appear longer blue before decolorizing occurrs.[47,48] The structural differences between cell walls of Gram-positive and Gram-negative bacteria will be described in the following. Since mycobacteria are not part of this work, they are mentioned in the interest of completeness but will not be discussed any further.

2.1.1 Cell wall of Gram-positive and Gram-negative bacteria

Cell walls of Gram-positive bacteria comprise a less complex structural organization than those of Gram-negative species although they are thicker (Figure 2.1).[18] They possess an open, hydrophilic structure mainly composed of peptidoglycan that represents approximately 50% of the weight of the wall and covers the cytoplasmic membrane.[18,46] The formation and structure of peptidoglycan will be presented in Chapter 2.1.2. Cell walls of Gram-positive bacteria exhibit a net negative charge due to the covalent binding of linear anionic polymers (teichoic acids) to peptidoglycan.[46] Lipoteichoic acid as one form of teichoic acids as well as multiple functionally relevant proteins bound to peptidoglycan are found in cell walls of Gram-positive bacteria.[46,49] They are important for interactions between cell walls and their environment. Charged moieties

of capsular polysaccharides loosely attached to the cell walls of Gram-positive bacteria form an additional barrier for antibiotics (electrostatic attraction or repulsion).[18,46] The cell wall of Gram-negative bacteria, on the other hand, is more complex in many aspects (Figure 2.1). In addition to a cytoplasmic membrane, this multilayered cell wall includes an outer membrane, externally located to the peptidoglycan layer and the cytoplasmic membrane, which exhibits an unusual, asymmetric structure.[18] The composition of the outer membrane of Gram-negative bacteria significantly differs from the cytoplasmic membrane as the latter is rich in phospholipids which are replaced by lipopolysaccharides in the outer membrane.[18] These lipids hamper the uptake of hydrophilic agents in Gram-negative bacteria. However, protein channels are incorporated into the outer membrane, thus allowing the elimination of waste products and the access of hydrophilic substances.[50] This so-called 'hydrophilic pathway' is very important since the majority of antibiotics exhibit hydrophilic properties.[18] In 1976, such a channel-forming protein was discovered and termed 'porin'.[51] Hereupon, porins were defined as a class of proteins that form non-specific diffusion channels. [50] They are found in every type of Gram-negative bacteria.[50] Between both membranes, a region called periplasm or periplasmic space with variable thickness is located, demonstrating the complexity of these cell walls.[52] Hence, drug entrance into Gram-negative bacteria is more challenging than into Gram-positive bacteria, especially for targets located in the periplasm and cytoplasm of Gram-negative bacteria. In the latter case, antibiotics need to cross the cytoplasmic membrane mainly by active transport mechanisms. Transport mechanisms and cellular uptake of antibiotics will be discussed in more detail in Chapter 2.3.

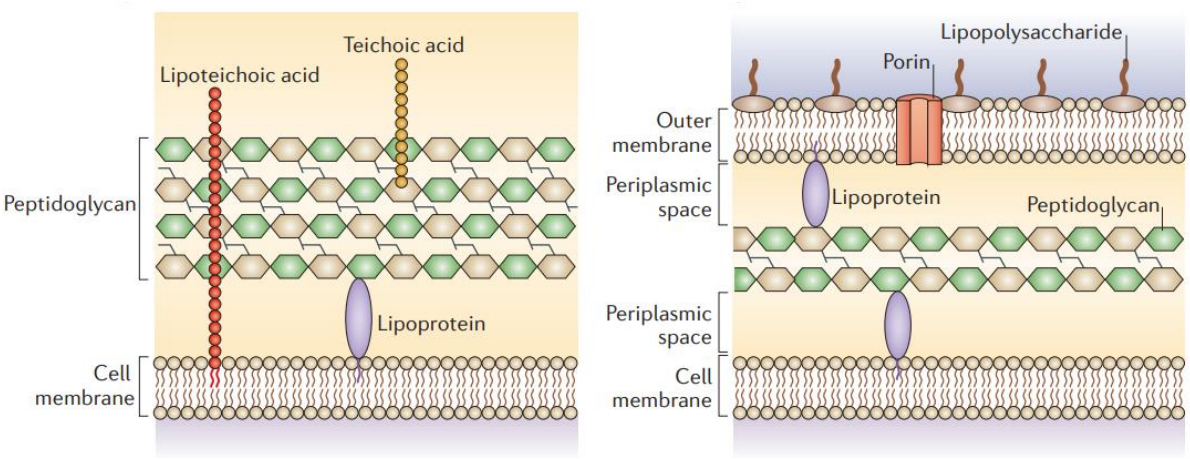

*Figure 2.1: Cell wall of Gram-positive bacteria (left) and Gram-negative bacteria (right) (taken from: Brown, Nature **2015**, 13, 620-630).[49]*

2.1.2 Peptidoglycan and its biosynthesis

Both Gram-positive and Gram-negative bacteria contain the heteropolymer peptidoglycan (also termed murein[22]) as an essential and specific component of their cell walls. The inhibition of its biosynthesis by antibacterial agents or its specific degradation by lysozymes leads to cell lysis,[22] demonstrating the significance of peptidoglycan as an attractive target for antibiotics. The covalent macromolecular structure of peptidoglycan[53] provides a closed, shaped layer around the cytoplasmic membrane and consists of linear glycan strands cross-linked by short peptides[22]. The structure of peptidoglycan for an exemplary amino acid composition is shown in Figure 2.2. Mature glycan strands of bacterial peptidoglycan contain alternating β-1,4-linked *N*-acetylmuramic acid (Mur*N*Ac) and *N*-acetylglucosamine (Glc*N*Ac) moieties.[54] Peptide units vary among different species but are most often comprised of L-Ala-γ-D-Glu-X-D-Ala-D-Ala with X usually being *meso*-2,6-diaminopimelic acid (DAP) in case of Gram-negative bacteria and L-Lys for Gram-positive species.[22] These peptides are attached to the D-lactoyl group of each Mur*N*Ac unit.[19,22,53] After being incorporated into the cell wall, glycan strands are often modified post-synthetically, with *N*-deacetylation, *N*-glycolylation and *O*-acetylation being most frequently observed.[54]

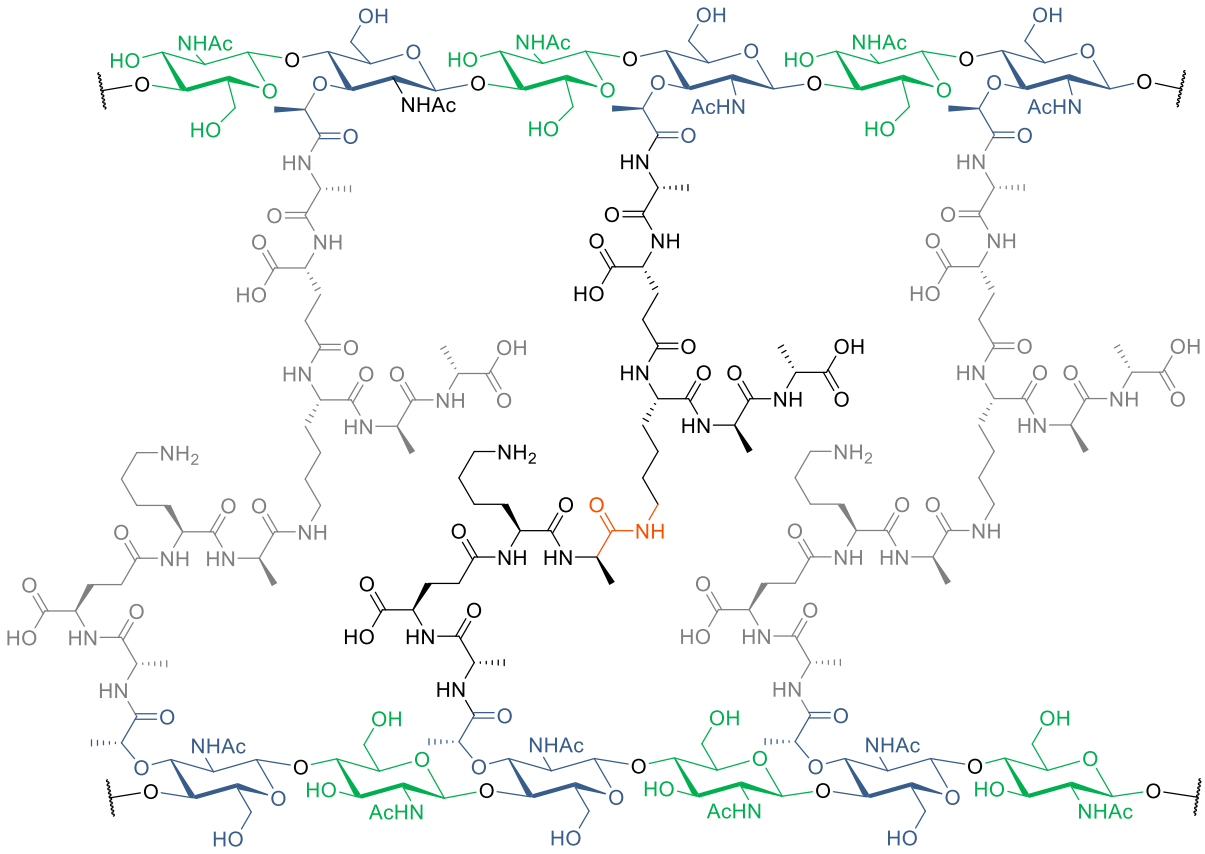

Figure 2.2: Structure of peptidoglycan, consisting of N-acetylmuramic acid (blue) and N-acetylglucosamine (green) glycoside units cross-linked with peptide chains (taken from: Wiegmann et al., Beilstein J. Org. Chem. ***2016****, 12, 769-795).*[55]

Bacterial cell wall biosynthesis has already been described in several reviews[53,56–60] and is therefore summarized very shortly in the following section. The biosynthesis of peptidoglycan includes a complex sequence that occurs in different parts of the bacteria. As schematically depicted in Figure 2.3, it can be divided into three major parts. Starting in the cytoplasm, nucleotide-activated precursors are synthesized (Figure 2.3, step A). This is followed by a membrane-associated sequence with transport of the intermediates to the extracellular side of the membrane (Figure 2.3, steps B and C). Finally, polymerization to oligosaccharides by cross-linking of the peptides takes place at the outer side of the cytosolic membrane (Figure 2.3, steps D and F).

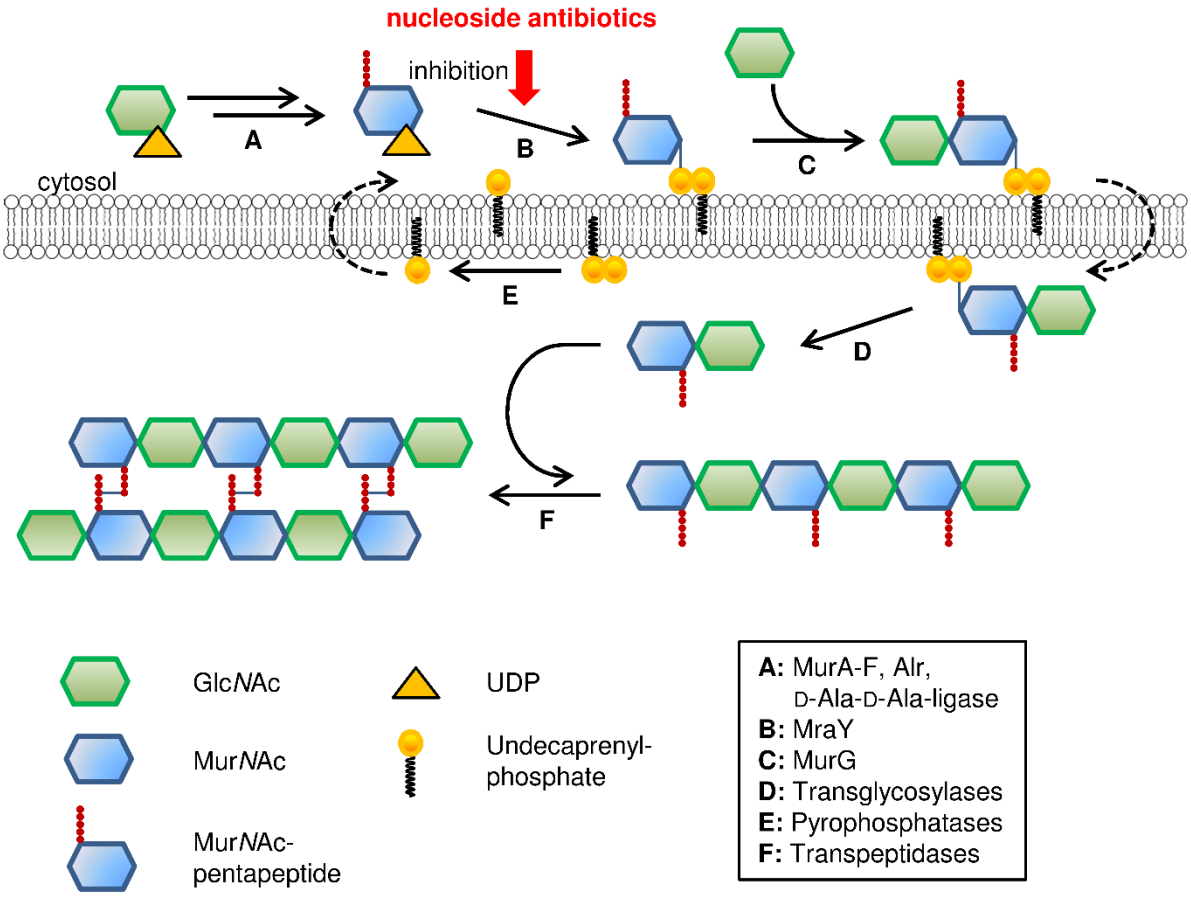

Figure 2.3: Schematic overview of bacterial cell wall biosynthesis (taken from: Wiegmann et al., Beilstein J. Org. Chem. ***2016****, 12, 769-795).*[55]

The first part of bacterial peptidoglycan biosynthesis is shown in more detail in Figure 2.4. It begins with the formation of uridine diphosphate (UDP)-*N*-acetylglucosamine (UDP-Glc*N*Ac) as one of the main cytoplasmic precursors from fructose-6-phosphate.[57] The biosynthesis of this nucleotide-activated sugar[57] includes four enzymatic reactions involving glucosamine synthetase GlmS[61], phosphoglucosamine mutase GlmM[62] and GlmU, the bifunctional glucosamine-1-phosphate acetyltransferase/*N*-acetylglucosamine-1-phosphate uridyltransferase[63,64]. Subsequently, UDP-Glc*N*Ac is transformed into uridine diphosphate-*N*-acetyl-

muramic acid (UDP-Mur*N*Ac) in two enzymatic reactions, catalyzed by MurA and MurB.[19,53] First, the enolpyruvate unit of phosphoenolpyruvate (PEP) is transferred to position 3 of the Glc*N*Ac residue by transferase MurA to obtain UDP-Glc*N*Ac-enolpyruvate. Subsequent reduction of the enolpyruvate moiety to a D-lactoyl unit by the reductase MurB yields UDP-Mur*N*Ac as the second unit for the polysaccharide backbone of peptidoglycan.[19] The next step includes the formation of UDP-Mur*N*Ac-peptides, catalyzed by the highly specific cytoplasmic amino acid ligases MurC, MurD, MurE and MurF (UDP-*N*-acetylmuramoyl-tripeptide-D-alanyl-D-alanine ligase).[19,53,57,65–69] These enzymes mediate the sequential ligation of L-Ala, D-Glu, *m*eso-DAP (or L-lysine) and a dipeptide most frequently consisting of D-Ala-D-Ala[53] to the D-lactoyl unit of UDP-Mur*N*Ac to assemble UDP-Mur*N*Ac-pentapeptide (Park's nucleotide)[70]. This sequence is depicted in step A of Figure 2.3.

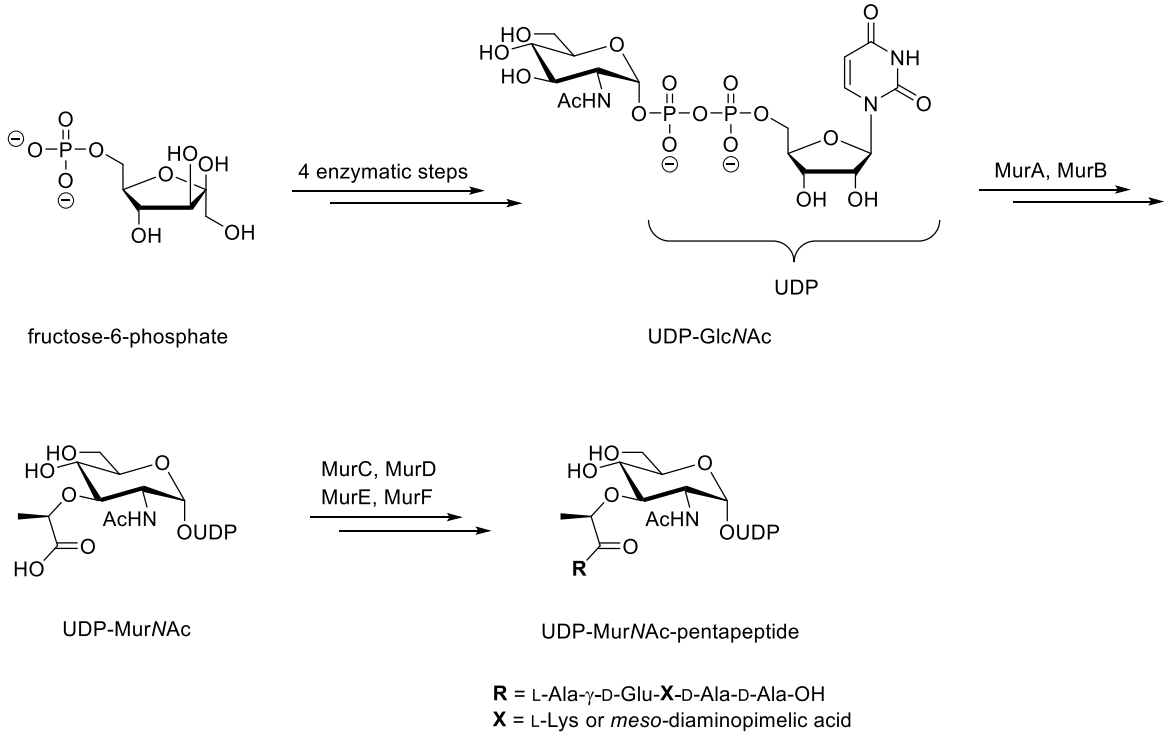

Figure 2.4: First part of peptidoglycan biosynthesis.

Subsequent formation of the lipid intermediates takes place at the inner side of the cytoplasmic membrane[53,57] and is schematically shown in Figure 2.5. The first membrane-associated step starts with the transfer of UDP-Mur*N*Ac-pentapeptide to undecaprenyl phosphate, i.e., a lipid carrier in the membrane, to yield Mur*N*Ac-(pentapeptide)pyrophosphoryl undecaprenol (lipid I).[19,53] This reaction is schematically depicted in part B of Figure 2.3. It is characterized by the substitution of uridine monophosphate (UMP) with undecaprenyl phosphate[71,72] and is catalyzed by a phospho-Mur*N*Ac-pentapeptide transferase (translocase I or MraY)[53,57]. MraY will be discussed in detail in Chapter 2.2.

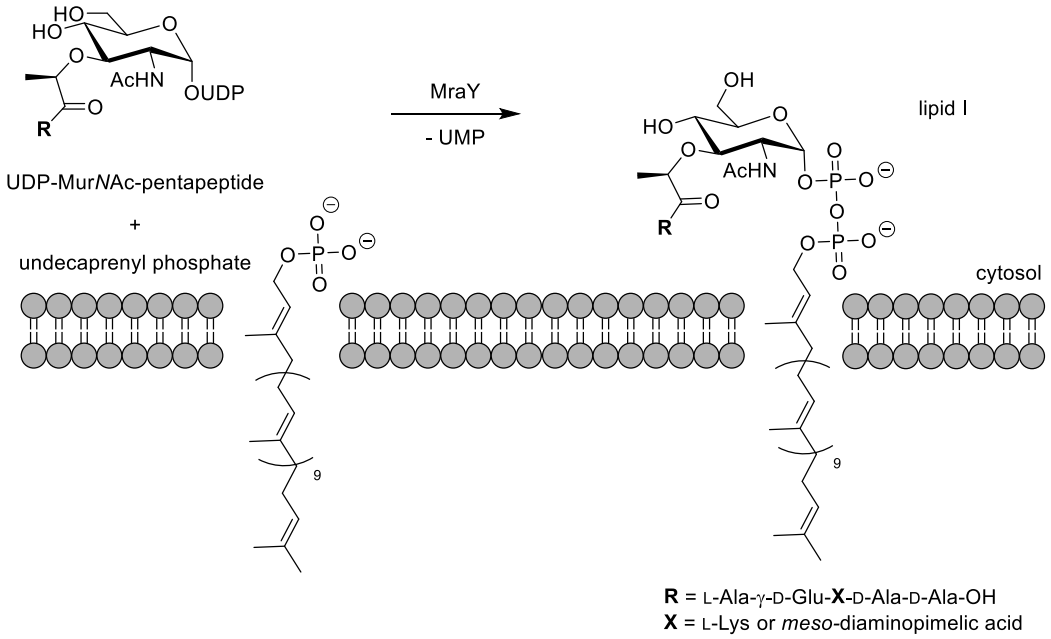

Figure 2.5: MraY-catalyzed reaction as second part of peptidoglycan biosynthesis.

Thereafter, the *N*-acetylglucosamine transferase MurG (translocase II) catalyzes the formation of Glc*N*Ac-Mur*N*Ac-pentapeptide-pyrophosphoryl undecaprenol (lipid II) by attaching a Glc*N*Ac unit of UDP-Glc*N*Ac to lipid I.[19,53] This last intracellular step is represented in step C in Figure 2.3 and schematically illustrated in Figure 2.6. After being moved to the outer side of the cytosolic membrane, lipid II is used as substrate for subsequent polymerization reactions (transglycosylation and transpeptidation) as depicted in steps D and F of Figure 2.3, thus forming mature peptidoglycan.[19,53] Across the cytoplasmic membrane, lipid II serves as substrate for many transferases in order to produce new glycan strands.[57]

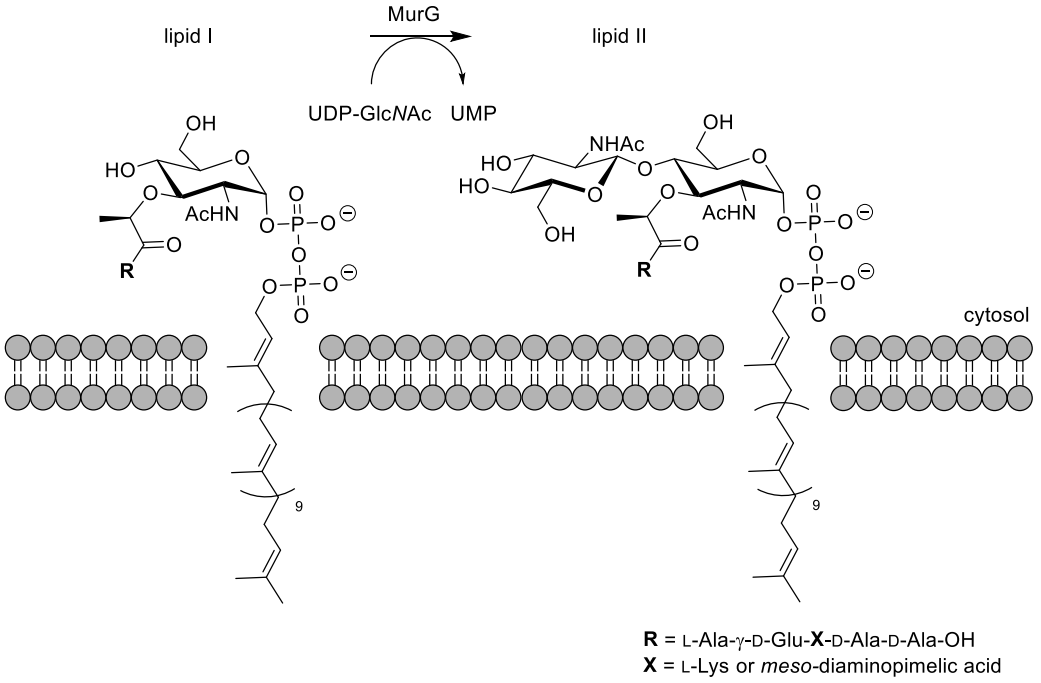

Figure 2.6: Third part of peptidoglycan biosynthesis.

2.2 MraY

MraY is a unique bacterial protein that plays a crucial role in cell growth as it is involved in peptidoglycan biosynthesis.[19,53,73] This membrane-bound enzyme, which is inhibited by a number of non-clinically used antibiotics (Chapter 2.4), has not significantly been targeted yet. Thus, it represents a promising target for the development of novel antibacterial agents. MraY belongs to the superfamily of prenyl sugar transferases[74] and is also known as phospho-*N*-acetylmuramoyl-pentapeptide transferase or translocase I. As mentioned (Chapter 2.1.2), Park's nucleotide and undecaprenyl phosphate serve as substrates of MraY for the formation of lipid I under UMP release.[71,72] The membrane-bound isoprenoid lipid is identitical in all bacteria whereas the cytosolic nucleotide substrate varies.[53] Within this enzymatic reaction, magnesium was identified to be an essential cofactor[75] providing the basis for the hypothesis of a two-step mechanism (Figure 2.7 **A**).[76] Based on kinetic studies and isotope labeling experiments, Heydanak, Neuhaus and coworkers postulated the formation of an initial enzyme-substrate complex by the reversible transphosphorylation of the nucleophilic center of MraY under UMP release.[77,78] This intermediate undergoes another transphosphorylation in a second step in the presence of undecaprenyl phosphate, leading to the formation of lipid I and the native form of MraY.[76] The authors used crude enzyme preparations due to the lack of protein isolation and purification methodologies.[76] This initial hypothesis was revised by Bouhss et al. in 2008 based on site-directed mutagenesis studies utilizing purified MraY from *Bacillus subtilis* ($MraY_{BS}$).[74] The MraY-catalyzed reaction proceeds in one step in which UDP-Mur*N*Ac-pentapeptide is attacked by the enzymatically activated undecaprenyl phosphate with release of UMP as a byproduct (Figure 2.7 **B**).

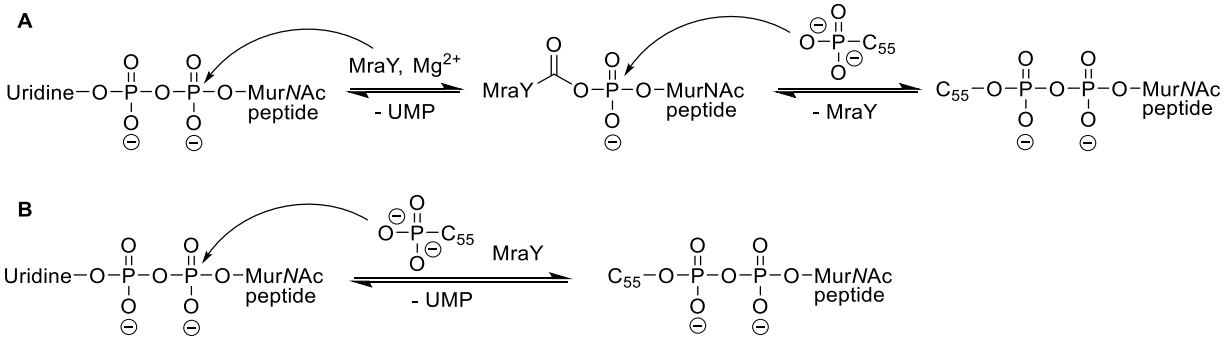

*Figure 2.7: Postulated mechanisms for the MraY-catalyzed reaction (taken from: Wiegmann et al., Beilstein J. Org. Chem. **2016**, 12, 769-795).[55] Two-step mechanism proposed by Heydanek et al. (**A**).[76] One-step mechanism presented by Bouhss et al. (**B**).[74]*

Genes encoding enzymes that are involved in bacterial peptidoglycan biosynthesis are located in discrete regions of chromosome-forming clusters in *E. coli* which Ikeda et al. termed *mra* (murein synthetic gene cluster a), with the largest of these gene clusters including the *mraY* gene encoding MraY.[79] The authors oberserved enhanced activity of MraY in membranes of

E. coli following the overexpression of the *mraY* gene.[79] This was in agreement with the observation of bacterial cell lysis as a result of MraY depletion made by Boyle and Donachie[73]. Moreover, a lipid environment is required for the activity of MraY with respect to its function as a membrane protein.[80–82] These findings led to the developement of a two-dimensional topology model that revealed alternating sequences of lipophilic and hydrophilic domains within the amino acid sequence of MraY (from *E. coli*).[83] Hence, MraY was identified as a protein with ten transmembrane helices, five cytoplasmic loops and six periplasmic domains including the N- and C-termini.[83] The active site of MraY is located at the cytosolic side of the membrane.[84] In 2004, Bouhss et al. described the overexpression, purification and characterization from $MraY_{BS}$ on a milligram scale[85], and a few years later, a cell-free overexpression of MraY was reported[86,87]. A first model of the active site of MraY was established by Bugg and coworkers, identifying three conserved aspartic acid (Asp) residues (Asp115, Asp116 and Asp267).[88] Mutations of these amino acids resulted in the loss of MraY activity, indicating these amino acids to be essential for catalytic activity.[88] While Asp115 and Asp116 were supposed to chelate the magnesium cofactor, Asp267 seemed to function as catalytic nucleophile.[88] A significant contribution regarding the structure of MraY was made by Chung et al. in 2013[89] which will be discussed in the next section.

2.2.1 X-ray crystal structure of MraY

A major breakthrough was achieved with the first X-ray crystal structure of MraY (at resolution 3.3 Å) from the extremophile *Aquifex aeolicus* ($MraY_{AA}$) in 2013, representing the first crystal structure of a member of the family of prenyl sugar transferases.[89] This structure of MraY significantly contributes to insights into catalytic mechanisms for this class of enzymes. Basically, the former topology model of MraY reported by Bouhss et al was confirmed.[83] Moreover, Chung et al. demonstrated that MraY crystallized as an asymmetric dimer with an oval-shaped tunnel at the center of the dimer which was surrounded mostly by lipophilic amino acids, providing space for hydrophobic units.[89] The existence of the protein as a dimer also applies to solutions as reported by Henrich and coworkers.[90] In addition, the magnesium ion was located within the proposed active site of the protein. Due to the location and binding mode of the magnesium ion, the two-step mechanism proposed by Heydanak et al. (Figure 2.7 **A**) has been increasingly questioned.[89] Although these X-ray crystallography experiments were remarkable, there was no progress in gaining further insights into MraY inhibition by nucleoside antibiotics. This changed three years later with the co-crystal structure of $MraY_{AA}$ in complex with a naturally occurring nucleoside antibiotic (muraymycin D2 **1**), at resolution 2.95 Å, published by the same research group.[91] Nucleoside antibiotics and their synthetic access, will be discussed in detail in Chapter 2.4. Chung et al. described the crystallized complex of $MraY_{AA}$ and muraymycin D2 **1** as a dimer, analogous to the previous structure of the ligand-

free apoprotein, and the active site was predicted to be on the cytosolic side of the membrane (Figure 2.8).[91,92]

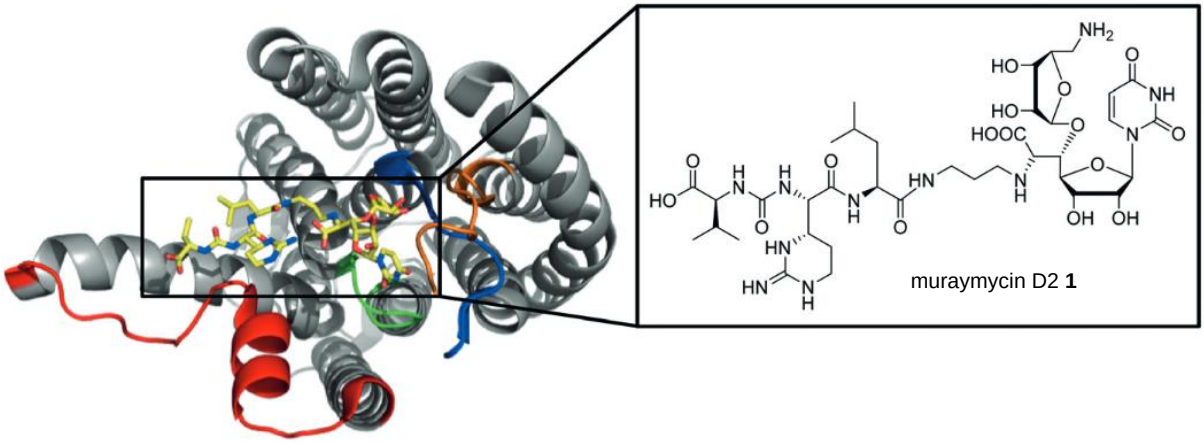

Figure 2.8: X-ray crystal structure of MraY from Aquifex aeolicus in complex with muraymycin D2 ***1*** *(structure shown on the right) from the cytosolic side. The backbone of muraymycin D2 is shown in yellow. The other colors represent parts of MraY that move long distances upon ligand binding. (taken from: Koppermann and Ducho, Angew. Chem. Int. Ed.* ***2016****, 55, 11722-11724).*[92]

However, binding of muraymycin D2 **1** to $MraY_{AA}$ resulted in significant conformational changes of the protein (Figure 2.9 and 2.10 **A**), in which some moieties move distances of 5-17 Å relative to the structure of the apoprotein, thus creating a peptide binding site next to a nucleoside-binding pocket.[91,92] The inhibitor binds to the nucleoside-binding pocket like a plug inserted into a socket, using the aminoribose and uridine moieties as molecular anchors and is additionally stabilized by further interactions in the peptide binding site, thus increasing its affinity for $MraY_{AA}$.[91]

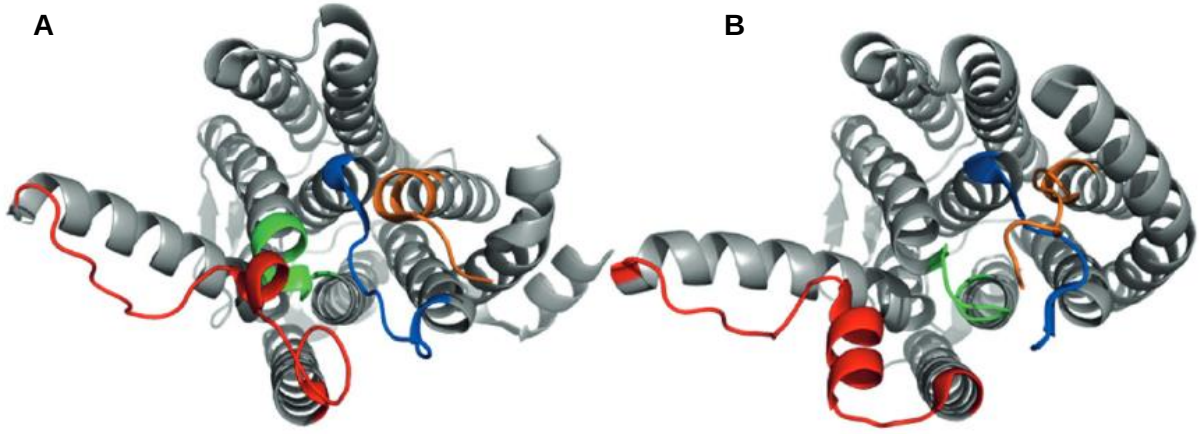

Figure 2.9: X-ray crystal structures of the apoprotein MraY from Aquifex aeolicus*, ligand-free (****A****) and in complex with muraymycin D2* ***1*** *without the ligand (****B****). The comparison between* ***A*** *and* ***B*** *demonstrates the significant conformational changes of the protein (taken from: Koppermann and Ducho, Angew. Chem. Int. Ed.* ***2016****, 55, 11722-11724).*[92]

As shown in Figure 2.10 **B**, two binding pockets for the 5'-aminoribosyl moiety and the uracil base of uridine were identified near the active site upon inhibitor binding. The peptide chain is located on the surface of the protein.[91] Surprisingly, muraymycin D2 **1** did not interact with either one of the three aspartate residues nor with magnesium, although all units are supposed to be required for catalytic activity (Chapter 2.2). This suggested a similar but somehow distinct binding of nucleoside inhibitors to MraY relative to its natural substrate UDP-Mur*N*Ac-pentapeptide which might explain the diversity of inhibitors targeting MraY. It should be noted that, to date, no structure of MraY bound to a substrate or substrate analogue is available.

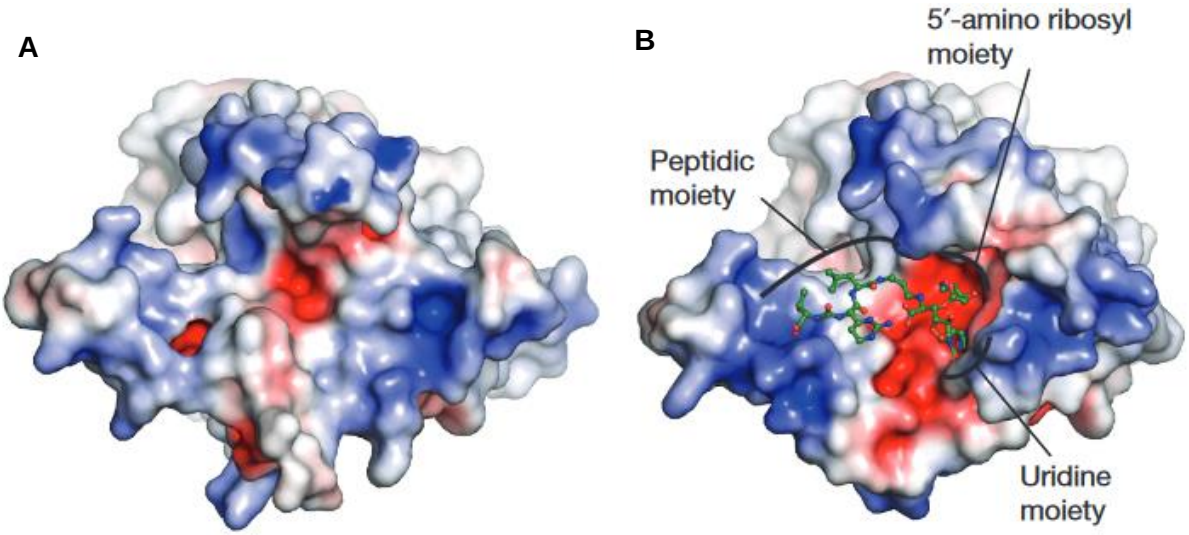

*Figure 2.10: Electrostatic surface representation of MraY from Aquifex aeolicus without (**A**) and in complex with (**B**) muraymycin D2 **1** (illustrated in green), both shown from the cytosolic side. (taken from: Chung et al., Nature. **2016**, 533, 557-560).[91]*

With these studies, Lee and coworkers provided important insights into the interaction of MraY and its inhibitors, thus facilitating the design of new MraY-inhibiting antibacterial drugs in the future. Nevertheless, the conformational plasticity of MraY as well as the aforementioned variety and the size of inhibitors explain the difficulty of reliable computational docking and molecular modeling studies. In the interest of completeness, the crystal structures of MraY in complex with five classes of naturally occurring nucleoside inhibitors reported by Mashalidis and coworkers in 2019 should be mentioned as well.[93]

Basically, two parameters serve as initial properties for the evaluation and characterization of drugs in antibiotics research: the inhibitory concentration at 50% (IC_{50}) *in vitro* for the respective target and IC_{50} values for bacterial growth inhibition. The former refers to inhibition of an enzyme *in vitro* and is defined as the concentration of any inhibitor at which an inhibition of 50% is observed.[94] The latter represent the lowest concentration of antibacterial agents inhibiting the visible bacterial growth.[95] Besides target interaction, IC_{50} values for bacterial growth inhibition provide additional useful information, e.g. about cellular uptake. However,

these data do not reflect target affinity in a direct manner, assays for the determination of inhibitory activities need to be considered separately.

The current state includes three types of established *in vitro* MraY assays. In 1996, Bugg et al. introduced a fluorescence-based enzyme assay with fluorescently labeled UDP-Mur*N*Ac-pentapeptide (dansylated Park's nucleotide).[96,97] This substrate was synthesized in our research group in 2016.[98,99] The assay monitors the change in fluorescence emission as a result of the formation of fluorescent lipid I. In contrast, Bouhss et al. described an MraY assay utilizing radioactively labeled UDP-Mur*N*Ac-pentapeptide.[85] A third MraY *in vitro* assay was published by Shapiro et al.[100] This novel assay takes advantage of Förster resonance energy transfer (FRET) as a FRET donor is linked to UDP-Mur*N*Ac-pentapeptide while a FRET acceptor is placed in detergent micelles containing undecaprenyl phosphate and MraY.[100]

2.2.2 Interactions of MraY with other proteins

Knowledge of functional interactions between proteins is essential for understanding cellular functions. This can be well illustrated with MraY which interacts with a variety of other membrane embedded proteins.[93,101–103] For the investigation of such interactions, an open source database called STRING represents a useful tool as it collects and integrates this information by consolidating known and predicted protein-protein interactions for numerous organisms.[104] STRING accesses information about direct physical interactions but also indirect functional interactions, as long as both are specific and biologically significant.[104] Besides evidence from real biochemical, biophysical and genetic experiments or databases of known metabolic pathways, STRING also includes phylogenetic distributions of orthologs of all proteins in a given organism among others. Furthermore, the genomic neighborhood as well as occurrence patterns of gene families and proteins whose genes are correlated in their expression are taken into account, thus resulting in a theoretical interaction network of the corresponding gene or protein.[104] An exemplary interaction map is schematically depicted for the *mraY* gene of *Aquifex aeolicus* VF5 in Figure 2.11

.

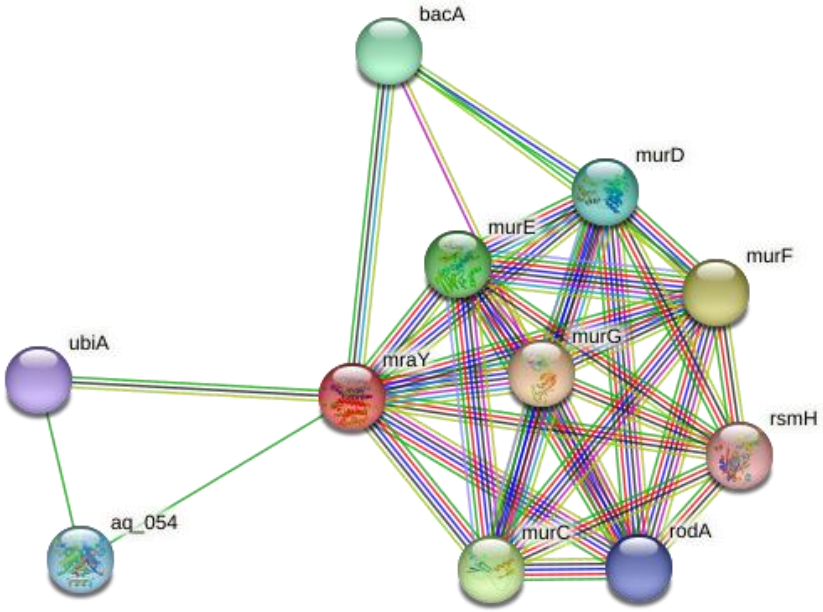

Figure 2.11: Interaction network of the mraY *gene of* Aquifex aeolicus *VF5 obtained from the bioinformatical software STRING.*

2.2.3 Interaction of MraY and nanobody 7

An artificially induced interaction between MraY and another protein was demonstrated by Mashalidis et al. in 2019.[93] As this interaction plays an important role in this work, it will be presented in the following. With the aim to stabilize crystals, the authors specifically raised an antibody against $MraY_{AA}$.[93] Such antibodies are generally termed nanobodies. They represent a novel class of naturally occurring antigen-binding fragments with beneficial properties like small size, high stability, water solubility and a strong antigen-binding affinity.[105] Nanobodies were first described in 1993 although they were not termed like this during this time.[106] They are derived from so-called heavy-chain-only (or single-chain) antibodies present in the serum of camelids such as, e.g., llamas, dromedaries or alpacas and can be considered as a smaller variant of antibodies.[93,105] While antibodies contain light- and heavy-chain domains, the former is absent in nanobodies, thus explaining their reduced size.[105] Up to date, various nanobodies are part of clinical studies concerning human diseases like breast cancer and enjoy the status of next-generation biodrugs.[105]

In their studies, Mashalidis et al. demonstrated the interaction of several high-affinity $MraY_{AA}$ nanobodies and $MraY_{AA}$, resulting in complexes that remained intact during size exclusion chromatography (SEC).[93] One nanobody in particular formed a tight complex with $MraY_{AA}$.[93] This nanobody was termed nanobody 7 (NB7) and its presence did not affect $MraY_{AA}$ enzymatic activity or inhibition by nucleoside antibiotics such as carbacaprazamycin, capuramycin or 3'-hydroxymureidomycin A.[93] NB7-$MraY_{AA}$-complexes were subjected to X-ray crystallography that identified $MraY_{AA}$ as a dimer with NB7 bound to each protomer on the periplasmatic site, away from the catalytic site (Figure 2.12).[93] This is consistent with its

oligomeric state.[93] The interaction between NB7 and $MraY_{AA}$ was exploited in one project of this work and will be discussed in Chapters 3 and 4.

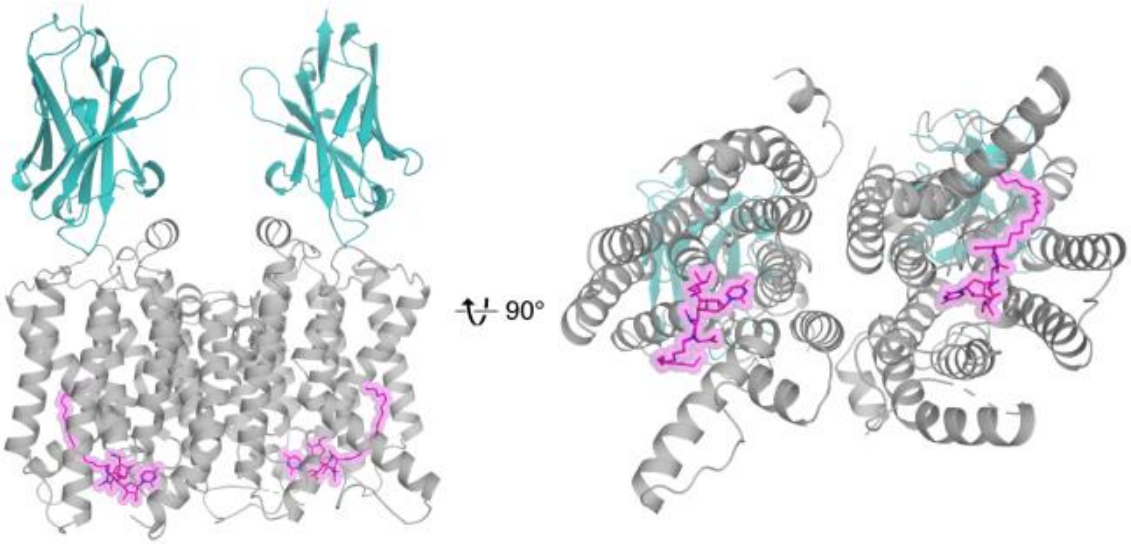

Figure 2.12: Complex between MraY from Aquifex aeolicus (gray) and nanobody 7 (teal) with carbacaprazamycin (purple) bound, shown from the membrane and cytoplasmic side (taken from: Mashalidis et al., Nat. Commun. ***2019****, 10****,*** *2917).*[93]

2.2.4 Nanodiscs and MraY

Membrane proteins, including MraY, play a major role in fundamental cellular and biophysical processes.[107] They vary greatly in terms of their size, structure and function and mostly require a phospholipid bilayer membrane for their structural stabilization.[107] Approximately 20-30% of all bacterial genes are estimated to encode membrane proteins[108], while only about 2% of all protein structures in the protein database are those of membrane proteins due to their non-trivial production in folded and active forms[109]. This difficulty mainly arises from the selection of an appropriate membrane-mimetic environment supporting the proteins' function and stability.[109] Detergent micelles have historically been used as a common tool to stabilize many membrane proteins.[110] However, the application of detergents may reduce enzymatic activity and/or ligand binding of membrane proteins, illustrating only a few disadvantages.[109] Membrane mimetic systems such as vesicles or liposomes are also associated with challenges.[111–113] Protein preparations prepared from liposomes, e.g., can become cloudy and viscous within a short period of time, caused by the protein's precipitation, indicating the system's instability.[107] Current investigations concerning alternative approaches for membrane stabilization provided detergent micelles,[114] detergent bicelles,[115] bilayers such as amphipols[116] or detergent-free nanometer scale lipid bilayers called nanodiscs,[107,109,117,118] all enabling structural insights into protein function and structure. The first two mentioned systems ultimately cause the same aforementioned problems due to the presence of detergents. Therefore, detergent-free nanodiscs came to the fore more recently and will be described in detail here as they play a major role in this work. Nanodiscs are self-assembled

molecular particles characterized by a discoidal phospholipid bilayer which is stabilized via encircling amphipathic helical membrane scaffold proteins (MSPs), overall leading to the mimicry of a native lipid environment.[107] The initial MSP sequences were derived from the human ApoA1 protein of high-density lipoprotein particles and have been optimized to form stable and useful bilayers with defined size and composition.[107,119,120] An empty nanodisc is schematically depicted in Figure 2.13.

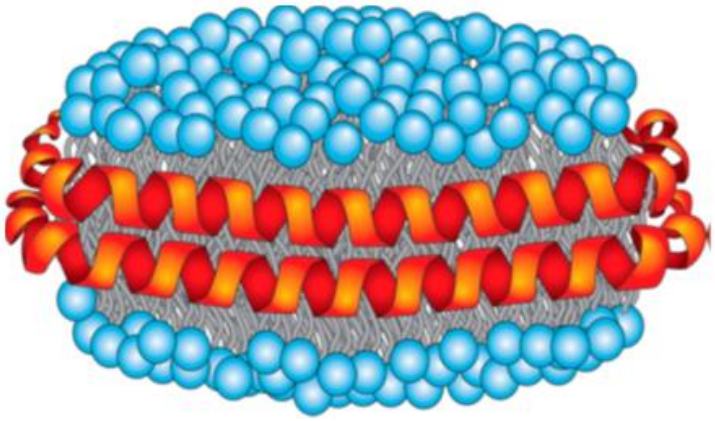

Figure 2.13: Schematic nanodisc assembly as phospholipid bilayer with its hydrophilic moieties (blue) and its unpolar units (grey) stabilized by encircling membrane scaffold proteins (red) in helical conformation (taken from: Denisov and Sligar, Chem. Rev. ***2017****, 117, 4669–4713).*[107]

The self-assembly of nanodiscs, i.e., detergent removal from membrane proteins solubilzed in detergent micelles, can be induced by adsorption on hydrophobic beads or by dialysis. The assembly success primarily depends on the ratio between the target protein, the lipid mixture and MSP as demonstrated by Hagn et al.[109]: an optimal ratio during assembly will provide monodisperse membrane proteins that can be studied in solution nuclear magnetic resonance (NMR) studies and/or other techniques. To further improve nanodisc size control and uniformity, covalently circularized nanodiscs (cNDs) were engineered for structural biology studies.[121] Besides their use in this advantageous spectroscopy tool, the permanent dynamic equilibrium of nanodiscs with their environment, their higher stability and more defined structure can be listed as additional benefits relative to other self-assembled systems like the aforementioned liposomes.[107,109]

In his dissertation, Dr. P. Fischer (Dana-Farber Cancer Institute, Arthanari Laboratory, Boston, USA) developed a detergent-free, lipid bilayer environment for MraY, the MraY nanodiscs.[122] In this system, solubilized $MraY_{AA}$, stabilized in decyl-β-D-maltopyranoside (DM) micelles, is used in a near-native lipid environment. Compared to crude membranes with overexpressed MraY, which is routinely used in inhibitory assays in our lab, isolated solubilized protein was purified and does not contain other membrane components which could influence the ligand-target-interaction. Since the size of the nanodisc is determined by which MSP is used, MSP1E3D1 was chosen for MraY.[122,123] MSP1E3D1 produces nanodiscs of 12-14 nm in

diameter, thus providing enough space for the homodimeric MraY (~ 80 kDa).[122,123] Considering the phospholipid mixture of membranes of *E. coli* which contains 75% phosphatidylethanolamine, 20% phosphatidylglycerol and 1-5% cardiolipin[124], a mixture of 85% 1,2-dioleoyl-*sn*-glycero-3-phosphoethanolamine (DOPE) and 15% 1,2-dimyristoyl-*sn*-glycero-3-phospho-*rac*-(1-glycerol) (DMPG) was used as phospholipid composition to keep the environment similar[122]. MraY-nanodisc formation was realized by combining solubilized $MraY_{AA}$, MSP1E3D1 and the aforementioned lipid mixture, followed by detergent removal using neutral macroporous polymeric beads.[122] The success of the MraY-nanodisc formation was shown by SEC followed by sodium dodecyl sulfate polyacrylamide gel electrophoresis (SDS-PAGE) analysis, transmission electron microscopy and the MraY inhibition assays (Chapter 7.1.2.3).[122]

The $MraY_{AA}$ nanodiscs were subjected to the MraY *in vitro* assay with one member of each series of the naturally occurring muraymycins (Chapter 2.4.1) as inhibitor: muraymycin A1, B2, C1 and D2 **1**. The inhibition data was determined as part of this work in collaboration with Dr. P. Fischer[122] and are depicted in Table 2.1. They will be discussed here compared to the previous data for which crude membranes of MraY from *Clostridium bolteae* ($MraY_{CB}$), solubilized $MraY_{CB}$ and solubilized $MraY_{AA}$ have been used.[84,122] It should be noted in the interest of completeness that crude membranes of $MraY_{SA}$ have been used in this series of measurements as well.[84] They are not presented in this context as the comparison between solubilized and crude membranes is in the fore and these data are available for $MraY_{CB}$. The inhibition data of muraymycin B2, C1 and D2 **1** using $MraY_{AA}$ nanodiscs are preliminary due to their rapid activity loss (Table 2.1). The measurements need to be repeated.

Table 2.1: Inhibition data from in vitro *MraY assays of naturally occurring muraymycins A1, B2, C1 and D2* ***1****.[84,122] *The inhibitory activities of muraymycin B2, C1 and D2* ***1*** *against* $MraY_{AA}$ *in nanodiscs are preliminary.*

	IC_{50} [nM]			
	Clostridium bolteae crude membrane	*Aquifex* solubilized	*Clostridium bolteae* solubilized	Nanodiscs
muraymycin A1	0.017 ± 0.004	0.11 ± 0.02	0.16 ± 0.04	3.5 ± 0.2
muraymycin B2	0.0083 ± 0.0006	0.11 ± 0.01	0.14 ± 0.01	0.87 ± 0.11*
muraymycin C1	0.093 ± 0.020	0.35 ± 0.04	0.45 ± 0.17	0.92 ± 0.16*
muraymycin D2 **1**	25 ± 4	46 ± 13	200 ± 30	1000 ± 200*

The inhibitory activity of muraymycin A1 using $MraY_{AA}$ nanodiscs decreased by a factor of ~ 200 (IC_{50} = 3.5 ± 0.2 nM) compared to crude membrane preparations of $MraY_{CB}$ (IC_{50} = 0.017 ± 0.004 nM). The difference of $MraY_{AA}$ nanodiscs to both solubilized MraY proteins, $MraY_{AA}$ (IC_{50} = 0.11 ± 0.02 nM) and $MraY_{CB}$ (IC_{50} = 0.16 ± 0.04 nM), is less pronounced, but nonetheless observable. The comparison between the inhibitory activity of muraymycin A1 in crude membrane preparations of $MraY_{CB}$ and in isolated purified $MraY_{CB}$

already demonstrates the high impact of enzyme preparation on the inhibitory potential: muraymycin A1 was less potent (factor ~ 10) against solubilized protein compared to the same homologue overexpressed in crude membranes (Table 2.1). This also applied for muraymycins B2, C1 and D2 **1** (Table 2.1) with muraymycin B2 showing the most pronounced differences with a factor of ~ 17. In summary, a previous trend could be observed for the tested muraymycins, although the data obtained for muraymycin B2, C1 and D2 should be interpreted with care as already mentioned: the highest IC_{50} values were obtained when using MraY-nanodiscs, while crude membrane preparations of $MraY_{CB}$ caused the lowest IC_{50} values. Taking the experimental uncertainty into account, both proteins in solubilized form, $MraY_{AA}$ and $MraY_{CB}$, elicited the same inhibitory data of the tested inhibitors (Table 2.1).

The reason for the differences in inhibitory activities using crude membranes and solubilized protein might be DM, a non-denaturing detergent, which is absent in crude membrane protein preparations. DM could affect the structural rearrangements of MraY required for an effective enzymatic inhibition by nucleoside antibiotics.[122] Moreover, the dynamic interplay between other components of crude membrane preparations should be kept in mind, which does not affect for solubilized proteins since they are free from impurities. It should also be considered that purification and solubilization of MraY in micelles could lead to partially misfolded protein. Hence, substrates were not quantitatively converted into dansylated lipid I and as a consequence higher concentrations of inhibitors would be needed to obtain IC_{50} values in the same range.[122] These considerations represent the basics for one of the projects of this work which will be presented in Chapter 3. With the MraY nanodiscs, Dr. P. Fischer provided a novel approach for our research group for elucidating integral membrane protein functions. The publication of Roos et al.[125] in 2012, however, needs to be mentioned here as well as the recently published work of Lui et al.[126] who focused on $MraY_{BS}$ in nanodisc systems.

2.3 Cellular uptake of antibiotics and corresponding assays

The bacterial cell wall functions as a barrier for all types of substances and needs to be crossed by many antibiotics, thus representing a major hurdle for their action. As already mentioned, there are different types of membrane transport mechanisms: mainly passive and active transport ways.[18] A general overview will be briefly given here. The simplest form of transport is the diffusion of small lipophilic molecules through biological membranes with concentration gradients as the driving force, thus generating an equilibrium between the intra- and extracellular space.[127] Such a passive transport takes place without any energy source being required. In contrast, active transport ways do not consider concentration gradients, but the corresponding transporters are dependent on pumps instead. They function as energy source for the (active) transport.[127] This points out the major differences between passive and active

transport mechanisms: the direction of the concentration gradient during transport and consequently the need of pumps as energy source.[127]

As cellular uptake of muraymycin analogues plays a major role in this work, cellular uptake of antibiotics as well as literature-known cellular uptake assays will be discussed in more detail here. In general, overcoming the cell wall is easier in Gram-positive bacteria than in Gram-negative pathogens due to their cell wall composition (Figure 2.1). The same applies for drugs with targets on the outside of the cytoplasmic membrane of Gram-negative bacteria as compared to those with cytoplasmic targets which need to pass two membranes for being effective.[18] Amongst others, cellular uptake of antibiotics varies with their physicochemical profile, such as size, charge and hydrophilicity besides cellular aspects like the number of porins or other transporting channels present in bacterial membranes.[18,128] Most agents with antibacterial activity possess hydrophilic properties, thus crossing bacterial cell walls through porins via the 'hydrophilic pathway' (Chapter 2.1.1).[18] In contrast, antibiotics with lipophilic moieties utilize the hydrophobic pathway by dissolving in the phospholipid bilayer.[18] Other chemical parameters which play an essential role in this context besides the polarity of drugs are properties such as the number of hydrogen bond acceptors or donors, the availability of polar surfaces and their molecular weight.[128] These properties guide antibiotics in terms of their antibacterial activity, i.e., if they are antimicrobially active against Gram-positive bacteria only or against Gram-negative bacteria. O'Shea and Moser showed that the polarity of antibiotics with Gram-negative antibacterial activity is higher than of those with Gram-positive activity only.[128] In addition, as compared to other drugs that served as reference group in these studies, antibiotics with Gram-negative antibacterial activity had higher molecular weights, however, there is a defined cut-off at 600 Dalton (Da).[128] The hydrophilic pathway illustrates the major entry route of drugs into Gram-negative bacteria, with antibiotics larger than 600 Da being directly excluded.[128] Interestingly, a cut-off regarding molecular weight was not found for antibiotics with Gram-positive bacteria activity only, in particular with targets in the peptidoglycan matrix or on the outer surface of the lipid layer as for e.g. the cell wall biosynthesis inhibitor vancomycin.[128] Moreover, additional studies by Hergenrother and coworkers assigned geometric parameters like flexibility and globularity as fundamental factors of cellular uptake and accumulation of antibiotics in Gram-negative bacteria.[129] Based on computational studies, the authors predicted small, rigid, amphiphilic, non-sterically hindered amine-containing antibiotics with a minor number of rotatable bonds (implying low flexibility) and with low globularity to exhibit best accumulation potential into Gram-negative *E. coli* (Figure 2.14, left).[129] Furthermore, drugs with activity against Gram-positive bacteria only significantly differ from those with activity against Gram-negative bacteria regarding charge, flexibility and globularity (Figure 2.14, right). Impressively, the application of their guidelines led to the conversion of a natural product with activity against Gram-positive bacteria only into

an antibiotic active against various resistant Gram-negative bacteria, indicating the importance of these 'eNTRY rules studies' for the development of novel antibiotics.[129] Therefore, the open-access web application 'eNTRYway' was developed for the prediction of compound accumulation potential in *E. coli* by the same research group.[130]

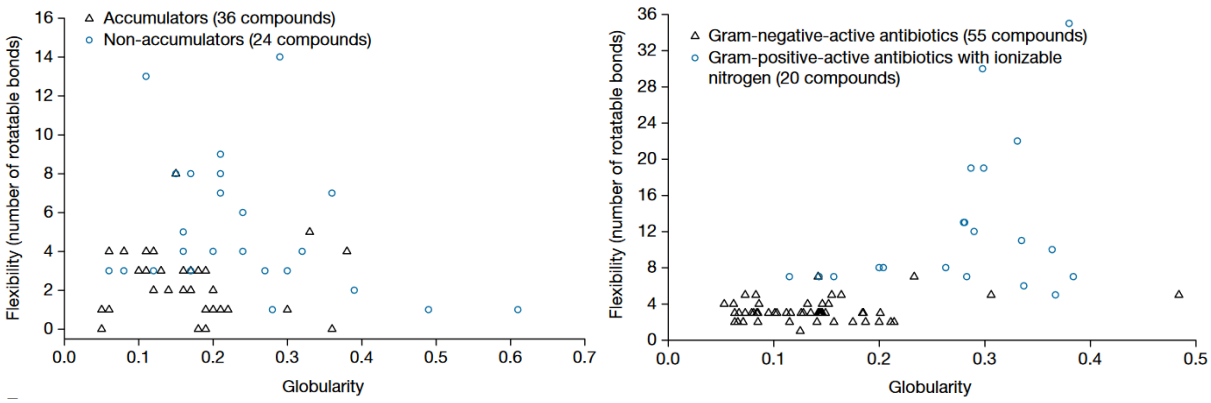

*Figure 2.14: Flexibility and globularity of antibacterially active drugs. Left: Accumulating drugs exhibit low flexibility and low globularity. Right: Proposed accumulation into Gram-positive and Gram-negative bacteria (taken from: Richter et al., Nature **2017**, 545, 299-304).[129]*

Besides cellular uptake of antibiotics through transport mechanisms, efflux of antimicrobial agents should not be neglected. After antibacterial agents have entered bacterial cells, the natural urge of bacteria is their direct removal via protein channels like TolC as the most prominent example (Chapter 1.2). Hence, cellular uptake and accumulation of antibiotics and efflux processes often compete.

In the last years, the investigation of cellular uptake and accumulation of drugs in bacteria has been extensively studied. The current state in terms of established cellular uptake and accumulation assays will be presented here with focus on different methodologies and publications with relevance for this work. Strikingly, cellular uptake and accumulation in Gram-negative bacteria (mostly *E. coli*) is more represented in the literature while the field does not cover Gram-positive bacteria well. In 2008, a liquid chromatography (LC)-mass spectrometry (MS)-based drug accumulation assay was developed by Cai et al. with *P. aeruginosa* as bacterial species.[131] First, they developed a fluorescence assay which was aimed to provide the assay conditions for the following rabiolabeled assay by measuring the time-dependant accumulation of a tracer.[131] Subsequent radiolabeled assay included ^{3}H-labeled antibiotics and was implemented in the LC-MS-based drug accumulation assay of this research group.[131] In general, radiolabeling cannot be carried out in many laboratories and is therefore not suitable for accumulation assays. Fluorescence, however, basically represents another tool that might be more appropriate compared to assays based on radiolabeling. This is due to their sensitivity and the optical 'read-out'.[132] But fluorescence-based models are also associated with disadvantages as derivatizations of drugs with fluorescent dyes would influence cellular

uptake due to altered physicochemical properties of the antibiotics. Until then, the most feasible method was published by Zhou et al. with their drug accumulation assay based on LC-MS.[133] This assay uses the theoretical calculation of intracellular amounts of drugs by comparing extracellular concentrations before and after the incubation with bacteria. Unlike a direct measurement of intracellular amounts, the authors measured the reduction of compound concentration in the external culture medium.[133] This protocol served as basic construct for the assays of J. Meiers during his diploma thesis in our research group.[134] The accumulation assay of J. Meiers is based on the incubation of a defined number of Gram-negative *E. coli* cells with antimicrobially active candidate compounds. After cell lysis, cellular uptake was quantified by LC-MS. Besides the determination of total intracellular drug concentrations, a distinction between cytoplasmic and periplasmic spaces is now feasible. Further detailed insights, especially additional developments and modifications of the assay that are performed in this dissertation, will be given in the corresponding chapters of this work (Chapters 2.4.4, 3 and 4.1.1). The same principle was applied by Brönstrup and coworkers in 2019 with the additional investigation of membrane components.[135] In the interest of completeness, a current protocol for the quantification of drug accumulation by LC-MS/MS by Geddes et al. in 2021 should be noted as well.[130] In general, comparisons between different assays and their outcome are difficult mainly due to different assay conditions like variations in media, growth conditions and bacterial strains and should therefore be interpreted with care.

2.4 Nucleoside antibiotics

Nucleoside antibiotics have been intensively reviewed by Bugg et al.[19,136], Ichikawa et al.[137] and our research group[55]. They are uridine-derived natural products representing a huge, promising class of novel antibacterial agents. Although they all share a nucleoside core structure, representatives of this class are structurally very diverse. Some selected examples of various nucleoside antibiotic classes are depicted in Figure 2.15. As already discussed (Chapters 2.1.2 and 2.2), nucleoside antibiotics exhibit the same mode of action as they target the bacterial membrane protein MraY, thereby inhibiting the formation of lipid I, a key intermediate of peptidoglycan biosynthesis. So far, there are no nucleoside antibiotics in clinical investigations,[53] underlining the importance of research in this field.

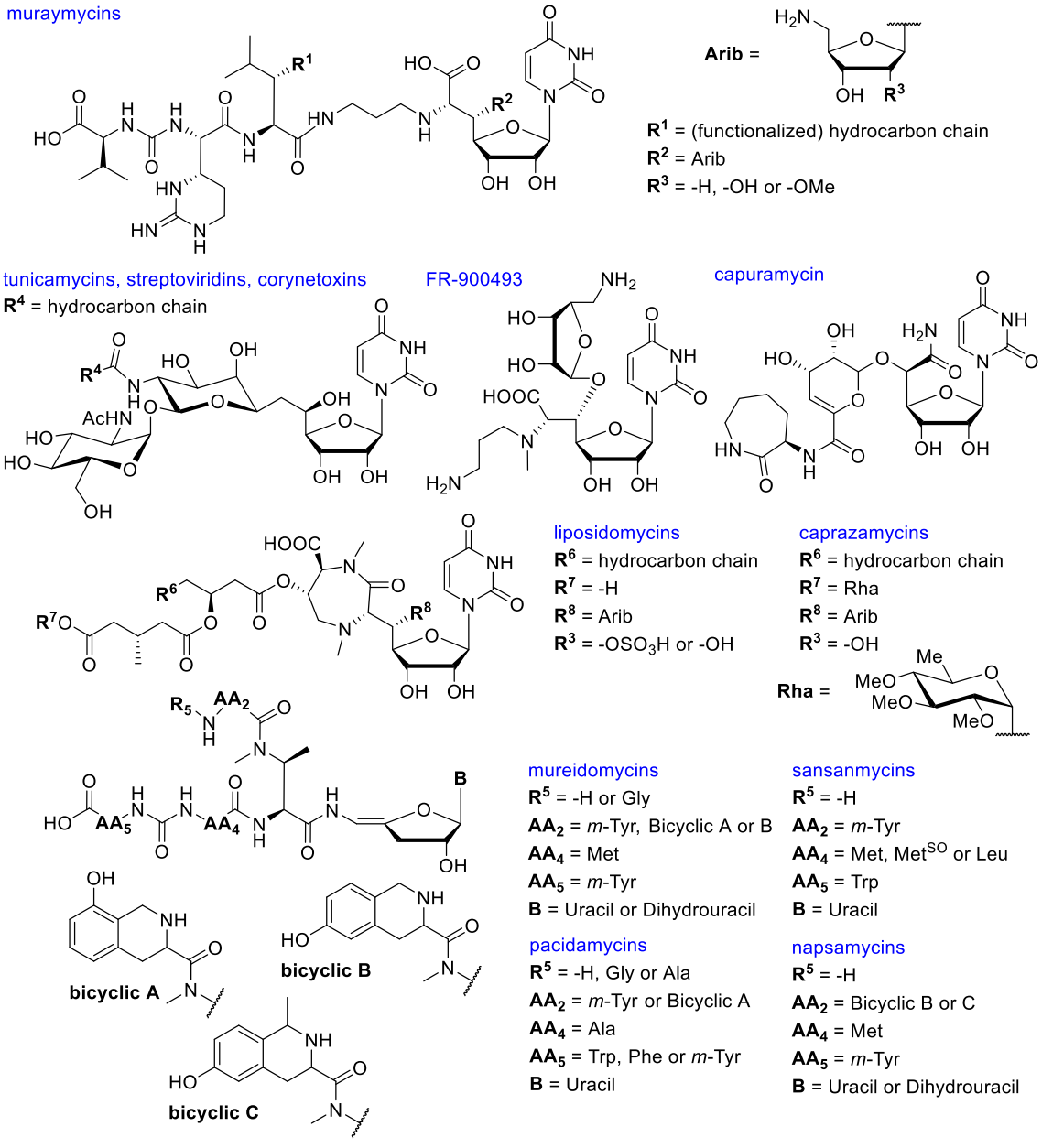

*Figure 2.15: Selected representative classes of nucleoside antibiotics (taken and modified from: Wiegmann et al., Beilstein J. Org. Chem. **2016**, 12, 769-795).[55]*

There are numerous potent naturally occurring inhibitors of MraY. The first class of nucleoside antibiotics, tunicamycins, was isolated in 1971 from *Streptomyces lysosuperfiscus* by Takatsuki and Tamura.[138–140] Members of this class consist of a uridine core structure and two *O*-glycosidically linked sugars (the so-called tunicamines) and a mostly unsaturated fatty acid chain (Figure 2.15). Tunicamycin was isolated as a mixture of homologous antibiotics.[141] A few years later, streptovirudins[142–144] and corynetoxins,[145] two structurally closely related families, were discovered (Figure 2.15). These classes show antibacterial activity against Gram-positive bacteria but are rather unattractive to be developed as drugs due to their pronounced cytotoxicity against human cells.[141]

Mureidomycins,[146–148] pacidamycins,[149–151] napsamycins[152] and sansanmycins[153,154] were discovered in 1989, 1994 and 2007/2008. These structurally closely related classes all consist of a 3'-deoxyuridine unit with an uncommon enamide linkage and the non-proteinogenic 2-amino-3-methylbutyric acid. Two other aromatic amino acids in positions AA_2 and AA_5 are connected to the core system: non-proteinogenic L-*m*-tyrosine in position AA_2 and proteinogenic L-tryptophan in position AA_5 in case of sansanmycins and L-*m*-tyrosine in both positions in case of mureidomycins (Figure 2.15). Mureidomycins, pacidamycins, napsamycins as well as sansanmycins are characterized by their specific anti-pseudomonal activity while lacking biological activity mainly against Gram-negative *E. coli* or Gram-positive *S. aureus.*[148,151,152,154] Pointing out a significant difference from the other classes, sansanmycins A and B showed pronounced antibacterial activity against *Mycobacterium tuberculosis* (*M. tuberculosis*).[154]

Two diazepanone ring-containing classes are liposidomycins, isolated in 1985 from *Streptomyces griseosporeus*,[155] and caprazamycins, discovered in 2003[156,157]. These representatives consist of an aminoribose unit attached to the 5'-position of the uridine moiety and a long hydrophobic side chain that is connected to the diazepanone ring (Figure 2.15). A rhamnose unit in position R^7 is present in case of caprazamycins (Figure 2.15). Impressively, liposidomycins exhibit activity against *Mycobacterium phlei* while being inactive against all other strains tested.[155] The family of caprazamycins is active against *M. tuberculosis* and against most Gram-positive bacteria.[156,158] Even before the discovery of caprazamycins, capuramycin was isolated from *Streptomyces grisus* in 1986. It only shares the nucleoside core with the other classes and is inactive against Gram-negative strains (Figure 2.15).[159–161] The only pronounced activity was seen against *Streptococcus pneumoniae* and *Mycobacterium smegmatis*.[160]

A truncated version of muraymycins, another class of nucleoside antibiotics, is represented by an antibacterial agent termed FR-900493 that was isolated in 1990 from *Bacillus cereus.*[162,163] In comparison to the class of muraymycins, FR-900493 exhibits a simplified structure as the urea dipeptide unit and the lipopeptidyl moiety are missing (Figure 2.15). It shows antimicrobial

activities against *S. aureus* und *Bacillus subtilis*.[163] Since muraymycins are a major part of this work, they will be discussed in detail in the next section.

In summary, certain structural units are present among these different classes of nucleoside antibiotics: A hydrocarbon chain is found in muraymycins, tunicamycins, streptovirudins, corynetoxins and caprazamycins. Muraymycins, liposidomycins and caprazamycins contain an aminoribose moiety, and a urea dipeptide is present in muraymycins, mureidomycins, sansanmycins, pacidamycins and napsamycins. As already mentioned, there are significant differences in terms of antibacterial activities of these nucleoside antibiotics which are poorly understood so far.

2.4.1 Naturally occurring muraymycins

In 2002, the family of muraymycins was isolated from a strain of *Streptomyces sp.* by McDonald et al.[164] Since then, Cui et al. discovered three new muraymycin congeners.[165] These currently known 22 naturally occurring muraymycins are depicted in Figure 2.16. Muraymycins are divided into four different subfamilies A-D with respect to their structural composition.[164] Basically, the family of muraymycins represents a class of nucleoside-lipopeptide antibiotics and shares a glycyl-uridine motif as core structure. This (5'*S*,6'*S*)-nucleosyl amino acid unit is *O*-glycosidically linked to an aminoribose unit at the 5'-hydroxy position in all muraymycins, except for muraymycins A5 and C4 **2** most likely as a result of hydrolysis during isolation.[164] Furthermore, the uridine core is linked via an aminopropyl linker to a urea dipeptide chain consisting of a leucine derivative, L-epicapreomycidine as a non-proteinogenic amino acid and L-valine. Varying structures of the leucine unit led to the division into groups A-D. Members of groups A and B contain a 3-hydroxy-L-leucine unit including lipophilic side chains with varying lengths. These lipophilic side chains are ω-functionalized with a guanidino or hydroxyguanidino unit for members of series A, while being terminally branched for muraymycins of series B. On the contrary, muraymycins of series C have an unfunctionalized 3-hydroxy-L-leucine unit, whereas proteinogenic L-leucine occurs in series D. One of the most active members is represented by muraymycin A1 with antibacterial activities against Gram-positive bacteria like *Staphylococci* (MIC = 2-16 µg/mL), *Enterococci* (MIC = 16 to > 64 µg/mL) and also against a few Gram-negative pathogens, e.g. *E. coli* (MIC = 8 to > 64 µg/mL).[164,166] It also showed pronounced activity against an *E. coli* mutant strain containing a reduced lipid bilayer (MIC < 0.03 µg/mL).[136,164] In addition, its inhibitory activity against its bacterial target MraY was determined to be in the low picomolar range (IC_{50} = 27 ± 3 pM).[84] Hence, the presence and structure of the fatty acid side chain seems to significantly affect antimicrobial properties of muraymycins.[84] In general, ester-containing muraymycins were antibacterially more active than non-acylated ones, especially when ω-functionalized guanidino or hydroxyguanidino side chains were present. Improved antibacterial activities were

generally obtained for muraymycins of series A with their long lipophilic side chains as compared to muraymycins C4 **2** and D2 **1**, for instance, in which these fatty acid chains are missing.[166] Furthermore, target inhibition of the latter was reduced with IC_{50} values in the low nanomolar range as compared to lipophilic side chain-containing muraymycins.[84] The importance of fatty acid side chains for bacterial cellular uptake and thus antimicrobial properties was confirmed in studies by Ducho and coworkers.[167,168]

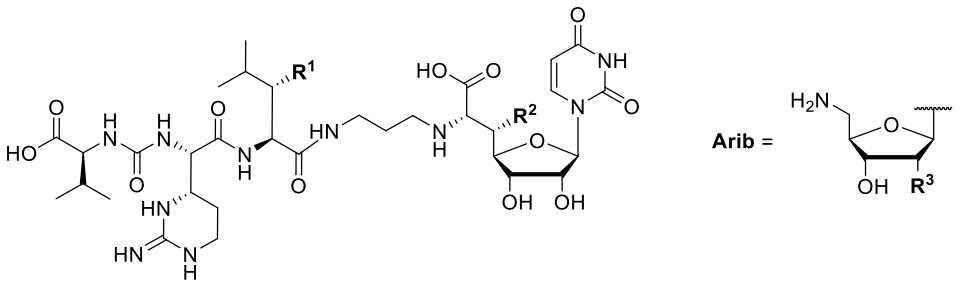

	R^1	R^2	R^3
A1	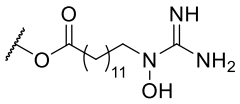	**Arib**	-OMe
A2	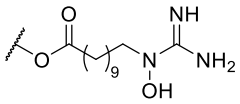	**Arib**	-OMe
A3	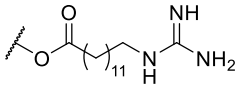	**Arib**	-OMe
A4	like **A1**	**Arib**	-OH
A5	like **A1**	-OH	
B1	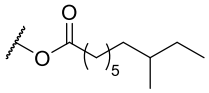	**Arib**	-OMe
B2	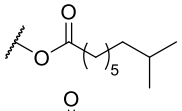	**Arib**	-OMe
B3	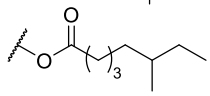	**Arib**	-OMe
B4	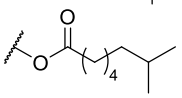	**Arib**	-OMe
B5	like **B4**	**Arib**	-OH
B6	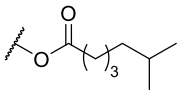	**Arib**	-OMe

	R^1	R^2	R^3
B7	like **B6**	**Arib**	-OH
B8*	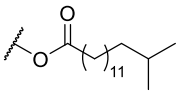	**Arib**	-OMe
B9*	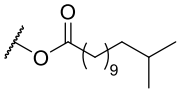	**Arib**	-OH
C1	-OH	**Arib**	-OMe
C2	-OH	**Arib**	-OH
C3	-OH	**Arib**	-H
C4 (2)	-OH	-OH	
C6*	-OH	-NAcArib	-OMe
D1	-H	**Arib**	-OMe
D2 (1)	-H	**Arib**	-OH
D3	-H	**Arib**	-H

Figure 2.16: Naturally occurring muraymycins isolated by McDonald et al.[164] and recently isolated muraymycins B8, B9* and C6* by Cui et al.[165]*

In 2018, Cui et al. reinvestigated two mutant *Streptomyces* strains, resulting in the isolation of three new muraymycin congeners termed muraymycin B8, B9 and C6 (Figure 2.16).[165]

Besides pronounced target inhibition in the low picomolar range (IC_{50} = 4-22 pM), congeners B8 and B9 exhibited antibacterial activities against Gram-positive *S. aureus* (MIC = 2-6 µg/mL) and efflux-deficient *E. coli* Δ*tolC* (MIC = 2-4 µg/mL).[165] An *N*-acetyl modification in R^2 characterizes the only difference of muraymycin C6 compared to analogue C1, thus reducing its inhibitory (IC_{50} = 93 ± 8 pM) and antibacterial activity against *S. aureus* (MIC > 32 µg/mL) and *E. coli* Δ*tolC* (MIC = 16 µg/mL).[84,165] This modification could be used for self-resistance of *Streptomyces* (will be discussed in Chapter 2.5). After the successful isolation of muraymycins, numerous attempts were made to establish synthetic access to these natural products and their simplified analogues. Those are described in the following sections.

2.4.2 Semisynthetic access to muraymycins

In 2002, Lin et al. reported semisynthetic approaches for SAR studies of 16 muraymycin derivatives, starting from muraymycin C1 (Figure 2.16) as a natural product.[169] They aimed for derivatizations of the amino function of the aminoribose moiety and the secondary amine in the 6'-position of the nucleosyl amino acid unit (Figure 2.17).

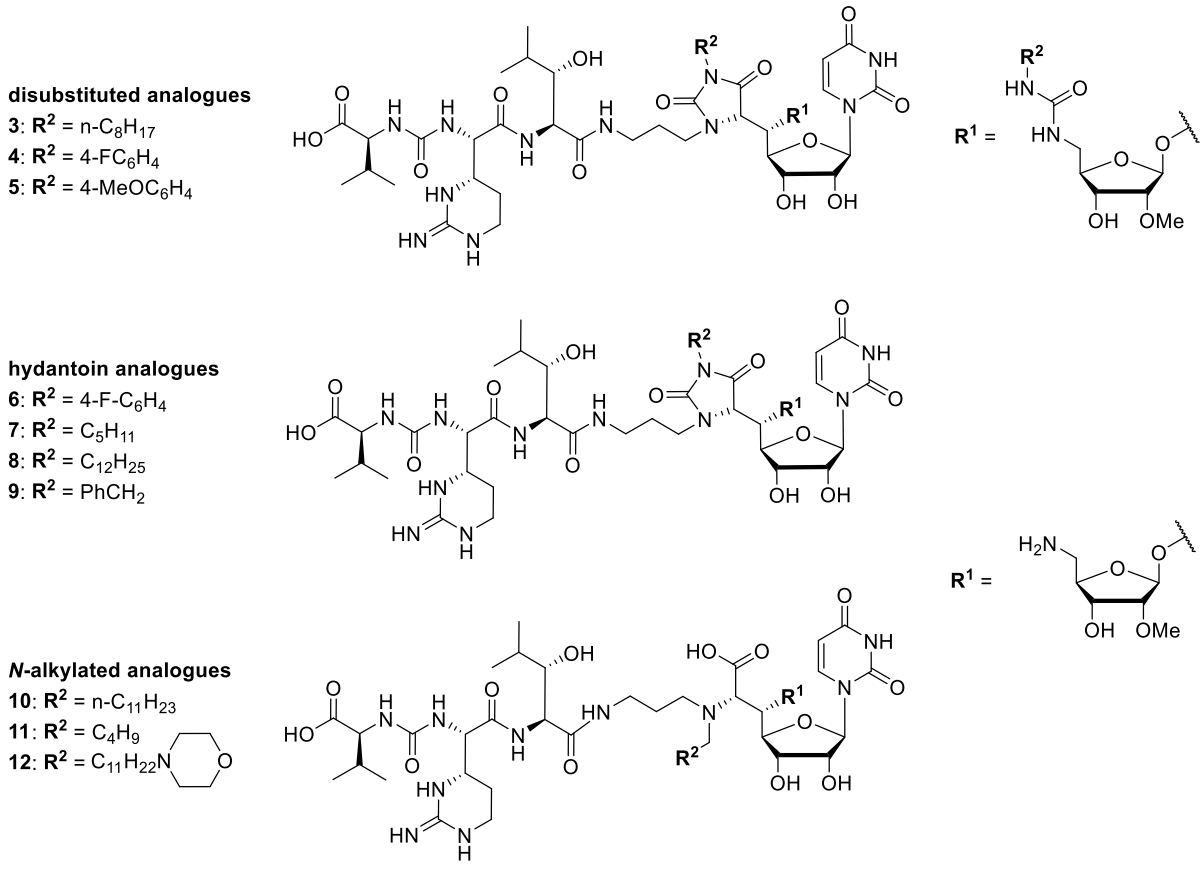

Figure 2.17: Selected semisynthetic analogues of muraymycin C1 reported by Lin et al.[169]

The analogues were tested for their inhibitory activity against MraY.[169] In the interest of completeness, it should be noted that MurG biochemical assays were performed by Lin et al. as well, but they will not be reported further here.[169] A modification of the aminoribose unit

due to disubstitution resulted in a complete loss of inhibitory activity as demonstrated with compounds **3**-**5**.[169] In contrast, target inhibition was slightly retained in the low micromolar range with increased lipophilicity of the substituents introduced.[169] This applied for hydantoin analogues **6**-**9** and *N*-alkylated analogues **10**-**12**.[169] These data demonstrated the significance of the free amine of the aminoribose in terms of inhibitory potential.[169] Generally, a certain degree of lipophilicity was assumed to enhance permeability and consequently cellular uptake. These findings concur to those of McDonald et al. for naturally occurring muraymycins.[164] However, a significant improvement of antibacterial activity or target inhibition of these semisynthetic analogues compared to the natural products could not be observed.

2.4.3 Synthetic access to muraymycins

The current state of synthetic access to muraymycins has been reviewed by Ducho and coworkers.[55] In this section, literature-known synthetic approaches relevant for this work will be presented. The first total synthesis of structurally simplified muraymycin analogues was described by Yamashita et al. in 2003 (route not shown).[170–174] These analogues lacked the lipophilic side chain and the aminoribose unit, but still contained a hydroxy moiety in 5'-position. Biological testing revealed a slight preference of analogues in (5'*S*)-configuration in terms of MraY inhibition, although the opposite trend was shown for antibacterial growth inhibition against various bacterial strains.[170] Strikingly, Yamashita et al. reported the pronounced antibacterial activity of truncated analogues, still bearing *tert*-butyldimethylsilyl (TBDMS) and other protection groups.[170] However, this seems doubtful as results from our research group imply.[175] Overall, these studies served as excellent starting point for the development of novel structurally simplified muraymycin analogues.The uridine-derived core structure of muraymycins is also part of the synthesis of (+)-caprazol and other caprazaymycin derivatives which was published by Ichikawa et al. in 2005 (routes not shown).[176–178] In these routes, a Sharpless stereoselective aminohydroxylation was used which was also applied in the total synthesis of muraymycin D2 **1**, its D-leucine epimer and lipidated analogues by the same research group (route not shown).[179–186] The central step in this synthesis was, however, an Ugi four-component reaction with an isocyanate, an amine, an aldehyde and a urea dipeptide. The latter was obtained via C-H activation as established by Ichikawa et al. (route also not shown).[179,180] Muraymycin D2 **1** and its epimer both exhibited *in vitro* target inhibition against $MraY_{BS}$ (IC_{50} = 0.01/0.09 µM), but no antibacterial activity (MIC > 64 µg/mL) against various bacterial strains, most likely due to limited cellular uptake.[181] Consequently, better biological properties were associated with enhanced bacterial membrane penetration resulting from increased lipophilicity of the analogue. Such lipidated muraymycin derivatives were described in further SAR studies by Ichikawa and coworkers in 2010 and 2011 (structures not shown). Their studies focused on variations in the peptide chain with different amino acids and truncated analogues lacking, e.g., the L-valine urea unit.[181,182] The exchange of

L-epicapreomycidine with L-capreomycidine, L-arginine or L-ornithine did not affect antibacterial properties.[181,182] Even the truncated analogues exhibited reasonable antimicrobial activities against pathogens such as *S. aureus* whilst leaving target affinity in terms of IC_{50} values unconsidered. These data strengthened the assumption that variations in the peptide chain of muraymycins seem to be well tolerated.[181,182] Furthermore, the beneficial impact of lipophilic side chains for enhanced cellular uptake was demonstrated.[181,182] This assumption was confirmed by SAR studies of our research group.[187] Our findings, however, suggest an interaction between lipophilic side chains and the target, which leads to enhanced target affinity as well as improved cellular uptake.

After the successful total synthesis of muraymycin D2 **1** in 2010, Kurosu and coworkers described synthetic access to muraymycin D1 and its amide analogues in 2016 (route not shown).[188] This route included a ring-opening reaction of a diastereomeric mixture as key step besides a β-selective ribosylation and Strecker reaction. Remarkably, muraymycin D1 showed antibacterial activity against *M. tuberculosis* (MIC = 1.56-6.25 µg/mL) and target inhibition against MraY from *Mycobacterium tuberculosis* ($MraY_{Mtb}$ or MurX), as well as against another bacterial phosphotransferase WecA in the low micromolar range (IC_{50} = 0.1-0.7 µM).[188,189]

Furthermore, an alternative route providing the naturally occurring uridine-derived muraymycin core structure **13** was established by Ducho and coworkers (Scheme 2.1).[190,191]

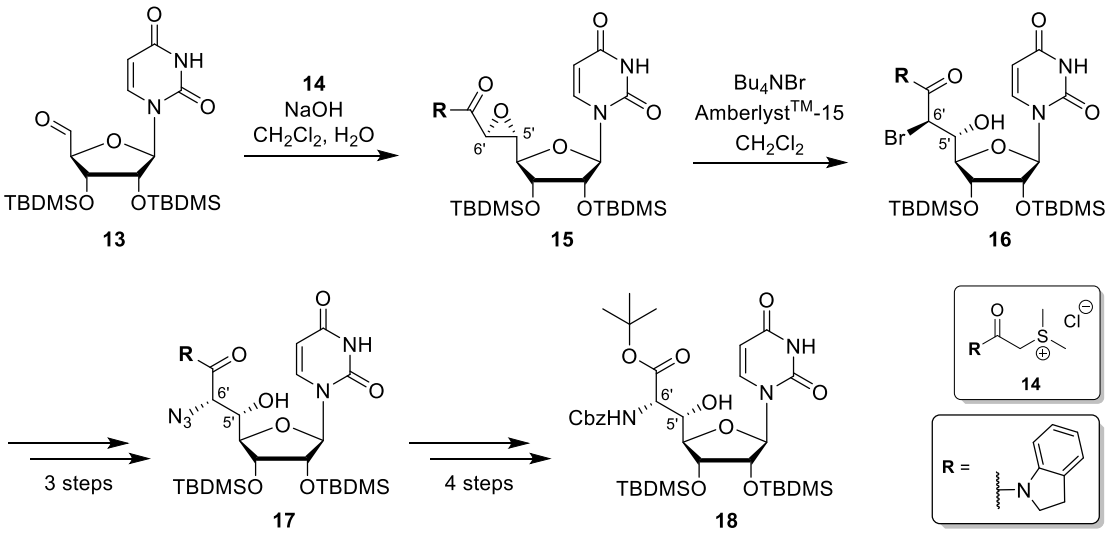

Scheme 2.1: Stereocontrolled synthesis of the uridine-derived nucleosyl amino acid core structure via sulfur ylides as reported by Ducho and coworkers.[190,191]

Initially, the stereocontrolled approach towards 5'-hydroxy amino acid **18** had been described by Sarabia et al.[192,193] Starting from uridine-5'-aldehyde **13**, they presented a substrate-controlled sulfur ylide reaction[194,195] as key step of their route, providing *trans*-epoxide **15** with high diastereoselectivity and without the need of chiral auxiliaries. The sulfur ylide **14** was generated *in situ* from sulfonium salts. The stereochemical configuration of **15** was predicted

as (5'*S*,6'*R*) by Sarabia et al., however, this was revised by Ducho and coworkers with X-ray chrystallographic data proving the (5'*R*,6'*S*) configuration of **15**.[191] The correct stereochemical information is depicted in the revised synthetic route presented in Scheme 2.1. The regioselective ring opening of **15** was performed with tetrabutylammonium, yielding the corresponding bromohydrine **16**. Subsequent protection of the hydroxy group in 5'-position, nucleophilic substitution at the 6'-position with sodium azide and oxidation with 2,3-dichloro-5,6-dicyano-1,4-benzoquinone furnished amide **17** by double inversion. The corresponding nucleosyl amino acid **18** was provided in four final steps. Based on these studies, Ducho and coworkers generated further 5'- and 6'-epimeric analogues of this nucleosyl amino acid **18** via suitable epoxide precursors (structures not shown).[196]

5'-Deoxy muraymycin analogues, which had been described by Ducho and coworkers in 2010, are synthetically much easier accessible.[190,197,198] These analogues lack the aminoribose unit in 5'-position as this moiety appeared not to be associated with enhanced biological activity of naturally occurring muraymycins. This can be demonstrated by comparing the inhibitory activities of the aminoribose-containing muraymycin A1 and the aminoribose-lacking muraymycin A5 (Figure 2.16).[164,166] Thus, 5'-deoxy muraymycin analogues represent a reasonable tool for SAR studies of this class of nucleoside antibiotics. As better activities of 5'-epimeric simplified muraymycin analogues compared to the corresponding derivatives with native 5'*S*,6'*S*-configuration have been reported,[170,171] further studies of 5'-deoxy muraymycin epimers with regard to the need of the hydroxy unit in 5'-position and the influence of the stereochemistry at the 6‘-position were performed in our research group.[197,198]

For the stereoselective synthesis of 5'-deoxy muraymycin C4 **27**, Ducho and coworkers developed a novel tripartite approach[190,197,198] in which a uridine-derived core structure of type **18** (Scheme 2.1), the L-hydroxyleucine-derived aldehyde **24**[199] and an epicapreomycidine-containing urea dipeptide **26**[190] served as building blocks (Scheme 2.2). The synthesis of aldehyde **24** was based on a strategy developed by Zhu et al.,[200] starting from D-serine which was stereoselectively converted into a protected amino alcohol by nucleophilic addition to an aldehyde intermediate (synthesis not shown). The synthesis of building block **26** started with a stereoselective Grignard reaction of a Garner aldehyde-derived imine as key step, followed by ozonolysis, reductive amination and formation of the guanidine unit (route not shown).[190] The synthetic access to the nucleosyl amino acid core will be described in detail as part of the stereocontrolled synthesis of structurally simplified 5'-deoxy muraymycin C4 **27** in which this novel tripartite approach was applied (Scheme 2.2).

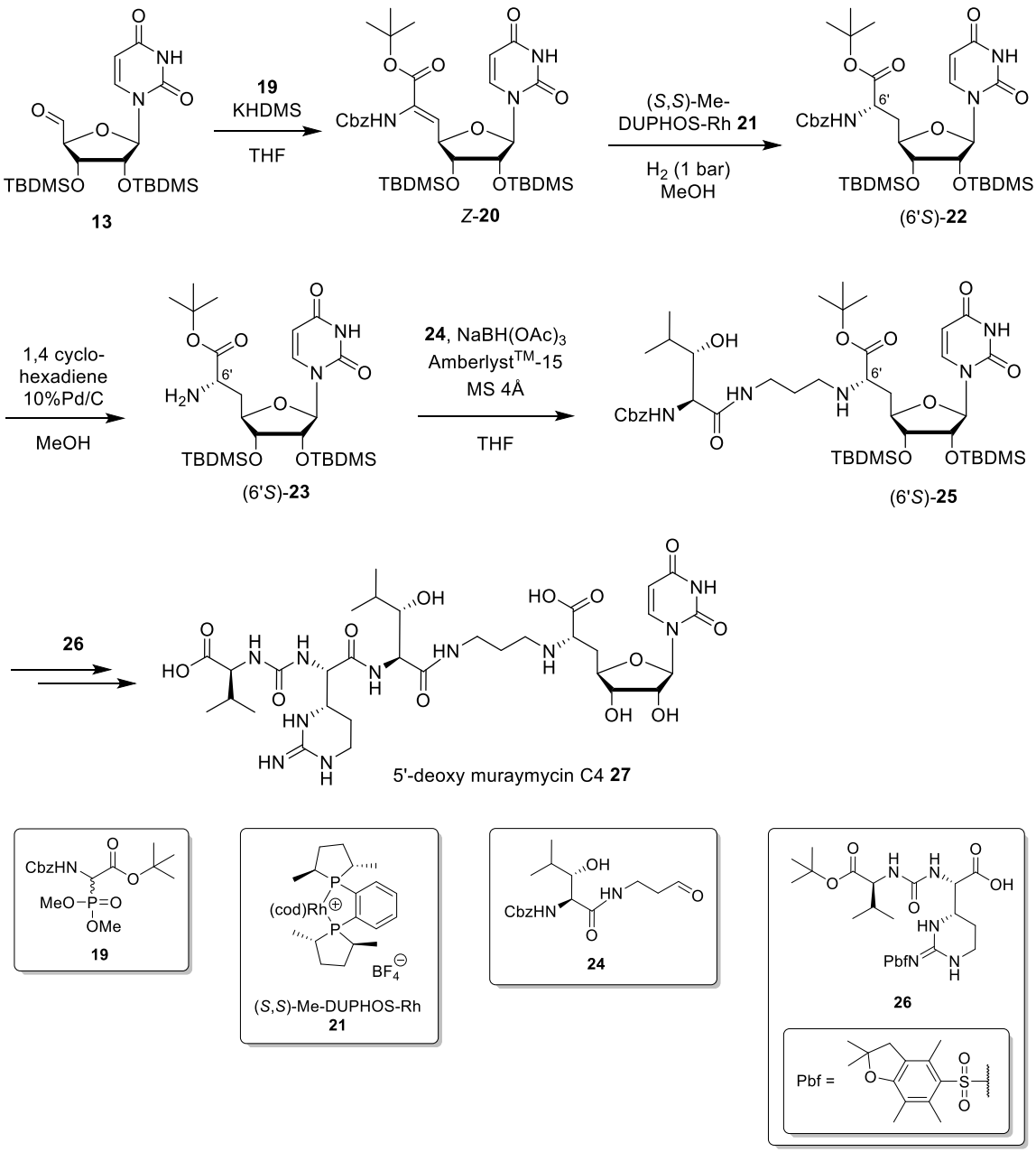

Scheme 2.2: Synthesis of 5'-deoxy muraymycin C4 ***27*** *by Ducho and coworkers.*[190,197,198]

The uridine-derived core structure **23** was constructed utilizing a *Z*-selective Wittig-Horner reaction[201,202] of uridine-5'-aldehyde **13** and phosphonate **19**[203–206] as a key step in this route, providing the olefin **20** with high diastereoselectivity. Subsequent asymmetric catalytic hydrogenation[207,208] with the chiral rhodium (I) catalyst (+)-1,2-Bis-((2*S*,5*S*)-2,5-dimethylphospholano)-benzene-(1,5-cyclooctadiene)-rhodium(I)-tetrafluoroborate ((*S*,*S*)-Me-DUPHOS-Rh) **21** furnished diastereomerically pure nucleosyl amino acid with (6'*S*)-configuration **22**[190,197]. A diastereoselectivity of > 98:2 was reported.[198] The corresponding (*R*)-isomer could also be obtained using (-)-1,2-Bis-((2*S*,5*S*)-2,5-dimethylphospholano)-benzene-(1,5-cyclooctadiene)-rhodium(I)-tetrafluoroborate ((*R*,*R*)-Me-DUPHOS-Rh) with the opposite configuration as catalyst. The deprotection of the benzyloxycarbonyl (Cbz) unit by transfer-hydrogenation to

nucleosyl amino acid **23** and reductive amination with aldehyde **24** yielded the corresponding 5'-deoxy nucleosyl amino acid **25** which was coupled with urea dipeptide **26**. Global deprotection provided 5'-deoxy muraymycin C4 **27** which exhibited moderate antibacterial activity against *E. coli* DH5α (MIC = 15 µg/mL) as well as good target inhibition against MraY (IC_{50} = 95 ± 19 nM).[84,190]

The tripartite approach was also used in our research group for the synthesis of further muraymycin analogues with fluorinated, C2'-deoxygenated and 5,6-didehydro-uracil-containing nucleoside structures (synthesis not shown).[209] Furthermore, it was applied to the synthesis of 5'-defunctionalized muraymycin D2 **30** by utilizing the uridine-derived core structure **23**, the aldehyde **28** and the urea dipeptide **26** (synthesis depicted in abbreviated form in Scheme 2.3).

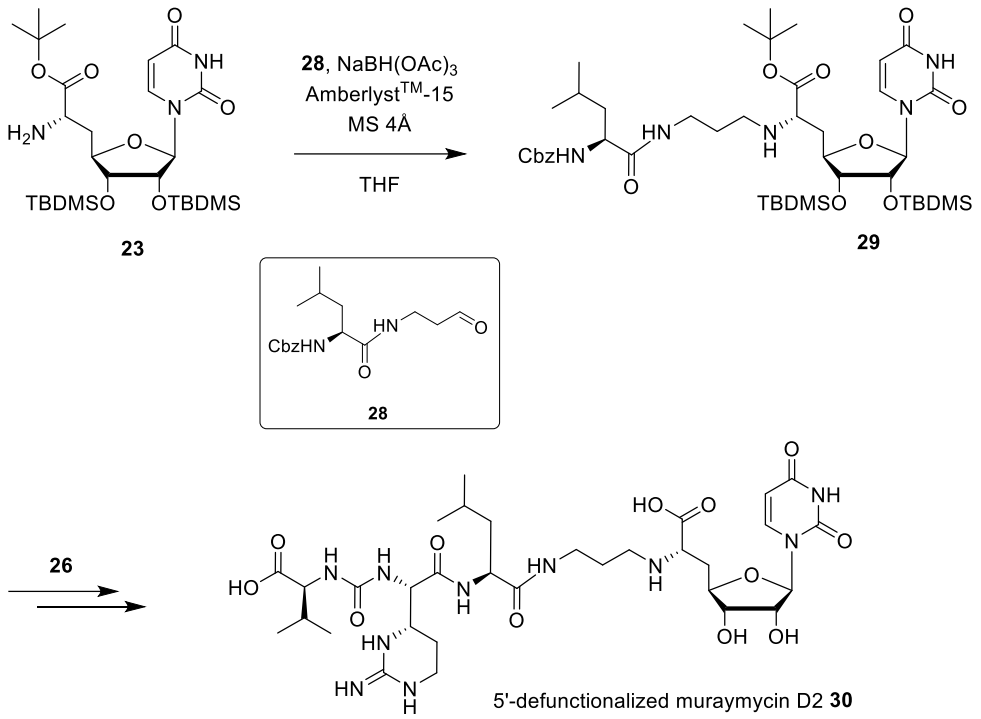

*Scheme 2.3: Tripartite approach for the synthesis of 5'-defunctionalized muraymycin D2 **30** by Ducho and coworkers.[210,211]*

5'-Defunctionalized muraymycin D2 **30** showed significantly reduced inhibitory activity against MraY (IC_{50} = 0.67 ± 0.12 µM[175]) relative to 5'-deoxy muraymycin C4 **27** (IC_{50} = 95 ± 19 nM), indicating that the hydroxy unit at the 3'-position of the leucine moiety contributes to target affinity. Remarkably, the absence of the aminoribose moiety led to decreased target affinity by the factor ~ 2000, demonstrated with an IC_{50} = 0.39 ± 0.11 nM[84] of muraymycin D2 **1**. As 5'-deoxy muraymycins are synthetically much easier accessible and retain biological activity to a certain extent, they represent a reasonable tool for further SAR studies, consequently.

In the interest of completeness, glycosylated (5'*S*,6'*S*)-nucleosyl amino acids synthesized by Ducho and coworkers should be mentioned as well. Beside the attachment of ribosylated alkyl moieties at the nitrogen atoms of either the uracil nucleobase or the 6'-position of uridine, Ducho and coworkers performed *O*-glycosylations at C-5' of uridine in addition.[212–214] The latter has been reported in the literature as part of the synthesis of (+)-caprazol[176] (synthesis not shown), caprazamycin analogues[215] (route not shown) and muraymycin D2 **1**[180], all utilizing a ribosyl fluoride as glycosyl donor. Another glycosylation donor was applied in 2016 by Kurosu et al. in the synthesis of muraymycin D1 with the use of a thioglycoside.[188] Further glycosylation studies by our research group included a modified version of the Koenigs-Knorr glycosylation method with a ribosyl bromide as glycosyl donor, furanose donors as part of Schmidt's tricholoracetimidate method and the use of *n*-pentenyl glycosides and thioglycoside donors.[214] General glycosylation conditions of all synthetic approaches vary.

In summary, several key interactions of muraymycins with the bacterial membrane protein MraY have been identified, impacting their biological relevance in terms of target inhibition and antibacterial activities. The co-crystal structure by Chung et al. revealed two binding pockets, one for uridine and one for the 5-aminoribosyl moiety.[91] A peptide-binding site provides an additional key interaction, although the peptide chain, which is located on the surface of the protein, can be truncated and some amino acids are exchangeable.[91] Furthermore, the lipophilic side chain might mediate another key interaction with the target, resulting in enhanced antimicrobial and inhibitory activity.[183] At least two of these interactions need to be addressed by the inhibitor for reasonable activity. These findings form a principle starting point for the development of novel muraymycin analogues in the course of SAR studies.

2.4.4 Prodrugs in medicinal chemistry and some selected concepts

One of the greatest challenges in the development of marketable drugs are biological membranes. They serve as barriers and provide, among others, stability, solubility, permeability, presystemic metabolism and targeting limitations.[216] Several strategies have been developed and applied in the pharmaceutical industry to address this issue with prodrug approaches being a growing trend.[217,218] A classification of drugs approved worldwide as prodrugs can be estimated with about 5-7%[217] and over the past 10 years, e.g., the US Food and Drug Administration has approved 30 prodrugs, representing 12% of all approved novel chemicals during this time[218]. Prodrugs are bioreversible molecules which contain structural modifications relative to their corresponding bioactive drugs.[216] They exhibit little or no pharmaceutical activity and are transformed into the active parent drug *in vivo* by enzymatic or chemical reactions or by a combination of the two.[218] The released active drug can then execute the desired pharmacological effect *in vivo*.[217] In the interest of completeness, it should be kept in mind that salts of active drugs, whose metabolites contribute to the pharmacological

response, are not included in this definition.[219] The simplified concept and principle of prodrugs is illustrated in Figure 2.18.

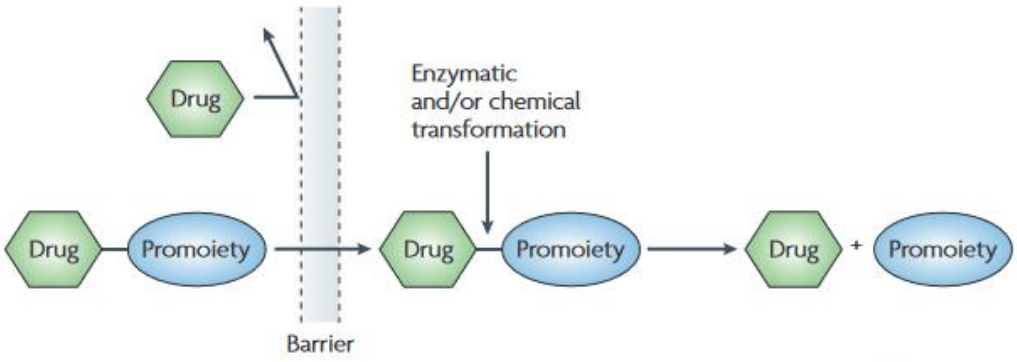

*Figure 2.18: Concept and principle of prodrugs in pharmaceutical and medicinal chemistry (taken from: Rautio et al., Nature Reviews **2008**, 7, 255-270).[217]*

The term “prodrug“ was originally introduced by Adrien Albert in 1958 although the principle had already been applied with methanamine in 1899.[219] At the same time, acetylsalicylic acid (Aspirin) was introduced to the market and caused a debate regarding its function as prodrug.[219] This is due to the fact that aspirin inhibits cyclooxygenase irreversibly while the parent drug salicylic acid only causes a weak enzymatic inhibition.[219] However, with the rapid hydrolysis of Aspirin to salicylic acid in the blood, the categorization of Aspirin as prodrug seems to be at least partially legitimated.[219] Another example can be given with prontosil, which was introduced in 1935 and initially not developed as a prodrug.[219] In the same year, however, it was shown that the potent form of prontosil is released by reductive enzymes, which led to its classification as a prodrug.[219]

The prodrug concept and their development have been implemented for enhancing physicochemical, biopharmaceutical or pharmacokinetic properties of pharmacologically active agents and thereby increasing the developability and usefulness of a potential drug.[217] Prodrugs are used to improve undesired properties of drugs in terms of absorption, distribution, metabolism and excretion (ADME).[217,219] Furthermore, reduced organ and tissue toxicity, increased target selectivity, improved oral bioavailability and enhanced hydro- or lipophilicity, as required, are sought.[219] Following, increased lipophilicity will be focused on as this plays a major role in this work in the synthesis of novel muraymycin prodrug approaches. Increasing lipophilicity of compounds can be generally performed by masking hydrophilic moieties with lipophilic units which will be cleaved intracellularly after diffusion through the bacterial membrane. Some of the most common hydrophilic functionalities are phosphates, phophonates, amines, hydroxyl or carboxylic groups.[217] These functionalities are targeted in the development of prodrugs to provide beneficial enzymatic cleavable moieties such as, e.g., esters, carbonates, carbamates, amides and oximes.[217] First, the use of pivaloyloxymethyl

(POM) moieties in terms of prodrugs will be presented in detail since masking of carboxylic moieties with POM units plays a major role in this work. This masking leads to the formation of ester units which will be cleaved after intracellular entrance of the prodrug. Especially in the field of antivirals, phosphate ester functionalities depict the most widely used unit for prodrugs, with the POM-containing nucleotide adefovir-dipivoxil as one prominent example. It is approved as bis-POM prodrug of adefovir **31** against hepatitis B and the human immunodeficiency virus (HIV).[220–225] Tenofovirdisoproxil, the bis-*iso*-propyl-oxymethylcarbonyl (POC) prodrug of tenofovir **32**, represents another nucleotide prodrug in this field, also targeting HIV.[220–225] Both prodrugs make use of intracellular esterases which release the potent drug after cleaving the ester functionalities.[220,221] The cleavage mechanism is briefly depicted in Scheme 2.4. The first POM unit is cleaved quickly and leads to an instable intermediate (Scheme 2.4, middle) which decomposes into the appropriate phosphate diester under formaldehyde elimination.[226] Due to net charges of the phosphate diester, its passive diffusion through cellular membranes is hampered.[226] The cleavage of the second POM unit is slower, but takes place in analogous fashion.[226] As a result, the desired mono phosphate is released, adefovir **31** in case of adefovir-dipivoxil.[226] For the POC-containing tenofovirdisoproxil, the first enzymatic cleavage provides a carboxylic acid derivative which decomposes into the same type of hemiacetale as mentioned before under release of carbon dioxide. Subsequent formaldehyde elimination and second POM cleavage leads to the release of tenofovir **32**.[226]

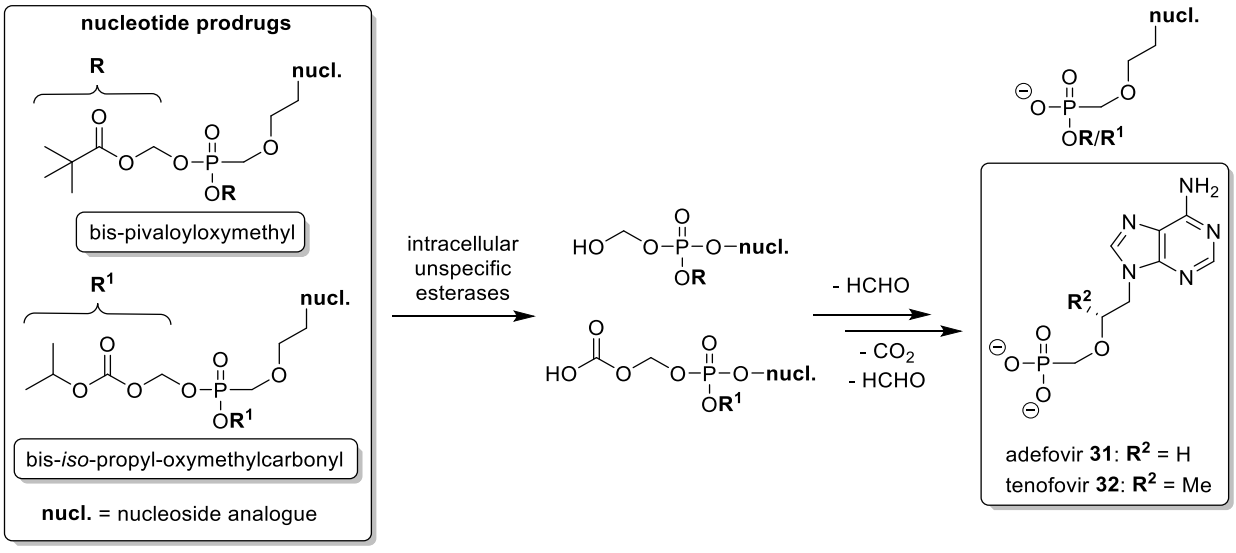

Scheme 2.4: Enzymatic cleavage mechanism of bis-pivaloyloxymethyl and bis-iso-propyl-oxymethylcarbonyl nucleotide prodrugs reported by Ducho.[226]

Another common prodrug strategy is the masking of hydrophilic amino functionalities which is elementary for this work as well. The enzymatic cleavage mechanism is exemplarily depicted in Scheme 2.5 for a carbamate-containing prodrug.[227] First, the corresponding ester of is

cleaved by esterases which takes place in analogy to the cleavage of POM units. This cleavage results in a *para*-hydroxybenzyl carbamate that spontaneously decomposes into an amine, carbon dioxide and *para*-quinone methide. Hydrolysis of the latter yields the non-toxic *para*-hydroxybenzyl alcohol (Scheme 2.5).

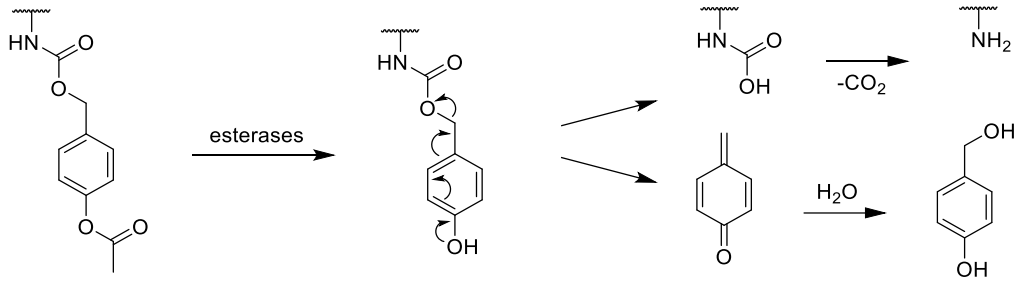

Scheme 2.5: Mechanism of cleavage of amine funtionalities masked as carbamate units reported by Nautiyal et al.[227]

So far, prodrug strategies cover a broad area in antiviral fields, but are rather underrepresented in antibiotics research. A few ester-containing prodrugs derived from β-lactam antibiotics such as penicillins (Chapter 1.3) have been developed. They lead to significantly increased oral bioavailability by masking polar acidic functionalities with the beneficial side effect of improved β-lactamase stability.[217,228] Amp and its prodrug pivampicillin are depicted as one example of such a drug-prodrug-couple in Figure 2.19.

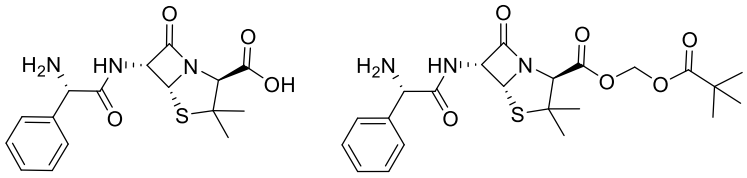

Figure 2.19: Ampicillin and its prodrug pivampicillin.[217]

A relatively novel prodrug approach reported by Cheng and Wuest targets cell permeation and cellular uptake of drugs in Gram-negative bacteria.[229] As cell permeation is generally hampered by the outer membrane (Chapter 2.3), off-target effects, toxicity and resistance development might be overcome by specifically addressing this issue.[229] Similar to antiviral prodrugs, POM- or POC-ester can be used as masking groups for acids, while, e.g., lactones or redox systems would be conceivable for amino functionalities.[230] Such an approach would be extremely promising for interfering in early steps of peptidoglycan biosynthesis (Chapter 2.1.2). However, there is no precedence known in the literature so far.

A prodrug approach in antibiotics research was investigated by Dr. D. Wiegmann in his dissertation within our research group.[212] Focus of his studies was the improvement of bacterial cellular uptake of muraymycin analogues with the structurally simplified muraymycin analogue **33** serving as parent drug. Relative to naturally occurring muraymycins (Figure 2.16),

compound **33** consists of L-lysine instead of epicapreomycidine, L-leucine instead of hydroxyleucine and a 5'-deoxy nucleosyl core structure instead of a hydroxy unit or aminoribose attached to the 5'-position. For the prodrug approach, target structures **34**-**36** with POM units attached were designed to increase the lipophilicity of **33**. They are depicted in Figure 2.20. The cleavage of the prodrugs **34**-**36** is carried out by esterases, thus releasing the parent drug **33** intracellularly.

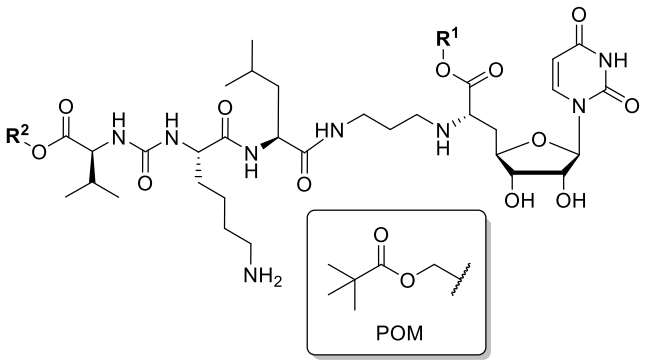

Compound	R^1	R^2
33	H	H
34	POM	POM
35	POM	H
36	H	POM

*Figure 2.20: Prodrug approaches **34**-**36** of structurally simplified muraymycin parent drug **33** by Dr. D. Wiegmann.[212,231]*

Prodrug **34** is termed “bis-POM prodrug“ and “mono-POM prodrug“ is used for prodrugs **35** and **36** in the following. The difference between both mono-POM prodrugs is the localization of the POM unit, which is attached to the carboxylic acid in prodrug **35**, whereas it masks the urea dipeptide moiety in prodrug **36**. Biological data (i.e. inhibitory and antibacterial activities) of compounds **33**-**36** completed the SAR studies of Dr. D. Wiegmann. They are listed in Table 2.2. The overall comparison of these data provided fundamental insights into the envisioned muraymycin prodrug concept. The parent drug **33** and mono-POM prodrug **35** showed inhibitory activity against $MraY_{SA}$ in the low micromolar range (IC_{50} (**33**) = 2.5 ± 0.6 µM, IC_{50} (**35**) = 5.7 ± 0.8 µM), whereas bis-POM prodrug **34** and mono-POM prodrug **36** were inactive (IC_{50} >100 µM). None of the compounds showed antibacterial activity against *E. coli* DH5α (MIC >100 µg/mL). In contrast, bis-POM prodrug **34** (MIC = 25 µg/mL) and mono-POM prodrug **35** (MIC = 32 µg/mL) showed improved antibacterial activity against the efflux-deficient Gram-negative *E. coli* Δ*tolC* relative to the parent drug **33** (MIC >100 µg/mL). Hence, the localization of the POM group in the molecule seems to play a role since mono-POM prodrug **36** did not display antibacterially activity against *E. coli* Δ*tolC* (MIC >100 µg/mL). Further evaluation regarding cellular uptake was not done as this subject was not examined in our research group at this time.

*Table 2.2: Biological activities of parent drug **33** and prodrugs **34**-**36**.[212]*

Compound	IC_{50} ($MraY_{SA}$) [µM]	MIC *E. coli* Δ*tolC* [µg/mL]	MIC *E. coli* DH5α [µg/mL]
33	2.5 ± 0.6	100	>100
34	>100	25	>100
35	5.7 ± 0.8	32	>100
36	>100	>100	>100

Meanwhile, cellular uptake assays for *E. coli* Δ*tolC* were developed in our research group by J. Meiers.[134] The parent drug **33** and the prodrugs **34** and **35** served, among others, as candidate compounds. Since mono-POM prodrug **36** did not show any biological activity (IC_{50} >100 µM, MIC >100 µg/mL), it was excluded from these studies. As mentioned (Chapter 2.3), a defined number of Gram-negative *E. coli* cells (Chapter 7.1.3.1.1) was incubated with the parent drug **33** and the prodrugs **34** and **35**, each in biological triplicates. Incubation was performed in a water bath, cell lysis was carried out by sonication (conditions as in Chapter 7.1.3.2.1). Following, porcine liver esterase (PLE) was added to prodrugs **34** and **35** to release the parent drug **33** and samples were incubated in a water bath (37 °C, 2 hours). Cellular uptake of compounds **33**-**35** was quantified by LC-MS after protein precipitation, centrifugation and lyophilization. The total intracellular concentration of the parent drug **33** and the prodrugs **34** and **35** was examined. The calibration by high resolution mass spectrometry (HRMS) was done with the parent drug **33** since the released analogue **33** will be quantified for the prodrugs **34** and **35**. Moreover, a cold osmotic shock (Chapter 7.1.3.2.2) was performed to distinct between cytoplasmic and periplasmic space. The obtained data for cellular uptake are presented in Table 2.3.[134]

*Table 2.3: Cellular uptake into E. coli Δ*tolC* of parent drug **33** and prodrugs **34** and **35**, depicted as sample concentration, measured in biological triplicates. The release of **33** was quantified. n.d. = not detectable. *Sample concentrations of **33**-**35** in periplasm were corrected with the factor 0.5 due to the assay procedure.[134]*

Compound	Sample concentration [nM]		
	Whole cells	Intracellular accumulation	Periplasmic accumulation*
33	64 ± 18	n.d.	14 ± 1
34	204 ± 8	127 ± 18	48 ± 5
35	99 ±13	2.1 ± 1.1	6.8 ± 0.6

Measured sample concentrations after complete cell lysis were in line with the antibacterial activities of **33**, **34** and **35** (Table 2.2). The intracellular accumulation of bis-POM prodrug **34** was the strongest (204 ± 8 nM) in the series relative to the parent drug **33** (64 ± 18 nM) and mono-POM prodrug **35** (99 ±13 nM). This data confirmed the success of this prodrug strategy as increased lipophilicity goes along with enhanced cellular uptake. The parent drug **33**

represents the most hydrophilic compound in this series and cellular accumulation was the lowest (64 ± 18 nM). In contrast, cellular uptake of bis-POM prodrug **34** as the most lipophilic analogue in this series was the highest (204 ± 8 nM). An overall comparison of the data reveals, however, that cellular uptake did not correlate directly with the antimicrobial activity of the analogues. In case of direct proportionality, cellular uptake of bis-POM prodrug **34** should be improved by factor ~ 4 relative to **33**. This is similar to mono-POM prodrug **35**, which should also accumulate to a greater extent (factor ~ 3) than the parent drug **33**. It still remained unclear, e.g., if both POM groups of the bis-POM prodrug **34** were released at the same rate. Initial accumulation studies focused on the overall cellular accumulation without consideration of periplasmic accumulation. Further investigations with regard to cytoplasmic and periplasmic accumulation delivered additional findings that confirmed the aforementioned tendency (Table 2.2): increased lipophilicity of the compound resulted in higher amounts in the cytosolic fraction. Bis-POM prodrug **34** mainly crossed the bacterial cell wall and cytosolic membrane and released the parent drug **33** into the cytosol to a greater extent (127 ± 18 nM) than into the periplasmic fraction (48 ± 5 nM). In contrast, mono-POM prodrug **35** showed periplasmic accumulation (6.8 ± 0.6 nM) and was detectable to a small extent in the cytoplasmic room (2.1 ± 1.1 nM). The same trend was observed for the parent drug **33** with periplasmic accumulation (14 ± 1 nM) and no detectable amounts in the cytosol. Therefore, periplasmatic accumulation without release into the cytoplasm could be an explanation for the lack of antibacterial activity for compound **33** (MIC >100 µg/mL). In the literature, a periplasmic binding site of muraymycins to MraY was previously reported by Rodolis et al.[232] The authors assumed improved cellular uptake upon binding to the periplasmic motif which would be an explanation for these cellular uptake data. However, a correlation between cellular uptake and antibacterial activities of the parent drug **33** and its prodrugs **34** and **35** needs to be handled with care. There are many uncertainties such as, e.g., the rate of release or the limitation of an effective concentration of parent drug **33** in bacterial cells.

2.5 Theory of self-resistance of *Streptomyces* species against muraymycins

As already mentioned, MraY is inhibited by muraymycins and other classes of nucleoside antibiotics produced as natural products in *Streptomyces* species (Chapter 2.4). Since the bacterial membrane protein is an essential part of peptidoglycan synthesis in all bacteria, the mechanism of self-resistance utilized by bacterial natural product producers is a topic of interest. In 2016, single-point mutations of MraY were reported with a focus on the two $MraY_{AA}$ mutants Asp193Asn and Phe262Ala. Both mutants still exhibited enzymatic activity but led to reduced inhibitory activity of muraymycin D2 **1** of ~ 75% at 1 µM.[91] These point mutations seem to prevent the interactions with the 5'-aminoribose and uracil moieties of muraymycin D2 **1**. Various other artificially induced point-mutations were performed by Chung et al., confirming these tendencies: Most of the mutants (with only a few exceptions such as, e.g.,

Asp193Ala) were enzymatically active but significantly weakened the inhibitors' inhibition ability.[91] Most recently, Cui et al. identified functionalized, covalently modified precursors of muraymycins, mostly phosphorylated or adenylated, which seem to be important in self-resistance.[233] The authors assumed that these precursors of muraymycins were produced extracellularly in *Streptomyces* species and were converted intracellularly into muraymycins. Remarkably, inhibitory activity of these precursors was still found in activity assays, although reduced compared to their parent compounds, suggesting additional mechanisms of self-resistance.[233]

In the past, protein mutations were rarely addressed as amino acid residues in the catalytic center of MraY between *Streptomyces sp.* and other isoforms are highly conserved. However, novel investigations on structural data of natural product binding modes indicate other residues involved in ligand binding.[91,93,234] In this context, Dr. P. Fischer made an alignment of MraY sequences of several bacteria (schematically depicted in abbreviated form in Figure 2.21). Remarkably, a triple histidine motif was standing out among almost all MraY isoforms (red box in Figure 2.21), except for *Streptomyces* MraY where a glutamine residue in the first position was found instead.[122]

Figure 2.21: Protein alignment of the C-terminal region of Streptomyces coelicolor *MraY with various other MraY isoforms via Clustal Omega by Dr. P. Fischer.*

With glutamine being present in *Streptomyces* MraY instead of histidine, the question arose if this single point mutation could interfere with the conformational flexibility and consequently interactions of MraY required for nucleoside antibiotics binding and substrate specificity, whilst retaining enzymatic activity. Since such a mechanism has already been described for other proteins in the literature,[235–238] Dr. P. Fischer created single point-mutations of *Streptomyces* and *S. aureus* MraY to gain further insights in nucleoside binding modes for MraY.[122] Therefore, histidine324 (H324) came into the fore as its conformational flexibility and importance was indicated by alignments of apo-MraY$_{AA}$ and MraY$_{AA}$ bound to muraymycin D2 **1**.[91] These considerations form the basis for one of the projects within the biological evaluation of muraymycin analogues of this work (Chapter 3).

3 Scope and aim of this work

The need for new antimicrobial agents steadily increases due to emerging resistances of bacterial strains. Particularly suitable in this context are naturally occurring antibiotics such as nucleoside antibiotics with novel or yet unexploited modes of action. Nucleoside antibiotics sometimes differ greatly in terms of their antibacterial potential which is poorly understood and not well investigated yet. As members of this class, muraymycin-derived antibiotics such as muraymycin D2 **1** or 5'-deoxy muraymycin analogue of the natural product C4 **27**, for instance, exhibit good target inhibition against $MraY_{BS}$ (nanomolar IC_{50}), but relatively weak antimicrobial activity against *S. aureus* and *Enterococcus faecalis* (micromolar MICs).[84,182] These data suggest a limited intracellular bacterial accumulation of muraymycin-derived antibiotics due to restricted cellular uptake as result of their polarity. This highlights the general strong contrast between good inhibitory activity and weak antibacterial properties as a major obstacle in current antibiotics research. Lipophilicity seems to contribute significantly to biological properties of muraymycin analogues as Matsuda et al. demonstrated in their studies.[182]

Therefore, this dissertation deals with the bacterial uptake of muraymycin analogues, biological studies for their evaluation and the synthesis of novel muraymycin analogues as part of a SAR study. The biological and synthetic projects, divided in two parts in this work, will provide further insights into the SAR of muraymycin analogues and a better understanding of bacterial cellular uptake.

3.1 Biological studies of nucleoside antibiotics

Biological studies of this work will be examined in the following chapters. They include cellular uptake assays, hemolysis assays and PLE assays. Studies regarding MraY as the bacterial target of nucleoside antibiotics, e.g., MraY inhibition assays and MraY quantification assays will be performed. $MraY_{Mtb}$ (MurX) will be investigated as part of a collaboration besides the theory of self-resistance mechanisms of *Streptomyces* species against muraymycins and the interaction between MraY and MurF, the preceding enzyme that produces the substrate for MraY.

3.1.1 Cellular uptake assays

To address biochemical properties of muraymycin-derived analogues like different bacterial cellular uptake and the impact of efflux effects, a robust LC-MS-based assay for Gram-negative *E. coli* has been developed in our research group in its basics.[134] The assay enables the investigation of cellular uptake of muraymycins and their analogues. This subject arose from controversial antibacterial growth inihibition data of 5'-deoxy muraymycin C4 **27** obtained in our research group.[190] Various parameters affect the antibacterial activity of a compound, e.g., cellular uptake, target interaction, intracellular stability, potential off-target interactions and

efflux effects. These factors demonstrate the complexity of different bacterial species and the biochemical processes involved in bacterial cellular uptake. The investigation of bacterial cellular uptake is therefore of special interest of this work.

On the one hand, the LC-MS-based uptake assay will be used to investigate the bacterial uptake of compounds synthesized in our research group and by collaborators. Compounds synthesized by Dr. G. Niro (**37** and **38**, Figure 3.1) served, amongst others, as test compounds to better understand their biological properties.[239] Both analogues **37** and **38** exhibit comparable antibacterial activity against *P. aeruginosa* in a low micromolar range, whereas their inhibitory potential against MraY significantly differed (factor ~ 1000).[239] The reasons for these biological differences could not be clarified yet. It was questioned if they correlate with (different) bacterial cellular uptake. Hence, the investigation of cellular uptake of compounds **37** and **38** will help to gain further insights and to optimize the development of novel target compounds for SAR studies of muraymycin analogues in the future.

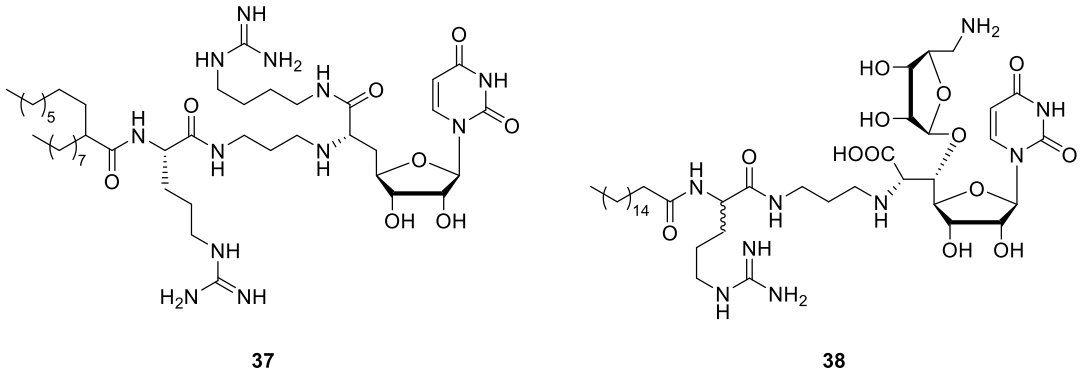

37 **38**

*Figure 3.1: Muraymycin analogues **37** and **38** synthesized by Dr. G. Niro.[239]*

Furthermore, the cellular uptake assay for *E. coli* will be modified as part of this work to investigate bacterial accumulation of selected compounds synthesized by Dr. C. Rohrbacher.[240] Studies of Dr. C. Rohrbacher dealt with muraymycin conjugates, i.e., muraymycin analogues that are either linked to other antibiotics which already exhibit an intrinsic ability to permeate the bacterial cell wall, e.g., streptomycin, or to cell-penetrating moieties such as a guanidinylated cube-octameric silsesquioxane scaffold (GuCOSS)[206] or known cell-penetrating peptides (CPP).[240] Cellular uptake into Gram-negative *E. coli* will be performed using two muraymycin conjugates, GuCOSS conjugate **39** and CPP conjugate **40,** that contain intracellularly cleavable carbamate units and disulfide bonds (Figure 3.2). The lysine reference **33** will be used as reference since cleavage of the aforementioned moieties in both conjugates **39** and **40** will result in the release of **33**. For this purpose, novel steps will be incorporated into the existing assay protocol to ensure a complete release of the parent drug **33**. These studies will gain further insights into this conjugate approach and will help to optimize the development of novel prodrug approaches of muraymycin analogues.

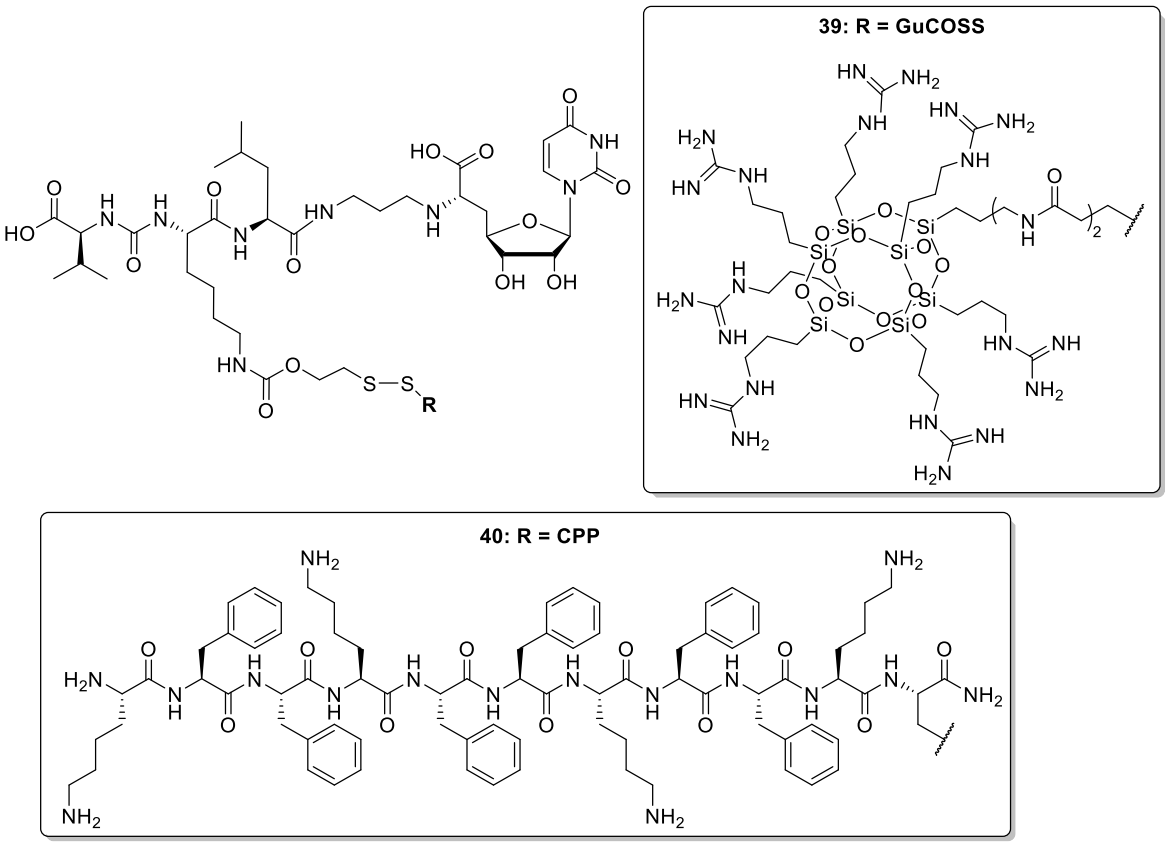

*Figure 3.2: Muraymycin conjugates **39** and **40** synthesized by Dr. C. Rohrbacher.[240]*

As part of the collaboration with the research group of Dr. S. Roy (Department of BioMolecular Sciences, The University of Mississippi, USA), cellular uptake of potential non-nucleoside compounds with broad spectrum activity including *M. tuberculosis* will be investigated (**41** and **42**, Figure 3.3). The research group of Dr. S. Roy works on a structure-based drug design approach targeting MraY, which plays a significant role in the MraY-related projects of this work. These projects will be discussed in greater detail in the corresponsing chapter (Chapter 3.1.2).

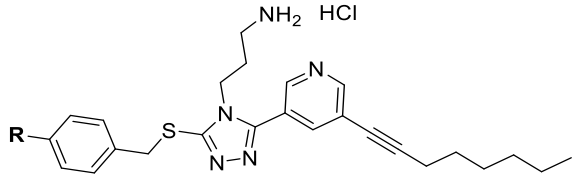

41: **R** = Cl
42: **R** = OH

*Figure 3.3: Potential non-nucleoside MraY inhibitors **41** and **42** with anti-tuberculosis activity provided by the research group of Dr. S. Roy.*

Further compounds for the cellular uptake assays were synthesized by Dr. R. Wadgy who provided MurA pyrazolidinone analogues **43**-**47** (Figure 3.4).[241] They all exhibit micromolar inhibitory activity against MurA of *E. coli* in the middle double-figures micromolar region, but

were antibacterially inactive against *E. coli* Δ*tolC*.[241] Contrary, they partially showed antimicrobial activity against *S. aureus*. Hence, the lack of growth inhibition against *E. coli* Δ*tolC* will be investigated in the cellular uptake assays to strengthen these findings. MurA pyrazolidinone analogue **47** with antibacterial activity against *E. coli* Δ*tolC* will serve as a positive control in this series.

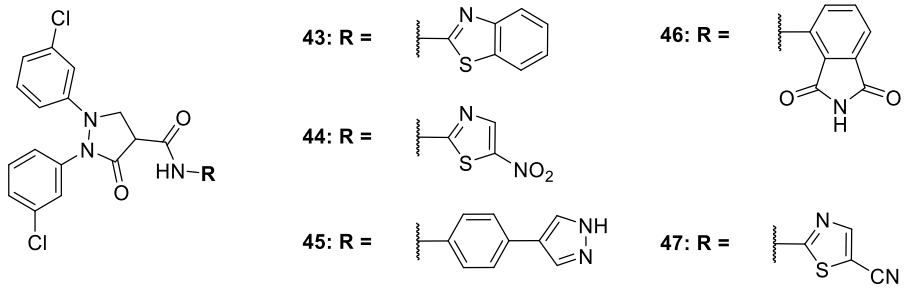

*Figure 3.4: MurA pyrazolidinone analogues **43**-**47** provided by Dr. R. Wagdy.[241]*

As mentioned, this dissertation will also contain the synthesis of novel muraymycin prodrugs (Figure 3.6), representing the extension of the POM prodrugs by Dr. D. Wiegmann (Figure 2.20).[212] Cellular uptake of these novel analogues into Gram-negative *E. coli* will be examined as well in the accumulation assay. The data will enable further evaluation regarding the entire POM prodrug strategy. This subject as well as the synthesis of these prodrugs will be focused on in greater detail in the second part of this chapter (Chapter 3.2).

Furthermore, an appropriate cellular uptake assay for *S. aureus* as a representative for a Gram-positive bacterium will be established. Unlike sonication that is used to lyse *E. coli*, the lysis of Gram-positive *S. aureus* requires an enzyme called lysostaphin. For its expression, a construct encoding lysostaphin in a pET-based vector system will be designed and commercially obtained. Subsequent plasmid transformation and protein expression, based on studies by Farhangnia et al.,[242] will be established and optimized in our research group as part of this project. The commercially available linezolid with antibacterial activity against *S. aureus* will be used for the validation of the assay. Predetermined compounds for this assay are selected *O*-acylated muraymycin analogues synthesized by Dr. M. Wirth with antimicrobial activity against *S. aureus* in a low micromolar region (**48** and **49**, Figure 3.5).[243] Moreover, naturally occurring muraymycins, in particular muraymycin A1 or B8 (Figure 2.16) with antibacterial activity against Gram-positive *S. aureus* in the low micromolar region, seem to be interesting for the envisioned assay.

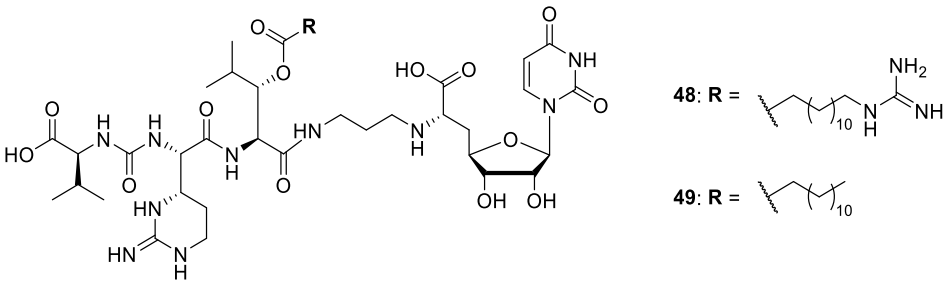

*Figure 3.5: O-acylated muraymycin analogues **48** and **49** synthesized by Dr. M. Wirth.[243]*

As an essential part for the cellular uptake data for both types of bacteria, a suitable calculation tool will be established. This calculation tool will help to evaluate data plausibility as it shall convert sample concentrations as result of the LC-MS measurements into absolute concentrations by taking cell numbers and cell volumes as well as the assay procedure, i.e., dilution and washing steps into account. This additional evaluation is based on studies by Brönstrup et al.[135] Nevertheless, sample contents are eminent values as the investigation of cellular uptake of the compounds itself is primary on focus. Relative comparisons in a series of compounds are envisioned.

3.1.2 MraY-related projects

MraY-related projects play an elementary role for our research group as MraY depicts the bacterial target of muraymycins and their analogues. Therefore, MraY inhibition assays[84,96,97,99,244] will be performed as part of this dissertation for elucidating the SAR of drug candidates synthesized in our research group and by collaborators. Collaborations included here are the research groups of Dr. S. Roy, Prof. Dr. S. Van Lanen (Pharmaceutical Sciences, College of Pharmacy, University of Kentucky, USA) and Prof. Dr. M. Kaiser (Center of Medical Biotechnology, Faculty of Biology, University of Duisburg-Essen). In addition, the research group of Prof. Dr. R. Müller (Department of Microbial Natural Products, Helmholtz-Institute for Pharmaceutical Research Saarland (HIPS) and Department of Pharmacy at Saarland University) provided compounds for the MraY-inhibition assay. So far, crude membrane preparations with overexpressed MraY from *S. aureus* were used in the MraY inhibition assays providing inhibition data of compounds (IC_{50}). These crude membrane preparations were adjusted with regard to overall protein concentrations, thus guaranteeing the assay comparability (gradient curves evaluated with Origin 2021/2022 served as criterion). The problem, however, arises from the fact that crude membrane preparations contain natural phospholipids and other membrane ingredients besides MraY. Consequently, overall protein concentrations vary in dependence of different batches of MraY. Therefore, the question arose if overexpression varies in general and which factors might cause these differences. Misfolded MraY, e.g., could be possibly incorporated into membranes, inducing these variations. In order to gain further insights into this matter, an assay enabling the quantification of MraY will be

developed in this work. This will be done in a semi-quantitative manner by performing Western Blots. They will make use of the MraY nanobody whose transformation and expression will be done in this work as well. This assay will be called “MraY quantification assay“, and will allow the quantification of MraY amounts in protein preparations utilized in our research group, such as crude membranes, solubilized protein and nanodiscs. The comparison of MraY amounts in the aforementioned different protein preparations should fundamentally help to better understand the obtained inhibitory data and to gain further insights into the molecular mechanisms of MraY. Therefore, MraY-nanodisc systems will be produced in this work using the method established by Dr. P. Fischer.

Regarding the MraY-related projects generally, $MraY_{Mtb}$ (MurX) came into the fore since the research group of Dr. S. Roy works on target-based discovery of chemotherapeutics against *M. tuberculosis* and other antibiotic-resistant bacterial infections. With a plasmid encoding MurX that was kindly provided by the research group of Prof. Dr. S. Van Lanen, studies on the expression of MurX will be carried out in this work. Unlike the plasmid of $MraY_{SA}$ which is expressed in a pET28a vector, the corresponding plasmid of MurX was supplied in a pET30a vector. For better comparison, subcloning of the MurX genes into a pET28a vector will be performed with following plasmid transformation and protein expression. The investigation of protein activity utilizing the MraY-inhibition assays will furnish a better understanding of the biological behavior of different bacterial MraY species.

Besides the aforementioned studies, multiple other projects involving MraY are included in this work in collaboration with Dr. P. Fischer. One of these projects deals with a multienzyme complex participating in peptidoglycan synthesis in which MraY is suggested to be involved in. This multienzyme complex of MraY, ligase MurF, flippase MurG and possibly other proteins is predicted to be used by bacteria to diminish the possible diffusion of intermediate products to the cytoplasm by a controlled channeling network. With the use of biochemical methods, Dr. P. Fischer showed an interaction between the membrane-bound MraY and soluble MurF. Studies concerning this interaction will be performed as part of this work since MurF represents one of the participating proteins that produces the substrate for MraY, i.e., Park’s nucleotide.

Furthermore, the role of amino acid conservation in self-resistance mechanisms of *Streptomyces* species against muraymycins will be examined. Since MraY is found in various isoforms in all classes of bacteria, functionalized precursors of muraymycins were investigated by the research group of Prof. Dr. S. Van Lanen. With regard to their suggested self-resistance mechanisms of muraymycins, Dr. P. Fischer performed a protein alignment in which a conserved histidine motif was standing out. This observation led to the design of MraY proteins with point mutations which will be investigated in terms of their biological activity. The appropriate plasmids were provided by Dr. P. Fischer.

3.1.3 Hemolysis assays

Novel muraymycin analogues of our research group include compounds with long lipophilic side-chains and anti-pseudomonal activity as mentioned (Chapter 3.1.1). They have been synthesized by Dr. G. Niro[239] and are exemplarily shown in Figure 3.1. During her studies, the question of possible toxic side-effects due to membrane disruption arose, leading to the development of an appropriate assay as part of this work. This assay utilizes the sensitivity of red blood cells (erythrocytes) to determine the capability of compounds to destroy biological membranes. Possible membrane-disruptive effects of the compounds will be determined by the investigation of the erythrocyte integrity after incubation with the compound. This assay will provide additional insights into biological properties and the mode of action of muraymycin analogues and is called “hemolysis assay“ hereafter. Further compounds synthesized in our research group and by collaborators will be examined in this assay in terms of membrane-disruptive modes of actions.

3.1.4 Porcine liver esterase assays

Besides the muraymycin-related projects mentioned so far, our research group is working on therapeutic oligonucleotides. Among others, prodrug approaches are one central topic in both fields, resulting in a collaboration with the research group of Prof. Dr. W. Dehaen (KU Leuven, Molecular Design and Synthesis, Belgium) for a further side project of this dissertation. They developed an enzymatic assay protocol using different dyes to target PLE activity. This assay will be adapted in this dissertation for our objectives as muraymycin and oligonucleotide prodrugs need to be cleaved intracellularly by the activity of unspecific esterases. The synthesis of antibacterial muraymycin prodrugs addresses improved bacterial cellular uptake, thus boosting their antibacterial activities. In contrast, the development of oligonucleotide prodrugs should provide potential anti-tumor active compounds in human cells. In both cases, however, the designed prodrugs need to undergo esterase cleavage. There is literature for the uptake of such prodrugs in human cells,[245–248] but nearly no previous example for a similar strategy applied to antibacterial analogues. As our data imply, esterase activity in bacterial cells might be lower than in human cells, thus leading to a slower conversion of the prodrugs. However, this is quite difficult to prove in a reliable manner. So far, LC-MS analysis is used in our research group to test the stability of compounds in bacterial or human cell lysate. Since LC-MS analysis is sometimes hampered by unspecific protein binding, the application of this PLE assay will provide a suitable and efficient tool for the determination of esterase activity in different biological media.

3.2 Synthetic studies of novel muraymycin prodrugs

The second part of this dissertation addresses novel synthetic prodrug approaches which continue and expand the studies of Dr. D. Wiegmann.[212] As already mentioned (Chapter 3), a general discrepancy between inhibitory activity and antibacterial potential of synthetic muraymycins and their simplified analogues exists. Therefore, the question arose if limited cell permeability could be circumvented or at least improved by increasing the lipophilicity of muraymycin analogues. In this context, Ichikawa and colleagues made initial synthetic studies by modifying the core of muraymycins with lipophilic units.[182] Although this modification resulted in better antibacterial activities, it decreased the inhibitory potential against $MraY_{BS}$ by a factor of ~ 3. Hence, cell permeation seems to play an important role regarding antibacterial activities of muraymycins. Obviously, the strategy by Tanino et al. yielded poorer binding of the drugs to MraY.[182] For prodrugs, on the other hand, no affinity loss is expected as the gain in lipophilicity is achieved by the addition of cleavable functionalities, resulting in the release of the parent compound with identical potency after cellular uptake.

Dr. D. Wiegmann has demonstrated the success of such a prodrug approach for muraymycin analogues (Table 2.2 and 2.3) with the synthesis of the POM muraymycin prodrugs **34**-**36** (Figure 2.20). These prodrugs represent the “first POM prodrug generation“. Cell permeation of muraymycin analogue **33** was hampered due to net charges of its two carboxyl and amino functionalities. Compounds protonation state generally occur in dependance of the pH value in a buffered system. Although being formally zwitterionic, compound **33** exhibits anionic properties at physiological pH as both amino units were balanced by trifluoracetates. Generally, negative charges present a greater hurdle for cell permeation than positive ones.[249] Functional moieties which mask these units, such as POM units, are therefore more promising, thus leading to the prodrug approach of Dr. D. Wiegmann with bis-POM prodrug **34** and mono-POM prodrugs **35** and **36** as target structures.[212] In order to verify a feasible correlation between antibacterial activities and cellular uptake, compounds **33**-**36** were investigated in cellular uptake assays by J. Meiers.[134] With a higher intracellular accumulation of bis-POM prodrug **34** relative to the parent drug **33** and mono-POM prodrug **35**, a basic trend of increased cellular uptake for more lipophilic compounds was substantiated. Contrary, the inhibitory activity of prodrug **34** (IC_{50} >0.1 mM) against MraY *in vitro* was significantly worse relative to the parent drug **33** (IC_{50} = 2.5 ± 0.6 µM). Encouraged by these results, efforts have been made to further investigate and improve this prodrug approach, leading to the design of the target structures of this work. They will be called “second POM prodrug generation“. These prodrugs should be even more lipophilic than those of Dr. D. Wiegmann in order to investigate the potential of increased cellular uptake with higher lipophilicity. The amino unit of the L-lysine side chain will be on focus by creating carbamate functionalities that can be cleaved by esterases in bacteria. The design of this “second POM prodrug“ series will be discussed in the

next section. At this point it needs to be clarified that the primary objective of this project is to examine the general correlation between antibacterial activities and cellular uptake. It should be investigated if the trend of the "first POM prodrug generation" can be confirmed with the more lipophilic ones of this "second generation". The synthesis of an oral applicable drug as novel antibiotics, e.g., has never been to the fore.

3.2.1 Design of target structures

The "second POM prodrug generation" include carbamate POM prodrugs **50**-**52** (Figure 3.6). They will be synthesized in analogy to the synthetic route established by Dr. D. Wiegmann[212], utilizing the aforementioned tripartite approach (Chapter 2.4.3) by Ducho and coworkers[55,190]. The target compounds **50**-**52** share the same core (Figure 3.6): The non-proteinogenic amino acid epicapreomycidine is replaced by L-lysine due to its easier synthetic accessibility (Chapter 2.4.1), L-leucine is used instead of hydroxy-leucine and the nucleoside uridine exhibited a 5'-deoxy modification. The only variation will exist in the residue of the carbamate containing moiety, with a methyl functionality in **50**, a *n*-butyl moiety in **51** and a *tert*-butyl unit in **52** (Figure 3.6).

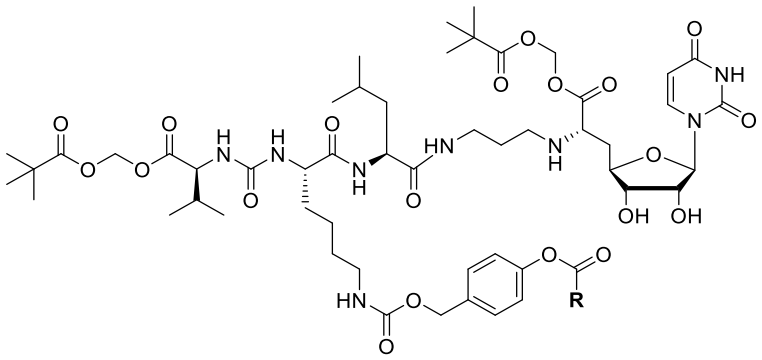

50: **R** = Me
51: **R** = *n*-Bu
52: **R** = *tert*-Bu

*Figure 3.6: Target compounds of this work: methyl-substituted carbamate bis-POM prodrug **50**, n-butyl substituted carbamate bis-POM prodrug **51** and tert-butyl subsituted carbamate bis-POM prodrug **52**.*

The enzymatic cleavage mechanisms of POM units and carbamate prodrugs that will be used for this prodrug approach have already been described (Chapter 2.4.4).[227] Target compounds **50**-**52** will be examined with regard to their inhibitory activity against the target protein MraY. Furthermore, antibacterial activities against *E. coli* DH5α, *E. coli* Δ*tolC* and *S. aureus* will be investigated. Cellular uptake assays utilizing *E. coli* Δ*tolC* will be performed to investigate the hypothesis of improved cellular uptake as a result of the higher lipophilicity of **50**-**52** relative the prodrugs of the "first POM prodrug generation" by Dr. D. Wiegmann.[212] Furthermore, the target compounds **50**-**52** will be investigated in cellular uptake assays with *S. aureus*. All these studies should gain further insights into prodrug approaches of muraymycins.

3.2.2 Retrosynthetic considerations

Carbamate POM prodrugs **50**-**52** can be retrosynthetically divided into three building blocks: the nucleosyl amino acid **53**, the urea dipeptide **54** and chloroformate derivatives **55**-**57** (Scheme 3.1). They will be synthesized by peptide coupling, subsequent carbamate formation and a final global acidic deprotection.

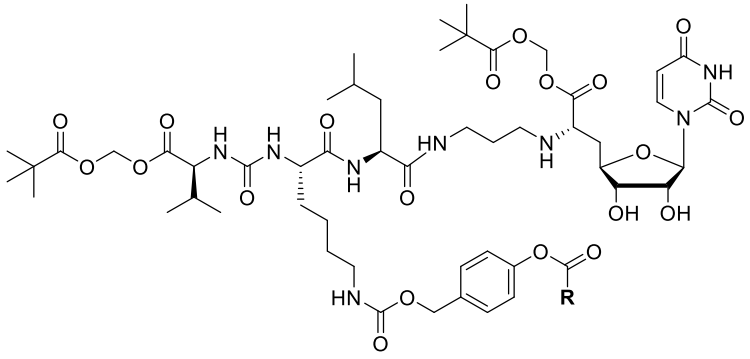

50: **R** = Me
51: **R** = *n*-Bu
52: **R** = *tert*-Bu

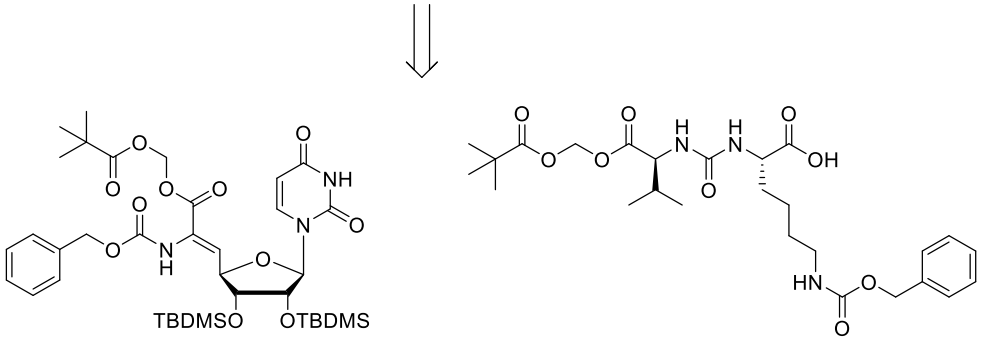

53 **54**

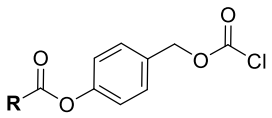

55: **R** = Me
56: **R** = *n*-Bu
57: **R** = *tert*-Bu

*Scheme 3.1: Retrosynthesis of carbamate prodrugs **50**-**52**.*

The nucleosyl amino acid **53** will be obtained by a Wittig-Horner reaction[201,202] utilizing uridine-5'-aldehyde **13** and the *N*-Cbz protected POM ester phosphonate **58** (Scheme 3.2), followed by asymmetric hydrogenation[207,208] with (*S*,*S*)-Me-DUPHOS-Rh **21** as chiral catalyst. The 2',3'-*O*-bis-(TBDMS)-uridine-5'-aldehyde **13** results from the 5'-selective TBMDS-deprotection of the fully TBDMS-protected uridine **59** with subsequent oxidation using 2-iodoxybenzoic acid (IBX) **60** (Scheme 3.2).[172,184] This route is well established in our research group and has already been described in Chapter 2.4.3. The POM ester phosphonate **58** will be synthesized

in four steps by saponification of the methyl ester phosphonate **61** and alkylation with pivaloyloxy methyl iodide (POM-I) **62**.[203–205,250] The nucleosyl amino acid **53** represents one of the two building blocks required for the formation of **63** which should be available after reductive amination of **53** with L-leucine derived aldehyde **28**.[212] The synthesis of the aminopropyl linker **28** will be conducted by peptide coupling of L-leucine **64**, which amine moiety will be previously Cbz-protected, and 1-amino-3,3-diethoxypropane **65**, thus forming amide **66**.[231,251] Subsequent cleavage under acidic conditions will provide the desired aldehyde **28** (Scheme 3.2).

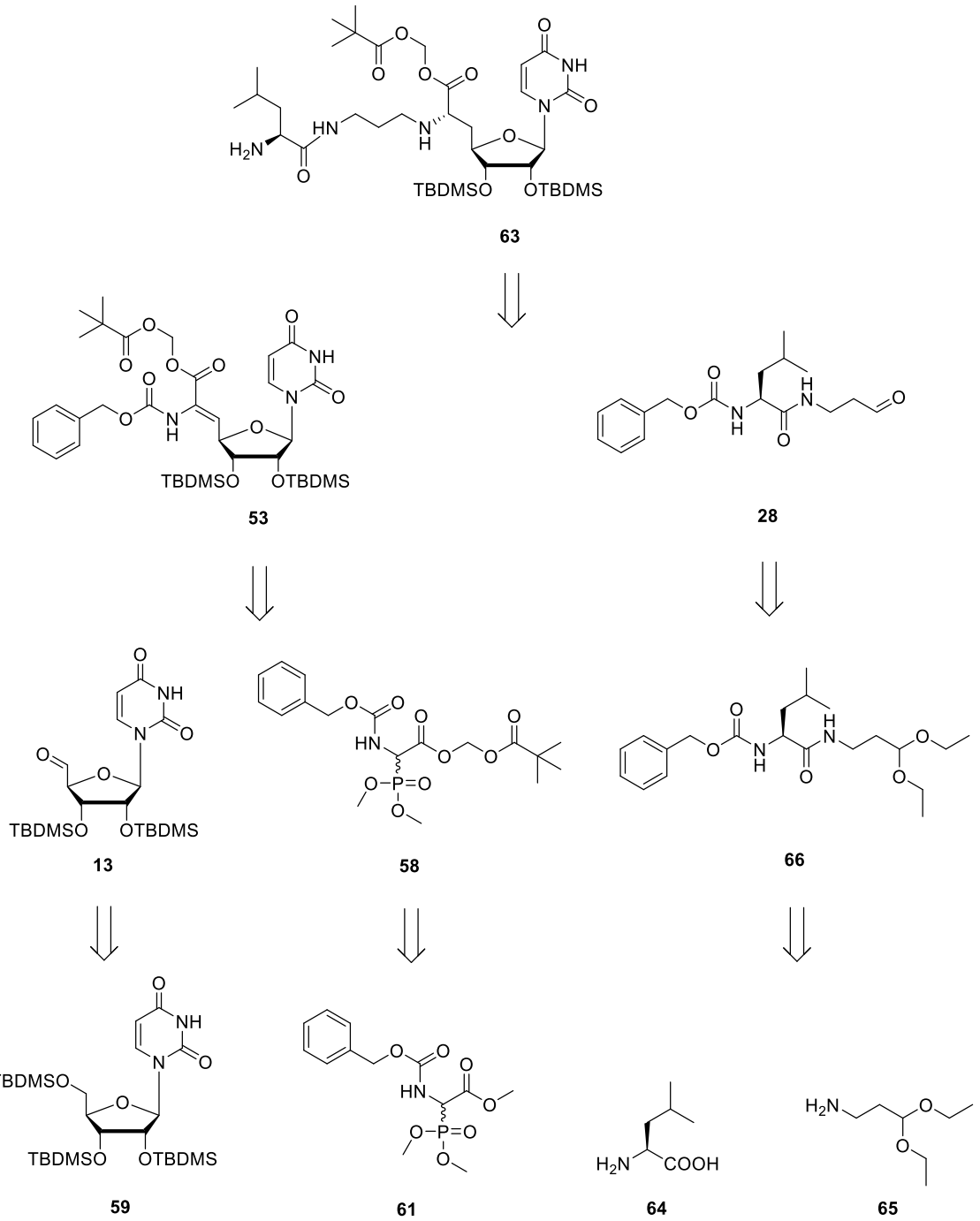

*Scheme 3.2: Retrosynthesis of nucleosyl amino acid **63**.*

The POM-modified urea dipeptide **54** will be synthesized in four steps (Scheme 3.3). First, the POM unit will be attached to *N*-Cbz-L-valine **67** under basic conditions utilizing POM-I **62**.[212] This functionalization will provide *N*-Cbz-l-valine POM ester **68**. Subsequent Cbz-deprotection and reaction with triphosgene will result in the instable isocyanate which will be converted into urea dipeptide **54** by adding N^{ε}-Cbz-L-lysine **69**.[212,252,253] Both amino acids **67** and **69** are commercially available.

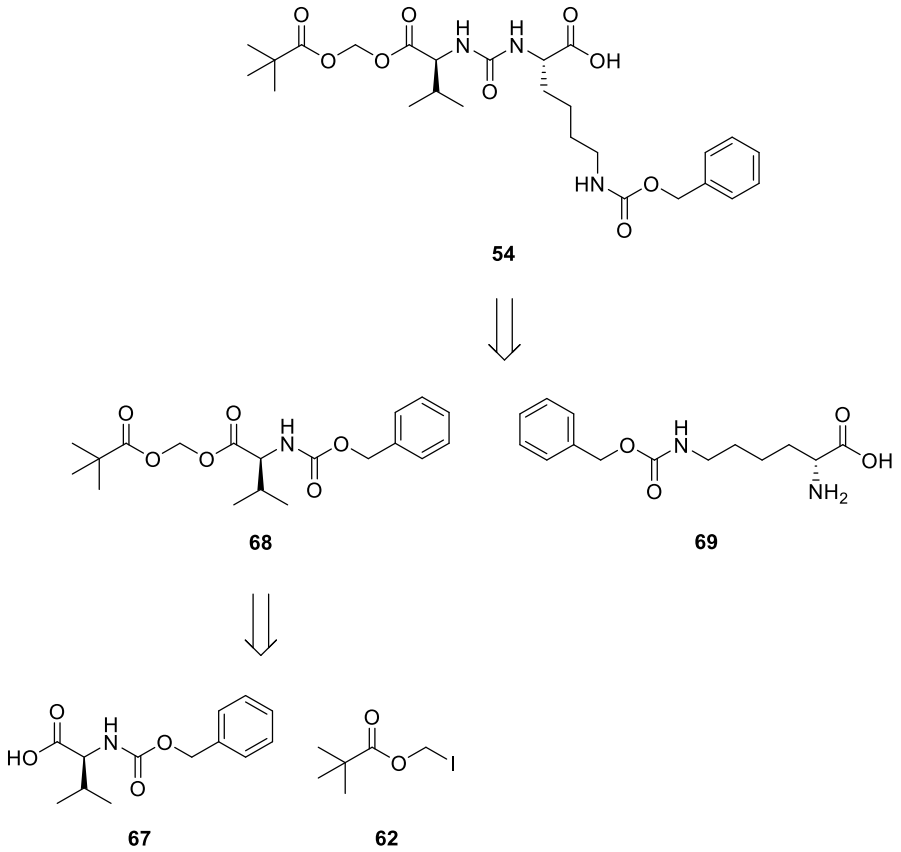

*Scheme 3.3: Retrosynthesis of urea dipeptide **54**.*

Chloroformates **55**-**57** will be obtained in a three-step sequence, starting with 4-hydroxybenzaldehyde **70** and the appropriate acyl chlorides **71**-**73** to form the ester.[254] Subsequent reduction with sodium borohydride and the reaction with triphosgene will furnish the desired compounds **55**-**57** (Scheme 3.4).[254,255]

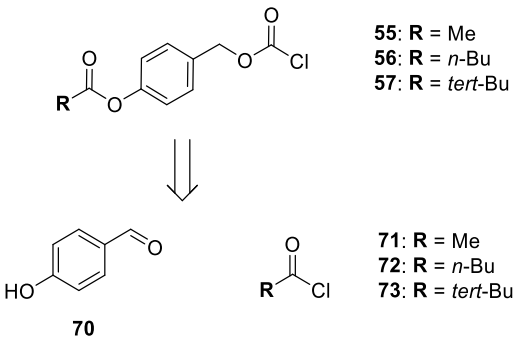

*Scheme 3.4: Retrosynthesis of chloroformates **55**-**57**.*

4 Results and discussion

The results of this dissertation will be presented in two parts. The first one includes the results of the biological studies. The synthesis of the novel muraymycin prodrugs will be presented and discussed in the second part of this chapter.

4.1 Biological studies

The following chapter focuses on biological studies for the evaluation of muraymycin analogues synthesized in our research group and other potential drug candidates by collaborators. Cellular uptake represents a major topic in this work and will be presented and discussed first. A basic procedure for the investigation of cellular uptake in Gram-negative *E. coli* is available in our research group and served as starting point for this work.[134] It was adapted and optimized for individual compounds in my studies and will be reported and discussed. The development of a corresponding cellular uptake assay for Gram-positive *S. aureus* will be presented thereafter, followed by a suitable calculation tool for the evaluation of cellular uptake data. Former accumulation data for Gram-negative *E. coli*[134] will be revised with this calculation tool and presented. In the following section, results of MraY inhibition assays and the preparation of the target protein in different biological environments will be reported, with focus on MraY in phospholipid nanodiscs. The development of a novel assay for the quantification of MraY will be presented and discussed. Subcloning results of the $MraY_{Mtb}$ (MurX) genes into different vectors will be reported, focusing on the biological behavior of different bacterial MraY isoforms. The last part of the MraY-related projects addresses a potential explanation for the self-resistance of muraymycins and initial results of the interaction between MurF and MraY are depicted. A hemolysis assay and an assay for the determination of PLE activity complete this chapter. Some of the represented results were obtained as part of my supervision of an internship by K. Ringle.

4.1.1 Cellular uptake assays

The following chapter presents the results of cellular uptake assays for Gram-negative *E. coli* (Chapter 4.1.1.1). The development of a corresponding assay for Gram-positive *S. aureus* will be presented afterwards (Chapter 4.1.1.2), followed by the calculation tool with the converted results of this work and revised former accumulation data (Chapter 4.1.1.3).

4.1.1.1 Assay for Gram-negative *E. coli*

Initial cellular uptake assays with Gram-negative *E. coli* were performed with commercially available ciprofloxacin (Figure 4.1). During assay development,[134] ciprofloxacin was chosen as a model compound to validate the assay for *E. coli* due to its broad antibacterial spectrum and its beneficial analytical properties.[134] Ciprofloxacin exhibits good detectablity by MS which

was used for analytics. Ciprofloxacin belongs to the family of fluoroquinolons and exploits hydrophilic and lipophilic pathways of cellular uptake in Gram-negative bacteria (Chapters 2.1.1 and 2.3). A charged state of ciprofloxacin exists at physiological pH, thus leading to an equilibrium between a zwitterionic, polar form and a completely uncharged form (Figure 4.1).

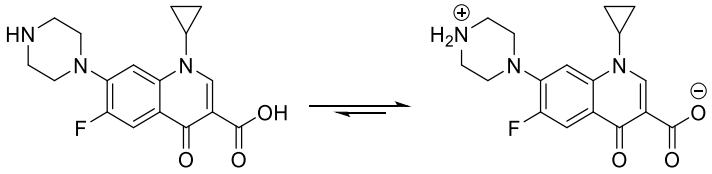

Figure 4.1: Ciprofloxacin in its uncharged, lipophilic form (left) and in its zwitterionic, strongly polar form (right).

Initial cellular uptake assays of this work were performed with ciprofloxacin in analogy to the former experiments during assay development and validation.[134] It should be noted that former accumulation data was obtained with the HRMS system of the research group of Prof. Dr. A. Luzhetskyy (Pharmaceutical Biotechnology, Saarland University),[134] whíle cellular uptake data of this work were obtained using the Thermo Scientific UHPLC system of our research group (Chapter 7.1.3.1.2). Different HRMS systems should, however, not cause significant differences. Due to intrinsic variance of the performed analytics, the obtained results should generally not be interpreted as absolute values, but always relative to results obtained from other compounds which were analyzed in an identical fashion.

Compound concentration determinations for cellular uptake assays with Gram-negative *E. coli* were calculated in dependence on their antibacterial growth inhibition results:[134] A final concentration of 1 µM was used for compounds with IC_{50} < 20 µg/mL, whereas a final concentration of 10 µM was taken for compounds with IC_{50} > 20 µg/mL.[134] This principle was utilized for all experiments of this work. Deviating concentrations have been applied by request of our collaborators in the individual projects of this work and will be listed in the corresponding chapters. Nevertheless, too high drug concentrations should be generally avoided in the assay since cell damage and changes in cell physiology might be induced by bacteriostatic antibiotics, while too high concentrated bactericidal drugs would directly cause bacterial death. In most cases, a straight distinction between bacteriostatic and bactericidal antibiotics is generally not possible due to their concentration-dependent effects.[256] However, cellular uptake data would be falsified regardless of the bacterial mode of action.

The cellular uptake assay with ciprofloxacin was performed as follows: A day culture of *E. coli* Δ*tolC* was prepared in lysogeny broth (LB) from an overnight culture and was grown to an optical density at 600 nm (OD_{600}) of ~ 0.6. Bacteria were subsequently harvested and washed twice with M9 medium. Last, an OD_{600} of ~ 4 was adjusted with M9 medium to yield the

bacterial suspension for the assay. The principle of preparing such bacterial suspensions was done in analogous fashion for all assays and will therefore not be described in detail hereafter. However, the initial OD_{600} and the volume of M9 medium that was used for adjusting the bacterial suspension to an OD_{600} of ~ 4 play a major role for the data conversion later on (Chapter 4.1.1.3). Subsequent assay procedure will be described for each compound due to individual required modifications resulting in varying assay protocols. Solvent volumes for washing can be found in Chapter 7.1.3.1.1 and will not be listed in this part, unless they deviate from the usual ones. The settings for centrifugations (speed, time, temperature) are listed in Chapter 7.1.3.1.1 as well.

Antibacterial growth inhibition of ciprofloxacin (IC_{50}) was determined with 0.3 µg/mL (≙ 0.9 µM) against *E. coli* Δ*tolC*.[134] Due to the compound concentration determinations (IC_{50} < 20 µg/mL), a final concentration of 1 µM was used in the assay with *E. coli* Δ*tolC*. A solution of ciprofloxacin in M9 medium (2 µM) was incubated with the bacterial suspension (equal volumes) in a water bath at 37 °C for 30 minutes. Mixtures were centrifuged and washed twice with M9 medium. The pellets were frozen overnight to facilitate lysis. Lysis was performed under usual conditions by sonication (Chapter 7.1.3.2.1) using lysis buffer (Chapter 7.1.1.9). Centrifugation, protein precipitation with acetonitrile (MeCN) and an incubation on ice (5 minutes) followed. Another centrifugation yielded the supernatants that were applied to MS, thus providing the whole lysate. The second approach implemented a cold osmotic shock (Chapter 7.1.3.2.2) that ensured a separation of the cytoplasmic and periplasmic fraction. The periplasmic fraction was frozen prior to MS measurements, while the cytoplasm was treated in analogous fashion as the whole lysate. The samples were lysed and centrifuged. A protein precipitation with MeCN was performed, followed by incubation on ice (5 minutes) and another centrifugation before applying the supernatants to MS. The results are presented as sample concentrations in Figure 4.2.

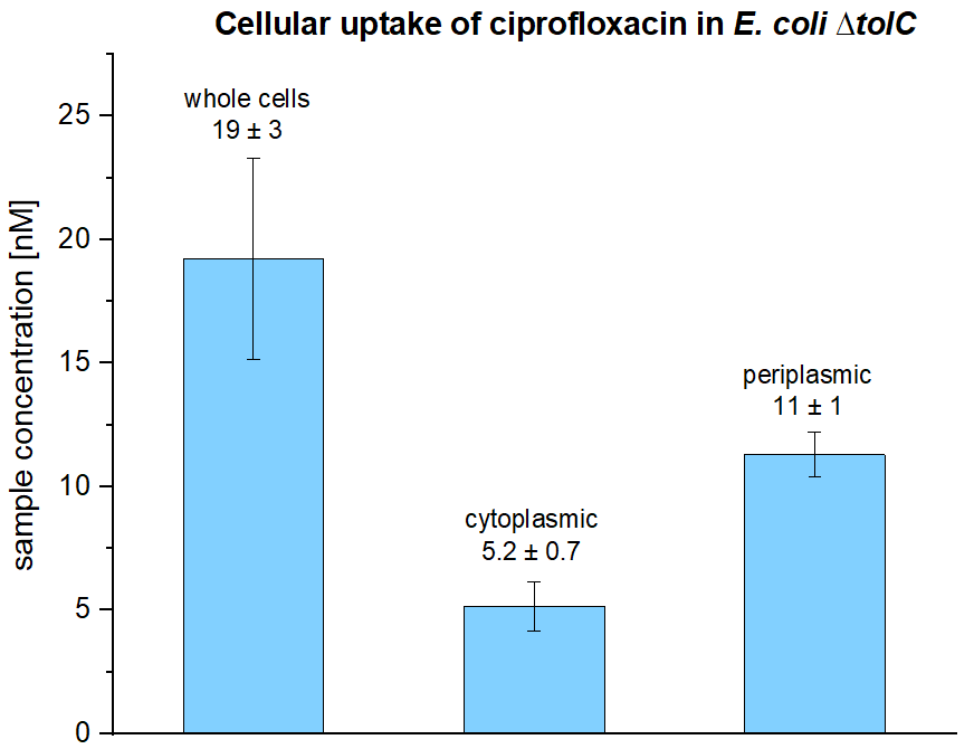

Figure 4.2: Cellular uptake of ciprofloxacin in E. coli ΔtolC depicted as sample concentrations for whole cell lysate ("whole cells"), cytoplasmic space and periplasmic space.

A sample concentration of 19 ± 3 nM was obtained for the whole cell lysate (Figure 4.2). The cold osmotic shock yielded sample concentrations of 5.2 ± 0.7 nM ciprofloxacin in the cytoplasm and 11 ± 1 nM in the periplasmic space (Figure 4.2). This data was in agreement with previous results.[134] Extraction procedures of the different cell compartments were performed with the same solvent volumes, thus enabling a direct comparison of the measured sample concentrations after data correction for the periplasmic space (MeCN treatment). Ciprofloxacin distributed equally between the periplasmic and cytoplasmic space after incubation. This is plausible due to its uptake mechanism. Due to its small size, ciprofloxacin is able to cross the outer membrane of Gram-negative bacteria through porins (Chapters 2.1.1 and 2.3) in its hydrophilic zwitterionic form (Figure 4.1). Once in the periplasm, it accumulates because only the uncharged form is able to pass the cytoplasmic membrane by passive diffusion and the equilibrium favors the zwitterionic site (Figure 4.1).[128] The robustness and consistency of the assay protocol was demonstrated. The obtained amounts of ciprofloxacin correspond to sample amounts and not to biological concentrations in the compartments (Chapter 4.1.1.3.1). Otherwise, the ciprofloxacin amounts in cytoplasmic space and periplasmic space should correlate to the whole cell lysate, assuming that no adhesion to the membranes occurred.

In general, different matrices, i.e. biological media but also the choice of solvent(s), and their effect on the analytics of the compounds need to be considered for the envisioned cellular uptake assays. Matrices can effect protonation state, ionizability and detectability due to the

formation of non-ionizable complexes or by side reactions of ions with co-eluted substances. Hence, all compounds were investigated using individual matrices prior to cellular uptake assays.

Cellular uptake of muraymycin analogues synthesized by our research group and by collaborators were examined and will be discussed in the following, including the modifications required for individual studies. The investigation of cellular uptake in Gram-negative *E. coli* Δ*tolC* of the envisioned target structures **50**-**52** of this work was not possible at this stage because their synthesis was ongoing.

4.1.1.1.1 Cellular uptake of compounds with anti-pseudomonal activity

Muraymycin analogue **37** and the literature-known reference compound **38**[183] synthesized by Dr. G. Niro[239] were investigated in the accumulation assay with *E. coli* Δ*tolC*. Both compounds **37** and **38** showed beneficial biological properties that are summarized in Figure 4.3.

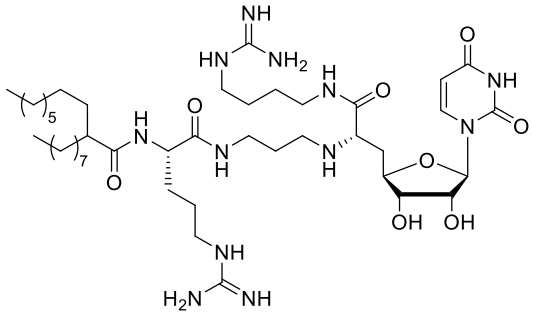

37

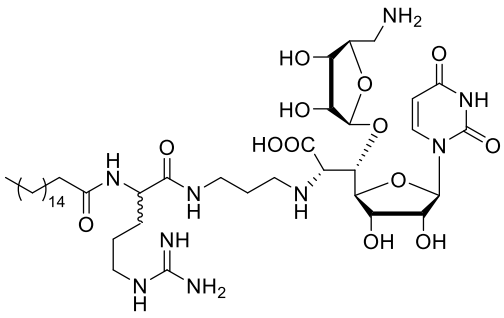

38

Compound	IC_{50} against MraY from *S. aureus* [µM]	MIC_{50} [µg/mL]
37	4.4 ± 1.3	*E. coli* DH5α 14 *E. coli* Δ*tolC* 3.9 *P. aeruginosa* 18 *S. aureus* 3.4
38	(2.3 ± 0.4) · 10^{-3}	*E. coli* DH5α 5.9 *E. coli* Δ*tolC* 5.1 *P. aeruginosa* 16 *S. aureus* 1.3

*Figure 4.3: Biological activities of muraymycin analogues **37** and **38** by Dr. G. Niro.[239]*

Analogues **37** and **38** exhibited antibacterial growth inhibition against Gram-positive *S. aureus* as well as against both Gram-negative *E. coli* strains, DH5α and Δ*tolC* (Figure 4.3).[239] Moreover, both analogues **37** and **38** are characterized by their antibacterial activity against the Gram-negative pathogen *P. aeruginosa* (Figure 4.3). The inhibitory activity of compounds **37** and **38** against MraY, however, varied in orders of magnitude: Analogue **37** displayed lower inhibition against MraY by a factor of ~ 1000 relative to the reference **38** (Figure 4.3).[239] The similarity in antibacterial activities in spite of different inhibitory potencies against MraY might be attributed to bacterial uptake, i.e., they might result from an improved uptake of compound

37 relative to compound **38**. This suggestion was examined with the cellular uptake assay with *E. coli* Δ*tolC*.

First, matrix effects were investigated for compounds **37** and **38** because previous biological studies revealed the compounds' tendency to precipitate in aqueous systems (e.g. MraY assays, cf. Chapter 7.1.2.3). Micelle formation as a result of the high amphiphilicity of both analogues **37** and **38** is potentially an important feature regarding our biological studies and demonstrate the compounds' potential to serve as detergents. This subject was investigated in the following studies and was especially important when the compounds were lyophilized at the latest stage of the assay. Lyophilization represents a gentle method to concentrate compounds without them being decomposed and to exchange solvents. An exchange of the lysis buffer would be required in case of lyophilization prior to MS measurements. The lysis buffer contains high amounts of salt (Table 7.2) which would be concentrated as well during lyophilization, resulting in insoluble solids in mixtures such as MeCN/H_2O (50/50) that is frequently used for HRMS measurements. Therefore, a $MgCl_2$ (5 mM) solution as an alternative solvent for lysis was considered during the experimental preparations prior to cellular uptake assays (adopted from former studies in our research group[134]). For the investigation of matrix effects, compounds **37** and **38** were dissolved in lysis buffer, $MgCl_2$ (5 mM), MeCN and in an acid-containing (1% HCOOH) mixture of MeCN/H_2O. Analytics were performed by HRMS. Measurements in lysis buffer and $MgCl_2$ (5 mM) could not be evaluated, likely due to low solubility. This applied for both muraymycin analogues and demonstrated solubility features of the compounds. Compounds **37** and **38** dissolved in MeCN and in 1% HCOOH-containing MeCN/H_2O (50/50), however, showed reproducible MS results. The studies further revealed that an addition of organic acid was beneficial for analytics. As a consequence, the envisioned cellular uptake assays will include a solvent exchange for both analogues **37** and **38** after cell lysis to improve the compounds' solubility for MS analytics.

For the following accumulation assay, a bacterial suspension (*E. coli* Δ*tolC*) was prepared using conditions described in Chapter 4.1.1.1. The final concentration of both analogues **37** and **38** was 1 µM each, according to their antibacterial activities (Figure 4.3). Compounds **37** and **38** were dissolved in M9 medium at a concentration of 2 µM and incubated with equal volumes of bacterial suspension in a water bath at 37 °C for 30 minutes. Mixtures were centrifuged and washed twice with M9 medium. The pellets were frozen overnight to facilitate lysis. Lysis was performed using $MgCl_2$ under usual conditions (Chapter 7.1.3.2.1). The samples were centrifuged and proteins were precipitated with MeCN, followed by incubation on ice (5 minutes). Another centrifugation yielded the supernatants that were applied to MS, thus providing the whole lysate. A cold osmotic shock (Chapter 7.1.3.2.2) was performed in a second approach and provided the cytoplasmic and periplasmic fraction. The periplasmic

fraction was frozen prior to MS measurements. The cytoplasmic fraction was treated in analogous fashion as described earlier for the whole lysate. The results are depicted as sample concentrations in Figure 4.4.

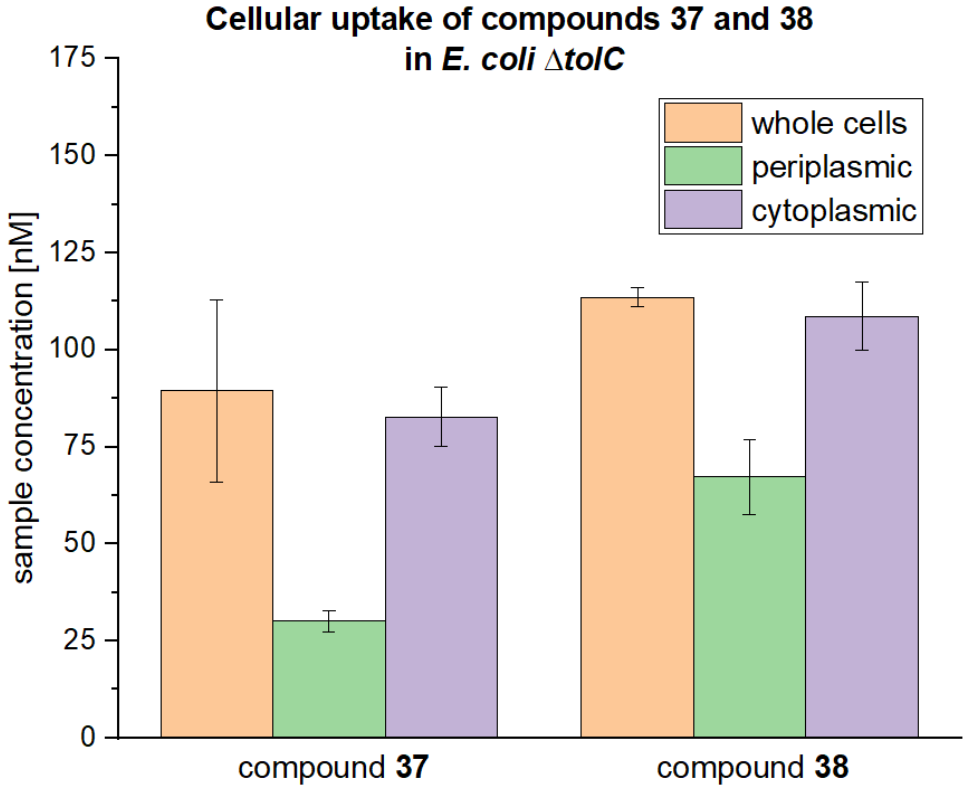

*Figure 4.4: Cellular uptake of compounds **37** and **38** in E. coli ΔtolC depicted as sample concentrations for whole cell lysate ("whole cells"), cytoplasmic space and periplasmic space.*

A sample concentration of 90 ± 24 nM was obtained for compound **37** in whole cell lysate (Figure 4.4). Periplasmic accumulation of compound **37** was significantly lower with a sample concentration of 30 ± 3 nM, while cytoplasm accumulation was measured as a sample concentration of 83 ± 8 nM (Figure 4.4). The same trend was observed for the literature-known reference **38**. Compound **38** was found in whole cell lysate in a sample concentration of 114 ± 3 nM (Figure 4.4). The application of the cold osmotic shock resulted in sample concentrations of 67 ± 10 nM in the periplasm and 109 ± 9 nM in the cytoplasm (Figure 4.4). In summary, cellular uptake of both compounds **37** and **38** in *E. coli* Δ*tolC* was comparable. The retention in antibiotic activity did consequently not result from vastly improved cellular uptake of muraymycin analogue **37** as it was suggested. *E. coli* Δ*tolC* does not capture drug efflux (Chapter 1.2) that might be an explanation for the discrepancy between the inhibitory and antibacterial activities of compounds **37** and **38**. Moreover, an alternative, additional or even secondary mode of action of compound **37** was considered. This suggestion, however, has not been unearthed yet, but will be examined in further studies by the research group of Prof. Dr. T. Lee (Department of Environmental Engieneering, Yonsei University, Republic of

Korea). A Raman-based spectroscopy approach is envisioned which enables a differentiation into different modes of action of drugs (e.g. cell wall biosynthesis inhibitor, protein biosynthesis inhibitors or targeting DNA gyrase). Commercially available antibiotics such as Amp (cell wall biosynthesis inhibitor), streptomycin (protein synthesis inhibitor) and ciprofloxacin (targeting DNA gyrase) serve, among others, as references in their studies.

4.1.1.1.2 Cellular uptake of muraymycin conjugates

Cellular uptake assays of the muraymycin GuCOSS conjugate **39** and the muraymycin CPP conjugate **40** synthesized by Dr. C. Rohrbacher[240] were performed. The lysine reference **33** was included in this series as the released parent drug. The comparison of the data from conjugates **39** and **40** to those from the lysine reference **33** was of special interest for the evaluation of the conjugation approach. The biological properties of the muraymycin lysine reference **33** and both muraymycin conjugates **39** and **40** are summarized in Figure 4.5.

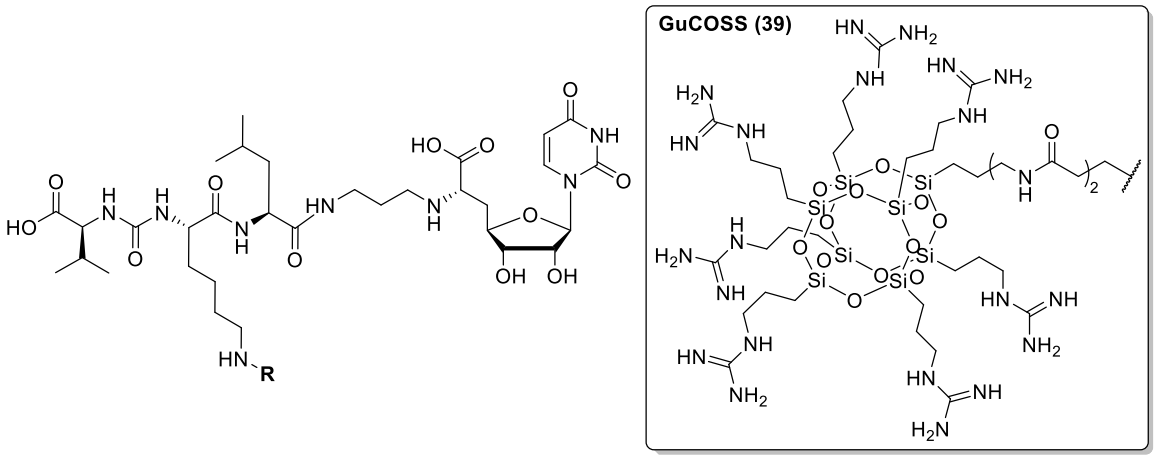

Compound	R	IC_{50} against MraY from *S. aureus* [µM]	IC_{50} [µg/mL]
33	H	2.5 ± 0.6	*E. coli* DH5α >100 *E. coli* Δ*tolC* 100
39	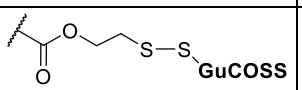	0.48 ± 0.03	*E. coli* DH5α 63 *E. coli* Δ*tolC* 6.5
40	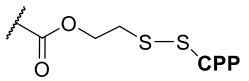	1.3 ± 0.2	*E. coli* DH5α 44 *E. coli* Δ*tolC* 6.4

*Figure 4.5: Biological activities of muraymycin lysine reference **33**[212,231] and muraymycin conjugates **39** and **40** by Dr. C. Rohrbacher[240].*

Conjugate **40** showed reduced inhibitory activity against MraY by a factor of ~ 2.5 relative to conjugate **39**, but still enhanced activity by a factor of ~ 2 relative to the parent lysine reference **33** (Figure 4.5).[240] Furthermore, both conjugates **39** and **40** are characterized by antibacterial growth inhibition against Gram-negative *E. coli* Δ*tolC* in contrast to the parent muraymycin drug **33** (Figure 4.5).[240]

The analytics for the investigation of compound **33** has previously been optimized by Dr. S. Boettcher in metabolic stability experiments[212] and was in principle adopted for the following studies. The detection limit was examined prior to the assays and was determined with <5 nM for compound **33** in a mixture of MeCN/H_2O (50/50) with acid (1% HCOOH). The analytical investigation of conjugates **39** and **40** showed a good solubility in a mixture of MeCN/H_2O (50/50). It was further demonstrated that the addition of organic acid (1% HCOOH) to both compounds was beneficial for analytics. A detection limit of <5 nM was obtained for both compounds **39** and **40**. Matrix effects or other distinctive features were not observed.

Both muraymycin conjugates **39** and **40** are characterized by a disulfide bond and a carbamate functionality (Figure 4.5).[240] The cleavage of these moieties results in the release of analogue **33** which will be used for calibration. Hence, a modification of the known assay procedure was required after incubation prior to analytics to completely convert both conjugates into the lysine reference **33** for the investigation of their cellular uptake. A disulfide cleavage yielded the corresponding thiol intermediate which would be unsuitable for analytics in any case due to its instability. Apart from that, it was not available in our laboratory for these studies. Metabolic stability assays by M. Jankowski revealed a slow carbamate cleavage, which would impact the envisioned assay. Hence, a complete conversion of the muraymycin conjugates into the parent muraymycin drug **33** was required for providing cellular uptake data for these compounds. The evaluation of the assays will be done by calibration using the parent muraymycin drug **33.**

The assay modifications were performed as follows: The known procedure was applied until bacterial lysis. After lysis, samples were treated with dithiothreitol (DTT) and incubated in a water bath to cleave the disulfide bond. Hereafter, the mixture was treated with sodium hydroxide during a second incubation in a water bath. The basic conditions were applied to cleave the carbamate unit, thereby releasing the parent muraymycin analogue **33**. It was decided to use sodium hydroxide in a high concentration (2 M) to ensure a complete cleavage. The remaining steps of the accumulation assay were performed as described earlier (Chapter 4.1.1.1).

Prior to cellular uptake assays with the conjugates, lysine reference **33** was used to investigate possible effects of DTT and sodium hydroxide on the assay, although there is no need for these treatments with regard to the chemical structure of analogue **33**. The final concentration of lysine reference **33** was 10 µM. A bacterial suspension (*E. coli* Δ*tolC*) was prepared and the

assay was performed as described before (Chapter 4.1.1.1) until lysis: Lysis was performed with $MgCl_2$ (5 mM)[134] followed by treatment with DTT (final concentration 2 mM) and sodium hydroxide (final concentration 2 M) and incubated in a water bath at 37 °C for 15 minutes. A cold osmotic shock was not performed in this series. The remaining procedure was performed as described before (Chapter 4.1.1.1). A sample concentration of 47 ± 15 nM was obtained for muraymycin parent drug **33** under these assay conditions, comparable to previous results and demonstrating assay consistency.[134] The use of DTT and sodium hydroxide did not seem to affect the assay.

Muraymycin GuCOSS conjugate **39** was used in the following cellular uptake assay. A bacterial suspension of *E. coli* Δ*tolC* was prepared as described before (Chapter 4.1.1.1). The final concentration of compound **39** was 1 µM according to its antibacterial activity against *E. coli* Δ*tolC* (Figure 4.5). An appropriate solution of compound **39** in M9 medium was prepared (2 µM) and incubated with an equal volume of bacterial suspension in a water bath at 37 °C for 30 minutes. Mixtures were centrifuged, washed twice with M9 medium and the corresponding pellets were frozen overnight to facilitate lysis. Lysis was performed in $MgCl_2$ (5 mM). Mixtures were treated with DTT (final concentration 2 mM) and incubated in a water bath for 15 minutes. Following, sodium hydroxide (final concentration 2 M) was added and the mixtures were incubated for additional 15 minutes. A sample concentration of 98 ± 2 nM was obtained for conjugate **39**, ~ 2 times higher in relation to the parent compound **33**.

To investigate the distribution of compounds into soluble and insoluble components, cell pellets and lysates were analyzed individually. Cytoplasm and periplasm represent the supernatant after lysis, while insoluble fragments such as membranes are found in the pellet (Chapter 2.1). The mostly negatively charged cell wall fragments are generally removable by centrifugation up to 17,000 x g, while membrane fragments require ultra-centrifugation of up to 180,000 x g to be harvested. To avoid an additional step of ultra-centrifugation (that cannot be performed in our laboratory), it was envisioned to modify the already adapted assay again as follows: The adapted assay procedure was applied in analogous fashion until lysis as described in the previous experiment. After lysis, cells were harvested by centrifugation as usual, followed by a deviating novel step: pellets and supernatants were separated and individually treated with DTT and sodium hydroxide as described before. The samples are termed “supernatants“ and “pellets“. However, HRMS measurements were performed with the supernatant of the redissolved pellets after an additional centrifugation. This novel modified assay procedure was applied for the GuCOSS conjugate **39**. The DTT and sodium hydroxide-treated pellet of conjugate **39** yielded a sample concentration of 23 ± 1 nM (Table 4.1). For the DTT and sodium hydroxide treated supernatant, a sample concentration of 82 ± 9 nM was obtained for conjugate **39** (Table 4.1). The results of this assay were in agreement to the previous assay

(no individual analysis of the cell pellets and lysates) with a sample concentration of 98 ± 2 nM for conjugate **39**, taking the measurement uncertainty into account.

The same adapted conditions were applied for the accumulation assay with muraymycin CPP conjugate **40**. A bacterial suspension of *E. coli* Δ*tolC* was prepared as described before (Chapter 4.1.1.1). According to its antibacterial activity against *E. coli* Δ*tolC* (Figure 4.5) and for comparability to the previous assay with GuCOSS conjugate **39**, an appropriate solution of compound **40** in M9 medium was prepared at a concentration of 2 µM. Incubation with equal volumes of bacterial suspension was performed in a water bath at 37 °C for 30 minutes. Mixtures were centrifuged, washed and the corresponding pellets were frozen overnight to facilitate lysis. Lysis was performed in $MgCl_2$ (5 mM). Pellets and supernatants obtained after centrifugation were individually treated with DTT (final concentration 2 mM) and incubated in a waterbath for 15 minutes followed by sodium hydroxide treatment (final concentration 2 M) and an additional incubation (37 °C, 15 minutes). The remaining steps were done in analogous fashion as usual (Chapter 4.1.1.1). A sample concentration of 25 ± 7 nM was obtained for the pellet and the DTT and sodium hydroxide treated supernatant of conjugate **40** resulted in a sample concentration of 38 ± 5 nM (Table 4.1).

*Table 4.1: Cellular uptake of compounds **33**, **39** and **40** in E. coli Δ*tolC* depicted as sample concentrations for the DTT and sodium hydroxide-treated pellets and supernatants. Calibration was done with the lysine reference **33** serving as released parent drug.*

Sample concentration [nM]	33	39	40
Pellet	47 ± 15	23 ± 1	25 ± 7
Supernatant		82 ± 9	38 ± 5

The supernatant distribution of released muraymycin analogue **33** for the GuCOSS-containing conjugate **39** was higher compared to the CPP conjugate **40** while the amounts of released muraymycin analogue **33** in the pellets of both conjugates were in the same range (Table 4.1). However, an evaluation should be handled with care with regard to a possible adsorption of these highly charged muraymycin conjugates to the outer membrane. Such a non-specific adsorption cannot be determined with this assay. To elucidate the different antibacterial growth inhibition behavior of the conjugates **39** and **40** relative to the parent drug **33**, additional studies need to be performed. Further modifications, especially with regard to the analytics (MS^2 analytics), would be necessary to gain more insights into this subject.

4.1.1.1.3 Cellular uptake of non-nucleoside MraY inhibitors

Cellular uptake in *E. coli* Δ*tolC* of the non-nucleoside compounds **41** and **42** with antituberculosis activity provided by the research group of Dr. S. Roy was investigated. Prior to accumulation assays, both analogues were examined towards their antimicrobial activities

against *E. coli* DH5α and Δ*tolC* in the antibacterial growth assays (established in our laboratory, Chapter 7.1.1.11). They showed similar antibacterial activities against both *E. coli* strains: Antibacterial growth inhibition of ~ 7 µM (≙ 3.7 µg/mL against *E. coli* DH5α, 3.5 µg/mL against Δ*tolC*) was obtained for compound **41** against *E. coli* DH5α and Δ*tolC* (Figure 4.6). Compound **42** resulted in an antibacterial growth inhibition of ~ 13 µM against *E. coli* DH5α (≙ 6.5 µg/mL) and ~ 7 µM against *E. coli* Δ*tolC* (≙ 3.3 µg/mL). In the interest of completeness, it should already be noted that both compounds were further examined for their inhibitory activities against MraY from *S. aureus* (overexpressed in *E. coli*) as crude membrane preparations (Chapter 4.1.2.1).

Following, analytics of compounds **41** and **42** were examined, because low solubility of selected provided compounds is known. In our hands, both compounds were soluble in a mixture of MeCN/H_2O (50/50) within solvent experiments and no distinctive solubility features could be observed. The addition of organic acid (1% HCOOH) was beneficial for the analytics of both compounds. A detection limit of ~ 5 nM was obtained for both compounds. According to the obtained antibacterial activity against *E. coli* Δ*tolC* (Figure 4.6), the incubation concentration in the cellular uptake assays was determined with 1 µM for both compounds **41** and **42**, thus allowing a direct comparison of the accumulation results.

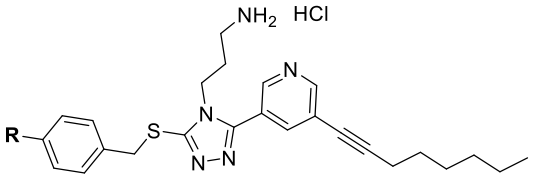

41: **R** = Cl
42: **R** = OH

Compound	IC_{50} against MraY from *S. aureus* @250 µM [%]	IC_{50} [µg/mL]
41	34	*E. coli* DH5α 3.7 *E. coli* Δ*tolC* 3.5
42	n.d.	*E. coli* DH5α 6.5 *E. coli* Δ*tolC* 3.3

*Figure 4.6: Biological activities of non-nucleoside compounds **41** and **42** by Dr. S. Roy. "n.d." = not detectable.*

The following accumulation assays were done under usual conditions to investigate the overall accumulation in Gram negative *E. coli* Δ*tolC* (Chapter 4.1.1.1). Modifications did not seem to be required according to the chemical structure of both compounds (Figure 4.6). A bacterial suspension (*E. coli* Δ*tolC*) and appropriate solutions of compounds **41** and **42** in M9 medium were prepared in a concentration of 2 µM each. The incubation with the bacterial suspension was performed in a water bath at 37 °C for 30 minutes. Mixtures were centrifuged and washed twice with M9 medium. A cold osmotic shock was done as described before (Chapter 4.1.1.1). Lysis of the whole cell lysate and the spheroblasts was performed with $MgCl_2$ (5 mM), followed

by centrifugation. Protein precipitation with MeCN, incubation on ice (5 minutes) and another centrifugation were done hereafter. The lysates were lyophilized and the remaining solids were redissolved in a mixture of MeCN/H_2O (50/50) including 1% HCOOH for HRMS measurements. The results are presented as sample concentrations in Figure 4.7.

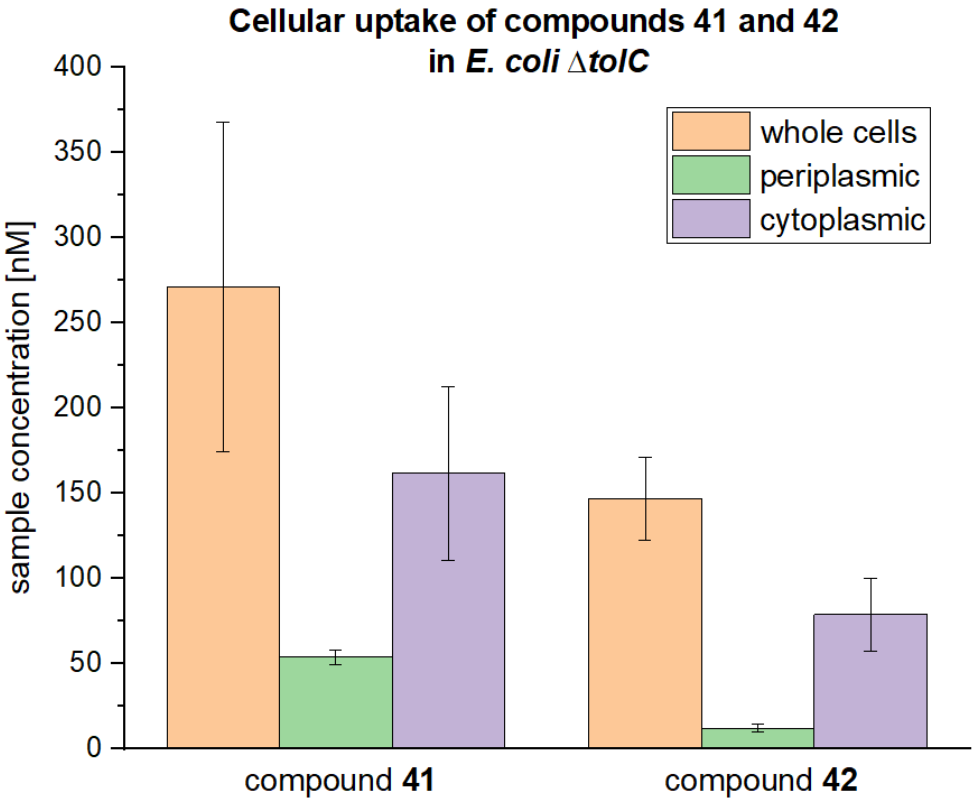

*Figure 4.7: Cellular uptake of compounds **41** and **42** in E. coli ΔtolC depicted as sample concentrations for whole cell lysate ("whole cells"), cytoplasmic space and periplasmic space.*

Compound **41** was detected with a sample concentration of 271 ± 97 nM in whole cell lysate (Figure 4.7). A sample concentration of 54 ± 4 nM was obtained in periplasm and cytoplasm yielded a sample concentration of 162 ± 51 nM (Figure 4.7). For compound **42**, the same accumulation trend was observed with a sample concentration of 147 ± 25 nM in whole cell lysate and sample concentrations of 12 ± 2 nM in periplasm and 79 ± 21 nM in cytoplasm after a cold osmotic shock (Figure 4.7). Taking the measurements uncertainty into account, cellular uptake of both compounds **41** and **42** in *E. coli ΔtolC* was comparable. The structurally similar compounds **41** and **42** only varied in one unit as part of a SAR study (Chapter 4.1.2.1, Figure 4.7). Compound **41** has a chloride in position **R**, while compound **42** has a hydroxy group (Figure 4.6). This difference affects polarity as the chloride unit enhances the hydrophobicity in contrast to the polar hydroxy unit. Enhanced lipophilicity would indeed lead to improved cellular uptake. A similar cellular accumulation, however, is in agreement to the antibacterial activities of both compounds that were in the same range (Figure 4.6). Nevertheless, the antibacterial activity of a compound is a function of various other factors

such as target interaction and efflux effects besides its cellular uptake. To complete the overall picture, further investigations are required.

4.1.1.1.4 Cellular uptake of MurA pyrazolidinone analogues

MurA-inhibiting pyrazolidinone analogues **43**-**47** provided by Dr. R. Wadgy[241] were used in further cellular uptake assays with *E. coli* Δ*tolC*. All analogues showed similar inhibitory activities against *E. coli* MurA (Figure 4.8). Antibacterial growth inhibition against *E. coli* Δ*tolC* below 40 µM was not observed for compounds **43**-**45** (Figure 4.8), while compounds **46** and **47** showed antibacterial activity against *E. coli* Δ*tolC* at a concentration of ~ 20 µM (Figure 4.8).[241] Compounds **44** and **47** represented the only two compounds in this series with antibacterial activity against *S. aureus* in the low micromolar region (Figure 4.8).[241]

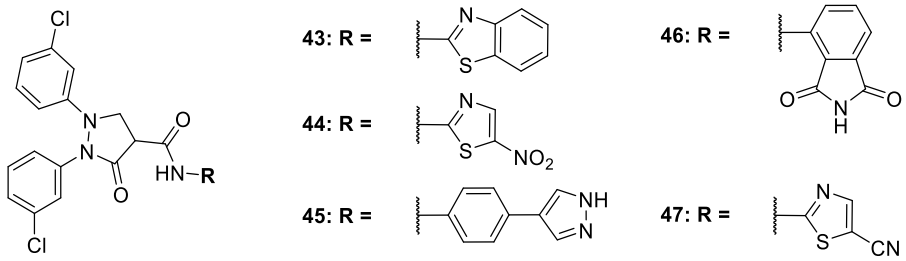

Compound	IC_{50} against *E. coli* MurA [µM]	MIC_{90} (*E. coli* Δ*tolC*) [µM]	MIC_{90} (*S. aureus*) [µM]
43	18	>40	>40
44	20	>40	8
45	13	>40	>40
46	13	17	>40
47	21	21	11

*Figure 4.8: Biological activities of MurA-inhibiting pyrazolidinone analogues **43**-**47** by Dr. R. Wagdy.[241]*

The lack of growth inhibition against *E. coli* Δ*tolC* indicated the inability of the corresponding compounds (**43**-**45**) to penetrate the Gram-negative cell wall. Previous experiments towards testing compound solubility revealed a high matrix impact for all analogues (reported by Dr. R. Wagdy[241]). For investigating solvent effects and solubility concerns, compound solutions were prepared in lysis buffer, $MgCl_2$ (5 mM), MeCN and a mixture of MeCN/H_2O (1% HCOOH was included for analogues **43** and **45** in accordance to HRMS measurements in positive mode (ESI^+)). Analytics were performed by HRMS. Measurements in lysis buffer and $MgCl_2$ (5 mM) could not be evaluated, likely due to low solubility. The use of organic solvent mixtures, however, led to reproducible results and yielded detection limits of 10 nM for all

analogues. Therefore, it was envisioned to perform the assays in principle in analogous fashion as for the compounds of Dr. G. Niro (Chapter 4.1.1.1.1).

The following cellular uptake assays were done under the conditions described above (Chapter 4.1.1.1). Bacterial suspensions (*E. coli* Δ*tolC*) and solutions of the analogues **43**-**47** in M9 medium were prepared at a concentration of 20 µM each. The incubation concentration was determined by Dr. R. Wagdy. Compound solutions were incubated with bacterial suspensions in a water bath at 37 °C for 30 minutes (equal volumes). Mixtures were centrifuged and washed twice with M9 medium. Lysis was performed with $MgCl_2$ (5 mM) followed by centrifugation, protein precipitation with MeCN, incubation on ice (5 minutes) and another centrifugation. Lyophilization was required due to low solubility. The volume for redissolving the solids differed from the other assays with 120 µL. Reproducible HRMS measurements were obtained for compounds **43** and **45** in positive mode (ESI^+) with 1% HCOOH in the solvent mixture, while acid-free conditions were beneficial for the analytics of analogues **44**, **46** and **47** (negative mode (ESI^-)). The results are presented as sample concentrations in Figure 4.9.

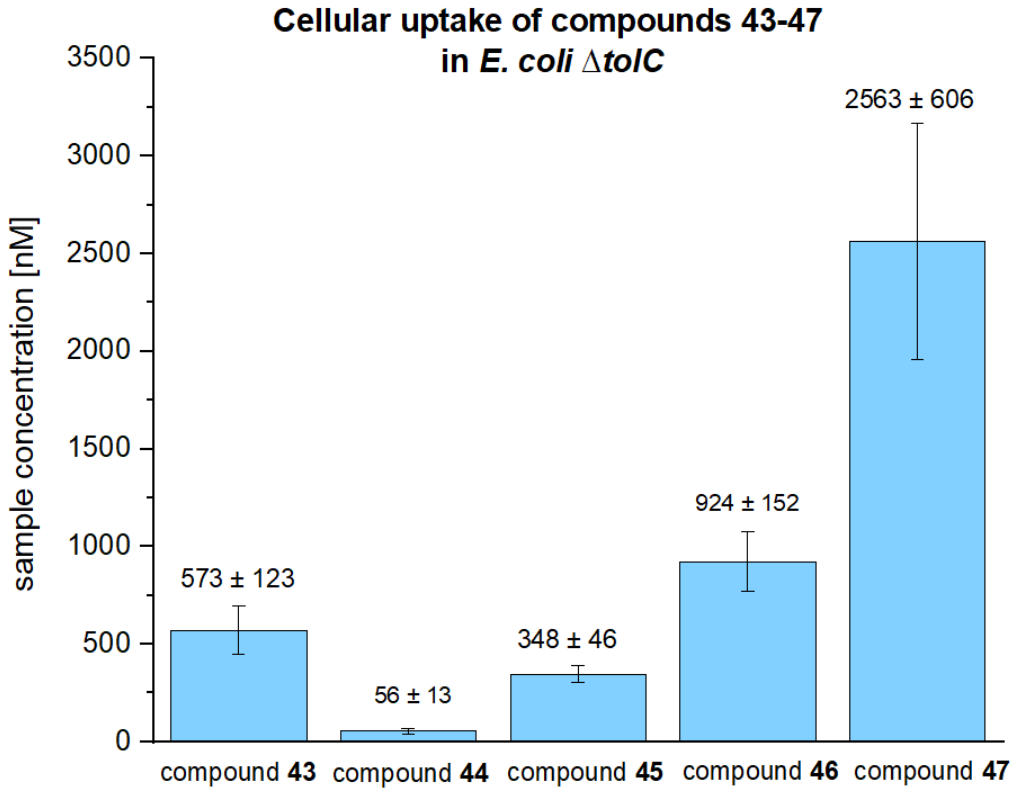

*Figure 4.9: Cellular uptake of compounds **43**-**47** in E. coli ΔtolC depicted as sample concentrations for whole cell lysate ("whole cells").*

The lowest cellular uptake within the series was observed for compound **44** with a sample concentration of 56 ± 13 nM (Figure 4.9). Cellular uptake of compounds **43** and **45** was comparable with obtained sample concentrations of 573 ± 123 nM for analogue **43** and 348 ±

46 nM for compound **45** (Figure 4.9). Compound **47** showed the highest cellular uptake into *E. coli* Δ*tolC* with a sample concentration of 2.56 ± 0.61 µM (Figure 4.9). A sample concentration of 924 ± 152 nM was obtained for compound **46** (Figure 4.9). Structurally similar compounds **44** and **47** exhibited comparable inhibitory activities against MurA and similar antibacterial potential against *S. aureus*, but significantly differed in their antibacterial activity against *E. coli* Δ*tolC*.[241] No growth inhibition against *E. coli* Δ*tolC* was observed for analogue **44** while compound **47** was active antibacterially against *E. coli* Δ*tolC* (Figure 4.8).[241] The only difference between the two compounds is the electron-withdrawing cyano group in compound **47** compared to an electron-withdrawing nitro unit in analogue **44** (Figure 4.8). A slightly higher distribution coefficient (logP) is known for nitro units, but this would indeed not explain the difference in cellular uptake by a factor of ~ 50. Sterical features might be further discussable in this context: the cyano unit is characterized by a triple bond, while the nitro unit exhibited a trigonal planar core. This different texture might affect bacterial uptake of these small sized analogues as well. Further investigations is required but nevertheless, the trend of bacterial cellular uptake agreed with the antibacterial activities of compounds **43**-**47**.

4.1.1.2 Assay for Gram-positive *S. aureus*

The establishment of a cellular uptake assay for Gram-positive *S. aureus* is presented in this chapter. A construct encoding for lysostaphin was designed as part of this work because this zinc metalloenzyme is required for lysis of *S. aureus*.[257,258] The expression of lysostaphin was performed based on studies by Farhangnia et al.[242] and is presented first (Chapter 4.1.1.2.1), followed by the development of an accumulation assay with *S. aureus* (Chapter 4.1.1.2.3).

4.1.1.2.1 Plasmid transformation and expression of lysostaphin

A codon-optimized plasmid encoding lysostaphin was designed in a bacterial pET-type vector (pET32a),[242] called pET-lys hereafter. The corresponding plasmid map is depicted in the Appendix. The purchased pET-lys was dissolved in Milli-Q® to a final concentration of 50 ng/µL. A plasmid transformation into chemically competent *E. coli* BL21(DE3) pLysS cells was performed according to the manufacturer with Amp and CAM as antibiotics. Lysostaphin expression was carried out in small scale (25 mL). The bacterial suspension was analyzed 2 and 4 hours after IPTG induction (1 mM) by SDS-PAGE analysis. An aliquot of bacterial suspension was taken before induction serving as negative control. SDS-PAGE analysis is depicted in Figure 4.10.

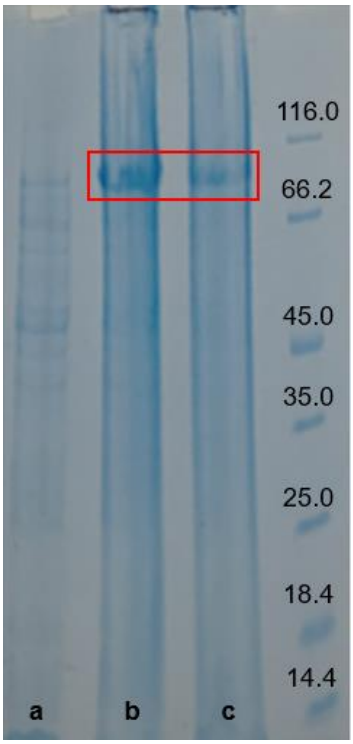

Figure 4.10: SDS-PAGE analysis of lysostaphin expression before induction with IPTG (a), 4 hours (b) and 2 hours after induction (c).

A protein band at a size between 66-116 kDa was obtained in both samples after IPTG induction (Figure 4.10, red box), but not before IPTG induction (sample (a)), indicating overexpression of lysostaphin. This protein band was more pronounced in sample (b) which was induced for 4 hours (Figure 4.10). Hence, a longer induction time seemed to be beneficial in terms of protein amounts. Farhangnia et al.performed similar experiments in terms of induction time during their studies. Their SDS-PAGE analysis is presented in Figure 4.11.[242]

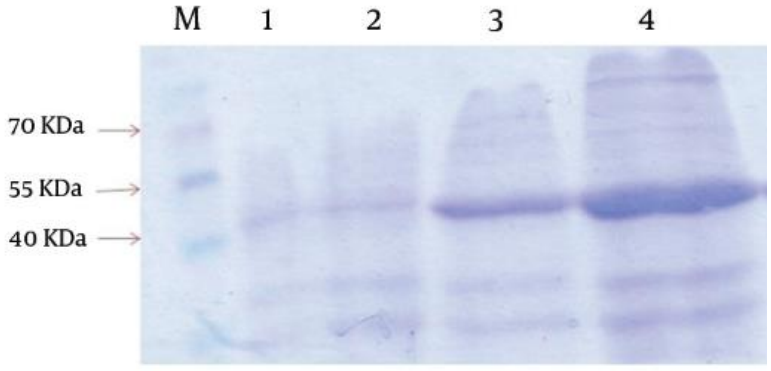

*Figure 4.11: SDS-PAGE analysis of lysostaphin expression with samples taken before induction (1, 2), 2 hours (3) and 4 hours after induction (4) beside the protein ladder (M) as reference (taken from: Farhangnia et al., Jundishapur J. Microbiol. **2004**, 7, e10009).[242]*

A comparison between the SDS-PAGE analysis by Farhangnia et al.[242] and those of this work showed differences in terms of protein size which depicted a major concern initially. SDS-

PAGE analysis by Farhangnia et al. revealed a protein band at a size between 40-55 kDa (Figure 4.11),[242] while a protein band with significantly higher weight was observed in this expression (Figure 4.10). In the literature, a molecular weight of 27 kDa was reported for lysostaphin, but this refers to mature lysostaphin.[255] The addition of IPTG, however, induces the overexpression of recombinant protein with a size of ~ 42 kDa which was observed by Farhangnia et al. (Figure 4.11).[242] Regarding SDS-PAGE analysis of this work, the obtained band (Figure 4.10) agrees with the expected size of recominbant lysostaphin taking the tags introduced by the pET32a vector into account.

Following, lysostaphin was expressed in larger scale (500 mL) with freshly transformed plasmid (chemically competent *E. coli* BL21(DE3) pLysS cells) and purified via Ni-NTA affinity chromatography. IPTG induction was done for 4 hours as evaluated in previous studies. Eluted protein was refolded overnight according to Farhangnia et al.[242] The SDS-PAGE analysis is depicted in Figure 4.12.

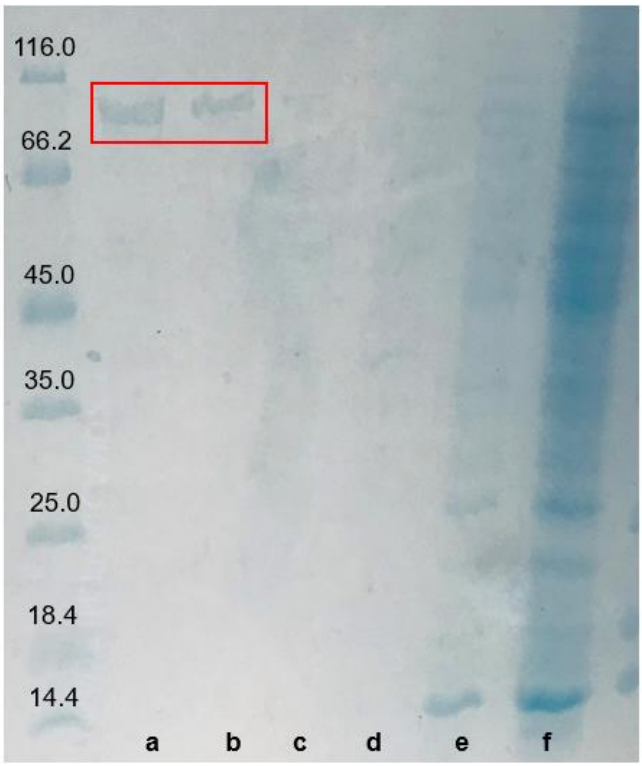

Figure 4.12: SDS-PAGE analysis of purified lysostaphin with samples of eluted protein (a) and (b) and samples taken during wash steps (d), (e) and (f).

Eluted protein, samples (a) and (b), revealed a protein band at a size between 66-116 kDa (Figure 4.12). Samples (d), (e) and (f) taken from other fractions during purification showed additional protein bands (Figure 4.12). The sample taken at the start of purification (sample (f)), i.e., the first wash step, showed intensive greasing (Figure 4.12). The observed protein band in samples (a) and (b) was in agreement to the previous studies (Figure 4.11) with a size between 66-116 kDa, thus confirming the success of lysostaphin expression and purification.

Protein preparations were aliquoted and flash frozen in liquid nitrogen for the storage at -80 °C. Lysostaphin concentration was determined with 1.4 mg/mL.

Purified lysostaphin was furthermore submitted to MS experiments (Dr. C. Bader, Department of Microbial Natural Products, Helmholtz-Institute for Pharmaceutical Research Saarland (HIPS) and Department of Pharmacy at Saarland University). A small amount of commercially available lysostaphin (Apollo Scientific Biochemicals) was purchased for comparison. It must be mentioned in advance that lysis of *S. aureus cells* was not successful with this batch of commercially available lysostaphin, thus questioning its functionality. A comparison of the MS data to the expressed and purified lysostaphin of this work was therefore focused on. Sections of both MS chromatograms in which peaks were found are depicted in Figure 4.13. Both obtained full MS chromatograms that revealed peaks are depicted in the Appendix.

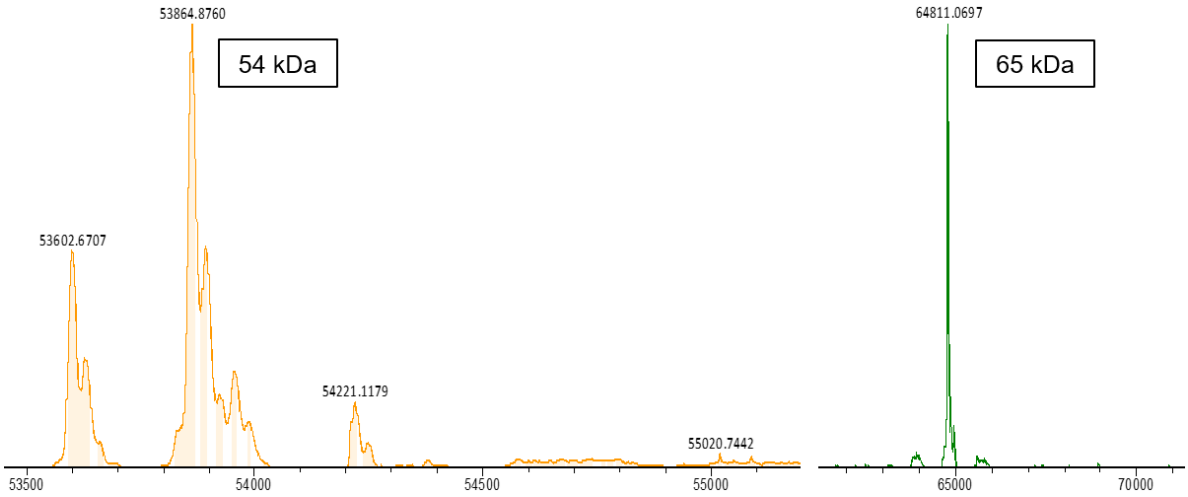

Figure 4.13: Sections of the chromatograms of MS experiments with obtained peaks for the purchased lysostaphin (left) and lysostaphin expressed and purified in this work (right).

The MS chromatograms of both protein samples revealed peaks with different sizes: For the purchased lysostaphin, several peaks within a range of ~ 53-55 kDa (Figure 4.13, left) were obtained, while the expressed and purified lysostaphin of this work showed one peak with a higher size (Figure 4.13, right). The commercially available lysostaphin displayed multiple impurities with a dominating peak at ~ 54 kDa (Figure 4.13, left). In contrast, lysostaphin of this work exhibited one dominant peak with a protein size of ~ 65 kDa (Figure 4.13, right) which was in accordance to all previous studies (Figure 4.11 and 4.17). The MS chromatogram of the expressed lysostaphin confirmed the protein's purity (Figure 4.13, right). It was used for subsequent lysis experiments with *S. aureus* which are presented next.

4.1.1.2.2 Lysis studies

Lysis of *S. aureus* is a crucial step in the development of the cellular uptake assays. It was investigated separately and decoupled from the assay itself. Nonetheless, the initial steps of the cellular uptake assay for *E. coli* (Chapter 4.1.1.1) were adopted for the lysis experiments with *S. aureus*, i.e., the procedure was performed in analogous fashion until lysis. It was envisioned to perform the lysis studies and subsequent experiments for developing the cellular uptake assay with a commercially available drug. Therefore, the oxazolidinone linezolid was chosen as a model compound. It exhibits antibacterial activity against multiple Gram-positive organisms including *S. aureus*.[259,260] Antibacterial growth inhibition between 1-4 µg/mL against various strains is reported, thus demonstrating its potent activity against Gram-positive bacteria.[259,260] Linezolid is depicted in Figure 4.14.

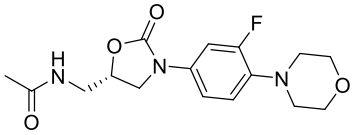

Figure 4.14: Linezolid as a model compound for cellular uptake assays with S. aureus.

Lysis experiments were performed as follows: A day culture of *S. aureus* Newman was prepared in Müller Hinton medium from the corresponding overnight culture (in Müller Hinton) and was grown until an OD_{600} of ~ 0.6 was reached. Bacteria were subsequently harvested and washed with M9 medium. The bacterial suspension was prepared by resuspending the pellet with M9 medium until an OD_{600} of ~ 4 was reached. The test antibiotic linezolid was incubated with this bacterial suspension in a water bath at 37 °C for 30 minutes. A linezolid concentration of 1 µM was used according to its antibacterial growth inhibition behavior (cf. Chapter 4.1.1.2.3 for further considerations in terms of incubation concentration). Mixtures were subsequently centrifuged and washed twice with M9 medium, followed by storage of the pellets at -20 °C overnight. Lysis experiments were performed in the following morning by enzymatic treatment with the expressed and purified lysostaphin presented before (Chapter 4.1.1.2.1). The OD_{600} was measured and evaluated relative to a sample without lysostaphin treatment to assess bacterial lysis. Because bacterial solutions appear clearly without turbity after lysostaphin incubation, samples were visually evaluated as a first indication of lysis success in accordance to the lysis studies of the research group of Prof. Dr. M. Bischoff (Hospital and Medical Faculty, Saarland University).

Initial lysis studies were performed to optimize the lysostaphin concentration. Pellets were resuspended with $MgCl_2$ (5 mM) and lysostaphin was added in the following concentrations:

(1) No lysostaphin ≙ negative control

(2) 21 nM lysostaphin (≙ 14 µg/mL)

(3) 105 nM lysostaphin (≙ 70 µg/mL)

(4) 210 nM lysostaphin (≙ 140 µg/mL)

(5) 525 nM lysostaphin (≙ 350 µg/mL)

(6) 1 µM lysostaphin (≙ 700 µg/mL)

Samples were incubated at 37 °C for 1 hour (180 rpm) with end-over-end tumbling of the tube by hand every 10 minutes. OD_{600} measurements were performed for evaluation. The results are presented in Figure 4.15. Lysostaphin incubation times were optimized at a later stage.

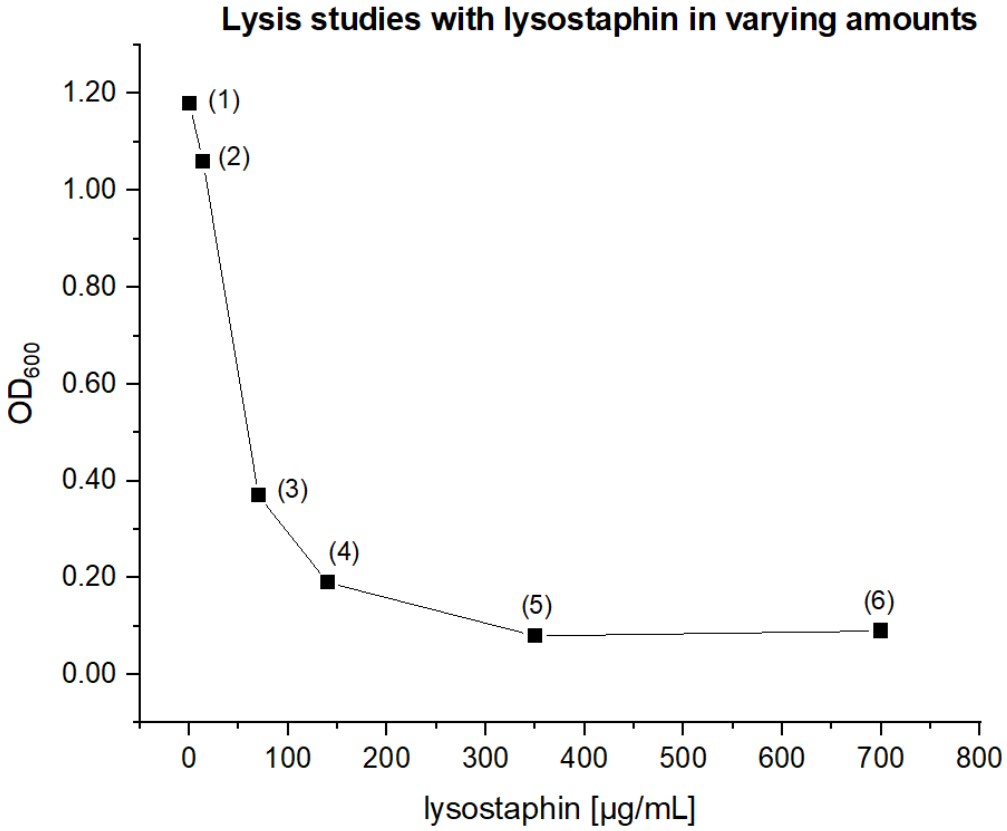

Figure 4.15: Lysis studies with lysostaphin in varying concentrations (samples 1-6) for cellular uptake assays with S. aureus. Sample 1 presented the negative control and lysostaphin concentrations increased from samples (2)-(6).

The OD_{600} decreased exponentially from samples (2)-(5), and reached a plateau for samples (5) and (6), indicating maximal possible lysis (Figure 4.15). Hence, the lysostaphin concentration used in sample (5) was utilized thereafter (350 µg/mL).

Next studies focused on the incubation time for enzymatic treatment. Previous studies were performed with an incubation of 1 hour. In the following experiments, periods of 20 minutes, 40 minutes and 1 hour were used to further validate lysis. The highest time point of 1 hour was set in accordance to studies of our collaborator Prof. Dr. M. Bischoff. Experimental conditions were kept identical otherwise. Lysostaphin was used at a concentration of 350 µg/mL. Samples

were evaluated by OD_{600} measurements after 20 minutes, 40 minutes and 1 hour. Insufficient lysis was observed by OD_{600} measurements for incubation times <1 hour. This result agrees with the studies of the research group of Prof. Dr. M. Bischoff. Thus, 1 hour incubation time was used in all further experiments. In summary, efficient lysis conditions for the envisioned accumulation studies with *S. aureus* were successfully determined. The development and establishment of a cellular uptake assay in *S. aureus* will be presented in the following chapter.

4.1.1.2.3 Development of a cellular uptake assay for *S. aureus*

Initially, the methodology of the cellular uptake assay with *E. coli* was used (Chapter 4.1.1.1) for developing an appropriate assay with *S. aureus*. However, this procedure was reevaluated due to the difference between *S. aureus* as a Gram-positive bacterium and the Gram-negative *E. coli* (Chapter 2.1.1). Test compounds were generally used at identical concentrations compared to the cellular uptake assay with *E. coli* (Chapter 4.1.1.1): According to the compound's antibacterial growth inhibition data for *S. aureus*, a final concentration of 1 µM (IC_{50} < 20 µg/mL) or 10 µM (IC_{50} > 20 µg/mL) was applied. For assay development with *S. aureus*, linezolid was used at a concentration of 1 µM (IC_{50} < 20 µg/mL).

Cellular uptake assays were performed as follows: A day culture of *S. aureus* Newman was prepared in Müller Hinton medium from the corresponding overnight culture (in Müller Hinton) and was grown until an OD_{600} of ~ 0.6 was reached. Bacteria were subsequently harvested and washed with M9 medium. The final bacterial suspension was prepared by resuspending the pellet with M9 medium until an OD_{600} of ~ 4 was reached. This procedure was applied for all following assays and will therefore not be described hereafter. However, the OD_{600} and the volume of M9 medium being used for adjusting the OD_{600} ~ 4 of M9 play a major role for the calculations later on (Chapter 4.1.1.3). Linezolid (in M9 medium) was incubated with the bacterial suspension in a water bath at 37 °C for 30 minutes. Centrifugation followed by washing of the pellets with M9 medium (twice) was performed. Pellets were stored at -20 °C overnight and resuspended in $MgCl_2$, (5 mM). Enzymatically induced lysis by lysostaphin (350 µg/mL) was performed at 37 °C for 1 hour. Samples were centrifuged and proteins were precipitated with iced MeCN (including HCOOH (1%)) followed by incubation on ice (5 minutes) and a second centrifugation. Lyophilization was performed and samples were analyzed by HRMS.

Analytics and matrix effects of linezolid were examined prior to cellular uptake assays. Linezolid dissolved well in a mixture of MeCN/H_2O (50/50). The addition of organic acid (1% HCOOH) was beneficial for analytics. A detection limit of <5 nM was obtained for linezolid and no matrix effects were observed. Initial cellular uptake assays investigated varying incubation times of linezolid. It was envisioned to examine the rate of cellular uptake in *S. aureus* compared to *E. coli.*

A bacterial suspension (*S. aureus* Newman) was prepared as described above. An appropriate solution of linezolid in M9 medium (2 µM) was incubated with bacterial suspension in a water bath at 37 °C for varying times. All approaches were performed in parallel using the same bacterial suspension:

(1) 0 minutes ≙ negative control

(2) 5 minutes

(3) 10 minutes

(4) 20 minutes

(5) 30 minutes

(6) 45 minutes

(7) 60 minutes

Longer incubation times (> 60 minutes) were rejected due to potential bacterial growth inhibition. Following incubation, mixtures were centrifuged, washed with M9 medium (twice) and the resulting pellets were stored at -20 °C overnight. In the next morning, lysis was performed with lysostaphin under the established conditions as described above. Samples were centrifuged. Proteins were precipitated with iced MeCN (including HCOOH (1%)) followed by sample incubation on ice (5 minutes) and a second centrifugation. Although a detection limit of <5 nM was determined for linezolid, lyophilization was included to account for lower cellular uptake during shorter incubation times. Resulting solids were resolved in a mixture of MeCN/H_2O (50/50) with HCOOH (1%) included. The results of MS measurements are presented in Figure 4.16.

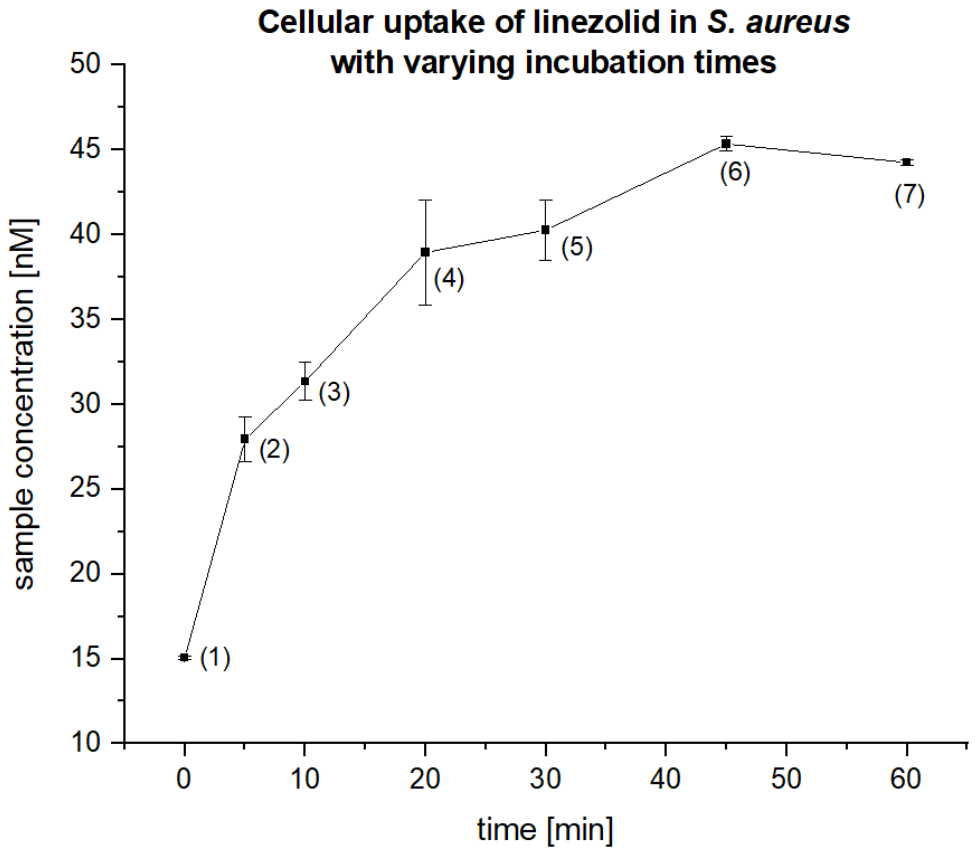

Figure 4.16: Cellular uptake of linezolid in S. aureus depicted as sample concentrations with incubation times from 0-60 minutes.

Increasing incubation yielded higher linezolid sample concentrations, resulting in a hyperbolic curve when plotted as a function of incubation time, reaching sample concentrations of ~ 45 nM (Figure 4.16). The comparison of intracellular linezolid amounts after incubations of 45 minutes (sample (6)) and 60 minutes (sample (7)) revealed no significant differences, comparable to the cellular uptake in Gram-negative *E. coli*.[134] An increase in the sample concentrations was observed between incubations of 30 minutes (samples (5)) and 45 minutes (sample (6)). Nonetheless, an incubation time of 30 minutes was decided on for the envisioned assays as a compromise to avoid potential bacterial growth inhibition because the cellular uptake of linezolid seems to be mostly done after 30 minutes (Figure 4.16).

Subsequent assays investigated concentration-dependent uptake effects of linezolid. A bacterial suspension (*S. aureus* Newman) was prepared under the conditions described above. Appropriate solutions of linezolid in M9 medium were prepared as follows:

(1) 6 µM (1x antibacterial growth inhibition)

(2) 3 µM (1/2x antibacterial growth inhibition)

(3) 1.5 µM (1/4x antibacterial growth inhibition)

(4) 0.75 µM (1/8x antibacterial growth inhibition)

(5) 0.3 µM (1/20x antibacterial growth inhibition)

Higher concentrations than 6 µM were ruled out to avoid bacterial disruption and death (Chapter 4.1.1.1). All approaches were done in parallel using the same bacterial suspension. Drug solutions were incubated with bacterial suspension in a water bath at 37 °C for 30 minutes. Mixtures were centrifuged and washed with M9 medium. Samples were stored at -20 °C overnight. Lysis was done with lysostaphin (350 µg/mL) under established conditions. Samples were centrifuged and protein precipitation with iced MeCN (including HCOOH (1%)) was performed. After incubation on ice (5 minutes) and a second centrifugation, samples were lyophilized overnight. The redissolved solids (HCOOH-including (1%) MeCN/H_2O (50/50)) were applied in MS measurements. The results are plotted as a function of offered concentration in Figure 4.17.

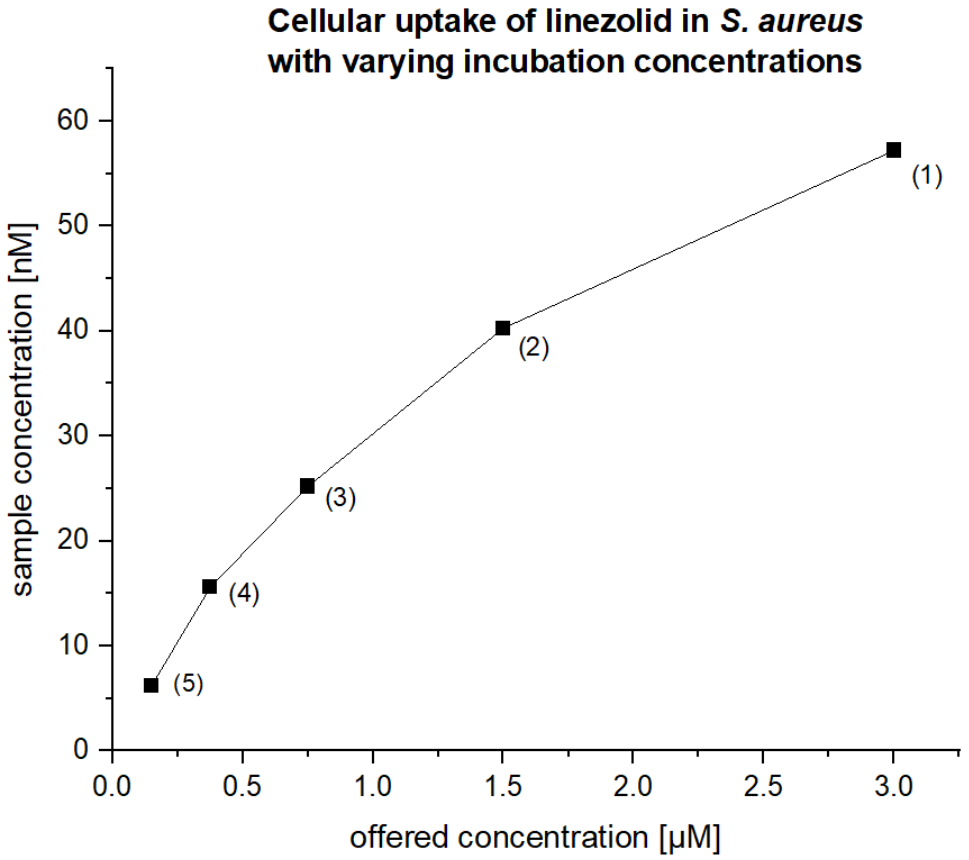

Figure 4.17: Cellular uptake of linezolid in S. aureus depicted as sample concentrations with 3 µM (1), 1.5 µM (2), 750 nM (3), 330 nM (4) and 150 nM (5) linezolid, plotted as a function of offered concentration.

Higher intracellular sample concentrations were obtained as result of increased offer, leading again to a hyperbolic curve (Figure 4.17). Linezolid was detected in the nanomolar region: Sample (5) led to a sample concentration in the single-digit nanomolar range (<10 nM), while

sample concentrations in the double-digit nanomolar region (15-60 nM) were obtained for all other samples (Figure 4.17). However, the results obtained for sample (1) containing the highest concentration in the assay should be evaluated with care (Figure 4.17). They differed notably most likely due to toxic effects of linezolid on the bacteria (also seen with direct comparison of R^2 with and without the corresponding data, not shown). The results of sample (2) were of special interest because the provided concentration of 1.5 µM was in the same magnitude of order as in previous experiments (1 µM). A sample concentration of ~ 40 nM was obtained for linezolid at 1.5 µM (Figure 4.17). This is in agreement to the previous results, thus confirming assay reproducibility. The incubation conditions for the accumulation assays with *S. aureus* were successfully examined and established.

4.1.1.2.4 Cellular uptake of compounds with activity against *S. aureus*

Cellular uptake of *O*-acylated muraymycin analogues **48** and **49** synthesized by Dr. M. Wirth[243] into *S. aureus* Newman was investigated. Their biological activities are summarized in Figure 4.18. Both analogues showed beneficial biological properties, in particular compound **49** with an antibacterial activity against *S. aureus* in the nanomolar region (Figure 4.18).

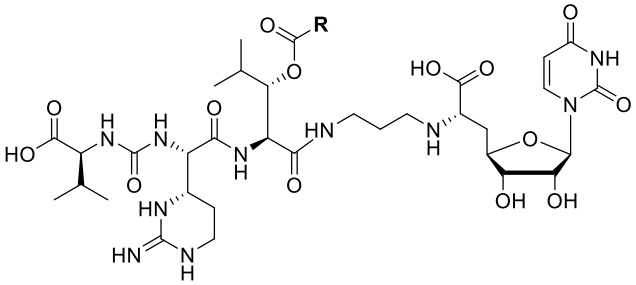

Compound	R	IC_{50} against MraY from *S. aureus* [nM]	MIC_{50} [µg/mL]
48	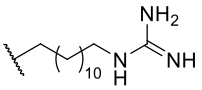	4.0 ± 0.7	*E. coli* DH5α n.a. *E. coli* Δ*tolC* <1 *P. aeruginosa* >100 *S. aureus* 11.4
49	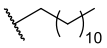	5.8 ± 0.5	*E. coli* DH5α n.a *E. coli* Δ*tolC* <1 *P. aeruginosa* - *S. aureus* 0.32*

*Figure 4.18: Biological activities of muraymycin analogues **48** and **49** by Dr. M. Wirth.[243] *Previous reported antibacterial activity, subsequent obtained data varied up to 50 µg/mL.*

Analytics of muraymycin analogues **48** and **49** showed solubility in a mixture of MeCN/H_2O (50/50). The addition of organic acid (1% HCOOH) is beneficial for both compounds. A detection limit of <5 nM was obtained for analogues **48** and **49**. Matrix effects were not observed.

A bacterial suspension (*S. aureus* Newman) was prepared as described above. Appropriate solutions of compounds **48** and **49** in M9 medium were prepared at a concentration of 2 µM according to their antibacterial activities (Figure 4.18) After incubation with bacterial suspension in a water bath at 37 °C for 30 minutes, mixtures were centrifuged and washed twice with M9 medium. Samples were stored at -20 °C overnight and lysostaphin-induced lysis (350 µg/mL) was performed in the next morning under established conditions. After centrifugation and protein precipitation with iced MeCN including HCOOH (1%)), samples were incubated on ice (5 minutes) and centrifuged. Samples were lyophilized to ensure valide quantification with regard to overall substance management. The resulting solids were redissolved in a mixture of MeCN/H_2O (50/50) with HCOOH (1%) included. The results of the MS measurements are presented as sample concentrations in Figure 4.19.

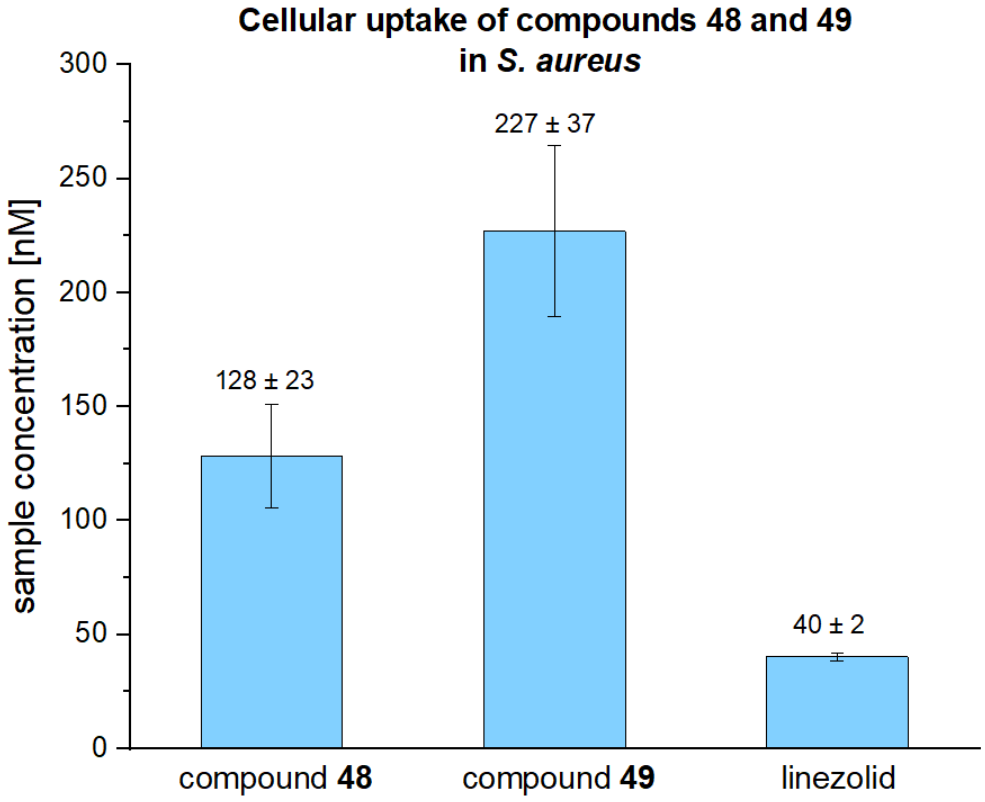

*Figure 4.19: Cellular uptake of compounds **48** and **49** in S. aureus Newman in comparison to cellular uptake of linezolid, depicted as sample concentrations.*

Analogue **48** was measured as a sample concentration of 128 ± 23 nM (Figure 4.19). Accumulation of compound **49** was higher by factor ~ 2 with a sample concentration of 227 ± 37 nM (Figure 4.19). The structurally similar compounds **48** and **49** vary in one functionality as part of a SAR study: Muraymycin analogue **49** has a terminally unbranched tridecanoyl unit and misses the polar guanidine moiety compared to analogue **48** (Figure 4.19). The fatty acid chain enhances the hydrophobicity in contrast to compound **48**. Because enhanced lipophilicity would lead to improved cellular uptake, a higher intracellular uptake of compound **49** would be expected. Adsorption to the membrane similar as suggested for the muraymycin conjugates

by Dr. C. Rohrbacher (cf. Chapter 4.1.1.1.2) is possible due to the structure of compounds **48** and **49**. Investigation of membrane fragments as done for the muraymycin conjugates (Chapter 4.1.1.1.2) can be applied in future experiments to explore this hypothesis. Further studies will be performed.

4.1.1.3 Calculation tool for cellular uptake assays

A calculation tool for the conversion of the sample obtained from the cellular uptake assays into intracompartmental concentrations will be presented in the following chapter. The conversion of the cellular uptake data utilizing Gram-negative *E. coli* will be discussed first (Chapter 4.1.1.3.1). Hereafter, sample concentrations of the cellular uptake assays with *S. aureus* will be equally converted according to the adapted assay procedure for this Gram-positive bacterium (Chapter 4.1.1.3.2). The converted sample concentrations are termed "biological concentration".

4.1.1.3.1 Gram-negative *E. coli*

The number of *E. coli* cells was calculated for each assay according to studies by Volkmer and Heinemann.[261] The authors demonstrated a correlation between the total cell volume in a sample and the OD_{600}.[261] They investigated cell parameters on different growth conditions and presented the following relation: 1 mL of *E. coli* in LB medium contains 7.8 x 10^8 cells at an OD_{600} ~ 1.[261] Based on this correlation, an initial equation (1) was set up to calculate the total number of cells. Day cultures were always prepared in 30 mL LB medium, thus providing the parameter *"V (bacterial suspension in mL)"* of equation (1). Bacterial growth of the day cultures resulted in the parameter *"specific OD_{600}"* of equation (1).

$$(1)\ Total\ number\ of\ cells = \frac{7.8\ x\ 10^8\ cells}{mL} \cdot\ specific\ OD_{600} \cdot V\ (bacterial\ suspension\ [mL])$$

$$[with\ OD_{600} = optical\ density\ at\ 600\ nm]$$

Following, bacteria were washed and resuspended in M9 medium until an OD_{600} of ~ 4 was reached. This procedure was implemented in a second equation (2) with the parameter "*V (ad)*". The incubation mixtures contained equal volumes (0.5 mL) of bacterial suspension and compound solution, thus resulting in the parameter „*V (inc)*" of equation (2):

$$(2)\ Number\ of\ cells\ in\ the\ assay = \frac{equation\ 1}{V\ (ad)} \cdot\ V\ (inc)$$

$$[with\ V\ (ad) =\ volume\ used\ to\ obtain\ an\ OD_{600} \sim 4\ for\ assay\ adjustment\ [mL],$$

$$V\ (inc) =\ incubation\ volume = 0.5\ mL]$$

Then, cell numbers were related to cell volumes followed by a recalculation to another unit (from µm³ to µL). The abstraction of a single *E. coli* cell to a cylinder which is flanked by two

hemispheres and further cell dimension calculations resulted in the differentiation into the subcellular compartments of *E. coli* cells.[135,262,263] This allowed calculations for *E. coli* cells as total cell unit (total volume) as well as calculations for the cytoplasmic and the periplasmic space after cold osmotic shock. Subcellular compartment volumes provided by Brönstrup et al.[135] were used for further calculations. They are presented in Table 4.2.

Table 4.2: Volumes of the subcellular compartments of E. coli cells.[135]

	Single *E. coli* cell (µm³)
Total volume	4.60
Volume of cytoplasm	4.08
Volume of periplasm	0.32

Calculated cell numbers were used to obtain subcellular compartment volumes for each assay individually based on the following conversions:

$$(3)\ Total\ volume\ [\mu L] = 4.6\ \mu m^3\ \cdot\ number\ of\ cells\ (equation\ (2))\ \cdot 10^{-9}$$

$$(4)\ Volume\ of\ cytoplasm\ [\mu L] = 4.08\ \mu m^3\ \cdot\ number\ of\ cells\ (equation\ (2))\ \cdot 10^{-9}$$

$$(5)\ Volume\ of\ periplasm\ [\mu L] = 0.32\ \mu m^3\ \cdot\ number\ of\ cells\ (equation\ (2))\ \cdot 10^{-9}$$

The volume for *E. coli* cells as whole unit ("whole cells") was calculated with equation (3). The cytoplasmic volume was calculated with equation (4) and equation (5) was used to calculate the volume for periplasm (final unit in µL).

A variance of 10-20% between cell numbers of different assays was decided on as tolerance for this work since systematic uncertainties were constant within the experiments and relative comparisons with the cellular uptake data were envisioned.

To calculate final intracompartmental biological concentrations for the accumulation assays, steps with volume changes, such as partially performed lyophilization (equation (6)) and protein precipitation with MeCN (equation (7), not applicable for periplasm) were considered:

$$(6)\ Factor\ by\ lyophilization = \frac{V\ (before\ lyophilization)\ [\mu L]}{V\ (after\ lyophilization)\ [\mu L]}$$

$$(7)\ Factor\ by\ protein\ precipitation = \frac{V\ (total)\ [\mu L]}{V\ (MeCN)\ [\mu L]} = 2$$

Lastly, the sample amounts were divided by the volume of each compartment (equations (3), (4) or (5)) to obtain biological concentrations ("calculated biological concentrations") using equation (8):

$$(8)\ Biological\ concentration\ [\mu M] = \frac{sample\ amount\ [pmol]}{total\ volume,\ cytoplasm\ or\ periplasm\ [\mu L]}$$

To rule out artifically induced high cell numbers in our assays, the following experiment was performed in addition to the data conversion of the obtained sample concentrations. Focus of this experiment was the relation of cell numbers in the linear range of OD_{600} ~ 0.2-1.2, i.e., the in particular investigation of proportionality due to the Lambert Beer Law. Bacterial suspensions of the cellular uptake assays were adjusted to an OD_{600} of ~ 4. This OD_{600} exceeds the linear OD_{600} area of ~ 0.2-1.2, so dilutions were measured. A bacterial suspension of *E. coli* was prepared as described in Chapter 4.1.1.1. However, the procedure will be described in detail because volumes and dilutions were focused on to evaluate the aforementioned concern. A day culture of *E. coli* (300 µL in 30 mL LB medium) was prepared from an appropriate overnight culture and was grown until an OD_{600} of ~ 0.6 was obtained. Bacteria were harvested and the resultant pellet was resuspended with M9 medium until an OD_{600} of ~ 4 was reached. Then, a serial dilution of this suspension was done to obtain a final solution with an OD_{600} <1 which was directly measured without further dilution. The number of cells was calculated for this sample. Based on this cell number, a calculation of cell numbers in the reverse way was performed for the other three samples considering the dilution steps.[261] The results of this experiment are depicted in Figure 4.20.

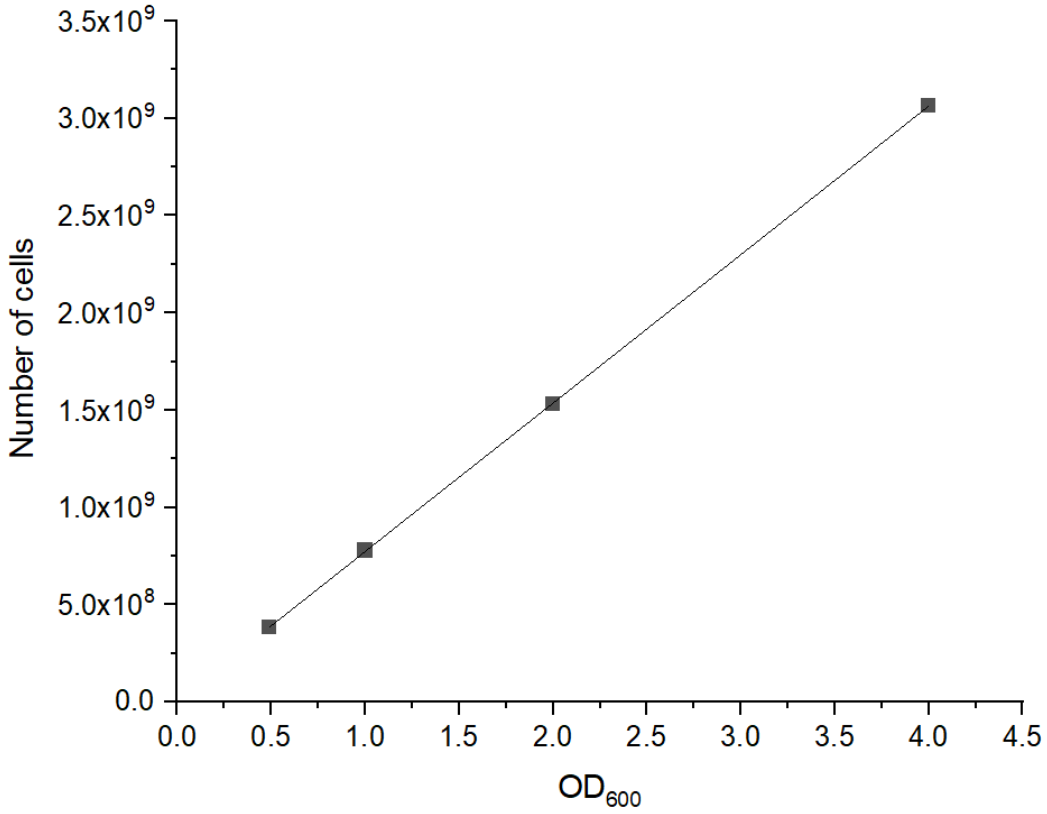

Figure 4.20: Calculation of the cell number (based on studies by Volkmer and Heinemann).

The calculation backwards yielded a proportionality between the OD_{600} and the cell number as demonstrated in Figure 4.20. Based on this experiment, a cell number of 1.53 x 10^9 cells was calculated for the bacterial suspension being used in our assays. This value was compared to the number of cells that was calculated according to the described steps above. The values are in good agreement, so that initial concerns in terms of falsified cell numbers could be ruled out. Data plausibility was confirmed.

Following, the calculated biological concentrations of the cellular uptake assays of this work are presented. Compounds which have been investigated in the same assay (same number of cells due to same bacterial suspension being used) will be reported together. A calculation of the cellular uptake data for the muraymycin lysine reference **33** and both POM prodrugs **34** and **35** obtained by J. Meiers[134] completes this chapter. Cell numbers of assays performed in this work were partially adopted for the revision of cellular uptake data by J. Meiers since no further information were available. This applied to ciprofloxacin, compound **33** and POM prodrugs **34** and **35** (the last two compounds were not examined in this dissertation). For calculations of these compounds, the cell number of the corresponding assay with lysine reference **33** was used since they represent one series of compounds with compound **33** serving as parent drug of the POM prodrugs **34** and **35.** The adoption of cell numbers is tolerable because we decided on a variance of 10-20% for bacterial cell numbers of different assays.

First, ciprofloxacin sample concentrations in *E. coli* Δ*tolC* were converted. The calculated biological concentrations of ciprofloxacin obtained in this work and by J. Meiers[134] are presented in Table 4.3. Cell number was determined with 1.55 x 10^9 cells (Table 4.3) that corresponds to ~ 7 µL total volume, ~ 6 µL cytoplasm and ~ 0.5 µL periplasm in relation to the cell volume. The sample concentration of ~ 20 nM for ciprofloxacin in whole *E. coli* lysate corresponds to a biological concentration of ~ 5 µM under consideration of 1.55 x 10^9 cells (Table 4.3). For cytoplasm, a lower biological concentration was obtained with ~ 2 µM, while calculations for periplasmic space resulted in ~ 23 µM ciprofloxacin (Table 4.3). Sample concentrations obtained by J. Meiers[134] were in the same range, therefore calculations yielded comparable results: biological concentrations of ~ 7 µM for whole cell lysate, ~ 3 µM for cytoplasm and ~ 30 µM for periplasm were obtained (Table 4.3). The volume of periplasm is described to be smaller by factor ~ 13 relative to cytoplasm (Table 4.2),[264] which explains the significantly higher compartmentable concentrations in periplasm obtained from sample concentrations in a similar range.

Table 4.3: Cellular uptake data of ciprofloxacin in E. coli ΔtolC obtained in this work (non-italics) and by J. Meiers (italics, no further information as listed available),[134] presented as mean sample concentrations and calculated biological concentrations under consideration of the cell number.

	Ciprofloxacin obtained in this work *obtained by J. Meiers*[134]		
	Cell volume (µL) per 1.55 x 10^9 cells	**Sample concentration (nM)**	**Calculated biological concentration (µM)**
total volume	7.1	19 ± 3 *26*	5.4 ± 0.8 *7.3*
volume cytoplasm	6.3	5.2 ± 0.7 *9.1*	1.6 ± 0.1 *2.9*
volume periplasm	0.5	11 ± 1 *16*	23 ± 1 *31*

The calculation results of the cellular uptake assays of muraymycin analogue **37** with activity against *P. aeruginosa* are depicted in Table 4.4 and yielded a cell number of 1.57 x 10^9 cells. This cell number corresponds to ~ 7 µL whole lysate, ~ 6 µL cytoplasm and ~ 0.5 µL periplasm related to the cell volume (Table 4.4). Considering 1.57 x 10^9 cells, the sample concentration of ~ 90 nM obtained for analogue **37** in whole *E. coli* lysate corresponds to a biological concentration of ~ 1.5 µM (Table 4.4). The biological concentration for cytoplasmic space was determined in the same micromolar range, whereas a higher biological concentration (by a factor of ~ 2.5) was obtained for periplasm due to its smaller volume (Table 4.4).

*Table 4.4: Cellular uptake data of compound **37** in E. coli ΔtolC presented as mean sample concentrations and calculated biological concentrations under consideration of the cell number.*

	Compound 37		
	Cell volume (µL) per 1.57 x 10^9 cells	**Sample concentration (nM)**	**Calculated biological concentration (µM)**
total volume	7.2	90 ± 24	1.5 ± 0.4
volume cytoplasm	6.4	83 ± 8	1.6 ± 0.3
volume periplasm	0.5	30 ± 3	3.6 ± 0.3

The calculation results of the cellular uptake assays with the literature-known reference **38** are presented in Table 4.5. The cell number was calculated as 1.66 x 10^9 cells (Table 4.5). Based on this cell number, the calculation of the sample concentrations for the whole *E. coli* cell lysate with ~ 114 nM and for cytoplasm with ~ 109 nM resulted in equal biological concentrations of ~ 2 µM (Table 4.5). A higher biological concentration with ~ 8 µM was calculated for the periplasmic space (Table 4.5). The effects of the smaller volume of the periplasm space compared to the cytoplasm were noticeably observable as for compound **37** (Table 4.4). The 2-fold higher accumulation of compound **38** in periplasm (Table 4.5) relative to compound **37**

(Table 4.4) described the most pronounced difference between both compounds in terms of cellular uptake.

*Table 4.5: Cellular uptake data of compound **38** in E. coli ΔtolC presented as mean sample concentrations and calculated biological concentrations under consideration of the cell number.*

Compound 38			
	Cell volume (µL) per 1.66 x 10^9 cells	**Sample concentration (nM)**	**Calculated biological concentration (µM)**
total volume	7.6	114 ± 3	1.8 ± 0.1
volume cytoplasm	6.8	109 ± 9	1.9 ± 0.2
volume periplasm	0.5	67 ± 10	7.6 ± 1.1

Cellular uptake assays performed with the muraymycin GuCOSS conjugate **39** contained 1.55 x 10^9 cells which corresponds to ~ 7 µL whole lysate (Table 4.6). The modified assay yielded a biological concentration of ~ 7 µM (sample concentration ~ 23 nM) of released lysine reference **33** for the pellet (Table 4.6). The corresponding supernatant showed a significantly higher biological concentration in the double-digit micromolar region with ~ 23 µM (Table 4.6).

*Table 4.6: Cellular uptake data of compound **39** in E. coli ΔtolC presented as mean sample concentrations and calculated biological concentrations under consideration of the cell number.*

Compound 39			
	Cell volume (µL) per 1.55 x 10^9 cells	**Sample concentration (nM)**	**Calculated biological concentration (µM)**
Pellet	7.2	23 ± 1	6.5 ± 0.2
Supernatant		82 ± 9	23 ± 3

The calculation results of the cellular uptake assays with CPP muraymycin conjugate **40** are presented in Table 4.7. A cell number of 1.71 x 10^9 cells (corresponds to ~ 8 µL whole lysate) was determined for this assay (Table 4.7). A biological concentration of ~ 6 µM was determined for the pellet after separation of the soluble and insoluble bacterial components (Table 4.7). The sample concentration of ~ 38 nM for the supernatant resulted in a biological concentration of ~ 10 µM (Table 4.7).

*Table 4.7: Cellular uptake data of compound **40** into E. coli ΔtolC presented as mean sample concentrations and calculated biological concentrations under consideration of the cell number.*

Compound 40			
	Cell volume (µL) per 1.71 x 10^9 cells	**Sample concentration (nM)**	**Calculated biological concentration (µM)**
Pellet	7.9	25 ± 7	6.3 ± 1.7
Supernatant		38 ± 5	9.7 ± 1.3

The calculation results of the cellular uptake assays with muraymycin lysine reference **33** are presented in Table 4.8. A cell number of 1.61 x 10^9 cells (corresponds ~ 7 µL for the whole lysate, ~ 7 µL cytoplasm and ~ 0.5 µL periplasm) was determined for this assay (Table 4.8). This yielded a biological concentration of ~ 700 nM corresponding to a sample concentration of ~ 50 nM for whole *E. coli* lysate (Table 4.8).

*Table 4.8: Cellular uptake data of compound **33** in E. coli ΔtolC, presented as mean sample concentrations and calculated biological concentrations under consideration of the cell number.*

Compound 33			
	Cell volume (µL) per 1.61 x 10^9 cells	**Sample concentration (nM)**	**Calculated biological concentration (µM)**
total volume	7.4	47 ± 15	0.7 ± 0.3

The calculation results of the cellular uptake assays with non-nucleoside compounds **41** and **42** are depicted in Table 4.9. A cell number of 1.63 x 10^9 cells was calculated that corresponds to ~ 8 µL whole lysate, ~ 7 µL cytoplasm and ~ 0.5 µL periplasm in relation to the cell volume (Table 4.9). A biological concentration of ~ 4 µM was calculated for compound **41** in whole *E. coli* lysate (Table 4.9). Compound **42** resulted in a biological concentration of ~ 2 µM in whole *E. coli* lysate (Table 4.9). The sample concentrations of ~ 162 nM for compound **41** and ~ 79 nM for compound **42** in cytoplasmic space correspond to biological concentrations in the range of ~ 1.5-3 µM (Table 4.9). Biological concentrations of ~ 6 µM for compound **41** and ~ 1 µM for compound **42** in periplasm depicted the most pronounced difference between the compounds which has already been discussed in Chapter 4.1.1.1.3.

*Table 4.9: Cellular uptake data of compounds **41** (non-italics) and **42** (italics) in E. coli ΔtolC presented as mean sample concentrations and calculated biological concentrations under consideration of the cell number.*

Compound 41 ***Compound 42***			
	Cell volume (µL) per 1.63 x 10^9 cells	**Sample concentration (nM)**	**Calculated biological concentration (µM)**
total volume	7.5	271 ± 97 *147 ± 25*	4.3 ± 1.5 *2.4 ± 0.4*
volume cytoplasm	6.7	162 ± 51 *79 ± 21*	2.9 ± 0.9 *1.4 ± 0.4*
volume periplasm	0.5	54 ± 4 *12 ± 2*	6.2 ± 0.5 *1.4 ± 0.3*

Cellular uptake assays performed with MurA pyrazolidinone analogues **43** and **45** contained 1.62 x 10^9 cells that correspond to ~ 7 µL for the whole cells in relation to the *E. coli* cell volume (Table 4.10). Compound **43** revealed a sample concentration of ~ 573 nM in whole *E. coli* cell lysate which was converted into a biological concentration of ~ 19 µM considering the number

of cells (Table 4.10). Lower accumulation data were obtained for analogue **45** with a biological concentration of ~ 11 µM (sample concentration of ~ 348 nM) relative to the number of cells number (Table 4.10).

*Table 4.10: Cellular uptake data of compounds **43** (non-italics) and **45** (italics) in E. coli ΔtolC presented as mean sample concentrations and calculated biological concentrations under consideration of the cell number.*

Compound 43 ***Compound 45***			
	Cell volume (µL) per 1.62 x 10^9 cells	**Sample concentration (nM)**	**Calculated biological concentration (µM)**
total volume	7.4	573 ± 123 *348 ± 46*	19 ± 4 *11 ± 2*

The calculation results of the assays with further MurA pyrazolidinone analogues **44**, **46** and **47** are depicted in Table 4.11. A cell number of 1.60 x 10^9 cells (corresponds to ~ 7 µL whole lysate) was determined for these assays (Table 4.11). Based on this cell number, the sample concentrations of ~ 56 nM for compound **44**, ~ 924 nM for compound **46** and ~ 3 µM for compound **47** in whole *E. coli* cell lysate resulted in biological concentrations of ~ 2 µM for compound **44**, ~ 30 µM for compound **46** and ~ 84 µM for compound **47** (Table 4.11).

*Table 4.11: Cellular uptake data of compounds **44** (non-italics), **46** (italics) and **46** (italics*) in E. coli ΔtolC presented as mean sample concentrations and calculated biological concentrations under consideration of the cell number.*

Compound 44 ***Compound 46*** ***Compound 47****			
	Cell volume (µL) per 1.60 x 10^9 cells	**Sample concentration (nM)**	**Calculated biological concentration (µM)**
total volume	7.4	56 ± 13 *924 ± 152* *2563 ± 606**	1.8 ± 0.4 *30 ± 5* *84 ± 20**

A calculation of the cellular uptake data obtained by J. Meiers[134] for the lysine reference **33**, bis-POM-prodrug **34** and mono-POM prodrug **35** was performed. The calculation results are presented in Table 4.12. A cell number of 1.61 x 10^9 cells (corresponds to ~ 7 µL whole lysate, ~ 7 µL cytoplasm and ~ 0.5 µL periplasm) was determined in this work (Table 4.12). This yielded a biological concentration of ~ 1 µM for compound **33** in whole *E. coli* lysate corresponding to a sample concentration of ~ 60 nM for (Table 4.12). Compound **33** was not detectable in cytoplasm and the obtained sample concentration of ~ 14 nM in periplasm corresponds to a biological concentration of ~ 2 µM (Table 4.12). Periplasmic accumulation of muraymycin lysine reference **33** was demonstrated. The intracellularly released parent drug **33** was detected in sample concentrations of ~ 204 nM for compound **34** and ~ 99 nM for

analogue **35** in whole *E. coli* cell lysate, thus resulting in biological concentrations of ~3 µM for bis-POM prodrug **34** and ~ 2 µM for mono-POM prodrug **35** (Table 4.12). The sample concentration of ~ 127 nM for compound **34** and ~ 2 nM for prodrug **35** in cytoplasm correspond to biological concentrations of ~ 2 µM for bis-POM prodrug **34** and ~ 1 µM for mono-POM prodrug **35** (Table 4.12). Compound **34** accumulated to a greater extent in periplasm than in as demonstrated with a biological concentration of ~ 11 µM. The same trend was observed for compound **35** with biological concentrations of ~ 1 µM in cytoplasm and ~ 4 µM in periplasm, thereby representing the most pronounced difference compared to bis-POM prodrug **34** (Table 4.12). The concept of the prodrug strategy was confirmed with this data as demonstrated by direct comparison with the cellular uptake data of compound **33**: the biological concentrations in the low single-digit micromolar region in whole cell lysate and periplasm were significantly lower (Table 4.12).

*Table 4.12: Cellular uptake data of compounds **33** (non-italics), **34** (italics) and **35** (italics*) in E. coli ΔtolC obtained by J. Meiers,[134] presented as mean sample concen-trations and calculated biological concentrations under consideration of the cell number. "n.d." = not detectable.*

Compound 33 ***Compound 34*** ***Compound 35****			
	Cell volume (µL) per 1.61 x 10^9 cells	**Sample concentration (nM)**	**Calculated biological concentration (µM)**
total volume	7.4	64 ± 19 *204 ± 8* *99 ± 1**	1.0 ± 0.3 *3.3 ± 0.1* *1.6 ± 0.2**
volume cytoplasm	6.6	n.d. *127 ± 18* *2.1 ± 1.1**	- *2.3 ± 0.3* *1.0 ± 0.1**
volume periplasm	0.5	14 ± 1 *96 ± 9* *32 ± 10**	1.6 ± 0.1 *11 ± 1* *3.7 ± 1.1**

4.1.1.3.2 Gram-positive *S. aureus*

The number of *S. aureus* cells was calculated based on studies by Hasanah et al.[265] As performed by Volkmer and Heinemann for *E. coli* cells,[261] the authors provided a correlation between the growth behavior of *S. aureus*, i.e., cell number, and the OD_{600}. This relation is presented in Figure 4.21.[265]

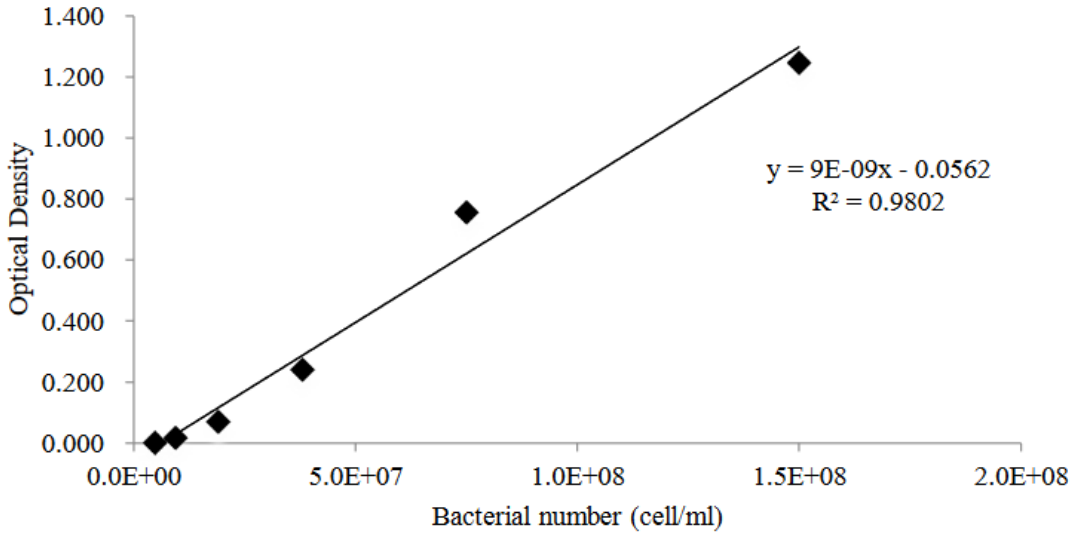

Figure 4.21: Correlation of cell number and OD_{600} of S. aureus (taken from U. Hasanah et al., IOP Conf. Ser.: Earth Environ. Sci. ***2008****, 187).*[265]

The following equation (9) provided by Hasanah et al. was used as a basis for the calculation of *S. aureus* cell numbers in this work:[265]

$$(9)\ y = 9\,x\,10^{-9} - 0.0562$$

The conversion to parameter "x" that corresponds to the number of *S. aureus* cells yielded equation (10). Parameter "y" represents the specific OD_{600} that resulted from bacterial growth of the day cultures of *S. aureus*:

$$(10)\ x = \frac{y + 0.0562}{9\,x\,10^{-9}}$$

$$[with\ y = OD_{600} = optical\ density\ at\ 600\ nm]$$

Equation (11) was set up to calculate the total number of cells. Day cultures of *S. aureus* were prepared in a total volume of 30 mL Müller Hinton medium, thus providing the parameter *"V (bacterial suspension [mL])*".

$$(11)\ Total\ number\ of\ cells = x \cdot V\ (bacterial\ suspension\ [mL])$$

Bacteria were washed and resuspended in M9 medium until an OD_{600} of ~ 4 was reached, thus yielding the parameter "*V (ad)*" of subsequent equation (12). The incubation mixtures were

prepared with equal volumes (0.5 mL) of bacterial suspension and compound solution, thus resulting in the parameter „*V (inc)*“ of equation (12):

$$(12)\ Number\ of\ cells\ in\ the\ assay = \frac{equation\ 11}{V\ (ad)} \cdot V\ (inc)$$

$$[with\ V\ (ad) =\ volume\ used\ to\ obtain\ an\ OD_{600} \sim 4\ \ for\ assay\ adjustment\ [mL],$$

$$V(inc) =\ incubation\ volume = 0.5\ mL]$$

In accordance to the accumulation assays for *E. coli* (Chapter 4.1.1.3.1), a variance of 10-20% for bacterial cell numbers of different assays with *S. aureus* was decided on as tolerance. Steps including volume changes, such as lyophilization (equation (13)) and protein precipitation with MeCN (equation (14)), were adressed in the calculations:

$$(13)\ Factor\ by\ lyophilization = \frac{V\ (before\ lyophilization)\ [\mu L]}{V\ (after\ lyophilization)\ [\mu L]}$$

$$(14)\ Factor\ by\ protein\ precipitation = \frac{V\ (total)\ [\mu L]}{V\ (MeCN)\ [\mu L]} = 2$$

Following, linezolid sample concentrations of the incubation studies (Chapter 4.1.1.2.3) were converted. The calculated biological concentrations of linezolid are depicted in Table 4.13. The obtained sample concentrations were observed in a range of 30-45 nM, thus corresponding to biological concentrations between 10-20 µM (Table 4.13).

Table 4.13: Cellular uptake data of linezolid in S. aureus, presented as mean sample concentrations and calculated biological concentrations under consideration of the cell number.

Linezolid		
Incubation time (min)	**Sample concentration (nM)**	**Calculated biological concentration (µM)**
5	28 ± 1	10 ± 1
10	31 ± 1	12 ± 1
20	39 ± 3	15 ± 1
30	40 ± 2	15 ± 1
45	45 ± 1	17 ± 1
60	44 ± 1	17 ± 1

Preliminary cellular uptake results obtained for the muraymycin analogues **48** and **49** were not converted because the assays need to be repeated (Chapter 4.1.1.2.4).

4.1.2 MraY-related projects

The following chapter presents the results of all projects related to MraY. The results of the MraY inhibition assays[84,96,97,99,244] performed in this dissertation will be discussed in detail for drug candidates provided by the research groups of Dr. S. Roy, Prof. Dr. M. Kaiser, Prof. Dr. S. Van Lanen and Prof. Dr. R. Müller (Chapter 4.1.2.1). The IC_{50} determination of muraymycin analogues synthesized in our research group, which was routinely done as part of this dissertation, will not be presented specifically here. The provided inhibitory activities of the compounds are or will be included in the works of Dr. G. Niro,[239] S. Rosinus,[266] A. Heib,[267] N. Stadler,[268] Dr. C. Rohrbacher[240] and S. Lauterbach (unpublished). Studies with MraY in different environments such as crude membrane preparations, in micelles and in nanodiscs will be discussed with focus on the latter (Chapter 4.1.2.2). The development of an appropriate assay for the quantification of MraY in different protein preparations will be presented hereafter (Chapter 4.1.2.3). Studies concerning MurX (Chapter 4.1.2.4), the theory of self-resistance of *Streptomyces* species against muraymycins (Chapter 4.1.2.5) and the interaction between MraY and MurF (Chapter 4.1.2.6) will complete this section.

4.1.2.1 MraY inhibition assays

Virtual screening hits of non-nucleoside chemotherapeutics with antibacterial activity against *M. tuberculosis* and other antibiotic-resistant bacteria provided by the research group of Dr. S. Roy were investigated in the *in vitro* MraY assays (established in our research group, Chapter 7.1.2.3). This structure-based drug design approach contains compounds that are characterized by their small size, mostly nitrogen-containing heterocycles and partially nucleoside-derived units. Compound structures cannot be presented due to confidentiality. The MraY inhibition assays using MraY from *S. aureus* (overexpressed in *E. coli*) as crude membrane preparations were performed under established conditions.[84,96,97,99,244] The percentage of inhibition of the compounds was calculated instead of IC_{50} determination. The following screening method was applied for these studies: an initial screening was performed with all compounds at a concentration of 100 µM. Depending on their inhibitory activity, they were divided into different groups as follows:

1) Group 1: compounds with inhibitory activity against MraY > 10%
2) Group 2: compounds with inhibitory activity against MraY between 7-10%
3) Group 3: compounds with inhibitory activity against MraY < 7%

Compounds of groups 1 and 2 were used in a next screening round with a concentration of 250 µM. Selected compounds with high structural similarity to naturally occurring muraymycins were further investigated at a concentration of 1 mM. An IC_{50} determination for selected compounds was done if requested by our collaborators, whereby compound solubility as well

as the compound's own fluorescence partially influenced the experiments (cf. later in this chapter). Prior to screening, assay consistency was demonstrated with commercially available tunicamycin as a positive control and two negative controls: One excluded MraY, the other one contained dimethyl sulfoxide (DMSO) to account for solvent effects. Tunicamycin showed an inhibitory activity against MraY in the low nanomolar range (IC_{50} = 19 ± 2 nM) that was in agreement with the IC_{50} ~ 16 nM measured by S. Koppermann.[84] The absence of enzyme resulted in a baseline, while a hyperbolic curve was obtained for the DMSO-containing mixture. The screening results are summarized in Table 4.14.

*Table 4.14: MraY inhibition screening results for non-nucleoside compounds as percentage of inhibition provided by the research group of Dr. S. Roy."-" Compounds were not investigated at this concentration. [1]No inhibition at a concentration of 100 µM. [2]IC_{50}-determination of compounds written in **bold** was not possible. [3]Several replications. [4]No evaluation possible. Compounds with high similarity to naturally occurring muraymycins are written in blue.*

Compound	MraY inhibition [%]		
	@100 µM	@250 µM	@1 mM
TB-VS0002	10	14	-
TB-VS0003	[1]	-	-
TB-VS0004	13	14	-
TB-VS0005	[1]	-	-
TB-VS0006	**10**	**33[2]**	-
TB-VS0007	<5	-	-
TB-VS0008	**8**	**20[2]**	-
TB-VS0010	[1]	-	-
TB-VS0011	<5	-	-
TB-VS0012	[1]	-	-
TB-VS0013	<5	-	-
TB-VS0014	[1]	-	-
TB-VS0015	9	13	-
TB-VS0016	**8**	**24[2]**	-
TB-SB0432	<5	-	9
TB-SB0403	[1]	-	-
TB-SB0421	[1]	-	-
TB-SB0417	<5	-	-
TB-SB0417	[1]	-	-
TB-SB0425	9	17	-
TB-SB0419	**18**	**30[2]**	-
TB-SB0438	[1]	-	-
TB-VS12-4	[1]	-	-
TB-VS12-7	[1]	-	-
TB-VS12-9	[1]	-	-
TB-VS12-14	[1]	-	-

Compound	MraY inhibition [%]		
	@100 µM	@250 µM	@1 mM
TB-VS12-15	**17**	**62[2]**	-
TB-VS12-16	7	-	-
TB-VS0012	6	-	-
TB-VS12-2	[1]	-	-
TB-VS12-3	8	13	-
TB-VS12-5	<5	-	-
TB-VS12-6	11	13	-
TB-VS12-8	<5	-	-
TB-VS12-10	**12**	**31[2]**	-
TB-VS12-11	[1]	-	-
TB-VS12-12	<5	-	-
TB-VS12-13	<5	-	-
TB-SB0440	[1]	-	57
TB-SB0441	**10**	**27[2]**	36
TB-SB0439	6	-	-
TB-VS12-17	[1]		-
TB-VS12-18	**6 – 20[3]**	**28[2]**	compound precipitated
TB-VS12-19	[1]		-
TB-VS12-20	4 – 10[3]	17	-
TB-VS12-21	**11**	**32[2]**	-
TB-VS12-22	2 – 17[3]	14	-
TB-VS12-23	[1]		-
TB-VS12-24	**7**	**34[2]**	-
TB-VS12-25	<5		-
TB-VS12-26	[1]	-	-
TB-VS12-27	[1]	-	-
TB-VS12-28	[1]	-	-
TB-VSII-2	[1]	-	-
TB-VSII-3	**18**	**36[2]**	-
TB-VSII-5	[1]	-	-
TB-VSII-6	[1]	-	-
TB-VSII-7	[1]	-	-
TB-ROY-NA2	6	-	38
TB-ROY-NA1	6	-	-[4]
TB-VS12-32	[1]	-	-
74	49	82	-
TB-VS12-34	33	49	-
TB-VS12-35	[1]	-	-
TB-VSII-1 (THF)	**17**	**60[2]**	-
TB-VSII-4 (THF)	**<10[3]**	**27[2]**	-

An IC_{50} determination of compounds **74**, TB-VS12-34, TB-VSII-1 and TB-VSII-4 was performed. Compound **74** and TB-VS12 34 showed an inhibitory activity against MraY in the triple-digit micromolar region: IC_{50} (**74**) = 136 ± 40 µM, IC_{50} (TB-VS12-34) = 171 ± 36 µM. The IC_{50} determination for compounds TB-VSII-1 and TB-VSII-4 turned out to be non-trivial. Both were almost insoluble in DMSO and were therefore dissolved in tetrahydrofuran (THF). Influences on enzyme activity due to this solvent change were ruled out before. Nevertheless, an IC_{50} determination of compounds TB-VSII-1 and TB-VSII-4 was not possible most likely due to their high fluorescence. The same applied for compound TB-VSII-3 (dissolved in DMSO). Overall, the obtained MraY inhibition screening results seemed positive: 15 out of 65 non-nucleoside compounds resulted in inhibitory activities in the double-figures percentage range at a concentration of 250 µM (Table 4.14). The screening hits of our collaborators could indeed result in a novel SAR study for potential drug candidates with inhibitory activity against MraY.

The research group of Prof. Dr. M. Kaiser provided callyaerin B which was examined in our MraY inhibition assay. Callyaerins represent naturally occurring cyclic peptides from *Callyspongia aerizusa*, the Indonesian marine sponge.[269] Callyaerin B is of special interest with its inhibitory activity against *M. tuberculosis* in the low micromolar region.[269] It is depicted in Figure 4.22.

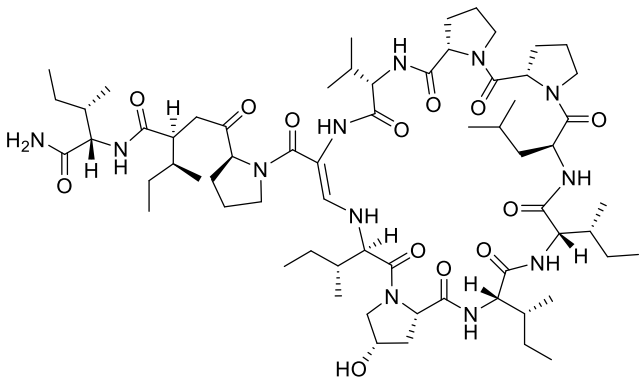

callyaerin B

Figure 4.22: Callyaerin B with antitubercular activity in the low micromolar range.[269]

The MraY inhibition assays using MraY from *S. aureus* (overexpressed in *E. coli*) as crude membrane preparations were performed under usual conditions. A screening was envisioned using callyaerin B at a concentration of 100 µM. No inhibitory activity against MraY was observed at this concentration. Additional investigations were not performed.

Further MraY assays were performed with a novel capuramycin from a bacterial strain isolated from a unique ecological niche provided by the research group of Prof. Dr. S. Van Lanen. Our standard procedure using MraY from *S. aureus* (overexpressed in *E. coli*) as crude membrane preparations was applied. In contrast to previous screening approaches, an IC_{50} determination was directly envisioned here since capuramycins are known as potent MraY inhibitors.[270,271]

Capuramycins A and F were used as controls in first experiments since this family of compounds has not been examined in our laboratory before. Both were provided by our collaborators and are depicted in Figure 4.23. The newly discovered compound cannot be presented in this dissertation for confidentiality reasons.

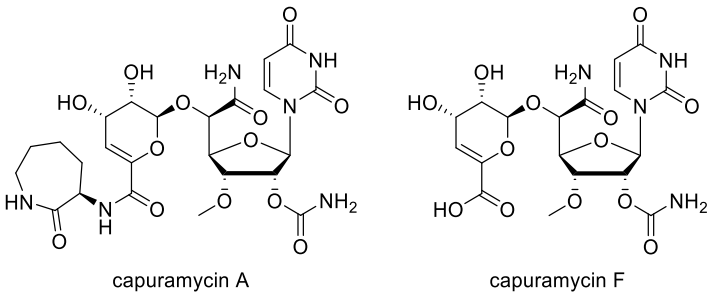

Figure 4.23: Capuramycins A and F.[271]

The inhibitory activity of capuramycin A against MraY was determined in the low nanomolar range (IC_{50} = 87 ± 15 nM). In contrast, capuramycin F showed significantly less inhibitory activity against MraY (IC_{50} = 1.7 ± 0.6 µM). These data seem to be in reasonable agreement with the literature (IC_{50} (capuramycin A) = 24 nM, IC_{50} (capuramycin F) = 17.9 µM) as MraY from *E. coli* has been used in this reference.[270,271] The discovered capuramycin was the most active one in the series with an IC_{50} = 13 ± 3 nM, thus identifying this novel compound as a promising lead structure for future optimization in medicinal chemistry. Within their studies, our collaborators identified a phosphotransferase that covalently modified the 3''-hydroxy unit of the sugar of the novel capuramycin. Enzymatic transformation resulted in the phosphorylated version of the novel capuramycin which was investigated in further assays. It showed significantly reduced inhibitory activity against MraY with an IC_{50} = 789 ± 124 nM relative to the unphosphorylated form (IC_{50} = 13 ± 3 nM). The expected reduced inhibitory activity against MraY as a result of phosphorylation was confirmed with these assays.

Further assays were performed with an extract that was provided by the research group of Prof. Dr. R. Müller. Within their studies, they obtained a myxobacterium which is hypothesized to produce muraymycins as indicated by HRMS. However, overall mass data did not allow any evaluations with regard to muraymycin group affiliation. Compounds of the extract could either belong to the heavier muraymycins of series A- or B or to the C- or D-series without the fatty acyl unit. An initial screening of this extract in our assay was performed since any muraymycin would display rather strong inhibitory properties towards MraY. A concentration of 500 µM (referred to a mean molecular weight of muraymycins B1, B3 and B4 due to our collaborators) was used. No inhibitory activity against MraY could be observed. The absence of inhibitory activity was in agreement with HRMS analysis of muraymycin B6 that was performed parallel at the research group of Prof. Dr. R. Müller. The fragmentation pattern of muraymycin B6 and the selected compounds in the collaborator‘s extract did not show any similarities. The overall

results led to the conclusion that none of the compounds in the extract belong to the family of muraymycins. No further investigations were performed.

4.1.2.2 Preparation of MraY in different systems

MraY was prepared as overexpressed protein in crude membrane preparation, as purified protein in detergent micelles and in nanodiscs. Plasmid transformation into competent *E. coli* Lemo21(DE3) cells and subsequent expression of $MraY_{SA}$ as crude membrane preparation was standardly performed as part of this dissertation based on our established protocol.[98] The integration of MraY into phospholipid nanodiscs depicts a central project of this work and will be focused on. Protein expressions of MSP1E3D1 and $MraY_{AA}$ (purified in detergent micelles) for the nanodisc assembly were performed according to the literature.[89,91,109]

The obtained fractions of the MSP1E3D1 expression[109] were analyzed by SDS-PAGE after dialysis overnight. SDS-PAGE analysis is depicted in Figure 4.24. One sample represents the so-called “inclusion bodies“ that are vesicles formed by the bacteria which coat the desired protein.[272] For releasing the target protein from the insoluble inclusion bodies, a denaturation is required as described in the literature.[109,272] This can be done with guanidine hydrochloride (GuHCl) that induces a refolding of MSP from its denatured state.[109] Coated MSP will be released in its native biologically active form.[272] Selective extraction of the desired protein is basically also feasible with urea, but higher concentrations are required for the same effect.[272] The use of GuHCl is therefore more convenient. To cleave off His-tags, Hagn et al. recommend a treatment with tabacco etch virus (TEV) protease after Ni-NTA purification.[109] However, this was not required for these studies because MraY did not contain a His-tag anymore.[109]

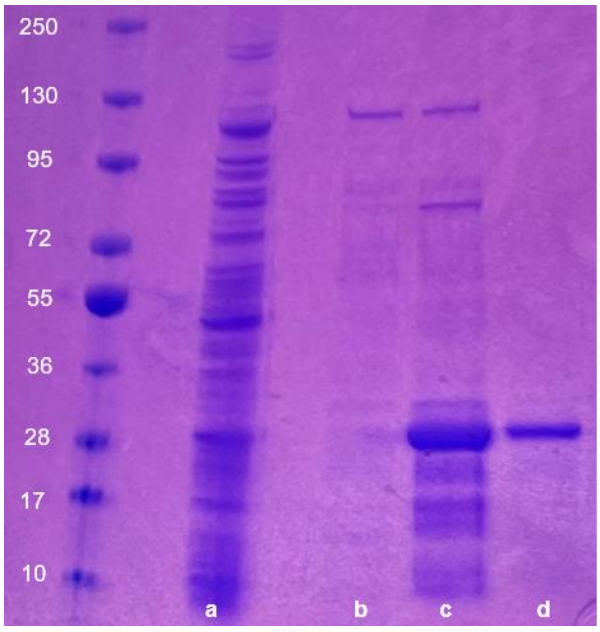

Figure 4.24: SDS-PAGE analysis of fractions obtained during MSP1E3D1 purification with samples of flow through (a), wash step after imidazol treatment (b) eluted protein (c) and inclusion bodies (d).

Samples (c) and (d) exhibited bands at the corresponding protein level of MSP (His-tag included) with a size of ~ 32 kDa (Figure 4.24). The band observed in sample (c) appeared more intense in relation to the band in sample (e). This makes sense because sample (d) is the sample of inclusion bodies. Intensive greasing was observed for the flow through-containing sample (Figure 4.24, b) which was significantly reduced after washing with imidazole (Figure 4.24, c). The success of MSP1E3D1 expression was confirmed.

The obtained fractions of the $MraY_{AA}$ expression[89,91] were analyzed by SDS-PAGE which is depicted in Figure 4.25. A protein band at a size between 40-55 kDa appeared in all fractions of gel 1 (Figure 4.25, green box) with reduced band intensity from samples (a1)-(i1). This was is good agreement to peak intensity of the SEC. A size of ~ 42 kDa corresponds to the decahistidine maltose-binding protein (MBP) tag and confirmed the success of $MraY_{AA}$ expression and purification. All fractions on gel 2 gel showed additional protein bands with sizes between 55-70 kDa, although they did not appear intensive (Figure 4.25, red box).

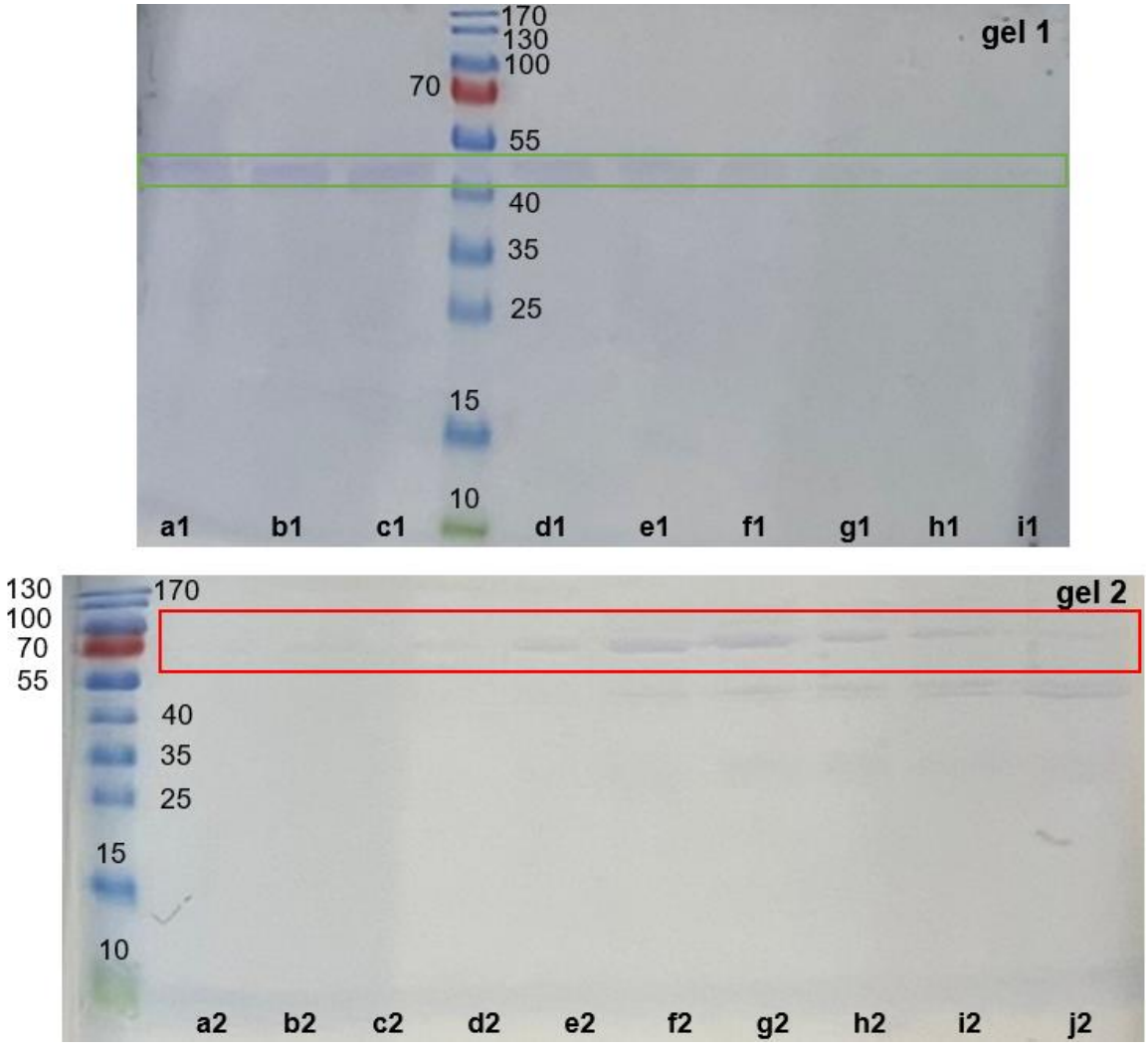

Figure 4.25: SDS-PAGE analysis of fractions obtained after SEC of $MraY_{AA}$ expression and purification with gel 1 (fractions (a1)-(c1), the protein ladder and fractions (d1)-(i1)) above and gel 2 (protein ladder and fractions (a2)-(j2)) below.

Nanodisc formation itself will be discussed in detail in the following. The $MraY_{AA}$-nanodisc assembly was performed with purified $MraY_{AA}$ and MSP1E3D1. A lipid mixture of DOPE (51 mM) and DMPG (9 mM) was prepared in chloroform in a ratio of 8.5/1.5. The lipid mixture was prepared in cholate buffer after chloroform evaporation under nitrogen gas. It was crucial to carefully turn the lipid mixture-containing tube while evaporating to create a dry thin film of lipids. $MraY_{AA}$ nanodiscs were prepared with purified MSP1E3D1 in 3-fold excess and the lipid mixture in 100-fold excess with respect to final concentration of purified $MraY_{AA}$. The correct order of pipetting was essential: MSP buffer, lipid mixture, purified MSP1E3D1, purified $MraY_{AA}$. Pipetting and subsequent incubation were carried out at room temperature to accommodate the phase transition temperatures of DOPE (10 °C) and DMPG (23 °C).[273] Beads (Biobeads SM-2) were added and the mixture was incubated with gentle shaking at room temperature overnight. Prior to nanodisc formation, beads were intensively washed with water because saturated beads are required. The nanodiscs-containing tube was washed with MSP buffer after beads were removed by centrifugation. Protein concentration, gel filtration and SDS-PAGE analysis was performed (depicted in Figure 4.26).

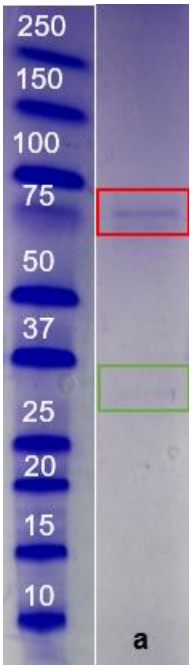

Figure 4.26: SDS-PAGE analysis of fraction (a) obtained after gel filtration of $MraY_{AA}$ in phospholipid nanodiscs. $MraY_{AA}$ appeared as dimer (red box). The other band (green box) revealed MSP.

Sample (a) resulted in two protein bands at sizes between 25-37 kDa and at ~ 75 kDa (Figure 4.26). The first one was affiliated to MSP with a protein size of ~ 32kDa (Figure 4.26, sample (a) green box). The second band should consequently be related to $MraY_{AA}$ (Figure 4.26, sample (a) red box). The presence of $MraY_{AA}$ as a dimer at ~ 70-75 kDa was observed before, but predominantly when using crude membrane preparations. Thus, SDS-PAGE analysis indicated the success of MraY-nanodisc formation but since the yields were

low in this approach (no quantification possible), a repetition of the nanodiscs assembly is necessary. This will be the connecting point for the dissertation of M. Lutz who will continue this project.

4.1.2.3 MraY quantification assays

This project takes advantage of the MraY-specific nanobody NB7 reported by Mashalidis et al.[93] It was envisioned to use this nanobody as a primary antibody in a Western Blot set-up to quantify MraY in different preparations (protein in crude membrane preparation, as purified protein in detergent micelles and in nanodiscs). The His_6-tag containing NB7 serves as primary antibody that will be recognized by another antibody, an anti His_6-tag that is coupled to the horseradish peroxidase (Hrp) for luminescence detection. A goat anti-rabbit antibody coupled to the Alexa Fluor 680 dye was chosen as a third antibody for fluorescence detection at 680 nm. First, this experimental set-up as described was evaluated after protein expression and purification of NB7.

The NB7 expression was performed as described by Mashalidis et al.[93] NB7 served as sample in this experiment since staining of NB7 by the Hrp-conjugated anti His_6-tag antibody and its detection by the goat-anti rabbit antibody was on focus of this experiment. The membrane was blocked, washed and incubated with the Hrp-conjugated antibody in 1:1,000 dilution. Membranes were washed, incubated with the goat anti-rabbit antibody in 1:10,000 dilution and washed again. The dilutions of both antibodies (applies for all experiments) were adopted from the research group of Prof. Dr. A. Kiemer (Pharmaceutical Biology, Saarland University). The visualized Western Blot is depicted in Figure 4.27.

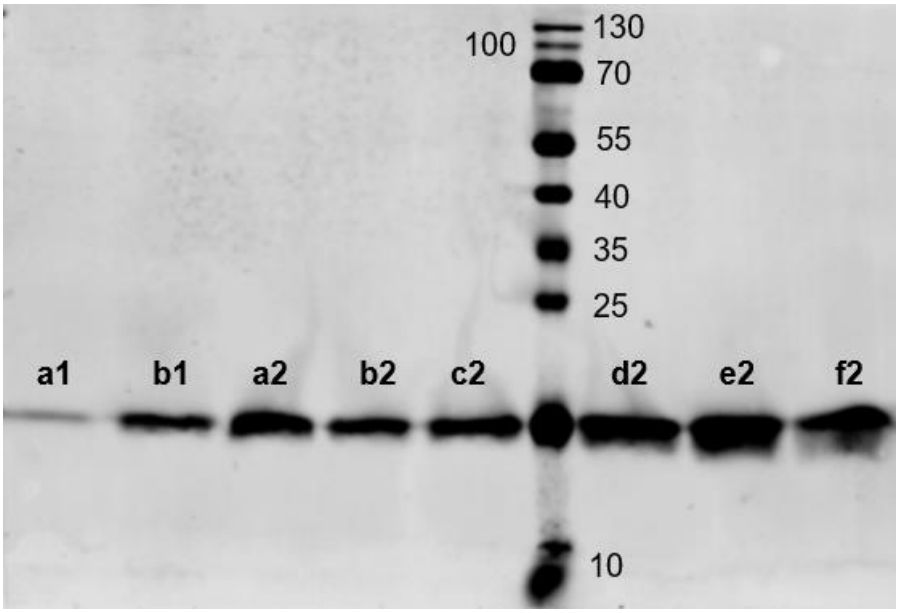

Figure 4.27: Western Blot with NB7-containing protein fractions obtained after gel filtration. The fourth line from the right depicts the protein ladder.

A protein band at a size of ~ 15 kDa was observed in all fractions (Figure 4.27) with enhanced band intensity from samples (c2)-(f2). NB7 was stained by the Hrp-conjugated antibody, thus confirming the proof of concept of this project (Figure 4.27). The band of fraction (a1) appeared to a less extent than the other ones, thus indication lower, but still observable protein amounts (Figure 4.27). The obtained size of NB7 with ~ 15 kDa was in accordance to studies by Mashalidis et al.[93] They reported the $MraY_{AA}$-NB7 complex at 50 kDa in SDS-PAGE as result of the molecular weights of $MraY_{AA}$ (~ 40 kDa) and free NB7 (~ 14 kDa).[93] Their SDS-PAGE analysis with samples of $MraY_{AA}$, NB7 and the $MraY_{AA}$-NB7 complex is depicted in Figure 4.28.

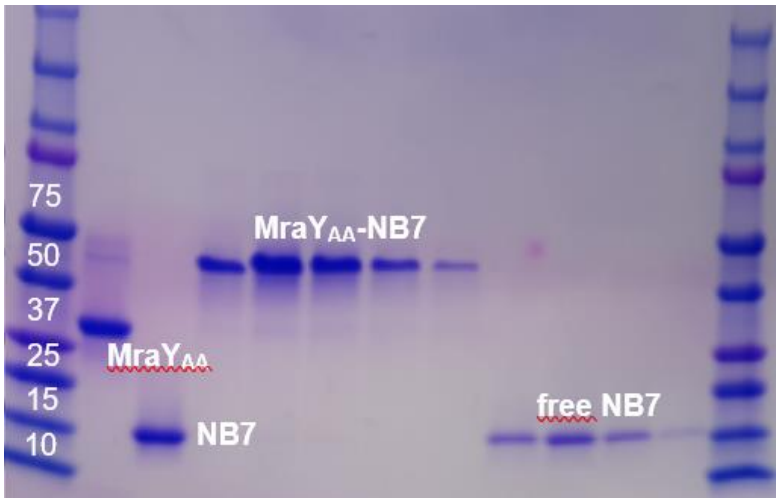

Figure 4.28: SDS-PAGE analysis of $MraY_{AA}$, NB7 and the $MraY_{AA}$-NB7-complex after gel filtration (visualization modified, originally taken from: Mashalidis et al., Nat. Commun. ***2019****, 10****,*** *2917).*[93]

Next experiments contained $MraY_{AA}$ in its function as sample to quantify protein amounts in differently prepared protein purification systems. The first experiment was performed to assess the optimal MraY amount and the experiment's sensitivity. Initial studies accessed $MraY_{AA}$ that has been expressed and purified by S. Koppermann. Later on, $MraY_{AA}$ was expressed and purified in this work for the formation of $MraY_{AA}$ in phospholipid nanosdiscs. This batch was used for all further studies of this project (Chapter 4.1.2.2). Dilutions of purified $MraY_{AA}$ were prepared as follows:

(1) 50 µL protein + 50 µL H_2O (1:2 dilution) ≙ 2 µg/mL $MraY_{AA}$

(2) 25 µL protein + 75 µL H_2O (1:4 dilution) ≙ 1 µg/mL $MraY_{AA}$

(3) 10 µL protein + 90 µL H_2O (1:10 dilution) ≙ 400 ng/mL $MraY_{AA}$

(4) 5 µL protein + 95 µL H_2O (1:20 dilution) ≙ 200 ng/mL $MraY_{AA}$

SDS-PAGE analysis was performed under usual conditions with the sample dilutions (1)-(4) and is depicted in Figure 4.29. A protein band at a size between 25-35 kDa (Chapter 4.1.2.2) appeared in all samples which was related to $MraY_{AA}$ (Figure 4.29). A dose dependency was observed with reduced protein band intensity from samples (1)-(4). Absolute protein amounts

of the samples were calculated based on the dilutions and sample loading on the SDS-PAGE gel.

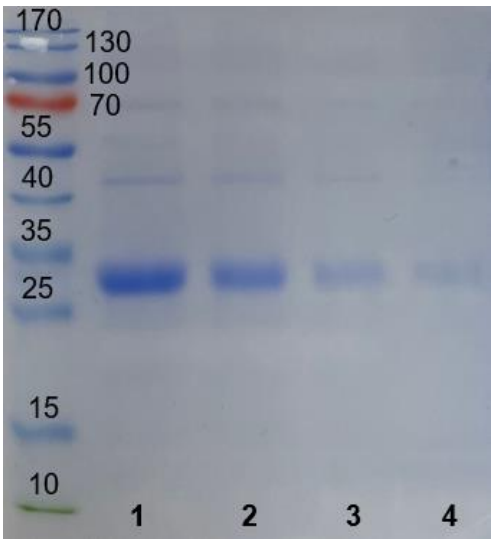

Figure 4.29: SDS-PAGE analysis of $MraY_{AA}$ in amounts of 60 ng (1), 30 ng (2), 12 ng (3) and 6 ng (4).

Protein transfer from SDS-PAGE gel to Western Blot membranes was performed overnight. After membrane blocking, NB7 was added and the membrane was incubated overnight. Sample (d2) was used (Figure 4.27) in 1:500-dilution (25 µL of sample (d2) in 12.5 mL blocking buffer (BB)) in this initial experiment (≙ 6 µg/mL). During assay establishment, NB7 concentration was on focus and will be discussed later on. Membranes were washed and incubated with Hrp-conjugated anti His_6-tag antibody in 1:1,000 dilution. Membranes were washed, incubated with the goat anti-rabbit antibody in 1:10,000 dilution and washed again. The Western Blot is depicted in Figure 4.30.

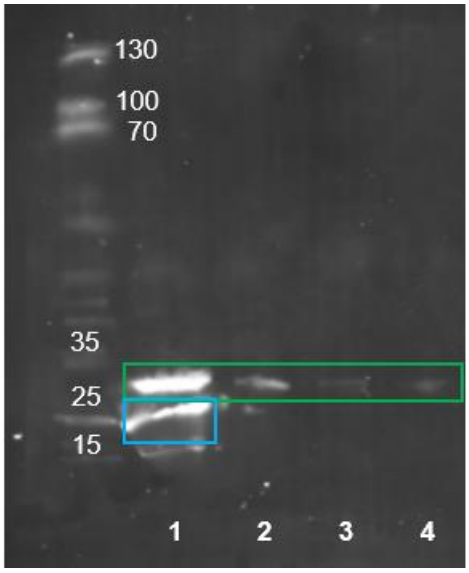

Figure 4.30: Western Blot of $MraY_{AA}$ in amounts of 60 ng (1), 30 ng (2), 12 ng (3) and 6 ng (4). $MraY_{AA}$ appeared as monomer (green box). The other band (blue box) could not be identified.

The Western Blot revealed $MraY_{AA}$ as a monomer at a size of ~ 30 kDa in all samples (Figure 4.30, green box), thus being in agreement to SDS-PAGE analysis (Figure 4.29). The previous dose dependency between the samples (1)-(4) was also seen on the blot (Figure 4.30). The presence of $MraY_{AA}$ as a dimer at a size of~ 70-75 kDa was not observed in the samples (Chapter 4.1.2.2). The highest concentrated sample (1) revealed an additional protein band below the one that corresponds to the $MraY_{AA}$ monomer (Figure 4.30, blue box), potentially indicating proteolysis. Strikingly, this additional band at a size of ~ 25 kDa only appeared in sample (1) and was not observed before by SDS-PAGE analysis (Figure 4.29). The experiment was repeated in analogous fashion to assess this additional band.

Sample dilutions (1)-(4) were prepared using a new aliquot of protein. SDS-PAGE analysis was performed and is presented in Figure 4.31. Previous results of SDS-PAGE analysis were confirmed (Figure 4.29): $MraY_{AA}$ appeared as monomer at a size of ~ 30 kDa in all samples (Figure 4.31) and the dose dependency between samples (1)-(4) was observed as well. An additional protein band was not discovered in sample (1) that was on focus of this experiment (Figure 4.31).

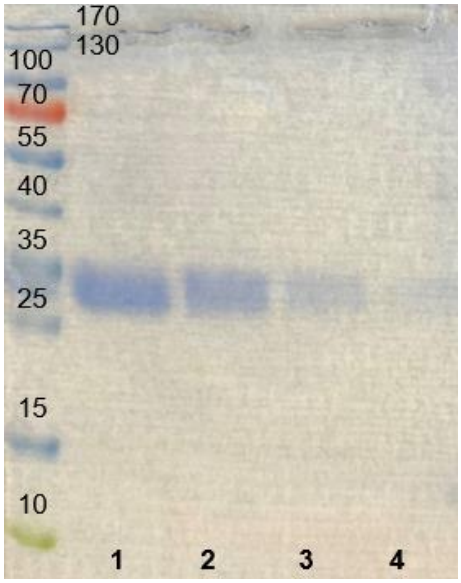

Figure 4.31: SDS-PAGE analysis of $MraY_{AA}$ in amounts of 60 ng (1), 30 ng (2), 12 ng (3) and 6 ng (4).

Western Blotting was performed in analogous fashion to the previous experiment using the same antibody dilutions. The visualized Western Blot is depicted in Figure 4.32.

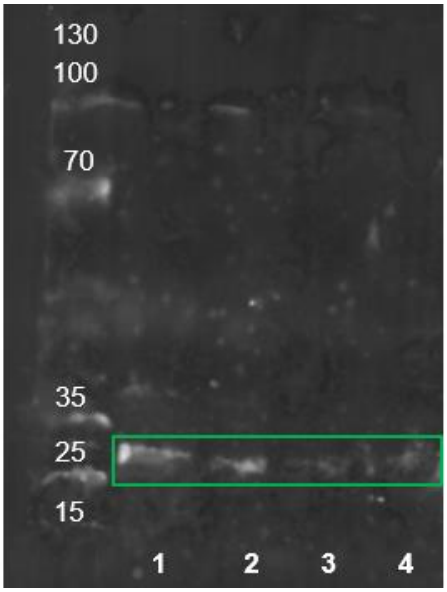

Figure 4.32: Western Blot of $MraY_{AA}$ in amounts of 60 ng (1), 30 ng (2), 12 ng (3) and 6 ng (4). $MraY_{AA}$ appeared as monomer (green box).

The obtained Western Blot (Figure 4.32) was comparable to the previous one (Figure 4.30). A protein band at a size of ~ 30 kDa was observed in all samples (green box) which corresponds to $MraY_{AA}$ (Figure 4.32). The additional non-identifiable band observed in sample (1) within the previous Western Blot (Figure 4.30) was not present here and was therefore attributed to technical issues during protein transfer before or proteolysis. Both Western Blots (Figure 4.30 and 4.38) indicated sample (2) to be sensitive and sufficient for the envisioned experiments. Sample (2) contained an absolute amount of 30 ng purified protein.

To evaluate assay practicability with regard to different protein environments, $MraY_{AA}$ in crude membrane preparations was used as sample. The experiments were performed in analogous fashion as with purified $MraY_{AA}$. The overall protein concentration in the crude membrane preparation was determined with 0.11 mg/mL and dilutions were prepared as follows:

(1) 50 µL protein + 50 µL H_2O (1:2 dilution) ≙ 55 µg/mL overall protein

(2) 25 µL protein + 75 µL H_2O (1:4 dilution) ≙ 27.5 µg/mL overall protein

(3) 10 µL protein + 90 µL H_2O (1:10 dilution) ≙ 110 µg/mL overall protein

(4) 5 µL protein + 95 µL H_2O (1:20 dilution) ≙ 5.5 µg/mL overall protein

SDS-PAGE analysis was performed as described above with the sample dilutions (1)-(4) and is depicted in Figure 4.33. The use of crude membrane preparations resulted in intensive greasing as expected (Figure 4.33). However, protein bands appeared in all samples at sizes of <35 kDa and between 70-100 kDa that would suit $MraY_{AA}$ (Figure 4.33). The dose dependency was observed with reduced band intensity from samples (1)-(4). Overall protein

amounts of the samples were calculated based on the dilutions and sample loading on the SDS-PAGE gel.

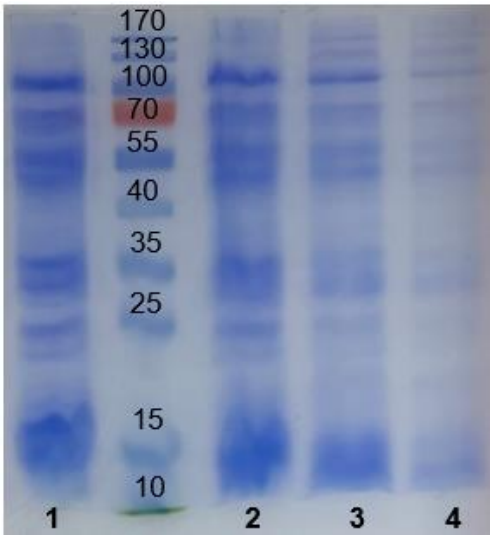

Figure 4.33: SDS-PAGE analysis of $MraY_{AA}$ as crude membrane preparation with an overall protein concentration of 0.11 mg/mL.

Subsequent Western Blotting was performed in analogous fashion to the previous experiment using the same antibody dilutions. The visualized Western Blot is depicted in Figure 4.34.

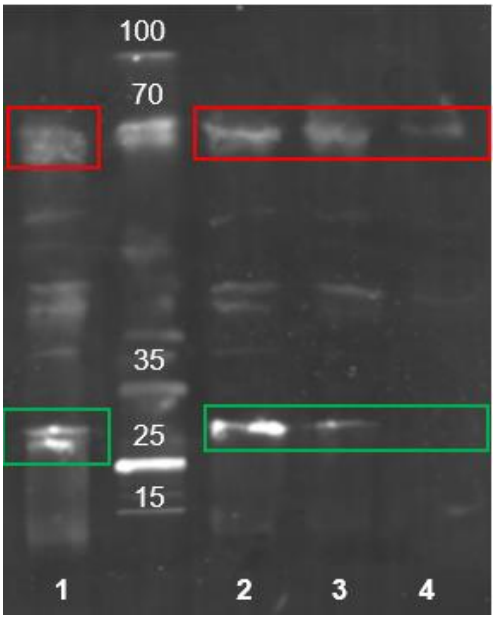

Figure 4.34: Western Blot of $MraY_{AA}$ as crude membrane preparation with an overall protein concentration of 0.11 mg/mL $MraY_{AA}$ appeared as monomer (green boxes) and as dimer (red boxes).

The Western Blot revealed $MraY_{AA}$ not only as a monomer at a size of ~ 30 kDa in all samples (Figure 4.34, green box), but also as a dimer at a size of ~ 70 kDa (Figure 4.34, red box). This was in good agreement to our experience because the visualization of MraY as a dimer was

predominantly observed when using crude membrane preparations (Chapter 4.1.2.2). Overall, the use of MraY as crude membrane preparation and in purified form was applicable in the experiments. Reproducible results were obtained, thus proving the principle of MraY quantification via Western Blot and leading to following optimization studies.

Next studies optimized the concentration of NB7. In previous experiments, 25 µL NB7 (sample d2, Figure 4.27) was used in 12.5 mL BB, i.e., a 1:500 dilution (6 µg/mL). Because NB7 is the primary antibody, the experimental set-up was planned as follows: SDS-PAGE experiments as well as protein transfer from SDS-PAGE gels to Western Blot membranes were performed as usual. $MraY_{AA}$ was used on the gel as 30 ng MraY purified in detergent micelles (sample 2a) and as crude membrane preparation (sample 2b, 825 ng overall protein). Individual membranes were incubated with NB7 antibody dilutions as follows:

(1) 250 µL NB7 in 12.5 mL BB ≙ 1:50 dilution (60 µg/mL)

(2) 125 µL NB7 in 12.5 mL BB ≙ 1:100 dilution (30 µg/mL)

(3) 25 µL NB7 in 12.5 mL BB ≙1:500 dilution (6 µg/mL)

(4) 12.5 µL NB7 in 12.5 mL BB ≙1:1000 dilution (3 µg/mL)

(5) 1.25 µL NB7 in 12.5 mL BB ≙ 1:10000 dilution (0.3 µg/mL)

SDS-PAGE and Western Blotting was carried out as described above with the adopted dilutions of the Hrp-conjugated anti His_6-tag antibody (1:1,000) and the goat anti-rabbit antibody (1:10,000) being used as before (Table 4.15).

Table 4.15: Scheme of SDS-PAGE gels for the investigation of varying NB7 amounts. One gel served as control gel.

gel 1								
Sample (2a)	*Sample (2b)*	*Protein ladder*	*Sample (2a)*	*Sample (2b)*	*Protein ladder*	*Sample (2a)*	*Sample (2b)*	*Protein ladder*
Control gel			*Dilution (1) of NB7 Western Blot I*			*Dilution (2) of NB7 Western Blot II*		

gel 2								
Sample (2a)	*Sample (2b)*	*Protein ladder*	*Sample (2a)*	*Sample (2b)*	*Protein ladder*	*Sample (2a)*	*Sample (2b)*	*Protein ladder*
dilution (3) of NB7 Western Blot III			*Dilution (4) of NB7 Western Blot IV*			*Dilution (5) of NB7 Western Blot V*		

The obtained control SDS-PAGE gel (Table 4.15) is presented in Figure 4.35. SDS-PAGE analysis was in agreement with all previous results: $MraY_{AA}$ appeared at a size of ~ 30 kDa in the purified sample (Figure 4.35, sample 2a). Using crude membrane preparations resulted in

greasing (Figure 4.35, sample 2b). However, protein bands appeared at sizes between 25-35 kDa and between 70-100 kDa display $MraY_{AA}$ (Figure 4.35, sample 2b).

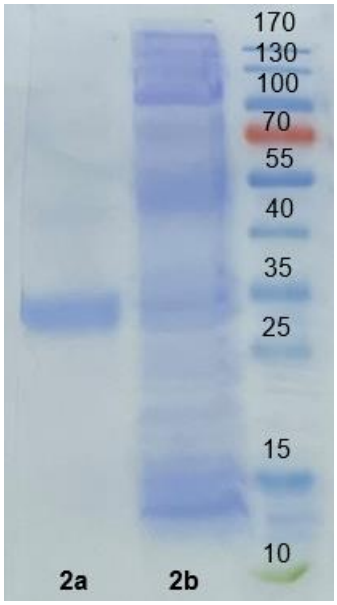

Figure 4.35: SDS-PAGE analysis of $MraY_{AA}$ purified in detergent micelles (sample 2a, 30 ng), as a crude membrane preparation (sample 2b, overall protein concentration 0.11 mg/mL.).

Western Blotting was performed as described in the experimental set-up before. Using the 1:10,000 NB7 dilution (0.3 µg/mL) yielded reproducible, sensitive results. The corresponding visualized Western Blot is depicted in Figure 4.36.

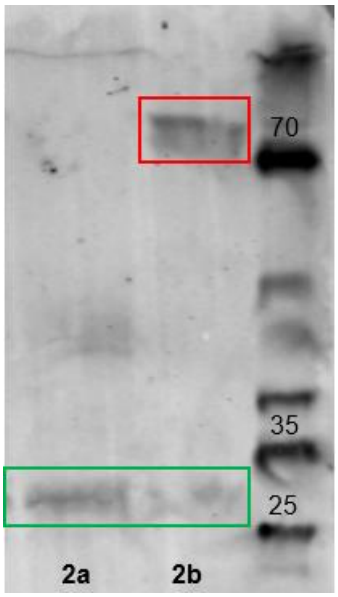

Figure 4.36: Western Blot of $MraY_{AA}$ purified in detergent micelles (sample 2a, 30 ng) and as crude membrane preparation (sample 2b, overall protein 825 ng) using a 1:10,000 NB7 dilution (0.3 µg/mL). $MraY_{AA}$ appeared as monomer (green boxes) and as dimer, but only in crude membrane preparations (red box).

Protein bands on the blot indicate the success of protein transfer (Figure 4.36). Protein bands of both samples were observed with a size of ~ 30 kDa which is in agreement with previous experiments (Figure 4.36). However, a continuous electricity supply was not guaranteed overnight due to technical issues. The results should therefore be handled with care since protein transfer might have been affected (Figure 4.36). A repetition of this experiment should be on focus of follow-up studies. In addition, the investigation of further dilutions of NB7 would be interesting regarding the method's sensitivity. This project will be continued by M. Lutz. Nevertheless, further assay parameters such as the antibody incubation times should be addressed.

4.1.2.4 MurX

The MurX plasmid (provided by the research group of Prof. Dr. S. Van Lanen in a pET30a vector) was transformed into *E. coli* Lemo21 (DE3) cells. Overexpression of the transformed MurX plasmid was performed analogous to $MraY_{SA}$ crude membrane preparations (in a pET28a vector, established in our research group, Chapter 7.1.2.3). The plasmid maps of both vectors pET30a and pET28a are depicted in the Appendix. MurX activity was investigated in the MraY activity assay.

Crude membrane preparations of $MraY_{SA}$ served as reference and two negative controls were used. For negative control 1, pET28a $MraY_{SA}$ was transformed into *E. coli* Lemo21 (DE3) cells, but induction with IPTG was omitted. Negative control 2 contained water instead of a plasmid and IPTG induction was included. The MraY activity assays were initially performed with undiluted crude membrane preparations to gain initial insights into protein activity. The results are presented in Figure 4.37.

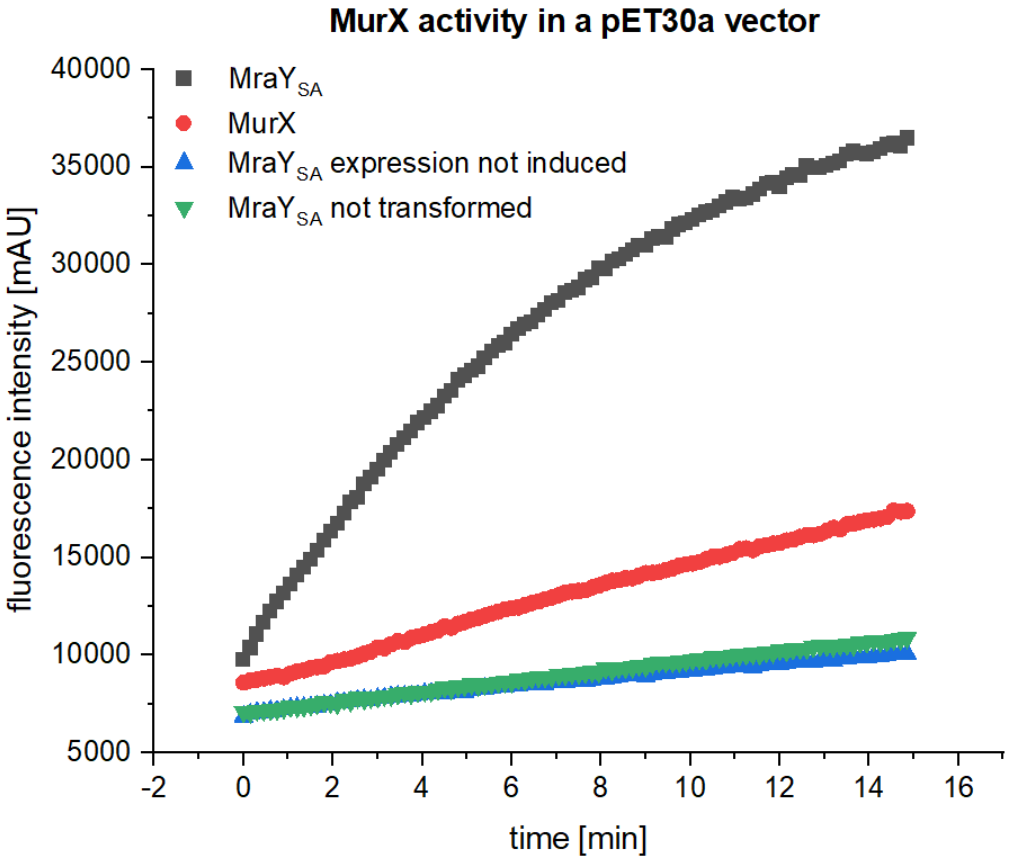

Figure 4.37: Investigation of MurX activity (in a pET30a vector) in the MraY activity assay. Activity of the crude membrane preparations of MraY$_{SA}$ (black), MurX (red) and the two negative controls (blue and green) are plotted as a function of time.

A hyperbolic curve was obtained when using crude membrane preparations of MraY$_{SA}$, thus confirming protein activity and the assay consistency (black curve, Figure 4.37). Both negative controls did not show enzymatic activity (blue and green curves, Figure 4.37). A slight increase compared to the negative controls was observed for the crude membrane preparation of MurX (red curve, Figure 4.37). To rule out expression issues, plasmid transformations and expressions of all approaches were repeated in analogous fashion. The initial results were confirmed (data not shown).

Because our laboratory routinely overexpresses MraY$_{SA}$ in a pET28a vector, subcloning of the MurX genes into this vector was performed to investigate the effects of the expression plasmid (Boston, USA). Subcloning experiments were performed using the *in vivo* assembly (IVA) cloning by polymerase chain reaction (PCR).[274] Samples were prepared with only insert (MurX) or vector (pET28a) and were termed “individual samples” in the following. Furthermore, insert and vector were combined in another tube (termed “combined approach”). Two approaches were performed for each sample with DMSO (1 µL) included (“+“) and excluded (“-“). Subcloning was analyzed by agarose gel electrophoresis which is depicted in Figure 4.38.

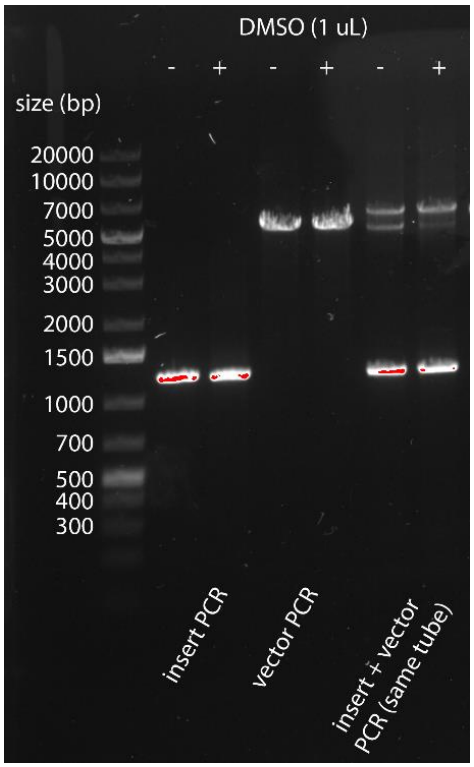

Figure 4.38: Agarose gel of subcloning of the MurX genes into a pET28a vector (Arthanari laboratory, Boston, USA). Samples were pipetted as follows: reference ladder, insert PCR, vector PCR and a combined approach. "+" refers to DMSO-containing samples, while DMSO was omitted in samples with "–".

Both "individual approaches" contained one band each: the insert PCR revealed a band between 1,000-1,500 bp, while a band between 5,000-7,000 bp was observed in the vector PCR (Figure 4.38). This was in agreement with the sizes of MurX with ~ 1,100-1,200 bp and the pET28a vector with 5,900 bp (Appendix). The "combined approach" yielded two bands at the corresponding sizes, thus confirming the results obtained in the "individual approaches" (Figure 4.38). Agarose gel electrophoresis confirmed the fragmentation by PCR.

The "individual approaches" were combined for following DpnI digestion to induce degradation of bacterial template DNA. The recombination of both amplified PCR products was achieved by transformation into *E. coli* DH5α as described before. A plasmid extraction was performed on single colonies prior to sequencing (Boston, USA). The obtained sequencing results confirmed the success of subcloning. The subcloned MurX plasmid was transformed into chemically competent *E. coli* Lemo21 (DE3) cells and crude membrane preparations were expressed as described before. Protein activity was investigated in the MraY activity assay. Undiluted MurX crude membrane preparations were used for an initial evaluation of protein activity. The results are depicted in Figure 4.39.

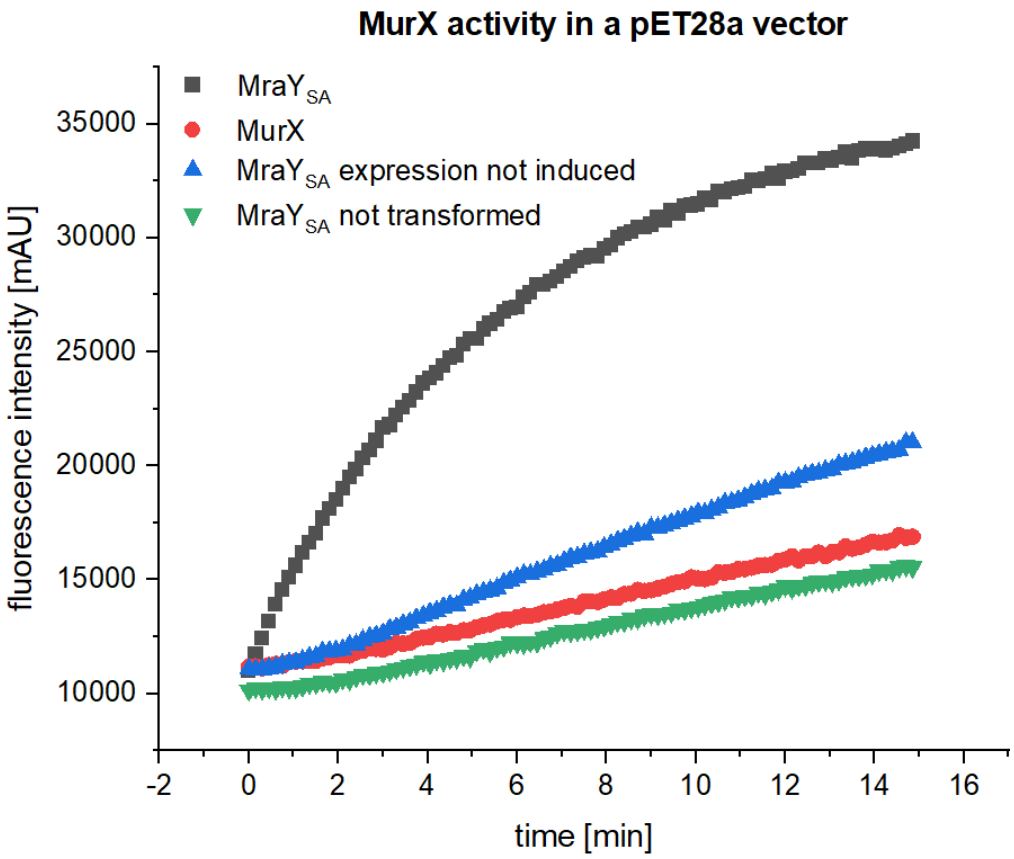

Figure 4.39: Investigation of MurX activity after subcloning of the MurX genes into a pET28a vector in the MraY activity assay. Activity of the crude membrane preparations of MraY$_{SA}$ (black), MurX (red) and the two negative controls (blue and green) are plotted as a function of time.

The hyperbolic trend of the crude membrane preparations of MraY$_{SA}$ demonstrated reasonable protein activity (black curve, Figure 4.39). Both negative controls did not show protein activity (blue and green curves, Figure 4.39). When using crude membrane preparations of MurX in a pET28a vector (red curve, Figure 4.39), a line comparable to both negative controls was obtained. The results were in agreement to previous experiment with MurX in a pET30a vector (red curve, Figure 4.37), no hyperbolic curve was observed (red curve, Figure 4.39).

Subcloning of the MurX genes into a pET28a vector did not result in a change of protein activity. This might be caused by various issues. The biological behavior of MraY in different bacterial species seems to be more complex than expected. It cannot be ruled out that the MurX genes are generally not expressed or that the Park's nucleotide is not recognized as a substrate. The choice of competent cells for plasmid transformation was also questioned. It primarily depends on the purification method of the proteins: Chemically competent *E. coli* Lemo21 (DE3) cells were used for the preparation of crude membrane preparations and competent *E. coli* C41 (DE3) cells for purified MraY (regardless of the bacterial species). However, instead of using different competent cells in further experiments, the idea of another subcloning experiment arose: Our laboratory routinely expresses MraY$_{AA}$ in a pET26a vector, thus leading to a further

subcloning of the pET28a vector containing MurX genes into a pET26a vector. The plasmid map of pET26a is presented in the Appendix. In analogy to purified $MraY_{AA}$, it was envisioned to purifiy MurX after expression.

Subcloning experiments were performed as before by IVA cloning.[274] Samples were prepared as “individual samples” with only insert (MurX) or vector (pET26a vector) besides a “combined approach” with insert and vector. PCR samples were prepared twice: one approach included DMSO (“+“), the other one excluded DMSO (“-“). Subcloning was analyzed by agarose gel electrophoresis which is depicted in Figure 4.40. One band appeared in both “individual approaches”. The insert PCR exhibited a band at ~ 1,000 bp (Figure 4.40). This agrees with the size of MurX with ~ 1,100-1,200 bp. A band between 5,000-6,000 bp was seen in the vector PCR (Figure 4.40), thus confirming the size of pET26a vector. Two bands at the corresponding sizes were obtained in both “combined approaches” which were in good agreement with the results of the “individual approaches” (Figure 4.40). Agarose gel electrophoresis confirmed the successful PCR fragmentation.

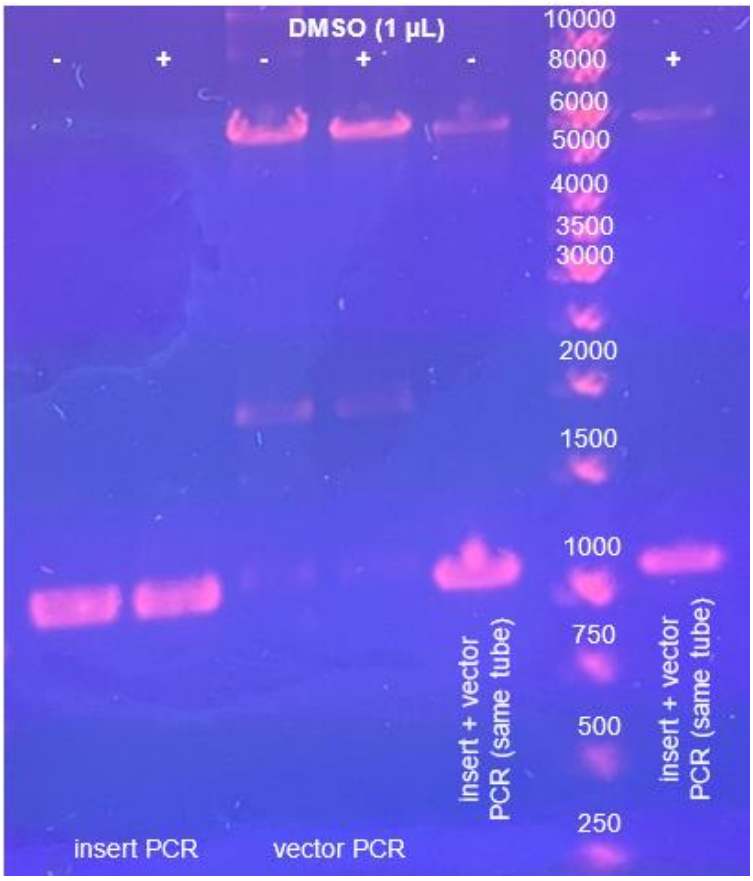

Figure 4.40: Agarose gel of subcloning of the MurX genes into a pET26a vector. Samples were pipetted as follows: Insert PCR, vector PCR and a combined approach with the reference ladder in between. “+” refers to DMSO-containing samples, while DMSO was omitted in samples with “–“.

DpnI digestion of the combined “individual approaches” was performed followed by plasmid transformation into competent *E. coli* DH5α cells and plasmid extraction as described before. The success of subcloning was confirmed by sequencing of the extracted plasmid. Following plasmid transformation, protein expression and purification will be continued by M. Lutz as part of his dissertation.

4.1.2.5 Self-resistance of *Streptomyces* species against muraymycins

First investigations concerning the role of amino acid conservation within the suggested self-resistance mechanism of *Streptomyces species* against muraymycins were performed with expressed crude membrane preparations of $MraY_{SA}$H287Q provided by Dr. P. Fischer.[122] Crude membrane preparations of $MraY_{SA}$ served as a reference and two negative controls were used. Negative control 1 contained transformed pET28a $MraY_{SA}$ into competent *E. coli* Lemo21(DE3) cells without IPTG induction. For negative control 2, water was used instead of a plasmid and IPTG induction was included. Protein activity was investigated in the *in vitro* MraY activity assay (established in our research group, Chapter 7.1.2.3). The assay results are presented in Figure 4.41.

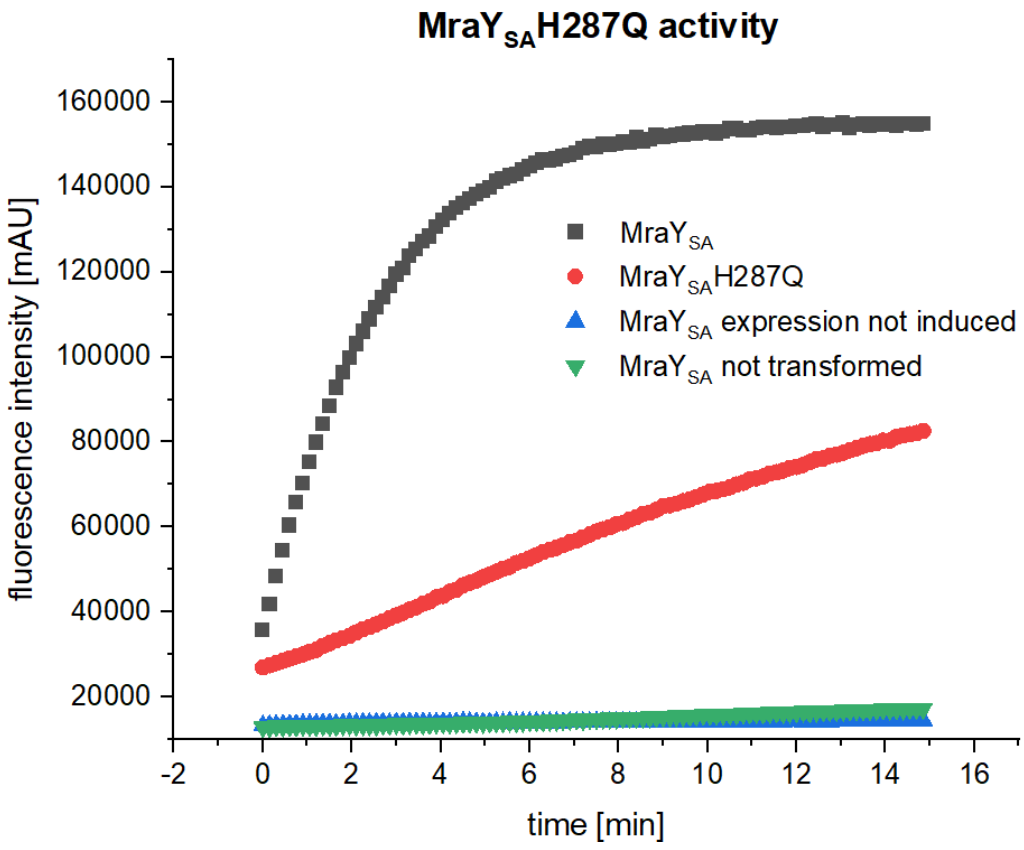

Figure 4.41: Investigation of protein activity in the MraY activity assays. Activity of the crude membrane preparations of $MraY_{SA}$ (black), $MraY_{SA}$H287Q (red) and the two negative controls (blue and green) was plotted as a function of time.

The use of crude membrane preparation of $MraY_{SA}$ resulted in a hyperbolic curve (black curve, Figure 4.41). The curve obtained for the mutant protein $MraY_{SA}$H287Q revealed significantly lower enzymatic activity (red curve, Figure 4.41). Both negative controls did not show protein activity (blue and green curves, Figure 4.41). The loss in activity most likely results from the mutagenesis of a highly conserved histidine in proximity to the active site, although other reasons such as lower overexpression levels or partial misfolding cannot be excluded.

However, since protein activity was still retained to a certain extent, preliminary MraY inhibition assays with selected MraY inhibitors were performed. Therefore, the guanidinylated muraymycin analogue **48** synthesized by Dr. M. Wirth,[243] compound **33** and commercially available tunicamycin were chosen. MraY activity assays were performed under established conditions (Chapter 7.1.2.3), but sigmoidal fitting for the evaluation of IC_{50} values was not possible for any of the compounds.

The experiments were repeated with transformations of the following plasmids (plasmid (1) was provided by Dr. P. Fischer[122]) into chemically competent *E. coli* Lemo21(DE3) cells and protein expression as crude membrane preparations:

(1) pET28a $MraY_{SA}$

(2) pET28a $MraY_{SA}$H287Q

(3) pET28a $MraY_{SA}$ without IPTG induction (negative control 1)

(4) no plasmid (water instead), with IPTG induction (negative control 2)

For comparability, plasmid transformations and protein expressions were performed in parallel as described before. Protein activity was investigated in subsequent MraY inhibition assays. The results were comparable to the previous ones (data not shown): no protein activity of the $MraY_{SA}$H287Q crude membrane preparations was observed, thus confirming the previous hypothesis.

Next experiments focused on the reaction time to investigate the different enzymatic kinetics of the MraY mutant. Therefore, the experimental set-up was modified: the number of cycles was increased to 250 (usual conditions: 100) and the number of flashes per well was increased from 9 to 20. This resulted an in an increase of the original measurement of 15 minutes to 40 minutes. The results are depicted in Figure 4.42.

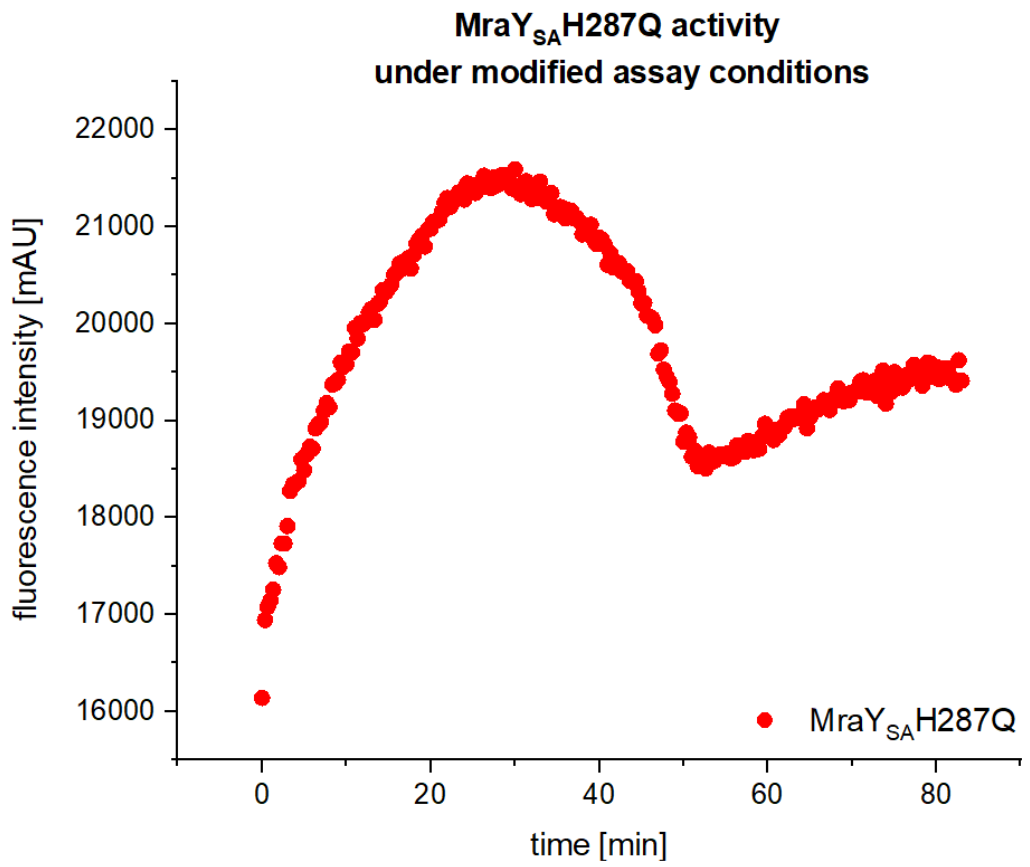

Figure 4.42: Investigation of protein activity in the MraY activity assays using crude membrane preparations of MraY$_{SA}$H287Q under modified assay conditions (number of cycles = 250, number of flashes and cycles per well = 20) plotted as a function of time.

An initial fluorescence increase was observed within the first ~ 35 minutes after reaction start followed by a sudden decrease afterwards. The results suggest potential reversibility of the MraY-catalyzed reaction. Different states of equilibrium as well as different binding affinities to the essential cofactor magnesium (Chapter 2.2) were considered. Moreover, substrate concentration might have an impact, thus altering the "Michaelis constant". The "Michaelis constant" characterizes enzyme affinities to their corresponding substrates[275] and was reported with a concentration of 18 µM for the non-dansylated substrate. This hypothesis was adressed in the next experiment.

The typical Park's nucleotide concentration used in our assay was 7.5 µM.[99] Subsequent assay was performed with a 10-fold higher substrate concentration to ensure the detection of activity changes of the mutant. The number of cycles was set as usually. However, increased Park's nucleoside concentration of 75 µM yielded the same results as before (curves not presented): as in all activity assays before, a straight line with a slight increase was obtained for MraY$_{SA}$H287Q instead of a hyperbolic trend.

Further studies included constructs coding for wild-type MraY from *Streptomyces platensis* (MraY$_{SP}$) and another mutant, MraY$_{SP}$Q316H. Both were cloned into pET28a vectors by Dr. P. Fischer[122] and provided for this dissertation. The mutant-containing protein MraY$_{SP}$Q316H

represented the isoform of MraY in which a back-mutation of glutamine to histidine was performed.[122] The plasmids of $MraY_{SP}$ and $MraY_{SP}$Q316H were transformed into competent *E. coli* Lemo21(DE3) cells and expression of the proteins as crude membrane preparations was performed under usual conditions. For comparability, $MraY_{SA}$ was transformed into competent *E. coli* Lemo21(DE3) cells and expressed as crude membrane preparations parallel. Activity of all proteins was examined in the assay. Two negative controls were performed as described above. The results are depicted in Figure 4.43.

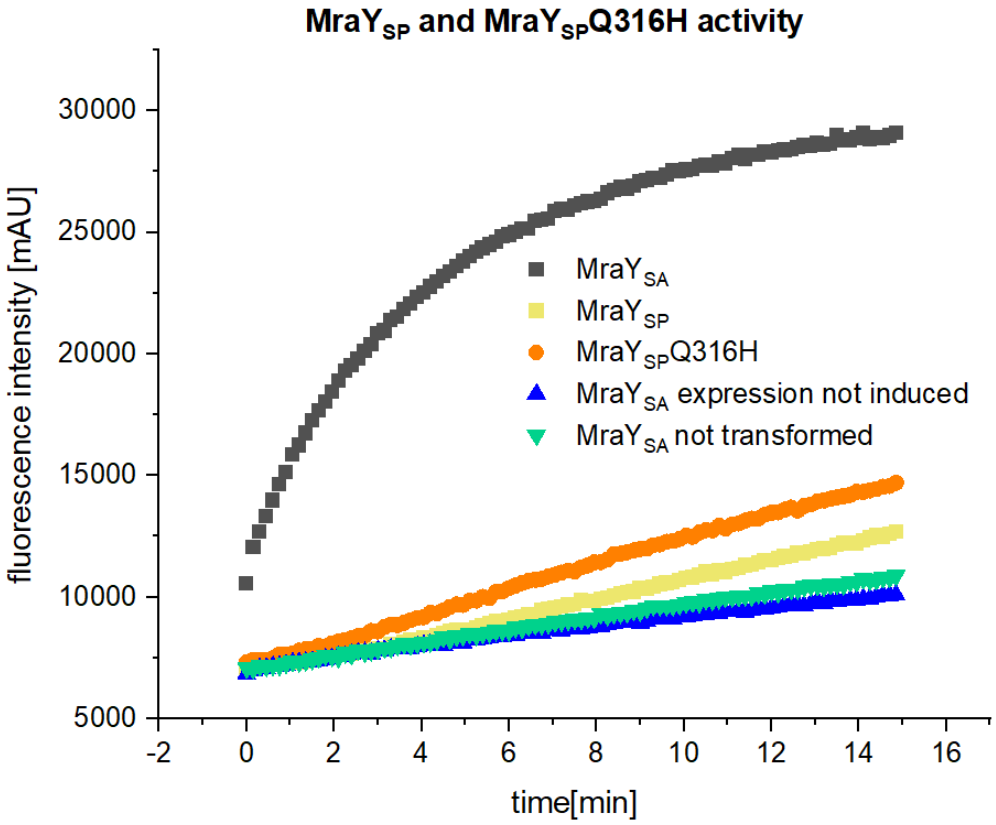

Figure 4.43: Investigation of protein activity in the MraY activity assays. Activity of the crude membrane preparations of $MraY_{SA}$ (black), $MraY_{SP}$ (yellow), $MraY_{SP}$Q316H (orange) and the two negative controls (blue and green) was plotted as a function of time.

A hyperbolic curve was observed with the use of crude membrane preparations of $MraY_{SA}$ (black curve, Figure 4.43). A line appeared for crude membrane preparations of $MraY_{SP}$ (yellow curve, Figure 4.43), indicating significantly lower enzymatic activity compared to $MraY_{SA}$. The use of $MraY_{SP}$Q316H resulted in the similar curve trend (orange curve, Figure 4.43). Both negative controls did not show protein activity (blue and green curves, Figure 4.43). No detectable enzymatic activity for $MraY_{SP}$Q316H was observed, indicating feasibility limitations in this assay system. Overall, the absence of histidine in both mutants, $MraY_{SP}$Q316H and $MraY_{SA}$H287Q, seems to result in protein activity loss. The reasons could not been elucidated within this dissertation. Further investigations regarding the role of specific amino acid residues will be performed by M. Lutz who will continue this project.

4.1.2.6 Interaction between MraY and MurF

The interaction between MraY and MurF demonstrated by Dr. P. Fischer[122] was investigated in our MraY activity assay (established in our research group, Chapter 7.1.2.3). First studies of this side project contained $MraY_{AA}$ purified in detergent micelles at a final concentration of 77.5 nM (provided by S. Koppermann) and purified MurF ligase provided by Dr. P. Fischer.[122] A serial dilution of MurF was prepared to investigate MraY activity in the presence of MurF. The results are presented in Figure 4.44.

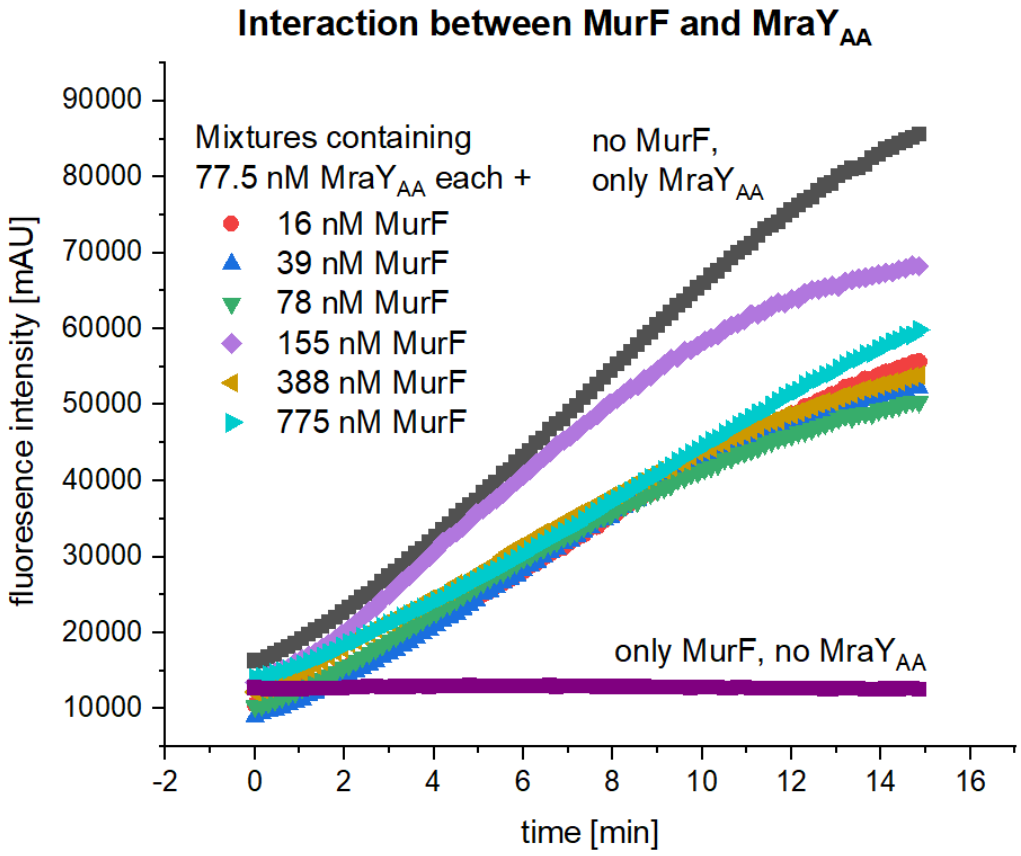

Figure 4.44: Investigation of the interaction between $MraY_{AA}$ and MurF in the MraY activity assays with 77.5 nM purified $MraY_{AA}$ (black) and purified MurF in varying concentrations (different colors). Activity was plotted as a function of time.

$MraY_{AA}$ in detergent micelles resulted in a hyperbolic curve (black curve, Figure 4.44). Varying MurF concentrations in the assay did not result in significant differences in the curves (Figure 4.44). However, the presence of MurF reduced MraY activity slightly. No protein activity was observed for the sample that contained only MurF and no $MraY_{AA}$ (purple, Figure 4.44). The experiment requires repetition due to protein precipitation prior to the MraY activity assay. Furthermore, higher MurF concentrations will be tested to accommodate the dissociation constant (K_D) of ~ 30 µM between MurF and MraY (determined by Dr. P. Fischer[122]).

Parallel on that, further assays were performed in collaboration with Dr. P. Fischer with purified $MraY_{AA}$ in phospholipid nanodiscs in the presence of muraymycin A1 as inhibitor and MurF in

varying concentrations. This data have been presented in the dissertation of Dr. P. Fischer.[122] In the interest of completeness, the obtained results are shortly summarized and discussed at this stage. Due to the rapid enzymatic activity loss of MraY in nanodiscs, however, the data need to be handled as preliminary. Inhibitory activity of muraymycin A1 against $MraY_{AA}$ in phospholipid nanodiscs was found in the low nanomolar range (preliminary IC_{50} = 3.5 ± 0.2 nM).[122] This concentration was used in the activity assays. The MurF concentrations varied in a range of 2-130 µM. No significant effect on MraY inhibition was observed when applying MurF in a triple-digits micromolar range in contrast to MurF concentrations in a single- to double-digit micromolar region. The most pronounced effect was observed at a MurF concentration of 8 µM with a hyperbolic curve being observed in the presence of muraymycin A1. MurF seemed to reverse the muraymycin A1-induced MraY inhibition as demonstrated with the data for $MraY_{AA}$ in the absence of MurF. A MurF concentration of 8 µM corresponded to a ratio between $MraY_{AA}$ and MurF of ~ 2:1. This indicates the binding between a MraY dimer and a MurF monomer. Lower MurF concentrations (<8 µM) resulted in MraY inhibition in a concentration-dependent manner, i.e., MraY activity was restored to a lesser extent. However, reduction of protein activity of the $MraY_{AA}$-nanodiscs system was already indicated as mentioned, thus demonstrating again the importance of nanodisc implementation into our laboratory which was done within this work (Chapter 4.1.2.2). To gain further insights into this protein interaction, M. Lutz will continue this project in collaboration with Dr. P. Fischer.

4.1.3 Hemolysis assays

This chapter deals with the development of a hemolysis assay for the investigation of possible toxic side-effects due to membrane disruption of muraymycins (Chapter 4.1.3.1). Hemolytic data of muraymycin analogues with antibacterial activity against Gram-negative *P. aeruginosa* (Chapter 4.1.3.2), analogues with anti-staphylococcal activity (Chapter 4.1.3.3), muraymycin conjugates (Chapter 4.1.3.4) and non-nucleoside chemotherapeutics with activity against *M. tuberculosis* (Chapter 4.1.3.5) will be presented and discussed.

4.1.3.1 Development and establishment of the assay

A commercially available kit provided by HaemoScan[276] was used for the establishment of a hemolysis assay in our laboratory. Previous experiments within this project were performed with commercially available human red blood cells. However, erythrocyte washing with phosphate-buffered saline (PBS) as reported in the literature[277] turned out to be non-trivial. Therefore, we decided to head over to the aforementioned kit that already contained buffers for erythrocyte washing.[276] The purchased kit served as basis for the development of a hemolysis assay, but is basically intended for daily blood contacting medical devices. In contrast, our objective was the investigation of hemolytic activites of potential drug candidates. Due to former concerns in terms of erythrocyte washing, we decided to use this kit as tool for the preparation of erythrocyte suspensions for our studies. The washing procedure and dilution of the provided erythrocyte concentrate has already been specified by the provider.[276] This will ensure not only the preparation of a suitable suspension of red blood cells but also a functionable erythrocyte amount. The kit itself was modified with regard to our objectives.

First steps during assay development addressed the thawing procedure of the erythrocyte concentrate. The erythrocyte concentrate was stored at -80 °C and for initial experiments, it was thawed in different ways: In one attempt, the erythrocyte concentrate was thawed on ice (0 °C) for 30 minutes. In a second attempt, a more rapid way was chosen by thawing the erythrocyte concentrate in a shaking water bath for 10 minutes at room temperature. Washing was performed according to the manufacturers protocol (Chapter 7.1.4).[276] It was observed that the resulting pellet was twice as big after the complete washing procedure when thawing the erythrocyte concentrate at room temperature compared to thawing on ice. The major benefit was achieved with the second and third washing. The preparation of an erythrocyte suspension to work with was significantly affected by the way of thawing of the concentrate and resulted in a thawing process at room temperature.

Focus of the kit is the investigation of haemocompatibility of medical devices as mentioned.[276] Medical devices such as one silicone elastomer, a polymer termed “Buna N“ and medical steel are therefore included as references. The hemolytically inactive silicone elastomer served as negative control, whereas “Buna N“ and the steel were reported to be hemolytically active.[276]

HaemoScan recommended to include at least two reference materials in each analysis.[276] Prior to protocol modifications with regard to our objectives, we decided to perform the kit in accordance to the kit with the use of these references. The procedure was carried out in analogy to the manufacturers protocol after preparation of the erythrocyte suspension.[276] The incubation of the erythocyte suspension with each of the three provided reference materials was carried out in syringes. Remaining air was carefully removed from the syringe. A syringe without material served as negativ control. Mixtures were incubated by end-over end rotation (37°C, 24 h) and transferred into tubes again followed by centrifugation (4,000 x g, 1 min, 23 °C). Assay buffer was added for OD measurement. A serial dilution of the hemoglobin standards was performed to obtain a calibration between 0.15-10 mg/mL. Wavelenghts at 415 nm, 450 nm and 380 nm were measured for the evaluation by Harboe as described with the following equation (15):

$$(15)\ Calculated\ OD\ =\ (2\ x\ OD\ at\ 415\ nm) - (OD\ at\ 450\ nm\ +\ OD\ at\ 380\ nm)$$

The calculated OD was plotted against the hemoglobin concentration of the standards. The obtained curve is presented in Figure 4.45.

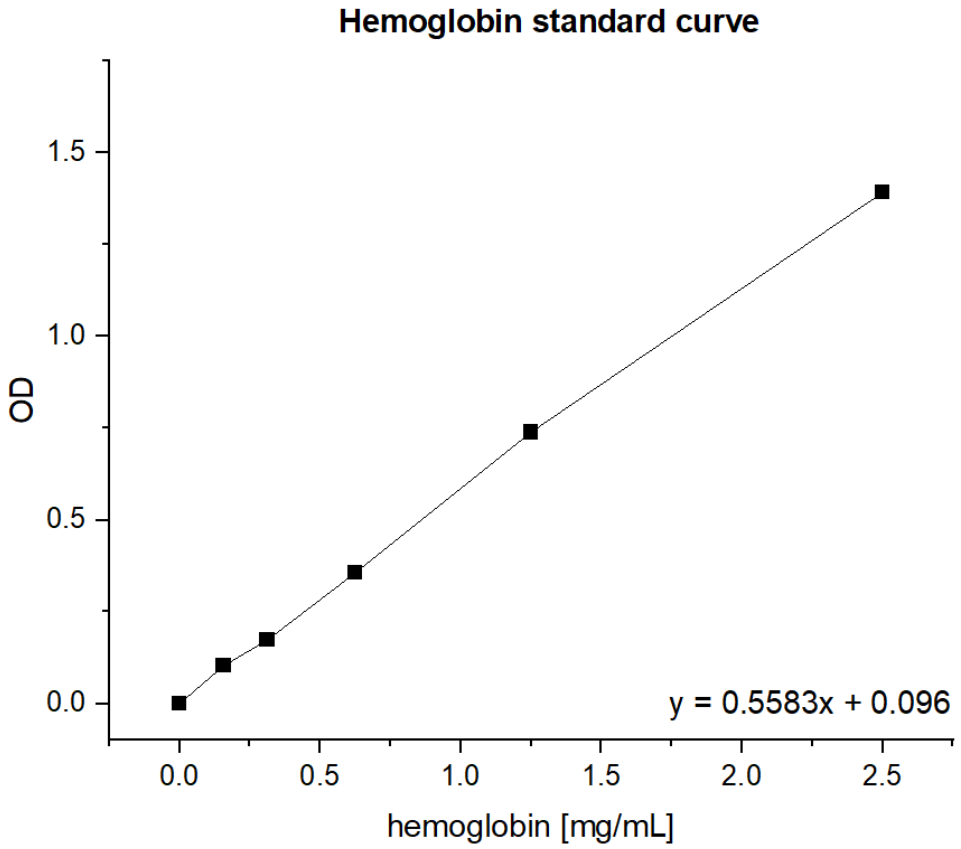

Figure 4.45: Hemoglobin standard curve according to the assay procedure by HaemoScan. The OD is plotted as a function of the hemoglobin concentration of the calibration standards.

A coefficient of determination (R^2) of the calibration curve ≥ 0.98 was provided by HaemoScan as assay criteria.[276] The obtained standard curve agrees well with this parameter within a hemoglobin concentration of 0-10 mg/mL. Hemolytic activities of the references (silicone elastomer, “Buna N“, medical steel) are presented in Table 4.16.

Table 4.16: Hemolytic activities of the silicone elastomer, the polymer “Buna N“ and the medical steel. Hemolytic activities of the references obtained by the supplier are presented for comparison. “n.d.” = not detectable.

	Hemolysis obtained as Hb [mg/mL]	
Reference	**Results of this work**	**Kit**
Silicone elastomer	n.d.	-0.1-0.1
Buna N	0.12	0.0-0.2
Medical steel	0.02	0.0-0.4

No hemolysis was observed for the negative control silicone elastomer. The highest degree of hemolysis was generated by the polymer “Buna N“ with a hemoglobin concentration of 0.12 mg/mL which was in accordance to the kit.[276] The hemolytic activity of the medical steel was expected to be in the same range as “Buna N“. This was not observed with the obtained hemoglobin concentration of 0.02 mg/mL. However, no further focus was placed on this result since this concentration agrees the manufacturer's data (0.0-0.4 mg/mL).[276] The hemolytic activity of the negative control was determined with ≤ 0.1% of the total hemoglobin concentration which was also in agreement with the results of the kit.[276] Overall, all obtained results agree with the data provided by HaemoScan.[276] In the interest of completeness, it should be mentioned that red blood cells turned brown after 24 h of incubation that was applied in this experiment (as performed by HaemoScan[276]). This is most likely due to oxidation of hemoglobin. However, an incubation time of 24 hours did not represent realistic conditions for our studies, so that no further focus was placed on this objective.

Fowlloing that, a hemolysis assays with regard to our objectives was developed. Hemolytic effects of membrane-active peptides with antibacterial activity have been reported in the literature by Sharma et al.[277] The principle of these studies served as basis for our assay: mixtures of human red blood cells and the samples in varying concentrations were incubated in a thermoshaker for 1 hour (37 °C), harvested and the absorbance of the supernatant was measured (414 nm).[277] Sharma et al. used Triton X-100 (0.1%) as a positive control and PBS as a negative control.[277] Both controls were adopted as standards for the studies of this work in accordance with the literature. Since relative comparisons between hemolytic activities of compounds were envisioned with the hemolysis assays, reference values for 0% and 100% hemolysis were sufficient. Therefore, first experiments focused on the determination of the amount of Triton X-100 representing 100% lysis.

The erythrocyte concentrate was thawed in a shaking waterbath. Washing and dilution of the erythrocyte concentrate was performed according to the reported procedure[276] which was successfully evaluated. Since this applied for all experiments, details in terms of washing and dilution will not be listed hereafter. The resulting solution is termed erythrocyte suspension. All approaches were prepared in a final volume of 100 µL, consisting of 95 µL erythrocyte suspension and 5 µL triton X-100 solution in varying dilutions. A negative control was performed with PBS. Triton X-100 solutions were prepared as follows:

(1) 0.1% (v/v %), final assay amount 0.05% (v/v %)

(2) 1% (v/v %), final assay amount 0.05% (v/v %)

(3) 2% (v/v %), final assay amount 0.1% (v/v %)

(4) 10% (v/v %), final assay amount 0.5% (v/v %)

Mixtures were incubated (37 °C, 1 hour), centrifuged and the absorbance of the supernatant was measured. The results are presented in Figure 4.46.

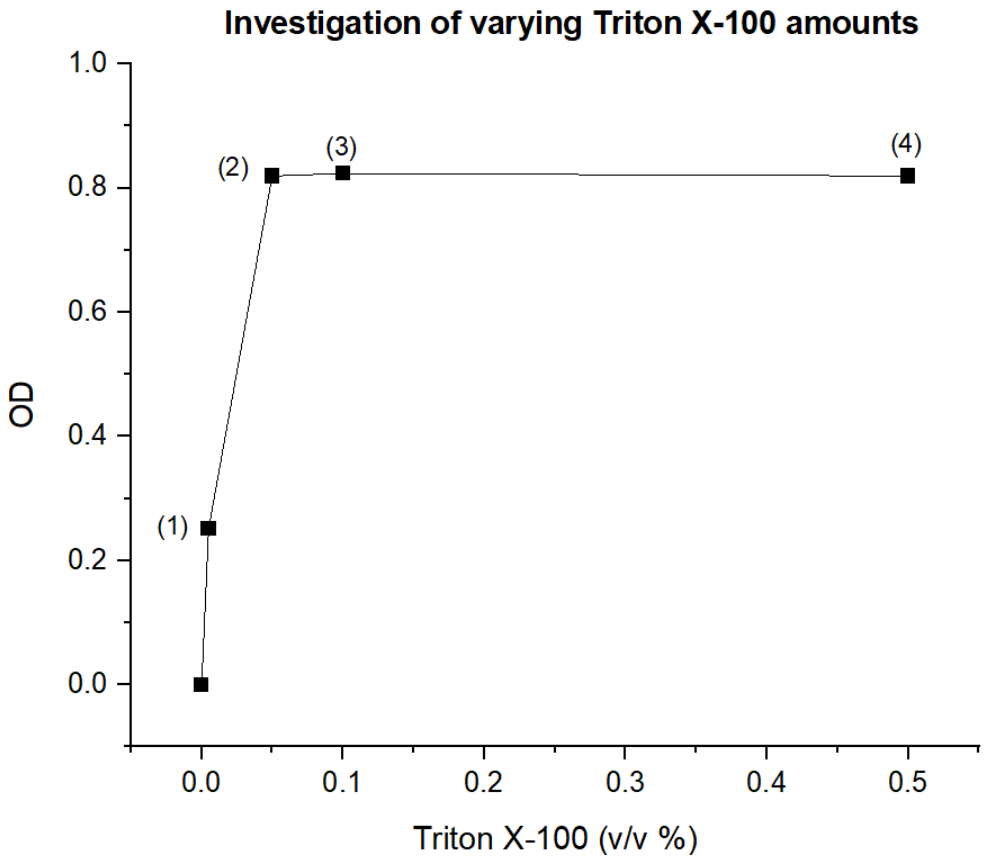

Figure 4.46: Investigation of varying Trion X-100 amounts for a positive control (100% lysis) in the hemolysis assays The OD is plotted against the Triton X-100 amounts.

The corrected OD obtained for sample (1) with the lowest Triton X-100 amount (0.1% v/v %) was significantly lower than the OD values obtained for samples (2), (3) and (4) that contain higher Triton X-100 amounts. Triton X-100 amounts within a range of 0.05-0.5 v/v % yielded a

plateau (Figure 4.46). During assay development, we decided on using an amount of 0.1% Triton X-100 as positive control (corresponding to sample (2)) to avoid too high amounts of Triton X-100 in the assay. This amount seemed to be efficient (Figure 4.46).

Possible effects of DMSO on the system were further examined since the majority of compounds in our research group is dissolved in DMSO. Therefore, two controls were prepared: PBS (as described in the lierature[277]) and a combination of PBS and DMSO. For the latter, it was basically envisioned to use the same amount of DMSO as for the compound solutions. With these two negative controls, the assay conditions were adapted and evaluated for each compound individually. DMSO-mediated hemolytic effects up to 5% final DMSO were ruled out.

Three approaches were considered in terms of the compound's final concentration. When conducting a series of compounds, a standard concentration of 20 µM was decided on, thus enabling relative comparisons. In addition, experiments with concentrations relative to the antibacterial growth inhibition data for the corresponding bacteria were envisioned (depending on previous results). Concentrations of ~ 1-fold MIC_{50} and ~ 4-fold MIC_{50} were decided on. Hemolysis of predetermined muraymycin analogues of our research group, such as those of Dr. G. Niro[239] or Dr. M. Wirth[243] with high lipophilicity, and selected compounds provided by collaborators were investigated. Controls were used as biological triplicates and compounds as biological quintuples due to erythrocyte sensitivity. Each experiment was performed with the following controls which will not be mentioned specifically hereafter:

(1) Positve control: Triton X-100 (0.1% (v/v %))

(2) Negative control 1: PBS

(3) Negative control 2: PBS + DMSO (adapted for each compound)

4.1.3.2 Hemolytic activity of compounds with anti-pseudomonal activity

Selected muraymycin analogues with anti-pseudomonal activity synthesized by Dr. G. Niro[239] (compounds **37**, **38** and **75**-**78**) were investigated towards their hemolytic activities to further examine their unspecific mode of action. They are presented in Figure 4.47.

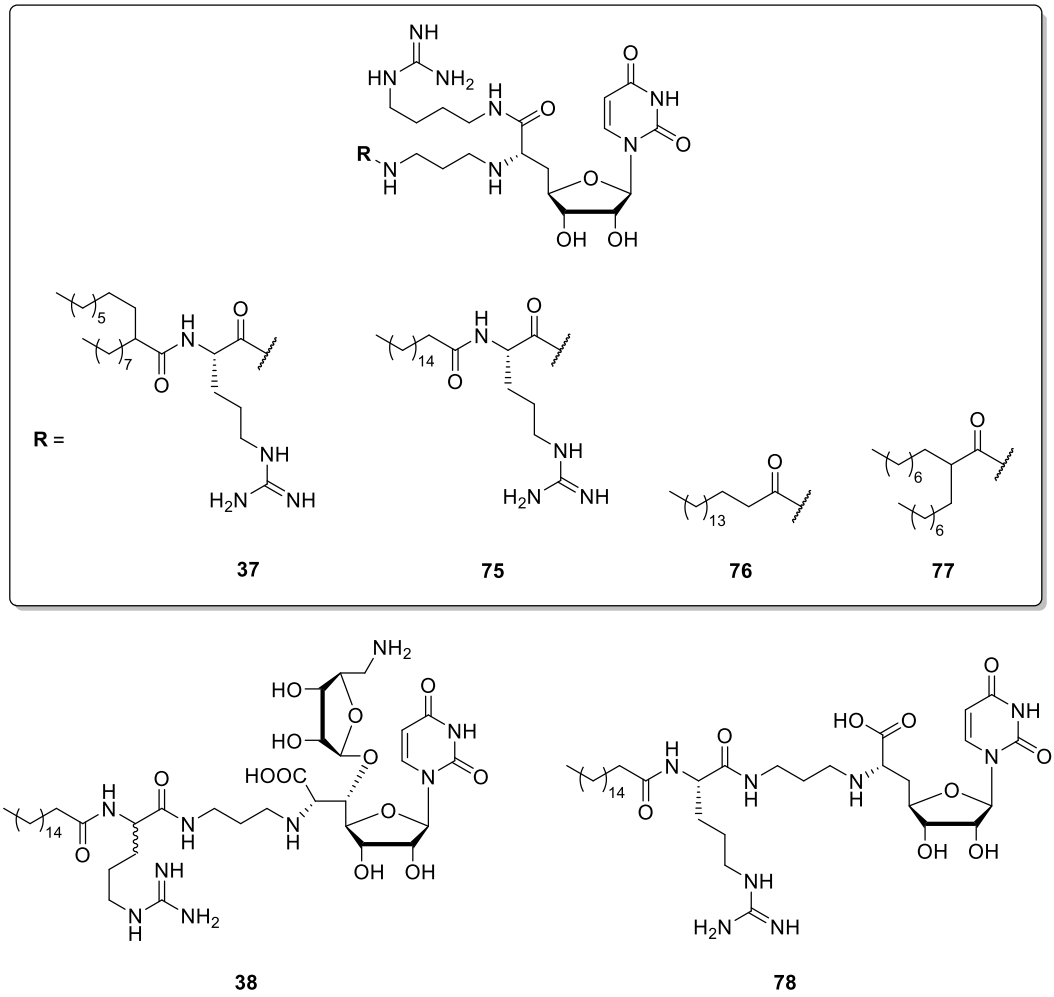

*Figure 4.47: Muraymycin analogues **37**, **38** and **75**-**78** by Dr. G. Niro for hemolysis assays.[239]*

An erythrocyte suspension was prepared as described before. Mixtures containing 95 µL erythrocyte suspension and 5 µL compound solution in PBS (final concentratiion = 20 µM) were incubated (37 °C, 1 hour). Mixtures were centrifuged and the absorbance of the supernatant was measured. The results are presented in Figure 4.48.

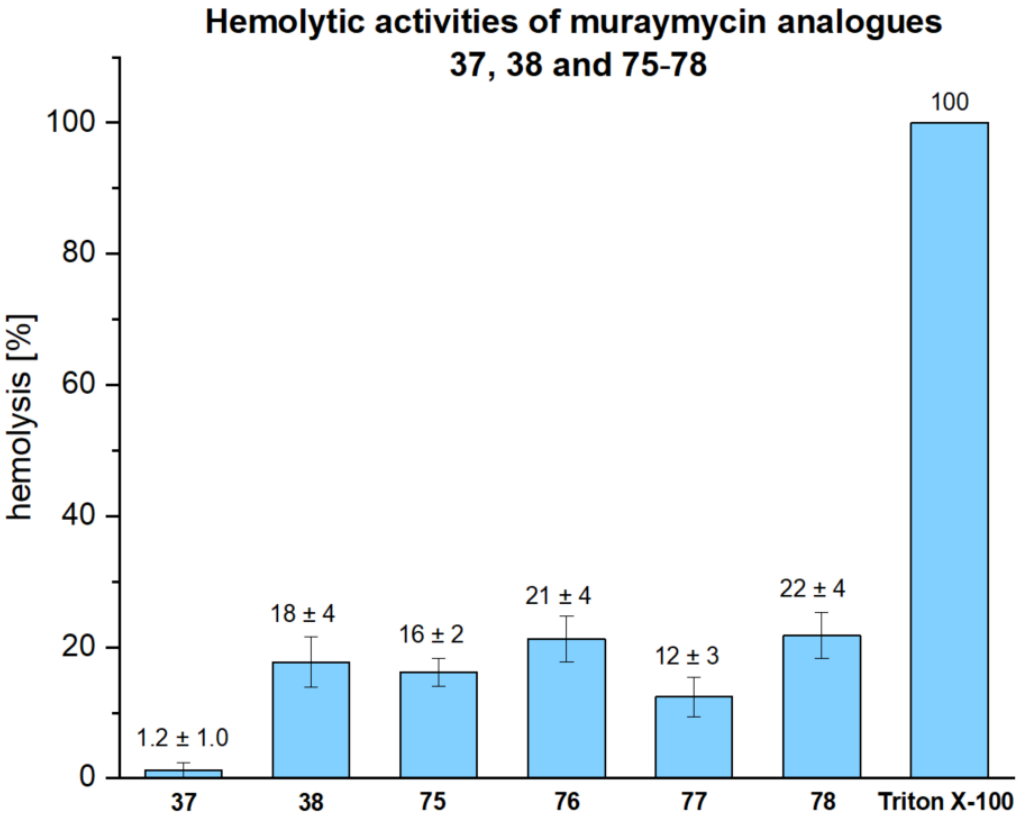

*Figure 4.48: Hemolytic activities of muraymycin analogues **37**, **38** and **75**-**78**[239] at a concentration of 20 µM.*

Compound **38** exhibited 18 ± 4% hemolysis at a concentration of 20 µM (Figure 4.48). This analogue has been reported by Ichikawa and Matsuda[183] and served as reference in this series. Muraymycin analogue **78**, which lacks the aminoribose in the 5'-position and bears a carboxylic unit instead (Figure 4.47), showed similar hemolytic effects (22 ± 4%). Hence, the presence or absence of the aminoribose moiety in the 5'-position did not seem to affect hemolysis. The second guanidine moiety which is seen in compound **75** compared to analogue **78** (Figure 4.47) resulted in a hemolytic activity in the same range (16 ± 2%). The replacement of an arginine unit in **R** and the insertion of a guanidine moiety in the 5'-position as offered in compound **76** (Figure 4.47) did also not increase hemolytic activity significantly (21 ± 4%). A minor decrease in hemolytic activity was observed for compound **77** with 12 ± 3% hemolysis at a concentration of 20 µM (Figure 4.48). Compound **77** displayed a branched alkyl chain in **R** compared to analogue **76** (Figure 4.47). Thus, a branching of the alkyl chain slightly decreases hemolysis. The presence of an additional arginine unit in **R** was observed to reduce hemolysis even further by a factor of ~ 10, as demonstrated with compound **37** with 1.2 ± 1.0% hemolysis (Figure 4.48). Despite displaying a similar cytotoxicity (assays performed by the research group Prof. Dr. Kiemer, Pharmaceutical biologay, Saarland University), the hemolytic activitiy of analogue **37** was negligible in contrast to the literature-known reference **38**. Hemolytic effects of DMSO amounts as contained in each compound solution were not observed. The hemolytic data identified compound **37** as 'best-in-class compound' within this SAR study.

Overall, membrane-disruptive effects seem to depend on two structural motifs for this series of compounds: On the one hand, the number of guanidine functions seems to influence hemolytic activity. On the other hand, the presence of branched lipophilic side chains seems to have an impact on hemolytic effects of these muraymycin analogues.

In addition to the assays with a standardized concentration of 20 µM, hemolytic activities of the compounds relative to their antibacterial activity against *P. aeruginosa* with final concentrations of ~ 1-fold and ~ 4-fold MIC_{50} were investigated. Hemolysis assays were performed as described before. The results are depicted in Table 4.17.

*Table 4.17: Hemolytic activities of muraymycin analogues **37**, **38** and **75**-**78**[239] relative to their antibacterial activity against P. aeruginosa. "-" measurement not possible.*

	Antibacterial growth inhibition against *P. aeruginosa*		**Hemolysis [%]**	
Compound	**[µg/mL]**	**[µM]**	**@1-fold MIC_{50}**	**@4-fold MIC_{50}**
37	18	15	<1	26 ± 7
38	16	13	6.6 ± 1.0	65 ± 5
75	71	58	78 ± 11	-
76	>100	>100	83 ± 3	86 ± 6
77	34	35	29 ± 4	93 ± 1
78	>50	52	38 ± 7	90 ± 5

Incubation with the corresponding compound in a final concentration of ~ 4-fold MIC_{50} resulted in significantly higher hemolytic activities as compared to the appropriate incubation in a final concentration of ~ 1-fold MIC_{50} for all compounds except for compound **76** (Table 4.17). This muraymycin analogue **76** exhibited the same hemolytic activity at concentrations of ~ 1-fold MIC_{50} (100 µM) with 83 ± 3% and ~ 4-fold MIC_{50} with 86 ± 6% hemolysis (Table 4.17). The most pronounced difference within a compound's measurement was observed for reference compound **38** with 6.6 ± 1.0% hemolytic activity at a concentration of ~ 1-fold MIC_{50} and 65 ± 5% hemolysis at a concentration of ~ 4-fold MIC_{50} (Table 4.17). Strikingly, hemolytic activities of analogues **75** and **78** significantly differed at ~ 1-fold MIC_{50} which is observed in the same micromolar concentration (Table 4.17). While compound **75** showed 78 ± 11% hemolysis at a concentration of ~ 1-fold MIC_{50}, 38 ± 7% hemolysis was observed for compound **78** (Table 4.17). Hemolysis assays with analogue **76** at a concentration of ~ 4-fold MIC_{50} was not possible because not enough material was available. No hemolytic activitiy was observed for the 'best-in-class compound' **37** at final concentration of ~ 1-fold MIC_{50} (15 µM). At a final concentration of ~ 4-fold MIC_{50} (60 µM), analogue **37** showed 26 ± 7% hemolysis (Table 4.17). This result was in the same range as for compounds **75** und **77** at a concentration of ~ 1-fold MIC_{50} (Table 4.17). This underlined the beneficial properties of compound **37**. The DMSO amounts in the samples did not reveal hemolytic effects in the assays. In summary, these

further studies confirmed the hypothesis of membrane-disruptive modes of action in terms of hemolytic effects.

4.1.3.3 Hemolytic activity of compounds with activity against *S. aureus*

Muraymycin analogues **48**, **49** and **79** provided by Dr. M. Wirth[243] were investigated towards their membrane-disruptive effects. Compound **80** was included in this series for completion of the SAR studies of Dr. M. Wirth[243] besides two naturally occurring muraymycins: The ω-hydroxyguanidino functionalized muraymycin **A1** (MIC_{50} = 18 µg/mL)[278] and muraymycin **B8** (respresenting the most antibacterially active compound against *S. aureus* with MIC_{50} = 2 µg/mL)[165]. The analogues are depicted in Figure 4.49**.**

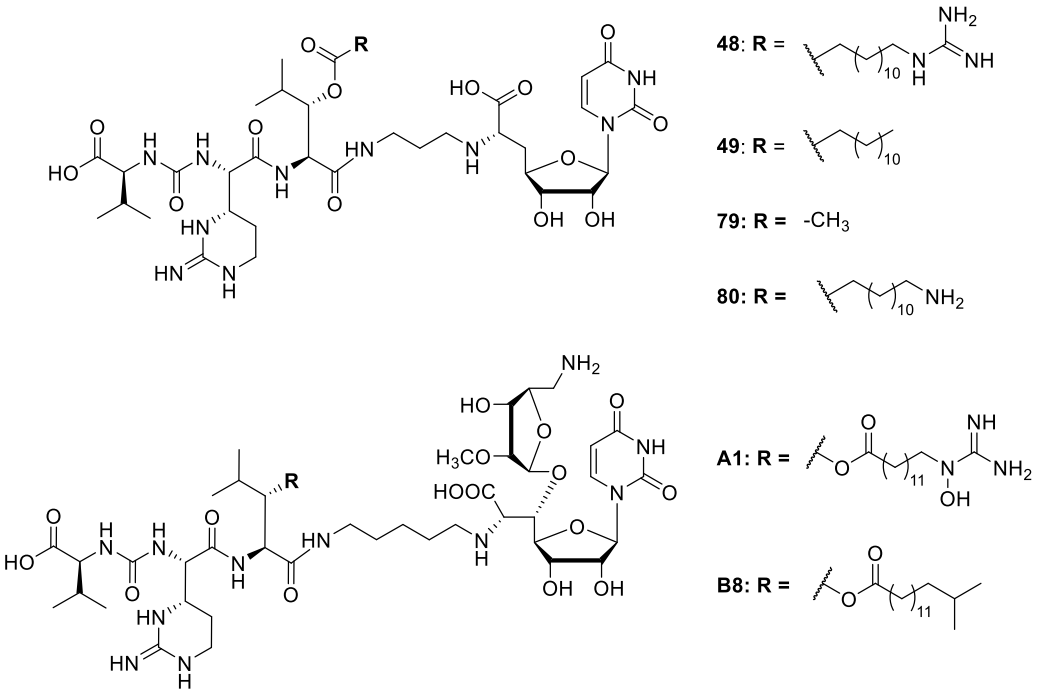

*Figure 4.49: Muraymycin analogues **48**, **49**, **79** and **80** by Dr. M. Wirth (above)[243] and naturally occurring muraymycins **A1** and **B8** (below)[164] for hemolysis assays.*

An erythrocyte suspension was prepared as described before. Mixtures containing 95 µL erythrocyte suspension and 5 µL compound solution in PBS (final concentration = 20 µM) were incubated (37 °C, 1 hour). Mixtures were centrifuged and the absorbance of the supernatant was measured. The results are presented in Table 4.18.

*Table 4.18: Hemolytic activities of muraymycin analogues **48**, **49**, **79** and **80**[243] and naturally occurring muraymycins **A1** and **B8**[164] at a concentration of 20 µM.*

Compound	Hemolysis [%] @20 µM
48	1.1 ± 0.1
49	<1
79	<1
80	<1
muraymycin A1	<1
muraymycin B8	1.2 ± 0.1

Hemolytic activities of analogues **79** and **80** were not observed (<1%) at a concentration of 20 µM (Table 4.18). Hemolysis assays with compound **48** resulted in 1.1 ± 0.1% hemolysis (Table 4.18). Muraymycin analogue **49** represented the 'best-in-class compound' within this SAR study with its antibacterial activity against *S. aureus* in the three-digit nanomolar range (Figure 4.18). Hemolytic activity was not observed for this compound (<1%) at a concentration of 20 µM (Table 4.18). The naturally occurring muraymycin **A1** did also not reveal a hemolytic activity (<1%) at a concentration of 20 µM (Table 4.18). For muraymycin **B8**, hemolysis was detected with 1.2 ± 0.1% at a concentration of 20 µM (Table 4.18). Both naturally occurring muraymycins were included in these assays due to high structural similarity to the target compounds of Dr. M. Wirth.[243] Muraymycin analogue **49** represented the simplified form of naturally occurring muraymycin **B8** (Figure 4.49). The beneficial properties of this 'best-in-class compound **49** would have been further improved in case of membrane-disruptive modes of action of naturally occurring muraymycin **B8**, which have not been observed. However, the abscence of hemolysis of muraymycin analogues **49** strenghtend its beneficial properties in any case. Hemolytic effects of DMSO amounts as contained in each compound‘s solution were not observed. In summary, muraymycin analogues **48**, **49**, **79** and **80** did not seem to act as membrane disrupters. The non-proteinogenic L-epicapreomycidine which is present in all compounds **48**, **49**, **79** and **80** did not influence hemolytic activities. Furthermore, variations in the peptide-containing moiety also seem to be well tolerated in terms of possible toxic side-effects caused by membrane disruption. Further hemolysis experiments in relation to the antibacterial growth inhibition data of the analogues were not performed.

4.1.3.4 Hemolytic activity of muraymycin conjugates

Hemolytic activities of selected muraymycin conjugates synthesized by Dr. C. Rohrbacher[240] were investigated in the following studies. Muraymycin streptomycin conjugates **81** and **82**, muraymycin GuCOSS conjugates **39** and **83** as well as muraymycin CPP conjugate **40** were used (Figure 4.50).[240]

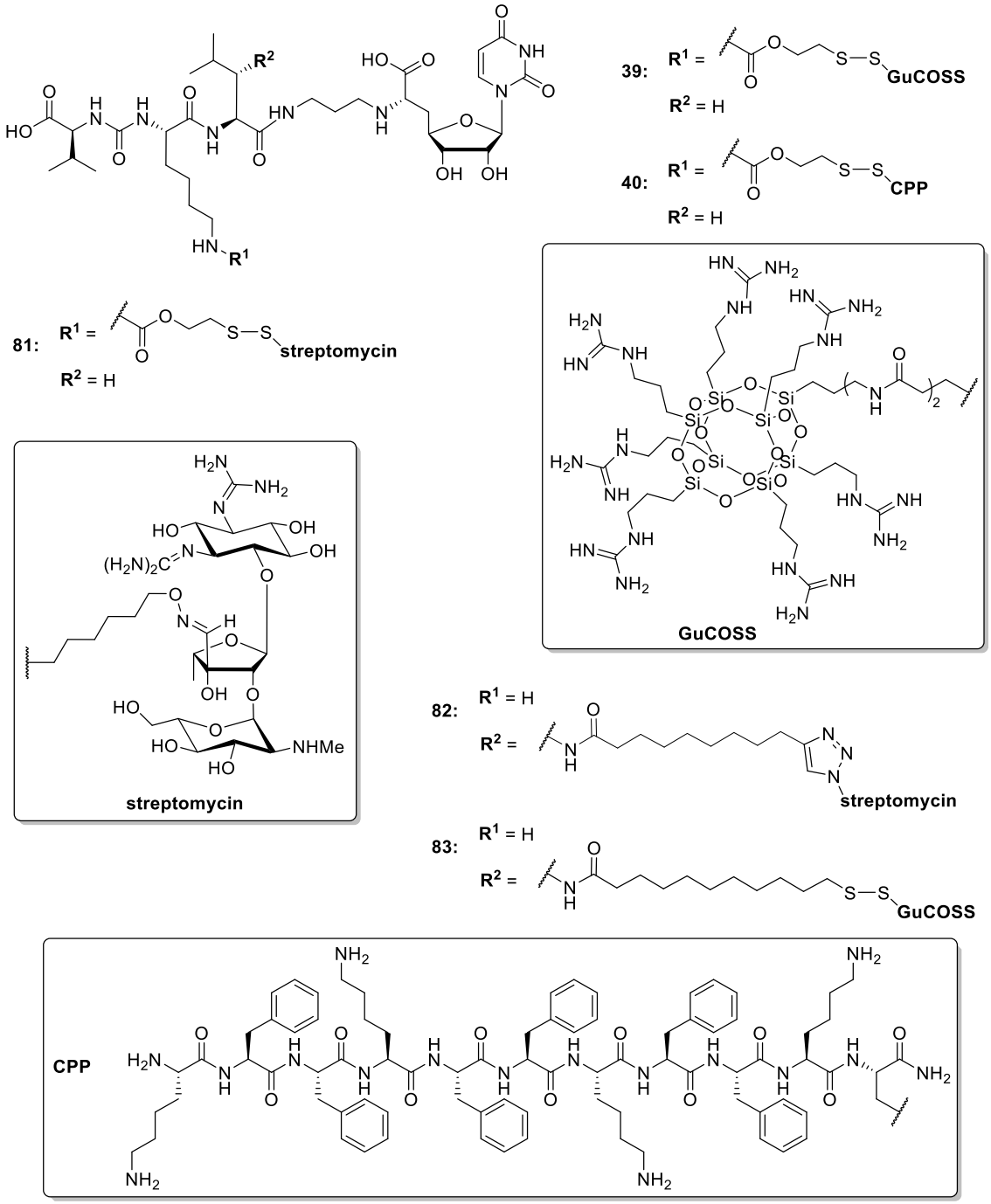

*Figure 4.50: Muraymycin streptomycin conjugates **81** and **82**, muraymycin GuCOSS conjugates **39** and **83** and muraymycin CPP conjugate **40** by Dr. C. Rohrbacher[240] for hemolysis assays.[240]*

The investigation of possible membrane-disruptive effects was of special interest because adsorption to membranes is possible for these conjugates (indicated by previous results for the GuCOSS conjugate **39** and the CPP conjugate **40**, cf. Chapter 4.1.1.1.2). This objective was related to the highly charged moieties being attached to the muraymycin core and was further evaluated in the hemolysis assays. The antibacterial growth inhibition data of these compounds underlined the importance of these experiments since they might be caused by unspecific binding to membranes as well.

An erythrocyte suspension was prepared as described before. Mixtures containing 95 µL erythrocyte suspension and 5 µL compound solution in PBS (final concentration = 20 µM) were incubated (37 °C, 1 hour). Mixtures were centrifuged and the absorbance of the supernatant was measured. The results are presented in Table 4.19.

*Table 4.19: Hemolytic activities of muraymycin streptomycin conjugates **81** and **82**, muraymycin GuCOSS conjugates **39** and **83** and muraymycin CPP conjugate **40**[240] at a concentration of 20 µM.*

Compound	Hemolysis [%] @20 µM
39	<1
40	<1
81	<1
82	<1
83	<1

Strikingly, hemolytic activity was not detected for any of the muraymycin conjugates (<1%) at a concentration of 20 µM (Table 4.19). The same applied for the DMSO amounts as contained in each compound solution. The absence of hemolytic effects strengthened the conjugate strategy. Further hemolysis experiments in relation to the antibacterial growth inhibition data of the analogues were not performed.

4.1.3.5 Hemolytic activity of non-nucleoside MraY inhibitors

The two non-nucleoside MraY inhibitors **41** and **42** with antibacterial activities were examined in the hemolysis assay. Compound **74** as another novel target compound was added to this series of measurements. All compounds were provided by the research group of Dr. S. Roy. Membrane-disruptive effects are possible because these compounds represent amphiphilic molecules. Compounds **41**, **42** and **74** vary in position **R**: analogue **41** bears a chloride, analogue **42** exhibits a hydroxy unit and analogue **74** contains a nitro group. The inhibitors are depicted in Figure 4.51.

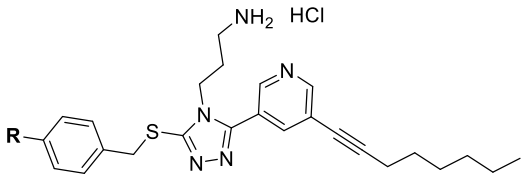

41: **R** = Cl
42: **R** = OH
74: R = NO_3

*Figure 4.51: Non-nucleoside MraY inhibitors **41**, **42** and **74** by the research group of Dr. S. Roy for hemolysis assays.*

An erythrocyte suspension was prepared as described before. Mixtures containing 95 µL erythrocyte suspension and 5 µL compound solution in PBS (final concentration = 20 µM) were incubated (37 °C, 1 hour). Mixtures were centrifuged and the absorbance of the supernatant was measured. The results are presented in Table 4.20.

*Table 4.20: Hemolytic activities of non-nucleoside MraY inhibitors **41**, **42** and **74** at a concentration of 20 µM.*

Compound	Hemolysis [%] @20 µM
41	<1
42	<1
74	<1

None of the compounds **41**, **42** and **74** exhibited hemolytic activities (<1%) at a concentration of 20 µM (Table 4.20). Hemolytic effects of DMSO amounts as contained in each compound solution were not observed. The beneficial biological properties of these analogues, i.e. broad spectrum activity and resonable bacterial cellular uptake into Gram-negative *E. coli* Δ*tolC*, were underlined with no hemolytic effects. This type of non-nucleoside analogues seems to be promising for the development of further potential MraY inhibitors as discussed before (Chapters 4.1.1.1.3 and 4.1.2.1). Further hemolysis studies in relation to the antibacterial growth inhibition data of the analogues were not performed.

4.1.4 Porcine liver esterase activity assays

Two compounds provided by the research group of Prof. Dr. W. Dehaen (Department of Chemistry, KU Leuven, Belgium) termed “dye 4” and “dye 6” were used at the beginning of the studies to demonstrate the proof of concept with regard to our objectives. Chemical structures of the dyes cannot be presented in this work due to confidentiality.

Each assay was performed as follows: A mixture of dye solution, PLE solution and phosphate buffer was prepared. Fluorescence intensity was measured at room temperature in 30 second intervals for 1 hour with orbital shaking before the first measurement and between the

measurements. Differing parameters or adaptions of this procedure will be individually listed for the experiments. The final concentration of PLE in phosphate buffer was 35 nM when using dye 4. For dye 6, PLE was applied in a final concentration of 1.3 µM. The concentration of PLE differed in the reaction mixture of both dyes in accordance to our collaborators. The first assay contained dye 4 in a final concentration of 10 µM. DMSO was used as a negative control. The results are presented in Figure 4.52.

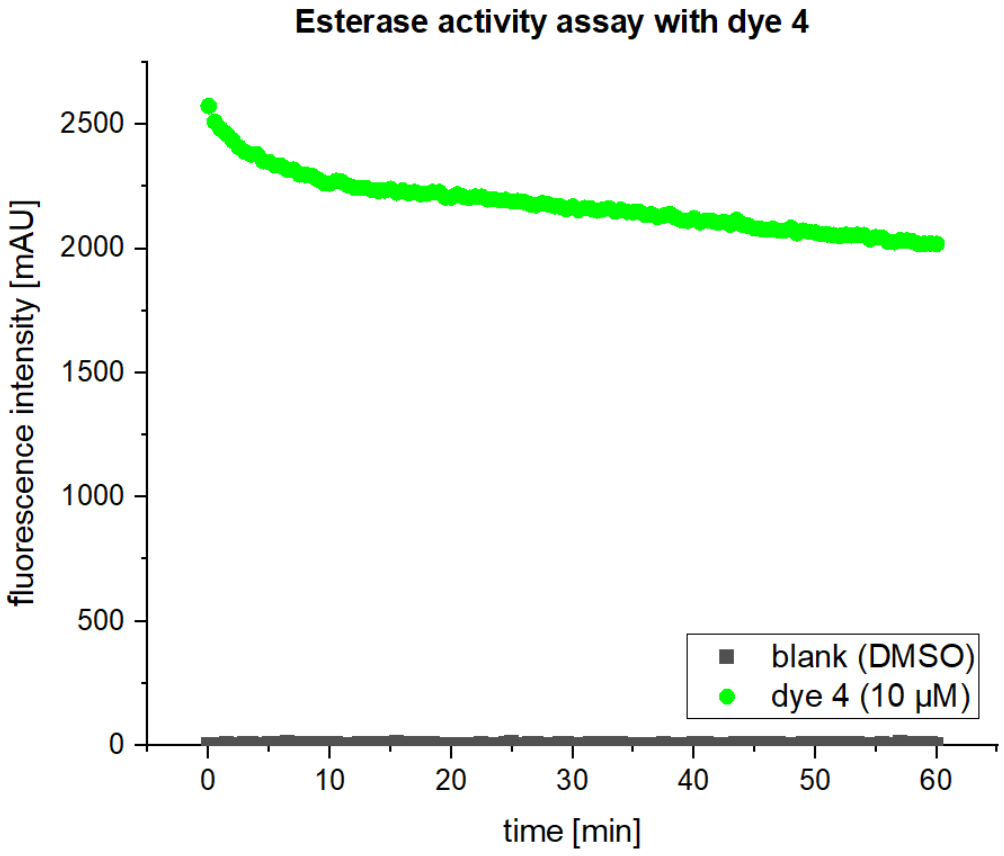

Figure 4.52: PLE assay with dye 4 in a concentration of 10 µM and PLE in a concentration of 35 nM. DMSO was used as a negative control.Fluorescence intensity was plotted as a function of time.

The application of dye 4 resulted in a logarithmic decay of fluorescence during the enzymatic reaction (Figure 4.52). However, the decay in fluorescence even after 1 hour of incubation time has already been noticed to be relatively limited regarding enzymatic reactions with esterases in general. Next experiment was performed in analogous fashion with dye 6 (10 µM). The results are presented in Figure 4.53 and revealed a hyperbolic fluorescence increase in contrast to dye 4 before. According to our collaborators, however, the intensity of fluorescence over time should decrease as well for dye 6.

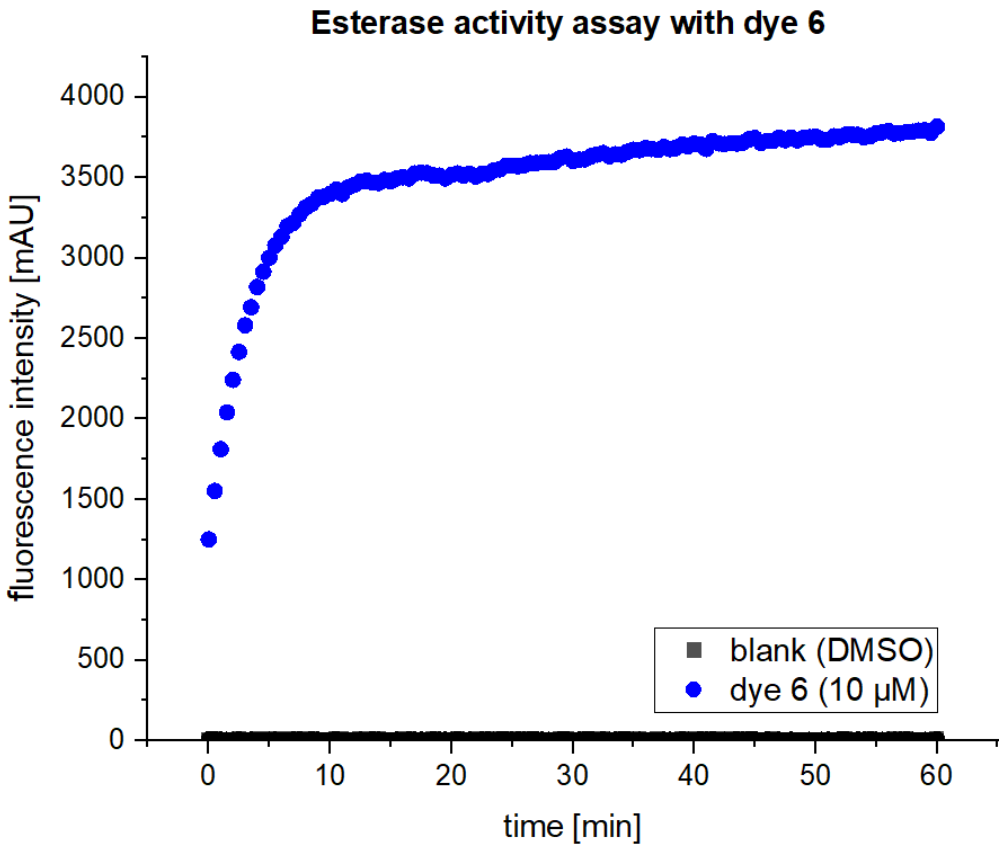

Figure 4.53: PLE assay with dye 6 in a concentration of 10 µM and PLE in a concentration of 13 µM. DMSO was used as a negative control. Fluorescence intensity was plotted as a function of time.

Due to the outcome of the performed experiments, a parameter on the plate reader termed ‘gain adjustment/value’ came into the fore. Initial experiments (Figure 4.52 and 4.53) were carried out with a low gain value in accordance to our collaborators who also used low gain values at their fluorimeter. The gain value was set to 400 at our plate reader, whereas no quantitative value was available at our collaborator's fluorimeter.

The next experiments therefore dealt with this parameter to examine its influence on the assay and the results. An increased ‘gain value’ was used for the following experiments. Otherwise, the experiments were performed as described before. The results are depicted in Figure 4.54 for both dyes. A fluorescence decrease was observed for dye 4 (Figure 4.54), thus confirming previous data (Figure 4.52). Fluorescence values were significantly higher in the experiment compared to the previous ones, whilst showing a comparable decay trend. However, the decay in fluorescence during the enzymatic reaction was comparable to the results before and still not pronounced (Figure 4.54). Fluorescence values obtained for dye 6 were slightly higher relative to dye 4, but showed a decay in fluorescence during the enzymatic reaction as it would be expected and confirmed by our collaborators (Figure 4.54). Nevertheless, the opposite result has been obtained in the assay before for dye 6 (Figure 4.53) with a lower ‘gain value’

of 400. Further modifications were performed in exchange with our collaborators. However, assay limitations were indicated.

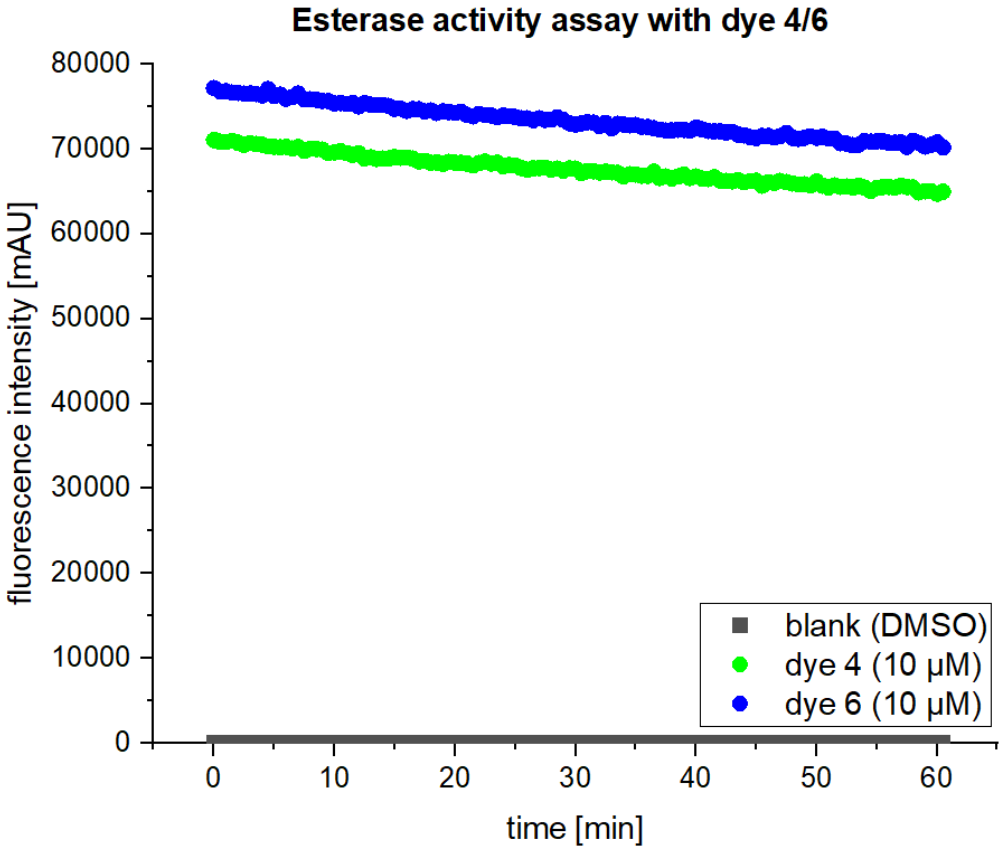

Figure 4.54: PLE assays with dyes 4 (green) and 6 (blue) in a concentration of 10 µM each. PLE concentration was 35 nM for dye 4 and 13 µM for dye 6. DMSO was used as a negative control. Fluorescence intensity was plotted as a function of time.

Next assays were performed in a detergent containing buffer. An improved solubility of both dyes as well as better product formation during the enzymatic reaction was envisioned with a detergent included in the buffer. Enhanced product formation would result in pronounced fluorescence changes during the enzymatic reaction that would be beneficial with regard to our objectives of the assay. Triton X-100 was used as detergent in a concentration of 0.5% (v/v). The investigation of possible interactions between Triton X-100 and different biological media such as cell lysates, in which we envision to determine esterase activity, would be required prior to final assay establishment in our laboratory. However, reproducible results in terms of fluorescence courses, i.e. increase or decrease, were initially focused on in the assays. Next experiments were performed as described before with the modified buffer, whilst leaving the higher ‘gain value’ of 700. The results are depicted in Figure 4.55 for both dyes.

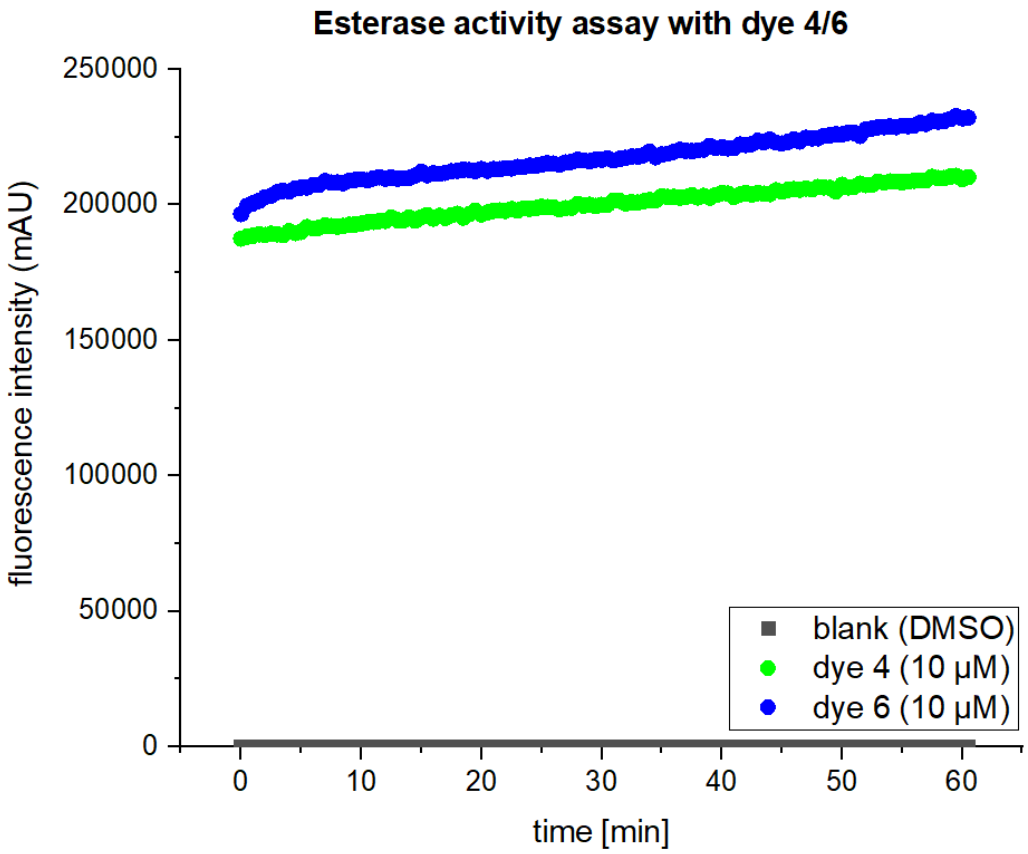

Figure 4.55: PLE assays with dyes 4 (green) and 6 (blue) in a concentration of 10 µM each. PLE concentration was 35 nM for dye 4 and 13 µM for dye 6. A Triton X-100-containing buffer was used. DMSO was used as a negative control.Fluorescence intensity was plotted as a function of time.

A fluorescence increase was observed for both dyes under these conditions (Figure 4.55). This was astonishing in many aspects. This behavior of dye 4 was observed for the first time while the other experiments resulted in fluorescence decrease (Figure 4.52 and 4.54). The inverted effect for dye 4 might be related to the implementation of Triton X-100 in the buffer which represented the only difference compared to previous assays. However, the results were not reproducible. The flourescence increase for dye 6 was in agreement to the experiment when using phosphate buffer without detergent (Figure 4.53). However, the results should be inverted as mentioned before. Overall, the results for dye 6 were also not consistent and reproducible.

Due to these variable results, we decided to terminate this project. The dependence of the dyes on multiple parameters was a major concern. Furthermore, the relatively limited decay in fluorescence was a major concern with regard to our objectives. The signal approaches a fairly high value of fluorescence even at a prolonged incubation period. A first suspected product inhibition was ruled out due to our collaborators since the product of the enzymatic reaction itself acts as fluorophor, but to a lesser extent than the substrate. In case of a 1 hour enzymatic reaction, e.g., the half-lives of the dyes in this experimental set-up could be estimated with

~ 10 minutes (dye 4) and <5 minutes (dye 6) based on the obtained data. This would characterize dye 6 as the more suitable compound for the determination of esterase activity as incubations with PLE should result in half-lives of a few minutes. However, a rather high fluorescence at the endpoint of the reaction might result in a bad signal-to-noise ratio when applying the sample to a complex mixture such as plasma or a cell lysate. The samples could be significantly more stable in complex biological media since incubations with PLE would represent an ideal setting for esterase-mediated reactions. Hence, the detection of a reliable fluorescence decay under these conditions might be limited. As demonstrated with these studies, an intensive optimization of the assay conditions would be required to accompany our objectives. The provided assay protocol by the research group of Prof. Dr. W. Dehean could not be accomplished within this work under these conditions. However, the assay represents a promising tool for prodrugs in the fields of muraymycins and therapeutic oligonucleotides and was therefore outsourced for separate studies.

4.2 Synthesis of novel muraymycin prodrugs

The following chapter deals with the synthesis of novel muraymycin prodrugs. It starts with the synthesis of required reagents and precursors followed by the synthesis of the three building blocks for the POM prodrug approaches: the urea dipeptide **54**, different chloroformates **55**-**57** and the nucleosyl amino acid building block **53**. The synthesis of the latter is well established in our research group. Nonetheless, it will be described in detail in the following since this building block served as a key intermediate in this work. It also represents a major part of this work and its synthesis was partially optimized. Some of the represented results were compiled as part of my supervision of the research assistant M. Ajdari Rad, a bachelor thesis by H. Rolshausen[279] and two internships by P. Ries and L. Thilmont.

4.2.1 Synthesis of reagents and precursors

Following, the synthesis of POM-I **62**, IBX **60** and the POM ester phosphonate **58** required for the nucleosyl building block will be described and discussed.

4.2.1.1 Synthesis of POM-I 62

Esterification of carboxylic acid moieties with POM units is characteristic for the design of the novel muraymycin prodrugs **50**-**52** in this work. This was realized with POM-I **62** which was obtained by a Finkelstein reaction of the less reactive pivaloyloxymethyl chloride (POM-Cl) **84** with sodium iodide in MeCN at room temperature for 21 hours.[280] The purification via distillation was performed in the absence of light due to the instability of POM-I **62** in order to avoid radical formation. The reaction is depicted in Scheme 4.1.

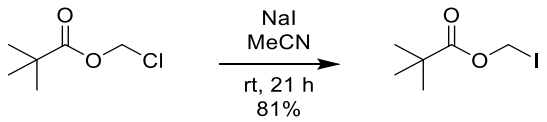

84 **62**

*Scheme 4.1: Synthesis of POM-I **62**.*

It is crucial to start the distillation under atmospheric pressure to remove MeCN first. Once the temperature has dropped, a vacuum rectification needs to be carried out under extreme caution. Considering this procedure, a slight carry-over of POM-I **62** by MeCN was observed, but this loss was neglectable and can be attributed to the complex distillation. No trace of POM-Cl **84** could be detected in the product by NMR spectroscopy. The equilibrium shift in Finkelstein reactions on the product side generally leads to good yields, being confirmed here with a yield of 81%. The product POM-I **62** was stored under inert gas at -26 °C to prevent decomposition.

4.2.1.2 Synthesis of IBX 60

IBX was used as oxidation reagent for the established mild oxidation of primary alcohols to their corresponding aldehydes. Its synthesis is based on a literature-known procedure with oxone® (2 $KHSO_5 \cdot KHSO_4 \cdot K_2SO_4$).[281] Therefore, 2-iodobenzoic acid **85** was heated with oxone® in water for 2.5 hours. The reaction mixture was cooled to 0 °C, leading to the precipitation of the desired product. Crystals were filtered off and IBX **60** was obtained in 69% yield. The reaction is depicted in Scheme 4.2.

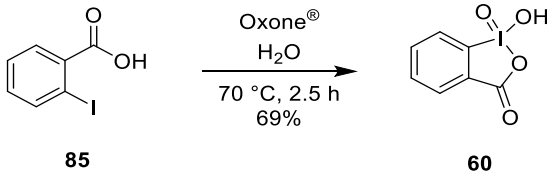

85 **60**

*Scheme 4.2: Synthesis of IBX **60**.*

This method is more convenient as a non-toxic reagent and solvent is used compared to the widely applied synthesis with potassium bromate.[282,283] IBX **60** was stored at -26 °C for several months without decomposition.

4.2.1.3 Synthesis of POM ester phosphonate 58

The POM ester phosphonate **58** is required for the Wittig-Horner reaction of the uridine-5'-aldehyde **13**, the key step within the synthesis of 5'-deoxy nucleosyl amino acids. Its synthesis is based on a literature-known method[202–205] and was further optimized by Dr. A. Spork[231] and Dr. D. Wiegmann[212]. It includes a Michaelis-Arbuzov-type reaction, followed by alkylation with POM-I **62** in four steps. The sequence is depicted in Scheme 4.3.

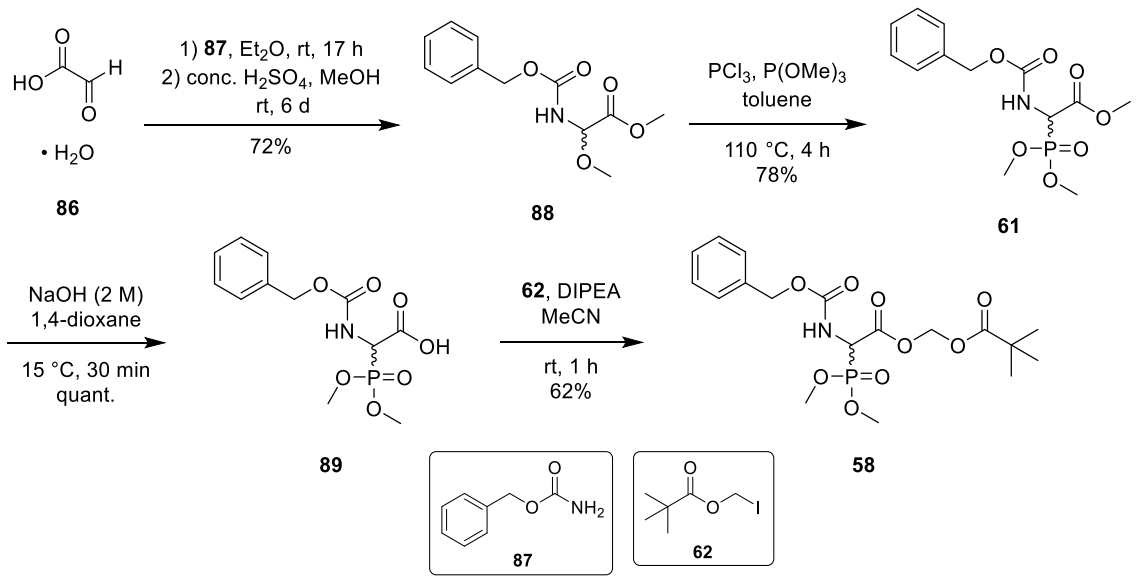

86 **88** **61** **89** **58** **87** **62**

*Scheme 4.3: Synthesis of POM ester phosphonate **58**.*

First, glyoxylic acid monohydrate **86** was combined in a condensation reaction with benzyl carbamate **87** in diethyl ether (Et_2O) at room temperature for 17 hours. Concentration of the solution *in vacuo* delivered a solid that was isolated by filtration. Methanol (MeOH) and catalytic amounts of concentrated sulfuric acid were added, and the reaction mixture was stirred at room temperature for 6 days. The desired methyl ester **88** was obtained in 72% yield. The following intermediate of this route, the *N*-Cbz-2-(dimethylphosphoryl) glycine methyl ester **61**, was synthesized by A. Heib[267] and E. Mareykin[284] and kindly provided for this work. Its synthesis is briefly described in the interest of completeness. Phosphorous trichloride was used as activation reagent to form a chlorinated intermediate, leading to the formation of **61** by a Michaelis-Arbuzov-type reaction with trimethylphosphite. The purification was done by recrystallization. Thereafter, the *N*-Cbz-2-(dimethylphosphoryl) glycine methyl ester **61** was saponified under basic conditions with aqueous sodium hydroxide in water and 1,4-dioxane as cosolvent to form **89**.[212] A full conversion was observed after 30 minutes by thin-layer chromatography (TLC). The pH value was adjusted with hydrochloric acid to pH = 2 during the aqueous workup, resulting in quantitative yields of the viscous intermediate **89**. Remaining solvents were completely removed by coevaporation with CH_2Cl_2 *in vacuo*. In a last step, the carboxylic acid of POM ester phosphonate **89** was deprotonated with *N*,*N*-diisopropylethyl-amine (DIPEA) and esterified with POM-I **62** by nucleophilic substitution to provide the desired POM ester phosphonate **58**. Initially, Dr. D. Wiegmann performed the esterification of the carboxylic acid with POM-Cl **84** and MeCN as solvent under light exclusion, resulting in a reaction time of 18 days and 17% yield.[212] The use of POM-I **62** instead led to an improvement of 1 hour reaction time and 63% yield.[212] These conditions were awere adopted for this work. Improving previous studies of Dr. D. Wiegmann,[212] pure CH_2Cl_2 was used instead of petroleum ether (PE):ethyl acetate (EtOAc) 4:6 to dissolve the crude product **58** for chromatographic purification with the aforementioned mixture of PE and EtOAc. The enhanced solubility in CH_2Cl_2 resulted in 62% yield of the desired POM ester phosphonate **58**. This yield was comparable to that of Dr. D. Wiegmann.[212] However, a lability of the POM ester phosphonate **58** towards acids was suggested since a greater loss was observed in attempts when sticking the product on silica gel during purification.

4.2.2 Synthesis of prodrug building blocks

Within this section, the synthesis of the three building blocks required for the formation of the POM prodrug approaches will be presented. First, the synthesis of the urea dipeptide **54** will be described. The synthesis of the chloroformates **55**-**57** with varying residues will be reported thereafter while the last part focusses on the synthesis of the nucleosyl amino acid **53**.

4.2.2.1 Synthesis of urea dipeptide 54

The L-valine- and L-lysine-containing urea dipeptide **54** was synthesized in four steps according to a route established by Dr. C. Schütz and Dr. D. Wiegmann.[212,252] An overview of the synthesis is given in Scheme 4.4.

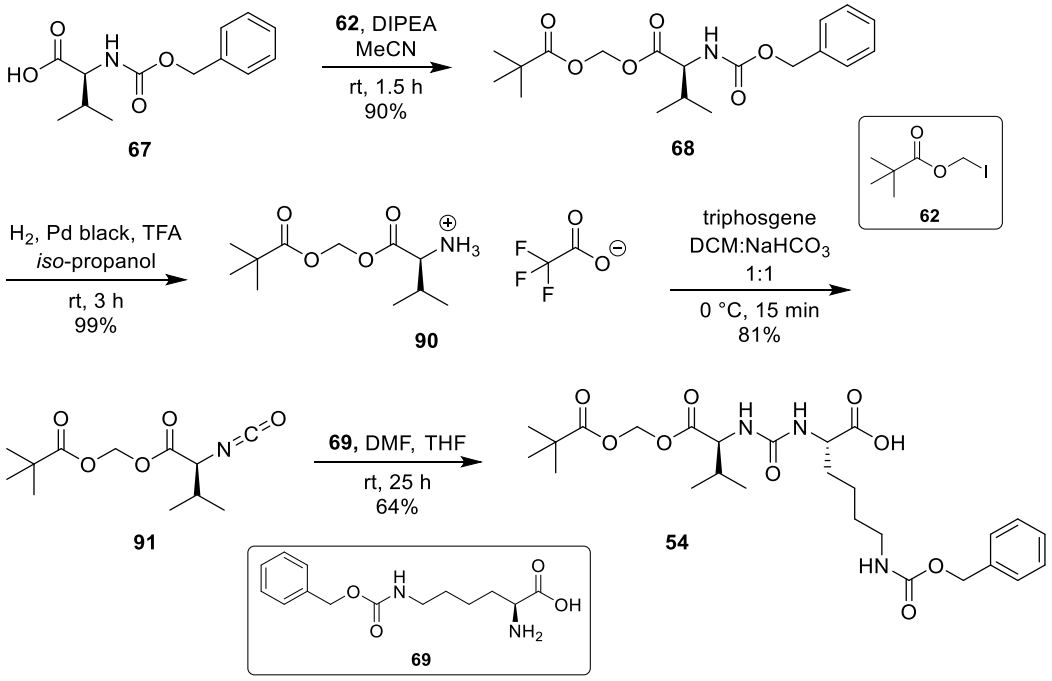

*Scheme 4.4: Synthesis of urea dipeptide **54**.*

In a first step, the POM functionality was added to the commercially available *N*-Cbz-protected L-valine **67**, leading to the formation of *N*-Cbz-L-valine POM ester **68**. This was realized by deprotonation of **67** with DIPEA and a subsequent nucleophilic substitution. The reaction was carried out at room temperature under light exclusion due to the photolability and radical formation of POM-I **62**. A full conversion was observed by TLC after 1.5 hours. The desired product **68** was obtained with 90% yield after chromatographic purification. Cbz-deprotection of the intermediate **68** was initially carried out under mild standard transfer hydrogenation conditions established in our research group, using 1,4-cyclohexadiene in *iso*-propanol under acidic conditions (TFA) to avoid the reduction of the nucleobase.[196] 1,4-cyclohexadiene serves as hydrogen source here. The use of *iso*-propanol circumvents cyclic side products as result of the formation of formaldehyde when MeOH served as solvent.[212] These conditions, however, resulted in impurities and an incomplete conversion of the desired product **90**, even after multiple hours of reaction time. Furthermore, partial decomposition of the desired product was observed after chromatographic purification. The reproducibility with regard to high purity and good yields demonstrated by Dr. D. Wiegmann could not be achieved here.[212] Therefore, adapted Cbz-deprotection conditions have been chosen. Since no other hydrogenable groups are present in compound **68**, a direct hydrogenation with hydrogen gas was chosen for the

reduction of the carbamate functionality of the Cbz-protecting group. For this step, TFA and catalytic amounts of palladium black were added to a solution of *N*-Cbz-L-valine POM ester **68** in *iso*-propanol under hydrogen atmosphere. A full conversion was indicated by TLC after a reaction time of 3 hours. The mixture was filtered through a syringe filter and the solvent was removed under reduced pressure. L-valine-POM-ester **90** was obtained in 99% yield as TFA salt, identified by ^{19}F NMR spectroscopy. As TFA salt, side reactions of the free primary amine of **90**, especially with the POM moiety, were suppressed in future reactions.[212] The next two steps of this sequence were established in our research group by Dr. C. Schütz.[252] The first one proceeded over an unstable isocyanate intermediate **91** by adding triphosgene under aqueous conditions with CH_2Cl_2 as cosolvent. Due to the toxicity of triphosgene which forms highly toxic phosgene *in situ*, the synthesis was carried out under extreme caution with equimolar amounts of triphosgene. The reaction mixture was stirred at 0° C for 20 minutes, extracted with CH_2Cl_2 and dried over sodium sulfate. *O*-POM-L-valine isocyanate **91** was obtained in 81% yield after carefully evaporating the solvent with the rotary evaporator at 50 mbar *in vacuo*. The crude product **91** was not dried in high vacuum as isocyanates are known to be volatile and unstable. Hence, the crude isocyanate **91** was directly converted into *O*-POM-L-valine-*N*-(C=O)-*N*-(*N*$^{\varepsilon}$-Cbz)-L-lysine **54** by coupling with the commercially available *N*$^{\varepsilon}$-Cbz-L-lysine **69**. Therefore, isocyanate **91** was dissolved in THF and a suspension of *N*$^{\varepsilon}$-Cbz-L-lysine **69** in *N*,*N*-dimethylformamide (DMF) was added dropwise. The reaction mixture was stirred at room temperature for 24 hours. After aqueous workup and chromatographic purification, the desired product **54** was obtained in 64% yield.

4.2.2.2 Synthesis of chloroformates 55-57

The carbamate functionality will be included in the target compounds **50**-**52** by synthesizing the benzyl chloroformates **55**-**57** in three steps according to the literature.[254,255] The reaction sequence includes an esterification (Scheme 4.5), a reduction (Scheme 4.6) and the formation of the corresponding acid chlorides (Scheme 4.7). The first two steps of this sequence will be described in detail for the acetate-containing derivative, respectively. The third step will be presented for the pivalate-containing derivative as model compound.

4.2.2.2.1 Synthesis of 4-formylphenyl derivatives 92-94

Acetyl chloride **71** and triethylamine were added to a solution of 4-hydroxybenzaldehyde **70** in THF. The reaction mixture was cooled to 0 °C and stirred at room temperature for 2.5 hours. After removing the solvent *in vacuo*, the desired product **92** was obtained in 99% yield without further purification. The reaction for each derivative is depicted in Scheme 4.5.

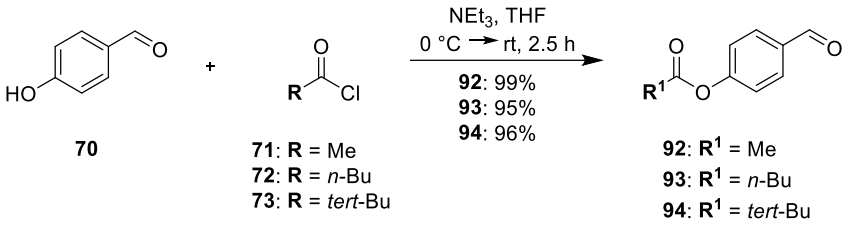

*Scheme 4.5: Synthesis of 4-formylphenylacetate **92**, -butyrate **93** and -pivalate **94**.*

The formation of 4-formylphenylbutyrate **93** was carried out with butyryl chloride **72**. The same reaction conditions provided the desired product **93** in 95% yield. Pivaloyl chloride **73** was used for the formation of 4-formylphenylpivalate **94** which was obtained in 96% yield.

4.2.2.2.2 Synthesis of 4-(hydroxymethyl)-phenyl derivatives 95-97

For subsequent reduction, 4-formylphenylacetate **92** was solved in THF and cooled to 0 °C. Sodium borohydride, serving as reducing agent, was added in excess (1.5 eq.) to the solution. The reaction mixture was allowed to warm to room temperature and stirred for 3 hours. After dilution with EtOAc, a saturated ammonium chloride solution was carefully added whilst the flask being cooled to counter the exothermic nature of the reaction. Following workup and purification by column chromatography delivered the desired 4-(hydroxymethyl)-phenylacetate **95** in 81% yield. The reaction for each derivative is presented in Scheme 4.6.

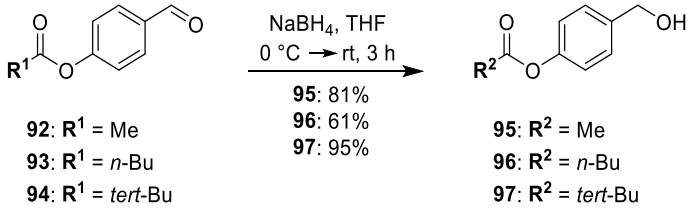

*Scheme 4.6: Synthesis of 4-(hydroxymethyl)-phenylacetate **95**, -butyrate **96** and -pivalate **97**.*

The same conditions provided the corresponding butyrate-containing derivative **96** in 61% yield. In contrast, 4-(hydroxymethyl)-phenylpivalate **97** was obtained in a yield of 95%. Although the same eluent mixture was used for the purification of **96**, multiple mixed fractions were obtained. These mixed fractions caused the loss in material compared to the two other phenyl derivatives **95** and **97** but since enough material was obtained, the chromatographic purification was not further optimized.

4.2.2.2.3 Synthesis of 4-(pivaloxy)-benzylchloroformate 57

The last step includes the chloroformate formation that is depicted in Scheme 4.7. Therefore, triphosgene was added to a solution of 4-formylphenylpivalate **97** in toluene. The synthesis was carried out under extreme caution due to the toxicity of triphosgene. The reaction mixture was stirred at room temperature for 3 days. After removing the solvent under inert gas, the crude product **57** was isolated in quantitative yields. A purification by column chromatography

as reported in the literature[255] has not been carried out to prevent the product's decomposition. Due to this matter, the desired 4-(pivaloxy)-benzylchloroformate **57** was always synthesized freshly and stored under inert gas at -26 °C before coupling with the nucleosyl amino acid core. With regard to its instability, storage time never exceeded a day.

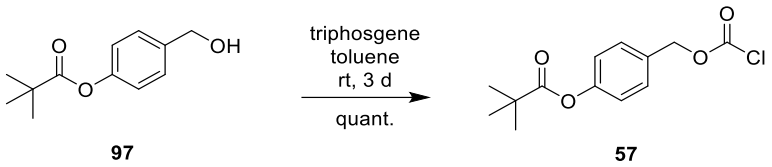

97 **57**

*Scheme 4.7: Synthesis of 4-(pivaloxy)-benzylchloroformate **57**.*

As mentioned, the suitability of the initial route for the assembly of the desired carbamate POM prodrugs (Chapter 3.2.2) was investigated in this work. Therefore, only the pivalate-containing chloroformate derivative **57** was synthesized in its final step. It served as model compound as it represents the most stable derivative in this series. This has been demonstrated in previous studies of our research group.[285] The methyl- and butyryl-containing derivatives, however, were stored in their reduced form (Chapter 4.2.2.2.2) at -26 °C. It has to be said in advance that this route seemed to be attributed with several difficulties overall and further optimization is required. The following studies have been outsourced during this work for a separate Master thesis performed by L. Thilmont.[286]

4.2.2.3 Synthesis of nucleoside building blocks

The 5'-deoxy nucleosyl amino acid **53** represents an essential building block for the desired target structures **50**-**52**. Its synthesis will be on focus in the following sections. Prior to this, the synthesis of the linker-aldehyde **28** will be dealt with since the reductive amination of the nucleosyl amino acid core with a suitable linker-aldehyde represents another key step in the synthesis of the envisioned carbamate prodrugs.

4.2.2.3.1 Synthesis of the aldehyde 28 for reductive amination

The linker-aldehyde **28** was synthesized in three steps according to a literature-known method that has been established in our research group by Dr. A. Spork.[171,231,251] An overview of the synthesis is given in Scheme 4.8.

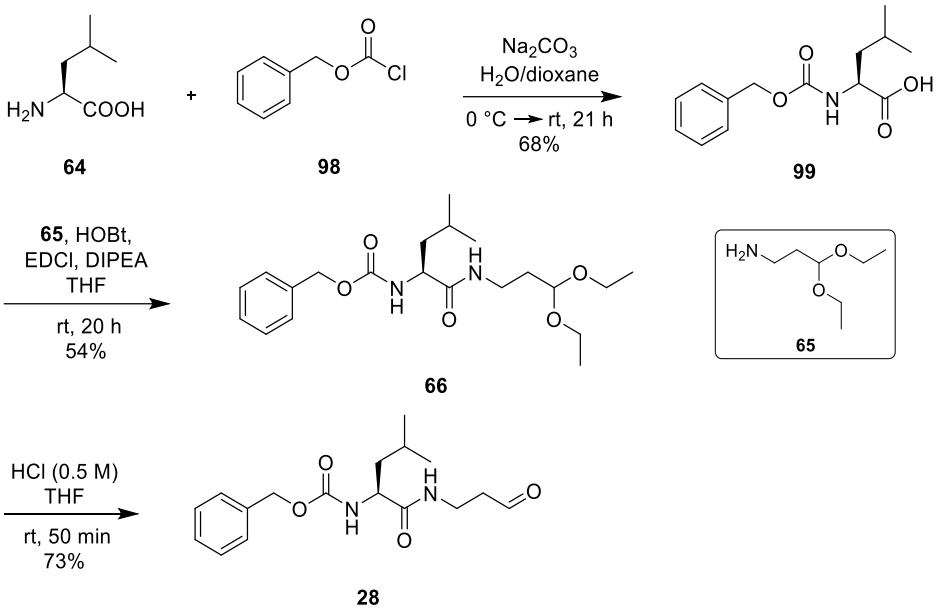

*Scheme 4.8: Synthesis of 2-N-(benzyloxycarbonyl)-1-N-(3'-oxopropyl)-L-leucine amide **28**.*

In a first step, L-leucine **64** was Cbz-protected in a mixture of 1,4-dioxane and water under basic conditions for providing N-Cbz-L-leucine **99**. Following, a solution of benzyloxycarbonyl chloride **98** in 1,4-dioxane was added dropwise at 0 °C within 30 minutes. The reaction mixture was allowed to warm to room temperature and stirred for 21 hours. The crude *N*-Cbz-L-leucine **99** was obtained in 68% yield without any further purification after workup. Next, the coupling reagents 1-hydroxybenzotriazole (HOBt) and 1-ethyl-3-(3-dimethylamino-propyl)carbodiimide (EDCl) hydrochloride were added to a solution of *N*-Cbz-L-leucine **99** in THF to form 2-*N*-Cbz-1-*N*-(3,3-diethoxypropyl)-L-leucine amide **66**. EDCI activates the carboxylic acid moiety of **99** which is subsequently converted into an ester by adding HOBt, thus preventing an irreversible acyl shift.[231] The resulting suspension was stirred at room temperature for 30 minutes. The envisioned acetal functionality in **66** was introduced by adding DIPEA and 1-amino-3,3-diethoxypropane **65** to the reaction mixture. The solution was stirred at room temperature for further 20 hours. After dilution, acidification of the organic layer with hydrochlorid acid and aqueous workup, the reaction mixture was dried over sodium sulfate. The solvent was removed *in vacuo* and the desired product **66** was obtained in 54% yield after column chromatography with triethylamine as modifier in the eluent mixture. As a last step, the acetal unit in **66** was cleaved under acidic conditions to yield the linker-aldehyde **28**. Therefore, intermediate **66** was dissolved in THF and aqueous hydrochloric acid (0.5 M) was added. The reaction mixture was stirred at room temperature for 50 minutes. For workup, the solution was diluted with saturated sodium bicarbonate, extracted with EtOAc and washed with brine. The reaction mixture was dried and the solvent was removed *in vacuo* for several hours. 2-*N*-(benzyloxycarbonyl)-1-*N*-(3'-oxopropyl)-L-leucine amide **28** was obtained with 73% yield after chromatographic purification and stored at -26 °C for several months without decomposition.

4.2.2.3.2 Synthesis of nucleoside amino acids

The most important building block of the tripartite approach for the stereoselective assembly of muraymycin analogues that has been developed in our research group (Chapter 2.4.3) is the uridine-derived 5'-deoxy-nucleosyl amino acid **53**. Its synthesis was carried out according to an optimized protocol and is described in Scheme 4.9.

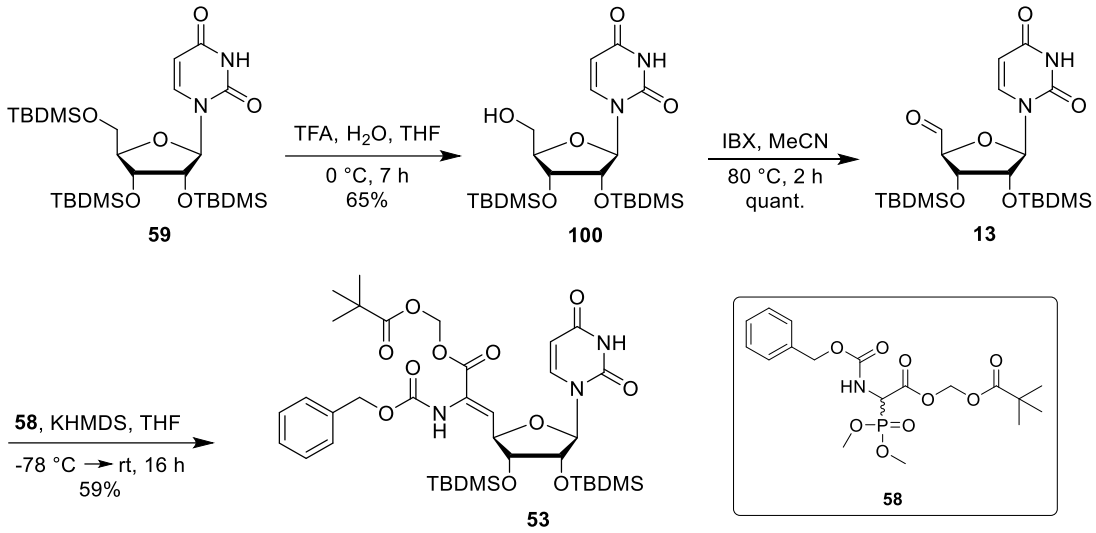

*Scheme 4.9: Synthesis of Z-uridinyl amino acid **53** from tris-TBDMS-protected uridine **59**.*

The fully TBDMS-protected uridine **59** was kindly provided by Dr. D. Wiegmann for this work.[212] In the interest of completeness, however, its synthesis will be briefly described. The commercially available uridine was coevaporated with the base pyridine. Subsequent silylation was performed with TBDMS chloride in excess (3.2 eq.). Imidazole served as activator. The reaction mixture was stirred at room temperature for 3 days. The fully TBDMS-protected uridine **59** was obtained after chromatographic purification.

The following selective TBDMS-deprotection of **59** in 5'-position was performed under acidic conditions with a mixture of TFA and water in equimolar amounts at 0 °C in THF according to the literature.[172] These conditions ensured the selective cleavage of the silyl ether at the primary hydroxy unit of uridine.[172] This reaction is upscalable to 10 g educt with reproducible yields as demonstrated by Dr. A. Spork in his studies.[231] The reaction was TLC-monitored and quenched with saturated sodium bicarbonate solution as soon as byproduct-formation was observed on the TLC plate. These byproducts correspond to the 2'- or 3'-desilylated product and occurred after a reaction time of 7 hours. The desired 2',3'-*O*-bis-TBDMS uridine-5'-alcohol **100** was obtained in 65% yield after workup and chromatographic purification (Scheme 4.9).

Subsequent oxidation to the inherently unstable uridine 5'-aldehyde **13** was carried out under mild, neutral conditions according to a method by Finney et al. with IBX as oxidizing agent.[184] Therefore, uridine-5'-alcohol **100** was dissolved in MeCN and IBX was added in excess

(2.5 eq.). The resulting suspension was heated under reflux. The reaction mixture was filtered, and the solvent was removed *in vacuo*. This workup was sufficient due to the insolubility of IBX and its side products in cold MeCN, also being beneficial regarding the instability of IBX. The labile uridine-5'-aldehyde **13** was obtained in quantitative yield and sufficient purity based on the ^{1}H NMR spectrum. To prevent its decomposition, subsequent Wittig-Horner reaction was always performed directly afterwards on the same day. Basic conditions were applied in the Wittig-Horner reaction, thus providing *Z*-olefin **53** out of uridine 5'-aldehyde **13** and POM-ester phosphonate **58**. Both educts were solved in THF and the solution of the latter was cooled to -78 °C. In parallel, a solution of the non-nucleophilic, sterically hindered base potassium hexamethyldisilazane in THF was prepared and also cooled to -78 °C. By combining both cooled solutions in equimolar amounts, the POM-ester phosphonate **58** was deprotonated. The reaction mixture was stirred at -78 °C for 10 minutes before adding the solution of 2',3'-*O*-bis-(*tert*-butyldimethylsilyl)-uridine-5'-aldehyde **13** in THF dropwise in excess (1.2 eq.). The *Z*-selectivity of this reaction with glycine-derived phophonates is described in the literature[287] and has also been confirmed in studies of our research group.[197] The excess of the labile aldehyde in the reaction mixture and a temperature of -78 °C prevent *E*/*Z*-isomerizations of the product. Furthermore, the *E*/*Z*-selectivity is extremely dependent on the rate of addition of the aldehyde to the reaction mixture, which needs to be performed slowly as Dr. A. Spork demonstrated in his studies.[231] The reaction mixture was allowed to warm to room temperature and stirred for 16 hours. After aqueous workup and chromatographic purification, (*Z*)-didehydro-POM-ester uridinyl-amino acid **53** was obtained in 59% yield (Scheme 4.9). None of the separated side products could be identified as *E*-isomer which is contrary to Wittig-Horner reactions with the *tert*-butyl ester phosphonate as Ducho et al. observed.[198] The Wittig-Horner reaction with the POM ester phosphonate **58** therefore seemed to work stereoselective in this work. This was contrary to studies by Dr. D. Wiegmann who observed the formation of both diastereomers (diastereomeric ratio (*d.r.*) 8:2 → 9:1) in several approaches under the same conditions.[212] In summary, the *Z*-configurated nucleosyl amino acid **53** was obtained in 35% yield over two steps.

The following homogenous asymmetric hydrogenation represented the most problematic reaction in this sequence. The stereochemical information in the 6'-position of the nucleosyl amino acid **53** was introduced in this step by applying the sensitive chiral rhodium(I) catalyst Me-DUPHOS-Rh in *S*-configuration **21** to yield (6'*S*)-6'*N*-Cbz-POM-ester uridinyl-amino acid **101**. The reaction is depicted in Scheme 4.10. The selective formation of L-amino acids from *Z*-olefins with (*S*,*S*)-Me-DUPHOS-Rh has been reported in the literature[207,208] and was confirmed by our research group via X-ray crystallography.[231] In contrast, the use of (*R*,*R*)-Me-DUPHOS-Rh with the *Z*-olefin leads to the formation of the corresponding D-amino acid. This combination legitimates the term „mismatched pair“ as the reaction takes significantly

longer and the required amount of catalyst increases.[207,208,231] However, good yields and high diastereoselectivity were still observed.[231]

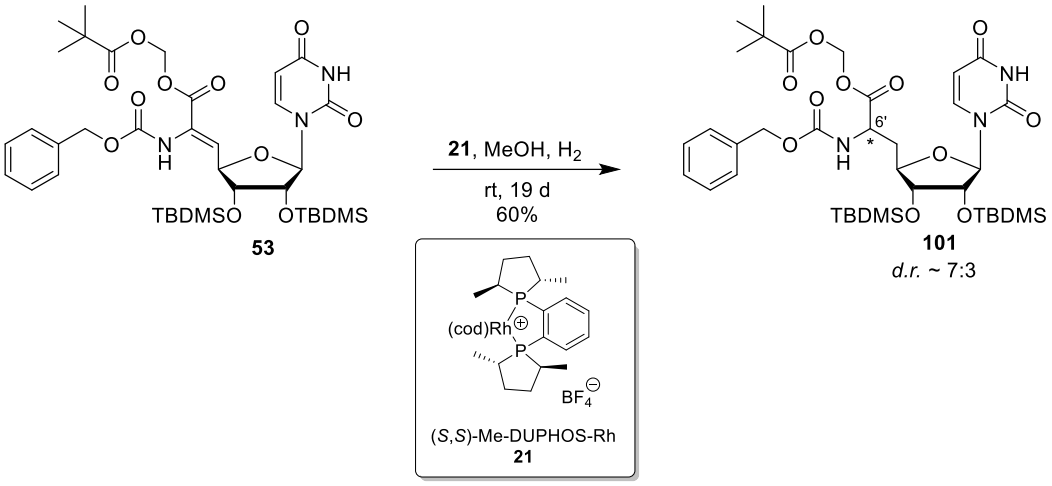

*Scheme 4.10: Synthesis of the (6'S)-nucleosyl amino acid **101** by asymmetric hydrogenation.*

Additional severe inert gas conditions were required for hydrogenation as (*S*,*S*)-Me-DUPHOS-Rh **21** is extremely labile towards oxygen and moisture. As a consequence, all glass equipment was dried multiple times by heating *in vacuo* and an argon atmosphere was used for flushing the flasks instead of nitrogen. The Z-olefin **53** was dissolved in MeOH and carefully degassed. A spatula tip of (*S*,*S*)-Me-DUPHOS-Rh **21** was added under an argon atmosphere. The flask was flushed with hydrogen (quality grade 6.0) and the reaction mixture was stirred at room temperature with a slight overpressure in the flask. The hydrogen atmosphere was renewed daily for avoiding any oxygen diffusion. Reaction control was done by ^{1}H NMR spectroscopy. The first NMR sample was taken after a reaction time of five days since hydrogenations with (*S*,*S*)-Me-DUPHOS-Rh usually take five to 14 days. For ^{1}H NMR spectroscopy, $CDCl_3$ was used as solvent contrary to Dr. D. Wiegmann who used benzene-d_6 in his studies.[212] This solvent replacement was due to a better comparison to the non-hydrogenated nucleosyl amino acid **53** whose ^{1}H NMR spectrum was recorded in $CDCl_3$ as well. Furthermore, the signals in the spectrum were better resolved. For $CDCl_3$ as solvent, a full conversion of **53** to **101** is indicated by a missing doublet (d) at around 6.13 ppm that corresponds to the proton at the 5'-position of the olefinic double bond. In case of incomplete conversion, an additional amount of (*S*,*S*)-Me-DUPHOS-Rh **21** was added to the flask which was again flushed with hydrogen and the reaction was further stirred at room temperature. As already mentioned, this reaction turned out to be a bottleneck for the synthesis of the three envisioned target structures **50**-**52** of this work. In a first attempt, the reaction was carried out in small scale (400 mg) with an older batch of the catalyst. A complete conversion was determined by ^{1}H NMR spectroscopy after 16 days of reaction time but the expected high stereoselectivity could not be achieved in this attempt. ^{1}H NMR spectroscopy of the purified product revealed a second set of signals that could be attributed to the formation of a different isomer (*d.r.* ~ 8:2). Since their separation

was not possible by column chromatography, the mixture was used for subsequent Cbz-deprotection and reductive amination with the linker-aldehyde **28**. It can already be mentioned in advance that a separation of the product mixture by chromatographic purification was possible after the latter. However, acidic silica gel induces decomposition of the dehydrogenated nucleosyl amino acid **101** which was also observed after long exposition to MeOH. These issues could explain the significant yield loss of this first attempt. Overall, the (6'*S*)-nucleosyl amino acid **101** was obtained in 21% yield. The reaction was repeated in bigger scale with freshly synthesized educts and a new batch of (*S*,*S*)-Me-DUPHOS-Rh **21** as well as new hydrogen gas. The glass equipment was dried as described above and the flasks were flushed with argon gas. This second approach was performed with ~ 2 g of nucleosyl amino acid **53** under the same conditions. However, even after a reaction time of 20 days with the catalyst being added twice and a daily renewal of the hydrogen atmosphere, only a small conversion of **53** could be observed. Hence, the reaction was interrupted and the educt was reisolated by column chromatography, resulting in the separation of two unidentified compounds which have never appeared before. Overscaling as an explanation was ruled out due to successful reactions performed by E. Mareykin at similar scales.[284] The third iteration was performed in analogy to the previous attempts, but again with a new batch of catalyst and a fast elution of the product on the silica gel to avoid decomposition. After 19 days of reaction time and a rapid chromatographic purification, the full conversion of **53** into its hydrogenated form was observed. Previous failures were attributed to low-grade catalyst batches, thus underlining the catalyst's sensitivity. The desired (6'*S*)-6'*N*-Cbz-POM-ester uridinyl-amino acid **101** was obtained in 60% yield in this attempt with a diasteroemeric ratio of *d.r.* ~ 7:3 based on ^{1}H NMR data. A section of the ^{1}H NMR spectrum of the (6'*S*)-nucleosyl amino acid **101** is shown in Figure 4.56. Strikingly, the proton of uridine in 6-position showed a low integration in the ^{1}H NMR spectrum (Figure 4.56) while the corresponding carbon atom was clearly detectable in the ^{13}C NMR spectrum. Since the NMR data indicated the *R*-isomer also being formed during hydrogenation and a bigger integration in the aromatic region was observed in the ^{1}H NMR spectrum, an overlay of the 6H-atom of the hydrogenated *Z*-olefin **91** and the aryl protons of the Cbz-protecting group was suggested (Figure 4.56).

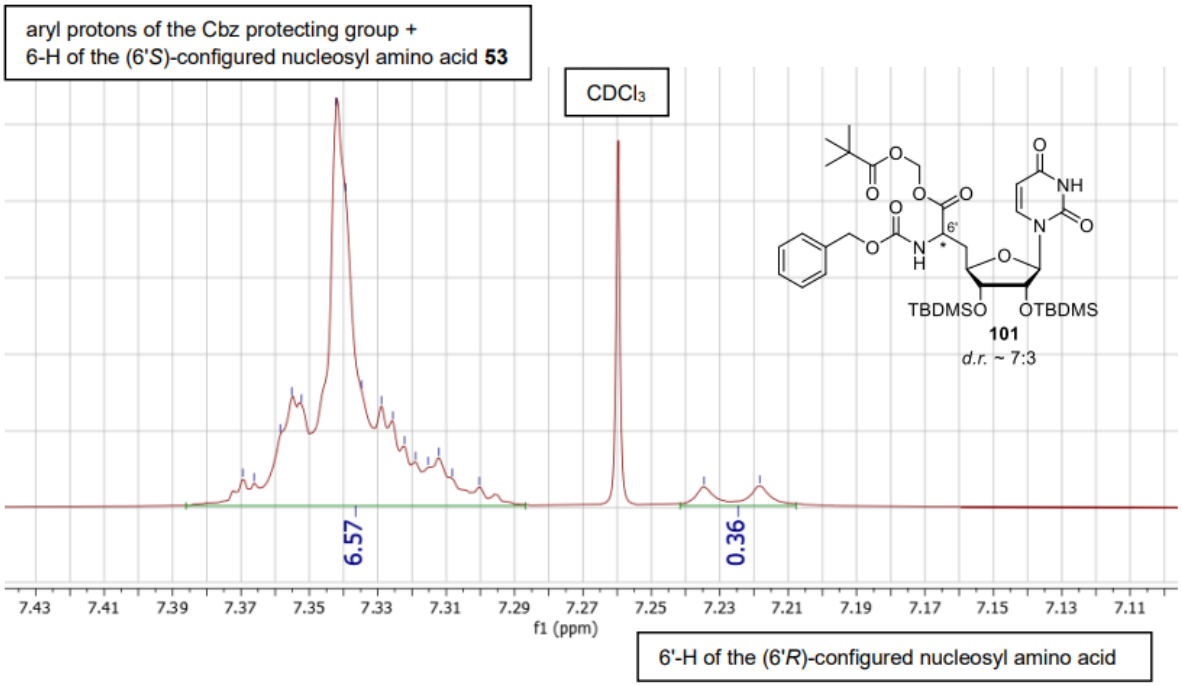

*Figure 4.56: Section of the ^{1}H NMR spectrum of the (6'S)-nucleosyl amino acid **101**.*

This assumption was confirmed as the signals of both isomers could be found and assigned in the ^{1}H NMR spectrum after subsequent Cbz-deprotection. The Cbz-deprotection of the (6'*S*)-nucleosyl amino acid **101** to the corresponding amine **102** is depicted in Scheme 4.11.

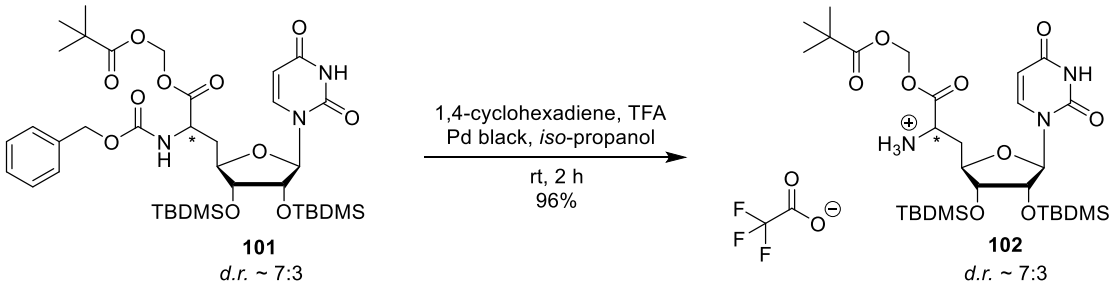

*Scheme 4.11: Synthesis of the (6'S)-O-POM-2',3'-O-bis-TBDMS-uridinyl-amino acid **102**.*

In this step, the aforementioned Cbz-deprotection conditions were applied (Chapter 4.2.2.1). A solution of dehydrogenated uridinyl-amino acid **101** in *iso*-propanol, 1,4-cyclohexadiene and palladium black was stirred under acidic catalysis (TFA) at room temperature for 2 hours. After filtration of the reaction mixture through a syringe filter and removing of the solvent *in vacuo*, the desired amine **102** was obtained in 96% yield. No further purification was needed. Again, amine **102** was provided as TFA salt to avoid decomposition due to the nucleophilic properties of free amino moieties (Chapter 4.2.2.1).

Following, the linker-containing nucleoside building block **103** was provided by a reductive amination of the nucleosyl amino acid **102** and the linker-aldehyde **28** according to an established method in our research group.[212] The synthesis is presented in Scheme 4.12.

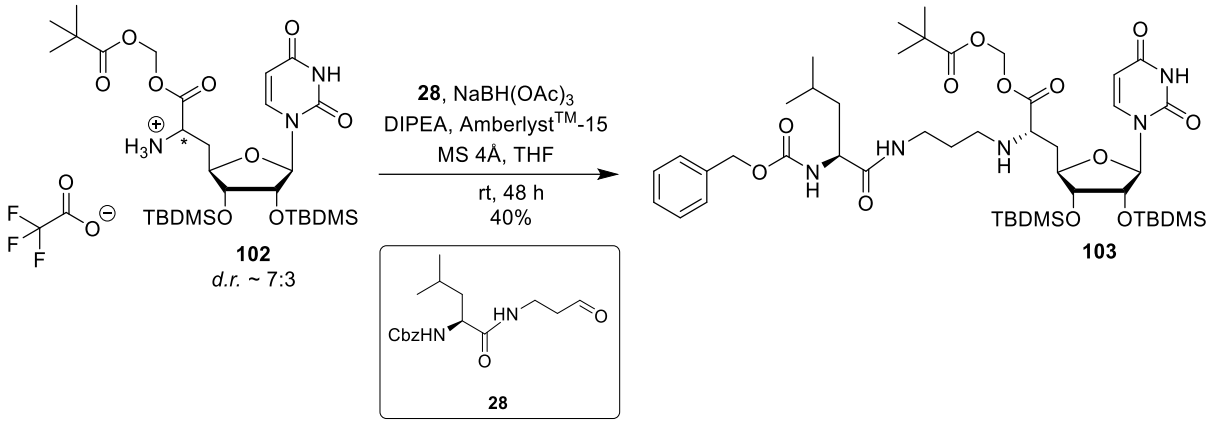

*Scheme 4.12: Synthesis of the linker-containing nucleoside **103**.*

Prior to the reaction, the glassware was dried *in vacuo* as described before but with molecular sieves (4 Å) in the flask during drying. The general use of molecular sieves is crucial due to an imine formation as first step of reductive aminations. The imine formation represents an equilibrium reaction that strongly depends on the amount of water, thus illustrating the water sensitivity of this reaction. Hence, molecular sieves were added in the flask for removing the water that is formed during the reaction. The free amine **102** was dissolved in THF over molecular sieves (4 Å) and the solution was stirred at room temperature for 10 minutes. The solvent was always freshly taken from the solvent purification system. The linker-aldehyde **28** and DIPEA were added and the reaction mixture was stirred at room temperature for further 23 hours. The nucleosyl amino acid **102** and the linker-aldehyde **28** were used in equimolar amounts. An excess of the latter would deliver a product mixture which is not separable by column chromatography, as Dr. A. Spork observed for a similar system.[231] Following, Amberlyst™-15 (0.33 eq.) and sodium triacetoxyborohydride (2.0 eq.) were added to the reaction mixture. Amberlyst™-15 serves as activating proton source in the reaction to capture the excess of DIPEA (2.0 eq.). Sodium triacetoxyborohydride represents the reducing agent and was dried for at least 12 hours *in vacuo* prior to use. The solution was stirred at room temperature for further 24 hours. After aqueous workup and chromatographic purification, the product **103** was obtained in 40% yield. The essential need of an aqueous workup of the reaction mixture for removing the boron salts was demonstrated by Dr. A. Spork as chromatographic purification directly afterwards led to a significant loss in yield.[231] As already mentioned, the separation of the (6'*R*)-configured isomer was possible during column chromatography, thus enabling all subsequent reactions to be performed with the desired pure isomer in (*S*)-configuration. Generally, reductive aminations represent a critical step in the whole synthesis of nucleosyl amino acids beside the asymmetric hydrogenation. This has been observed within several studies in our research group. The success as well as the yields of reductive aminations varied greatly in our research group although the same conditions have

always been applied. The use of a new batch of sodium triacetoxyborohydride should therefore always be kept in mind, if necessary.

A final Cbz-deprotection of the linker-containing nucleoside **103** provided Cbz-deprotected nucleosyl amino acid **63** as bis-TFA salt. Therefore, the Cbz-protecting group of **103** was cleaved under standard transfer hydrogenation conditions using 1,4-cyclohexadiene, palladium black and TFA in *iso*-propanol at room temperature for 1.5 hours. The reaction is depicted in Scheme 4.13. The desired deprotected nucleosyl amino acid **103** was obtained in 99% yield after filtration through a syringe filter and the solvent being removed *in vacuo*. No further purification was needed.

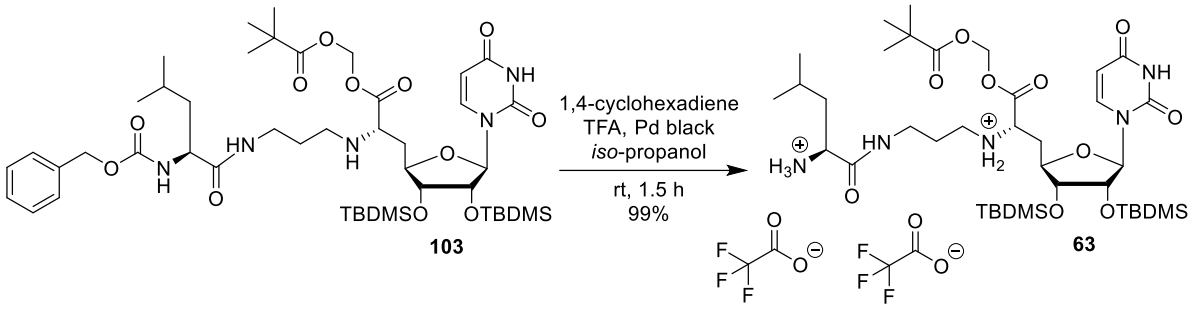

*Scheme 4.13: Synthesis of L-leucine-propyl-5'-deoxy-POM ester nucleosyl amino acid **63**.*

With the successful syntheses of urea dipeptide **54**, the pivaloyl-substituted chloroformate **57** and the nucleosyl amino acid core **63**, all building blocks required for the assembly of the target structure **52** were available. The reaction sequence providing prodrug **52** will be described in the following. This included an amide coupling, a Cbz-deprotection, a carbamate formation and a final acidic global deprotection.

4.2.2.3.3 Attempted synthesis of bis-POM prodrug approach 52

The synthesis of the fully protected bis-POM prodrug **104** was carried out by a peptide coupling of the (6'*S*)-configured L-leucine-propyl-5'-deoxy-POM ester nucleosyl amino acid **63** and the POM ester containing urea dipeptide **54**. The reaction is depicted in Scheme 4.14. It could be demonstrated in former studies of our research group that higher yields of amide couplings are generally obtained with the use of the nucleosyl amino acid as TFA salt.[212] The reaction was performed according to an established method of Dr. D. Wiegmann and Dr. A. Spork.[212,231]

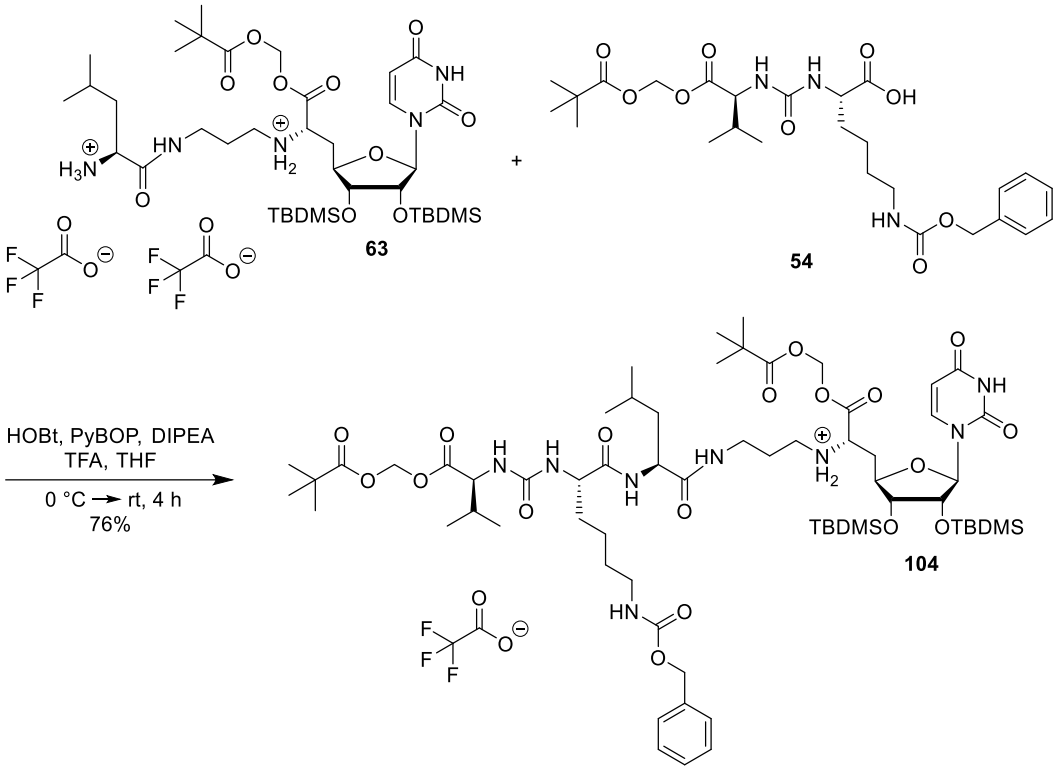

*Scheme 4.14: Synthesis of fully protected bis-POM-5'-deoxy muraymycin analogue **104**.*

The peptide coupling of the urea dipeptide to the nucleoside moiety was carried out with HOBt and benzotriazol-1-yl-oxytripyrrolidinophosphonium hexafluorophosphate (PyBOP) as coupling reagents. Both were added to a solution of **54** in THF in the presence of DIPEA. The reaction mixture was stirred at room temperature for 30 minutes. After cooling to 0 °C, a solution of the nucleosyl amino acid **63** in THF was added dropwise. The reaction mixture was stirred at 0 °C for 1 hour and at room temperature for further 3 hours. The solution was acidified with TFA, leading to the salt formation of the desired bis-POM-5'-deoxy muraymycin analogue **104**. After stirring the reaction mixture at room temperature for further 15 minutes, the solvent was removed *in vacuo*. Due to the high complexity of this full-length analogue, the identity of the obtained product was only confirmed by LC-MS kindly performed in the research group of Prof. Dr. U. Kazmaier. A second compound was observed in this approach, which likely was tripyrrolidinophosphine oxide. It is a known byproduct of amide couplings with PyBOP and only removable by reversed phase HPLC with isocratic conditions. The unsuccessful isolation by column chromatography here strengthened this suggestion. Nevertheless, the desired protected bis-POM-5'-deoxy muraymycin analogue **104** was suggested to be detected by LC-MS analysis with a measured value of m/z = 1335 [M+H$^+$]. The chromatogram and the MS spectrum are depicted in Figure 4.57. Although this value reflects a rounded one and no further zooming was performed, it agreed well with the calculated m/z = 1333.74 [M+H$^+$] of compound **104** within the limits of accuracy in this method. Especially for huge compounds such as this one, the probability of high ^{13}C ratios within the compound seems likely, thus leading to the

detection of higher m/z values. The success of the peptide coupling towards the desired product **104** was assumed, however, a yield was not determined.

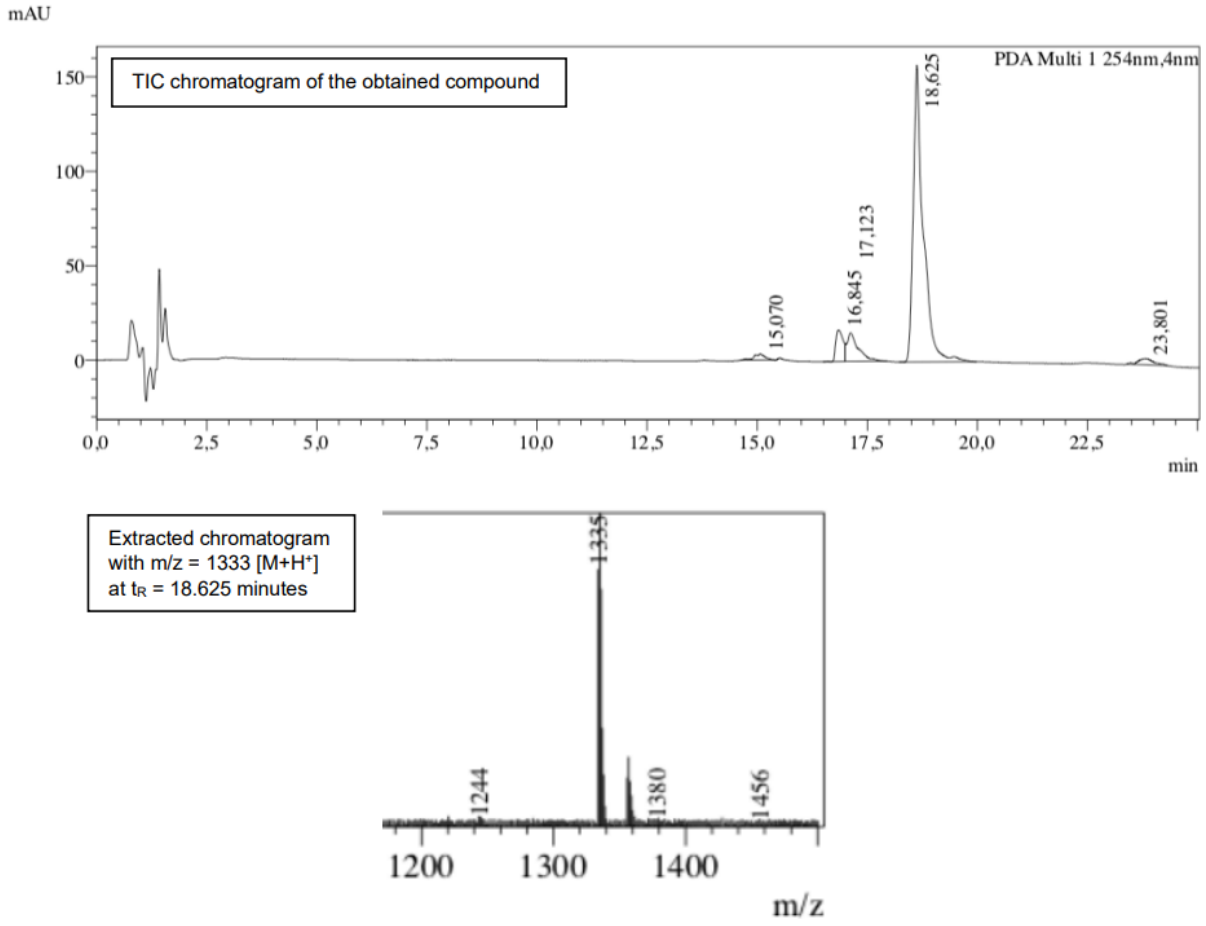

Figure 4.57: LC-MS analysis of the obtained compound after peptide coupling.

In a second iteration, peptide coupling was performed in the same scale utilizing the same conditions. After a full conversion was observed by TLC after 4 hours, the solvent was carefully removed *in vacuo*. Chromatographic purification provided a white foam that was analyzed by LC-MS. LC-MS analysis of this approach was performed in our reserach group. The compound could be identified as fully protected bis-POM prodrug **104** with m/z = 1333.85 [M+H$^+$] in 76% yield. A sufficient purity for subsequent reactions was verified by the UV chromatogram (λ = 254 nm) of the LC-MS analysis. The chromatogram and the MS spectrum are depicted in Figure 4.58.

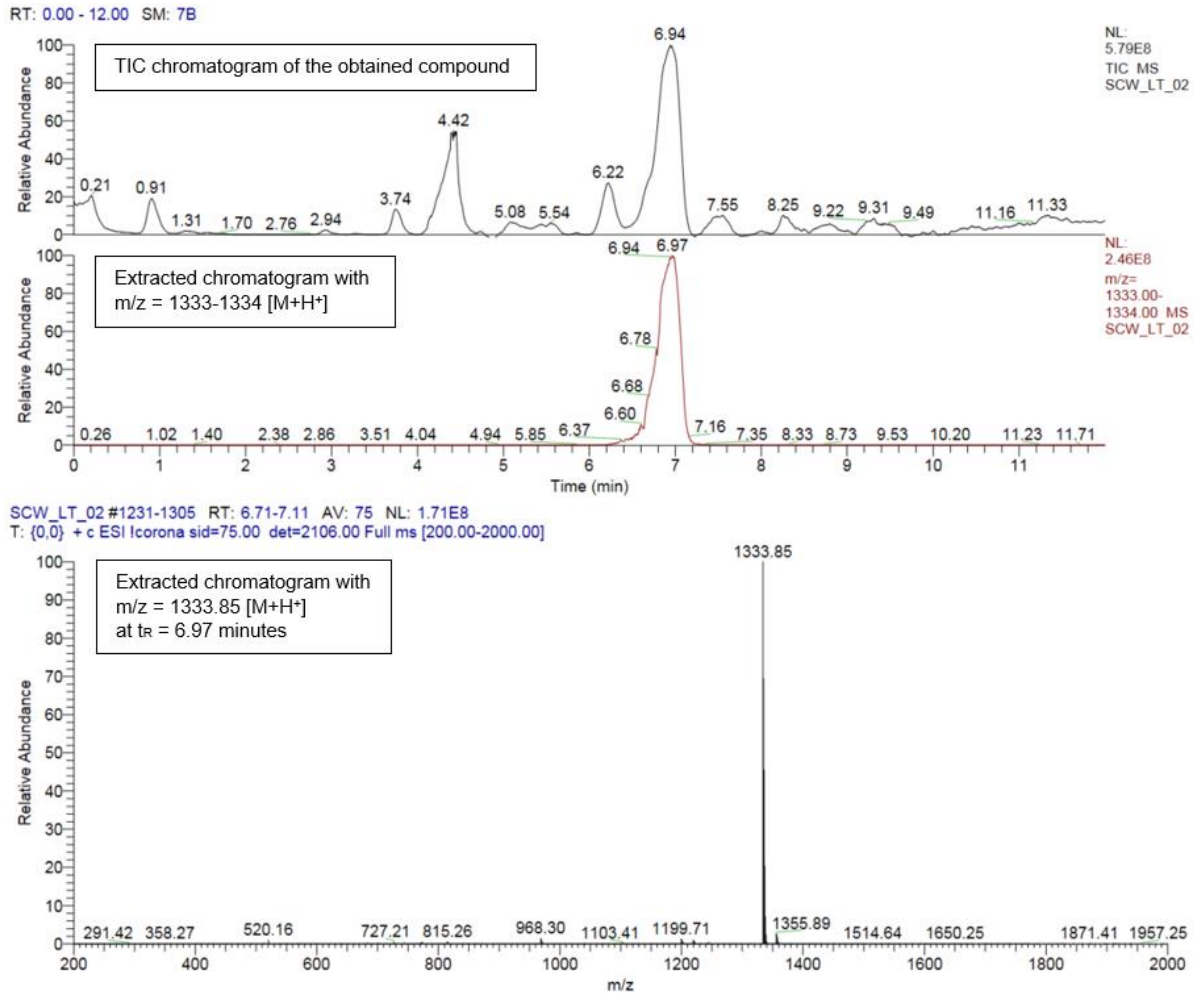

Figure 4.58: LC-MS analysis of the obtained compound after peptide coupling.

Next, the Cbz-protecting group of **104** was cleaved under transfer hydrogenation conditions leading to the full-length *N*-Cbz-deprotected bis-POM-5'-deoxy muraymycin analogue **105**. The reaction is depicted in Scheme 4.15.

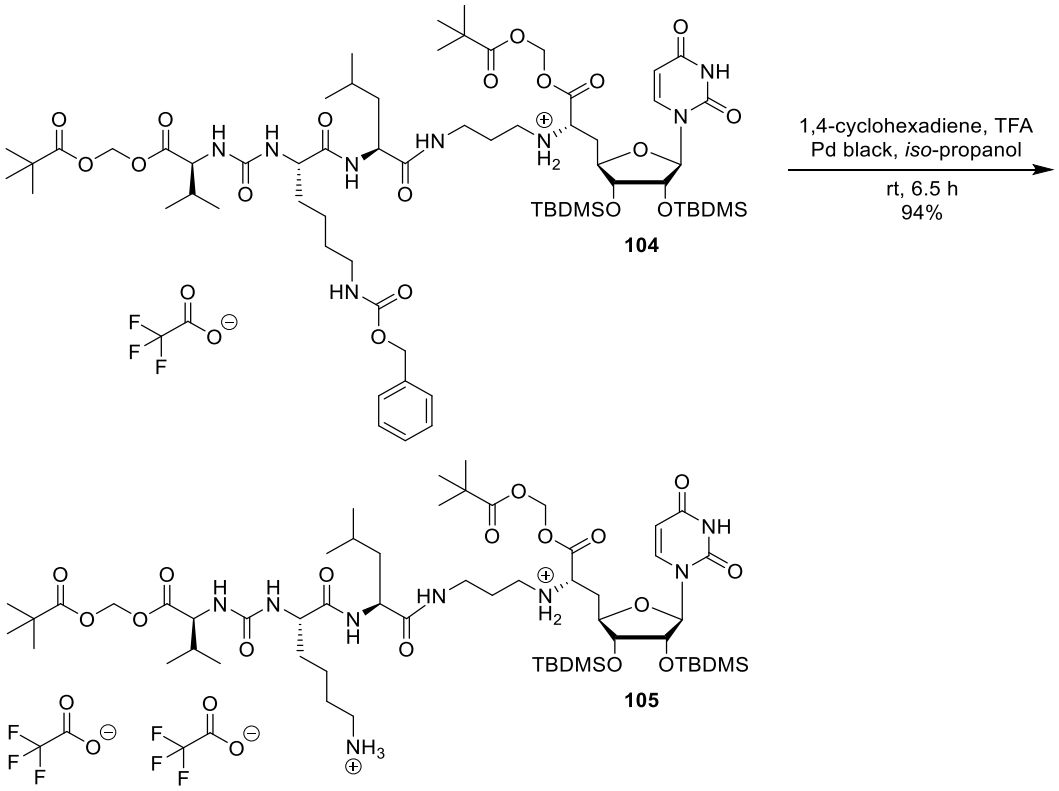

*Scheme 4.15: Synthesis of Cbz-deprotected bis-POM-5'-deoxy muraymycin analogue **105**.*

The Cbz-protected nucleosyl amino acid **104** was dissolved in *iso*-propanol and 1,4-cyclohexadiene, palladium black and TFA were added. The reaction mixture was stirred at room temperature. A full conversion was observed by TLC after 1,4-cyclohexadiene and palladium black have been added three additional times during 6.5 hours of reaction time. The desired nucleosyl amino acid **105** was obtained in 94% yield after filtration of the reaction mixture through a syringe filter and solvent-removing. No further purification was required and amine **105** was provided as TFA salt. The identity of **105** was shown by LC-MS due to its structural complexity. The measured value of m/z = 1199.63 [M+H$^+$] agreed well with the calculated m/z = 1200.71 [M+H$^+$] of compound **105** within the limits of accuracy in this method [M+H]$^+$. A sufficient purity for subsequent reactions was verified by the UV chromatogram (λ = 254 nm) of the LC-MS analysis. The chromatogram and the MS spectrum are depicted in Figure 4.59.

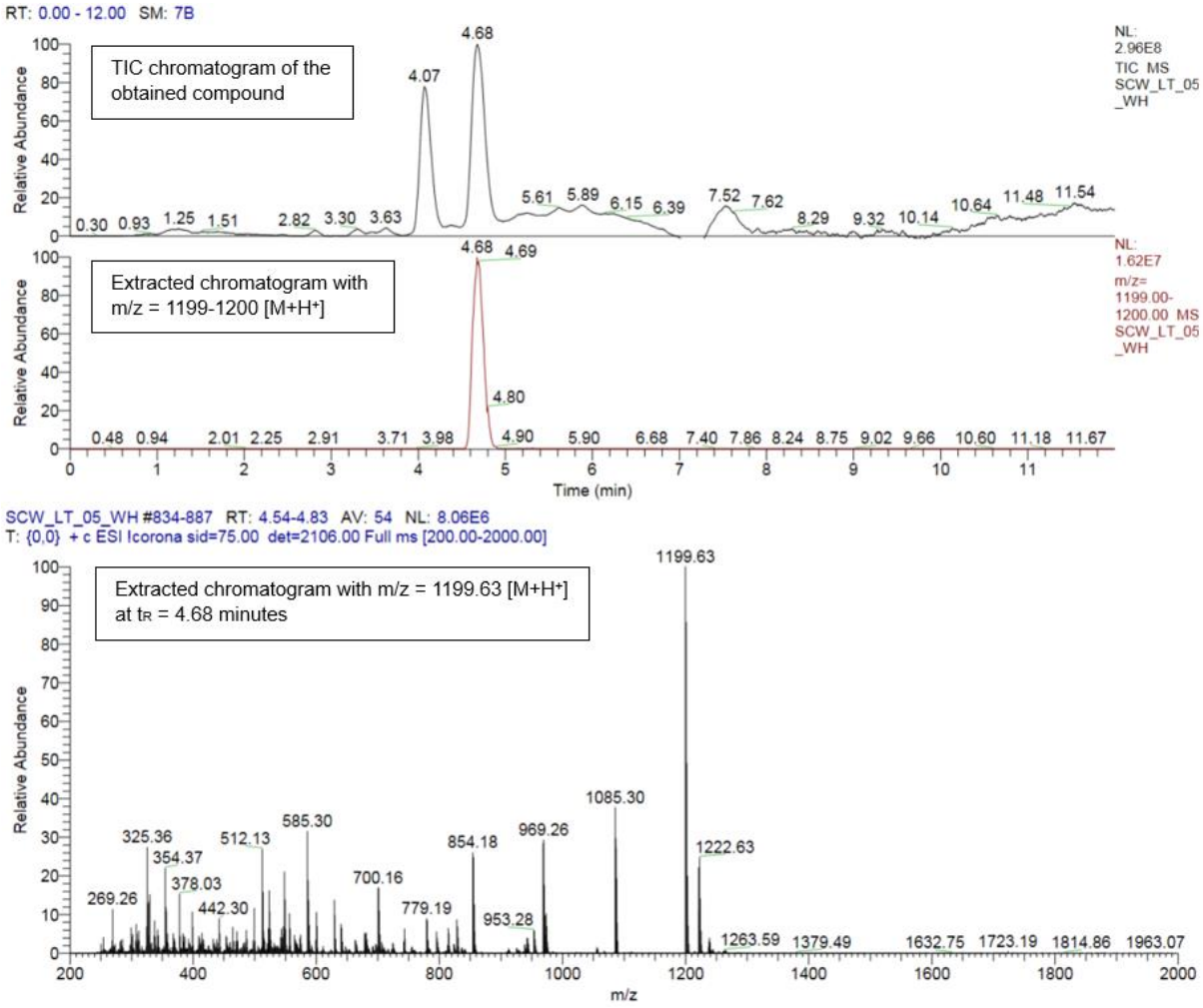

Figure 4.59: LC-MS analysis of the obtained compound after Cbz deprotection.

The next step represented the carbamate formation which is depicted as first reaction in Scheme 4.16. The *N*-Cbz-deprotected analogue **105** was dissolved in THF. Chloroformate **57** (3.2 eq.) and DIPEA (2.0 eq.) were added in excess to provide the fully protected carbamate prodrug **106**. This sytnthesis was a first attempt to investigate the success and efficiency of this route as mentioned (Chapter 4.2.2.2.3), After stirring the solution at room temperature for 21 hours, the solvent was removed *in vacuo*. The obtained crude product **106** was directly used for subsequent global deprotection presented as second reaction in Scheme 4.16.

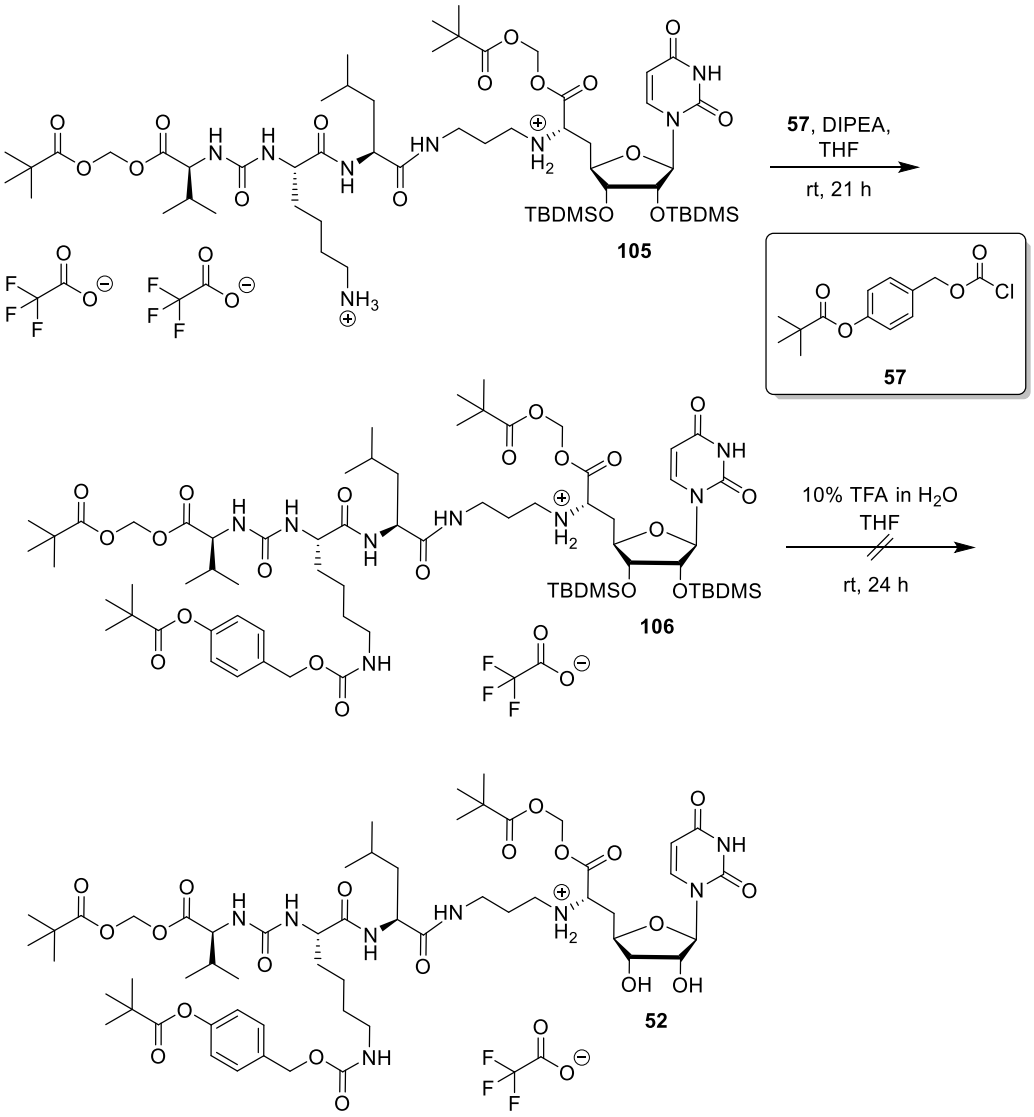

*Scheme 4.16: Attempted synthesis of target compound **52**.*

The conditions for global deprotection of muraymycin analogues with TFA and the amount needed to selectively cleave different protecting groups have been intensively studied in our research group:[212] Dr. D. Wiegmann demonstrated the cleavage of TBDMS-ethers with 20% TFA in water and THF as cosolvent. *Tert*-butyl esters stayed intact under these conditions while POM esters partially decomposed after a reaction time up to 20 hours. Hence, Dr. D. Wiegmann established the global acidic deprotection conditions for his POM muraymycin prodrugs with the use of 10% TFA in water within a reaction time of 24 hours.[212] These mild conditions were applied. Nucleoside **106** was dissolved in THF and TFA was added as a 10% solution in water. The reaction mixture was stirred at room temperature for 24 hours. After removing the solvent by freeze dying, the crude product was purified by semi-preparative HPLC (Chapter 7.2.1.5). This attempt yielded a white foam insufficient for full analytical characterization. However, an attempt to provide NMR data was made. The ^{1}H NMR spectrum of the obtained compound (depicted in Figure 4.60) did not show expected signals, thus concluding failure of the synthesis. Typically, the aromatic ring system of carbamates appears

as multiplet at ~ 7.0-7.2 ppm in the ^{1}H NMR spectrum. This multiplet was completely missing here and two weakly integrated, not assignable doublets appeared at 7.0 ppm and 7.35 ppm instead (Figure 4.60). A detailed evaluation of the ^{1}H NMR spectrum was not needed since initial inspection of the spectrum was sufficient to conclude absence of the desired product (Figure 4.60).

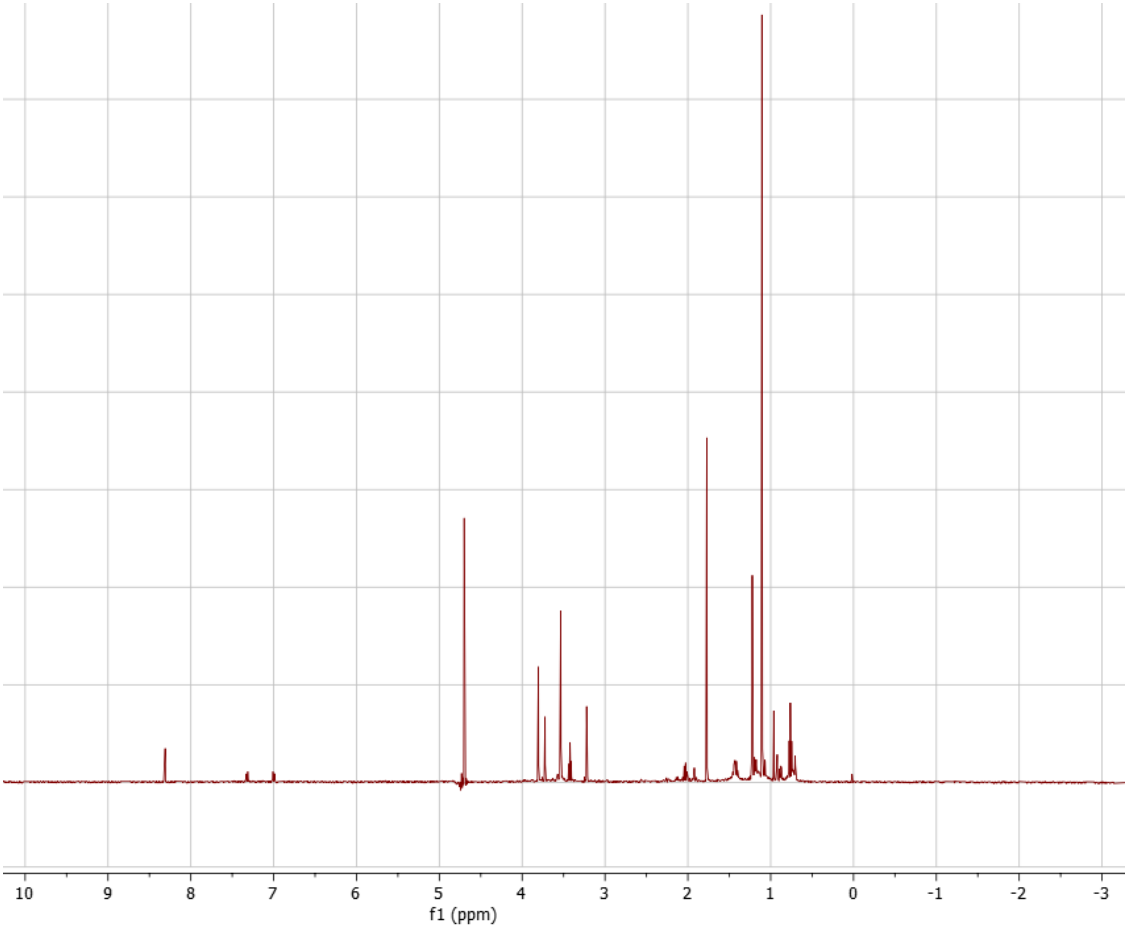

*Figure 4.60: ^{1}H NMR spectrum of the failed synthesis of bis-POM prodrug **52**.*

As already mentioned, the chloroformate **57** was present in excess in the first reaction within this two-step synthesis. This excess could have induced undesired side reactions between the chloroformate and the nucleosyl amino acid core. The reactivity of chloroformates should be kept in mind generally for further approaches, also in terms of adaptions of the synthesis. Hydrolysis to the corresponding alcohol would be possible as well, thus hampering the formation of the desired product. A decomposition of the desired prodrug **52** during global deprotection might also be possible. However, this possibility seems to be less likely since mild deprotection conditions have been applied that have been intensively investigated by Dr. D. Wiegmann in his studies.[212] The desired target compound **52** should be stable enough during the reaction. Overall, the synthesis has to be repeated and further studies should keep other synthetic routes in hand for launching the carbamate moiety to the nucleosyl amino acid core.

5 Summary and conclusion

The aim of this dissertation was the investigation of bacterial uptake of muraymycin-derived nucleoside antibiotics, further biological studies for their evaluation and the synthesis of novel muraymycin analogues addressing a prodrug approach.

5.1 Biological studies

Cellular uptake assays, a hemolysis assay and an assay for the quantification of MraY amounts in different preparations were successfully established. Calculations of the accumulation data were made based on the cell volume and cell numbers to obtain intracellular biological concentrations. The calculation tool was successfully established in our research group for cellular uptake assays for *E. coli* and *S. aureus*. Investigations on MurX, the hypothesis of self-resistance of *Streptomyces* species against muraymycins and the interaction between MraY and MurF gained deeper insights into the biological behaviour of MraY and helped with the development of novel nucleoside antibiotics towards potential antibacterial drug candidates.

A cellular uptake assay for Gram-positive *S. aureus* was successfully developed in this work. During assay development, bacterial lysis proved critical. To lyse *S. aureus* cells, the endopeptidase lysostaphin was required for specific cleavage of the polyglycine bonds in the peptidoglycan layer of *S. aureus* cell walls.[242] Expression and purification of lysostaphin were successfully optimized in this dissertation. Lysostaphin identity was confirmed by sequencing, native mass spectrometry studies and biochemical methods such as SDS-PAGE analysis. The commercially available linezolid with activity against *S. aureus* was used as a drug to ensure representative assay conditions. Lysostaphin amounts and incubation times at 37 °C were optimized during lysis studies and resulted in a lysostaphin concentration of 350 µg/mL and an incubation time of 1 hour as sufficient conditions. After the successful optimization and validation of bacterial lysis, further studies addressed the incubation time and concentration of test antibiotics. Studies regarding varying incubation times with linezolid resulted in higher intracellular drug sample concentrations as a result of longer incubation times. Moreover, the experiments revealed that cellular uptake was not completed after an incubation period of 10 minutes. The sample concentrations of linezolid significantly differed compared to longer incubation times (> 30 minutes). The experiments revealed an incubation time of 30 minutes to be reasonable for the cellular uptake assays with *S. aureus*. Subsequent concentration-dependant studies revealed higher intracellular linezolid amounts as a result of an increased offer. Bacteriostatic or bactericidal effects which have already been observed during assay development for *E. coli*[134] were also seen for *S. aureus* with linezolid concentrations higher than its IC_{50} value for growth inhibition. In summary, studies towards time and concentration of the test antibiotics yielded plausible results and confirmed the assay consistency.

After the successful development of the assay, cellular uptake of *O*-acylated muraymycin analogues **48** and **49** by Dr. M. Wirth[243] was examined since both revealed antibacterial activity against *S. aureus* in the nanomolar range (Figure 5.1). Accumulation of compound **49** was observed to greater extent compared to analogue **48** (Figure 5.1). However, the obtained results are preliminary and experiments need to be repeated.

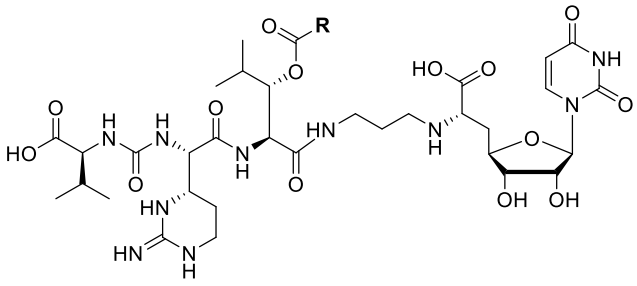

Compound	R	IC_{50} against MraY from *S. aureus* [nM]	MIC_{50} [µg/mL]	Cellular uptake in *S. aureus* Sample concentration [nM]
48	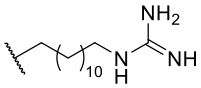	4.0 ± 0.7	*E. coli* DH5α n.a. *E. coli* Δ*tolC* <1 *P. aeruginosa* >100 *S. aureus* 11.4	128 ± 23
49	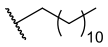	5.8 ± 0.5	*E. coli* DH5α n.a *E. coli* Δ*tolC* <1 *P. aeruginosa* - *S. aureus* 0.32*	227 ± 37

*Figure 5.1: Biological activities of muraymycin analogues **48** and **49** by Dr. M. Wirth.[243] The inhibitory activity against MraY, antibacterial growth inhibition data ("-" = no evaluation possible, "n.a." = data not available) and preliminary cellular uptake data in S. aureus Newman as sample concentrations are presented. *Previous reported antibacterial activity, subsequent obtained data varied up to 50 µg/mL.*

Accumulation assays for Gram-negative *E. coli* that slightly differ from the known procedure[134] were successfully established. Modifications of the previously established LC-MS-based assay were performed for each of the compounds investigated in this work as required.

Cellular uptake of muraymycin analogue **37** and the literature-known reference **38** by Dr. G. Niro[239] in *E. coli* Δ*tolC* was investigated. Both compounds were antibacterially active against *E. coli* DH5α, *E. coli* Δ*tolC*, *P. aeruginosa* and *S. aureus*, but differed in their inhibitory activity against MraY by a factor of ~ 1000 (Figure 5.2). The difference in inhibitory activity, however, could not be related to different bacterial cellular uptake as demonstrated with the accumulation assay. The same trend of cellular accumulation was observed for both compounds **37** and **38**. They revealed higher biological concentrations in periplasmic space relative to cytoplasmic space as a result of the lower periplasmic volume (Figure 5.2).

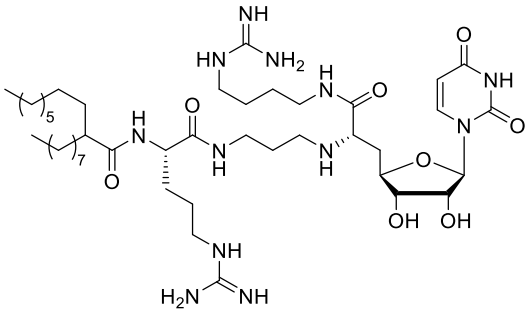

37

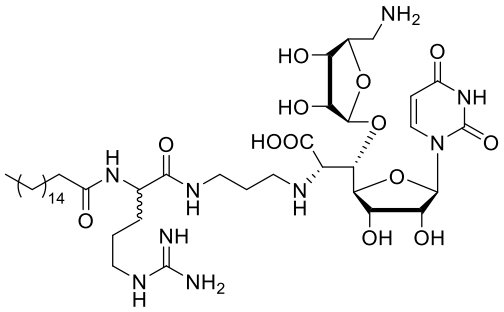

38

Compound	IC_{50} against MraY from *S. aureus* [µM]	MIC_{50} [µg/mL]	Cellular uptake in *E. coli* Δ*tolC* Sample concentration [nM] / *Biological concentration [µM]*
37	4.4 ± 1.3	*E. coli* DH5α 14 *E. coli* Δ*tolC* 3.9 *P. aeruginosa* 18 *S. aureus* 3.4	whole cells: 90 ± 24 */ 1.5 ± 0.4* cytoplasm: 83 ± 8 */ 1.6 ± 0.3* periplasm: 30 ± 3 */ 3.6 ± 0.3*
38	$(2.3 \pm 0.4) \cdot 10^{-3}$	*E. coli* DH5α 5.9 *E. coli* Δ*tolC* 5.1 *P. aeruginosa* 16 *S. aureus* 1.3	whole cells: 114 ± 3 */ 1.8 ± 0.1* cytoplasm: 109 ± 9 */ 1.9 ± 0.2* periplasm: 67 ± 10 */ 7.6 ± 1.1*

*Figure 5.2: Biological activities of muraymycin analogues **37** and **38** by Dr. G. Niro.[239] The inhibitory activity against MraY, antibacterial growth inhibition data and cellular uptake data in E. coli ΔtolC are depicted. The cellular uptake data is presented as sample concentrations for the whole cell lysate ("whole cells"), cytoplasmic space and periplasmic space. The biological concentrations are calculated under consideration of the cell number.*

A preferential cellular uptake of muraymycin analogue **37** as an explanation for the retention in antibiotic activity (since MraY is an transmembrane target on the bacterial membrane) could not be demonstrated with the cellular uptake assays. To investigate a different mode of action, further investigation is required.

Cellular accumulation of the guanidinylated cube-octameric silsesquioxane scaffold (GuCOSS)-containing muraymycin conjugate **39** and the cell-penetrating peptide (CPP)-containing muraymycin conjugate **40** by Dr. C. Rohrbacher[240] was investigated. Both conjugates bear a carbamate unit and a disulfide bond (Figure 5.3). Due to analytics, a full conversion of both muraymycin conjugates into the parent drug **33** was necessary. A modification of the assay was done after bacterial lysis. Differing from the usual procedure, pellet and supernatant were separated and treated individually. To induce cleavage of the aforementioned units, two novel steps were included, thus releasing the parent drug **33**. Samples were treated with dithiothreitol (DTT) to cleave the disulfide bond followed by sodium hydroxide treatment for carbamate hydrolysis. Strong basic conditions were applied to cleave the carbamate moiety. Both chemicals did not affect the assay itself as demonstrated in prior experiments with lysine reference **33**. The released lysine reference **33** was detected to a greater extent in the supernatant of the muraymycin GuCOSS conjugate **39** compared to the muraymycin CPP conjugate **40** (Figure 5.3). Biological pellet concentrations were obtained in

the same range for both conjugates **39** and **40** (Figure 5.3). Concentrations of released muraymycin analogue **33** for both conjugates were higher in comparison to those of the parent, non-conjugated muraymycin analogue **33**. However, a possible adsorption of these highly charged muraymycin conjugates to the outer membrane could not be ruled out. Reliable evaluations regarding improved cellular uptake should therefore be handled with care. Non-specific binding was suggested as an explanation for the high accumulation data. However, this concern cannot be captured with this assay. Further investigation is required to address this subject.

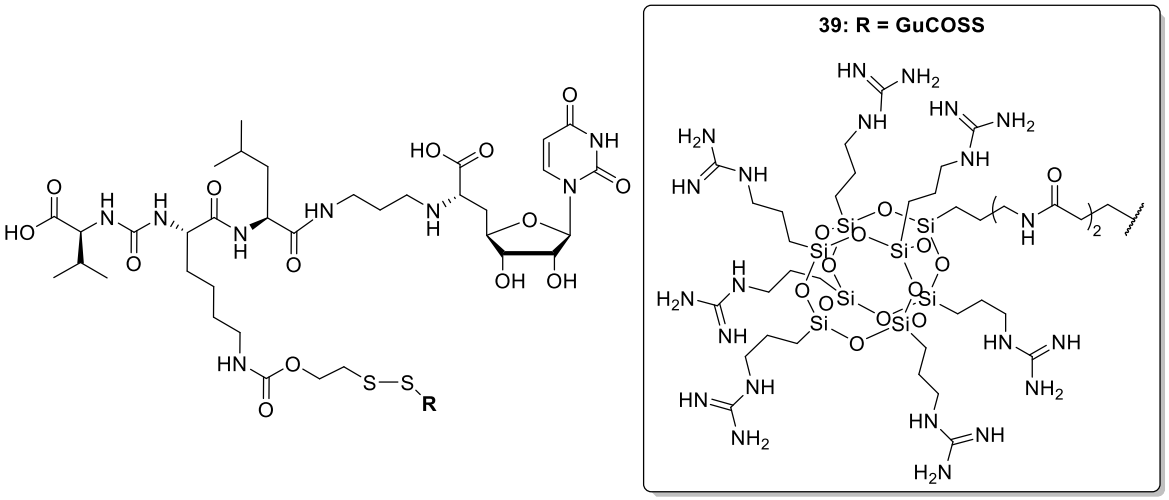

Compound	IC_{50} against MraY from *S. aureus* [µM]	IC_{50} [µg/mL]	Cellular uptake in *E. coli* Δ*tolC* Sample concentration [nM] / *Biological concentration [µM]*
39	0.48 ± 0.03	*E. coli* DH5α 63 *E. coli* Δ*tolC* 6.5 *S- aureus* >100	pellet: 23 ± 1 / *6.5 ± 0.2* supernatant: 82 ± 9 / *23 ± 3*
40	1.3 ± 0.2	*E. coli* DH5α 45 *E. coli* Δ*tolC* 6.4 *S. aureus* >50	pellet: 25 ± 7 / *6.3 ± 1.7* supernatant: 38 ± 5 / *9.7 ± 1.3*

*Figure 5.3: Biological activities of muraymycin analogues **39** and **40** by Dr. C. Rohrbacher.[240] The inhibitory activity against MraY, antibacterial growth inhibition data and cellular uptake data in E. coli ΔtolC are depicted. The cellular uptake data is presented as sample concentrations for the pellets and the supernatants after harvesting the bacteria following lysis. The biological concentrations are calculated under consideration of the cell number.*

Accumulation studies of MurA pyrazolidinone analogues **43**-**47** provided by Dr. R. Wagdy[241] were successfully performed. The compounds are structurally similar, but differ greatly in terms of their biological properties (Figure 5.4). All analogues in this series show inhibitory activity against *E. coli* MurA in the low double-digit micromolar range (Figure 5.4). In contrast, antibacterial growth inhibition of *E. coli* Δ*tolC* was only observed for analogues **46** and **47**, while compounds **43**-**45** were antibacterially inactive against this strain (Figure 5.4). Analogues **44** and **47** showed additional antibacterial activity against *S. aureus* (Figure 5.4). The hypothesis that compound **44** might not be able to diffuse through Gram-negative cell wall was strenghtened with the cellular uptake assays. A reasonable explanation for the lack of growth inhibition against *E. coli* Δ*tolC* was provided with the lowest biological concentration in cell lysate of *E. coli* Δ*tolC* (Figure 5.4). Higher amounts were observed for analogues **43** and **45**, exceeded by analogue **47** with the highest data (Figure 5.4). Cellular uptake of compound **46** was in between the other compounds (Figure 5.4). The cellular uptake studies gained further insights and contributed to the development of future structure activity relationship (SAR) studies for this class of compounds.

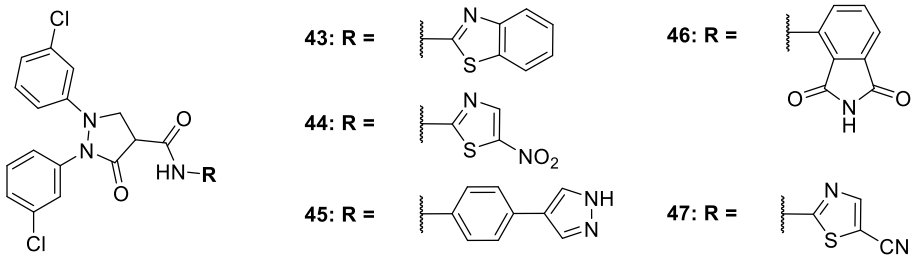

Compound	IC_{50} against *E. coli* MurA [µM]	MIC_{90} [µM]	Cellular uptake in *E. coli* Δ*tolC* Sample concentration [nM] / *Biological concentration [µM]*
43	18	*E. coli* Δ*tolC* >40 *S. aureus* >40	whole cells: 573 ± 123 / *19 ± 4*
44	20	*E. coli* Δ*tolC* >40 *S. aureus* 8	whole cells: 56 ± 13 / *1.8 ± 0.4*
45	13	*E. coli* Δ*tolC* >40 *S. aureus* >40	whole cells: 348 ± 46 / *11 ± 2*
46	13	*E. coli* Δ*tolC* 17 *S. aureus* >40	whole cells: 924 ± 152 / *30 ± 5*
47	21	*E. coli* Δ*tolC* 21 *S. aureus* 11	whole cells: 2563 ± 606 / *84 ± 20*

*Figure 5.4: Biological activities of MurA pyrazolidinone analogues **43**-**47** by Dr. R. Wagdy.[241] The inhibitory activity against MurA, antibacterial growth inhibition data and cellular uptake data in E.coli Δ*tolC* are depicted. The cellular uptake data is presented as sample concentrations. The biological concentrations are calculated under consideration of the cell number.*

Studies concerning MraY as the bacterial target of muraymycins and their analogues were successfully performed and helped to gain further insights into the protein's inhibition. The investigation and evaluation of inhibitory activities as a result of the *in vitro* MraY inhibition

assays[84,96,97,99,244] contributed to the SAR studies of our research group. Candidate compounds provided by collaborators were successfully investigated. As shown before, it was demonstrated that differences in inhibitory activities depend on the purification method or isoform of MraY that was used in the MraY inhibition assays.[84] So far, crude membrane preparations with overexpressed MraY from *S. aureus* and MraY purified in detergent micelles were available in our laboratory. As part of this dissertation, the MraY-nanodisc system as a compromise of isolated protein in a near-native environment was successfully established. The combination of MSP1E3D1, solubilzed $MraY_{AA}$ in micelles and a phospholipid mixture of 1,2-dioleoyl-*sn*-glycero-3-phosphoethanolamine (DOPE) and 1,2-dimyristoyl-*sn*-glycero-3-phospho-*rac*-(1-glycerol) (DMPG) resulted in $MraY_{AA}$ incorporated in nanodiscs. The success of MraY-nanodisc formation was confirmed by SEC and SDS-PAGE analysis. $MraY_{AA}$ in nanodiscs served as beneficial environment for MraY besides crude membrane preparations and protein in micelles.

A quantification assay for MraY was successfully started. This assay focused on the interaction of the His_6-tagged nanobody 7 (NB7) and MraY which was used for the (semi-) quantification of MraY amounts by Western Blotting. MraY was captured with NB7 as a primary antibody, which was then visualized using antibodies that recognize the His tag. The proof of concept was successfully confirmed. An $MraY_{AA}$ amount of 30 ng purified protein was sensitive and sufficient as demonstrated during assay development. Initial investigations regarding NB7 concentration revealed the highest NB7 dilution (1:10,000) to still be too concentrated, thus demonstrating the high potential of this project, especially in terms of method sensitivity. This project will shed light onto inhibitory activities of drug candidates in different MraY preparations with knowledge about absolute MraY amounts, thus providing further insights into MraY inhibition. This project will be taken over by M. Lutz as part of his dissertation.

MraY crude membrane preparations with the plasmid encoding MurX in a pET30a vector were successfully expressed for studying the biological behavior of different bacterial MraY species. Activity analysis revealed protein activities that were not comparable to those of the crude membrane preparations of $MraY_{SA}$. However, activity was still observed for MurX to a smaller extent. Additionally, subcloning of the MurX gene into a pET28a vector by *in vivo* assembly (IVA) cloning was successfully performed. MraY activity assays yielded similar results. A second subcloning by IVA cloning was performed into pET26a to provide a suitable system for protein purification in detergent micelles. In further studies, purification of MurX in pET26a in micelles will be carried out to investigate enzymatic activity of this isoform. The project will be taken over by M. Lutz.

Further experiments addressed the role of hypothesized self-resistance of *Streptomyces* species against muraymycins in the target protein MraY. Notable retention in inhibitory activity that was observed for covalently modified precursors and varying amino acids were considered

to cause such self-resistance mechanisms.[233] The role of $MraY_{SA}$H324 was examined with constructs coding for $MraY_{SA}$H287Q, $MraY_{SP}$ and $MraY_{SP}$Q316H which were cloned into pet28a vectors (provided by Dr. P. Fischer[122]). Overexpression of MraY as crude membranes into *E. coli* Lemo21(DE3) was performed. MraY activity assays provided further insights by direct comparison of the mutant proteins with the crude membrane preparations of $MraY_{SA}$ which is routinely overexpressed in our laboratory. Protein activity of all mutants, however, was not observed. Further investigation is required to gain deeper insights into this subject. This project will be continued by M. Lutz.

A further side project dealt with the interaction between MraY and MurF. Activity analysis with purified MraY in nanodiscs in the presence of purified MurF (provided by Dr. P. Fischer[122]) and muraymycin A1 as an inhibitor demonstrated a concentration-dependant effect of MurF on MraY inhibition. The presence of MurF in single-digit micromolar concentration regions retained MraY activity in the presence of an inhibitor. Furthermore, it could be successfully demonstrated that high MurF concentrations did not impact MraY activity. Because enzymatic activity of MraY in nanodiscs rapidly declines, these results should be considered preliminary and the experiments need to be repeated. However, launching these studies successfully demonstrated the dynamic interplay between both proteins which will be further investigated by M. Lutz.

The next project of this work focused on toxic side-effects due to membrane disruption. The capability of compounds to destroy biological membranes was investigated in an assay using sensitive erythrocytes. Such a hemolysis assay was successfully developed and established in this work. Initial hemolysis studies using a purchased kit were successfully performed as demonstrated with the references included.[276] Subsequent studies focused on the development of a procedure regarding our objectives. A specific final concentration of 20 µM was chosen for the investigation of a series of compounds. Additional approaches dealt with concentrations in dependance on antibacterial growth inhibition data of the drugs. Triton X-100 was used as a positive control and phosphate-buffered saline (PBS) as a negative control. Studies of this work revealed a Triton X-100 concentration of 2% (v/v solution) to be efficient for quantitative lysis (100% lysis). PBS alone or PBS mixed with the same amount of dimethylsulfoxide (DMSO) as contained in the compound solutions were used as negative controls, ruling out negative hemolytic effects of DMSO. The assay consistency was confirmed. Following, predetermined compounds of our research group and selected compounds of collaborators were successfully examined in the established hemolysis assay. Muraymycin analogues **37**, **38** and **75**-**78** with long lipophilic side-chains by Dr. G. Niro[239] were of special interest for these studies (Figure 5.5). All muraymycin analogues of this series exhibited hemolytic activities in the middle double-digit percentage at a standard concentration of 20 µM except for one: the arginine and guanidine containing compound **37** (Figure 5.5). The

beneficial properties of analogue **37** were remarkable with ~ 1% hemolysis at a concentration of 20 µM since the literature-known reference **38** showed a higher hemolytic activity (Figure 5.5).

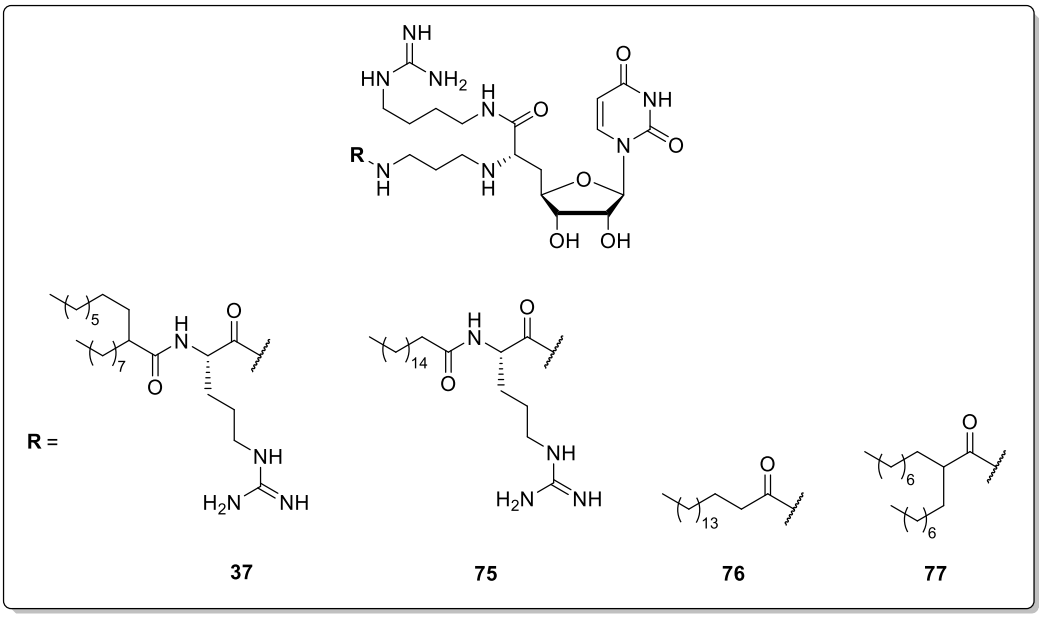

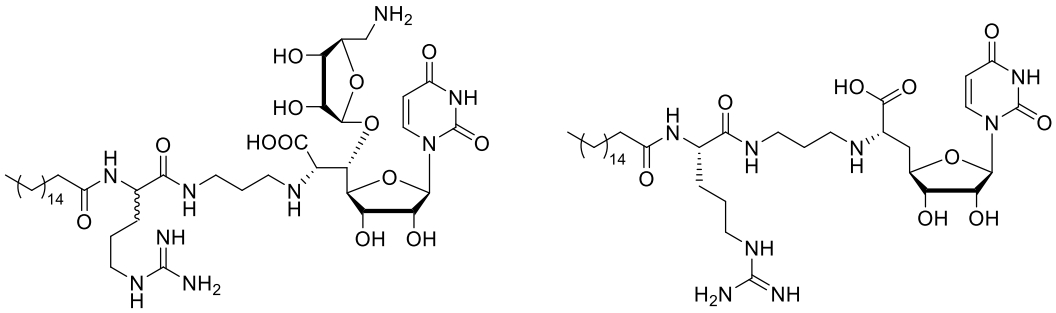

38 **78**

Compound	IC_{50} against MraY from *S. aureus* [µM]	MIC_{50} [µg/mL] *P. aeruginosa*	Hemolysis [%] @20 µM	Hemolysis [%] @1-fold MIC	Hemolysis [%] @4-fold MIC
37	4.4 ± 1.3	18	1.2 ± 1.0	n.d.	26 ± 7
38	(2.3 ± 0.4) · 10^{-3}	16	18 ± 4	6.6 ± 1.0	65 ± 5
75	1.6 ± 0.7	71	16 ± 2	78 ± 11	-
76	3.8 ± 0.8	>100	21 ± 4	83 ± 3	86 ± 6
77	18 ± 10	34	12 ± 3	29 ± 4	93 ± 1
78	2.7 ± 0.5	>50	22 ± 4	38 ± 7	90 ± 5

*Figure 5.5: Hemolytic activities of muraymycin analogues **37**, **38** and **75**-**78** by Dr. G. Niro[239] in a concentration of 20 µM and in concentrations relative to their antibacterial activity against P. aeruginosa. n.d. = not detectable.*

Concentrations relative to their antibacterial activity against *P. aeruginosa* yielded higher hemolytic activities of the compounds in the experiments with ~ 4-fold MIC_{50} compared to ~ 1-fold MIC_{50} (Figure 5.5). This was observed for all analogues except for compound **76** which exhibited hemolysis in the high double-digit percentage in both experiments (Figure 5.5). The

beneficial properties of analogue **37** were confirmed with these further studies (Figure 5.5). In summary, it could be demonstrated that membrane-disruptive modes of action for this series of muraymaycin analogues seem to be affected by two functionalities: The number of guanidine units and the presence of branched lipophilic side chains are influencing parameters in terms of membrane disruption for these compounds. The expected toxic effects of these long lipophilic side-chains-containing analogues were confirmed by the hemolysis assay.

In further hemolysis assays, muraymycin analogues **48**, **49**, **79** and **80** by Dr. M. Wirth[243] were investigated at a concentration of 20 µM. The two naturally occurring muraymycins **A1** and **B8** were included in this series due to structural similaries. Hemolysis assays with compound **48** resulted in 1.1 ± 0.1% hemolysis (Figure 5.6). A similar result was obtained for muraymycin **B8** with 1.2 ± 0.1% hemolysis (Figure 5.6). The other compounds of this series did not show hemolytic effects (<1%) at this concentration (Figure 5.6). The overall beneficial properties of the 'best-in-class compound' **49** were further confirmed with these studies.

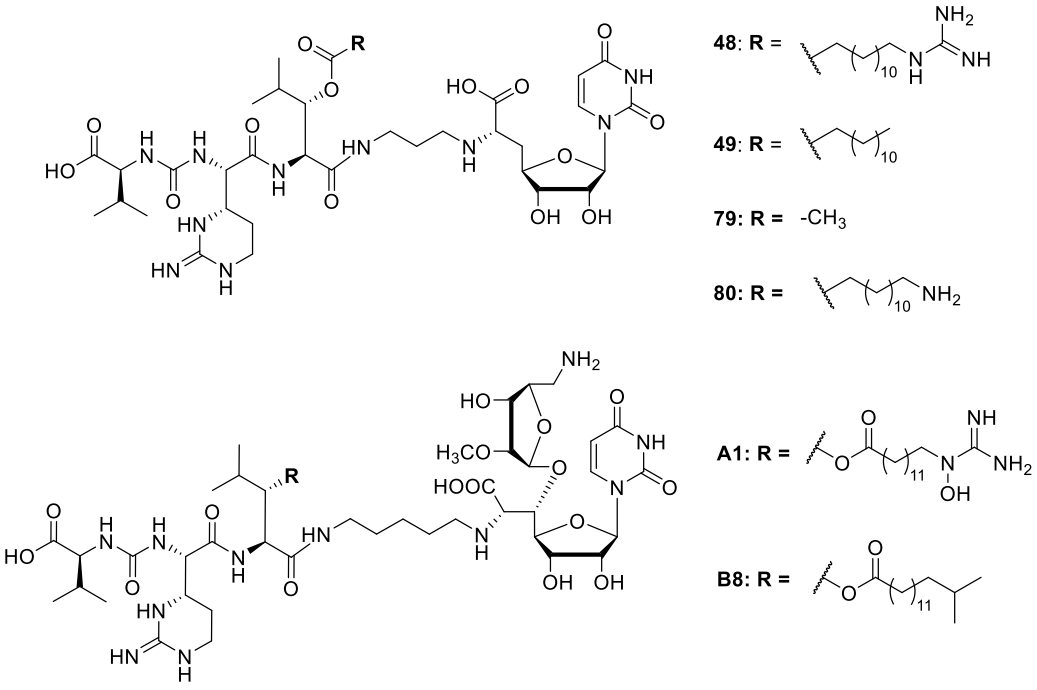

Compound	IC_{50} against MraY from *S. aureus* [nM]	MIC_{50} [µg/mL] *S. aureus*	Hemolysis [%] @20 µM
48	4.0 ± 0.7	11.4	1.1 ± 0.1
49	5.8 ± 0.5	0.32*	<1
79	82 ± 12	>100	<1
80	4.5 ± 0.3	40	<1
A1	0.027 ± 0.003	18	<1
B8	0.004 ± 0.0007	2	1.2 ± 0.1

*Figure 5.6: Hemolytic activities of muraymycin analogues **48**, **49**, **79** and **80** by Dr. M. Wirth[243] and naturally occurring muraymycins **A1** and **B8**[164] in a concentration of 20 µM. *Previous reported antibacterial activity, subsequent obtained data varied up to 50 µg/mL.*

Hemolytic activities of muraymycin streptomycin conjugates **81** and **82**, GuCOSS conjugates **39** and **83** and CPP conjugate **40** by Dr. C. Rohrbacher[240] were investigated in the hemolysis assays. All compounds were hemolytically inactive (<1%) at a concentration of 20 µM (Figure 5.7). Possible membrane-disruptive effects as a result of this conjugation, in particular for the GuCOSS conjugates **39** and **83**, were not observed in these studies. The absence of hemolysis further confirmed the conjugate strategy and strengthened the expansion of the different conjugation approaches.

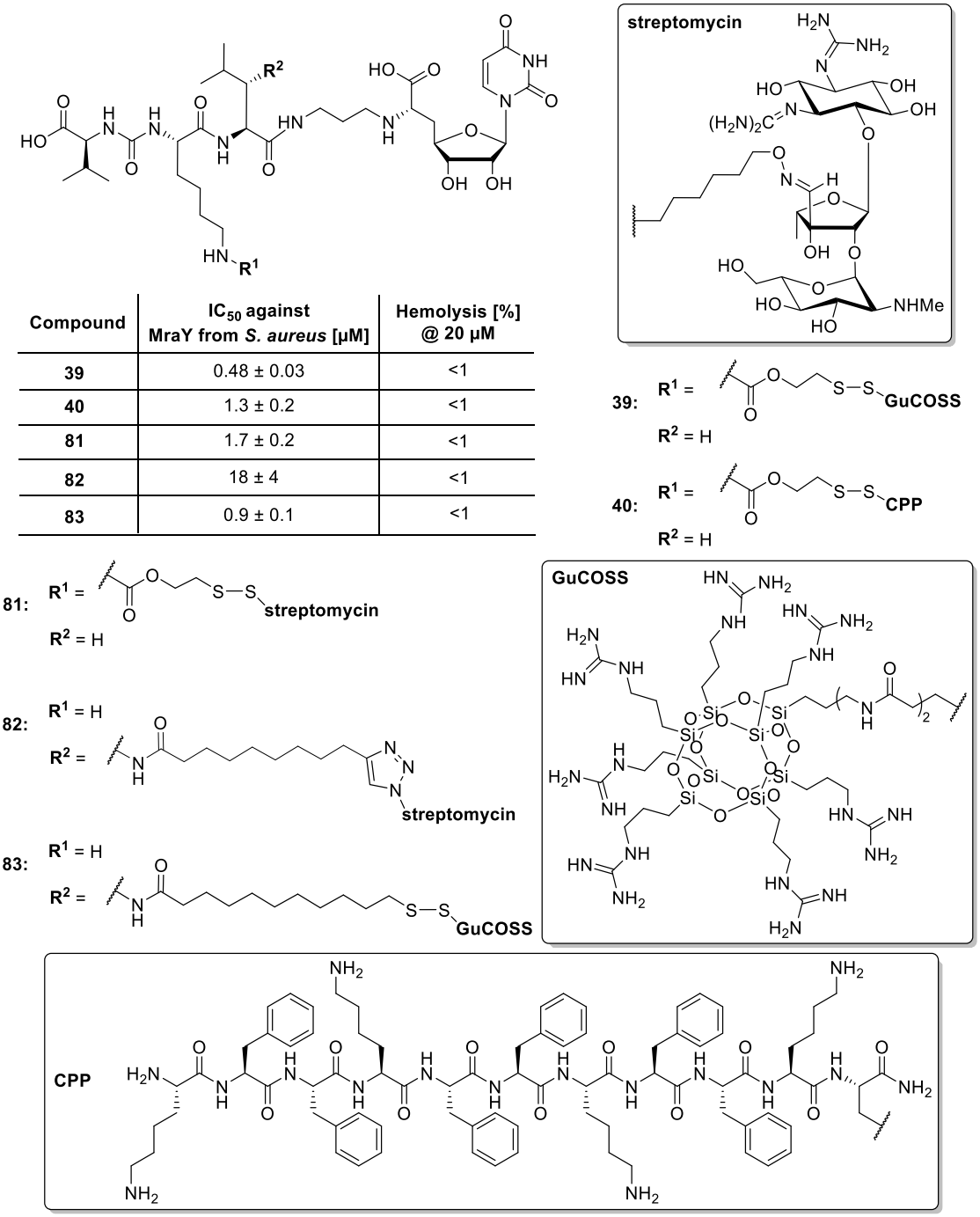

Compound	IC_{50} against MraY from *S. aureus* [µM]	Hemolysis [%] @ 20 µM
39	0.48 ± 0.03	<1
40	1.3 ± 0.2	<1
81	1.7 ± 0.2	<1
82	18 ± 4	<1
83	0.9 ± 0.1	<1

*Figure 5.7: Hemolytic activities of muraymycin streptomycin conjugates **81** and **82**, muraymycin GuCOSS conjugates **39** and **83** and muraymycin CPP conjugate **40** by Dr. C. Rohrbacher[240] in a concentration of 20 µM.*

In summary, the hemolysis assay of this work provided additional insights into biological properties of potential drug candidates of our research group.

Further studies were performed as part of several collaborations. A series of compounds provided by the research group of Dr. S. Roy was examined. Our collaborators work on a structure-based drug design approach targeting MraY and provided multiple compounds for the activity assays. Furthermore, selected compounds were investigated in cellular uptake and hemolysis assays. In terms of MraY inhibition assays, a screening was performed resulting in the successful identification of potential hit compounds. IC_{50} determination could be carried out for at least two compounds with inhibitory activities observed in the triple-digit micromolar range (not depicted). These studies strengthened our collaborator's screening and synthetic approach and contributed to the development of further compounds.

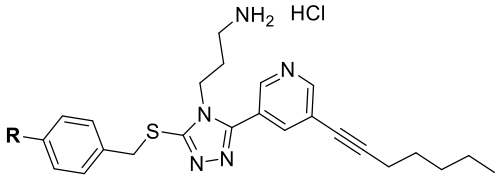

41: **R** = Cl
42: **R** = OH
74: R = NO_3

Compound	IC_{50} against MraY from *S. aureus* @250 µM [%]	IC_{50} [µg/mL]	Cellular uptake in *E. coli* Δ*tolC* Sample concentration [nM] / *Biological concentration [µM]*	Hemolysis [%] @20 µM
41	34	*E. coli* DH5α 3.7 *E. coli* Δ*tolC* 3.5	whole cells: 271 ± 97 / *4.3 ± 1.5* cytoplasm: 162 ± 5 / *2.9 ± 0.9* periplasm: 54 ± 4 / *6.2 ± 0.5*	<1
42	n.d.	*E. coli* DH5α 6.5 *E. coli* Δ*tolC* 3.3	whole cells: 147 ± 25 / *2.4 ± 0.4* cytoplasm: 79 ± 21 / *1.4 ± 0.4* periplasm: 12 ± 2 / *1.4 ± 0.3*	<1
74	82	not investigated	not investigated	<1

*Figure 5.8: Biological activities of non-nucleoside compounds **41, 42** and **74** by the research group of Dr. S. Roy. The inhibitory activity against MraY, antibacterial growth inhibition data, cellular uptake data in E. coli ΔtolC and hemolytic activities are depicted. The cellular uptake data is presented as sample concentrations for whole cell lysate ("whole cells"), cytoplasmic space and periplasmic space. The biological concentrations are calculated under consideration of the cell number.*

Accumulation studies were successfully performed for compounds **41** and **42** and revealed the same trend: Accumulation in the cytoplasm was higher compared to periplasmic accumulation (Figure 5.8). Nonetheless, cellular uptake of both compounds was comparable taking the measurement's uncertainty into account. Further investigation with regard to an additional mode of action might be interesting. Both compounds **41** and **42** were additionally examined in the hemolysis assay to address possible membrane-disruptive effects as a result of their amphiphilic properties. Compound **74** was included in this series of measurements (by request

of our collaborators). Hemolytic activity of all three compounds was determined with <1% at a concentration of 20 µM (Figure 5.8). In summary, the experiments complemented the biological data of potential novel drug candidates with anti-tuberculosis activity and helped our collaborators to gain further insights with regard to further SAR studies.

More compounds by collaborators were investigated in this work in terms of inhibitory activity against MraY. The research group of Prof. Dr. M. Kaiser provided callyaerin B that showed antitubercular activity in the low micromolar range. A screening was performed, but no inhibitory activity against *S. aureus* MraY (overexpressed in *E. coli*) as crude membrane preparations was detected. A novel capuramycin and its phosphorylated analogue provided by the research group of Prof. Dr. S. Van Lanen was examined in the MraY inhibition assay. Capuramycins A and F were utilized as references since no inhibitory data of this class of antibiotics was available in our laboratory. The obtained inhibitory activities of capuramycins A and F were comparable to those found in literature. Inhibition assays with the novel capuramycin revealed the strongest inhibitory activity against MraY compared to capuramycins A and F. The expected reduced inhibitory activity of the phosphorylated analogue was furthermore confirmed. The research group of Prof. Dr. R. Müller provided an extract for the investigation of MraY inhibition. The suggested presence of muraymycins in this extract could, however, be ruled out since no inhibitory activity was observed in the activity assay. Overall, the investigation of inhibitory activities with potential drug candidates provided by collaborators contributed to their overall biological evaluation and gave direction to the development of novel approaches.

In the interest of completeness, it should be noted that the adaption and establishment of the envisioned assay for the determination of porcine liver esterase activity in different biological media remained unsuccessful.

5.2 Synthesis

The synthesis project focused on the novel muraymycin pivaloyloxymethyl (POM) prodrugs **50**-**52**. The tripartite approach established in our reserach group was applied.[190,197,198] The uridine-derived 5'-deoxy-nucleosyl amino acid **53** represented the most important building block in this stereoselective route. It was succesfully synthesized according to our established procedure in 49% yield over two steps starting from the 2',3'-*O*-bis-*tert*-butyldimethylsilyl (TBDMS) uridine-5'-alcohol **100** (Figure 5.9). A selective oxidation in 5'-position of 2',3'-*O*-bis-*tert*-butyldimethylsilyl (TBDMS) uridine-5'-alcohol **100** followed by Wittig-Horner reaction with the POM ester phosphonate **58** resulted in the *Z*-configurated nucleosyl amino acid **53**. POM ester phosphonate **58** was obtained in four steps starting from glyoxylic acid monohydrate **86** by condensation, Michaelis-Arbuzov-type reaction and alkylation with POM-I **62** (not depicted, cf. Scheme 4.3). Subsequent homogeneous asymmetric hydrogenation with the chiral rhodium(I) catalyst Me-DUPHOS-Rh delivered the desired (6'S) stereocenter in the nucleoside building block (not depicted, cf. Scheme 4.10). Limited steroselectivity, however, resulted in a diastereomeric ratio of *d.r.* ~ 7:3 based on ^{1}H NMR analysis (Figure 4.56). The asymmetric hydrogenation of the nucleosyl amino acid **53** was examined in more detail in this work, thus contributing to further optimization of this step in the future. Following, Cbz deprotection and reductive amination were performed. Amines were generally provided as TFA salts to avoid decomposition as a result of the nucleophilic properties of free amino moieties in combination with POM functionalities. As a consequence, the reductive amination of the nucleosyl amino acid **102** with the leucine-derived aldehyde **28** was performed with a slight excess of DIPEA (2.0 eq.). The synthesis of the linker-containing aldehyde **28** was performed in 75% yield over three steps according to a literature-known method (not depicted, cf. Scheme 4.8). The nucleosyl amino acid **103** was obtained in 21% yield over three steps (Figure 5.9). Subsequent Cbz deprotection and peptide coupling with the urea dipeptide **54** delivered analogue **104** in 17% yield over two steps (Figure 5.9). Standard amide coupling conditions with the coupling reagents HOBt and PyBOP were applied. Tripyrrolidinophosphine oxide as a known byproduct of peptide couplings with PyBOP was removed by reversed phase HPLC under isocratic conditions at a later stage within this route. The L-valine- and L-lysine-containing urea dipeptide **54** was synthesized according to our established procedure and was successfully obtained in 36% yield over four steps (not depicted, cf. Scheme 4.4).[212,252,253] Overall, the fully protected bis-POM-5'-deoxy muraymycin **104** was successfully synthesized as the first key intermediate over nine steps starting from the 2',3'-*O*-bis-TBDMS uridine-5'-alcohol **100** (Figure 5.9). Hereafter, the Cbz-protection group was cleaved under our established transfer hydrogenation conditions to obtain bis-POM-5'-deoxy muraymycin analogue **105** in 17% (Figure 5.9). This analogue served as a starting point for the implementation of the carbamate functionaility into the target compound **52** (Figure 5.11).

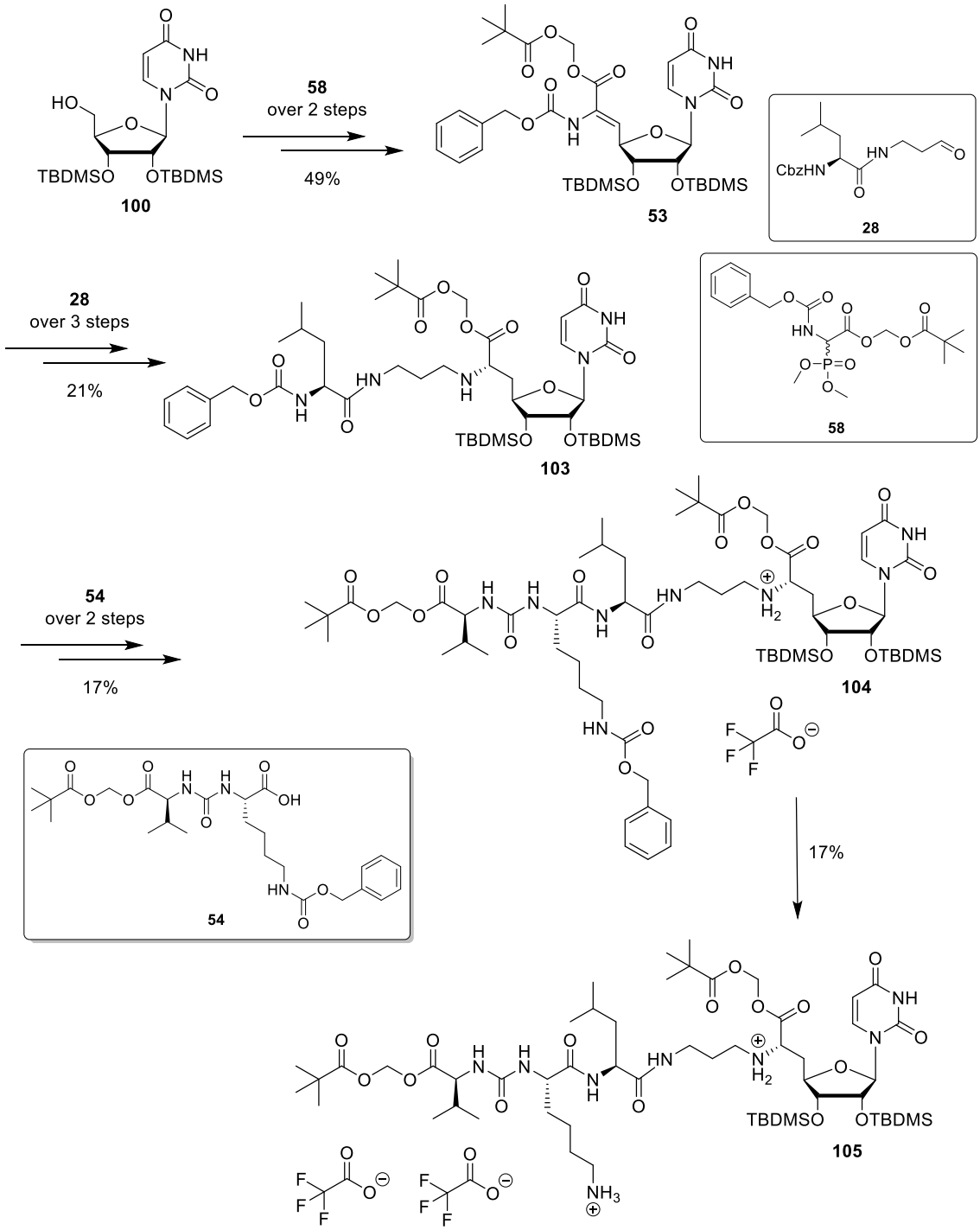

*Figure 5.9: Synthesis of bis-POM-5'-deoxy muraymycin analogue **105.***

The carbamate unit in the desired target compound **52** was introduced with the corresponding benzyl chloroformate **57** in three steps according to the literature (Figure 5.10).[254,255] The reaction sequence included an esterification, a reduction and the final formation of the corresponding acid chloride. Starting from 4-hydroxybenzaldehyde **70**, chloroformate **57** was successfully synthesized in 16% yield over three steps. Since the investigation of efficiency and suitability of this route was focused on, only the pivalate-containing chloroformate derivative **57** was synthesized in its final step. This formation was directly performed prior to

coupling with the nucleosyl amino acid core due to the known instability of chloroformates.[254,255] For the same reason, column chromatography as reported in the literature was avoided.[255] 4-(hydroxymethyl)-phenylacetate **86** was obtained in 78% over two steps. The synthesis of 4-(hydroxymethyl)-phenylbutyrate **87** resulted in 56% yield over two steps. The loss in yield of compound **87** was attributed to the purification by column chromatography. However, no further optimization of purification was performed since enough material was synthesizied. Both intermediates **86** and **87** were successfully synthesized (Figure 5.10). In summary, chloroformate intermediates at different stages were successfully synthesized.

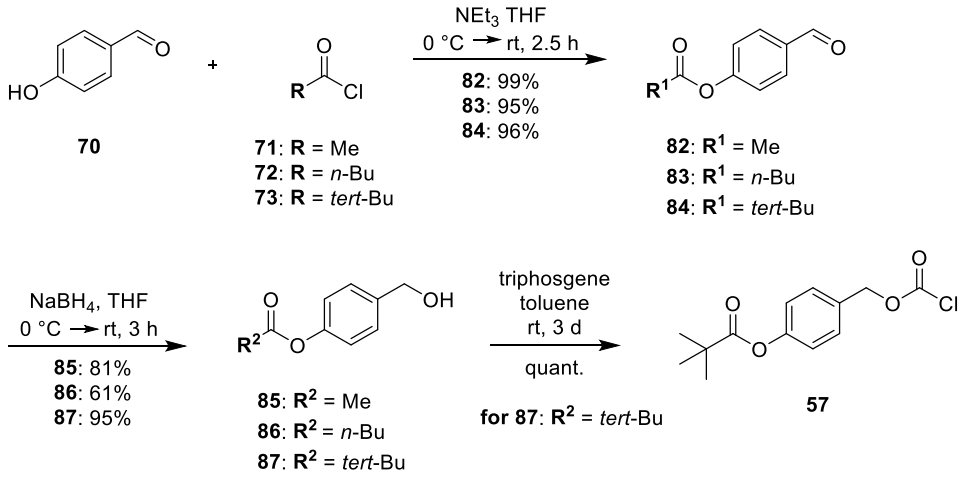

*Figure 5.10: Synthesis of chloroformate **57**.*

The final steps towards the target compound **52** consisted of the carbamate formation followed by global deprotection starting from the *N*-Cbz-deprotected Bis-POM-5'-deoxy muraymycin analogue **105** (Figure 5.11). Both reactions were performed in one step without analytics in between. Mild acidic conditions were applied for global deprotection to avoid decomposition of the POM moieties. The purification by semi-preparative HPLC, however, yielded insufficient amounts for a full analytical characterization. Nonetheless, NMR data indicated failure of the synthesis. The synthesis of the desired target compound remained unsuccessful, most likely due to the applied route of carbamate implementation. Further investigation is required.

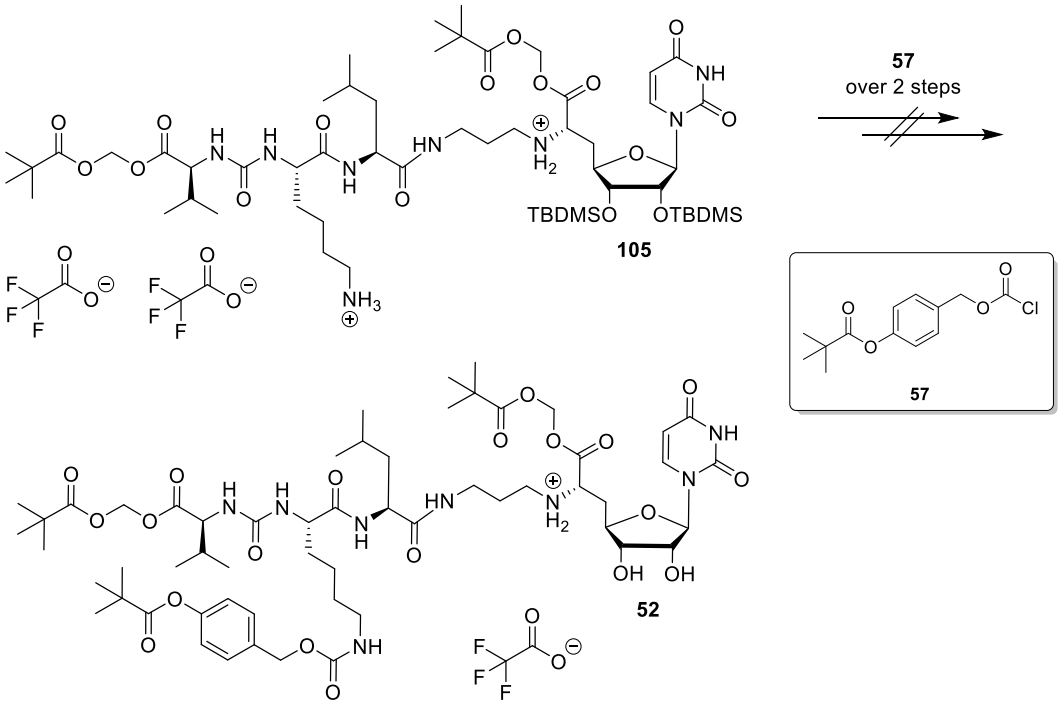

*Figure 5.11: Attempted synthesis of target compound **52**.*

In summary, the synthesis towards the desired muraymycin POM prodrug **52** had to be considered as failed. Nevertheless, synthesis studies of this work provided important findings which will contribute to the optimization of future work. In particular, asymmetric hydrogenation was extensively investigated. Reproducibility of the results obtained by Dr. D. Wiegmann were confirmed except for this reaction.[212] This synthesis project will be taken over to L. Thilmont as part of her dissertation.

6 Outlook

Analysis of cellular accumulation of potential drug candidates has become increasingly important. With cellular uptake assays for Gram negative *E. coli* and Gram-positive *S. aureus* in hand, other bacterial species, in particular species of the so-called “ESKAPE“ pathogens, will be of interest for further accumulation assays. Strains of *Enterobacter, Acinetobacter baumannii*, *Klebsiella pneumoniae*, *Enterococcus faecium* and *P. aeruginosa* beside *S. aureus* belong to this group that pose tremendous challenges to global healthcare.[288] A comparison of cellular uptake data between different bacterial species would enable deeper insights about different cellular barriers. In particular, *P. aeruginosa* would be of particular interest since the muraymycin analogues synthesized by Dr. G. Niro showed antibacterial activity against this strain.[239] Furthermore, a biofilm formation is observed for *P. aeruginosa* to protect itself against exogenous effects, thereby consequently representing an additional barrier.[12] Cellular uptake data would be attractive to evaluate the influence of this biofilm. The investigation of cellular uptake of the naturally occurring muraymycins should be kept in mind still, especially with regard to the enormous bacterial variety. It is not clearified yet if, e.g., cellular uptake of these compounds is challenging to a similar extent for other microorganisms as well. However, the focus should generally be placed on the lipidated muraymycin derivatives of the series A and B to investigate the impact of their fatty acid chains on cellular uptake. Matsuda and Ichikawa already associated these lipophilic properties with enhanced cellular uptake.[183] Accumulation data of the naturally occurring muraymycins would provide a deeper understanding of the physicochemical mechanisms in general. This information would be advantegous because they would specifically enable the design of novel derivatives with improved cellular uptake. Additional investigations of potential drug cadidates in permeation assays utilizing an artifical membrane model would also be interesting to compare these data with the uptake data performed with bacteria.[169] Such a membrane-mimetic assay was was primarily developed for clinically active drugs. However, since it is already published, adaption of these experiments can be implemented rapily.[169] In general, it would be interesting to investigate if selected bacterial strains are more resistant to selected compounds with antibacterial activity due to limited cellular uptake. These subjects have not been evaluated yet, thus demonstrating the high potential of this field.

In this context, the possibility of a compound’s adsorption to bacterial membranes should be noted. This subject came into the fore during the cellular uptake assays of this work in case of muraymycin conjugates with highly charged moieties and muraymycin analogues predominantly bearing lipophilic moieties. Cellular uptake could be simulated due to high accumulation data as a result of non-specific binding of the compounds to the bacterial membrane. Therefore, it would be beneficial to focus on membrane fragments in the cellular uptake assays. Modifications of the typical assay procedure were already performed in this

work for the corresponding compounds. However, more adaptions with special focus on the membrane (membrane fragments) would be helpful for evaluation of cellular uptake results. Experiments by Brönstrup et al. have already been performed.[135] However, the investigation of membrane fragments also requires an optimization of the analytics towards MS^2 analytics (as performed by Brönstrup et al.[135]). MS^2 analytics would enable the detection of low compound amounts. Contrary, sufficient amounts of the compounds are required for method optimization which can be problematic for compounds produced in limited quantities. An assay which enables the determination of membrane interactions would be a compromise. Initial efforts have been made in this work which were not further pursued in our laboratory. Incubation of bacteria with a membrane-interacting agent such as propidium iodide should result in the integration of this agent into membranes. The detection of fluorescence changes after the application of the compounds should enable an evaluation in terms of membrane interaction. Such an assay would provide further insights into this subject and should therefore be kept in mind for further studies.

Further experiments regarding the MraY quantification assay started in this work would be desirable. Follow-up studies in terms of the nanobody concentration should be envisioned. Moreover, parameters such as incubation times with the different antibodies should be evaluated and optimized for the further development of the assay. With all parameters optimized, MraY amounts in different preparations such as crude membrane preparations, MraY protein in detergent micelles and the MraY nanodiscs should be investigated. Evaluations in terms of inhibitory activities of drug candidates against their bacterial target MraY will be improved with specific MraY activity data and absolute MraY amounts in hand. The inhibitory activities of selected naturally occurring muraymycins provided by Koppermann et. al can be examined in more detail.[84]

Further studies should focus on the optimization of the synthesis towards the desired pivaloyloxymethyl (POM)-carbamate prodrugs. First, the synthesis should be performed in analogous fashion to obtain higher amounts of precursors. A complete modification of the synthetic route to increase yields should be considered. For instance, it is reported that chloroformates can also be prepared *in situ* without work-up or solvent removal.[227] Another approach could be the introduction of the carbamate functionality prior to the introduction of the urea dipeptide. A complete biological evaluation, i.e. assays for the investigation of MraY inhibition, antibacterial growth inhibition, metabolic stability and cellular uptake should be performed. The latter would be focused on since the success of enhanced lipophility of the POM-carbamate prodrugs of this work relative to the POM prodrugs by Dr. D. Wiegmann in terms of cellular uptake should be evaluted.[212] This data will be decisive to further conceptual studies in terms of the muraymycin prodrug approach. Moreover, it would be desirable to investigate other masking groups for the carboxylic acids and/or amino moiety of the

muraymycin core (encircled in Figure 6.1). Addditional esterase-cleavable masking groups would be, e.g., *iso*-propyl-oxycarbonyl-oxymethyl (POC), acetoxymethyl (AM), acetoxybenzyl (AB) or acetoxybenzyloxycarbonyl (ABC) units (Figure 6.1). The effects on the biological properties of muraymycin prodrugs bearing a combination of different masking groups would also be interesting. Overall, the projects of this dissertation represent a basis for further studies in terms of the presented subjects.

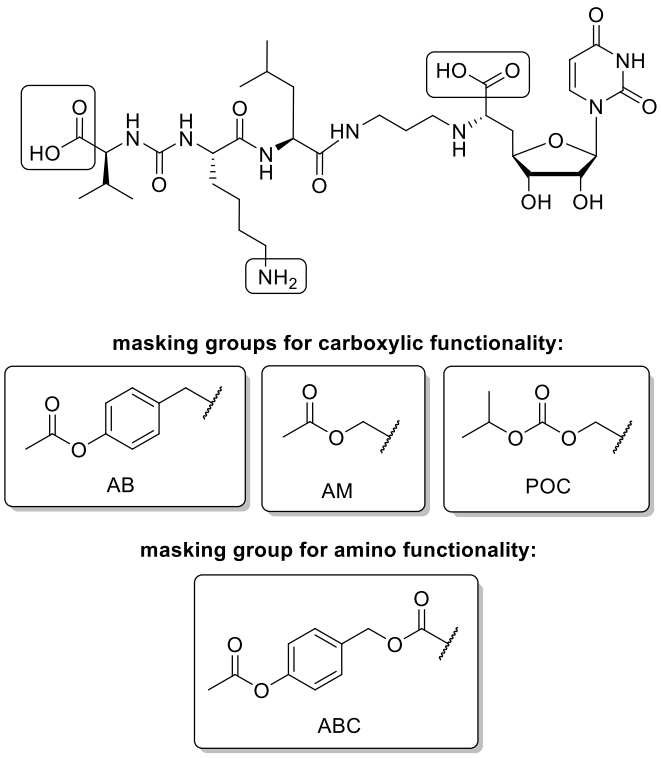

Figure 6.1: Different masking groups for the extension of the muraymycin prodrug strategy.

7 Experimental section

7.1 Biological studies

7.1.1 General methods and procedures

In the following section, general methods and procedures for the biological studies of this work will be presented.

7.1.1.1 Bacterial strains

All bacterial strains used in this work, *E. coli* DH5α, *E. coli* Δ*tolC* and *S. aureus* Newman, were obtained from the Helmholtz Institute for Pharmaceutical Research Saarland from the research groups Prof. Dr. R. Müller or Prof. Dr. A. K. H. Hirsch. All bacteria were stored at -80 °C as glycerol stocks (termed 'Stammsammlung AK Ducho').

Chemically competent *E. coli* DH5α(DE3) cells, *E. coli* Lemo21(DE3) cells, *E. coli* C41(DE3) cells, *E. coli* BL21(DE3) and *E. coli* BL21(DE3) pLysS cells used in this work were purchased from New England BioLabs and Promega.

7.1.1.2 Plasmids

All plasmids were either obtained from S. Koppermann or designed in the course of this work. In the latter case, corresponding sequences will be listed in the appropriate section. The pET32a(+) vector required for the expression of lysostaphin was purchased from Merck. Subsequent design of the lysostaphin plasmid included codon optimization and the plasmid was ordered as specific gene synthesis from Eurofins (Chapter 7.1.3.3.1).

7.1.1.3 Chemicals and solvents

All chemicals and solvents used in this work were purchased from ABCR, Alfa Aesar, Merck, Roth, Sigma Aldrich, VWR, Thermo Scienfitic and Carbosynth. Organic solvents were used in ultrapure quality ('HPLC grade'). If not indicated otherwise, highly pure water obtained from a TKA GenPure water purification system (Milli-Q®) was used throughout.

7.1.1.4 Autoclave

All media and solutions required sterile were autoclaved at 120 °C (Fedegari Autoklavi) if not indicated otherwise.

7.1.1.5 Sterile work

Sterile working procedures were carried out with disinfected gloves under the sterile bench (Thermo Scientific MSC-Advantage™ in S1 laboratory, Holten LaminAir in S2 laboratory). All

media and solutions required sterile were disinfected before being placed in the sterile bench and opened only under laminar flow.

7.1.1.6 Pipetting

Pipetting up to 1 mL was performed with calibrated microliter pipettes and the appropriate TipOne® tips from STARLAB. For larger volumes, autoclaved glassware or sterile serological pipettes were used.

7.1.1.7 SDS-PAGE

Denaturing SDS-PAGE was used for the separation of protein mixtures and as expression control. Gels (12% for separation, 5% for stacking) were prepared as listed in Table 7.1.

Table 7.1: Composition of separation and stacking gel for SDS-PAGE.

Separation gel (12%)	Composition	Stacking gel (5%)
3.3 mL	Milli-Q® water	1.4 mL
4.0 mL	Acrylamide (30%)	330 µL
2.5 mL	1.5 M Tris-HCl buffer pH 8.8	-
-	1.5 M Tris-HCl buffer pH 6.8	250 µL
100 µL	SDS (10%)	20 µL
280 µL	APS (10%)	56 µL
16 µL	TEMED	8 µL

Page Ruler™ Prestained Protein ladder from Thermo Scientific was used as reference. Sample preparations were performed differently depending on the purpose of the gel and are therefore mentioned in the corresponding chapters. SDS-PAGE gels were stained with a Coomassie solution consisting of solution A (50 mL water + 10 mL acetic acid 99%) and solution B (0.5 g Coomassie Brilliant Blue G-250 in 40 mL MeOH). Destaining was carried out with a solution consisting of MeOH (40%) and acetic acid (10%) in water.

7.1.1.8 Agarose gels

Agarose gels (1%) were performed to verify product formation of subcloning PCRs. Therefore, agarose (1.0 g) was suspended in Tris-acetate-EDTA (TAE) buffer (100 mL) and heated in the microwave for 90 s. As reference peqGOLD 1kb DNA ladder from Thermo Scientific was used. Samples were prepared differently and are listed in the corresponding chapters. Agarose gels were stained with a solution of ethidiumbromide (30 µL) in TAE buffer (600 mL) for 30 min and destained with water for 10 min. Visualizing was performed under UV light.

7.1.1.9 Media and buffers

All media and buffers used in this work are listed in Table 7.2 including their composition. Müller Hinton medium required for the cultivation of *S. aureus* was purchased from Carl Roth, dissolved in water and autoclaved according to the instructions prior to use.

Table 7.2: List of media and buffer used in this work.

Media / buffer	**Composition**
LB medium *for bacterial growth*	5.0 g NaCl 10.0 g peptone 5.0 g yeast extract in 1.0 L water
TB medium *for bacterial growth*	Solution 1: 24.0 g peptone 48.0 g yeast extract 8.0 mL glycerol in 1.8 L water Solution 2: 4.62 KH_2PO_4 25.08 g K_2PO_4 in 200 mL water Solution 1 and 2 were mixed, 2.0 L total volume
TAE buffer (50x) *for agarose gels*	242 g Tris-HCl 57.1 mL acetic acid 100 mL EDTA (500 mM) in 1 L water (adjusted to pH = 8.0)
buffer A *for MraY protein expressions* *(crude membrane preparations)*	BME (2 mM), $MgCl_2$ (1 mM), Tris-HCl pH = 7.5 (50 mM)
elution buffer *for MraY protein expressions* *(purified protein)*	BME (2 mM) DDM (1 mM) imidazole (250 mM) NaCl (150 mM) Tris-HCl pH = 8.0 (50 mM)
resuspension buffer *for MraY protein expressions* *(purified protein)*	BME (2 mM) NaCl (150 mM) Tris-HCl pH = 8.0 (50 mM)
size exclusion buffer *for MraY protein expressions* *(purified protein)*	DM (5 mM) DTT (2 mM) NaCl (150 mM) Tris-HCl pH = 8.0 (20 mM)
wash buffer *for MraY protein expressions* *(purified protein)*	BME (2 mM) DDM (1 mM) imidazole (10 mM) NaCl (150 mM) Tris-HCl pH = 8.0 (50 mM)

Media / buffer	**Composition**
MSP buffer *for MSP protein expression (purified protein) and nanodisc assembly*	EDTA (0.5 mM) NaCl (100 mM) Tris-HCl pH = 7.5 (20 mM)
MSP resuspension buffer *for MSP protein expression (purified protein)*	EDTA (1 mM) NaCl (500 mM) Tris-HCl pH = 8.0 (50 mM) Triton X-100 (1%)
buffer B *for MSP protein expression (purified protein)*	NaCl (500 mM) Tris-HCl pH = 8.0 (50 mM)
dialysis buffer *for MSP protein expression (purified protein)*	EDTA (0.5 mM) NaCl (0.2 mM) Tris-HCl pH = 8.0 (50 mM)
cholate buffer *for nanodisc assembly*	EDTA (0.5 mM) NaCl (100 mM) sodium cholate (100 mM) Tris-HCl pH = 7.5 (20 mM)
nanodisc buffer *for nanodisc assembly*	DTT (2 mM) $MgCl_2$ (10 mM) NaCl (150 mM) Tris-HCl pH = 8.0 (50 mM)
4-fold buffer *for MraY assays*	KCl (800 mM) $MgCl_2$ (40 mM) Tris-HCl pH = 7.5 (400 mM)
lysis buffer *for cellular uptake assays*	200 µL EDTA pH = 8.0 (500 mM) 2 mL NaCl (5 M) 10 mL Tris-HCl pH = 7.5 (1 M) in 100 mL water (adjusted to pH = 7.5)
M9 medium *for cellular uptake assays*	0.1 mL $CaCl_2$ (1 M) 10 mL glucose solution (20%) 200 mL M9 salts (5x) 2 mL $MgSO_4$ (1 M) in 1.0 L water
M9 salts (5x) *for cellular uptake assays*	15.0 g KH_2PO_4 2.5 g NaCl 5.0 g NH_4Cl 85.5 g Na_2HPO_4 x 12 H_2O in 1.0 L water
sucrose buffer *for cellular uptake assays*	2.0 g sucrose 100 µL EDTA pH = 8.0 (500 mM) 300 µL Tris-HCl pH = 7.5 (1 M) in 10 mL water
elution buffer *for lysostaphin expression*	imidazole (750 mM) NaCl (250 mM) Tris-HCl pH = 8.0 (20 mM)
resuspension buffer *for lysostaphin expression*	imidazole (5 mM) NaCl (250 mM) Tris-HCl pH = 8.0 (20 mM)

Media / buffer	**Composition**
wash buffer *for lysostaphin expression*	imidazole (20 mM) NaCl (250 mM) Tris-HCl pH = 8.0 (20 mM)
elution buffer *for NB7 expression*	imidazole (200 mM) NaCl (150 mM) Tris-HCl pH = 8.0 (50 mM)
osmotic lysis buffer *for NB7 expression*	imidazole (10 mM) NaCl (150 mM) Tris-HCl pH = 8.0 (50 mM) protease inhibitor tablet (one tablet) DNAse (one spatula tip)
resuspension buffer *for NB7 expression*	NaCl (150 mM) sucrose (20%) Tris-HCl pH = 8.0 (50 mM)
size exclusion buffer *for NB7 expression*	NaCl (150 mM) Tris-HCl (50 mM)
wash buffer *for NB7 expression*	imidazole (10 mM) NaCl (150 mM) Tris-HCl pH = 8.0 (50 mM)
running buffer (10x) *for SDS-PAGE and Western Blotting*	140.4 g glycine 30.0 g Tris-HCl in 1 L water
running buffer *for SDS-PAGE and Western Blotting*	100 mL running buffer (10x) 10 mL SDS (10%) 900 mL water
TBS buffer (10x) *for Western Blotting*	80.1 g NaCl 24.2 g Tris HCl in 1 L water (adjusted pH = 7.5)
TBST *for Western Blotting*	100 mL TBS buffer (10x) 1 mL Tween 900 mL water
transfer buffer *for Western Blotting*	200 mL MeOH 100 mL running buffer (10x) 5 mL SDS (10%) in 1 L water

The solutions of glucose (20%), $MgSO_4$ (1 M) and $CaCl_2$ (1 M) required for the M9 medium were prepared separately with water (100 mL each). The glucose solution was additionally sterile filtered (pore size 0.22 µM). All media were autoclaved and stored in the sterile bench. All buffers were sterile filtered (pore size 0.22 µM) and stored at room temperature in the laboratory.

7.1.1.10 Overnight and day cultures

To prepare overnight cultures of bacterial strains, a pipette tip of the corresponding bacterial strain in glycerol or one to five colonies from suitable LB agar plates was incubated in medium (10 mL) at 37 °C overnight (180 rpm) in a shaking incubator (Infors HT). A day culture was set up from the overnight culture in the following morning by providing a 1:100 dilution using fresh medium. Day cultures for cellular uptake assays (Chapter 7.1.3.1.1) were performed with 300 µL overnight culture in 30 mL medium, while 100 µL overnight culture in 10 mL medium were used in antibacterial growth inhibition assays (Chapter 7.1.1.11). Day cultures were grown at 37 °C and 180 rpm in a shaking incubator (Infors HT) until an OD_{600} of ~ 0.6 was obtained.

7.1.1.11 Antibacterial growth assays

Determination of antibacterial growth inhibition was performed prior to cellular uptake assays and is part of routine biological testing in our research group. It is based on the procedure "SOP-HIPS_04" provided by the Helmholtz Institute for Pharmaceutical Research Saarland. A day culture of the bacterial strain was prepared from the corresponding overnight culture as described (Chapter 7.1.1.10). Bacterial culture was diluted to an OD_{600} ~ 0.06 ('bacterial suspension'). Compounds were dissolved in DMSO or water (depending on the compound's solubility) at a concentration of 10 mg/mL. After testing the compound's precipitation tendency in solution, a 96-well plate was prepared as follows, utilizing LB medium for *E. coli* and Müller Hinton medium for *S. aureus*:

- row B3-10: medium (196 µL)
- rows C to G 3-10: medium (100 µL)
- all unused wells: water (200 µL)

The solution of the test compound in DMSO or water (4 µL) was pipetted into row B 3-10 and mixed properly. As a control, DMSO or water (4 µL) was used. 100 µL of row B was transferred into row C. After mixing properly, 100 µL were again transferred to the next row, row C. This process was repeated up to the last medium row, row G. 100 µL of row G were discarded. Bacterial suspension with OD_{600} ~ 0.06 (100 µL) was added to rows B to G 3-10. Absorption was measured at 600 nm ('A1') and the well plate was incubated in a shaking incubator (Infors HT) at 37 °C overnight (50 rpm). The following morning, absorbance at 600 nm was measured ('A2'). Compounds were tested as biological duplicates. Evaluation of the assays was done using Excel. First, the difference between mean values of A1 and A2 was plotted against the concentration of the tested antibiotics, with an example given in Figure 7.1.

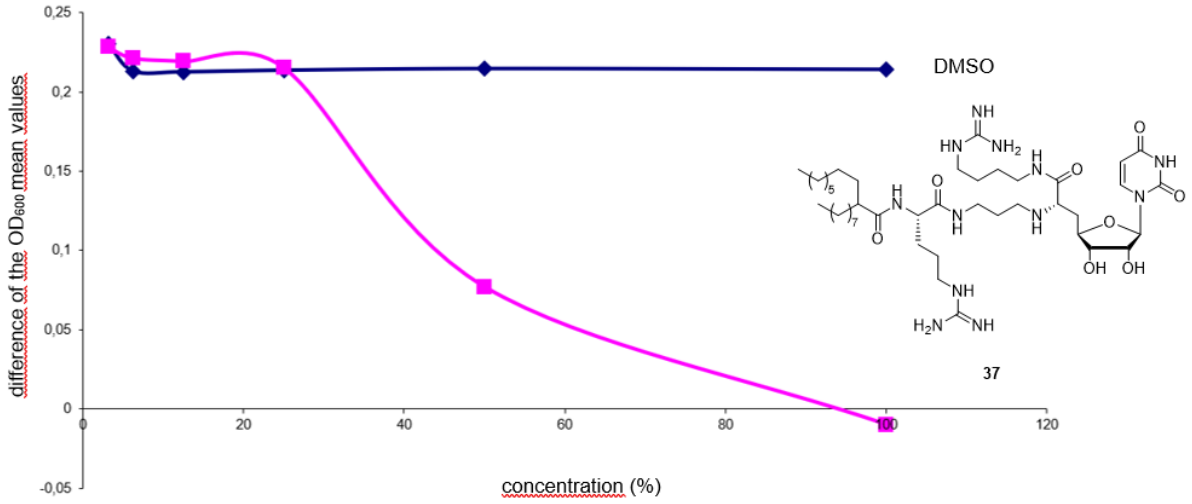

*Figure 7.1: Antibacterial growth assays for compound **37** (randomly picked) by Dr. G. Niro.*[239]

The following steps were done manually. An average trend line was drawn through the control, y-axis spacing was measured and another line was inserted halfway up (y/2). The point of intersection with the tested compound was determined and a straight line from the point of intersection to the x-axis was drawn. IC_{50} values for growth inhibition were obtained by forming the ratio and multiplying it with the highest test concentration used in the assay.

7.1.2 Methods and assays for MraY

All plasmid transformations and subsequent protein expressions of MraY in different bacterial strains will be presented in the following section.

7.1.2.1 Plasmid transformations into chemically competent *E. coli*

Plasmid transformations into chemically competent cells were performed as follows: An aliquot of competent cells (25-50 µL) was thawed on ice for 10 minutes. For subsequent plasmid injection (1 µL, ~ 50 ng) was important to not pipette up and down but rather go all the way down and pipette everything into the tube in one step. The mixture was placed back on ice and incubated for 30 minutes. A heat shock was performed at 42 °C for 45 seconds to transform the plasmid into the bacteria. After another incubation on ice for 2 minutes, sterile LB medium (200 µL) was added and the mixture was incubated in a shaking incubator (Infors HT) at 37 °C for 1 hour. 50 µL of the culture was plated on LB agar plates supplemented with appropriate antibiotics depending on the project. Plates were incubated at 37 °C overnight.

According to the general procedure, the following plasmids were transformed into chemically competent cells as listed:

- pET28a $MraY_{SA}$ was transformed into *E. coli* Lemo21(DE3) using LB agar plates supplemented with KAN (50 µg/mL) and CAM (30 µg/mL).

- pET28a $MraY_{SA}$ was transformed into *E. coli* C41(DE3) using LB agar plates supplemented with KAN (50 µg/mL).
- pET26a $MraY_{AA}$ was transformed into *E. coli* Lemo21(DE3) using LB agar plates supplemented with KAN (50 µg/mL) and CAM (30 µg/mL).
- pET26a $MraY_{AA}$ was transformed into *E. coli* C41(DE3) using LB agar plates supplemented with KAN (50 µg/mL).
- $MraY_{AA}$ (NB7) in an expression vector with a His6x tag and pelB sequence (obtained from the research group of Prof. Dr. S.-Y. Lee, Department of Biochemistry, Duke University Medical Center, USA) was transformed into *E. coli* C41(DE3) using LB agar plates supplemented with KAN (50 µg/mL).
- pET30a $MraY_{Mtb}$ (obtained from the research group of Prof. Dr. S. Van Lanen) was transformed into *E. coli* Lemo21(DE3) using LB agar plates supplemented with KAN (50 µg/mL) and CAM (30 µg/mL).
- pET28a $MraY_{Mtb}$ was transformed into *E. coli* Lemo21(DE3) using LB agar plates supplemented with KAN (50 µg/mL) and CAM (30 µg/mL).
- pET26a $MraY_{Mtb}$ was transformed into *E. coli* Lemo21(DE3) using LB agar plates supplemented with KAN (50 µg/mL) and CAM (30 µg/mL).
- pET28a $MraY_{SA}$H287Q was transformed into *E. coli* Lemo21(DE3) using LB agar plates supplemented with KAN (50 µg/mL) and CAM (30 µg/mL).
- pET26a $MraY_{SP}$ was transformed into *E. coli* Lemo21(DE3) using LB agar plates supplemented with KAN (50 µg/mL) and CAM (30 µg/mL).
- pET26a $MraY_{SP}$Q316H was transformed into *E. coli* Lemo21(DE3) using LB agar plates supplemented with KAN (50 µg/mL) and CAM (30 µg/mL).
- pET26a $MraY_{SP}$I291E was transformed into *E. coli* Lemo21(DE3) using LB agar plates supplemented with KAN (50 µg/mL) and CAM (30 µg/mL).
- pET26a $MraY_{SP}$I291E+Q316H was transformed into *E. coli* Lemo21(DE3) using LB agar plates supplemented with KAN (50 µg/mL) and CAM (30 µg/mL).
- pET28a MSP was transformed into *E. coli* BL21(DE3) using LB agar plates supplemented with KAN (35 µg/mL)

Negative controls were either performed without plasmid transformation or without induction.

7.1.2.2 Protein expressions

7.1.2.2.1 Crude membrane MraY protein preparations

Based on the expression protocol by Ducho et al.,[98] one to five colonies from the LB agar plates were used to prepare an overnight culture in LB medium (10 mL) supplemented with appropriate antibiotics depending on the project (180 rpm, 37 °C) for the expression of crude membrane MraY protein preparations. In the next morning, LB medium supplemented with appropriate antibiotics and L-rhamnose (1 mM) for controlling the overexpression rate was inoculated with overnight culture (1:100 dilution). The expression culture was incubated in a shaking incubator until an OD_{600} of ~ 0.6 (180 rpm, 37 °C, ~ 4-6 hours). Protein expression was induced with IPTG (1 mM) for 3.5 hours (180 rpm, 37 °C). Bacteria were harvested by centrifugation (5,750 x g, 20 minutes, 4 °C) and cell pellets were resuspended in buffer A (15 mL total volume), including lysozyme (one spatula tip), DNAse I (one spatula tip) and cOmplete™ EDTA-free protease inhibitor cocktail (Merck; one tablet). It was important to always prepare the buffer freshly. Cells were lysed by sonication (Bandelin Sonopuls HD 60, 15 minutes, 30% amplitude, 1 s on pulse, 2 s off pulse) and incubated at 4 °C for 30 minutes. The lysate was centrifuged (20,000 x g, 45 minutes, 4 °C) and the supernatant was centrifuged to harvest crude membrane preparations with overexpressed MraY (180,000 x g, 1 hour, 4 °C). The resultant pellet was resuspended in buffer A (1.7 mL total volume). Protein preparations were aliquoted (20 µL) and flash frozen in liquid nitrogen for storage at -80 °C.

7.1.2.2.2 Purified MraY protein in detergent micelles

According to the expression protocol by Chung et el.,[89,91] one to five colonies from the LB agar plates were used to prepare an overnight culture in LB medium supplemented with appropriate antibiotics depending on the project (180 rpm, 37 °C) for the expression of purified MraY protein. In the next morning, a culture of TB medium (2 L) was inoculated with overnight culture (20 mL) and KAN (35 µg/mL) and incubated until an OD_{600} of ~ 0.9-1.0 was reached (180 rpm, 37 °C, ~ 4 hours). Protein expression was induced with IPTG (0.4 mM) for 4 hours (180 rpm, 37 °C). Bacteria were harvested by centrifugation (5,750 x g, 15 minutes, 4 °C). Cell pellets were either stored at -80 °C overnight or immediately prepared for purification. Pellets were thawed on ice, incubated with resuspension buffer (20 mL per 1 L expression culture), including lysozyme (one spatula tip), DNAse I (one spatula tip) and cOmplete™ EDTA-free protease inhibitor cocktail (Merck; one tablet) at 4 °C for 1 hour before resuspending. Cells were lysed by sonication (Bandelin Sonopuls HD 60, 15 minutes, 30% amplitude, 1 s on pulse, 2 s off pulse). DDM was added to a final concentration of 30 mM and the mixture was stirred vigorously for 2 hours at 4 °C. Cellular debris was pelleted by centrifugation (20,000 x g, 45 minutes, 4 °C). The lysate was incubated with Co^{2+}-resin (Talon superflow resin, GE

Healthcare, 1.5 mL final bead volume for 1-2 L culture), preequilibrated with wash buffer, at 4 °C overnight. The following morning, the resin was washed with wash buffer until no protein was detected by Bradford test (10 µL eluent + 50 µL Bradford reagent). Bound protein was eluted with elution buffer (10 mL). DTT (1 mM final concentration), EDTA (1 mM final concentration) and PPX (3C Protease, 1:10 molar ratio) were added and the mixture was incubated at 4 °C overnight. 3C Protease stored at -80 °C was kindly provided by Dr. P. Fischer. Protein solution was concentrated using a 50 kDa cut off centrifugal filter (4,600 x g, 10 minutes, 4 °C) before gel filtration with size exclusion buffer (500 mL) using a Superdex 200 10/300 GL column (GE, Äkta System). Protein fractions were analyzed by SDS-PAGE (Chapter 7.1.1.7) and fractions containing MraY were combined. Protein preparations were aliquoted (20 µL) and flash frozen in liquid nitrogen for storage at -80 °C.

7.1.2.2.3 Purified membrane scaffold protein

Expression and purification of MSP1E3D1 for nanodisc assembly was performed in Boston based on the expression protocol by Wagner and coworkers.[109] In our laboratory in Germany, purified MSP1E3D1 protein was kindly provided by Dr. P. Fischer based on the same protocol. One to five colonies from the LB agar plates were used to prepare an overnight culture in LB medium supplemented with appropriate antibiotics depending on the project (180 rpm, 37 °C) for the expression of purified MraY protein. In the next morning, a culture of LB medium (2 L) was inoculated with overnight culture (20 mL) and KAN (35 µg/mL) and incubated until an OD_{600} of ~ 0.6-0.8 was reached (180 rpm, 37 °C, ~ 3 hours). Protein expression was induced with IPTG (1.0 mM) for 4 hours (180 rpm, 37 °C). Bacteria were harvested by centrifugation (6,000 x g, 15 minutes, 4 °C). Cell pellets were stored at -80 °C overnight. Pellets were thawed on ice, incubated with MSP resuspension buffer (max. 15 mL), including lysozyme (one spatula tip), DNAse I (one spatula tip) and cOmplete™ protease inhibitor cocktail (one tablet) at 4 °C for 1 hour before resuspending. Cells were lysed by sonication (15 minutes, 30% amplitude, 2 s on pulse, 4 s off pulse). $MgCl_2$ was added (5 mM) and the mixture was stirred 4 °C for 30 minutes at 4°C. Cellular debris was pelleted by centrifugation (30,000 x g, 45 minutes, 4 °C). The lysate was incubated with Ni-NTA agarose resin (Qiagen, 1 mL final bead volume for 1 L culture), preequilibrated with water and buffer B containing Triton X-100 (1%), at 4 °C for 2 hours. The resin was subsequently washed with buffer B containing Triton X-100 (1%), buffer B containing cholate (50 mM), buffer B and buffer B containing imidazole (20 mM). Washing was performed until no protein was detected by Bradford test (10 µL eluent + 50 µL Bradford reagent). Bound protein was eluted with buffer B containing imidazole (500 mM). Resulting pellet after lysis (“inclusion bodies“) was treated with buffer B containing GuHCl (6 M) to release MSP coated by the insoluble inclusion bodies. Purification by Ni-NTA agarose resin, preequilibrated with water and GuHCl (6 M), of the inclusion bodies was performed under same conditions. The expressed protein was dialyzed with dialysis buffer (2 L) at 4 °C overnight.

Protein solution was concentrated using a 50 kDa cut off centrifugal filter (4,600 x g, 10 minutes, 4 °C). Protein fractions were analyzed by SDS-PAGE (Chapter 7.1.1.7) and fractions containing MSP1E3D1 were concentrated to ~ 700 µM by 50 kDa cut off centrifugal filter (4,600 x g, 10 minutes, 4 °C). Protein preparations were aliquoted (20 µL) and flash frozen in liquid nitrogen for storage at -80 °C.

7.1.2.2.4 Nanodisc assembly

$MraY_{AA}$ nanodiscs were prepared based on the protocol by Dr. P. Fischer.[122] A lipid mixture of DOPE and DMPG in a ratio of 8.5/1.5, MSP1E3D1 (Chapter 7.1.2.2.3) and purified $MraY_{AA}$ (Chapter 7.1.2.2.2). Stock solutions of DOPE and DMPG in chloroform were combined in a tube to a final concentration of DOPE (51 mM) and DMPG (9 mM). Chloroform was evaporated under nitrogen gas followed by dissolving the lipid mixture in cholate buffer (final volume 200 µL, final concentration 60 mM). The $MraY_{AA}$-nanodisc system was prepared in a ratio of 3 (MSP1E3D1) : 1 (purified $MraY_{AA}$) : 100 (lipid mixture) in a volume of 500 µL. It was essential to follow the correct order of pipetting (at room temperature) as listed: MSP buffer, lipid mixture, purified MSP1E3D1, purified $MraY_{AA}$. After incubation at room temperature for 1 hour, ~ 500 mg saturated Biobeads SM-2 (BIO RAD) were added and the mixture was incubated with gentle shaking (IKA vibrax VXR shaker, VX8) at room temperature overnight. The next morning, beads were removed by centrifugation (4,600 x g, 10 minutes, 4 °C). The $MraY_{AA}$-nanodiscs-containing tube should be washed with MSP buffer. Nanodiscs were concentrated using a 10 kDa cut off centrifugal filter before subjecting to SEC using a Superdex 200 5/150 GL column (GE, Äkta System) preequilibrated with nanodisc buffer. Protein fractions were analyzed by SDS-PAGE (Chapter 7.1.1.7) and fractions containing $MraY_{AA}$ nanodiscs were combined and flash frozen in liquid nitrogen for storage at -80 °C.

7.1.2.3 *In vitro* MraY assays

According to Bugg's fluorescence-based method,[96,97,244] *in vitro* MraY assays used in our research group as well as the determination of IC_{50} values were carried out as described before.[84,99]

"*In vitro* MraY assays were performed using our previously reported adapted version of Bugg's fluorescence-based method. Fluorescence intensity over time was measured at λ_{ex} = 355 nm and λ_{em} = 520 nm (BMG Labtech POLARstar Omega, 384-well plate format). Each well contained a total volume of 20 µL with 100 mM TRIS-HCl buffer (pH 7.5), 200 mM KCl, 10 mM $MgCl_2$, 0.1% Triton X-100, 0-5% DMSO, 50 mM undecaprenyl phosphate, 7.5 mM dansylated Park's nucleotide (synthetic or semisynthetic), a protein preparation (*vide infra*) and the potential inhibitor at various concentrations. The amount of DMSO in the assay mixture depended on the solubility of the inhibitor, and inhibitor-free control assays with different DMSO

content (up to 5%) showed no change in MraY activity. For MraY from *S. aureus*, 1 µL of a crude membrane preparation with a total protein concentration of 1.0 mg/mL was used and the reaction was initiated by the addition of the protein preparation. […] All protein preparations showed comparable MraY activity in the absence of inhibitors. MraY activity at a certain inhibitor concentration was determined by a linear fit of the fluorescence intensity curve from 0 to 2 min. This measure of enzymatic activity was plotted against the logarithmic inhibitor concentration and fitted with a sigmoidal fit using the formula shown below, thus furnishing IC_{50} values.

$$y = A1 + \frac{(A2 - A1)}{1 + 10^{log\,((x_0 - x)\cdot p)}}$$

[…] The validity of the inhibitory activities was confirmed using the commercially available nucleoside antibiotic tunicamycin (mixture of compounds with different fatty acyl units, obtained from Sigma-Aldrich) as a reference MraY inhibitor. Under our assay conditions and with MraY from *S. aureus* in crude membranes, this tunicamycin mixture inhibited MraY with IC_{50} = 13.6 ± 1.2 ng/mL. If one assumes the four main components of the tunicamycin mixture to be present in equimolar amounts, this corresponds to an estimated IC_{50} value of ~ 16 nM. This result was in the same order of magnitude as previously reported IC_{50} values for MraY inhibition by tunicamycin, which were obtained with a different, FRET-based assay method.“

(Quote taken from Supporting Information of Koppermann et al., *ChemMedChem* **2018**, *13*, 779-784.)

A fitted curve for MraY activity is shown as an example in Figure 7.2.

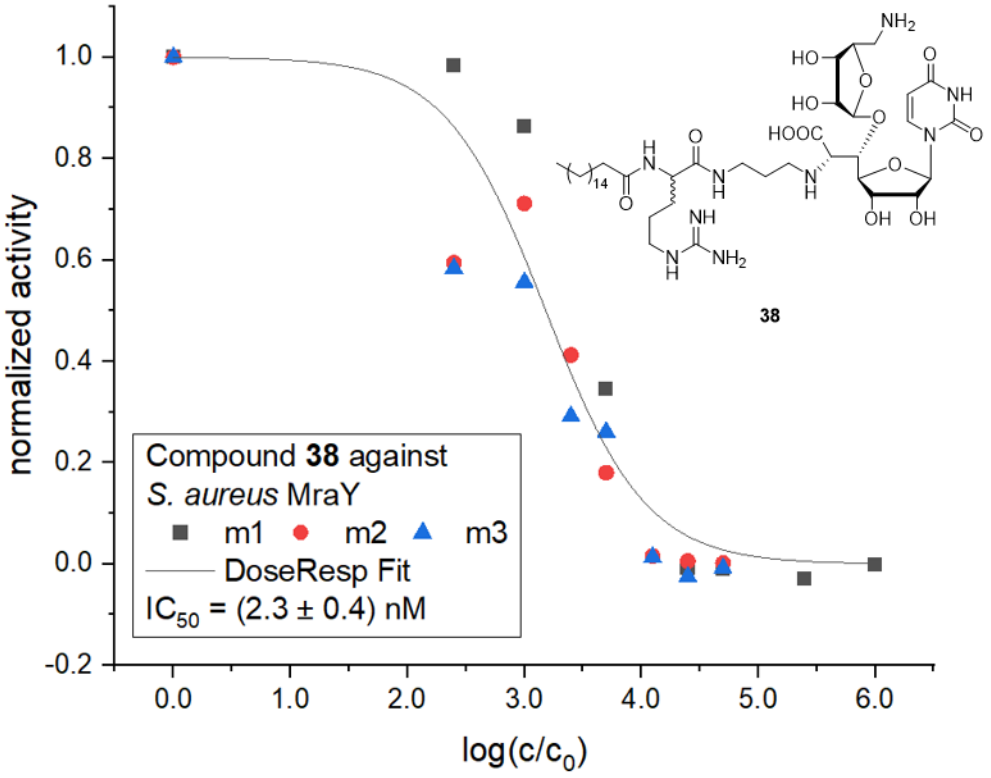

*Figure 7.2: Sigmoidal fit for IC_{50} determination (original triplicate data shown as individual series of measurements) of compound **38** (randomly picked) by Dr. G. Niro.*[239]

For compounds obtained from the laboratory of Dr. S. Roy a percentage of inhibition was determined at specific concentrations. Generally, this was also done for compounds synthesized in our research group with no or weak inhibition observed in the MraY assays. This was performed with a linear fit of the fluorescence intensity curve from 0-2 minutes using Origin as described above and subsequent calculations. Inhibition of the MraY-catalyzed reaction for tested compounds was calculated compared to blank (no inhibition, 100%) and percentage of inhibition was obtained from Excel as summarized below:

$$Percentage\ of\ inhibition\ (\%) = 100\% - \left(\frac{100\%}{Slope\ of\ blank} \cdot Slope\ of\ compound\right)$$

7.1.2.4 Subcloning by IVA method

Subcloning experiments were performed by IVA cloning according to the protocol by García-Nafría and coworkers.[274] The advantage of this cloning method is the simultaneous amplification of the vector which can either be empty or contain another gene and the insert, the gene of interest. Homologous regions to the amplified vector should be implemented at the 5'- and 3'-ends of the amplified insert. The principle is schematically depicted in Figure 7.3.

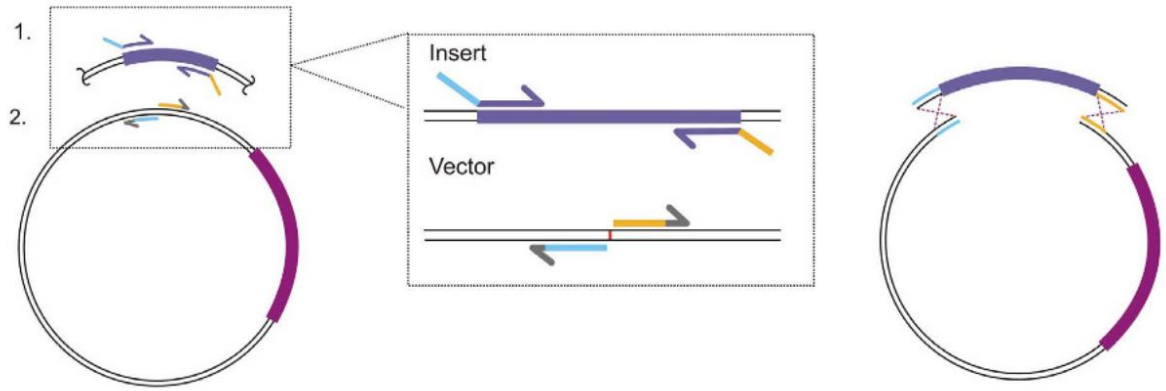

Figure 7.3: Principle of subcloning by IVA method utilizing four primers: two insert and two vector primers, forward and reverse each. The insert forward (reverse) primer includes the homologous region complementary to the vector reverse (forward) primer, shown in light blue (orange), and the template binding region, shown in magenta. Two vector primers with template binding regions are illustrated in grey/orange and grey/light blue. (taken from: García-Nafría et al., Sci. Rep. ***2016****, 6, 27459).[274]*

Four different primers, two vector and two insert primers which consisted of one forward (fwd) and one reverse (rev) primer each, were designed. To determine the right positions for subcloning, corresponding DNA sequences were translated into amino acid sequences by Expasy (includes nucleotide sequence, no spaces). Starting point for the design of the fwd vector primer was the region where the 3'-end of the gene of interest was going to be inserted. The melting temperature (T_m) value of this primer was adjusted to 60 °C by the tool 'T_m calculator' of New England BioLabs which was applied for all primer designs. The corresponding complementary rev vector primer was located at the 5'-end of where the gene of interest was going to be inserted with a T_m value of 60 °C as well. The general procedure for designing both insert primers was the same except for one addition: Both primers contained a nucleotide sequence which was complementary to the homologous region of the corresponding fwd or rev vector primer with a T_m value of 47-52 °C in order to avoid a simultaneous annealing during PCR. Vector, insert and primer sequences required and specifically ordered for this work are listed in Chapters 7.1.2.4.1 and 7.1.2.4.2. Subsequent PCR clean-up is described in detail in Chapter 7.1.2.4.3. PCR reactions were set up as described below in Table 7.3.

Table 7.3: General composition of PCR reactions.

PCR ingredients	Amount (µL)
template	1 (~ 3-5 ng DNA)
primer mix	1 (100 nM)
DMSO	0/1
Phusion High-Fidelity PCR master mix	12.5
water (to fill up to total volume)	varies depending on the approach (Table 7.4)
total volume	25

Individual PCR approaches were performed in separate tubes while 'combined approaches' were carried out in one single tube as presented in Table 7.4. Fwd and rev primers of insert and vector were mixed before (2.5 µM each). The addition of DMSO in PCR approaches may sometimes result in better amplifications, thus each approach was carried out twice (including and excluding DMSO).

Table 7.4: Pipetting scheme of 'individual approaches' and 'combined approach'.

	Amount (µL)	
PCR ingredients	**'Individual approach' insert/vector**	**'Combined approach'**
template	1	2 (insert and vector)
primer mix	1	2
DMSO	0/1	0
Phusion High-Fidelity PCR master mix	12.5	12.5
water (to fill up to total volume)	10.5/9.5	8.5
total volume	25	25

PCRs were performed overnight using a thermocycler from BIO RAD (T100™ Thermal Cycler) as described in Table 7.5

Table 7.5: PCR protocol.

PCR process	Temperature (°C)	Time (s)
initial denaturation	98	30
denaturation	98	10
annealing	60	30
extention	72	20/kb.
(repeat from 2, 19 times)		
final extention	72	5

Agarose gel analysis was used with all approaches after subcloning (Chapter 7.1.1.8). A PCR clean-up was done (Chapter 7.1.2.4.3) before amplified PCR products were transformed into *E. coli* DH5α (Chapter 7.1.2.1) in order to produce the vector including the gene of interest *in cellulo*.

7.1.2.4.1 pET30a $MraY_{Mtb}$ into pET28a $MraY_{Mtb}$

Sequence of pET28a $MraY_{SA}$:

ATCCGGATATAGTTCCTCCTTTCAGCAAAAAACCCCTCAAGACCCGTTTAGAGGCCCCA
AGGGGTTATGCTAGTTATTGCTCAGCGGTGGCAGCAGCCAACTCAGCTTCCTTTCGGG
CTTTGTTAGCAGCCGGATCTCAGTGGTGGTGGTGGTGGTGCTCGAGATGCACTCCAAT
CCATAAACCGATTAAACCTGAAATCAGACCAACAGCCCAAAATACTGTAACTACTTTCCA
TTCACTCCAACCTATCAATTCAAAATGATGATGAATCGGACTCATTTTAAATATACGCTTT
CCAGTCAATTTAAAGCTAGCGACTTGTAACATAACAGATAATGTTTCAATTACGAATACTA
AACCTATAAAAATTAATGATAATTCCTGATTAAGCATGATTGAAATCGTAGCAAATATACC
ACCTAAAGCTAAGCTACCTGTATCTCCCATAAACACTTTAGCAGGGTTAATGTTATATGG
TAAAAATCCTAAAAGTGCAAACAACATAATGATACAGAAAATACCAATCGCCGTTTCTCC
TAACACAAAGCTCATGATGGCATACATTGTAAATCCGATAATTGACAGTCCAGTTGCTAA
TCCATCTAAACCATCTGTTAAATTTACCGCATTAGAAAAACCTACTTGCCAAAAAACAATG
AAAATAACATATGCAAATGATAGTGGGATTGCTACATTCGTAAATGGAATATGTATGCTC
GTAGAAAAATTCACCAAATGAAATACATTACTTAAAACAAAGAAAATAATCGCAATACCAA
TTTGCGCCAAAAACTTCTGTTTACTTGTTAAACCTTGGTTATTCTTTTTAACAACAATAATA
TAATCATCTATAAAACCAATTAACCCAAAACCAATCGTCACAAATAATAACAGTATGATTG
GATTAGCTTGATCTACAAATATAATAGCCACCAAAGACGTTATCACAATACTTAATAGAAA
TGTTAGTCCACCCATCGTTGGTGTACCAGTCTTCTTCATATGGCTTTGTGGGCCTTCTTC
TCGAATACTTTGACCAAATTTCATCCTTTTTAATGTAGGTATTAAAACAGGTACCAAAACA
AATGTAATCACTAGCGCTAATAACGCATATACAAAAACCATGGTATATCTCCTTCTTAAAG
TTAAACAAAATTATTTCTAGAGGGGAATTGTTATCCGCTCACAATTCCCCTATAGTGAGT
CGTATTAATTTCGCGGGATCGAGATCTCGATCCTCTACGCCGGACGCATCGTGGCCGG
CATCACCGGCGCCACAGGTGCGGTTGCTGGCGCCTATATCGCCGACATCACCGATGGG
GAAGATCGGGCTCGCCACTTCGGGCTCATGAGCGCTTGTTTCGGCGTGGGTATGGTGG
CAGGCCCCGTGGCCGGGGGACTGTTGGGCGCCATCTCCTTGCATGCACCATTCCTTGC
GGCGGCGGTGCTCAACGGCCTCAACCTACTACTGGGCTGCTTCCTAATGCAGGAGTCG
CATAAGGGAGAGCGTCGAGATCCCGGACACCATCGAATGGCGCAAAACCTTTCGCGGT
ATGGCATGATAGCGCCCGGAAGAGAGTCAATTCAGGGTGGTGAATGTGAAACCAGTAA
CGTTATACGATGTCGCAGAGTATGCCGGTGTCTCTTATCAGACCGTTTCCCGCGTGGTG
AACCAGGCCAGCCACGTTTCTGCGAAAACGCGGGAAAAAGTGGAAGCGGCGATGGCG
GAGCTGAATTACATTCCCAACCGCGTGGCACAACAACTGGCGGGCAAACAGTCGTTGC
TGATTGGCGTTGCCACCTCCAGTCTGGCCCTGCACGCGCCGTCGCAAATTGTCGCGGC
GATTAAATCTCGCGCCGATCAACTGGGTGCCAGCGTGGTGGTGTCGATGGTAGAACGA
AGCGGCGTCGAAGCCTGTAAAGCGGCGGTGCACAATCTTCTCGCGCAACGCGTCAGTG
GGCTGATCATTAACTATCCGCTGGATGACCAGGATGCCATTGCTGTGGAAGCTGCCTGC
ACTAATGTTCCGGCGTTATTTCTTGATGTCTCTGACCAGACACCCATCAACAGTATTATT

TTCTCCCATGAAGACGGTACGCGACTGGGCGTGGAGCATCTGGTCGCATTGGGTCACC
AGCAAATCGCGCTGTTAGCGGGCCCATTAAGTTCTGTCTCGGCGCGTCTGCGTCTGGC
TGGCTGGCATAAATATCTCACTCGCAATCAAATTCAGCCGATAGCGGAACGGGAAGGC
GACTGGAGTGCCATGTCCGGTTTTCAACAAACCATGCAAATGCTGAATGAGGGCATCGT
TCCCACTGCGATGCTGGTTGCCAACGATCAGATGGCGCTGGGCGCAATGCGCGCCATT
ACCGAGTCCGGGCTGCGCGTTGGTGCGGATATCTCGGTAGTGGGATACGACGATACCG
AAGACAGCTCATGTTATATCCCGCCGTTAACCACCATCAAACAGGATTTTCGCCTGCTG
GGGCAAACCAGCGTGGACCGCTTGCTGCAACTCTCTCAGGGCCAGGCGGTGAAGGGC
AATCAGCTGTTGCCCGTCTCACTGGTGAAAAGAAAAACCACCCTGGCGCCCAATACGCA
AACCGCCTCTCCCCGCGCGTTGGCCGATTCATTAATGCAGCTGGCACGACAGGTTTCC
CGACTGGAAAGCGGGCAGTGAGCGCAACGCAATTAATGTAAGTTAGCTCACTCATTAGG
CACCGGGATCTCGACCGATGCCCTTGAGAGCCTTCAACCCAGTCAGCTCCTTCCGGTG
GGCGCGGGGCATGACTATCGTCGCCGCACTTATGACTGTCTTCTTTATCATGCAACTCG
TAGGACAGGTGCCGGCAGCGCTCTGGGTCATTTTCGGCGAGGACCGCTTTCGCTGGAG
CGCGACGATGATCGGCCTGTCGCTTGCGGTATTCGGAATCTTGCACGCCCTCGCTCAA
GCCTTCGTCACTGGTCCCGCCACCAAACGTTTCGGCGAGAAGCAGGCCATTATCGCCG
GCATGGCGGCCCCACGGGTGCGCATGATCGTGCTCCTGTCGTTGAGGACCCGGCTAG
GCTGGCGGGGTTGCCTTACTGGTTAGCAGAATGAATCACCGATACGCGAGCGAACGTG
AAGCGACTGCTGCTGCAAAACGTCTGCGACCTGAGCAACAACATGAATGGTCTTCGGTT
TCCGTGTTTCGTAAAGTCTGGAAACGCGGAAGTCAGCGCCCTGCACCATTATGTTCCGG
ATCTGCATCGCAGGATGCTGCTGGCTACCCTGTGGAACACCTACATCTGTATTAACGAA
GCGCTGGCATTGACCCTGAGTGATTTTTCTCTGGTCCCGCCGCATCCATACCGCCAGTT
GTTTACCCTCACAACGTTCCAGTAACCGGGCATGTTCATCATCAGTAACCCGTATCGTG
AGCATCCTCTCTCGTTTCATCGGTATCATTACCCCCATGAACAGAAATCCCCCTTACACG
GAGGCATCAGTGACCAAACAGGAAAAAACCGCCCTTAACATGGCCCGCTTTATCAGAAG
CCAGACATTAACGCTTCTGGAGAAACTCAACGAGCTGGACGCGGATGAACAGGCAGAC
ATCTGTGAATCGCTTCACGACCACGCTGATGAGCTTTACCGCAGCTGCCTCGCGCGTTT
CGGTGATGACGGTGAAAACCTCTGACACATGCAGCTCCCGGAGACGGTCACAGCTTGT
CTGTAAGCGGATGCCGGGAGCAGACAAGCCCGTCAGGGCGCGTCAGCGGGTGTTGGC
GGGTGTCGGGGCGCAGCCATGACCCAGTCACGTAGCGATAGCGGAGTGTATACTGGC
TTAACTATGCGGCATCAGAGCAGATTGTACTGAGAGTGCACCATATATGCGGTGTGAAA
TACCGCACAGATGCGTAAGGAGAAAATACCGCATCAGGCGCTCTTCCGCTTCCTCGCTC
ACTGACTCGCTGCGCTCGGTCGTTCGGCTGCGGCGAGCGGTATCAGCTCACTCAAAGG
CGGTAATACGGTTATCCACAGAATCAGGGGATAACGCAGGAAAGAACATGTGAGCAAAA
GGCCAGCAAAAGGCCAGGAACCGTAAAAAGGCCGCGTTGCTGGCGTTTTTCCATAGGC
TCCGCCCCCCTGACGAGCATCACAAAAATCGACGCTCAAGTCAGAGGTGGCGAAACCC
GACAGGACTATAAAGATACCAGGCGTTTCCCCCTGGAAGCTCCCTCGTGCGCTCTCCT

GTTCCGACCCTGCCGCTTACCGGATACCTGTCCGCCTTTCTCCCTTCGGGAAGCGTGG
CGCTTTCTCATAGCTCACGCTGTAGGTATCTCAGTTCGGTGTAGGTCGTTCGCTCCAAG
CTGGGCTGTGTGCACGAACCCCCCGTTCAGCCCGACCGCTGCGCCTTATCCGGTAACT
ATCGTCTTGAGTCCAACCCGGTAAGACACGACTTATCGCCACTGGCAGCAGCCACTGG
TAACAGGATTAGCAGAGCGAGGTATGTAGGCGGTGCTACAGAGTTCTTGAAGTGGTGG
CCTAACTACGGCTACACTAGAAGGACAGTATTTGGTATCTGCGCTCTGCTGAAGCCAGT
TACCTTCGGAAAAAGAGTTGGTAGCTCTTGATCCGGCAAACAAACCACCGCTGGTAGCG
GTGGTTTTTTTGTTTGCAAGCAGCAGATTACGCGCAGAAAAAAAGGATCTCAAGAAGAT
CCTTTGATCTTTTCTACGGGGTCTGACGCTCAGTGGAACGAAAACTCACGTTAAGGGAT
TTTGGTCATGAACAATAAAACTGTCTGCTTACATAAACAGTAATACAAGGGGTGTTATGA
GCCATATTCAACGGGAAACGTCTTGCTCTAGGCCGCGATTAAATTCCAACATGGATGCT
GATTTATATGGGTATAAATGGGCTCGCGATAATGTCGGGCAATCAGGTGCGACAATCTA
TCGATTGTATGGGAAGCCCGATGCGCCAGAGTTGTTTCTGAAACATGGCAAAGGTAGC
GTTGCCAATGATGTTACAGATGAGATGGTCAGACTAAACTGGCTGACGGAATTTATGCC
TCTTCCGACCATCAAGCATTTTATCCGTACTCCTGATGATGCATGGTTACTCACCACTGC
GATCCCCGGGAAAACAGCATTCCAGGTATTAGAAGAATATCCTGATTCAGGTGAAAATA
TTGTTGATGCGCTGGCAGTGTTCCTGCGCCGGTTGCATTCGATTCCTGTTTGTAATTGT
CCTTTTAACAGCGATCGCGTATTTCGTCTCGCTCAGGCGCAATCACGAATGAATAACGG
TTTGGTTGATGCGAGTGATTTTGATGACGAGCGTAATGGCTGGCCTGTTGAACAAGTCT
GGAAAGAAATGCATAAACTTTTGCCATTCTCACCGGATTCAGTCGTCACTCATGGTGATT
TCTCACTTGATAACCTTATTTTTGACGAGGGGAAATTAATAGGTTGTATTGATGTTGGAC
GAGTCGGAATCGCAGACCGATACCAGGATCTTGCCATCCTATGGAACTGCCTCGGTGA
GTTTTCTCCTTCATTACAGAAACGGCTTTTTCAAAAATATGGTATTGATAATCCTGATATG
AATAAATTGCAGTTTCATTTGATGCTCGATGAGTTTTTCTAAGAATTAATTCATGAGCGGA
TACATATTTGAATGTATTTAGAAAAATAAACAAATAGGGGTTCCGCGCACATTTCCCCGA
AAAGTGCCACCTGAAATTGTAAACGTTAATATTTTGTTAAAATTCGCGTTAAATTTTTGTT
AAATCAGCTCATTTTTTAACCAATAGGCCGAAATCGGCAAAATCCCTTATAAATCAAAAG
AATAGACCGAGATAGGGTTGAGTGTTGTTCCAGTTTGGAACAAGAGTCCACTATTAAAG
AACGTGGACTCCAACGTCAAAGGGCGAAAAACCGTCTATCAGGGCGATGGCCCACTAC
GTGAACCATCACCCTAATCAAGTTTTTTGGGGTCGAGGTGCCGTAAAGCACTAAATCGG
AACCCTAAAGGGAGCCCCCGATTTAGAGCTTGACGGGGAAAGCCGGCGAACGTGGCG
AGAAAGGAAGGGAAGAAAGCGAAAGGAGCGGGCGCTAGGGCGCTGGCAAGTGTAGCG
GTCACGCTGCGCGTAACCACCACACCCGCCGCGCTTAATGCGCCGCTACAGGGCGCG
TCCCATTCGCCA

Partial sequence of $MraY_{Mtb}$ (T7 for fwd primer):

ATGCACCATCATCATCATCATTCTTCTGGTCTGGTGCCACGCGGTTCTGGTATGAAAGA
AACCGCTGCTGCTAAATTCGAACGCCAGCACATGGACAGCCCAGATCTGGGTACCGGT
GGTGGCTCCGGTATTGAGGGTCGCATGAGGCAGATCCTTATCGCCGTTGCCGTAGCGG
TGACGGTGTCCATCTTGCTGACCCCGGTGCTGATCCGGTTGTTCACTAAGCAGGGCTTC
GGCCACCAGATCCGTGAGGATGGCCCGCCCAGCCACCACACCAAGCGCGGTACGCCG
TCGATGGGCGGGGTGGCGATTCTGGCCGGCATCTGGGCGGGCTACCTGGGCGCCCAC
CTAGCGGGCCTGGCGTTTGACGGTGAAGGCATCGGCGCATCGGGTCTGTTGGTGCTG
GGCCTAGCCACCGCTTTGGGCGGCGTCGGGTTCATCGACGATCTGATCAAGATCCGCA
GGTCGCGCAATCTCGGGTTGAACAAGACGGCCAAGACCGTCGGGCAGATCACCTCCG
CCGTGCTGTTTGGCGTGCTGGTGCTGCANTTCCGGAATGCTGCCGGCCTGACACCGGG
CAGCGCGGATCTGTCCTACGTGCGTGAG

Partial sequence of $MraY_{Mtb}$ (T7-term for rev primer):

TTTGTTAGCAGCCGGATCTCAGTGGTGGTGGTGGTGGTGCTCGAGTGCGGCCGCAAGC
TTGTCGACGGAGCTCGAATTCGGATCCGATATCGCCAT

Table 7.6: Sequences of designed insert and vector primers, forward and reverse each.

Primer	Sequence
insert fwd	AACTTTAAGAAGGAGATATACCATGAGGCAGATCCTTATCGCC
insert rev	GCAGCCGGATCTCA TCAGTGGTGGTGGTGGTG
vector fwd	TGAGATCCGGCTGCTAACAAAG
vector rev	GGTATATCTCCTTCTTAAAGTTAAACAAAATTATTTCT

7.1.2.4.2 pET28a $MraY_{Mtb}$ into pET26a $MraY_{Mtb}$

Sequence of pET26a $MraY_{AA}$:

TTGGCGAATGGGACGCGCCCTGTAGCGGCGCATTAAGCGCGGCGGGTGTGGTGGTTA
CGCGCAGCGTGACCGCTACACTTGCCAGCGCCCTAGCGCCCGCTCCTTTCGCTTTCTT
CCCTTCCTTTCTCGCCACGTTCGCCGGCTTTCCCCGTCAAGCTCTAAATCGGGGGCTCC
CTTTAGGGTTCCGATTTAGTGCTTTACGGCACCTCGACCCCAAAAAACTTGATTAGGGT
GATGGTTCACGTAGTGGGCCATCGCCCTGATAGACGGTTTTTCGCCCTTTGACGTTGGA
GTCCACGTTCTTTAATAGTGGACTCTTGTTCCAAACTGGAACAACACTCAACCCTATCTC
GGTCTATTCTTTTGATTTATAAGGGATTTTGCCGATTTCGGCCTATTGGTTAAAAAATGAG
CTGATTTAACAAAAATTTAACGCGAATTTTAACAAAATATTAACGTTTACAATTTCAGGTG
GCACTTTTCGGGGAAATGTGCGCGGAACCCCTATTTGTTTATTTTTCTAAATACATTCAA
ATATGTATCCGCTCATGAATTAATTCTTAGAAAAACTCATCGAGCATCAAATGAAACTGC
AATTTATTCATATCAGGATTATCAATACCATATTTTTGAAAAAGCCGTTTCTGTAATGAAG
GAGAAAACTCACCGAGGCAGTTCCATAGGATGGCAAGATCCTGGTATCGGTCTGCGATT
CCGACTCGTCCAACATCAATACAACCTATTAATTTCCCCTCGTCAAAAATAAGGTTATCA
AGTGAGAAATCACCATGAGTGACGACTGAATCCGGTGAGAATGGCAAAAGTTTATGCAT
TTCTTTCCAGACTTGTTCAACAGGCCAGCCATTACGCTCGTCATCAAAATCACTCGCATC
AACCAAACCGTTATTCATTCGTGATTGCGCCTGAGCGAGACGAAATACGCGATCGCTGT
TAAAAGGACAATTACAAACAGGAATCGAATGCAACCGGCGCAGGAACACTGCCAGCGC
ATCAACAATATTTTCACCTGAATCAGGATATTCTTCTAATACCTGGAATGCTGTTTTCCCG
GGGATCGCAGTGGTGAGTAACCATGCATCATCAGGAGTACGGATAAAATGCTTGATGGT
CGGAAGAGGCATAAATTCCGTCAGCCAGTTTAGTCTGACCATCTCATCTGTAACATCATT
GGCAACGCTACCTTTGCCATGTTTCAGAAACAACTCTGGCGCATCGGGCTTCCCATACA
ATCGATAGATTGTCGCACCTGATTGCCCGACATTATCGCGAGCCCATTTATACCCATATA
AATCAGCATCCATGTTGGAATTTAATCGCGGCCTAGAGCAAGACGTTTCCCGTTGAATAT
GGCTCATAACACCCCTTGTATTACTGTTTATGTAAGCAGACAGTTTTATTGTTCATGACC
AAAATCCCTTAACGTGAGTTTTCGTTCCACTGAGCGTCAGACCCCGTAGAAAAGATCAA
AGGATCTTCTTGAGATCCTTTTTTTCTGCGCGTAATCTGCTGCTTGCAAACAAAAAAACC
ACCGCTACCAGCGGTGGTTTGTTTGCCGGATCAAGAGCTACCAACTCTTTTTCCGAAGG
TAACTGGCTTCAGCAGAGCGCAGATACCAAATACTGTCCTTCTAGTGTAGCCGTAGTTA
GGCCACCACTTCAAGAACTCTGTAGCACCGCCTACATACCTCGCTCTGCTAATCCTGTT
ACCAGTGGCTGCTGCCAGTGGCGATAAGTCGTGTCTTACCGGGTTGGACTCAAGACGA
TAGTTACCGGATAAGGCGCAGCGGTCGGGCTGAACGGGGGGTTCGTGCACACAGCCC
AGCTTGGAGCGAACGACCTACACCGAACTGAGATACCTACAGCGTGAGCTATGAGAAA
GCGCCACGCTTCCCGAAGGGAGAAAGGCGGACAGGTATCCGGTAAGCGGCAGGGTCG
GAACAGGAGAGCGCACGAGGGAGCTTCCAGGGGGAAACGCCTGGTATCTTTATAGTCC

TGTCGGGTTTCGCCACCTCTGACTTGAGCGTCGATTTTTGTGATGCTCGTCAGGGGGG
CGGAGCCTATGGAAAAACGCCAGCAACGCGGCCTTTTTACGGTTCCTGGCCTTTTGCTG
GCCTTTTGCTCACATGTTCTTTCCTGCGTTATCCCCTGATTCTGTGGATAACCGTATTAC
CGCCTTTGAGTGAGCTGATACCGCTCGCCGCAGCCGAACGACCGAGCGCAGCGAGTC
AGTGAGCGAGGAAGCGGAAGAGCGCCTGATGCGGTATTTTCTCCTTACGCATCTGTGC
GGTATTTCACACCGCATATATGGTGCACTCTCAGTACAATCTGCTCTGATGCCGCATAGT
TAAGCCAGTATACACTCCGCTATCGCTACGTGACTGGGTCATGGCTGCGCCCCGACAC
CCGCCAACACCCGCTGACGCGCCCTGACGGGCTTGTCTGCTCCCGGCATCCGCTTACA
GACAAGCTGTGACCGTCTCCGGGAGCTGCATGTGTCAGAGGTTTTCACCGTCATCACC
GAAACGCGCGAGGCAGCTGCGGTAAAGCTCATCAGCGTGGTCGTGAAGCGATTCACAG
ATGTCTGCCTGTTCATCCGCGTCCAGCTCGTTGAGTTTCTCCAGAAGCGTTAATGTCTG
GCTTCTGATAAAGCGGGCCATGTTAAGGGCGGTTTTTTCCTGTTTGGTCACTGATGCCT
CCGTGTAAGGGGGATTTCTGTTCATGGGGGTAATGATACCGATGAAACGAGAGAGGAT
GCTCACGATACGGGTTACTGATGATGAACATGCCCGGTTACTGGAACGTTGTGAGGGTA
AACAACTGGCGGTATGGATGCGGCGGGACCAGAGAAAAATCACTCAGGGTCAATGCCA
GCGCTTCGTTAATACAGATGTAGGTGTTCCACAGGGTAGCCAGCAGCATCCTGCGATG
CAGATCCGGAACATAATGGTGCAGGGCGCTGACTTCCGCGTTTCCAGACTTTACGAAAC
ACGGAAACCGAAGACCATTCATGTTGTTGCTCAGGTCGCAGACGTTTTGCAGCAGCAGT
CGCTTCACGTTCGCTCGCGTATCGGTGATTCATTCTGCTAACCAGTAAGGCAACCCCGC
CAGCCTAGCCGGGTCCTCAACGACAGGAGCACGATCATGCGCACCCGTGGGGCCGCC
ATGCCGGCGATAATGGCCTGCTTCTCGCCGAAACGTTTGGTGGCGGGACCAGTGACGA
AGGCTTGAGCGAGGGCGTGCAAGATTCCGAATACCGCAAGCGACAGGCCGATCATCGT
CGCGCTCCAGCGAAAGCGGTCCTCGCCGAAAATGACCCAGAGCGCTGCCGGCACCTG
TCCTACGAGTTGCATGATAAAGAAGACAGTCATAAGTGCGGCGACGATAGTCATGCCCC
GCGCCCACCGGAAGGAGCTGACTGGGTTGAAGGCTCTCAAGGGCATCGGTCGAGATC
CCGGTGCCTAATGAGTGAGCTAACTTACATTAATTGCGTTGCGCTCACTGCCCGCTTTC
CAGTCGGGAAACCTGTCGTGCCAGCTGCATTAATGAATCGGCCAACGCGCGGGGAGAG
GCGGTTTGCGTATTGGGCGCCAGGGTGGTTTTTCTTTTCACCAGTGAGACGGGCAACA
GCTGATTGCCCTTCACCGCCTGGCCCTGAGAGAGTTGCAGCAAGCGGTCCACGCTGGT
TTGCCCCAGCAGGCGAAAATCCTGTTTGATGGTGGTTAACGGCGGGATATAACATGAGC
TGTCTTCGGTATCGTCGTATCCCACTACCGAGATATCCGCACCAACGCGCAGCCCGGA
CTCGGTAATGGCGCGCATTGCGCCCAGCGCCATCTGATCGTTGGCAACCAGCATCGCA
GTGGGAACGATGCCCTCATTCAGCATTTGCATGGTTTGTTGAAAACCGGACATGGCACT
CCAGTCGCCTTCCCGTTCCGCTATCGGCTGAATTTGATTGCGAGTGAGATATTTATGCC
AGCCAGCCAGACGCAGACGCGCCGAGACAGAACTTAATGGGCCCGCTAACAGCGCGA
TTTGCTGGTGACCCAATGCGACCAGATGCTCCACGCCCAGTCGCGTACCGTCTTCATG
GGAGAAAATAATACTGTTGATGGGTGTCTGGTCAGAGACATCAAGAAATAACGCCGGAA

CATTAGTGCAGGCAGCTTCCACAGCAATGGCATCCTGGTCATCCAGCGGATAGTTAATG
ATCAGCCCACTGACGCGTTGCGCGAGAAGATTGTGCACCGCCGCTTTACAGGCTTCGA
CGCCGCTTCGTTCTACCATCGACACCACCACGCTGGCACCCAGTTGATCGGCGCGAGA
TTTAATCGCCGCGACAATTTGCGACGGCGCGTGCAGGGCCAGACTGGAGGTGGCAAC
GCCAATCAGCAACGACTGTTTGCCCGCCAGTTGTTGTGCCACGCGGTTGGGAATGTAAT
TCAGCTCCGCCATCGCCGCTTCCACTTTTTCCCGCGTTTTCGCAGAAACGTGGCTGGCC
TGGTTCACCACGCGGGAAACGGTCTGATAAGAGACACCGGCATACTCTGCGACATCGT
ATAACGTTACTGGTTTCACATTCACCACCCTGAATTGACTCTCTTCCGGGCGCTATCATG
CCATACCGCGAAAGGTTTTGCGCCATTCGATGGTGTCCGGGATCTCGACGCTCTCCCTT
ATGCGACTCCTGCATTAGGAAGCAGCCCAGTAGTAGGTTGAGGCCGTTGAGCACCGCC
GCCGCAAGGAATGGTGCATGCAAGGAGATGGCGCCCAACAGTCCCCCGGCCACGGGG
CCTGCCACCATACCCACGCCGAAACAAGCGCTCATGAGCCCGAAGTGGCGAGCCCGAT
CTTCCCCATCGGTGATGTCGGCGATATAGGCGCCAGCAACCGCACCTGTGGCGCCGGT
GATGCCGGCCACGATGCGTCCGGCGTAGAGGATCGAGATCTCGATCCCGCGAAATTAA
TACGACTCACTATAGGGGAATTGTGAGCGGATAACAATTCCCCTCTAGAAATAATTTTGT
TTAACTTTAAGAAGGAGATATACATATGAAATACCTGCTGCCGACCGCTGCTGCTGGTCT
GCTGCTCCTCGCTGCCCAGCCGGCGATGGCCATGGATATCGGAATTAATTCGGATCCG
AATTCGAGCTCACATCACCATCACCATCACCATCACCATCACCCCATGAAAATCGAAGAA
GGTAAACTGGTAATCTGGATTAACGGCGATAAAGGCTATAACGGTCTCGCTGAAGTCGG
TAAGAAATTCGAGAAAGATACCGGAATTAAAGTCACCGTTGAGCATCCGGATAAACTGG
AAGAGAAATTCCCACAGGTTGCGGCAACTGGCGATGGCCCTGACATTATCTTCTGGGCA
CACGACCGCTTTGGTGGCTACGCTCAATCTGGCCTGTTGGCTGAAATCACCCCGGACA
AAGCGTTCCAGGACAAGCTGTATCCGTTTACCTGGGATGCCGTACGTTACAACGGCAAG
CTGATTGCTTACCCGATCGCTGTTGAAGCGTTATCGCTGATTTATAACAAAGATCTGCTG
CCGAACCCGCCAAAAACCTGGGAAGAGATCCCGGCGCTGGATAAAGAACTGAAAGCGA
AAGGTAAGAGCGCGCTGATGTTCAACCTGCAAGAACCGTACTTCACCTGGCCGCTGATT
GCTGCTGACGGGGGTTATGCGTTCAAGTATGAAAACGGCAAGTACGACATTAAAGACGT
GGGCGTGGATAACGCTGGCGCGAAAGCGGGTCTGACCTTCCTGGTTGACCTGATTAAA
AACAAACACATGAATGCAGACACCGATTACTCCATCGCAGAAGCTGCCTTTAATAAAGG
CGAAACAGCGATGACCATCAACGGCCCGTGGGCATGGTCCAACATCGACACCAGCAAA
GTGAATTATGGTGTAACGGTACTGCCGACCTTCAAGGGTCAACCATCCAAACCGTTCGT
TGGCGTGCTGAGCGCAGGTATTAACGCCGCCAGTCCGAACAAAGAGCTGGCAAAAGAG
TTCCTCGAAAACTATCTGCTGACTGATGAAGGTCTGGAAGCGGTTAATAAAGACAAACC
GCTGGGTGCCGTAGCGCTGAAGTCTTACGAGGAAGAGTTGGCGAAAGATCCACGTATT
GCCGCCACTATGGAAAACGCCCAGAAAGGTGAAATCATGCCGAACATCCCGCAGATGT
CCGCTTTCTGGTATGCCGTGCGTACTGCGGTGATCAACGCCGCCAGCGGTCGTCAGAC
TGTCGATGAAGCCCTGAAAGACGCGCAGACTCCGGGTAGCCTGGAAGTTCTGTTCCAG

GGGCCCGCGGTACCTAGGATGCTGTATCAACTGGCTCTGCTGCTGAAAGATTATTGGTT
CGCCTTTAACGTCCTGAAATATATCACCTTCCGCTCGTTTACTGCCGTTCTGATCGCCTT
CTTCCTGACACTGGTTCTGAGTCCGTCCTTTATTAACCGTCTGCGCAAAATCCAACGCCT
GTTTGGTGGCTATGTTCGTGAGTATACCCCGGAAAGCCATGAAGTGAAAAAATATACGC
CGACCATGGGTGGTATTGTGATCCTGATTGTGGTTACCCTGAGCACACTGCTGCTGATG
CGCTGGGATATCAAATATACCTGGGTGGTTCTGCTGTCTTTTCTGAGCTTTGGCACCAT
CGGTTTTTGGGACGACTATGTGAAACTGAAAAACAAAAAAGGCATCTCCATCAAAACCAA
ATTTCTGCTGCAGGTGCTGTCAGCATCTCTGATTAGCGTGCTGATCTATTATTGGGCCG
ACATCGACACGATTCTGTATTTCCCGTTCTTCAAAGAGCTGTATGTGGATCTGGGAGTC
CTGTATCTGCCGTTCGCTGTGTTTGTGATTGTTGGTAGCGCCAATGCCGTCAATCTGAC
CGACGGGCTGGATGGCCTGGCAATTGGACCGGCAATGACTACTGCTACTGCCCTGGGT
GTTGTTGCTTATGCCGTGGGACATTCGAAAATCGCCCAGTATCTGAATATTCCGTATGTT
CCATATGCTGGTGAACTGACCGTGTTCTGCTTTGCTCTGGTGGGTGCTGGTCTGGGGTT
TCTGTGGTTCAACTCCTTCCCGGCTCAAATGTTTATGGGGGATGTGGGTAGCCTGAGTA
TTGGAGCGTCACTGGCAACTGTGGCACTGCTGACCAAAAGCGAGTTCATCTTCGCCGTT
GCCGCTGGAGTGTTCGTTTTTGAAACCATCTCCGTGATTCTGCAAATCATCTATTTCCGC
TGGACAGGTGGAAAACGTCTGTTCAAACGTGCCCCGTTTCATCATCACCTGGAACTGAA
TGGTCTGCCTGAACCGAAAATTGTTGTCCGTATGTGGATTATTAGCATCCTGCTGGCCA
TTATCGCCATTTCAATGCTGAAACTGCGTTAACTCGAGCACCACCACCACCACCACTGA
GATCCGGCTGCTAACAAAGCCCGAAAGGAAGCTGAGTTGGCTGCTGCCACCGCTGAGC
AATAACTAGCATAACCCCTTGGGGCCTCTAAACGGGTCTTGAGGGGTTTTTTGCTGAAA
GGAGGAACTATATCCGGA

Partial sequence of $MraY_{Mtb}$ (T7 for fwd primer):

NNNNNNNNNNNNNNNTCCCCTCTAGAATAATTTTGTTTAACTTTAAGAAGGAGATATAC
CATGAGGCAGATCCTTATCGCCGTTGCCGTAGCGGTGACGGTGTCCATCTTGCTGACC
CCGGTGCTGATCCGGTTGTTCACTAAGCAGGGCTTCGGCCACCAGATCCGTGAGGATG
GCCCGCCCAGCCACCACACCAAGCGCGGTACGCCGTCGATGGGCGGGGTGGCGATTC
TGGCCGGCATCTGGGCGGGCTACCTGGGCGCCCACCTAGCGGGCCTGGCGTTTGACG
GTGAAGGCATCGGCGCATCGGGTCTGTTGGTGCTGGGCCTAGCCACCGCTTTGGGCG
GCGTCGGGTTCATCGACGATCTGATCAAGATCCGCAGGTCGCGCAATCTCGGGTTGAA
CAAGACGGCCAAGACCGTCGGGCAGATCACCTCCGCCGTGCTGTTTGGCGTGCTGGT
GCTGCAGTTCCGGAATGCTGCCGGCCTGACACCGGGCAGCGCGGATCTGTCCTACGT
GCGTGAGATCGCCACCGTCACATTGGCGCCGGTGCTGTTCGTGTTGTTCTGCGTGGTC
ATCGTCAGCGCCTGGTCGAACGCGGTCAACTTCACCGATGGCCTGGACGGGCTGGCC
GCCGGCACCATGGCGATGGTCACCGCCGCCTACGTGCTGATCACCTTCTGGCAGTACC
GCAACGCGTGCGTGACGGCGCCGGGCCTGGGCTGCTACAACGTGCGCGACCCGCTG

GACCTGGCGCTCATCGCGGCCGCAACCGCTGGCGCCTGCATCGGTTTTTTGTGGTGGA
ACGCCGCGCCCGCCAAGATCTTCATGGGTGACACTGGGTCGCTGGCGTTGGGCGGCG
TCATCGCGGGGTTGTCGGTGACCAGCCGCACCGAGATCCTTGCGGTGGTGCTGGGTG
CGCTGTTCGTCGCCGANATCACCTCGGTGGTGTTGCAAATCCTGACCTTCCGGACCAC
CGGGCGCCNGGATGTTTCNGATGGCGCCCTTTCCACCACCATTTCNANTTGGGTCNGN
TTGGGCTGAAACCACGGTCATCATCCGGNTTCTNGN

Partial sequence of $MraY_{Mtb}$ (T7-term for rev primer):

NNNNNNNNNNNNNNNNTCGGGCTTTGTTAGCAGCCGGATCTCATCAGTGGTGGTGGT
GGTGGTGCTCGAGTGCGGCCGCAAGCTTGTCGACGGAGCTCGAATTCGGATCCGATAT
CGCCATGGCCAGAGGAGAGTTAGAGCCTCAGGCACCGACCGCGGCAAGCCACTCACC
GTAGAACAAGGCCACGCCCAGACCGCAGGTGATCGCGGTGAGCAGCCAGAACCGGAT
GATGACCGTGGTTTCAGCCCAACCGACCAACTCGAAATGGTGGTGGAAGGGCGCCATC
CGAAACATCCGGCGCCCGGTGGTCCGGAAGGTCAGGATTTGCAACACCACCGAGGTG
ATCTCGGCGACGAACAGCGCACCCAGCACCACCGCAAGGATCTCGGTGCGGCTGGTC
ACCGACAACCCCGCGATGACGCCGCCCAACGCCAGCGACCCAGTGTCACCCATGAAG
ATCTTGGCGGGCGCGGCGTTCCACCACAAAAAACCGATGCAGGCGCCAGCGGTTGCG
GCCGCGATGAGCGCCAGGTCCAGCGGGTCGCGCACGTTGTAGCAGCCCAGGCCCGG
CGCCGTCACGCACGCGTTGCGGTACTGCCAGAAGGTGATCAGCACGTANGCGGCGGT
GACCATCGCCATGGTGCCGGCGGCCAGCCCGTCCAGGCCATCGGTGAAGTTGACCGC
GTTCGACCAGGCGCTGACGATGACCACGCAGAACNACACGAACAGCACCGGCGCCAAT
GTGACGGTGGCGATCTCACGCACGTAGGACAGATCCCGCGCTGCCCGGTGTCAGNCG
GCAGCATTCCGGAACTGCAGCACCAGCACGCCAAACAGCACGGCGGAGGTGATCTGN
CCGACGGTCTTGGCCGNCTTGNTCNACCCGAGATTGCNCGACCTGCGNATNTTGATCN
NATCGTCGATGAA

Table 7.7: Sequences of designed insert and vector primers, forward and reverse each.

Primer	Sequence
insert fwd	CCGCGGTACCTAGGATGAGGCAGATCCTTATCGCC
insert rev	GTGGTGCTCGAGTTATCAGGCACCGACCGCG
vector fwd	TAACTCGAGCACCACCACCA
vector rev	CCTAGGTACCGCGGGCC

7.1.2.4.3 PCR clean-up, plasmid transformation and plasmid extraction

PCR clean-up was done according to the kit 'NucleoSpin Gel and PCR Clean-up, Mini kit for gel extraction and PCR clean up' from Macherey-Nagel with a few modifications. All 'individual approaches' were combined in one tube (4 x 20 µL) and mixed with buffer NTI (160 µL). The total amount (240 µL) was loaded onto a NucleoSpin Gel and PCR clean-up column and

centrifuged (17,000 x g, 1 minute, 4 °C). After discarding the flow-through, the column was washed with buffer NT3 (2 x 700 µL) and centrifuged (17,000 x g, 1 minute, 4 °C). Flow-through was discarded and to remove remaining ethanol from buffer NT3, columns inserted in the collection tubes were centrifuged again (17,000 x g, 1 minute, 4 °C). Prior to DNA elution, samples were incubated with CutSmart (30 µL, 1:10 diluted with water) for 1 min at rt. A last centrifugation (17,000 x g, 1 minute, 4 °C) yielded the eluted DNA. DpnI (1 µL) was added to the tube and incubated for 40 minutes at 37 °C. Following agarose gel analysis, the PCR product was transformed into chemically competent *E. coli* DH5α (Chapter 7.1.2.1) and a plasmid extraction was performed on single colonies prior to sequencing, using the GenElute™ HP Plasmid Miniprep Kit from Sigma Aldrich without any modifications. Sequencing was carried out at Eurofins.

7.1.2.5 MraY quantification assays

Plasmid transformation and expression of NB7 required for MraY quantification assays was carried out based on the work of Lee and colleagues who kindly provided the plasmid of NB7 for this work (Chapter 7.1.2.1).[93]

7.1.2.5.1 Plasmid transformation of NB7

An aliquot of competent *E. coli* C41(DE3) cells (50 µL) was thawed on ice for 10 min. The NB7 plasmid (1 µL) was injected and incubated on ice for 30 minutes. A heat shock at 42 °C for 45 seconds and another incubation on ice for further 2 minutes followed. After adding sterile LB medium (200 µL), the mixture was incubated in a shaking incubator (Infors HT) at 37 °C for 1 hour. 50 µL of the culture was plated on LB agar plates supplemented with KAN (50 µg/mL) and incubated at 37 °C overnight.

7.1.2.5.2 Expression and purification of NB7

LB medium (10 mL) supplemented with KAN (50 µg/mL) was inoculated with one to five colonies from the LB agar plates and was incubated overnight (180 rpm, 37 °C). The following morning, LB medium (1 L) supplemented with KAN (35 µg/mL) was inoculated with overnight culture (10 mL) and incubated at 37 °C (180 rpm). Then, temperature was reduced to 20 °C at an OD_{600} of ~ 0.4 (~ 2.5 hours). After reaching an OD of ~ 0.6-0.8, the mixture was induced with IPTG (1 mM) and grown overnight. Bacteria were harvested by centrifugation (6,000 g, 15 minutes, 4 °C) and cell pellets were stored at -80 °C overnight. Pellets were thawed on ice and resuspended in resuspension buffer (20 mL per 1 L expression culture). Bacterial suspension was rotated at room temperature for 30 minutes and centrifuged (13,000 x g, 10 minutes, 4 °C). The resulting pellet was resuspended rapidly on ice with ice-cold osmotic lysis buffer (0 °C, max. 20 mL per 1 L expression culture). Bacterial suspension was rotated again at room temperature for 30 minutes and centrifuged (13,000 x g, 10 minutes, 4 °C). The

lysate was incubated with Ni-NTA agarose resin (Qiagen, 1 mL final bead volume for 1 L culture), preequilibrated with wash buffer, at 4 °C for 1 hour. The resin was washed with wash buffer until no protein was detected by Bradford test (10 µL eluent + 50 µL Bradford reagent). Bound protein was eluted with elution buffer (10 mL). Protein solution was concentrated using a 50 kDa cut off centrifugal filter (4,600 x g, 10 minutes, 4 °C) prior to gel filtration using a Superdex 200 10/300 GL column (GE, Äkta System), preequilibrated with size exclusion buffer. Protein fractions were analyzed by SDS-PAGE (Chapter 7.1.1.7) and fractions containing $MraY_{AA}$ NB7 were combined. Protein preparations were aliquoted (20 µL) and flash frozen in liquid nitrogen for the storage at -80 °C.

7.1.2.5.3 Western Blots as tool for MraY quantification

SDS-PAGE experiments were done as described before (Chapter 7.1.1.7). One SDS-PAGE was used as control in every experiment. Protein transfer from SDS-PAGE gels to Western Blot membranes (Merck, Immobilon®-FL PVDF membranes, pore size 0.45 µm) was performed with transfer buffer at 4 °C overnight. To prevent unspecific protein binding, membranes were blocked with blocking buffer (BB) purchased from Rockland (Blocking Buffer for Fluorescent Western Blotting, 25 mL) at 4 °C for 1.5 hours in the following morning. Membranes were incubated with NB7 (first antibody) at 4 °C overnight (varying concentrations in BB tested in the course of this work). Membranes were washed with TBST (three times, 4 °C) and incubated with a Hrp-conjugated anti His_6-tag antibody (1:1,000 diluted with BB, Rockland) at 4 °C for 4 hours. Membranes were washed with TBST (three times, 4 °C), incubated with goat anti-rabbit IgG (H+L) Cross-Adsorbed Secondary Antibody, Alexa Fluor™ 680 (Thermo Scienfitic) at room temperature for 1 hour (1:10,000 diluted with BB) and washed again with TBST (three times, room temperature). Western Blots were visualized by the Odyssee CLx LI-COR Near Infrared Imaging System and quantified with the ImageLab software. Western Blots were wrapped in paper and stored at room temperature.

7.1.3 Cellular uptake assays

This section will focus on cellular uptake assays for both types of bacteria. Furthermore, the plasmid transformation and protein expression of lysostaphin will be described which is specifically required for Gram-positive bacteria (Chapter 7.1.3.3.2).

7.1.3.1 General procedure for Gram-positive and Gram-negative bacteria

The basic assay procedure for Gram-negative *E. coli* DH5α and *E. coli* Δ*tolC* had been established by J. Meiers.[134] Principles of these assays were used for the investigation of cellular uptake of compounds from our research group and for the establishment of the corresponding assay in Gram-positive *S. aureus*.

7.1.3.1.1 Assay procedure

As described in Chapter 7.1.1.10, appropriate day cultures of bacteria were prepared from overnight cultures. Bacteria with an OD_{600} of ~ 0.6 were harvested (4,000 x g, 10 minutes, 4 °C) and the resultant pellet was washed with M9 medium (30 mL). Resuspended bacteria were centrifuged (4,000 x g, 10 minutes, 4 °C). After discarding the supernatant, bacteria were resuspended in M9 medium until an OD_{600} of ~ 4 was reached. This suspension is termed 'bacterial suspension'. Following that, bacteria suspension (500 µL) and compound solution (500 µL) were incubated in a water bath at 37 °C for 30 minutes. Samples were measured as biological triplicates. Incubation concentrations varied depending on the project:

a) Specific defined incubation concentration (mostly 2 µM or 20 µM)

b) Incubation concentration ~ IC_{50} value for growth inhibition of one candidate compound

c) Incubation concentration ~ IC_{50} value for growth inhibition of the candidate compound with the highest uptake (belated adaption)

After incubation, mixtures were centrifuged (6,000 x g, 10 minutes, 4 °C) and the resulting pellets were washed twice with ice-cold M9 medium (1 mL, 0 °C). To improve lysis, pelleted bacteria were frozen overnight (-20 °C). After thawing the pellets on ice, bacteria were lysed ('whole cells'). In general, lysis between Gram-negative and Gram-positive bacteria differs and will therefore be discussed separately in Chapters 7.1.3.2 and 7.1.3.3. Following lysis, insoluble cell components were separated by centrifugation (17,000 x g, 30 minutes, 4 °C), the resulting supernatants were mixed with one equivalent (v/v) MeCN (with or without 1% HCOOH, depending on the tested compound) and incubated on ice for 5 min. Samples were centrifuged again (17,000 x g, 30 minutes, 4 °C). Depending on the tested compound, the corresponding supernatants (1 mL) were lyophilized overnight and the resultant solids were dissolved in a mixture (60 µL) of water/MeCN (1:1), with or without 1% HCOOH, for MS measurements. MS methods are listed in the following chapter for each compound of which cellular uptake was investigated in the course of this work.

7.1.3.1.2 Instrumental analytics

Data for cellular uptake were measured as high resolution mass spectra (HRMS) on an Ultimate 3000 system by Thermo Scientific with a Dionex UltiMate 3000 UHPLC system that comprised an automated autosampler, a pump, a column department, a detector (diode array) and a Thermo Scientific Q Exactive OrbiTrap. A Thermo Accucore™ phenyl-X (2.1 µm, 3 x 100 mm) column was employed for UHPLC separation prior to detection. As the column system was modified in our research group, the terms 'column 1' (Thermo Accucore™ phenyl-X (2.1 µm, 3 x 100 mm, used until summer 2020 for ESI^+ and ESI^-) and 'column 2' (Macherey-Nagel EC 100/3 NUCLEOSHELL Phenyl-Hexyl (2.7 µm, 3 x 100 mm, used since

summer 2020 for ESI^+) will be used. Solvents A (water + 0.1% HCOOH) and B (MeCN + 0.1% HCOOH) were used for MS measurements in positive mode (ESI^+), water (C) and MeCN (D) were used for measurements in negative mode (ESI^-). Methods as well as mass-to-charge ratios (m/z) and retention times (t_R) for each compound are listed in Table 7.8 and 7.9.

Table 7.8: High resolution mass spectrometry methods for cellular uptake assays of compounds measured in positive mode (ESI^+).

t (min)	solvent A (%)	solvent B (%)
ciprofloxacin ('column 1')		
method name: _Steffi_CIPRO_200bis2000_UV		
t_R = 2.75 ± 0.05 min, m/z= 332.13-332.15, flow: 0.55 mL/min		
0	95	5
5	50	50
6	1	99
8.1	95	5
10	95	5
linezolid ('column 1')		
method name: _Steffi_LINEZOLID_200bis800_UV		
t_R = 4.92 ± 0.05 min, m/z= 338.14-338.16, flow: 0.50 mL/min		
0	95	5
5	50	50
6	1	99
8.1	95	5
10	95	5
compound 33 ('column 1')		
method name: 20180523_HighRes_Pos_ACN_FA_250bis1300		
t_R = 2.90 ± 0.05 min, m/z= 372.19-372.21, flow: 0.50 mL/min		
0	95	5
5.5	0	100
7.0	0	100
7.2	95	5
8.0	95	5
compound 33 ('column 2')		
method name: 20210413_PheHex50_Pos_ACN_FA_100bis1000		
t_R = 1.80 ± 0.05 min, m/z= 372.19-372.21, flow: 0.70 mL/min		
0	95	5
1.25	0	100
2.8	0	100
2.85	95	5
3.5	95	5

t (min)	solvent A (%)	solvent B (%)
compound 37 ('column 1')		
method name: 20180523_HighRes_Pos_ACN_FA_250bis1300_sv_GN246		
t_R = 3.95 ± 0.05 min, m/z= 447.31-447.33.15, flow: 0.55 mL/min		
0	95	5
5.5	0	100
7.0	0	100
7.2	95	5
8.0	95	5
compound 38 ('column 1')		
method name: 20180523_HighRes_Pos_ACN_FA_250bis1300_sv_GN246		
t_R = 4.28 ± 0.05 min, m/z= 457.77-457.79.15, flow: 0.55 mL/min		
0	95	5
5.5	0	100
7.0	0	100
7.2	95	5
8.0	95	5
compound 43 ('column 1')		
method name: 20190724_HighRes_Pos_ACN_FA_80bis800_KV_ohneUV		
t_R = 8.54 ± 0.05 min, m/z= 483.04-483.05, flow: 0.55 mL/min		
0	98	2
5	60	40
7.3	1	99
9.1	98	2
10	98	2
compound 45 ('column 1')		
method name: 20190724_HighRes_Pos_ACN_FA_80bis800_KV_ohneUV		
t_R = 8.11 ± 0.05 min, m/z= 492.09-492.11, flow: 0.55 mL/min		
0	98	2
5	60	40
7.3	1	99
9.1	98	2
10	98	2
compound 41 ('column 1')		
method name: 20180523_HighRes_Pos_ACN_FA_150bis1300		
t_R = 4.56 ± 0.05 min, m/z= 468.19-468.21, flow: 0.5 mL/min		
0	95	5
5.5	0	100
7	0	100
7.2	95	5
8	95	5

t (min)	solvent A (%)	solvent B (%)
compound 42 ('column 1') method name: 20180523_HighRes_Pos_ACN_FA_150bis1300 t_R = 4.46 ± 0.05 min, m/z= 450.22-450.24, flow: 0.5 mL/min		
0	95	5
5.5	0	100
7	0	100
7.2	95	5
8	95	5
compound 39 ('column 2') method name: 20210413_PheHex50_Pos_ACN_100bis1000 t_R = 1.78 ± 0.05 min, m/z= 372.19-372.21; 743.39-743.40, flow: 0.7 mL/min		
0	95	5
1	0	100
1.25	0	100
2.85	95	5
3.5	95	5
compound 40 ('column 1') method name: 20180523_HighRes_Pos_ACN_FA_150bis1300 t_R = 2.87 ± 0.05 min, m/z= 372.19-372.21; 743.39-743.40, flow: 0.5 mL/min		
0	95	5
5.5	0	100
7	0	100
7.2	95	5
8	95	5
compound 40 ('column 2') method name: 20210413_PheHex50_Pos_ACN_100bis1000 t_R = 2.74 ± 0.05 min, m/z= 372.19-372.21; 743.39-743.40, flow: 0.7 mL/min		
0	95	5
1	0	100
1.25	0	100
2.85	95	5
3.5	95	5

Table 7.9: High resolution mass spectrometry methods for cellular uptake assays of compounds measured in negative mode (ESI^-).

t (min)	solvent C (%)	solvent D (%)
compound 47 ('column 1') method name: 20190218_HighRes_Neg_ACN_200bis1000_NA t_R = 6.10 ± 0.05 min, m/z= 456.00-456.02; flow: 0.7 mL/min		
0	95	5
5.5	0	100
7	0	100
7.2	95	5
8	95	5
compound 44 ('column 1') method name: 20190218_HighRes_Neg_ACN_200bis1000_NA t_R = 6.22 ± 0.05 min, m/z= 475.99-476.01, flow: 0.7 mL/min		
0	95	5
5.5	0	100
7	0	100
7.2	95	5
8	95	5
compound 46 ('column 1') method name: 20190218_HighRes_Neg_ACN_200bis1000_NA t_R = 5.79 ± 0.05 min, m/z= 493.04-493.06, flow: 0.7 mL/min		
0	95	5
5.5	0	100
7	0	100
7.2	95	5
8	95	5

A full SIM (single ion monitoring) method was applied. For the investigation of cellular uptake of the compounds, an external calibration was used by plotting integrated peak areas (Gauss fit through seven points) of known standards over their concentrations. After fitting (quadratic fit) and forcing the resultant curve through the origin, concentrations in the samples were calculated ('sample concentration'). The coefficient of determination (R^2) of the calibration curves was greater than 0.99 in all cases.

7.1.3.1.3 Calculations

Sample concentrations resulting from HRMS measurements were converted into “biological concentrations“ by taking bacterial cell numbers into account,[135,261,265] as described with following equations which have been set up as part of this work:

$$Cell\ number\ (E.coli) = \frac{7.8\ x\ 10^{8}\ \cdot\ exact\ OD_{600}\ after\ growing\ until\ OD_{600} \sim 0.6\ \cdot 30\ mL}{(V(M9)\ for\ \ OD_{600} \sim 4\ [mL]\ /\ 0.5\ mL)}$$

$$Cell\ number\ (S.aureus) = \frac{y\ \cdot 30\ mL}{(V(M9)\ for\ OD_{600}\ of \sim 4\ [mL]\ /\ 0.5\ mL)}$$

$$with\ y = \frac{exact\ OD_{600}\ after\ growing\ until\ OD_{600} \sim 0.6 + 0.0562}{9\ x\ 10^{-9}}$$

Relative comparisons between cellular uptake of compounds were performed with calculated concentrations.

7.1.3.2 Specific procedures for Gram-negative bacteria

7.1.3.2.1 Lysis

For Gram-negative *E. coli* DH5α and efflux-deficient *E. coli* Δ*tolC* lysis was carried out by sonication (Bandelin Sonopuls HD 60; 50% amplitude, 5/10 s pulse, 5/10 s pause for 5 minutes) with cells on ice.

7.1.3.2.2 Differentiation between cytoplasm and periplasm

A cold osmotic shock[289] was applied to differentiate between cytoplasm and periplasm of Gram-negative bacteria. Therefore, pelleted bacteria were resuspended in ice-cold sucrose buffer (1 mL, 0 °C), incubated (10 minutes, 4 °C) with gentle shaking (Benchmark Benchrocker 2D) and centrifuged (6,000 x g, 10 min, 4 °C). Pellets were resuspended in ice-cold water (1 mL, 0 °C), incubated (10 minutes, 4 °C) with gentle shaking (Benchmark Benchrocker 2D) and centrifuged again (6,000 x g, 10 minutes, 4 °C). The resultant supernatants contained the periplasmic fractions ('periplasm') which were not subjected to lysis and frozen prior to MS measurements. The corresponding spheroblasts-containing pellets ('cytoplasm') were lysed using standard conditions (Chapter 7.1.3.2.1).

7.1.3.3 Lysis as specific procedure for Gram-positive bacteria

Lysis of *S. aureus* Newman as one representative of Gram-positive bacteria was performed with lysostaphin, which was expressed as part of this work (Chapter 4.1.1.2.1) based on a publication by Farhangnia et al.[242] The designed codon-optimized lysostaphin plasmid is called pET-lys. Lysis procedure was investigated and optimized (Chapter 4.1.1.2.2).

7.1.3.3.1 Design of lysostaphin plasmid

The lysostaphin plasmid was cloned into a pET32a(+) vector obtained from Merck: 10 µg pET32a(+) vector (5,900 bp) with a concentration of 0.5 µg/µL (20 µL as total volume). The vector contained three tags: a Trx-tag (~ 12 kDa), a His-tag (6xHis-tag + thrombin site (~ 1.9 kDa)) and an S-tag (S-tag + TEV site (~ 4 kDa)). 10 µL of pET32a(+) vector were sent to Eurofins Genomics for gene synthesis of pET32a(+)-lysostaphin (1,332 bp) using BamHI (5'-restriction site) and XhoI (3'-restriction site) as restriction enzymes, in frame with the mentioned tags and Amp as antibiotic resistance.

Gene sequence of the pET32a(+) vector (bp):

ATCCGGATATAGTTCCTCCTTTCAGCAAAAAACCCCTCAAGACCCGTTTAGAGGCCCCA
AGGGGTTATGCTAGTTATTGCTCAGCGGTGGCAGCAGCCAACTCAGCTTCCTTTCGGG
CTTTGTTAGCAGCCGGATCTCAGTGGTGGTGGTGGTGGTGCTCGAGTGCGGCCGCAAG
CTTGTCGACGGAGCTCGAATTCGGATCCGATATCAGCCATGGCCTTGTCGTCGTCGTC
GGTACCCAGATCTGGGCTGTCCATGTGCTGGCGTTCGAATTTAGCAGCAGCGGTTTCTT
TCATACCAGAACCGCGTGGCACCAGACCAGAAGAATGATGATGATGATGGTGCATATG
GCCAGAACCAGAACCGGCCAGGTTAGCGTCGAGGAACTCTTTCAACTGACCTTTAGACA
GTGCACCCACTTTGGTTGCCGCCACTTCACCGTTTTTGAACAGCAGCAGAGTCGGGATA
CCACGGATGCCATATTTCGGCGCAGTGCCAGGGTTTTGATCGATGTTCAGTTTTGCAAC
GGTCAGTTTGCCCTGATATTCGTCAGCGATTTCATCCAGAATCGGGGCGATCATTTTGC
ACGGACCGCACCACTCTGCCCAGAAATCGACGAGGATCGCCCCGTCCGCTTTGAGTAC
ATCCGTGTCAAAACTGTCGTCAGTCAGGTGAATAATTTTATCGCTCATATGTATATCTCC
TTCTTAAAGTTAAACAAAATTATTTCTAGAGGGGAATTGTTATCCGCTCACAATTCCCCTA
TAGTGAGTCGTATTAATTTCGCGGGATCGAGATCGATCTCGATCCTCTACGCCGGACGC
ATCGTGGCCGGCATCACCGGCGCCACAGGTGCGGTTGCTGGCGCCTATATCGCCGAC
ATCACCGATGGGGAAGATCGGGCTCGCCACTTCGGGCTCATGAGCGCTTGTTTCGGCG
TGGGTATGGTGGCAGGCCCCGTGGCCGGGGGACTGTTGGGCGCCATCTCCTTGCATG
CACCATTCCTTGCGGCGGCGGTGCTCAACGGCCTCAACCTACTACTGGGCTGCTTCCT
AATGCAGGAGTCGCATAAGGGAGAGCGTCGAGATCCCGGACACCATCGAATGGCGCAA
AACCTTTCGCGGTATGGCATGATAGCGCCCGGAAGAGAGTCAATTCAGGGTGGTGAAT
GTGAAACCAGTAACGTTATACGATGTCGCAGAGTATGCCGGTGTCTCTTATCAGACCGT
TTCCCGCGTGGTGAACCAGGCCAGCCACGTTTCTGCGAAAACGCGGGAAAAAGTGGAA
GCGGCGATGGCGGAGCTGAATTACATTCCCAACCGCGTGGCACAACAACTGGCGGGC
AAACAGTCGTTGCTGATTGGCGTTGCCACCTCCAGTCTGGCCCTGCACGCGCCGTCGC
AAATTGTCGCGGCGATTAAATCTCGCGCCGATCAACTGGGTGCCAGCGTGGTGGTGTC
GATGGTAGAACGAAGCGGCGTCGAAGCCTGTAAAGCGGCGGTGCACAATCTTCTCGCG
CAACGCGTCAGTGGGCTGATCATTAACTATCCGCTGGATGACCAGGATGCCATTGCTGT

GGAAGCTGCCTGCACTAATGTTCCGGCGTTATTTCTTGATGTCTCTGACCAGACACCCA
TCAACAGTATTATTTTCTCCCATGAAGACGGTACGCGACTGGGCGTGGAGCATCTGGTC
GCATTGGGTCACCAGCAAATCGCGCTGTTAGCGGGCCCATTAAGTTCTGTCTCGGCGC
GTCTGCGTCTGGCTGGCTGGCATAAATATCTCACTCGCAATCAAATTCAGCCGATAGCG
GAACGGGAAGGCGACTGGAGTGCCATGTCCGGTTTTCAACAAACCATGCAAATGCTGA
ATGAGGGCATCGTTCCCACTGCGATGCTGGTTGCCAACGATCAGATGGCGCTGGGCGC
AATGCGCGCCATTACCGAGTCCGGGCTGCGCGTTGGTGCGGACATCTCGGTAGTGGG
ATACGACGATACCGAAGACAGCTCATGTTATATCCCGCCGTTAACCACCATCAAACAGG
ATTTTCGCCTGCTGGGGCAAACCAGCGTGGACCGCTTGCTGCAACTCTCTCAGGGCCA
GGCGGTGAAGGGCAATCAGCTGTTGCCCGTCTCACTGGTGAAAAGAAAAACCACCCTG
GCGCCCAATACGCAAACCGCCTCTCCCCGCGCGTTGGCCGATTCATTAATGCAGCTGG
CACGACAGGTTTCCCGACTGGAAAGCGGGCAGTGAGCGCAACGCAATTAATGTAAGTT
AGCTCACTCATTAGGCACCGGGATCTCGACCGATGCCCTTGAGAGCCTTCAACCCAGT
CAGCTCCTTCCGGTGGGCGCGGGGCATGACTATCGTCGCCGCACTTATGACTGTCTTC
TTTATCATGCAACTCGTAGGACAGGTGCCGGCAGCGCTCTGGGTCATTTTCGGCGAGG
ACCGCTTTCGCTGGAGCGCGACGATGATCGGCCTGTCGCTTGCGGTATTCGGAATCTT
GCACGCCCTCGCTCAAGCCTTCGTCACTGGTCCCGCCACCAAACGTTTCGGCGAGAAG
CAGGCCATTATCGCCGGCATGGCGGCCCCACGGGTGCGCATGATCGTGCTCCTGTCGT
TGAGGACCCGGCTAGGCTGGCGGGGTTGCCTTACTGGTTAGCAGAATGAATCACCGAT
ACGCGAGCGAACGTGAAGCGACTGCTGCTGCAAAACGTCTGCGACCTGAGCAACAACA
TGAATGGTCTTCGGTTTCCGTGTTTCGTAAAGTCTGGAAACGCGGAAGTCAGCGCCCTG
CACCATTATGTTCCGGATCTGCATCGCAGGATGCTGCTGGCTACCCTGTGGAACACCTA
CATCTGTATTAACGAAGCGCTGGCATTGACCCTGAGTGATTTTTCTCTGGTCCCGCCGC
ATCCATACCGCCAGTTGTTTACCCTCACAACGTTCCAGTAACCGGGCATGTTCATCATCA
GTAACCCGTATCGTGAGCATCCTCTCTCGTTTCATCGGTATCATTACCCCCATGAACAGA
AATCCCCCTTACACGGAGGCATCAGTGACCAAACAGGAAAAAACCGCCCTTAACATGGC
CCGCTTTATCAGAAGCCAGACATTAACGCTTCTGGAGAAACTCAACGAGCTGGACGCG
GATGAACAGGCAGACATCTGTGAATCGCTTCACGACCACGCTGATGAGCTTTACCGCAG
CTGCCTCGCGCGTTTCGGTGATGACGGTGAAAACCTCTGACACATGCAGCTCCCGGAG
ACGGTCACAGCTTGTCTGTAAGCGGATGCCGGGAGCAGACAAGCCCGTCAGGGCGCG
TCAGCGGGTGTTGGCGGGTGTCGGGGCGCAGCCATGACCCAGTCACGTAGCGATAGC
GGAGTGTATACTGGCTTAACTATGCGGCATCAGAGCAGATTGTACTGAGAGTGCACCAT
ATATGCGGTGTGAAATACCGCACAGATGCGTAAGGAGAAAATACCGCATCAGGCGCTCT
TCCGCTTCCTCGCTCACTGACTCGCTGCGCTCGGTCGTTCGGCTGCGGCGAGCGGTAT
CAGCTCACTCAAAGGCGGTAATACGGTTATCCACAGAATCAGGGGATAACGCAGGAAA
GAACATGTGAGCAAAAGGCCAGCAAAAGGCCAGGAACCGTAAAAAGGCCGCGTTGCTG
GCGTTTTTCCATAGGCTCCGCCCCCCTGACGAGCATCACAAAAATCGACGCTCAAGTCA

GAGGTGGCGAAACCCGACAGGACTATAAAGATACCAGGCGTTTCCCCCTGGAAGCTCC
CTCGTGCGCTCTCCTGTTCCGACCCTGCCGCTTACCGGATACCTGTCCGCCTTTCTCCC
TTCGGGAAGCGTGGCGCTTTCTCATAGCTCACGCTGTAGGTATCTCAGTTCGGTGTAGG
TCGTTCGCTCCAAGCTGGGCTGTGTGCACGAACCCCCCGTTCAGCCCGACCGCTGCGC
CTTATCCGGTAACTATCGTCTTGAGTCCAACCCGGTAAGACACGACTTATCGCCACTGG
CAGCAGCCACTGGTAACAGGATTAGCAGAGCGAGGTATGTAGGCGGTGCTACAGAGTT
CTTGAAGTGGTGGCCTAACTACGGCTACACTAGAAGGACAGTATTTGGTATCTGCGCTC
TGCTGAAGCCAGTTACCTTCGGAAAAAGAGTTGGTAGCTCTTGATCCGGCAAACAAACC
ACCGCTGGTAGCGGTGGTTTTTTTGTTTGCAAGCAGCAGATTACGCGCAGAAAAAAAGG
ATCTCAAGAAGATCCTTTGATCTTTTCTACGGGGTCTGACGCTCAGTGGAACGAAAACT
CACGTTAAGGGATTTTGGTCATGAGATTATCAAAAAGGATCTTCACCTAGATCCTTTTAA
ATTAAAAATGAAGTTTTAAATCAATCTAAAGTATATATGAGTAAACTTGGTCTGACAGTTA
CCAATGCTTAATCAGTGAGGCACCTATCTCAGCGATCTGTCTATTTCGTTCATCCATAGT
TGCCTGACTCCCCGTCGTGTAGATAACTACGATACGGGAGGGCTTACCATCTGGCCCC
AGTGCTGCAATGATACCGCGAGACCCACGCTCACCGGCTCCAGATTTATCAGCAATAAA
CCAGCCAGCCGGAAGGGCCGAGCGCAGAAGTGGTCCTGCAACTTTATCCGCCTCCATC
CAGTCTATTAATTGTTGCCGGGAAGCTAGAGTAAGTAGTTCGCCAGTTAATAGTTTGCG
CAACGTTGTTGCCATTGCTGCAGGCATCGTGGTGTCACGCTCGTCGTTTGGTATGGCTT
CATTCAGCTCCGGTTCCCAACGATCAAGGCGAGTTACATGATCCCCCATGTTGTGCAAA
AAAGCGGTTAGCTCCTTCGGTCCTCCGATCGTTGTCAGAAGTAAGTTGGCCGCAGTGTT
ATCACTCATGGTTATGGCAGCACTGCATAATTCTCTTACTGTCATGCCATCCGTAAGATG
CTTTTCTGTGACTGGTGAGTACTCAACCAAGTCATTCTGAGAATAGTGTATGCGGCGAC
CGAGTTGCTCTTGCCCGGCGTCAATACGGGATAATACCGCGCCACATAGCAGAACTTTA
AAAGTGCTCATCATTGGAAAACGTTCTTCGGGGCGAAAACTCTCAAGGATCTTACCGCT
GTTGAGATCCAGTTCGATGTAACCCACTCGTGCACCCAACTGATCTTCAGCATCTTTTAC
TTTCACCAGCGTTTCTGGGTGAGCAAAAACAGGAAGGCAAAATGCCGCAAAAAAGGGAA
TAAGGGCGACACGGAAATGTTGAATACTCATACTCTTCCTTTTTCAATATTATTGAAGCAT
TTATCAGGGTTATTGTCTCATGAGCGGATACATATTTGAATGTATTTAGAAAAATAAACAA
ATAGGGGTTCCGCGCACATTTCCCCGAAAAGTGCCACCTGAAATTGTAAACGTTAATATT
TTGTTAAAATTCGCGTTAAATTTTTGTTAAATCAGCTCATTTTTTAACCAATAGGCCGAAA
TCGGCAAAATCCCTTATAAATCAAAAGAATAGACCGAGATAGGGTTGAGTGTTGTTCCA
GTTTGGAACAAGAGTCCACTATTAAAGAACGTGGACTCCAACGTCAAAGGGCGAAAAAC
CGTCTATCAGGGCGATGGCCCACTACGTGAACCATCACCCTAATCAAGTTTTTTGGGGT
CGAGGTGCCGTAAAGCACTAAATCGGAACCCTAAAGGGAGCCCCCGATTTAGAGCTTG
ACGGGGAAAGCCGGCGAACGTGGCGAGAAAGGAAGGGAAGAAAGCGAAAGGAGCGG
GCGCTAGGGCGCTGGCAAGTGTAGCGGTCACGCTGCGCGTAACCACCACACCCGCCG
CGCTTAATGCGCCGCTACAGGGCGCGTCCCATTCGCCA

Gene sequence of lysostaphin (bp):

GGATCCATGGATGTGAGCAAGAAAGTCGCAGAAGTGGAAACCAGCAAACCGCCCGTGG
AAAACACCGCAGAGGTTGAAACGAGTAAAGCGCCGGTGGAGAACACTGCGGAGGTGG
AAACTTCGAAAGCCCCGGTTGAAAACACCGCCGAGGTGGAAACCTCCAAGGCGCCAGT
CGAAAACACGGCCGAAGTCGAAACCAGTAAAGCACCGGTGGAAAATACGGCCGAAGTG
GAAACGTCCAAAGCGCCGGTCGAAAATACGGCAGAAGTTGAAACATCAAAAGCCCCTG
TGGAAAATACTGCGGAAGTAGAAACATCGAAGGCCCCTGTTGAGAATACCGCTGAGGTA
GAAACTAGCAAGGCACCGGTTGAGAATACTGCCGAGGTGGAGACTAGCAAGGCCCCAG
TGGAGAATACCGCAGAAGTAGAAACCTCTAAAGCGCCCGTTGAGAACACCGCGGAAGT
CGAAACTAGCAAAGCTCCAGTTGAAAATACCGCGGAAGTTGAAACGTCTAAAGCACCTG
TGGAGAATACGGCGGAGGTAGAAACCTCGAAAGCGCTGGTGCAGAATCGCACAGCTCT
TCGTGCGGCTACGCATGAACACTCTGCTCAGTGGCTGAACAACTACAAGAAAGGCTATG
GATATGGTCCGTATCCCTTGGGTATCAATGGCGGGATTCACTACGGTGTGGATTTCTTC
ATGAACATTGGCACCCCTGTAAAGGCTATTTCCAGCGGCAAAATCGTGGAAGCGGGTTG
GAGTAACTATGGTGGCGGCAATCAGATTGGCCTGATCGAAAATGACGGCGTTCATCGC
CAGTGGTATATGCATCTGAGCAAATACAACGTGAAAGTAGGTGACTATGTCAAAGCAGG
CCAGATTATTGGGTGGTCGGGGAGTACCGGGTATTCTACCGCGCCGCATTTACACTTTC
AACGGATGGTTAACTCGTTTAGCAACTCAACAGCGCAAGATCCGATGCCGTTCCTGAAA
AGCGCAGGCTATGGTAAAGCCGGAGGTACCGTAACGCCGACGCCAAACACCGGGTGG
AAAACCAACAAATACGGTACCCTGTACAAAAGCGAATCCGCCAGTTTTACCCCGAACAC
TGACATCATCACACGTACCACAGGACCGTTTCGTTCAATGCCACAATCAGGCGTTCTGA
AAGCCGGTCAGACCATCCACTATGATGAGGTCATGAAACAGGATGGCCATGTCTGGGT
GGGCTACACCGGTAATTCCGGCCAACGCATTTACCTCCCGGTCCGCACATGGAACAAA
TCTACGAACACGTTGGGTGTCTTATGGGGAACGATTAAATAACTCGAG

Sequence of lysostaphin (amino acids):

MSDKIIHLTDDSFDTDVLKADGAILVDFWAEWCGPCKMIAPILDEIADEYQGKLTVAKLNIDQ
NPGTAPKYGIRGIPTLLLFKNGEVAATKVGALSKGQLKEFLDANLAGSGSGHMHHHHHHSS
GLVPRGSGMKETAAAKFERQHMDSPDLGTENLYFQSMADIGSMDVSKKVAEVETSKPPVE
NTAEVETSKAPVENTAEVETSKAPVENTAEVETSKAPVENTAEVETSKAPVENTAEVETSKA
PVENTAEVETSKAPVENTAEVETSKAPVENTAEVETSKAPVENTAEVETSKAPVENTAEVET
SKAPVENTAEVETSKAPVENTAEVETSKAPVENTAEVETSKALVQNRTALRAATHEHSAQW
LNNYKKGYGYGPYPLGINGGIHYGVDFFMNIGTPVKAISSGKIVEAGWSNYGGGNQIGLIEN
DGVHRQWYMHLSKYNVKVGDYVKAGQIIGWSGSTGYSTAPHLHFQRMVNSFSNSTAQDP
MPFLKSAGYGKAGGTVTPTPNTGWKTNKYGTLYKSESASFTPNTDIITRTTGPFRSMPQSG
VLKAGQTIHYDEVMKQDGHVWVGYTGNSGQRIYLPVRTWNKSTNTLGVLWGTIK

7.1.3.3.2 Plasmid transformation of lysostaphin

An aliquot (50 µL) of competent *E. coli* BL21(DE3) pLysS cells was thawed on ice for 10 min. After injecting the pET-lys vector (1 µL) into the strain, the mixture was incubated on ice for 30 minutes. A heat shock was performed at 42 °C for 45 seconds, followed by another incubation on ice for 2 minutes. After adding sterile LB medium (200 µL), the mixture was incubated in a shaking incubator (Infors HT) at 37 °C for 1 hour, plated (50 µL) on LB agar plates supplemented with Amp (100 µg/mL) and CAM (34 µg/mL) and incubated at 37 °C overnight.

7.1.3.3.3 Expression of lysostaphin

LB medium (10 mL) supplemented with Amp (100 µg/mL) and CAM (34 µg/mL) was inoculated with one to five colonies from the LB agar plates and was incubated overnight (180 rpm, 37 °C). The following morning, a culture of LB medium (500 mL) was inoculated with overnight culture (5 mL) and Amp (100 µg/mL) and incubated until an OD_{600} of ~ 0.6 was reached (180 rpm, 37 °C, ~ 5 hours). The expression of lysostaphin was induced with IPTG (1 mM) for 4 h (200 rpm, 37 °C). The induction time was investigated as part of this work (Chapter 4.1.1.2.1). Bacteria were harvested by centrifugation (5,750 x g, 15 minutes, 4 °C) and cell pellets were stored at -80 °C overnight. Pellets were thawed on ice, incubated with resuspension buffer (20 mL total volume) including EDTA-free protease inhibitor cocktail (Merck; one tablet) at 4 °C for 1 hour before resuspending. Cells were lysed by sonication (Bandelin Sonopuls HD 60, 10 minutes, 30% amplitude, 1 s on pulse, 2 s off pulse). Cellular debris was pelleted by centrifugation (20,000 x g, 45 minutes, 4 °C). The lysate was incubated with Ni-NTA agarose resin (Qiagen, 1 mL final bead volume for 500 mL culture), preequilibrated with resuspension buffer, at 4 °C for 2 hours. The resin was washed with wash buffer until no protein was detected by Bradford test (10 µL eluent + 50 µL Bradford reagent). Bound protein was eluted with elution buffer (8 mL). The expressed protein was dialyzed and refolded with PBS (pH = 7.2) containing PMSF (0.2 mM) at 4 °C overnight. Protein fractions were analyzed by SDS-PAGE (Chapter 7.1.1.7) and fractions containing lysostaphin were combined. Protein preparations were aliquoted (20 µL) and flash frozen in liquid nitrogen for the storage at -80 °C.

7.1.4 Hemolysis assays

For the investigation of hemolytic activities of compounds, an erythrocyte suspension was prepared following a reported procedure.[276] The protocol adapted in the course of this work consisted of a final volume of 100 µL, mixing erythrocyte suspension (95 µL) and compound solution (5 µL diluted compound, dilution in PBS (pH 7.2) from a stock (20 mM) in DMSO). It was crucial to avoid any mechanical pressure and air bubbles when pipetting. Several approaches regarding compound incubation concentrations were employed:

a) Specific defined incubation concentration (400 µM)

b) Incubation concentration ~ 20-fold antibacterial growth inhibition

c) Incubation concentration ~ 80-fold antibacterial growth inhibition

Mixtures were incubated (500 rpm, 60 minutes, 37 °C) in a thermoshaker (PEQLAB, TS-100). Following incubation, samples were centrifuged (17,000 x g, 5 minutes, 23 C) and the release of hemoglobin was detected by measuring the absorbance of the supernatant at 414 nm using a plate reader (BMG Labtech POLARstar Omega, 96-well plate format, F-bottom). PBS (pH 7.2) alone or PBS (pH 7.2) mixed with the same amount of DMSO as contained in the compound solutions served as negative controls. Triton X-100 (2% v/v stock solution, 0.1% v/v final concentration) was used as positive control. Controls were measured as biological triplicates, compounds as biological quintuples. Hemolytic activity of compounds was determined by setting the mean absorbance of the erythrocyte suspension treated with compounds, considering the negative control including PBS and DMSO, in relation to the mean absorbance of the erythrocyte suspension treated with Triton X-100 (100% hemolysis).

7.1.5 Porcine liver esterase activity assays

According to the procedure by the research group of Prof. Dr. W. Dehaen (unpublished), PLE assays consist of esterase, testing dye 4 or 6 (both were found to represent the best assay conditions) and phosphate buffer. A suspension of PLE in ammonium sulfate (Sigma Aldrich, 3.2 M, pH = 8) was used and diluted in phosphate buffer (10 mM, pH = 7.4) to a final concentration of 38 µM. Depending on the testing dye, different intermediate concentrations of PLE in phosphate buffer were prepared: 350 nM for dye 4 or 13 µM for dye 6. Stock solutions of dyes 4 and 6 (10 mM) were prepared in DMSO and diluted to 1 mM. For the enzymatic reaction, dye solution (2 µL, 1 mM in DMSO), intermediate PLE solution (20 µL) and phosphate buffer (178 µL, 10 mM, pH = 7.4, 0.5% Triton-X) were mixed in a 96-black well plate (F-bottom). Fluorescence intensity was measured at λ_{ex} = 438 nm and λ_{em} = 520 nm (BMG Labtech POLARstar Omega) at room temperature in 30 seconds intervals for 1 hour with orbital shaking before the first measurement and between measurements. Fluorescence intensity was plotted as a function of time.

7.2 Synthesis

7.2.1 General methods

7.2.1.1 General working methods

Reactions under exclusion of moisture and oxygen were carried out with nitrogen as inert gas ('Schlenk technique') using anhydrous solvents, if not stated otherwise. Prior to use, the glass equipment was dried by heating *in vacuo*. The nitrogen used was dried over orange gel and phosphorus pentoxide. Suitable freezing mixtures (ice in water, ice and sodium chloride or liquid nitrogen in acetone) were used for reactions which required lower temperatures. A 'Christ Alpha2-4 LDplus' was used for lyophilization of compounds.

7.2.1.2 Starting materials and reagents

All chemicals and solvents used in this work were purchased from Acros Organics, Alfa Aesar, Fluka, GL Biochem, Honeywell, Iris Biotech, Merck, Roth, Sigma Aldrich and VWR or from the Zentrales Chemikalienlager of Saarland University in quality “for synthesis“ or “for analysis“ and used without further purification. Some reagents and starting materials were synthesized by Dr. D. Wiegmann (**59** and **60**), A. Heib (**61**) and E. Mareykin (**59**, **61**, **66** and **79**) who kindly provided them for this work.[212,267,284]

7.2.1.3 Solvents

CH_2Cl_2, EtOAc and PE (boiling range 40-60 °C) were purchased in technical quality, distilled and used for column chromatography, workups, extractions and reactions without inert gas conditions. All other solvents were purchased in p.a. quality and used without further purification, if not indicated otherwise. Deionized water was used directly from the water conduit. Highly pure water was obtained from a TKA GenPure water purification system (Milli-Q®).

7.2.1.4 Anhydrous solvents

Anhydrous solvents were obtained freshly from an MB SPS 800 solvent purification system by MBRAUN using solvents in ultrapure quality ('HPLC grade') or purchased in technical quality and dried as listed below.

- CH_2Cl_2: dried and purified by SPS.
- DMF: dried and purified by SPS.
- Et_2O: dried and purified by SPS.
- *Iso*-propanol: purchased as absolute solvent in sealed septum bottle.
- MeCN: dried and purified by SPS.

- MeOH: degassed and stored over molecular sieves (3 Å).
- THF: dried and purified by SPS.
- Toluene: purchased as absolute solvent in sealed septum bottle.

7.2.1.5 Chromatography

TLC:

TLC was performed on aluminum plates precoated with silica gel 60 F_{254} (VWR). Spots on the TLC were visualized via UV light (254 nm) and staining with suitable TLC stains, listed below, while heating.

- $KMnO_4$ solution (dissolved in water, 100 mL): 1.0 g $KMnO_4$, 6.0 g K_2CO_3 and 1.5 mL sodium hydroxide (5%, aq.) (w/v).
- Ninhydrin solution (dissolved in 1-butanol, 100 mL): 0.3 g ninhydrin, 3.0 mL AcOH.
- Vanillin/sulfuric acid solution (VSS) (dissolved in MeOH, 680 mL): 4.0 g vanillin, 25 mL H_2SO_4 (conc.), 80 mL AcOH.

Column chromatography:

For column chromatography silica gel 60 (40-63 µm, 230-400 mesh ASTM, VWR) was used.

HPLC:

Mixtures of MeCN or MeOH in ultrapure quality ('HPLC grade') and highly pure water were used as eluents for all HPLC applications. If necessary, both eluents were mixed with 0.1% trifluoroacetic acid (TFA 'HPLC grade', Sigma Aldrich). For analytical HPLC, a Thermo Scientific Spectra System including an SN 4000 controller, an SCM 1000 mixer, a P4000 pump system, an AS3000 autosampler, an UV2000 detector and a Surveryor MSQ Plus ESI-mass spectrometer (Finnigan) was used. For semipreparative HPLC, an Agilent Technologies 1200 Series HPLC system consisting of an Agilent 1100/1200 Quarternary Pump and a LiChroCart® Purospher® STAR RP18 column (5 µm, 10 x 250 mm, VWR) was used. Dead time corrections were not included in the stated retention times (t_R) [min]

Semi-preparative HPLC method:

Flow rate: 3 mL/min

Eluent: A (water + 0.1% TFA), B (MeCN + 0.1% TFA)

t [min]	0	30	34	44	44.1
B [%]	25	70	100	100	25

7.2.2 Instrumental analytics

NMR spectroscopy:

NMR spectra were measured at the NMR facilities of the Departments of Pharmacy and Chemistry at Saarland University. Therefore, the following NMR spectrometers by Bruker were used: Avance I 500 with a B ACS 60 auto sampler, Avance DRX 500 or Avance III 500 with a TCI cryo probe head for ^{1}H NMR spectra at 500 MHz and ^{13}C NMR spectra at 126 MHz, a fourier 300 for ^{1}H NMR spectra at 300 MHz and ^{13}C NMR spectra at 76 MHz and an avance II 400 for ^{31}P NMR spectra at 162 MHz and ^{19}F NMR spectra at 376 MHz. ^{13}C NMR spectra are ^{1}H-decoupled. Correlation 2D spectra (^{1}H,^{1}H-COSY, ^{1}H,^{13}C-HSQC, ^{1}H,^{13}C-HMBC) were measured for the correct assignment of signals. NMR spectra were recorded at room temperature unless indicated otherwise. Chemical shifts are given in units of [ppm] with reference to the non-deuterated solvent as internal standard. Coupling constants *J* are given in Hertz [Hz]. Diastereotopic protons are marked with the indices 'a' (upfield shifted proton) and 'b' (downfield shifted proton). The following abbreviations were used for multiplicities: s (singlet), d (doublet), t (triplet), q (quartet), quin (quintet), m (multiplet) and their combinations (e.g. dt (doublet of triplets)).

MS:

Low resolution mass spectra were recorded on a LC-MS Surveyor MSQ Plus integrating an electrospray ionization (ESI) unit, an AS3000 autosampler and a UV2000 detector (all from Finnigan). A Nucleodur® 100-5 C18 (5 µm, 3 x 125 mm) column was used for LC separation prior to detection.

High resolution mass spectra (HRMS) were recorded on an Ultimate 3000 system by *Thermo Scientific* with a *Dionex* UltiMate 3000 UHPLC system. It consisted of an automated autosampler, a pump, a column department, a detector (diode array) and a *Thermo Scientific* Q Exactive OrbiTrap. A Thermo Accucore™ phenyl-X (2.1 µm, 3 x 100 mm) column was adopted for UHPLC separation prior to detection.

7.2.3 General procedures

Procedure 1: Synthesis of 4-formylphenyl aldehydes[254,290]

The reaction was carried out without any inert gas conditions. A solution of 4-hydroxybenzaldehyde (1.0 eq.) in THF was cooled to 0 °C and triethylamine (1.5 eq.) and the corresponding acyl chloride (1.5 eq.) were added. The reaction mixture was stirred at room temperature for 2.5 hours, diluted with EtOAc and washed with saturated ammonium chloride solution (1 x). The aqueous phase was extracted with EtOAc (2 x). The combined organic layers were washed with water (1 x) and saturated brine (1 x) successively, dried over sodium sulfate and filtered. The product was obtained after removing the solvent *in vacuo* and directly used in the subsequent reduction to the corresponding alcohols (procedure 2).

Procedure 2: Synthesis of 4-hydroxymethylbenzyl alcohols[254,290]

The reaction was carried out without any inert gas conditions. A solution of 4-formylphenyl aldehyde (1.0 eq.) in THF was cooled to 0 °C and sodium borohydride (1.5 eq.) was added. The solution was stirred at room temperature for 3 hours and diluted with EtOAc. Saturated ammonium chloride solution (1 x) was carefully added while cooling (0 °C). The aqueous phase was extracted with EtOAc (2 x). The combined organic layers were washed with water (1 x) and saturated brine (1 x) successively, dried over sodium sulfate and filtered. The solvent was removed *in vacuo* and the crude product was purified by column chromatography (PE:EtOAc 3:1).

Procedure 3: *N*-Cbz-deprotections

Procedure 3.1: *iso*-propanol, palladium black, 1,4-cyclohexadiene

1,4-cyclohexadiene (10.0 eq.) and TFA (diluted to 10% in *iso*-propanol, 1.1 eq.) were added to a solution of *N*-Cbz-protected amine (1.0 eq.) in *iso*-propanol. Palladium black (one to three spatula tips) was added and the resulting solution was stirred at room temperature for 0.5-3 hours. Palladium black was filtered off through a syringe filter which was washed with preheated *iso*-propanol after a full conversion had been observed by TLC. The deprotected amine was obtained after removing the solvent *in vacuo*.

Procedure 3.2: *iso*-propanol, palladium black, hydrogen atmosphere

Palladium black (one to three spatula tips) and TFA (diluted to 10% in *iso*-propanol, 1.1 eq.) were added to a solution of *N*-Cbz-protected amine (1.0 eq.) in *iso*-propanol. The inert gas atmosphere was exchanged to a hydrogen atmosphere and the reaction mixture was stirred at room temperature for 3 hours. Palladium black was filtered through a syringe filter which was washed with preheated MeOH after a full conversion had been observed by TLC. The deprotected amine was obtained after removing the solvent *in vacuo*.

7.2.4 Synthesis of reagents and precursors

POM-I 62[280]

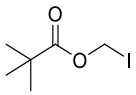

62

The reaction was carried out under light exclusion to avoid product decomposition. POM-Cl **84** (5.75 mL, 40.0 mmol, 1.0 eq.) was added dropwise to a solution of sodium iodide (6.00 g, 40.0 mmol, 1.0 eq.) in MeCN (30 mL). The reaction mixture was stirred at room temperature for 21 hours. The solvent was removed via distillation at 82 °C. Salts were removed by a vacuum rectification (boiling point: 50 °C at $1.9 \cdot 10^{-2}$ mbar). The product was stored at -20 °C under light exclusion and inert gas atmosphere. Beside the NMR spectroscopic characterization in which **62** was clearly detected no further analytics were done due to the rapid decomposition of **62**.

Yield (62): 7.80 g (32.2 mmol, 81%) as a yellow liquid.

^{1}H NMR (500 MHz, $CDCl_3$): δ [ppm] = 1.19 (s, 9 H, $\underline{C}(CH_3)_3$), 5.92 (s, 2 H, CH_2).

^{13}C NMR (126 MHz, $CDCl_3$): δ [ppm] = 26.65 ($C(\underline{C}H_3)_3$), 31.55 ($\underline{C}(CH_3)_3$), 39.01 (CH_2), 176.47 (C=O).

$C_6H_{11}IO_2$ (242.06 g/mol)

IBX 60[282]

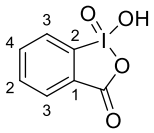

60

The reaction was carried out without any inert gas conditions. To a solution of oxone ($2\ KHSO_5 \cdot KHSO_4 \cdot K_2SO_4$, 68.6 g, 223 mmol, 3.0 eq.) in water (250 mL), 2-iodobenzoic acid **85** (18.5 g, 74.6 mmol, 1.0 eq.) was added. The reaction mixture was heated to 70 °C for 2.5 hours. The resulting suspension was cooled to 0 °C overnight. Precipitated crystals were filtered off, washed with ice-cold water (1 x 250 mL, 0 °C) and ice-cold acetone (2 x 250 mL, 0 °C). The product was dried *in vacuo* for several days. Due to poor solubility, NMR spectroscopic characterization was found to be sufficient.

Yield (60): 14.3 g (51.1 mmol, 69%) as a white solid.

^{1}H NMR (300 MHz, DMSO-d_6): δ [ppm] = 7.84 (ddd, *J* = 7.4 Hz, *J* = 1.0 Hz, 1 H, 5-H), 8.00 (ddd, *J* = 8.0 Hz, *J* = 7.3 Hz, *J* = 1.5 Hz, 1 H, 4-H), 8.03 (dd, *J* = 7.5 Hz, *J* = 1.0 Hz, 1 H, 6-H), 8.14 (dd, *J* = 7.4 Hz, 1 H, 3-H).

^{13}C NMR (75 MHz, DMSO-d_6): δ [ppm] = 125.03 (C-3), 130.11 (C-6), 131.45 (C-1), 132.97 (C-5), 133.42 (C-4), 146.57 (C-2). 167.56 (C=O).

$C_7H_5IO_4$ (280.02 g/mol)

POM ester phosphonate

***N*-Cbz-2-methoxyglycinmethylester 88**[203,204]

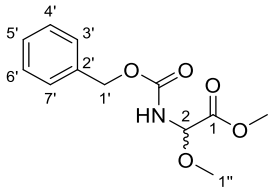

88

A solution glyoxylic acid monohydrate **86** (20.7 g, 224 mmol, 1.1 eq.) and benzyl carbamate **87** (30.9 g, 204 mmol, 1.0 eq.) in Et_2O (200 mL) was stirred at room temperature for 17 hours. The reaction mixture was concentrated *in vacuo*. The resulting suspension was filtered and washed with Et_2O (2 x 40 mL) at 0 °C. The solid was dried *in vacuo* and dissolved in MeOH (450 mL) at 0 °C. Sulfuric acid (6 mL) was added and the reaction mixture was stirred at rt for 6 d. Sodium hydrogen carbonate solution (350 mL) was slowly added to the reaction mixture at 0 °C. The aqueous layer was extracted with EtOAc (4 x 300 mL), the combined organic layers were dried over sodium sulfate and filtered. The solvent was removed *in vacuo* and PE (300 mL) was added to the resulting solid at 0 °C. The resulting suspension was filtered and washed with PE at 0 °C (2 x 50 mL). The product was dried *in vacuo* for several days.

Yield (88): 32.9 g (145 mmol, 72%) as a white solid.

^{1}H NMR (500 MHz, CD_3OD): δ [ppm] = 3.37 (s, 3 H, 1''-H), 3.76 (s, 3 H, $COOCH_3$), 5.13 (s, 2 H, 1'-H), 5.23 (s, 1 H, 2-H), 7.29-7.39 (m, 5 H, 3'-H, 4'-H, 5'-H, 6'-H, 7'-H).

^{13}C NMR (126 MHz, CD_3OD): δ [ppm] = 53.05 ($COO\underline{C}H_3$), 55.83 (C-1''), 67.95 (C-1'), 82.04 (C-2), 128.95 (C-3', C-7'), 129.15 (C-5'), 129.51 (C-4', C-6'), 137.89 (C-2'), 158.23 (NC(=O)O), 169.77 (C-1).

MS (ESI^+): m/z = 275.99 $[M+Na]^+$.

$C_{12}H_{15}NO_5$ (253.25 g/mol)

***N*-Cbz-2-(dimethylphosphoryl)-glycin-pivaloyloxymethylester 58**[212,250]

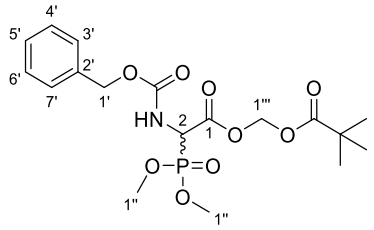

58

The first reaction was carried out without any inert gas conditions. *N*-Cbz-2-(dimethyl-phosphoryl) glycine methyl ester **61** (4.00 g, 12.2 mmol, 1.0 eq.)[204,205], kindly provided by A. Heib[267] and E. Mareykin[284], was dissolved in 1,4-dioxane (12 mL) and cooled to 15 °C. Sodium hydroxide solution (2 M, 6.04 mL, 12.1 mmol, 1.0 eq.) was added dropwise. The reaction mixture was stirred at 15 °C for 30 minutes. The solution was cooled to 0 °C and acidified to pH ~ 2 with hydrochloric acid (5 M). Water (40 mL) and EtOAc (80 mL) were added. The aqueous layer was extracted with EtOAc (4 x 40 mL), the combined organic layers were dried over sodium sulfate and filtered. The solvent was removed *in vacuo* to afford the intermediate **89** without further purification. The resulting solid (1.92 g, 6.04 mmol, 1.0 eq.) was dissolved in MeCN (20 mL). POM-I **62** (920 µL, 6.04 mmol, 1.0 eq.) and DIPEA (1.04 mL, 12.1 mmol, 1.0 eq.) were added dropwise under light exclusion. The solution was stirred at room temperature for 1 hour. The yellow solid was washed with a mixture of PE and EtOAc (1:1, 100 mL) and purified by column chromatography (EtOAc).

Yield (58): 1.62 g (3.76 mmol, 62%) as a colorless solid.

TLC: R_f = 0.59 (EtOAc).

^{1}H NMR (500 MHz, DMSO-d_6): δ [ppm] = 1.14 (s, 9 H, C(=O)C(CH_3)$_3$), 3.67 (d, $^3J_{PH}$ = 2.7 Hz, 3 H, 1''-H_a), 3.71 (d, $^3J_{PH}$ = 2.9 Hz, 3 H, 1''-H_b), 4.86 (dd, $^2J_{PH}$ = 24.4 Hz, J = 9.0 Hz, 1 H, 2-H), 5.08 (s, 2 H, 1'-H), 5.73 (d, J = 6.0 Hz, 1 H, 1'''-H_a), 5.82 (d, J = 6.0 Hz, 1 H, 1'''-H_b), 7.30-7.39 (m, 5 H, C-3', C-4', C-5', C-6', C-7'), 8.44 (dd, $^4J_{PH}$ = 9.0 Hz, J = 2.8 Hz, 1 H, NH).

^{13}C NMR (126 MHz, DMSO-d_6): δ [ppm] = 26.46 (C(=O)C(<u>C</u>H_3)$_3$), 38.18 (C(=O)<u>C</u>(CH_3)$_3$), 52.04 (d, $^1J_{CP}$ = 147.6 Hz, C-2), 53.70 (d, $^2J_{CP}$ = 7.3 Hz, C-1$_a$''), 53.77 (d, $^2J_{CP}$ = 6.4 Hz, C-1$_b$''), 66.11 (C-1'), 79.62 (C-1'''), 127.71, 127.91, 128.35 (C-3', C-4', C-5', C-6', C-7'), 136.58 (C-2'), 156.22 (NC(=O)O), 165.95 ($^2J_{CP}$ = 3.7 Hz, C-1), 175.95 (<u>C</u>(=O)C(CH_3)$_3$).

^{31}P NMR (162 MHz, DMSO-d_6): δ [ppm] = 17.96.

MS (ESI$^+$): m/z = 454.14 $[M+Na]^+$.

$C_{18}H_{26}NO_9P$ (431.38 g/mol)

7.2.5 Synthesis of prodrug building blocks

7.2.5.1 Synthesis of urea dipeptide

***N*-Cbz-L-valine POM ester 68**[212]

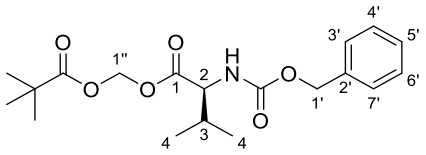

68

N-Cbz-L-valine **67** (2.10 g, 8.37 mmol, 1.0 eq.) was dissolved in MeCN (40 mL). POM-I **62** (1.20 mL, 7.98 mmol, 1.0 eq.) and DIPEA (1.36 mL, 7.97 mmol, 1.0 eq.) were added under light exclusion. The reaction mixture was stirred at room temperature for 1.5 hours and diluted with CH_2Cl_2 (500 mL). The organic layer was washed with saturated sodium bicarbonate solution (1 x 450 mL), dried over sodium sulfate and filtered. The solvent was removed *in vacuo*. The crude product was purified by column chromatography (PE:EtOAc 8:2).

Yield (68): 2.53 g (7.17 mmol, 90%) as a yellow oil.

TLC: R_f = 0.58 (PE:EtOAc 7:3).

^{1}H NMR (300 MHz, C_6D_6): δ [ppm] = 0.70 (d, *J* = 6.9 Hz, 3 H, 4-H_a), 0.81 (d, *J* = 6.8 Hz, 3 H, 4-H_b), 1.11 (s, 9 H, C(=O)C(CH_3)$_3$), 1.97 (m, *J* = 6.8 Hz, 1 H, 3-H), 4.50 (dd, *J* = 8.9 Hz, *J* = 5.0 Hz, 1 H, 2-H), 5.12 (d, *J* = 2.3 Hz, 1 H, 1'-H), 5.26 (d, 1 H, NH), 5.47 (d, *J* = 5.5 Hz, 1 H, 1''-H_a), 5.70 (d, *J* = 5.5 Hz, 1 H, 1''-H_b), 7.06-7.31 (m, 5 H, 3'-H, 4'-H, 5'-H, 6'-H, 7'-H).

^{13}C NMR (75 MHz, C_6D_6): δ [ppm] = 17.41 (C_a-4), 18.85 (C_b-4), 26.87 (C(=O)C(<u>C</u>H_3)$_3$), 31.03 (C-3), 38.72 (C(=O)<u>C</u>(CH_3)$_3$), 59.41 (C-2), 67.18 (C-1'), 79.53 (C-1''), 128.25, 128.51, 128.68 (C-3', C-4', C-5', C-6', C-7'), 137.07 (C-2'), 156.46 (NC(=O)O), 171.03 (C-1), 176.37 (<u>C</u>(=O)C(CH_3)$_3$).

MS (ESI^+): 388.19 $[M+Na]^+$.

$C_{19}H_{27}NO_6$ (365.43 g/mol)

L-valine POM ester 90[212]

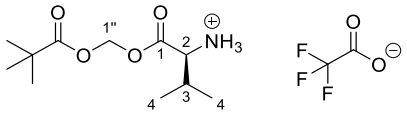

90

The reaction was carried out according to procedure 3.2 utilizing a solution of *N*-Cbz-L-valine-POM ester **68** (1.38 g, 3.77 mmol, 1.0 eq.) in *iso*-propanol (33 mL), TFA (317 µL, 4.15 mmol, diluted to 10% in *iso*-propanol, 1.1 eq.) and several spatula tips of palladium black

Yield (90): 1.29 g (3.74 mmol, 99%) as a white solid.

^{1}H NMR (500 MHz, CD_3OD): δ [ppm] = 1.07 (d, *J* = 7.0 Hz, 6 H, 4-H), 1.22 (s, 9 H, C(=O)C(CH_3)$_3$), 2.29 (dsept, *J* = 7.0 Hz, *J* = 4.5 Hz, 1 H, 3-H), 4.02 (d, *J* = 4.4 Hz, 1 H, 2-H), 5.79 (d, *J* = 5.7 Hz, 1 H, 1'-H_a), 5.99 (d, *J* = 5.7 z, 1 H, 1'-H_b).

^{13}C NMR (126 MHz, CD_3OD): δ [ppm] = 18.17 (C_a-4), 18.40 (C_b-4), 27.36 (C(=O)C(<u>C</u>H_3)$_3$), 31.11 (C-3), 39.93 (C(=O)<u>C</u>(CH_3)$_3$), 59.24 (C-2), 81.71 (C-1'), 169.34 (C-1), 178.19 (<u>C</u>(=O)C(CH_3)$_3$).

^{19}F NMR (282 MHz, CD_3OD): δ = -76.98.

MS (ESI^+): 232.12 $[M+H]^+$.

$C_{11}H_{21}NO_4$ (231.29 g/mol)

$C_{11}H_{21}NO_4 \cdot CF_3COOH$ (345.32 g/mol)

***O*-POM-L-valine isocyanate 91**[212,252,253]

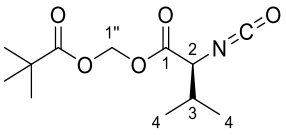

91

The reaction was carried out without any inert gas conditions. L-valine-POM ester **90** (960 mg, 2.78 mmol, 1.0 eq.) was dissolved in a mixture of CH_2Cl_2 (28 mL) and saturated sodium bicarbonate solution (28 mL) and cooled to 0 °C. Triphosgene (276 mg, 930 µmol, 1.0 eq.) was added and the reaction mixture was stirred at 0 °C for 20 minutes. The aqueous layer was extracted with CH_2Cl_2 (4 x 20 mL). The combined organic layers were dried over sodium sulfate and filtered. The solvent was removed *in vacuo* to afford the product without further purification.

Yield (91): 582 mg (2.26 mmol, 81%) as a white solid.

^{1}H NMR (500 MHz, $CDCl_3$): δ [ppm] = 0.91 (d, *J* = 6.8 Hz, 3 H, 4-H_a), 1.04 (d, *J* = 6.8 Hz, 3 H, 4-H_b), 1.23 (s, 9H, C(=O)C(CH_3)$_3$), 2.25 (dsept, *J* = 6.8 Hz, *J* = 3.6 Hz, 1 H, 3-H), 3.99 (d, *J* = 3.7 Hz, 1 H, 2-H), 5.80 (d, *J* = 5.4 Hz, 1 H, 1'-H_a), 5.91 (d, *J* = 5.4 Hz, 1 H, 1'-H_b).

^{13}C NMR (126 MHz, $CDCl_3$): δ [ppm] = 16.32 (C_a-4), 19.62 (C_b-4), 28.83 (C(=O)C(<u>C</u>H_3)$_3$), 31.73 (C-3), 38.78 (C(=O)<u>C</u>(CH_3)$_3$), 61.87 (C-2), 80.21 (C-1'), 126.83 (N=C=O), 169.90 (C-1), 176.88 (<u>C</u>(=O)C(CH_3)$_3$).

MS (ESI^+): 258.94 $[M+H]^+$.

$C_{12}H_{19}NO_5$ (257.29 g/mol)

***O*-POM-L-valine-*N*-(C=O)-N-($N^ε$-Cbz)-L-lysine 54**[212]

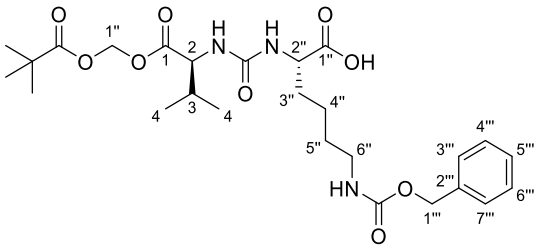

54

The reaction was carried out without any inert gas conditions. *O*-POM-L-valine isocyanate **91** (582 mg, 2.26 mmol, 1.1 eq.) was dissolved in THF (24 mL). A suspension of ($N^ε$-Cbz)-L-lysine **69** (589 mg, 2.10 mmol, 1.0 eq.) in DMF (116 mL) was added dropwise. The reaction mixture was stirred at room temperature for 25 hours. The reaction mixture was diluted with EtOAc (200 mL) and washed with hydrochloric acid (1 M, 3 x 300 mL). The combined organic layers were dried over sodium sulfate and filtered. The solvent was removed *in vacuo* and the crude product was purified by column chromatography (CH_2Cl_2:EtOAc 4:6 + 1% HCOOH).

Yield (54): 725 mg (1.35 mmol, 64%) as a white solid.

TLC: R_f = 0.27 (CH_2Cl_2:EtOAc 4:6 + 1% HCOOH).

^{1}H NMR (500 MHz, CD_3OD): δ [ppm] = 0.93 (d, *J* = 6.9 Hz, 3 H, 4-H_a), 0.98 (d, *J* = 6.8 Hz, 3 H, 4-H_b), 1.19 (s, 9 H, C(=O)C(CH_3)$_3$), 1.39-1.45 (m, 2 H, 4''-H), 1.50-1.56 (s, 2 H, 5''-H), 1.62-1.70 (m, 1 H, 3''-H_a), 1.80-1.86 (m, 1 H, 3''-H_b), 2.29 (dsept, *J* = 6.9 Hz, *J* = 5.0 Hz, 1 H, 3-H), 3.12 (t, *J* = 6.8 Hz, 2 H, 6''-H), 4.22 (d, *J* = 5.1 Hz, 1 H, 2-H), 4.25 (dd, *J* = 8.2 Hz, *J* = 5.0 Hz, 1 H, 2''-H), 5.06 (s, 2 H, 1'''-H), 5.69 (d, *J* = 5.6 Hz, 1 H, 1'-H_a), 5.84 (d, *J* = 5.6 Hz, 1 H, 1'-H_b), 7.28-7.38 (m, 5 H, 3'''-H, 4'''-H, 5'''-H, 6'''-H, 7'''-H).

^{13}C NMR (126 MHz, CD_3OD): δ [ppm] = 18.11 (C_a-4), 19.61 (C_b-4), 23.97 (C-4''), 27.41 (C(=O)C($\underline{C}H_3)_3$), 30.62 (C-3), 31.99 (C-5''), 33.43 (C-3''), 39.90 (C(=O)$\underline{C}(CH_3)_3$), 41.76 (C-6''), 54.10 (C-2''), 59.52 (C-2), 67.49 (C-1'''), 80.94 (C-1'), 128.91, 129.08, 129.60 (C-3''', C-4''', C-5''', C-6''', C-7'''), 138.52 (C-2'''), 159.06 (NC(=O)N), 160.37 (NC(=O)O), 173.00 (C-1), 176.48 (C-1''), 178.33 ($\underline{C}$(=O)C$(CH_3)_3$).

MS (ESI^+): 538.18 $[M+H]^+$.

$C_{26}H_{39}N_3O_9$ (537.61 g/mol)

7.2.5.2 Synthesis of chloroformates

4-Formylphenylacetate 92[254]

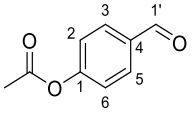

92

The reaction was carried out according to procedure 1 utilizing 4-hydroxybenzaldehyde **70** (10.0 g, 81.9 mmol, 1.0 eq.) in THF (250 mL), triethylamine (17.0 mL, 123 mmol, 1.5 eq.) and acetyl chloride **71** (8.76 mL, 123 mmol, 1.5 eq.). The reaction mixture was diluted with EtOAc (200 mL). Saturated ammonium chloride solution (1 x 350 mL), EtOAc (2 x 300mL), water (1 x 1 L) and saturated brine (1 x 1 L) were used for workup.

Yield (92): 13.2 g (80.7 mmol, 99%) as a brown liquid.

^{1}H NMR (300 MHz, $CDCl_3$): δ [ppm] = 2.34 (s, 3 H, CH_3), 7.28 (d, *J* = 8.6 Hz, 2 H, 2-H, 6-H), 7.92 (d, *J* = 8.6 Hz, 2 H, 3-H, 5-H), 10.00 (s, 1 H, 1'-H).

^{13}C NMR (75 MHz, $CDCl_3$): δ [ppm] = 21.27 (CH_3), 122.49 (C-2, C-6), 131.33 (C-3, C-5), 134.11 (C-4), 155.45 (C-1), 168.83 ($\underline{C}$(=O)CH_3), 191.04 (C-1').

$C_9H_8O_3$ (164.16 g/mol)

4-Formylphenylbutyrate 93[254]

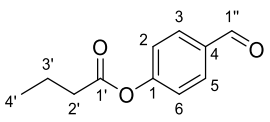

93

The reaction was carried out according to procedure 1 utilizing 4-hydroxybenzaldehyde **70** (10.0 g, 81.9 mmol, 1.0 eq.) in THF (250 mL), triethylamine (17.0 mL, 123 mmol, 1.5 eq.) and butyryl chloride **72** (12.7 mL, 123 mmol, 1.5 eq.). The reaction mixture was diluted with EtOAc

(200 mL). Saturated ammonium chloride solution (1 x 350 mL), EtOAc (2 x 300 mL), water (1 x 1 L) and saturated brine (1 x 1 L) were used for workup.

Yield (93): 14.6 g (77.8 mmol, 95%) as a light brown liquid.

^{1}H NMR (300 MHz, $CDCl_3$): δ [ppm] = 1.06 (t, *J* = 7.4 Hz, 3 H, 4'-H), 1.80 (tq, *J* = 7.4 Hz, 2 H, 3'-H), 2.58 (t, *J* = 7.4 Hz, 2 H, 2'-H), 7.27 (d, *J* = 8.6 Hz, 2 H, 2-H, 6-H), 7.92 (d, *J* = 8.5 Hz, 2 H, 3-H, 5-H), 9.99 (s, 1 H, 1''-H).

^{13}C NMR (75 MHz, $CDCl_3$): δ [ppm] = 13.65 (C-4'), 18.19 (C-3'), 36.34 (C-2'), 122.53 (C-2, C-6), 131.35 (C-3, C-5), 134.04 (C-4), 155.61 (C-1), 171.58 (C-1'), 191.11 (C1'').

$C_{12}H_{14}O_3$ (192.21 g/mol)

4-Formylphenylpivalate 94[254]

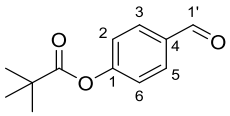

94

The reaction was carried out according to procedure 1 utilizing 4-hydroxybenzaldehyde **70** (10.0 g, 81.9 mmol, 1.0 eq.) in THF (250 mL), triethylamine (17.0 mL, 123 mmol, 1.5 eq.) and pivaloyl chloride **73** (15.1 mL, 123 mmol, 1.5 eq.). The reaction mixture was diluted with EtOAc (200 mL). Saturated ammonium chloride solution (1 x 350 mL), EtOAc (2 x 300 mL), water (1 x 1 L) and saturated brine (1 x 1 L) were used for workup.

Yield (94): 16.3 g (78.9 mmol, 96%) as a light brown liquid.

^{1}H NMR (300 MHz, $CDCl_3$): δ [ppm] = 1.35 (s, 9 H, C(=O)C($\underline{C}H_3)_3$), 7.22 (d, *J* = 8.4 Hz, 2 H, 2-H, 6-H), 7.90 (d, *J* = 8.5 Hz, 2 H, 3-H, 5-H), 9.97 (s, 1 H, 1'-H).

^{13}C NMR (75 MHz, $CDCl_3$): δ [ppm] = 27.17 (C(=O)C($\underline{C}H_3)_3$), 39.38 (C(=O)$\underline{C}(CH_3)_3$), 122.47 (C-2, C-6), 131.32 C-3, C-5), 133.98 (C-4), 156.06 (C-1), 176.57 ($\underline{C}$(=O)C(CH_3)), 191.15 (C-1').

$C_{12}H_{14}O_3$ (206.24 g/mol)

4-(Hydroxymethyl)-phenylacetate 95[254]

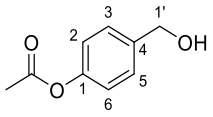

95

The reaction was carried out according to procedure 2 utilizing 4-formylphenylacetate **92** (13.0 g, 79.2 mmol, 1.0 eq.) in THF (400 mL) and sodium borohydride (4.50 g, 119 mmol, 1.5 eq.). diluted with EtOAc (300 mL). The reaction mixture was diluted with EtOAc (300 mL). Saturated ammonium chloride solution (1 x 500 mL), EtOAc (2 x 500 mL), water (1 x 1.5 L) and saturated brine (1 x 1.5 L) were used for workup.

Yield (95): 10.7 g (64.2 mmol, 81%) as a colorless oil.

TLC: R_f (PE:EtOAc 3:2) = 0.19.

^{1}H NMR (500 MHz, $CDCl_3$): δ [ppm] = 2.29 (s, 3 H, CH_3), 4.65 (s, 2 H, 1'-H), 7.06 (d, *J* = 8.5 Hz, 2 H, 2-H, 6-H), 7.36 (d, *J* = 8.6 Hz, 2 H, 3-H, 5-H).

^{13}C NMR (126 MHz, $CDCl_3$): δ [ppm] = 21.22 (CH_3), 64.77 (C-1'), 121.76 (C-2, C-6), 128.18 (C-3, C-5), 138.67 (C-4), 150.13 (C-1), 169.76 (C(=O)CH_3).

HRMS (ESI$^+$): calc. for $C_9H_{11}O_3^+$: 167.0703, found: 167.0704 $[M+H]^+$.

$C_9H_{10}O_3$ (166.18 g/mol)

4-(Hydroxymethyl)-phenylbutyrate 96[254]

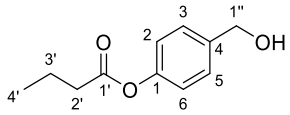

96

The reaction was carried out according to procedure 2 utilizing 4-formylphenylbutyrate **93** (15.0 g, 77.8 mmol, 1.0 eq.) in THF (400 mL) and sodium borohydride (4.41 g, 117 mmol, 1.5 eq.). The reaction mixture was diluted with EtOAc (300 mL). Saturated ammonium chloride solution (1 x 500 mL), EtOAc (2 x 500 mL), water (1 x 1.5 L) and saturated brine (1 x 1.5 L) were used for workup.

Yield (96): 9.15 g (47.1 mmol, 61 %) as a white solid.

TLC: R_f (PE:EtOAc 3:2) = 0.32.

^{1}H NMR (500 MHz, $CDCl_3$): δ [ppm] = 1.04 (t, *J* = 7.4 Hz, 3 H, 4'-H), 1.78 (tq, *J* = 7.4 Hz, *J* = 7.4 Hz 2 H, 3'-H), 2.54 (t, *J* = 7.4 Hz, 2 H, 2'-H), 4.66 (s, 2 H, 1''-H), 7.05-7.07 (m, 2 H, 2-H, 6-H), 7.35-7.38 (m, 2 H, 3-H, 5-H).

^{13}C NMR (126 MHz, $CDCl_3$): δ [ppm] = 13.76 (C-4'), 18.58 (C-3'), 36.34 (C-2'), 64.86 (C-1''), 121.81 (C-2, C-6), 128.18 (C-3, C-5), 138.53 (C-4), 150.25 (C-1), 172.39 (C-1').

HRMS (ESI$^+$): calc. for $C_{11}H_{15}O_3^+$: 195.1016, found: 195.1016 $[M+H]^+$.

$C_{11}H_{14}O_3$ (194.23 g/mol)

4-(Hydroxymethyl)-phenylpivalate 97[254]

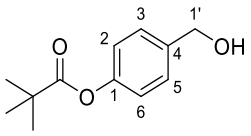

97

The reaction was carried out according to procedure 2 utilizing 4-formylphenylpivalate **94** (16.0 g, 77.8 mmol, 1.0 eq.) in THF (400 mL) and sodium borohydride (4.41 g, 117 mmol, 1.5 eq.). The reaction mixture was diluted with EtOAc (300 mL). Saturated ammonium chloride solution (1 x 500 mL), EtOAc (2 x 500 mL), water (1 x 1.5 L) and saturated brine (1 x 1.5 L) were used for workup.

Yield (97): 15.4 g (73.9 mmol, 95 %) as a white solid.

TLC: R_f (PE:EtOAc 3:2) = 0.32.

^{1}H NMR (500 MHz, $CDCl_3$): δ [ppm] = 1.35 (s, 9 H ($C(=O)C(CH_3)_3$), 4.67 (s, 2 H, 1'-H), 7.03 (d, *J* = 8.5 Hz, 2 H, 2-H, 6-H), 7.36 (d, *J* = 8.6 Hz, 2 H, 3-H, 5-H).

^{13}C NMR (126 MHz, $CDCl_3$): δ [ppm] = 27.26 ($C(=O)C(\underline{C}H_3)_3$), 39.18 ($C(=O)\underline{C}(CH_3)_3$), 64.90 (C-1'), 121.72 (C-2, C-6), 128.14 (C-3, C-5), 138.39 (C-4), 150.65 (C-1), 177.31 ($\underline{C}(=O)C(CH_3)_3$).

HRMS (ESI^+): calc. for $C_{12}H_{17}O_3^+$: 209.1172, found: 209.1173 $[M+H]^+$.

$C_{12}H_{16}O_3$ (208.26 g/mol)

4-(Pivaloxy)-benzylchloroformate 57[255]

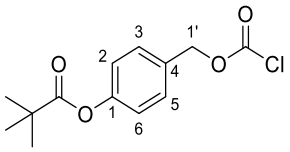

57

4-formylphenylpivalate **97** (585 mg, 2.81 mmol, 1.0 eq.) was dissolved in toluene (24 mL). Triphosgene (748 mg, 2.52 mmol, 1.0 eq.) was added and the reaction mixture was stirred at room temperature for 3 days. The solvent was removed under inert gas and EtOAc (15 mL) was added to the residue. The solvent was removed *in vacuo* to afford the product without further purification.

Yield (57): 567 mg (2.48 mmol, quant.) as a yellow oil.

^{1}H NMR (500 MHz, $CDCl_3$): δ [ppm] = 1.36 (s, 9 H (C(=O)C(CH_3)$_3$), 5.28 (d, *J* = 2.6 Hz, 2 H, 1'-H), 7.10 (d, *J* = 8.2 Hz, 2 H, 2-H, 6-H), 7.40-7.44 (m, 2 H, 3-H, 5-H).

^{13}C NMR (126 MHz, $CDCl_3$): δ [ppm] = 27.24 (C(=O)C(<u>C</u>H_3)$_3$), 39.26 (C(=O)<u>C</u>(CH_3)$_3$), 71.09 (C-1'), 122.15 (C-2, C-6), 130.19 (C-3, C-5), 130.42 (C-4), 147.96 (C-1), 151.94 (C(=O)Cl), 177.03 (<u>C</u>(=O)C(CH_3)$_3$).

MS (ESI^+): m/z = 271.26 $[M+H]^+$.

$C_{13}H_{15}ClO_4$ (270.71 g/mol)

7.2.5.3 Synthesis of nucleoside building blocks

7.2.5.3.1 Synthesis of aldehyde for reductive amination

***N*-Cbz-L-Leucin 99**[251]

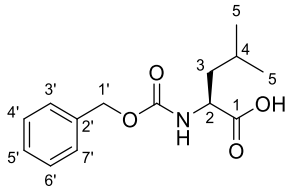

99

The reaction was carried out without any inert gas conditions. L-leucine **64** (3.03 g, 23.1 mmol, 1.0 eq.) and sodium carbonate (7.28 g, 68.7 mmol, 3.0 eq.) were dissolved in mixture of 1,4-dioxane and water (1:1, 150 mL). A solution of benzyloxycarbonyl chloride (3.60 mL, 25.7 mmol, 3.0 eq.) in 1,4-dioxane (20 mL) was added dropwise at 0 °C within 30 minutes. The reaction mixture was warmed to room temperature and stirred for 21 hours. The reaction mixture was concentrated *in vacuo* and washed with Et_2O (3 × 50 mL). The aqueous layer acidified to pH ~ 2 with hydrochloric acid (25 mL, 3 M) and extracted with Et_2O (2 x 100 mL). The combined organic layers were washed with brine (100 mL), dried over sodium sulfate and filtered. The solvent was removed *in vacuo* and the resulting product was dried *in vacuo* for several days.

Yield (99): 4.18 g (15.7 mmol, 68%) as a yellow oil.

^{1}H NMR (300 MHz, $CDCl_3$): δ [ppm] = 0.89-0.98 (m, 6 H, 5-H), 1.50-1.60 (m, 1 H, 3-H_a), 1.65-1.74 (m, 2 H, 3-H_b, 4-H), 4.40 (ddd, *J* = 4.7 Hz, *J* = 8.6 Hz, 1 H, 2-H), 5.11 (s, 2 H, 1'-H), 5.23 (d, *J* = 8.6 Hz, 1 H, NH), 7.28-7.39 (m, 5 H, 3'-H, 4'-H, 5'-H, 6'-H, 7'-H), 8.73 (s, 1 H, COOH).

^{13}C NMR (75 MHz, $CDCl_3$): δ [ppm] = 21.84 (C_a-5), 22.97 (C_b-5), 24.87 (C-4), 41.59 (C-3), 52.49 (C-2), 67.15 (C-1'), 127.82, 128.23, 128.35, 136.26 (C-2', C-3', C-4', C-5', C-6', C-7'), 156.28 (NC(=O)O), 177.78 (C-1).

MS (ESI$^+$): m/z = 266.10 $[M+H]^+$, 288.11 $[M+Na]^+$.

$C_{14}H_{19}NO_4$ (265.31 g/mol)

2-*N*-Cbz-1-*N*-(3,3-diethoxypropyl)-L-leucine amide 66[231]

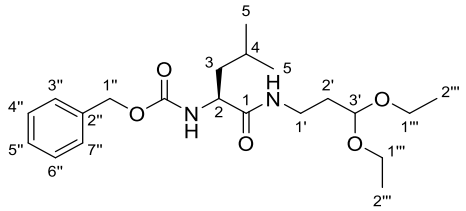

66

To a solution of *N*-Cbz-L-leucine **99** (4.01 g, 15.1 mmol, 1.0 eq.) in THF (75 mL), HOBt (2.04 g, 15.1 mmol, 1.0 eq.) and EDCl (2.94 g, 15.4 mmol, 1.0 eq.) were added. The resulting suspension was stirred at room temperature for 30 minutes. DIPEA (2.60 mL, 15.3 mmol, 1.0 eq.) and 1-amino-3,3-diethoxypropane **65** (2.40 mL, 14.8 mmol, 1.0 eq.) were added and the solution was stirred at rt for 20 h. The reaction mixture was diluted with EtOAc and water (1:1, 150 mL). The organic layer was washed with hydrochloric acid (0.5 M, 1 X 75 mL, 0 °C), saturated sodium bicarbonate solution (2 x 75 mL) and water (2 x 100 mL), dried over sodium sulfate and filtered. The solvent was removed *in vacuo* and the crude product was purified by column chromatography (PE:EtOAc 7:3 + 1% triethylamine).

Yield (66): 3.21 g (8.14 mmol, 54%) as a colorless oil.

TLC: R_f = 0.12 (PE:EtOAc 7:3 + 1% triethylamine).

^{1}H NMR (300 MHz, $CDCl_3$): δ [ppm] = 0.92 (d, *J* = 6.3 Hz, 6 H, 5-H), 1.21 (td, *J* = 3.0 Hz, *J* = 7.0 Hz, 6 H, 2'''-H_a, 2'''-H_b), 1.47-1.53 (m, 1 H, 3-H_a), 1.60-1.68 (m, 2 H, 3-H_b, 4-H), 1.78-1.86 (m, 2 H, 2'-H), 3.31-3.41 (m, 2 H, 1'-H), 3.44-3.55 (m, 2 H, 1'''-H_a, 1'''-H_b), 3.60-3.71 (m, 2 H, 1'''-H_c, 1'''-H_d), 4.08-4.17 (m, 1 H, 2-H), 4.55 (t, *J* = 5.0 Hz, 1 H, 3'-H), 5.10 (s, 2 H, 1''-H_a), 5.22 (d, *J* = 8.3 Hz, 1 H, 2-NH), 6.53 (s, 1 H, 1-NH), 7.31-7.38 (m, 5 H, 2''-H, 3''-H, 4''-H, 5''-H, 6''-H, 7''-H).

^{13}C NMR (75 MHz, $CDCl_3$): δ [ppm] = 15.48 (C-2'''), 22.13 (C_a-5), 23.08 (C_b-5), 24.82 (C-4), 32.95 (C-2'), 35.61 (C-1'), 42.21 (C-3), 53.76 (C-2), 62.21 (C-1_a''', C-1_b'''), 67.13 (C-1''), 102.62 (C-3'), 128.19 (C-3'', C-7''), 128.32 (C-5''), 128.67 (C-4'', C-6''), 136.36 (C-2''), 156.36 (NC(=O)O), 171.85 (C-1).

MS (ESI$^+$): m/z = 417.22 $[M+Na]^+$.

$C_{21}H_{34}N_2O_5$ (394.51 g/mol)

2-*N*-(Benzyloxycarbonyl)-1-*N*-(3'-oxopropyl)-L-leucine amide 28[251]

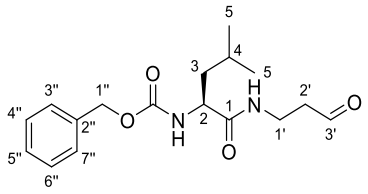

28

The reaction was carried out without any inert gas conditions. To a solution of 2-*N*-(benzyloxycarbonyl)-1-*N*-(3,3-diethoxypropyl)-L-leucine amine **66** (961 mg, 2.43 mmol, 1.0 eq.) in THF (10 mL), hydrochloric acid (0.5 mL, 0.5 M) was added and the resulting solution was stirred at room temperature for 50 minutes. The reaction mixture was diluted with saturated sodium bicarbonate solution (150 mL) and extracted with EtOAc (3 x 150 mL). The combined organic layers were washed with brine (200 mL), dried over sodium sulfate and filtered. The solvent was removed *in vacuo* and the crude product was purified by column chromatography (CH_2Cl_2:EtOAc 7:3 → 6:4).

Yield (28): 568 mg (1.77 mmol, 73%) as a white solid.

TLC: R_f = 0.25 (CH_2Cl_2:EtOAc 6:4).

^{1}H NMR (300 MHz, $CDCl_3$): δ [ppm] = 0.91 (d, *J* = 6.3 Hz, 6 H, 5-H), 1.44-1.54 (m, 1 H, 3-H_a), 1.57-1.67 (m, 2 H, 3-H_b, 4-H), 2.70 (t, *J* = 5.2 Hz, 2 H, 2'-H), 3.43-3.58 (m, 2 H, 1'-H), 4.00-4.18 (m, 1 H, 2-H), 5.09 (s, 2 H, 1''-H), 5.18 (d, *J* = 8.1 Hz, 1 H, 2-NH), 6.48 (s, 1 H, 1-NH), 7.27-7.40 (m, 5 H, 3''-H, 4''-H, 5''-H, 6''-H, 7''-H), 9.76 (s, 1 H, 3'-H).

^{13}C NMR (75 MHz, $CDCl_3$): δ [ppm] = 23.05 (C_a-5, C_b-5), 24.84 (C-4), 33.07 (C-1'), 41.57 (C-3), 43.69 (C-2'), 53.74 (C-2), 67.27 (C-1''), 128.24 (C-3'', C-7''), 128.38 (C-5''), 128.69 (C-4'', C-6''), 136.26 (NC(=O)O), 172.4 (C-1), 201.26 (C-3').

MS (ESI^+): m/z = 343.13 $[M+Na]^+$.

$C_{17}H_{24}N_2O_4$ (320.39 g/mol)

7.2.5.3.2 Synthesis of nucleoside amino acids

2',3'-*O*-bis-TBDMS uridine-5'-alcohol 100[172]

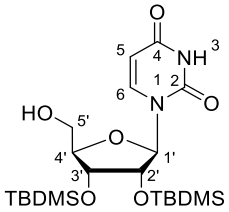

100

The reaction was carried out without any inert gas conditions. A solution of 2',3',5'-*O*-tris-*tert*-TBDMS-uridine **59** (6.50 g, 11.1 mmol, 1.0 eq.), kindly provided by Dr. D. Wiegmann,[212] in THF (125 mL) was cooled to 0 °C. A solution of TFA (30 mL) in water (30 mL) was added dropwise and the resulting solution was stirred at 0 °C for 7 hours being TLC controlled. Saturated sodium bicarbonate solution (500 mL) was added to the reaction mixture. The pH value was adjusted to 9 using sodium bicarbonate. EtOAc (1 L) was added to the solution. The organic layer was washed with saturated sodium bicarbonate solution (200 mL), dried over sodium sulfate and filtered. The solvent removed *in vacuo* and the crude product was purified by column chromatography (CH_2Cl_2:EtOAc 75:25).

Yield (100): 3.39 g (7.18 mmol, 65%) as a white solid.

TLC: R_f = 0.30 (CH_2Cl_2:EtOAc 75:25).

^{1}H NMR (500 MHz, DMSO-d_6): δ [ppm] = -0.03 (s, 3 H, $SiCH_3$), 0.02 (s, 3 H, $SiCH_3$), 0.08 (s, 3 H, $SiCH_3$), 0.09 (s, 3 H, $SiCH_3$), 0.83 (s, 9 H, $SiC(CH_3)_3$), 0.88 (s, 9 H, $SiC(CH_3)_3$), 3.58 (ddd, *J* = 12.4 Hz, *J* = 4.5 Hz, *J* = 3.0 Hz, 1 H, 5'-H_a), 3.63 (ddd, *J* = 12.4 Hz, *J* = 4.5 Hz, *J* = 3.0 Hz, 1 H, 5'-H_b), 3.88 (ddd, *J* = 3.3 Hz, *J* = 3.3 Hz, *J* = 3.0 Hz, 1 H, 4'-H), 4.13 (dd, *J* = 4.3 Hz, *J* = 2.9 Hz, 1 H, 3'-H), 4.25 (dd, *J* = 5.8 Hz, *J* = 4.6 Hz, 1 H, 2'-H), 5.24 (dd, *J* = 4.8 Hz, 1 H, OH), 5.69 (d, *J* = 8.1 Hz, 1 H, 5-H), 5.81 (d, *J* = 6.0 Hz, 1 H, 1'-H), 7.93 (d, *J* = 8.1 Hz, 1 H, 6-H).

^{13}C NMR (126 MHz, DMSO-d_6): δ = -5.02 ($SiCH_3$), -4.38 ($SiCH_3$), -4.27 ($SiCH_3$), -4.15 ($SiCH_3$), 17.64 ($SiC(CH_3)_3$), 17.79 ($SiC(CH_3)_3$), 25.62 ($SiC(CH_3)_3$), 25.74 ($SiC(CH_3)_3$), 60.43 (C-5'), 71.95 (C-3'), 74.55 (C-2'), 85.57 (C-4'), 86.84 (C-1'), 102.06 (C-5), 140.38 (C-6), 150.79 (C-2), 163.01 (C-4).

MS (ESI^+): m/z = 473.13 $[M+H]^+$.

$C_{21}H_{40}N_2O_6Si_2$ (472.73 g/mol)

2',3'-*O*-bis-(TBDMS)-uridine-5'-aldehyde 13[184]

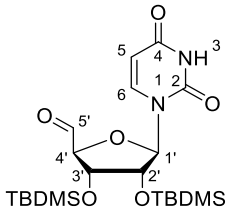

13

IBX **60** (2.96 g, 10.6 mmol, 2.5 eq.) was added to a suspension of 2',3'-*O*-bis-TBDMS uridine-5'-alcohol **100** (2.00 g, 4.23 mmol, 1.0 eq.) in MeCN (40 mL). The reaction mixture was heated under reflux for 2 h and then cooled to 0 °C. The resulting solid was filtered and washed with EtOAc (250 mL). The aldehyde **13** was obtained after removing the solvent *in vacuo* and was directly used without any further purification. Due to the known instability of uridine 5'-aldehydes, no further analytics were done beside ^{1}H NMR spectra. Purity of the aldehyde was determined to be >90% based on ^{1}H NMR.

Yield (13): 1.99 g (4.23 mmol, quant.) as a white solid.

^{1}H NMR (500 MHz, $CDCl_3$): δ [ppm] = 0.02 (s, 3 H, $SiCH_3$), 0.06 (s, 3 H, $SiCH_3$), 0.13 (s, 3 H, $SiCH_3$), 0.13 (s, 3 H, $SiCH_3$), 0.88 (s, 9 H, $SiC(CH_3)_3$), 0.94 (s, 9 H, $SiC(CH_3)_3$), 4.25 (dd, *J* = 4.0 Hz, *J* = 3.4 Hz, 1 H, 3'-H), 4.33 (dd, *J* = 5.5 Hz, *J* = 4.2 Hz, 1 H, 2'-H), 4.56 (d, *J* = 3.3 Hz, 1 H, 4'-H), 5.74 (d, *J* = 5.6 Hz, 1 H, 1'-H), 5.82 (dd, *J* = 8.2 Hz, *J* = 2.2 Hz, 1 H, 5-H), 7.70 (d, *J* = 8.2 Hz, 1 H, 6-H), 8.66 (s, 1 H, NH), 9.83 (s, 1 H, 5'-H).

$C_{21}H_{38}N_2O_6Si_2$ (470.71 g/mol)

(*Z*)-Didehydro-POM-ester uridinyl-amino acid 53[201,202]

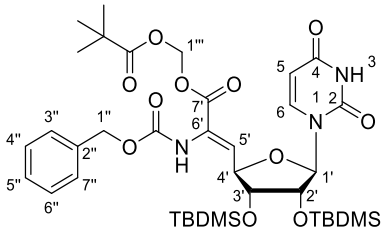

53

A solution of potassium bis(trimethylsilyl)amide (0.5 M in toluene, 7.05 mL, 3.52 mmol, 1.0 eq.) in THF (50 mL) was cooled to 0 °C. A solution of POM phosphonate **58** (1.52 g, 3.52 mmol, 1.0 eq.) in THF (40 mL) was added and the reaction mixture was stirred at -78 °C for 10 minutes. A solution of 2',3'-*O*-bis-(TBDMS)-uridine-5'-aldehyde **13** (1.99 g, 4.23 mmol, 1.2 eq.) in THF (60 mL) was added dropwise and the resulting solution was stirred for 16 hours, slowly warming to room temperature over this period. The reaction mixture was cooled to 0 °C.

MeOH (10 mL) was added for quenching the reaction and the solution was stirred for 5 minutes. The reaction mixture was diluted with EtOAc (300 mL), washed with half-saturated brine (3 x 150 mL), dried over sodium sulfate and filtered. The solvent was removed *in vacuo* and the crude product was purified by column chromatographic (PE:EtOAc 6:4).

Yield (53): 1.60 g (2.06 mmol, 59%) as a white foam.

TLC: R_f = 0.32 (PE:EtOAc 6:4).

^{1}H NMR (500 MHz, $CDCl_3$): δ [ppm] = 0.06 (s, 3 H, $SiCH_3$), 0.09 (s, 3 H, $SiCH_3$), 0.10 (s, 3 H, $SiCH_3$), 0.12 (s, 3 H, $SiCH_3$), 0.89 (s, 9 H, $SiC(CH_3)_3$), 0.90 (s, 9 H, $SiC(CH_3)_3$), 1.23 (s, 9 H, $(CH_3)_3$), 3.97 (dd, *J* = 6.3 Hz, *J* = 4.0 Hz, 1 H, 3'-H), 4.35 (dd, *J* = 3.6 Hz, *J* = 3.5 Hz, 1 H, 2'-H), 4.90 (dd, *J* = 7.2 Hz, *J* = 6.6 Hz, 1 H, 4'-H), 5.14 (d, *J* = 1.1 Hz, 2 H, 1''-H), 5.57 (d, *J* = 3.1 Hz, 1 H, 1'-H), 5.75 (dd, *J* = 8.2 Hz, *J* = 2.2 Hz, 1 H, 5-H), 5.84 (s, 2 H, 1'''-H), 6.41 (d, *J* = 7.5 Hz, 1 H, 5'-H), 6.84 (s, 1 H, 6'-NH), 7.24 (d, *J* = 8.1 Hz, 1 H, 6-H), 7.31-7.40 (m, 5 H, 3''-H, 4''-H, 5''-H, 6''-H, 7''-H), 8.79 (s, 1 H, 3-NH).

^{13}C NMR (126 MHz, $CDCl_3$): δ [ppm] = -4.87 ($SiCH_3$), -4.84 ($SiCH_3$), -4.46 ($SiCH_3$), -4.46 ($SiCH_3$), 17.98 ($SiC(CH_3)_3$), 18.03 ($SiC(CH_3)_3$), 25.74 ($SiC(CH_3)_3$), 25.80 ($SiC(CH_3)_3$), 26.84 ($C(=O)C(CH_3)_3$), 38.77 ($C(=O)C(CH_3)_3$), 67.71 (C-1''), 74.52 (C-2'), 75.98 (C-3'), 79.01 (C-4'), 80.19 (C-1'''), 93.02 (C-1'), 102.48 (C-5), 127.44 (C-5'), 128.16, 128.39, 128.56 (C-3'', C-4'', C-5'',C-6'', C-7''), 129.43 (C-6'), 135.52 (C-2''), 140.38 (C-6), 149.72 (C-2), 153.40 (NC(=O)O), 162.37 (C-4), 162.86 (C-7'), 176.96 ($C(=O)C(CH_3)_3$).

MS (ESI^+): m/z = 798.41 $[M+Na]^+$.

$C_{37}H_{57}N_3O_{11}Si_2$ (776.04 g/mol)

(6'*S*)-6'*N*-Cbz-POM-ester uridinyl-amino acid 101[190,198,212]

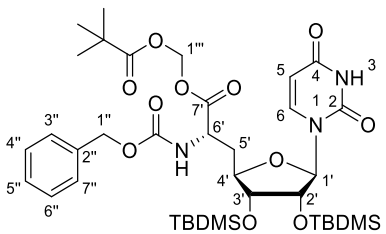

101

The reaction was carried out under an argon atmosphere. (*Z*)-Didehydro-POM-ester uridinyl-amino acid **53** (704 mg, 907 µmol, 1.0 eq.) was dissolved in MeOH (25 mL) and degassed with argon. Three spatula tips of (*S*,*S*)-Me-DUPHOS-Rh **21** were added and the resulting solution was stirred under hydrogen (6.0, 1 bar) for 19 days being ^{1}H NMR controlled every five days. The hydrogen atmosphere was renewed every day via flushing the flask with hydrogen (6.0, 1 bar) and (*S*,*S*)-Me-DUPHOS-Rh **21** was added if necessary (one spatula tip). The solvent

was removed *in vacuo*. The crude product was purified by column chromatography (PE:EtOAc 65:35).

Yield (101): 425 mg (546 µmol, 60%, *d.r.* ~ 7:3) as a white foam.

TLC: R_f = 0.22 (PE:EtOAc 65:35).

^{1}H NMR (500 MHz, $CDCl_3$): δ [ppm] = 0.07 (s, 3 H, $SiCH_3$), 0.08 (s, 3 H, $SiCH_3$), 0.08 (s, 3 H, $SiCH_3$), 0.09 (s, 3 H, $SiCH_3$), 0.89 (s, 9 H, $SiC(CH_3)_3$), 0.90 (s, 9 H, $SiC(CH_3)_3$), 1.21 (s, 9 H, $(CH_3)_3$), 2.05-2.12 (m, 1 H, 5'-H_a), 2.29-2.33 (m, 1 H, 5'-H_b), 3.72 (dd, *J* = 5.4 Hz, *J* = 4.4 Hz, 1 H, 3'-H), 4.15 (ddd, *J* = 11.0 Hz, *J* = 5.4 Hz, *J* = 2.5 Hz, 1 H, 4'-H), 4.25 (dd, *J* = 4.3 Hz, *J* = 4.2 Hz, 1 H, 2'-H), 4.56 (dd, *J* = 12.3 Hz, *J* = 6.0 Hz, 1 H, 6'-H), 5.11 (s, 2 H, 1''-H), 5.56 (d, *J* = 6.9 Hz, 1 H, 1'''-H_a), 5.65 (d, *J* = 6.9 Hz,1 H, 1'''-H_b), 5.73 (d, *J* = 5.7 Hz, 1 H, 6'-NH), 5.77-5.82 (m, 2 H, 5-H, 1'-H), 7.31-7.38 (m, 6 H, 6-H, 3''-H, 4''-H, 5''-H, 6''-H, 7''-H), 8.88 (s, 1 H, 3-NH).

^{13}C NMR (126 MHz, $CDCl_3$): δ [ppm] = -4.81 ($SiCH_3$), -4.76 ($SiCH_3$), -4.63 ($SiCH_3$), -4.26 ($SiCH_3$), 17.97 ($SiC(CH_3)_3$), 18.00 ($SiC(CH_3)_3$), 25.76 ($SiC(CH_3)_3$), 25.79 ($SiC(CH_3)_3$), 26.80 ($C(=O)C(CH_3)_3$), 34.88 (C-5'), 38.71 ($C(=O)C(CH_3)_3$), 51.93 (C-6'), 67.11 (C-1''), 74.36 (C-2'), 75.22 (C-3'), 80.25 (C-1'''), 80.40 (C-4'), 92.20 (C-1'), 102.32 (C-5), 128.09, 128.26, 128.54 (C-3'', C-4'', C-5'', C-6'', C-7''), 136.05 (C-2''), 140.56 (C-6), 149.90 (C-2), 155.65 (Cbz-C=O), 163.00 (C-4), 170.41 (C-7'), 176.88 ($C(=O)C(CH_3)_3$).

MS (ESI^+): m/z = 779.61 $[M+H]^+$.

$C_{37}H_{59}N_3O_{11}Si_2$ (778.06 g/mol)

(6'*S*)-O-POM-2',3'-O-Bis-TBDMS-uridinyl-amino acid 102[212]

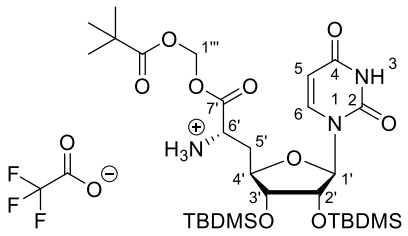

102

The reaction was carried out according to procedure 3.1 utilizing a solution of (6'*S*)-6'*N*-Cbz-POM-ester uridinyl-amino acid **101** (420 mg, 540 µmol, 1.0 eq.) in *iso*-propanol (36 mL), 1,4-cyclohexadiene (0.51 mL, 5.4 mmol, 10.0 eq.), TFA (42 µL, 0.54 mmol, diluted to 1% in *iso*-propanol, 1.0 eq.) and several spatula tips of palladium black. The reaction mixture was stirred at room temperature for 2 hours.

Yield (102): 392 mg (517 µmol, 96%) as a colorless foam.

^{1}H NMR (500 MHz, CD_3OD): δ [ppm] = 0.08 (s, 3 H, $SiCH_3$), 0.11 (s, 3 H, $SiCH_3$), 0.14 (s, 3 H, $SiCH_3$), 0.16 (s, 3 H, $SiCH_3$), 0.92 (s, 9 H, $SiC(CH_3)_3$), 0.95 (s, 9 H, $SiC(CH_3)_3$), 1.22 (s, 9 H, $(CH_3)_3$), 2.14-2.26 (m, 1 H, 5'-H_a), 2.40 (ddd, *J* = 14.6 Hz, *J* = 6.0 Hz, *J* = 2.3 Hz, 1 H, 5'-H_b), 4.03 (t, *J* = 4.9 Hz, 1 H, 3'-H), 4.23 (ddd, *J* = 11.6 Hz, *J* = 5.1 Hz, *J* = 2.3 Hz, 1 H, 4'-H), 4.31-4.35 (m, 1 H, 6'-H), 4.52 (dd, *J* = 4.6 Hz, *J* = 4.5 Hz, 1 H, 2'-H), 5.65 (d, *J* = 4.4 Hz, 1 H, 1'-H), 5.74 (d, *J* = 8.0 Hz, 1 H, 5-H), 5.83 (d, *J* = 5.7 Hz, 1 H, 1''-H_a), 5.87 (d, *J* = 5.7 Hz, 1 H, 1''-H_b), 7.60 (d, *J* = 8.1 Hz, 1 H, 6-H).

^{13}C NMR (126 MHz, CD_3OD): δ [ppm] = -4.32 ($SiCH_3$), -4.26 ($SiCH_3$), -4.22 ($SiCH_3$), -3.88 ($SiCH_3$), 19.01 ($SiC(CH_3)_3$), 19.08 ($SiC(CH_3)_3$), 26.52 ($SiC(CH_3)_3$), 26.60 ($SiC(CH_3)_3$), 27.39 ($C(CH_3)_3$), 34.73 (C-5'), 39.91 ($C(CH_3)_3$), 52.49 (C-6'), 74.88 (C-2'), 76.54 (C-3'), 82.30 (C-1''), 82.43 (C-4'), 94.57 (C-1'), 103.30 (C-5), 144.20 (C-6), 152.35 (C-2), 166.02 (C-4), 169.27 (C-7'), 178.12 ($C(=O)C(CH_3)_3$).

^{19}F NMR (282 MHz, CD_3OD): δ [ppm] = -75.64.

MS (ESI^+): m/z = 644.21 $[M+H]^+$.

$C_{29}H_{53}N_3O_9Si_2$ (643.93 g/mol)

$C_{29}H_{53}N_3O_9Si_2 \cdot CF_3COOH$ (757.95 g/mol)

***N*-Cbz-protected L-leucine-propyl-5'-deoxy-POM ester nucleosyl amino acid 103**[212]

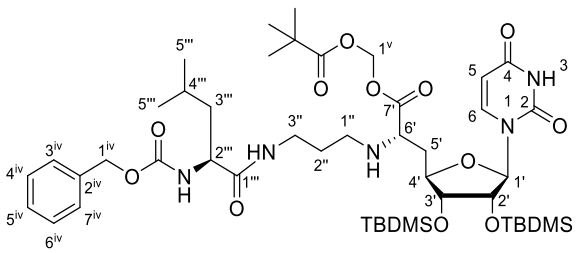

103

To a solution of (6'*S*)-*O*-POM-2',3'-O-Bis-TBDMS-uridinyl-amino acid **102** (360 mg, 475 µmol, 1.0 eq.) in THF (35 mL) over freshly activated molecular sieves (4 Å) 2-*N*-Cbz-1-*N*-(3'-oxopropyl)-L-leucine amide **28** (152 mg, 475 µmol, 1.0 eq.) and DIPEA (164 µL, 960 µmol, 1.0 eq.) were added and the resulting solution was stirred at room temperature for 23 hours. Amberlyst^{TM}-15 (23 mg) and sodium triacetoxyborohydride (204 mg, 962 µmol, 2.0 eq.) were added. The reaction mixture was stirred at room temperature for further 24 hours. The molecular sieves were filtered off and washed thoroughly with EtOAc (80 mL). The organic layer was washed with saturated sodium carbonate solution (3 x 50 mL) and the aqueous layer was extracted with EtOAc (3 x 100 mL). The combined organic layers were dried over sodium sulfate and filtered. The solvent was removed *in vacuo*. The crude product was purified by column chromatography (CH_2Cl_2:EtOAc 2:8).

Yield (103): 180 mg (190 µmol, 40%) as a white foam.

TLC: R_f = 0.21 (CH_2Cl_2:EtOAc 2:8).

^{1}H NMR (500 MHz, $CDCl_3$): δ [ppm] = 0.02 (s, 3 H, $SiCH_3$), 0.06 (s, 3 H, $SiCH_3$), 0.08 (s, 3 H, $SiCH_3$), 0.09 (s, 3 H, $SiCH_3$), 0.88 (s, 9 H, $SiC(CH_3)_3$), 0.91 (s, 9 H, $SiC(CH_3)_3$), 0.94-0.95 (m, 6 H, 5'''-H), 1.21 (s, 9 H, $C(=O)C(CH_3)_3$), 1.47-1.54 (m, 1 H, 3'''-H_a), 1.57-1.70 (m, 4 H, 2''-H, 3'''-H_b, 4'''-H), 1.87-1.90 (m, 1 H, 5'-H_a), 2.09-2.13 (m, 1 H, 5'-H_b), 2.56-2.61 (m, 1 H, 1''-H_a), 2.67-2.71 (m, 1 H, 1''-H_b), 3.31-3.41 (m, 2 H, 3''-H), 3.44-3.49 (m, 1 H, 6'-H), 3.83 (dd, *J* = 4.1 Hz, *J* = 3.5 Hz, 1 H, 3'-H), 4.04 (ddd, *J* = 10.7 Hz, *J* = 3.5 Hz, *J* = 3.2 Hz, 1 H, 4'-H), 4.25-4.31 (m, 1 H, 2'''-H), 4.65 (t, *J* = 4.7 Hz, 1 H, 2'-H), 5.14 (s, 2 H, 1^{iv}-H), 5.38 (d, *J* = 5.0 Hz, 1 H, 1'-H), 5.45 (d, *J* = 8.8 Hz, 2 H, 1'-H, 2'''-NH), 5.72 (d, *J* = 7.9 Hz, 1 H, 5-H), 5.77 (d, *J* = 5.4 Hz, 2 H, 1^{v}-H_a), 5.79 (d, *J* = 5.4 Hz, 1 H, 1^{v}-H_b), 7.15 (s, 1 H, 1'''-NH), 7.22 (d, *J* = 8.2 Hz, 1 H, 6-H), 7.29-7.38 (m, 5 H, 3^{iv}-H, 4^{iv}-H, 5^{iv}-H, 6^{iv}-H, 7^{iv}-H), 9.30 (s, 1 H, 3-NH).

^{13}C NMR (126 MHz, $CDCl_3$): δ [ppm] = -4.82 ($SiCH_3$), -4.66 ($SiCH_3$), -4.66 ($SiCH_3$), -4.41 ($SiCH_3$), 17.92 ($SiC(CH_3)_3$), 18.03 ($SiC(CH_3)_3$), 22.06 (C_a-5'''), 22.99 (C_b-5'''), 24.74 (C-4'''), 25.73 ($SiC(CH_3)_3$), 25.80 ($SiC(CH_3)_3$), 26.85 ($C(=O)C(CH_3)_3$), 28.67 (C-2''), 36.33 (C-5'), 38.51 ($C(=O)C(CH_3)_3$), 38.73 (C-3''), 41.82 (C-3'''), 46.29 (C-1''), 53.57 (C-2'''), 58.93 (C-6'), 67.13 ($C\text{-}1^{iv}$), 72.48 (C-2'), 75.65 (C-3'), 79.83 ($C\text{-}1^{v}$), 82.73 (C-4'), 94.82 (C-1'), 102.42 (C-5), 128.15, 128.21, 128.48 ($C\text{-}3^{iv}$, $C\text{-}4^{iv}$, $C\text{-}5^{iv}$, $C\text{-}6^{iv}$, $C\text{-}7^{iv}$), 136.27 ($C\text{-}2^{iv}$), 142.62 (C-6), 149.96 (C-2), 156.40 (NC(=O)O), 162.95 (C-4), 172.17 (C-1'''), 173.01 (C-7'), 177.08 ($C(=O)C(CH_3)_3$).

MS (ESI^+): m/z = 948.29 $[M+H]^+$.

$C_{46}H_{77}N_5O_{12}Si_2$ (948.32 g/mol)

L-leucine-propyl-5'-deoxy-POM ester nucleosyl amino acid 63[212]

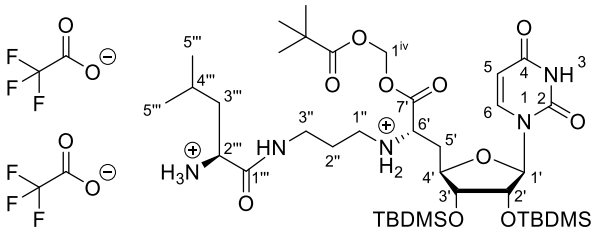

63

The reaction was carried out according to procedure 3.1 utilizing a solution of *N*-Cbz-protected L-leucine-propyl-5'-deoxy-POM ester nucleosyl amino acid **103** (175 mg, 185 µmol, 1.0 eq.) in *iso*-propanol (10 mL), 1,4-cyclohexadiene (175 µL, 1.85 mmol, 10.0 eq.), TFA (29 µL, 0.37 mmol, diluted to 1% in *iso*-propanol, 2.0 eq.) and several spatula tips of palladium black. The reaction mixture was stirred at room temperature for 1.5 hours.

Yield (63): 190 mg (182 µmol, 99%) as a white foam.

^{1}H NMR (500 MHz, CD_3OD): δ [ppm] = 0.05 (s, 3 H, $SiCH_3$), 0.10 (s, 3 H, $SiCH_3$), 0.14 (s, 3 H, $SiCH_3$), 0.16 (s, 3 H, $SiCH_3$), 0.90 (s, 9 H, $SiC(CH_3)_3$), 0.95 (s, 9 H, $SiC(CH_3)_3$), 0.99 (d, *J* = 5.8 Hz, 3 H, 5'''-H_a), 1.01 (d, *J* = 5.4 Hz, 3 H, 5'''-H_b), 1.22 (s, 9 H, $C(=O)C(CH_3)_3$), 1.64-1.72 (m, 3 H, 3'''-H, 4'''-H), 1.90-1.98 (m, 2 H, 2''-H), 2.28-2.35 (m, 1 H, 5'-H_a), 2.37-2.45 (m, 1 H, 5'-H_b), 3.15 (dd, *J* = 7.2 Hz, *J* = 7.0 Hz, 2 H, 1''-H), 3.32-3.34 (m, 2 H, 3''-H), 3.84-3.87 (m, 1 H, 2'''-H), 4.06 (dd, *J* = 4.3 Hz, *J* = 4.0 Hz, 1 H, 3'-H), 4.19 (ddd, *J* = 11.8 Hz, *J* = 3.2 Hz, *J* = 2.9 Hz, 1 H, 4'-H), 4.31 (dd, *J* = 8.1 Hz, *J* = 4.9 Hz, 1 H, 6'-H), 4.65 (t, *J* = 5.1 Hz, 1 H, 2'-H), 5.65 (d, *J* = 5.6 Hz, 1 H, 1'-H), 5.76 (d, *J* = 8.0 Hz, 1 H, 5-H), 5.85 (d, *J* = 5.8 Hz, 2 H, 1^{iv}-H_a), 5.90 (d, *J* = 5.8 Hz, 2 H, 1^{iv}-H_b), 7.68 (d, *J* = 8.1 Hz, 1 H, 6-H).

^{13}C NMR (126 MHz, CD_3OD): δ [ppm] = -4.48 ($SiCH_3$), -4.21 ($SiCH_3$), -4.16 ($SiCH_3$), -4.02 ($SiCH_3$), 19.00 ($SiC(CH_3)_3$), 19.08 ($SiC(CH_3)_3$), 22.25 (C-5_a'''), 23.15 (C-5_b'''), 25.67 (C-4'''), 26.51 ($SiC(CH_3)_3$), 26.60 ($SiC(CH_3)_3$), 27.41 ($C(=O)C(CH_3)_3$), 27.60 (C-2''), 34.29 (C-5'), 37.68 (C-3''), 39.95 ($C(=O)C(CH_3)_3$), 41.81 (C-3'''), 45.76 (C-1''), 53.26 (C-2'''), 58.53 (C-6'), 74.18 (C-2'), 76.65 (C-3'), 82.38 (C-4'), 82.60 (C-1^{iv}), 94.62 (C-1'), 103.49 (C-5), 144.93 (C-6), 152.43 (C-2), 166.01 (C-4), 168.71 (C-7'), 171.50 (C-1'''), 178.01 ($C(=O)C(CH_3)_3$).

^{19}F NMR (282 MHz, CD_3OD): δ [ppm] = -76.90.

MS (ESI^+): m/z = 814.96 $[M+H]^+$.

$C_{38}H_{71}N_5O_{10}Si_2$ (814.18 g/mol)

$C_{38}H_{71}N_5O_{10}Si_2 \cdot 2\ CF_3COOH$ (1042.23 g/mol)

7.2.5.4 Synthesis of POM prodrug

Fully protected Bis-POM-5'-deoxy muraymycin analogue 104

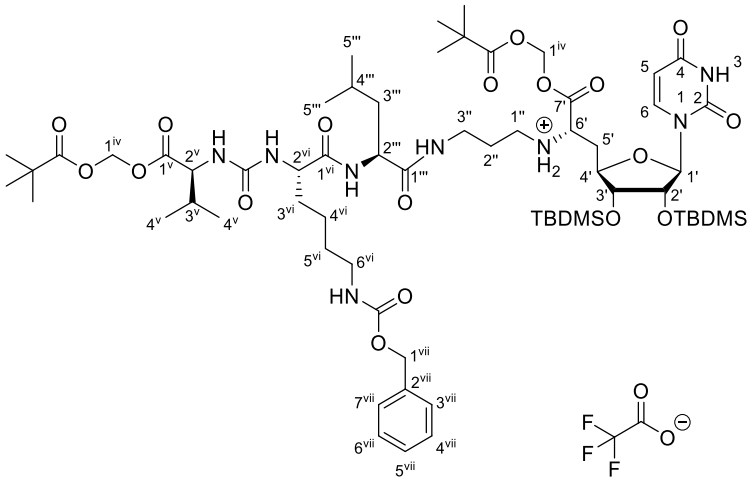

104

To a solution *O*-POM-L-valine-*N*-(C=O)-*N*-(N$^{\varepsilon}$-Cbz)-L-lysine **54** (24.2 mg, 45.0 µmol, 1.1 eq.) in THF (5 mL), DIPEA (15.0 µL, 88.2 µmol, 2.2 eq.), HOBt (6.10 mg, 45.1 µmol, 1.1 eq.) and PyBOP (23.4 mg, 45.0 µmol, 1.1 eq.) were added. The solution was stirred at room temperature for 30 minutes. The reaction mixture was cooled to 0 °C and a solution of L-leucine-propyl-5'-deoxy-POM ester nucleosyl amino acid **103** (42.0 mg, 40.3 µmol, 1.0 eq.) in THF (4 mL) was added dropwise. The reaction mixture was stirred at 0 °C for 1 hour and at room temperature for further 4 hours. TFA (6.0 µL, 77 µmol, 2.0 eq.) was added and the solution was stirred at room temperature for 15 minutes. The solvent was removed *in vacuo* and the crude product was purified by column chromatography (CH_2Cl_2:MeOH 9:1).

Yield (104): 46.0 mg as a white foam (100% yield: 58.3 mg).

Compound **104** was only identified by LC-MS analysis due to the complexity of the NMR spectrum. A sufficient purity for subsequent syntheses was assumed based on the purification by column chromatography, verified by the UV chromatogram (λ = 254 nm) of the LC-MS analysis.

TLC: R_f = 0.49 (CH_2Cl_2:MeOH 9:1).

MS (ESI$^+$): calc. for $C_{64}H_{109}N_8O_{18}Si_2^+$: m/z = 1333.74, found: m/z = 1333.85 $[M+H]^+$.

$C_{64}H_{108}N_8O_{18}Si_2$ (1333.78 g/mol)

$C_{64}H_{108}N_8O_{18}Si_2 \cdot CF_3COOH$ (1447.80 g/mol)

***N*-Cbz-deprotected Bis-POM-5'-deoxy muraymycin analogue 105**

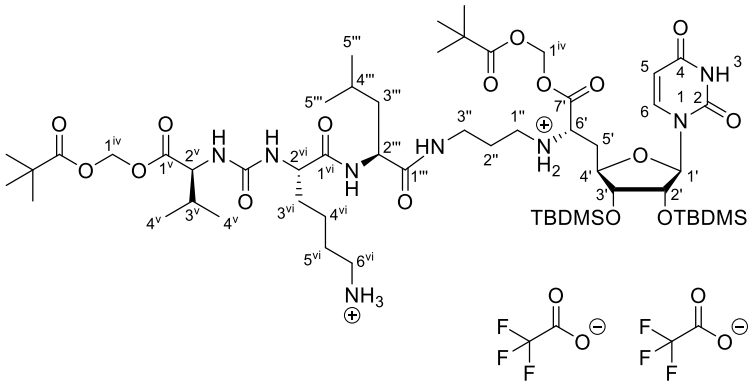

105

The reaction was carried out according to procedure 3.1 utilizing a solution of the fully protected Bis-POM-5'-deoxy muraymycin analogue **104** (8.00 mg, 5.53 µmol, 1.0 eq.) in *iso*-propanol (600 µL), 1,4-cyclohexadiene (6.50 µL, 68.7 µmol, 10.0 eq.), TFA (1.1 µL, 14 µmol, diluted to 1% in *iso*-propanol, 2.0 eq.) and several spatula tips of palladium black. The reaction mixture was stirred at room temperature for 2 hours. Since no full conversion had been observed by TLC, the same amounts of *iso*-propanol, 1,4-cyclohexadiene and TFA were added. The reaction mixture was stirred at room temperature for 6.5 hours in total.

Yield (105): 7.2 mg as a white foam (100% yield: 7.9 mg).

Compound **105** was only identified by LC-MS analysis due to the complexity of the NMR spectrum. A sufficient purity for subsequent syntheses was assumed based on the purification by column chromatography, verified by the UV chromatogram (λ = 254 nm) of the LC-MS analysis.

TLC: R_f = 0.35 (CH_2Cl_2:MeOH 9:1).

MS (ESI$^+$): calc. for $C_{64}H_{109}N_8O_{18}Si_2^+$: m/z = 1200.71, found: m/z = 1199.63 $[M+H]^+$.

$C_{56}H_{102}N_8O_{16}Si_2$ (1199.64 g/mol)

$C_{56}H_{102}N_8O_{16}Si_2 \cdot 2\ CF_3COOH$ (1427.69 g/mol)

Fully protected Bis-POM-5'-deoxy 4-(pialoxy)-benzylchloroformate muraymycin analogue 106

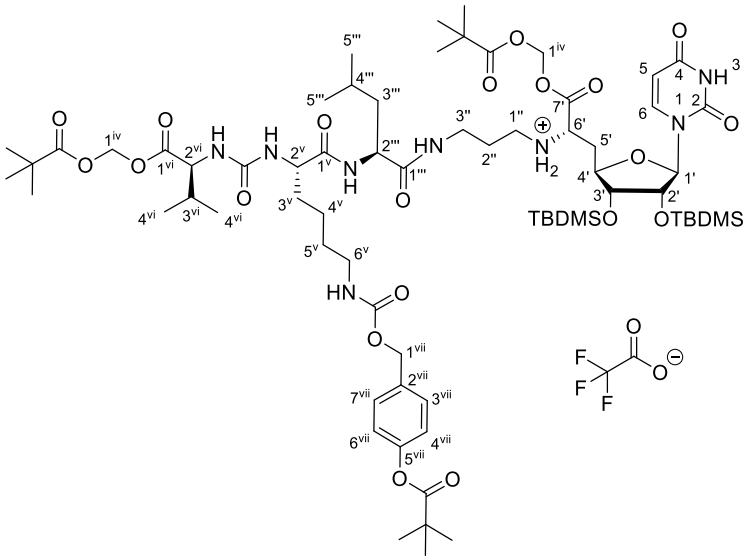

106

To a solution of the N-Cbz-deprotected bis-POM-5'-deoxy muraymycin analogue **105** (7.40 mg, 5.18 µmol, 1.0 eq.) in THF (1.0 mL), chloroformate **57** (4.60 mg, 17.0 µmol, 3.2 eq.) and DIPEA (6.00 µL, 10.4 µmol, 2.0 eq.) were added and the reaction mixture was stirred at room temperature for 21 hours. The solvent was removed in vacuo. The crude product was directly used for subsequent global deprotection.

Yield (106): 19.2 mg as a colorless solid with impurities included (100% yield: 8.0 mg).

$C_{69}H_{116}N_8O_{20}Si_2$ (1433.89 g/mol)

$C_{69}H_{116}N_8O_{20}Si_2 \cdot CF_3COOH$ (1547.92 g/mol)

Bis-POM-5'-deoxy 4-(pivaloxy)-benzylchloroformate muraymycin analogue 52

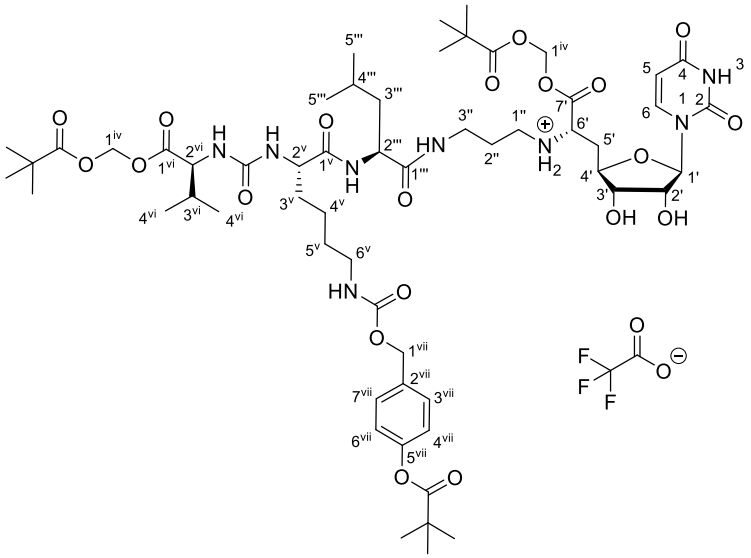

52

The reaction was carried out without any inert gas conditions. Solutions of the protected muraymycin analogue **106** (8.02 mg, 5.18 µmol, 1.0 eq.) in THF (600 µL) and TFA in water (2.5 mL, 10%) were cooled to 0 °C, combined and stirred at room temperature for 24 hours. The reaction mixture was diluted with water after a full conversion had been observed by TLC. The solvent was removed by freeze dying. The crude product was purified by semi-preparative HPLC (method shown in Chapter 7.2.1.5).

Yield (52): <1 mg as a colorless solid (100% yield: 7.4 mg).

No further characterization could be done since target compound **52** could not be weighted out properly.

HPLC (semi-preparative): t_R = 23.5 min (injection concentration: 19.7 mg in water/MeCN 95:5 (1.0 mL)).

$C_{57}H_{88}N_8O_{20}$ (1205.37 g/mol)

$C_{57}H_{88}N_8O_{20} \cdot CF_3COOH$ (1319.39 g/mol)

Bibliography

[1] T. A. Wencewicz; New antibiotics from Nature's chemical inventory; *Bioorg. Med. Chem.* **2016**, *24*, 6227–6252.

[2] F. von Nussbaum, M. Brands, B. Hinzen, S. Weigand, D. Häbich; Antibacterial Natural Products in Medicinal Chemistry - Exodus or Revival?; *Angew. Chem. Int. Ed.* **2006**, *45*, 5072–5129.

[3] P. Vuillemin; Antibiose et symbiose; *Assoc. Franc Pour l'Avanc. des sciences* **1889**, *2*, 525–542.

[4] S. A. Waksman; What is an antibiotic or antibiotic substance?; *Mycologia* **1947**, *39*, 565–569.

[5] S. A. Waksman; History of the word 'Antibiotic'; *J. Hist. Med. Allied Sci.* **1973**, *28*, 284–286.

[6] A. Fleming; On the antibacterial action of cultures of a penicillium, with special reference to their use in the isolation of *B. influenzae*; *Br. J. Exp. Pathol.* **1929**, *10*, 226.

[7] E. Chain, H. W. Florey, A. D. Gardner, N. G. Heatley, M. A. Jennings, J. Orr-Ewing, A. G. Sanders; Penicillin as a chemotherapeutic agent; *Lancet* **1940**, *236*, 226–228.

[8] B. Spellberg, B. Taylor-Blake; On the exoneration of Dr. William H. Stewart: debunking an urban legend; *Infect Dis. Poverty* **2013**, *2*.

[9] A. Raja, J. LaBonte, J. Lebbos, P. Kirkpatrick; Daptomycin; *Nat. Rev.* **2003**, *2*, 943–944.

[10] A. E. Clatworthy, E. Pierson, D. T. Hung; Targeting virulence: a new paradigm for antimicrobial therapy; *Nat. Chem. Biol.* **2007**, *3*, 541–548.

[11] *RÖMPP Online: Antibiotika-Resistenz*, Georg Thieme Verlag, Stuttgart, **2022**.

[12] W. C. Reygaert; An overview of the antimicrobial resistance mechanisms of bacteria; *AIMS Microbiol.* **2018**, *4*, 482–501.

[13] E. G. Pamer; Resurrecting the intestinal microbiota to combat antibiotic-resistant pathogens; *Science* **2016**, *352*, 535–538.

[14] M. J. Bonten, R. Willems, R. A. Weinstein; Vancomycin-resistant enterococci: why are they here, and where do they come from?; *Lancet Infect. Dis.* **2001**, *1*, 314–325.

[15] J. F. Barrett; MRSA: status and prospects for therapy? An evaluation of key papers on the topic of MRSA and antibiotic resistance; *Expert Opin. Ther. Targets* **2004**, *8*, 515–519.

[16] J. M. Munita, C. A. Arias; Mechanisms of Antibiotic Resistance; *Microbiol. Spectr.* **2016**, *4*.

[17] J. M. A. Blair, M. A. Webber, A. J. Baylay, D. O. Ogbolu, L. J. V. Piddock; Molecular mechanisms of antibiotic resistance; *Nat. Rev. Microbiol.* **2015**, *13*, 42–51.

[18] O. Cars, W. A. Craig; Pharmacodynamics of Antibiotics-Consequences for Dosing: Proceedings of a Symposium Held in Stockholm, June 7–9, 1990; *Scand. J. Infec. Dis.* **1990**, *22*, 1–284.

[19] K. Kimura, T. D. H. Bugg; Recent advances in antimicrobial nucleoside antibiotics targeting cell wall biosynthesis; *Nat. Prod. Rep.* **2003**, *20*, 252–273.

[20] Z. A. Popper, G. Michel, C. Hervé, D. S. Domozych, W. G. T. Willats, M. G. Tuohy, B. Kloareg, D. B. Stengel; Evolution and Diversity of Plant Cell Walls: From Algae to Flowering Plants; *Annu. Rev. Plant Biol.* **2011**, *62*, 567–590.

[21] S. M. Levitz; Innate Recognition of Fungal Cell Walls; *PLoS Pathog* **2010**, *6*, e1000758.

[22] W. Vollmer, D. Blanot, M. A. D. Pedro; Peptidoglycan structure and architecture; *FEMS Microbiol. Rev.* **2008**, *32*, 149–167.

[23] C. Walsh; Where will new antibiotics come from?; *Nat. Rev. Microbiol.* **2003**, *1*, 65–70.

[24] S. Melnikov, A. Ben-Shem, N. Garreau de Loubresse, L. Jenner, G. Yusupova, M. Yusupov; One core, two shells: bacterial and eukaryotic ribosomes; *Nat. Struct. Mol. Biol.* **2012**, *19*, 560–567.

[25] A. P. Carter, W. M. Clemons, D. E. Brodersen, R. J. Morgan-Warren, B. T. Wimberly, V. Ramakrishnan; Functional insights from the structure of the 30S ribosomal subunit and its interactions with antibiotics; *Nature* **2000**, *407*, 340–348.

[26] A. Garett, S. R. Douthwaite, A. Liljas, A. T. Matheson, P. B. Moore, H. F. Noller; *The Ribosome: Structure, Function, Antibiotics, and Cellular Interactions*, ASM Press, Washington, **2000**.

[27] F. Schlünzen, R. Zarivach, J. Harms, A. Bashan, A. Tocilj, R. Albrecht, A. Yonath, F. Franceschi; Structural basis for the interaction of antibiotics with the peptidyl transferase centre in eubacteria; *Nature* **2001**, *413*, 814–821.

[28] S. Baumann, J. Herrmann, R. Raju, H. Steinmetz, K. I. Mohr, S. Hüttel, K. Harmrolfs, M. Stadler, R. Müller; Cystobactamids: Myxobacterial Topoisomerase Inhibitors Exhibiting Potent Antibacterial Activity; *Angew. Chem. Int. Ed.* **2014**, *53*, 14605–14609.

[29] L. A. Mitscher; Bacterial Topoisomerase Inhibitors: Quinolone and Pyridone Antibacterial Agents; *Chem. Rev.* **2005**, *105*, 559–592.

[30] A. Bermingham, J. P. Derrick; The folic acid biosynthesis pathway in bacteria: evaluation of potential for antibacterial drug discovery; *BioEssays* **2002**, *24*, 637–648.

[31] M. G. Page; Cephalosporins in clinical development; *Expert Opin. Investig. Drugs* **2004**, *13*, 973–985.

[32] J. H. Steele, B. W. Frost; The structure of plankton communities; *Phil. Trans. R. Soc. Lond. B.* **1977**, *280*, 485–534.

[33] R. B. Sykes, C. M. Cimarusti, D. P. Bonner, K. Bush, D. M. Floyd, N. H. Georgopapadakou, W. H. Koster, W. C. Liu, W. L. Parker, P. A. Principe, et al.; Monocyclic P·lactam antibiotics produced by bacteria; *Nature* **1981**, *291*, 489–491.

[34] D. M. Floyd, A. W. Fritz, J. Pluscec, E. R. Weaver, C. M. Cimarusti; Monobactams. Preparation of (S)-3-amino-2-oxoazetidine-1-sulfonic acids from L-.alpha.-amino-.beta.-hydroxy acids via their hydroxamic esters; *J. Org. Chem.* **1982**, *47*, 5160–5167.

[35] G. S. Singh; β-Lactams in the New Millennium. Part-II: Cephems, Oxacephems, Penams and Sulbactam; *Mini-Rev. Med. Chem.* **2003**, *4*, 93–109.

[36] P. E. Reynolds; Structure, biochemistry and mechanism of action of glycopeptide antibiotics; *Eur. J. Clin. Microbiol. Infect. Dis.* **1989**, *8*, 943–950.

[37] A. Forge, J. Schacht; Aminoglycoside Antibiotics; *Auditol. Neurootol.* **2000**, *5*, 3–22.

[38] S. A. Waksman, E. Bugie, A. Schatz; Isolation of Antibiotic Substances from Soil Micro-Organisms, with special reference to Streptothricin and Streptomycin.; *Proc. Staff Meet. Mayo Clin.* **1944**, *19*, 537–48.

[39] A. Schatz, E. Bugle, S. A. Waksman; Streptomycin, a Substance Exhibiting Antibiotic Activity Against Gram-Positive and Gram-Negative Bacteria.; *Proc. Soc. Exp. Biol. Med.* **1944**, *55*, 66–69.

[40] I. Chopra, M. Roberts; Tetracycline Antibiotics: Mode of Action, Applications, Molecular Biology, and Epidemiology of Bacterial Resistance; *Microbiol. Mol. Biol. Rev.* **2001**, *65*, 232–260.

[41] S. Schwarz, J. Shen, K. Kadlec, Y. Wang, G. Brenner Michael, A. T. Feßler, B. Vester; Lincosamides, Streptogramins, Phenicols, and Pleuromutilins: Mode of Action and Mechanisms of Resistance; *Cold Spring Harb. Perspect. Med.* **2016**, *6*, a027037.

[42] I. Kanfer, M. F. Skinner, R. B. Walker; Analysis of macrolide antibiotics; *J. Chrom. A.* **1998**, *812*, 255–286.

[43] P. M. Hawkey; Mechanisms of quinolone action and microbial response; *J. Antimicrob. Chemother.* **2003**, *51*, 29–35.

[44] R. J. Henry; The Mode of Action of Sulfonamides; *Bacteriol. Rev.* **1943**, *7*, 175–262.

[45] G. M. Brown; The Biosynthesis of Folic Acid II. Inhibition of sulfonamides; *J. Biol. Chem.* **1962**, *237*, 536–540.

[46] P. A. Lambert; Cellular impermeability and uptake of biocides and antibiotics in Gram-positive bacteria and mycobacteria; *J. Appl. Microbiol.* **2002**, *92*, 46S-54S.

[47] H. C. Gram; Über die isolierte Färbung der Schizomyceten in Schnitt- und Trockenpräparaten; *Fortschr. Med.* **1884**, *2*, 185–189.

[48] A. Mayr; Medizinische Mikrobiologie, Infektions- und Seuchenlehre. 4.2 Aufbau und Anpassungsmechanismen der Bakterien; *Thieme Verlag* **2007**, *8., überarbeitete Auflage*, 346.

[49] L. Brown, J. M. Wolf, R. Prados-Rosales, A. Casadevall; Through the wall: extracellular vesicles in Gram-positive bacteria, mycobacteria and fungi; *Nat. Rev. Microbiol.* **2015**, *13*, 620–630.

[50] H. Nikaido; Molecular Basis of Bacterial Outer Membrane Permeability Revisited; *Microbiol. Mol. Biol. Rev.* **2003**, *67*, 593–656.

[51] T. Nakae; Outer membrane of Salmonella. Isolation of protein complex that produces transmembrane channels.; *J. Biol. Chem.* **1976**, *251*, 2176–2178.

[52] C. W. Forsberg, J. W. Costerton, R. A. Mac Leod; Separation and Localization of Cell Wall Layers of a Gram-Negative Bacterium; *J. Bacteriol.* **1970**, *104*, 1338–1353.

[53] J. van Heijenoort; Recent advances in the formation of the bacterial peptidoglycan monomer unit; *Nat. Prod. Rep.* **2001**, *18*, 503–519.

[54] W. Vollmer; Structural variation in the glycan strands of bacterial peptidoglycan; *FEMS Microbiol. Rev.* **2008**, 20.

[55] D. Wiegmann, S. Koppermann, M. Wirth, G. Niro, K. Leyerer, C. Ducho; Muraymycin nucleoside-peptide antibiotics: uridine-derived natural products as lead structures for the development of novel antibacterial agents; *Beilstein J. Org. Chem.* **2016**, *12*, 769–795.

[56] M. J. Osborn; Structure and Biosynthesis of the Bacterial Cell Wall; *Annu. Rev. Biochem.* **1969**, *38*, 501–538.

[57] A. J. F. Egan, W. Vollmer; The physiology of bacterial cell division; *Ann. N. Y. Acad. Sci.* **2013**, *1277*, 8–28.

[58] A. Gautam, R. Vyas, R. Tewari; Peptidoglycan biosynthesis machinery: A rich source of drug targets; *Crit. Rev. Biotechnol.* **2011**, *31*, 295–336.

[59] A. Bouhss, A. E. Trunkfield, T. D. H. Bugg, D. Mengin-Lecreulx; The biosynthesis of peptidoglycan lipid-linked intermediates; *FEMS Microbiol. Rev.* **2008**, *32*, 208–233.

[60] H. Barreteau, A. Kovač, A. Boniface, M. Sova, S. Gobec, D. Blanot; Cytoplasmic steps of peptidoglycan biosynthesis; *FEMS Microbiol. Rev.* **2008**, *32*, 168–207.

[61] B. Badet, P. Vermoote, P. Y. Haumont, F. Lederer, F. Le Goffic; Glucosamine synthetase from *Escherichia coli*: purification, properties, and glutamine-utilizing site location; *Biochemistry* **1987**, *26*, 1940–1948.

[62] D. Mengin-Lecreulx, J. van Heijenoort; Characterization of the essential gene glmM encoding phosphoglucosamine mutase in Escherichia coli; *J. Biol. Chem.* **1996**, *271*, 32–39.

[63] A. M. Gehring, W. J. Lees, D. J. Mindiola, C. T. Walsh, E. D. Brown; Acetyltransfer Precedes Uridylyltransfer in the Formation of UDP-*N*-acetylglucosamine in Separable Active Sites of the Bifunctional GlmU Protein of Escherichia coli; *Biochemistry* **1996**, *35*, 579–585.

[64] J. Rodríguez-Díaz, A. Rubio-del-Campo, M. J. Yebra; Regulatory insights into the production of UDP-N-acetylglucosamine by Lactobacillus casei; *Bioengineered* **2012**, *3*, 339–342.

[65] A. Bouhss, D. Mengin-Lecreulx, D. Blanot, J. van Heijenoort, C. Parquet; Invariant Amino Acids in the Mur Peptide Synthetases of Bacterial Peptidoglycan Synthesis and Their Modification by Site-Directed Mutagenesis in the UDP-MurNAc: L -Alanine Ligase from *Escherichia coli*; *Biochemistry* **1997**, *36*, 11556–11563.

[66] H. Jin, J. J. Emanuele, R. Fairman, J. G. Robertson, M. E. Hail, H.-T. Ho, P. J. Falk, J. J. Villafranca; Structural studies of Escherichia coli UDP-*N*-acetylmuramate: L-alanine ligase; *Biochemistry* **1996**, *35*, 1423–1431.

[67] C. Michaud, D. Blanot, B. Flouret, J. Heijenoort; Partial purification and specificity studies of the D-glutamate-adding and D-alanyl-D-alanine-adding enzymes from *Escherichia coli* K12; *Eur. J. Biochem.* **1987**, *166*, 631–637.

[68] E. Gordon; Crystal Structure of UDP-*N*-acetylmuramoyl-L-alanyl-D-glutamate: meso-Diaminopimelate Ligase from *Escherichia Coli*; *J. Biol. Chem.* **2001**, *276*, 10999–11006.

[69] Y. Yan, S. Munshi, B. Leiting, M. S. Anderson, J. Chrzas, Z. Chen; Crystal structure of Escherichia coli UDPMurNAc-tripeptide d-alanyl-d-alanine-adding enzyme (MurF) at 2.3 A resolution; *J. Mol. Biol.* **2000**, *304*, 435–445.

[70] J. T. Park; Uridine-5'-pyrophosphate derivatives; *J. Biol. Chem.* **1952**, *194*, 877–884.

[71] W. G. Struve, F. C. Neuhaus; Evidence for an Initial Acceptor of UDP-NAc-Muramyl-Pentapeptide in the Synthesis of Bacterial Mucopeptide; *Biochem. Biophys. Res. Commun.* **1965**, *18*, 6–12.

[72] J. S. Anderson, M. Matsuhashi, M. A. Haskin, J. L. Strominger; Lipid-Phosphoacetylmuramyl-pentapeptide and Lipid-Phosphodisaccharide-pentapeptide: Presumed Membrane Transport Intermediates in Cell Wall Synthesis; *Proc. Natl. Acad. Sci. USA* **1965**, *53*, 881–889.

[73] D. S. Boyle, W. D. Donachie; *mraY* Is an Essential Gene for Cell Growth in *Escherichia coli*; *J. Bacteriol.* **1998**, *180*, 6429–6432.

[74] B. Al-Dabbagh, X. Henry, M. E. Ghachi, G. Auger, D. Blanot, C. Parquet, D. Mengin-Lecreulx, A. Bouhss; Active Site Mapping of MraY, a Member of the Polyprenyl-phosphate *N*-Acetylhexosamine 1-Phosphate Transferase Superfamily, Catalyzing the First Membrane Step of Peptidoglycan Biosynthesis; *Biochemistry* **2008**, *47*, 8919–8928.

[75] W. G. Struve, R. K. Sinha, F. C. Neuhaus, M. S. Prime; On the Initial Stage in Peptidoglycan Synthesis. Phospho-*N*-acetylmuramyl-pentapeptide Translocase; *Biochemistry* **1966**, *5*, 82–93.

[76] M. G. Heydanek Jr, W. G. Struve, F. C. Neuhaus; Initial state in peptidoglycan synthesis. III. Kinetics and uncoupling of phospho-*N*-acetylmuramyl-pentapeptide translocase; *Biochemistry* **1969**, *8*, 1214–1221.

[77] F. C. Neuhaus; Initial Translocation Reaction in the Biosynthesis of Peptidoglycan by Bacterial Membranes; *Acc. Chem. Res.* **1971**, *4*, 297–303.

[78] D. D. Pless, F. C. Neuhaus; Initial Membrane Reaction in Peptidoglycan Synthesis, Lipid Dependence of Phospho-*N*-Acetylmuramyl-pentapeptide Translocase; *J. Biol. Chem.* **1973**, *248*, 1568–1576.

[79] M. Ikeda, M. Wachi, H. K. Jung, F. Ishino, M. Matsuhashi; The Escherichia coli *mraY* gene encoding UDP-*N*-acetylmuramoyl-pentapeptide: undecaprenyl-phosphate phospho-*N*-acetylmuramoyl-pentapeptide transferase.; *J. Bacteriol.* **1991**, *173*, 1021–1026.

[80] J. N. Umbreit, J. L. Strominger; Isolation of the Lipid Intermediate in Peptidoglycan Biosynthesis from *Escherichia coli*; *J. Bacteriol.* **1972**, *112*, 1306–1309.

[81] A. Geis, R. Plapp; Phospho-N-acetylmuramoyl-pentapeptide-transferase of Escherichia coli K12 Properties of the membrane-bound and the extracted and partially purified enzyme; *Biochim. Biophys. Acta Enzymol.* **1978**, *527*, 414–424.

[82] W. A. Weppner, F. C. Neuhaus; Initial Membrane Reaction in Peptidoglycan Synthesis. Interaction of lipid with phospho-N-acetylmuramyl-peptapeptidase translocase.; *Biochim. Biophys. Acta* **1979**, *552*, 418–427.

[83] A. Bouhss, D. Mengin-Lecreulx, D. Le Beller, J. Van Heijenoort; Topological analysis of the MraY protein catalysing the first membrane step of peptidoglycan synthesis; *Mol. Microbiol.* **1999**, *34*, 576–585.

[84] S. Koppermann, Z. Cui, P. D. Fischer, X. Wang, J. Ludwig, J. S. Thorson, S. G. Van Lanen, C. Ducho; Insights into the Target Interaction of Naturally Occurring Muraymycin Nucleoside Antibiotics; *ChemMedChem* **2018**, *13*, 779–784.

[85] A. Bouhss, M. Crouvoisier, D. Blanot, D. Mengin-Lecreulx; Purification and Characterization of the Bacterial MraY Translocase Catalyzing the First Membrane Step of Peptidoglycan Biosynthesis; *J. Biol. Chem.* **2004**, *279*, 29974–29980.

[86] Y. Ma, D. Munch, T. Schneider, H.-G. Sahl, A. Bouhss, U. Ghoshdastider, J. Wang, V. Dotsch, X. Wang, F. Bernhard; Preparative Scale Cell-free Production and Quality Optimization of MraY Homologues in Different Expression Modes; *J. Biol. Chem.* **2011**, *286*, 38844–38853.

[87] E. Henrich, Y. Ma, I. Engels, D. Münch, C. Otten, T. Schneider, B. Henrichfreise, H.-G. Sahl, V. Dötsch, F. Bernhard; Lipid Requirements for the Enzymatic Activity of MraY Translocases and in Vitro Reconstitution of the Lipid II Synthesis Pathway; *J. Biol. Chem.* **2016**, *291*, 2535–2546.

[88] A. J. Lloyd, P. E. Brandish, A. M. Gilbey, T. D. H. Bugg; Phospho-*N*-Acetyl-Muramyl-Pentapeptide Translocase from *Escherichia coli*: Catalytic Role of Conserved Aspartic Acid Residues; *J. Bacteriol.* **2004**, *186*, 1747–1757.

[89] B. C. Chung, J. Zhao, R. A. Gillespie, D.-Y. Kwon, Z. Guan, J. Hong, P. Zhou, S.-Y. Lee; Crystal Structure of MraY, an Essential Membrane Enzyme for Bacterial Cell Wall Synthesis; *Science* **2013**, *341*, 1012–1016.

[90] E. Henrich, O. Peetz, C. Hein, A. Laguerre, B. Hoffmann, J. Hoffmann, V. Dötsch, F. Bernhard, N. Morgner; Analyzing native membrane protein assembly in nanodiscs by combined non-covalent mass spectrometry and synthetic biology; *eLife* **2017**, *6*, e20954.

[91] B. C. Chung, E. H. Mashalidis, T. Tanino, M. Kim, A. Matsuda, J. Hong, S. Ichikawa, S.-Y. Lee; Structural insights into inhibition of lipid I production in bacterial cell wall synthesis; *Nature* **2016**, *533*, 557–560.

[92] S. Koppermann, C. Ducho; Natural Products at Work: Structural Insights into Inhibition of the Bacterial Membrane Protein MraY; *Angew. Chem. Int. Ed.* **2016**, *55*, 11722-11724. Naturstoffe bei der Arbeit: strukturelle Einblicke in die Inhibition des bakteriellen Membranproteins MraY; *Angew. Chem. Int. Ed*. **2016**, *128*, 11896-11898.

[93] E. H. Mashalidis, B. Kaeser, Y. Terasawa, A. Katsuyama, D.-Y. Kwon, K. Lee, J. Hong, S. Ichikawa, S.-Y. Lee; Chemical logic of MraY inhibition by antibacterial nucleoside natural products; *Nat. Commun.* **2019**, *10*, 2917.

[94] J. L. Sebaugh; Guidelines for accurate EC50/IC50 estimation; *Pharmaceut. Statist.* **2011**, *10*, 128–134.

[95] J. M. Andrews; Determination of minimum inhibitory concentrations; *J. Antimicrob. Chemother.* **2001**, *48*, 5–16.

[96] P. E. Brandish, K. I. Kimura, M. Inukai, R. Southgate, J. T. Lonsdale, T. D. H. Bugg; Modes of action of tunicamycin, liposidomycin B, and mureidomycin A: inhibition of

phospho-N-acetylmuramyl-pentapeptide translocase from Escherichia coli.; *Antimicrob. Agents Chemother.* **1996**, *40*, 1640–1644.

[97] P. E. Brandish, M. K. Burnham, J. T. Lonsdale, R. Southgate, M. Inukai, T. D. H. Bugg; Slow Binding Inhibition of Phospho-*N*-acetylmuramyl-pentapeptide-translocase (*Escherichia coli*) by Mureidomycin A; *J. Biol. Chem.* **1996**, *271*, 7609–7614.

[98] S. Wohnig; Synthese des dansylierten Park-Nucleotids und vereinfachter Analoga der Muraymycin-Antibiotika, Dissertation, Georg-August-University Göttingen; **2013**.

[99] S. Wohnig, A. P. Spork, S. Koppermann, G. Mieskes, N. Gisch, R. Jahn, C. Ducho; Total Synthesis of Dansylated Park's Nucleotide for High-Throughput MraY Assays; *Chem. Eur. J.* **2016**, *22*, 17813–17819.

[100] A. B. Shapiro, H. Jahić, N. Gao, L. Hajec, O. Rivin; A High-Throughput, Homogeneous, Fluorescence Resonance Energy Transfer-Based Assay for Phospho-*N*-acetylmuramoyl-pentapeptide Translocase (MraY); *J. Biomol. Screen.* **2012**, *17*, 662–672.

[101] S. Tanaka, W. M. Clemons Jr; Minimal requirements for inhibition of MraY by lysis protein E from bacteriophage ΦX174: A mutational analysis of phiX174 gene E mediated cell lysis; *Mol. Microbiol.* **2012**, *85*, 975–985.

[102] S. Mendel, J. M. Holbourn, J. A. Schouten, T. D. H. Bugg; Interaction of the transmembrane domain of lysis protein E from bacteriophage ϕX174 with bacterial translocase MraY and peptidyl-prolyl isomerase SlyD; *Microbiology* **2006**, *152*, 2959–2967.

[103] C. L. White, A. Kitich, J. W. Gober; Positioning cell wall synthetic complexes by the bacterial morphogenetic proteins MreB and MreD: Control of cell shape in bacteria; *Mol. Microbiol.* **2010**, *76*, 616–633.

[104] D. Szklarczyk, J. H. Morris, H. Cook, M. Kuhn, S. Wyder, M. Simonovic, A. Santos, N. T. Doncheva, A. Roth, P. Bork, et al.; The STRING database in 2017: quality-controlled protein–protein association networks, made broadly accessible; *Nucleic Acids Res.* **2017**, *45*, D362–D368.

[105] I. Jovčevska, S. Muyldermans; The Therapeutic Potential of Nanobodies; *BioDrugs* **2020**, *34*, 11–26.

[106] C. Hamers-Casterman, T. Atarhouch, S. Muyldermans, G. Robinson, C. Hammers, E. B. Songa, N. Bendahman, R. Hammers; Naturally occurring antibodies devoid of light chains; *Nature* **1993**, *363*, 446–448.

[107] I. G. Denisov, S. G. Sligar; Nanodiscs in Membrane Biochemistry and Biophysics; *Chem. Rev.* **2017**, *117*, 4669–4713.

[108] A. Krogh, B. Larsson, G. von Heijne, E. L. L. Sonnhammer; Predicting transmembrane protein topology with a hidden markov model: application to complete genomes11Edited by F. Cohen; *Journal of Molecular Biology* **2001**, *305*, 567–580.

[109] F. Hagn, M. L. Nasr, G. Wagner; Assembly of phospholipid nanodiscs of controlled size for structural studies of membrane proteins by NMR; *Nat. Protoc.* **2018**, *13*, 79–98.

[110] D. Linke; Detergents: an overview; *Methods Enzymol.* **2009**, 603–617.

[111] F. Szoka, D. Papahadjopoulos; Comparative Properties and Methods of Preparation of Lipid Vesicles (Liposomes); *Annu. Rev. Biophys. Bioeng.* **1980**, *9*, 467–508.

[112] J.-L. Rigaud, B. Pitard, D. Levy; Reconstitution of membrane proteins into liposomes: application to energy-transducing membrane proteins; *Biochimica et Biophysica Acta (BBA) - Bioenergetics* **1995**, *1231*, 223–246.

[113] G. D. Eytan; Use of liposomes for reconstitution of biological functions.; *Biochim. Biophys. Acta* **1982**, *694*, 185–202.

[114] A. Helenius, K. Simons; Solubilization of membranes by detergents; *Biochim. Biophys. Acta Biomembr.* **1975**, *415*, 29–79.

[115] D. Lee, K. F. A. Walter, A.-K. Brückner, C. Hilty, S. Becker, C. Griesinger; Bilayer in Small Bicelles Revealed by Lipid−Protein Interactions Using NMR Spectroscopy; *J. Am. Chem. Soc.* **2008**, *130*, 13822–13823.

[116] P. S. Chae, S. G. F. Rasmussen, R. R. Rana, K. Gotfryd, A. C. Kruse, A. Manglik, K. H. Cho, S. Nurva, U. Gether, L. Guan, et al.; A New Class of Amphiphiles Bearing Rigid Hydrophobic Groups for Solubilization and Stabilization of Membrane Proteins; *Chem. Eur. J.* **2012**, *18*, 9485–9490.

[117] K. Dalal, F. Duong; Reconstitution of the SecY translocon in nanodiscs; *Methods Mol. Biol.* **2010**, *619*, 145–156.

[118] K. K. Hoi, J. F. Bada Juarez, P. J. Judge, H.-Y. Yen, D. Wu, J. Vinals, G. F. Taylor, A. Watts, C. V. Robinson; Detergent-free Lipodisq Nanoparticles Facilitate High-Resolution Mass Spectrometry of Folded Integral Membrane Proteins; *Nano Lett.* **2021**, *21*, 2824–2831.

[119] P. T. Duong, H. L. Collins, M. Nickel, S. Lund-Katz, G. H. Rothblat, M. C. Phillips; Characterization of nascent HDL particles and microparticles formed by ABCA1-mediated efflux of cellular lipids to apoA-I; *Journal of Lipid Research* **2006**, *47*, 832–843.

[120] C. G. Brouillette, G. M. Anantharamaiah, J. A. Engler, D. W. Borhani; Structural models of human apolipoprotein A-I: a critical analysis and review; *Biochimica et Biophysica Acta (BBA) - Molecular and Cell Biology of Lipids* **2001**, *1531*, 4–46.

[121] M. L. Nasr, D. Baptista, M. Strauss, Z.-Y. J. Sun, S. Grigoriu, S. Huser, A. Plückthun, F. Hagn, T. Walz, J. M. Hogle, et al.; Covalently circularized nanodiscs for studying membrane proteins and viral entry; *Nat. Methods* **2017**, *14*, 49–52.

[122] P. Fischer; Structural and Functional Investigations to Address Challenging Drug Targets, Dissertation, Saarland University; **2021**.

[123] I. G. Denisov, Y. V. Grinkova, A. A. Lazarides, S. G. Sligar; Directed Self-Assembly of Monodisperse Phospholipid Bilayer Nanodiscs with Controlled Size; *J. Am. Chem. Soc.* **2004**, *126*, 3477–3487.

[124] C. R. H. Raetz; Molecular genetics of membrane phospholipid synthesis; *Annu. Rev. Genet.* **1986**, *20*, 253–295.

[125] C. Roos, M. Zocher, D. Müller, D. Münch, T. Schneider, H.-G. Sahl, F. Scholz, J. Wachtveitl, Y. Ma, D. Proverbio, et al.; Characterization of co-translationally formed nanodisc complexes with small multidrug transporters, proteorhodopsin and with the E.

coli MraY translocase; *Biochimica et Biophysica Acta (BBA) - Biomembranes* **2012**, *1818*, 3098–3106.

[126] Y. Liu, E. C. C. M. Moura, J. M. Dörr, S. Scheidelaar, M. Heger, M. R. Egmond, J. A. Killian, T. Mohammadi, E. Breukink; Bacillus subtilis MraY in detergent-free system of nanodiscs wrapped by styrene-maleic acid copolymers; *PLoS ONE* **2018**, *13*, e0206692.

[127] B. Alberts, D. Bray, K. Hopkin, A. D. Johnson, J. Lewis, M. Raff, K. Roberts, P. Walter; Lehrbuch der molekularen Zellbiologie; *Wiley-VCH* **2005**, *5. Auflage*, 427–430.

[128] R. O'Shea, H. E. Moser; Physicochemical Properties of Antibacterial Compounds: Implications for Drug Discovery; *J. Med. Chem.* **2008**, *51*, 2871–2878.

[129] M. F. Richter, B. S. Drown, A. P. Riley, A. Garcia, T. Shirai, R. L. Svec, P. J. Hergenrother; Predictive compound accumulation rules yield a broad-spectrum antibiotic; *Nature* **2017**, *545*, 299–304.

[130] E. J. Geddes, Z. Li, P. J. Hergenrother; An LC-MS/MS assay and complementary web-based tool to quantify and predict compound accumulation in *E. coli*; *Nat. Protoc.* **2021**, *16*, 4833–4854.

[131] H. Cai, K. Rose, L.-H. Liang, S. Dunham, C. Stover; Development of a liquid chromatography/mass spectrometry-based drug accumulation assay in *Pseudomonas aeruginosa*; *Anal. Biochem.* **2009**, *385*, 321–325.

[132] D. Bednarczyk; Fluorescence-based assays for the assessment of drug interaction with the human transporters OATP1B1 and OATP1B3; *Anal. Biochem.* **2010**, *405*, 50–58.

[133] Y. Zhou, C. Joubran, L. Miller-Vedam, V. Isabella, A. Nayar, S. Tentarelli, A. Miller; Thinking Outside the "Bug": A Unique Assay To Measure Intracellular Drug Penetration in Gram-Negative Bacteria; *Anal. Chem.* **2015**, *87*, 3579–3584.

[134] J. Meiers; Entwicklung eines HPLC-MS-basierten Assays zur Evaluierung der bakteriellen Zellaufnahme, Diploma Thesis, Saarland University; **2017**.

[135] H. Prochnow, V. Fetz, S.-K. Hotop, M. A. García-Rivera, A. Heumann, M. Brönstrup; Subcellular Quantification of Uptake in Gram-Negative Bacteria; *Anal. Chem.* **2019**, *91*, 1863–1872.

[136] M. Winn, R. J. M. Goss, K. Kimura, T. D. H. Bugg; Antimicrobial nucleoside antibiotics targeting cell wall assembly: Recent advances in structure–function studies and nucleoside biosynthesis; *Nat. Prod. Rep.* **2010**, *27*, 279–304.

[137] S. Ichikawa, M. Yamaguchi, A. Matsuda; Antibacterial Nucleoside Natural Products Inhibiting Phospho-Mur*N*Ac-Pentapeptide Translocase; Chemistry and Structure-Activity Relationship.; *Curr. Med. Chem.* **2015**, *22*, 3951–3979.

[138] A. Takatsuki, K. Arima, G. Tamura; Tunicamycin, a new antibiotic. I. Isolation and characterization of tunicamycin; *J. Antibiot.* **1971**, *24*, 215–223.

[139] A. Takatsuki, G. Tamura; Tunicamycin, a new antibiotic. II. Some biological properties of the antiviral activity of tunicamycin; *J. Antibiot.* **1971**, *24*, 224–231.

[140] A. Takatsuki, G. Tamura; Effect of tunicamycin on the synthesis of macromolecules in cultures of chick embryo fibroblasts infected with Newcastle disease virus; *J. Antibiot.* **1971**, *24*, 785–794.

[141] W. C. Mahoney, D. Duksin; Biological activities of the two major components of tunicamycin.; *J. Biol. Chem.* **1979**, *254*, 6572–6576.

[142] K. Eckardt, H. Thrum, G. Bradler, E. Tonew, M. Tonew; Streptovirudins, new antibiotics with antibacterial and antiviral activity. II. Isolation, chemical characterization and biological activity of streptovirudins A1, A2, B1, B2, C1, C2, D1, and D2; *J. Antibiot.* **1975**, *28*, 274–279.

[143] H. Thrum, K. Eckardt, G. Bradler, R. Fügner, E. Tonew, M. Tonew; Streptovirudins, new antibiotics with antibacterial and antiviral activity. I. Culture taxonomy, fermentation and production of streptovirudin complex; *J. Antibiot.* **1975**, *28*, 514–521.

[144] K. Eckardt, W. Ihn, D. Tresselt, D. Krebs; The chemical structures of streptovirudins; *J. Antibiot.* **1981**, *34*, 1631–1632.

[145] P. Vogel, D. S. Petterson, P. H. Berry, J. L. Frahn, N. Anderton, P. A. Cockrum, J. A. Edgar, M. V. Jago, G. W. Lanigan, A. L. Payne, et al.; Isolation of a group of glycolipid toxins from seedheads of annual ryegrass Lolium rigidum Gaud.) infected by Corynebacterium rathayi; *Aust. J. Exp. Biol. Med. Sci.* **1981**, *59*, 455–467.

[146] M. Inukai, F. Isono, S. Takahashi, R. Enokita, Y. Sakaida, T. Haneishi; Mureidomycins A-D, novel peptidylnucleoside antibiotics with spheroplast forming activity. I. Taxonomy, fermentation, isolation and physico-chemical properties.; *J. Antibiot.* **1989**, *42*, 662–666.

[147] M. Inukai, F. Isono, S. Takahashi, T. Haneishi; Mureidomycins A-D, novel peptidylnucleoside antibiotics with spheroplast forming activity. II. Structural Elucidation; *J. Antibiot.* **1989**, *42*, 667–673.

[148] M. Inukai, F. Isono, S. Takahashi, T. Haneishi; Mureidomycins A-D, novel peptidylnucleoside antibiotics with spheroplast forming activity. III. Biological Properties; *J. Antibiot.* **1989**, *42*, 674–679.

[149] J. P. Karwowski, M. Jackson, R. J. Theriault, R. H. Chen, G. J. Barlow, M. L. Maus; Pacidamycins, a novel series of antibiotics with anti-*Pseudomonas aeruginosa* activity. I. Taxonomy of the producing organism and fermentation.; *J. Antibiot.* **1989**, *42*, 506–511.

[150] R. H. Chen, A. M. Buko, D. N. Whittern, J. B. McAlpine; Pacidamycins, a novel series of antibiotics with anti-Pseudomonas aeruginosa activity. II. Isolation and structural elucidation; *J. Antibiot.* **1989**, *42*, 512–520.

[151] P. B. Fernandes, R. N. Swanson, D. J. Hardy, C. W. Hanson, L. Coen, R. R. Rasmussen, R. H. Chen; Pacidamycins, a novel series of antibiotics with anti-*Pseudomonas aeruginosa* activity. III. Microbiologic profile.; *J. Antibiot.* **1989**, *42*, 521–526.

[152] S. Chatterjee, S. R. Nadkarni, E. K. Vijayakumar, M. V. Patel, B. N. Ganguli, H. W. Fehlhaber, L. Vertesy; Napsamycins, new *Pseudomonas* active antibiotics of the mureidomycin family from *Streptomyces sp.* HIL Y-82,11372; *J. Antibiot.* **1994**, *47*, 595–598.

[153] Y. Xie, R. Chen, S. Si, C. Sun, H. Xu; A New Nucleosidyl-peptide Antibiotic, Sansanmycin; *J. Antibiot.* **2007**, *60*, 158–161.

[154] Y. Xie, H. Xu, S. Si, C. Sun, R. Chen; Sansanmycins B and C, New Components of Sansanmycins; *J. Antibiot.* **2008**, *61*, 237–240.

[155] K. Isono, M. Uramoto, H. Kusakabe, K.-I. Kimura, K. Izaki, C. C. Nelson, J. A. Mccloskey; Lipisidomycins: Novel nucleoside antibiotics which inhibit bacterial peptidoglycan synthesis; *J. Antibiot.* **1985**, *38*, 1617–1621.

[156] M. Igarashi, N. Nakagawa, N. Doi, S. Hattori, H. Naganawa, M. Hamada; Caprazamycin B, a Novel Anti-tuberculosis Antibiotic, from *Streptomyces sp.*; *J. Antibiot.* **2003**, *56*, 580–583.

[157] M. Igarashi, Y. Takahashi, T. Shitara, H. Nakamura, H. Naganawa, T. Miyake, Y. Akamatsu; Caprazamycins, Novel Lipo-nucleoside Antibiotics, from Streptomyces sp.; *J. Antibiot.* **2005**, *58*, 327–337.

[158] H. Naganawa, M. Hamada, M. Igarashi, T. Takeuchi; *Antibiotic Caprazamycins and Process for Producing the Same*, **2001**, Patent No. CA2388050 A1.

[159] H. Seto, N. Otake, S. Sato, H. Yamaguchi, K. Takada, M. Itoh, H. S. M. Lu, J. Clardy; The structure of a new nucleoside antibiotic, capuramycin; *Tetrahedron Lett.* **1988**, *29*, 2343–2346.

[160] H. Yamaguchi, S. Sato, S. Yoshida, K. Takada, M. Itoh, H. Seto, N. Otake; Capuramycin, a new nucleoside antibiotic. Taxonomy, fermentation, isolation and characterization.; *J. Antibiot.* **1986**, *39*, 1047–1053.

[161] W. Cai, A. Goswami, Z. Yang, X. Liu, K. D. Green, S. Barnard-Britson, S. Baba, M. Funabashi, K. Nonaka, M. Sunkara, et al.; The Biosynthesis of Capuramycin-type Antibiotics Identification of the A-102396 Biosynthetic Gene Cluster, Mechanism of Self-Resistance, and Formation of Uridine-5'-Carboxamide; *J. Biol. Chem.* **2015**, *290*, 13710–13724.

[162] S. Hirano, S. Ichikawa, A. Matsuda; Total synthesis of (+)-FR-900493 and establishment of its absolute stereochemistry; *Tetrahedron* **2007**, *63*, 2798–2804.

[163] K. Ochi, M. Ezaki, M. Iwami, T. Komori, M. Kohsaka; *FR-900493 Substance, a Process for Its Production and a Pharmaceutical Composition Containing the Same*, **1990**, Patent No. US4950605 A.

[164] L. A. McDonald, L. R. Barbieri, G. T. Carter, E. Lenoy, J. Lotvin, P. J. Petersen, M. M. Siegel, G. Singh, R. T. Williamson; Structures of the Muraymycins, Novel Peptidoglycan Biosynthesis Inhibitors; *J. Am. Chem. Soc.* **2002**, *124*, 10260–10261.

[165] Z. Cui, X. Wang, S. Koppermann, J. S. Thorson, C. Ducho, S. G. Van Lanen; Antibacterial Muraymycins from Mutant Strains of *Streptomyces* sp. NRRL 30471; *J. Nat. Prod.* **2018**, *81*, 942–948.

[166] G. T. Carter, J. A. Lotvin, L. A. McDonald; *Antibiotics Aa-896*, **2002**, Patent No. WO2002085310 A3.

[167] O. Ries, C. Carnarius, C. Steinem, C. Ducho; Membrane-interacting properties of the functionalised fatty acid moiety of muraymycin antibiotics; *Med. Chem. Commun.* **2015**, *6*, 879–886.

[168] F. Graef, B. Vukosavljevic, J.-P. Michel, M. Wirth, O. Ries, C. De Rossi, M. Windbergs, V. Rosilio, C. Ducho, S. Gordon, et al.; The bacterial cell envelope as delimiter of anti-infective bioavailability – An *in vitro* permeation model of the Gram-negative bacterial inner membrane; *J. Controlled Release* **2016**, *243*, 214–224.

[169] Y.-I. Lin, Z. Li, G. D. Francisco, L. A. McDonald, R. A. Davis, G. Singh, Y. Yang, T. S. Mansour; Muraymycins, novel peptidoglycan biosynthesis inhibitors: semisynthesis and SAR of their derivatives; *Bioorg. Med. Chem. Lett.* **2002**, *12*, 2341–2344.

[170] A. Yamashita, E. Norton, P. J. Petersen, B. A. Rasmussen, G. Singh, Y. Yang, T. S. Mansour, D. M. Ho; Muraymycins, novel peptidoglycan biosynthesis inhibitors: synthesis and SAR of their analogues; *Bioorg. Med. Chem. Lett.* **2003**, *13*, 3345–3350.

[171] A. Yamashita, E. Norton; *Antibiotic AA 896 Analogs*, **2005**, Patent No. WO/2002/086139.

[172] X.-F. Zhu, H. J. Williams, A. I. Scott; Facile and highly selective 5′-desilylation of multisilylated nucleosides; *J. Chem. Soc. Perkin Trans. 1* **2000**, 2305–2306.

[173] A. G. Myers, D. Y. Gin, D. H. Rogers; Synthetic studies of the tunicamycin antibiotics. Preparation of (+)-tunicaminyluracil,(+)-tunicamycin-V, and 5'-epi-tunicamycin-V; *J. Am. Chem. Soc.* **1994**, *116*, 4697–4718.

[174] L. Banfi, S. Cardani, D. Potenza, C. Scolastico; Stereoselective synthesis of t-butyl 2-amino-2,5-dideoxy-L-LYXO-pentanoate: Formal synthesis of L-daunosamine; *Tetrahedron* **1987**, *43*, 2317–2322.

[175] K. Leyerer; Muraymycin Nucleoside Antibiotics: Novel SAR Insights and Synthetic Approaches, Dissertation, Saarland University; **2018**.

[176] S. Hirano, S. Ichikawa, A. Matsuda; Total Synthesis of Caprazol, a Core Structure of the Caprazamycin Antituberculosis Antibiotics; *Angew. Chem.* **2005**, *117*, 1888–1890.

[177] S. Hirano, S. Ichikawa, A. Matsuda; Development of a Highly β-Selective Ribosylation Reaction without Using Neighboring Group Participation: Total Synthesis of (+)-Caprazol, a Core Structure of Caprazamycins; *J. Org. Chem.* **2007**, *72*, 9936–9946.

[178] S. Hirano, S. Ichikawa, A. Matsuda; Synthesis of Caprazamycin Analogues and Their Structure−Activity Relationship for Antibacterial Activity; *J. Org. Chem.* **2008**, *73*, 569–577.

[179] T. Tanino, S. Hirano, S. Ichikawa, A. Matsuda; Synthetic study of muraymycins using Ugi-four component reaction; *Nucleic Acids Symp. Ser.* **2008**, *52*, 557–558.

[180] T. Tanino, S. Ichikawa, M. Shiro, A. Matsuda; Total Synthesis of (−)-Muraymycin D2 and Its Epimer; *J. Org. Chem.* **2010**, *75*, 1366–1377.

[181] T. Tanino, S. Ichikawa, B. Al-Dabbagh, A. Bouhss, H. Oyama, A. Matsuda; Synthesis and Biological Evaluation of Muraymycin Analogues Active against Anti-Drug-Resistant Bacteria; *ACS Med. Chem. Lett.* **2010**, *1*, 258–262.

[182] T. Tanino, B. Al-Dabbagh, D. Mengin-Lecreulx, A. Bouhss, H. Oyama, S. Ichikawa, A. Matsuda; Mechanistic Analysis of Muraymycin Analogues: A Guide to the Design of MraY Inhibitors; *J. Med. Chem.* **2011**, *54*, 8421–8439.

[183] Y. Takeoka, T. Tanino, M. Sekiguchi, S. Yonezawa, M. Sakagami, F. Takahashi, H. Togame, Y. Tanaka, H. Takemoto, S. Ichikawa, et al.; Expansion of Antibacterial Spectrum of Muraymycins toward *Pseudomonas aeruginosa*; *ACS Med. Chem. Lett.* **2014**, *5*, 556–560.

[184] J. D. More, N. S. Finney; A Simple and Advantageous Protocol for the Oxidation of Alcohols with *o* -Iodoxybenzoic Acid (IBX); *Org. Lett.* **2002**, *4*, 3001–3003.

[185] G. Wittig, G. Geissler; Zur Reaktionsweise des Pentaphenyl-phosphors und einiger Derivate; *Liebigs Ann. Chem* **1953**, *580*, 44–57.

[186] B. Tao, G. Schlingloff, K. B. Sharpless; Reversal of regioselection in the asymmetric aminohydroxylation of cinnamates; *Tetrahedron Lett.* **1998**, *39*, 2507–2510.

[187] C. Rohrbacher; Synthese lipophil derivatisierter 5'-Desoxy-Muraymycin-Analoga, Master Thesis, Saarland University; **2017**.

[188] K. Mitachi, B. A. Aleiwi, C. M. Schneider, S. Siricilla, M. Kurosu; Stereocontrolled Total Synthesis of Muraymycin D1 Having a Dual Mode of Action against Mycobacterium tuberculosis; *J. Am. Chem. Soc.* **2016**, *138*, 12975–12980.

[189] B. A. Aleiwi, C. M. Schneider, M. Kurosu; Synthesis of Ureido-Muraymycidine Derivatives for Structure Activity Relationship Studies of Muraymycins; *J. Org. Chem.* **2012**, *77*, 3859–3867.

[190] A. P. Spork, M. Büschleb, O. Ries, D. Wiegmann, S. Boettcher, A. Mihalyi, T. D. H. Bugg, C. Ducho; Lead Structures for New Antibacterials: Stereocontrolled Synthesis of a Bioactive Muraymycin Analogue; *Chem. Eur. J.* **2014**, *20*, 15292–15297.

[191] A. P. Spork, S. Koppermann, B. Dittrich, R. Herbst-Irmer, C. Ducho; Efficient synthesis of the core structure of muraymycin and caprazamycin nucleoside antibiotics based on a stereochemically revised sulfur ylide reaction; *Tetrahedron: Asymmetry* **2010**, *21*, 763–766.

[192] F. Sarabia, L. Martín-Ortiz, F. J. López-Herrera; A Convergent Synthetic Approach to the Nucleoside-Type Liposidomycin Antibiotics; *Org. Lett.* **2003**, *5*, 3927–3930.

[193] F. Sarabia, L. Martín-Ortiz; Synthetic studies on nucleoside-type muraymycins antibiotics based on the use of sulfur ylides. Synthesis of bioactive 5′-epimuraymycin analogues; *Tetrahedron* **2005**, *61*, 11850–11865.

[194] V. K. Aggarwal, J. N. Harvey, J. Richardson; Unraveling the Mechanism of Epoxide Formation from Sulfur Ylides and Aldehydes; *J. Am. Chem. Soc.* **2002**, *124*, 5747–5756.

[195] V. K. Aggarwal, J. G. Ford, A. Thompson, R. V. Jones, M. C. Standen; Direct asymmetric epoxidation of aldehydes using catalytic amounts of enantiomerically pure sulfides; *J. Am. Chem. Soc.* **1996**, *118*, 7004–7005.

[196] A. Spork, C. Ducho; Stereocontrolled Synthesis of 5′- and 6′-Epimeric Analogues of Muraymycin Nucleoside Antibiotics; *Synlett* **2013**, *24*, 343–346.

[197] A. P. Spork, C. Ducho; Novel 5′-deoxy nucleosyl amino acid scaffolds for the synthesis of muraymycin analogues; *Org. Biomol. Chem.* **2010**, *8*, 2323–2326.

[198] A. P. Spork, D. Wiegmann, M. Granitzka, D. Stalke, C. Ducho; Stereoselective Synthesis of Uridine-Derived Nucleosyl Amino Acids; *J. Org. Chem.* **2011**, *76*, 10083–10098.

[199] O. Ries, M. Büschleb, M. Granitzka, D. Stalke, C. Ducho; Amino acid motifs in natural products: synthesis of *O*-acylated derivatives of (2*S*,3*S*)-3-hydroxyleucine; *Beilstein J. Org. Chem.* **2014**, *10*, 1135–1142.

[200] T. Laib, J. Chastanet, J. Zhu; Diastereoselective Synthesis of g-Hydroxy-α-amino Alcohols and (2*S*,3*S*)-α-Hydroxyleucine from Chiral D-(*N*,*N*-Dibenzylamino)serine (TBDMS) Aldehyde; *J. Org. Chem.* **1998**, *63*, 1709–1713.

[201] L. Horner, H. Hoffmann, H. G. Wippel; Phosphororganische Verbindungen, XII. Phosphinoxyde als Olefinierungsreagenzien; *Chem. Ber.* **1958**, *91*, 61–63.

[202] W. S. Wadsworth, W. D. Emmons; The utility of phosphonate carbanions in olefin synthesis; *J. Am. Chem. Soc.* **1961**, *83*, 1733–1738.

[203] U. Zoller, D. Ben-Ishai; Amidoalkylation of mercaptans with glyoxylic acid derivatives; *Tetrahedron* **1975**, *31*, 863–866.

[204] R. G. Vaswani, A. R. Chamberlin; Stereocontrolled Total Synthesis of (−)-Kaitocephalin; *J. Org. Chem.* **2008**, *73*, 1661–1681.

[205] U. Schmidt, A. Lieberknecht, J. Wild; Amino Acids and Peptides; XLIII. Dehydroamino Acids; XVIII. Synthesis of Dehydroamino Acids and Amino Acids from *N*-Acyl-2-(dialkyloxyphosphinyl)-glycin Esters; II; *Synthesis* **1984**, *1*, 53–60.

[206] S. Hörner, S. Knauer, C. Uth, M. Jöst, V. Schmidts, H. Frauendorf, C. M. Thiele, O. Avrutina, H. Kolmar; Nanoscale Biodegradable Organic–Inorganic Hybrids for Efficient Cell Penetration and Drug Delivery; *Angew. Chem. Int. Ed.* **2016**, *55*, 14842–14846.

[207] M. J. Burk; C2-symmetric bis (phospholanes) and their use in highly enantioselective hydrogenation reactions; *J. Am. Chem. Soc.* **1991**, *113*, 8518–8519.

[208] T. Masquelin, E. Broger, K. Müller, R. Schmid, D. Obrecht; Synthesis of Enantiomerically Pure D-and L-(Heteroaryl) alanines by asymmetric hydrogenation of (Z)-α-amino-αβ-didehydro esters; *Helv. Chim. Acta* **1994**, *77*, 1395–1411.

[209] A. Heib, G. Niro, S. C. Weck, S. Koppermann, C. Ducho; Muraymycin Nucleoside Antibiotics: Structure-Activity Relationship for Variations in the Nucleoside Unit; *Molecules* **2020**, *25*, 22.

[210] D. Wiegmann; Synthetische Untersuchungen zur Nucleosid-Einheit von Muraymycin-Antibiotika und ihren Analoga, Master Thesis, University of Paderborn; **2012**.

[211] K. Leyerer; Arbeiten zur Synthese neuer Analoga der Muraymycin-Antibiotika, Master Thesis, University of Paderborn; **2013**.

[212] D. Wiegmann; Neue Strategien zur Entwicklung von Derivaten der Muraymycin-Antibiotika mit verbesserter biologischer Aktivität, Dissertation, Saarland University; **2016**.

[213] D. Wiegmann, S. Koppermann, C. Ducho; Aminoribosylated Analogues of Muraymycin Nucleoside Antibiotics; *Molecules* **2018**, *23*, 3085.

[214] D. Wiegmann, A. Spork, G. Niro, C. Ducho; Thieme Chemistry Journals Awardees – Where Are They Now? -Ribosylation of an Acid-Labile Glycosyl Acceptor as a Potential Key Step for the Synthesis of Nucleoside Antibiotics; *Synlett* **2018**, *29*, 440–446.

[215] K. Ii, S. Ichikawa, B. Al-Dabbagh, A. Bouhss, A. Matsuda; Function-Oriented Synthesis of Simplified Caprazamycins: Discovery of Oxazolidine-Containing Uridine Derivatives as Antibacterial Agents against Drug-Resistant Bacteria; *J. Med. Chem.* **2010**, *53*, 3793–3813.

[216] V. J. Stella; Prodrugs as therapeutics; *Expert Opinion on Therapeutic Patents* **2004**, *14*, 277–280.

[217] J. Rautio, H. Kumpulainen, T. Heimbach, R. Oliyai, D. Oh, T. Järvinen, J. Savolainen; Prodrugs: design and clinical applications; *Nat. Rev. Drug Discov.* **2008**, *7*, 255–270.

[218] J. Rautio, N. A. Meanwell, L. Di, M. J. Hageman; The expanding role of prodrugs in contemporary drug design and development; *Nat. Rev. Drug Discov.* **2018**, *17*, 559–587.

[219] K. M. Huttunen, H. Raunio, J. Rautio; Prodrugs—from Serendipity to Rational Design; *Pharmacol. Rev.* **2011**, *63*, 750–771.

[220] D. Farquhar, D. N. Srivastva, N. J. Kuttesch, P. P. Saunders; Biologically Reversible Phosphate-Protective Groups; *J. Pharm. Sci.* **1983**, *72*, 324–325.

[221] J. K. Sastry, P. N. Nehete, S. Khan, B. J. Nowak, W. Plunkett, R. B. Arlinghaus, D. Farquhar; Membrane-Permeable Dideoxyuridine 5'-Monophosphate Analogue Inhibits Human Immunodeficiency Virus Infection; *Mol. Pharmacol.* **1992**, *41*, 441–445.

[222] A. Pompon, I. Lefebvre, J.-L. Imbach, S. Kahn, D. Farquhar; Decomposition pathways of the mono-and bis (pivaloyloxymethyl) esters of azidothymidine 5′-monophosphate in cell extract and in tissue culture medium: an application of the 'on-line ISRP-cleaning'HPLC technique; *Antivir. Chem. Chemother.* **1994**, *5*, 91–98.

[223] R. V. Srinivas, B. L. Robbins, M. C. Connelly, Y. F. Gong, N. Bischofberger, A. Fridland; Metabolism and in vitro antiretroviral activities of bis (pivaloyloxymethyl) prodrugs of acyclic nucleoside phosphonates.; *Antimicrob. Agents Chemother.* **1993**, *37*, 2247–2250.

[224] D. Farquhar, R. Chen, S. Khan; 5'-[4-(Pivaloyloxy)-1,3,2-dioxaphosphorinan-2-yl]-2'-deoxy-5-fluorouridine: A Membrane-Permeating Prodrug of 5-Fluoro-2'-deoxyuridylic Acid (FdUMP); *J. Med. Chem.* **1995**, *38*, 488–495.

[225] B. L. Robbins, R. V. Srinivas, C. Kim, N. Bischofberger, A. Fridland; Anti-human immunodeficiency virus activity and cellular metabolism of a potential prodrug of the acyclic nucleoside phosphonate 9-R-(2-phosphonomethoxypropyl) adenine (PMPA), bis (isopropyloxymethylcarbonyl) PMPA; *Antimicrob. Agents Chemother.* **1998**, *42*, 612–617.

[226] C. Ducho; *cyclo*Sal-Nucleotide - Ansätze zur Optimierung eines Wirkstoffsystems, Dissertation, University of Hamburg; **2005**.

[227] M. Nautiyal, B. Gadakh, S. De Graef, L. Pang, M. Khan, Y. Xun, J. Rozenski, A. Van Aerschot; Synthesis and Biological Evaluation of Lipophilic Nucleoside Analogues as Inhibitors of Aminoacyl-tRNA Synthetases; *Antibiotics* **2019**, *8*, 180.

[228] L. Mizen, G. Burton; The use of esters as prodrugs for oral delivery of beta-lactam antibiotics.; *Pharm. Biotechnol.* **1998**, *11*, 345–365.

[229] A. V. Cheng, W. M. Wuest; Signed, Sealed, Delivered: Conjugate and Prodrug Strategies as Targeted Delivery Vectors for Antibiotics; *ACS Infect. Dis.* **2019**, *5*, 816–828.

[230] A. Simplício, J. Clancy, J. Gilmer; Prodrugs for Amines; *Molecules* **2008**, *13*, 519–547.

[231] A. Spork; Synthetische Untersuchungen zur Nucleosid-Einheit von Muraymycin-Antibiotika, Dissertation, Georg-August-University Göttingen; **2012**.

[232] M. T. Rodolis, A. Mihalyi, C. Ducho, K. Eitel, B. Gust, R. J. M. Goss, T. D. H. Bugg; Mechanism of action of the uridyl peptide antibiotics: an unexpected link to a protein–protein interaction site in translocase MraY; *Chem. Commun.* **2014**, *50*, 13023–13025.

[233] Z. Cui, X.-C. Wang, X. Liu, A. Lemke, S. Koppermann, C. Ducho, J. Rohr, J. S. Thorson, S. G. Van Lanen; Self-Resistance during Muraymycin Biosynthesis: a Complementary Nucleotidyltransferase and Phosphotransferase with Identical Modification Sites and Distinct Temporal Order; *Antimicrob. Agents Chemother.* **2018**, *62*, e00193-18.

[234] J. K. Hakulinen, J. Hering, G. Brändén, H. Chen, A. Snijder, M. Ek, P. Johansson; MraY–antibiotic complex reveals details of tunicamycin mode of action; *Nat. Chem. Biol.* **2017**, *13*, 265–267.

[235] P. Oelschlaeger, S. L. Mayo, J. Pleiss; Impact of remote mutations on metallo-β-lactamase substrate specificity: implications for the evolution of antibiotic resistance; *Protein Sci.* **2005**, *14*, 765–74.

[236] W. Wehrli; Rifampin: Mechanisms of Action and Resistance; *Clinical Infectious Diseases* **1983**, *5*, S407–S411.

[237] R. M. Peterson, T. Huang, J. D. Rudolf, M. J. Smanski, B. Shen; Mechanisms of Self-Resistance in the Platensimycin- and Platencin-Producing Streptomyces platensis MA7327 and MA7339 Strains; *Chemistry & Biology* **2014**, *21*, 389–397.

[238] A. Fabbretti, R. Çapuni, A. M. Giuliodori, L. Cimarelli, A. Miano, V. Napolioni, A. La Teana, R. Spurio; Characterization of the Self-Resistance Mechanism to Dityromycin in the *Streptomyces* Producer Strain; *mSphere* **2019**, *4*, e00554-19.

[239] G. Niro; Studies on the Selectivity of Nucleoside Antibiotics, Dissertation, Saarland University; **2019**.

[240] C. Rohrbacher; Synthese neuartiger Muraymycin-Konjugate zur Verbesserung der bakteriellen Zellaufnahme, Dissertation, Saarland University; **2023**.

[241] R. A. W. M. Afifi; Design and synthesis of novel Mur enzymes inhibitors and their evaluation as antibacterial agents, Dissertation, German University Cairo; **2021**.

[242] L. Farhangnia, E. Ghaznavi- Rad, N. Mollaee, H. Abtahi; Cloning, Expression, and Purification of Recombinant Lysostaphin From Staphylococcus simulans; *Jundishapur J. Microbiol.* **2014**, *7*, e10009.

[243] M. Wirth; Untersuchungen zur Membranpermeabilität von *O*-acylierten Muraymycinen, Dissertation, Saarland University; **2019**.

[244] T. Stachyra, C. Dini, P. Ferrari, A. Bouhss, J. van Heijenoort, D. Mengin-Lecreulx, D. Blanot, J. Biton, D. Le Beller; Fluorescence Detection-Based Functional Assay for High-Throughput Screening for MraY; *Antimicrob. Agents Chemother.* **2004**, *48*, 897–902.

[245] G. Tosquellas; The pro-oligonucleotide approach: solid phase synthesis and preliminary evaluation of model pro-dodecathymidylates; *Nucleic Acids Research* **1998**, *26*, 2069–2074.

[246] R. P. Iyer, D. Yu, S. Agrawal; Prodrugs of Oligonucleotides: The Acyloxyalkyl Esters of Oligodeoxyribonucleoside Phosphorothioates; *Bioorg. Chem.* **1995**, *23*, 1–21.

[247] P. D. Iyer, N. Ho, D. Yu, S. Agrawal; Bioreversible oligonucleotide conjugates by site-specific derivatization; *Bioorg. Med. Chem. Lett.* **1997**, *7*, 871–876.

[248] R. P. Mauritz, F. S. Schmelz, C. Meier; Elucidation of the Hydrolytical Properties of α-Hydroxybenzylphosphonates as a New Potential Pro-Oligonucleotide Concept; *Nucleosides and Nucleotides* **1999**, *18*, 1417–1418.

[249] A. E. Cardenas, R. Shrestha, L. J. Webb, R. Elber; Membrane Permeation of a Peptide: It Is Better to be Positive; *J. Phys. Chem. B* **2015**, *119*, 6412–6420.

[250] R. Hamzavi, F. Dolle, B. Tavitian, O. Dahl, P. E. Nielsen; Modulation of the Pharmacokinetic Properties of PNA: Preparation of Galactosyl, Mannosyl, Fucosyl, *N*-Acetylgalactosaminyl, and *N*-Acetylglucosaminyl Derivatives of Aminoethylglycine Peptide Nucleic Acid Monomers and Their Incorporation into PNA Oligomers; *Bioconjugate Chem.* **2003**, *14*, 941–954.

[251] M. Y. H. Lai, M. A. Brimble, D. J. Callis, P. W. R. Harris, M. S. Levi, F. Sieg; Synthesis and pharmacological evaluation of glycine-modified analogues of the neuroprotective agent glycyl-l-prolyl-l-glutamic acid (GPE); *Bioorg. Med. Chem.* **2005**, *13*, 533–548.

[252] C. Schütz; Inhibitoren der bakteriellen Translocase und Collagenase als potentielle Antibiotika, Master Thesis, Saarland University; **2016**.

[253] J. H. Tsai, L. R. Takaoka, N. A. Powell, J. S. Nowick; Synthesis of amino acid ester isocyanates: methyl (S)-2-isocyanato-3-phenylpropanoate; *Org. Synth.* **2002**, *78*, 220.

[254] J. S. Zakhari, I. Kinoyama, M. S. Hixon, A. Di Mola, D. Globisch, K. D. Janda; Formulating a new basis for the treatment against botulinum neurotoxin intoxication: 3,4-Diaminopyridine prodrug design and characterization; *Bioorg. Med. Chem.* **2011**, *19*, 6203–6209.

[255] E. Nägele, M. Schelhaas, N. Kuder, H. Waldmann; Chemoenzymatic Synthesis of N-*Ras* Lipopeptides; *J. Am. Chem. Soc.* **1998**, *120*, 6889–6902.

[256] F. Silva, O. Lourenço, J. A. Queiroz, F. C. Domingues; Bacteriostatic versus bactericidal activity of ciprofloxacin in Escherichia coli assessed by flow cytometry using a novel far-red dye; *J Antibiot* **2011**, *64*, 321–325.

[257] W. Ablain, S. Hallier Soulier, D. Causeur, M. Gautier, F. Baron; A simple and rapid method for the disruption of *Staphylococcus aureus* , optimized for quantitative reverse transcriptase applications: Application for the examination of Camembert cheese; *Dairy Sci. Technol.* **2009**, *89*, 69–81.

[258] J. K. Kumar; Lysostaphin: an antistaphylococcal agent; *Appl Microbiol Biotechnol* **2008**, *80*, 555–561.

[259] D. C. Draghi, D. J. Sheehan, P. Hogan, D. F. Sahm; In Vitro Activity of Linezolid against Key Gram-Positive Organisms Isolated in the United States: Results of the LEADER 2004 Surveillance Program; *Antimicrob Agents Chemother* **2005**, *49*, 5024–5032.

[260] R. E. Mendes, P. A. Hogan, J. M. Streit, R. N. Jones, R. K. Flamm; Update on Linezolid *In Vitro* Activity through the Zyvox Annual Appraisal of Potency and Spectrum Program, 2013; *Antimicrob Agents Chemother* **2015**, *59*, 2454–2457.

[261] B. Volkmer, M. Heinemann; Condition-Dependent Cell Volume and Concentration of Escherichia coli to Facilitate Data Conversion for Systems Biology Modeling; *PLoS ONE* **2011**, *6*, e23126.

[262] O. Pierucci; Dimensions of Escherichia coli at various growth rates: model for envelope growth; *J Bacteriol* **1978**, *135*, 559–574.

[263] M. Heldal, S. Norland, O. Tumyr; X-ray microanalytic method for measurement of dry matter and elemental content of individual bacteria; *Appl Environ Microbiol* **1985**, *50*, 1251–1257.

[264] J. B. Stock, B. Rauch, S. Roseman; Periplasmic space in Salmonella typhimurium and Escherichia coli.; *Journal of Biological Chemistry* **1977**, *252*, 7850–7861.

[265] U. Hasanah, H. Widhiastuti, Syaefudin; Potency of Ethanol Extract from Berenuk (Crescentia cujete L.) Fruit Rind and Flesh as Antibacterial Agents; *IOP Conf. Ser.: Earth Environ. Sci.* **2018**, *187*, 012001.

[266] S. Rosinus; Synthese von Muraymycin-Analoga mit Variationen in der Peptidkette, Master Thesis, Saarland University; **2020**.

[267] A. Heib; Synthese von Muraymycin-Analoga mit Variationen in der Nucleosid-Einheit, Master Thesis, Saarland University; **2018**.

[268] N. Stadler; Muraymycin-Analoga mit potenzieller Aktivität gegen *Pseudomonas aeruginosa*, Master Thesis, Saarland University; **2021**.

[269] *RÖMPP Online: Planta Media*, Georg Thieme Verlag, **2023**.

[270] M. Muramatsu, M. Ishii Miyazawa, M. Inukai; Studies on Novel Bacterial Translocase I Inhibitors, A-500359s II. Biological Activities of A-500359 A, C, D and G; *J Antibiot* **2003**, *56*, 253–258.

[271] A. Muramatsu, T. Ohnuki, M. Ishii Miyazawa, M. Kizuka, R. Enokita, S. Miyakoshii, T. Takatsu, M. Inukai; A-503083 A, B, E and F, Novel Inhibitors of Bacterial Translocase I, Produced by Streptomyces sp. SANK 62799; *J Antibiot* **2004**, *57*, 639–646.

[272] I. Palmer, P. T. Wingfield; Preparation and Extraction of Insoluble (Inclusion-Body) Proteins from *Escherichia coli*; *CP Protein Science* **2004**, *38*, DOI 10.1002/0471140864.ps0603s38.

[273] J. R. Silvius; Thermotropic phase transitions of pure lipids in model membranes and their modifications by membrane proteins. Lipid protein-interactions; *John Wiley & Sons* **1982**.

[274] J. García-Nafría, J. F. Watson, I. H. Greger; IVA cloning: A single-tube universal cloning system exploiting bacterial In Vivo Assembly; *Sci. Rep.* **2016**, *6*, 27459.

[275] K. A. Johnson, R. S. Goody; The Original Michaelis Constant: Translation of the 1913 Michaelis–Menten Paper; *Biochemistry* **2011**, *50*, 8264–8269.

[276] HaemoScan BV; Biomaterial hemolytic assay kit insert; *https://www.haemoscan.com/products/hemolysis/* **2018**, *opened on 11/27/2018*.

[277] K. K. Sharma, I. K. Maurya, S. I. Khan, M. R. Jacob, V. Kumar, K. Tikoo, R. Jain; Discovery of a Membrane-Active, Ring-Modified Histidine Containing Ultrashort Amphiphilic Peptide That Exhibits Potent Inhibition of *Cryptococcus neoformans*; *J. Med. Chem.* **2017**, *60*, 6607–6621.

[278] S. Koppermann, Z. Cui, P. D. Fischer, X. Wang, J. Ludwig, J. S. Thorson, S. G. Van Lanen, C. Ducho; Insights into the Target Interaction of Naturally Occurring Muraymycin Nucleoside Antibiotics; *ChemMedChem* **2018**, *13*, 779–784.

[279] H. Rolshausen; Arbeiten zur Synthese neuer Prodrugs von Muraymycin-Analoga, Bachelor Thesis, Saarland University; **2019**.

[280] H. Jessen; Untersuchungen zur intrazellulären Freisetzung von Nucleosidphosphaten, Dissertation, University of Hamburg; **2008**.

[281] M. Frigerio, M. Santagostino, S. Sputore; A User-Friendly Entry to 2-Iodoxybenzoic Acid (IBX); *J. Org. Chem.* **1999**, *64*, 4537–4538.

[282] R. K. Boeckman, Jr. Shao P., J. J. Mullins; The Dess-Martin Periodinane: 1,1,1-Triacetoxy-1,1-dihydro-1,2-benziodoxol-3(1H)-one; *Org. Synth.* **2000**, *77*, 141.

[283] D. B. Dess, J. C. Martin; Readily accessible 12-I-5 oxidant for the conversion of primary and secondary alcohols to aldehydes and ketones; *J. Org. Chem.* **1983**, *48*, 4155–4156.

[284] E. Mareykin; Synthese neuer Prodrugs von Analoga der Muraymycin-Antibiotika, Master Thesis, Saarland University; **2018**.

[285] V. Böttner; Untersuchungen zu Synthese und Eigenschaften von Oligonucleotid Prodrugs, Dissertation, Saarland University; **2019**.

[286] L. Thilmont; Prodrugs von Muraymycin-Nucleosid-Antibiotika, Master Thesis, Saarland University; **2021**.

[287] R. Mazurkiewicz, A. Kuznik, M. Grymel, N. Kuznik; 1H NMR spectroscopic criteria for the configuration of *N*-acyl-alpha,beta-dehydro-alpha-amino acid esters; *Magnetic Resonance in Chemistry* **2005**, *43*, 36–40.

[288] S. Santajit, N. Indrawattana; Mechanisms of Antimicrobial Resistance in ESKAPE Pathogens; *BioMed Research International* **2016**, *2016*, 1–8.

[289] C. Neu, A. Heppel; The Release of Enzymes from Kwherichia coli by Osmotic Shock and during the Formation of Spheroplasts; *J. Biol. Chem.* **1965**, *240*, 9.

[290] O. Khersonsky, D. S. Tawfik; Structure−Reactivity Studies of Serum Paraoxonase PON1 Suggest that Its Native Activity Is Lactonase; *Biochemistry* **2005**, *44*, 6371–6382.

Appendix

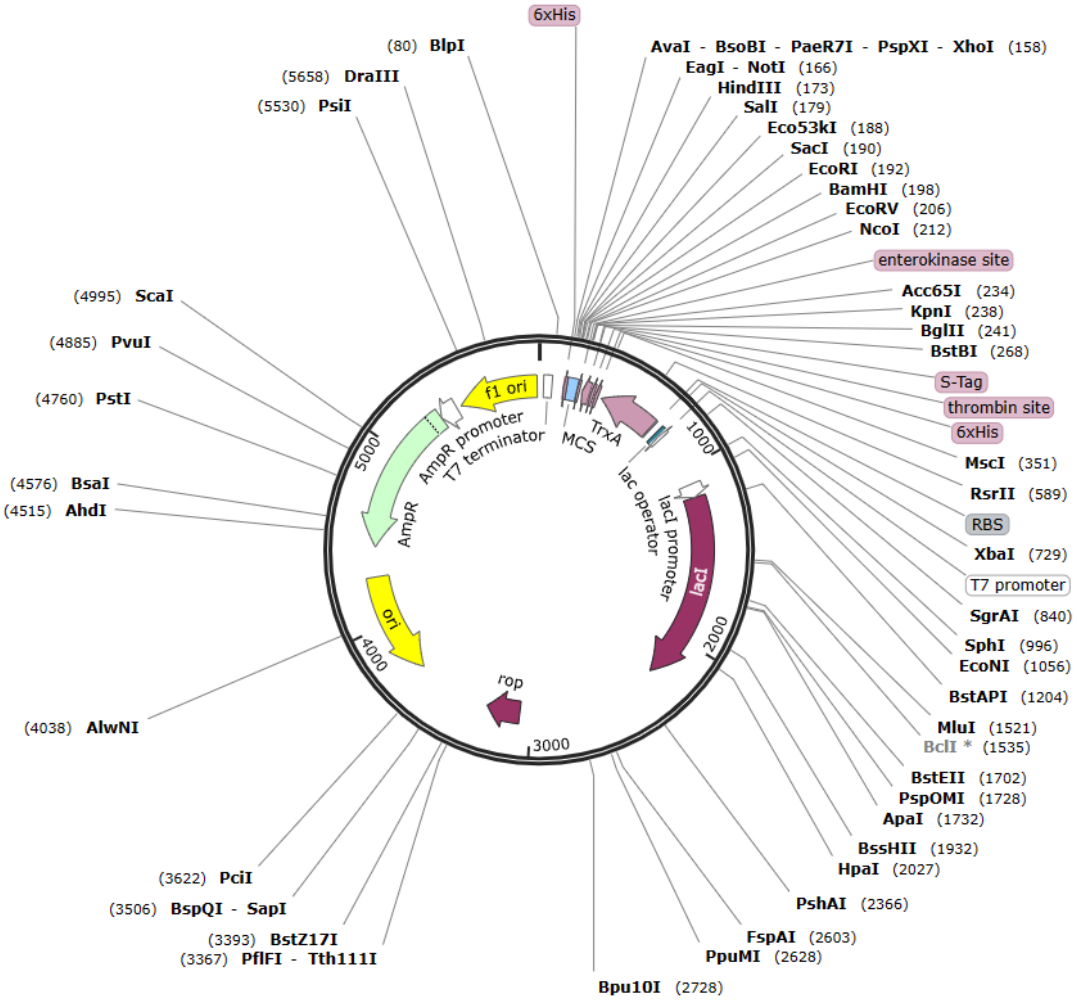

Appendix I: Plasmid map of pET32a (5900 bp) for design of codon-optimized lysostaphin plasmid (taken from: SnapGene).

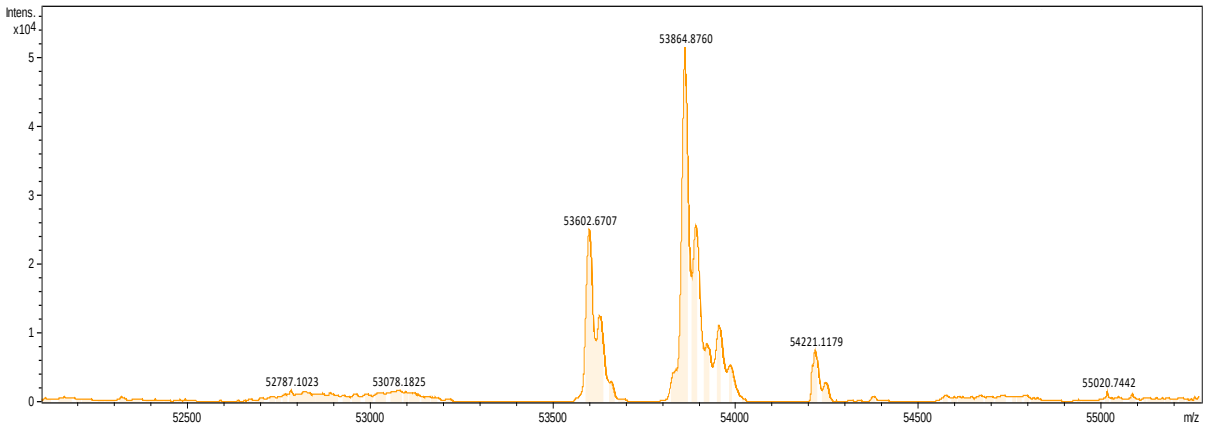

Appendix II: Full chromatogram of MS experiment with obtained peaks for the purchased lysostaphin.

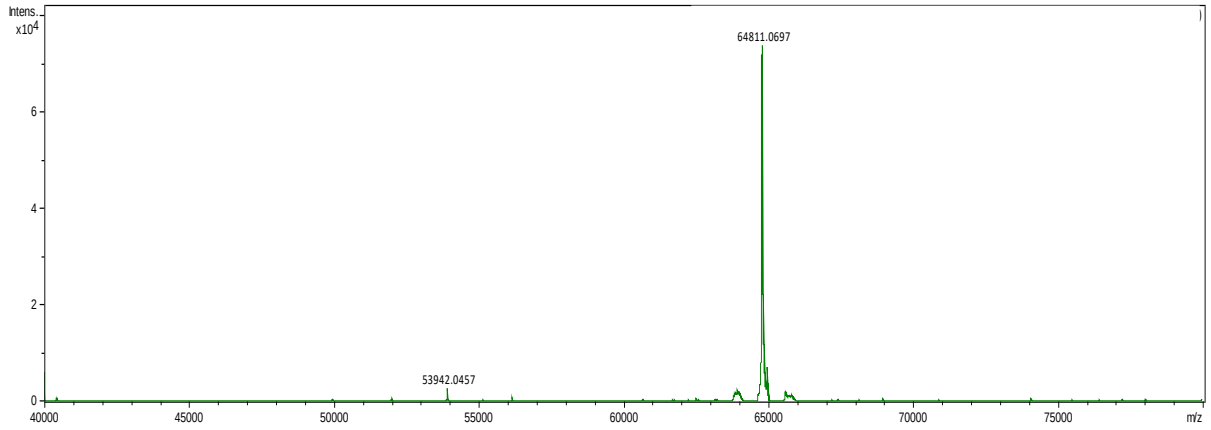

Appendix III: Full chromatogram of MS experiment with obtained peaks for the expressed and purified lysostaphin in this work

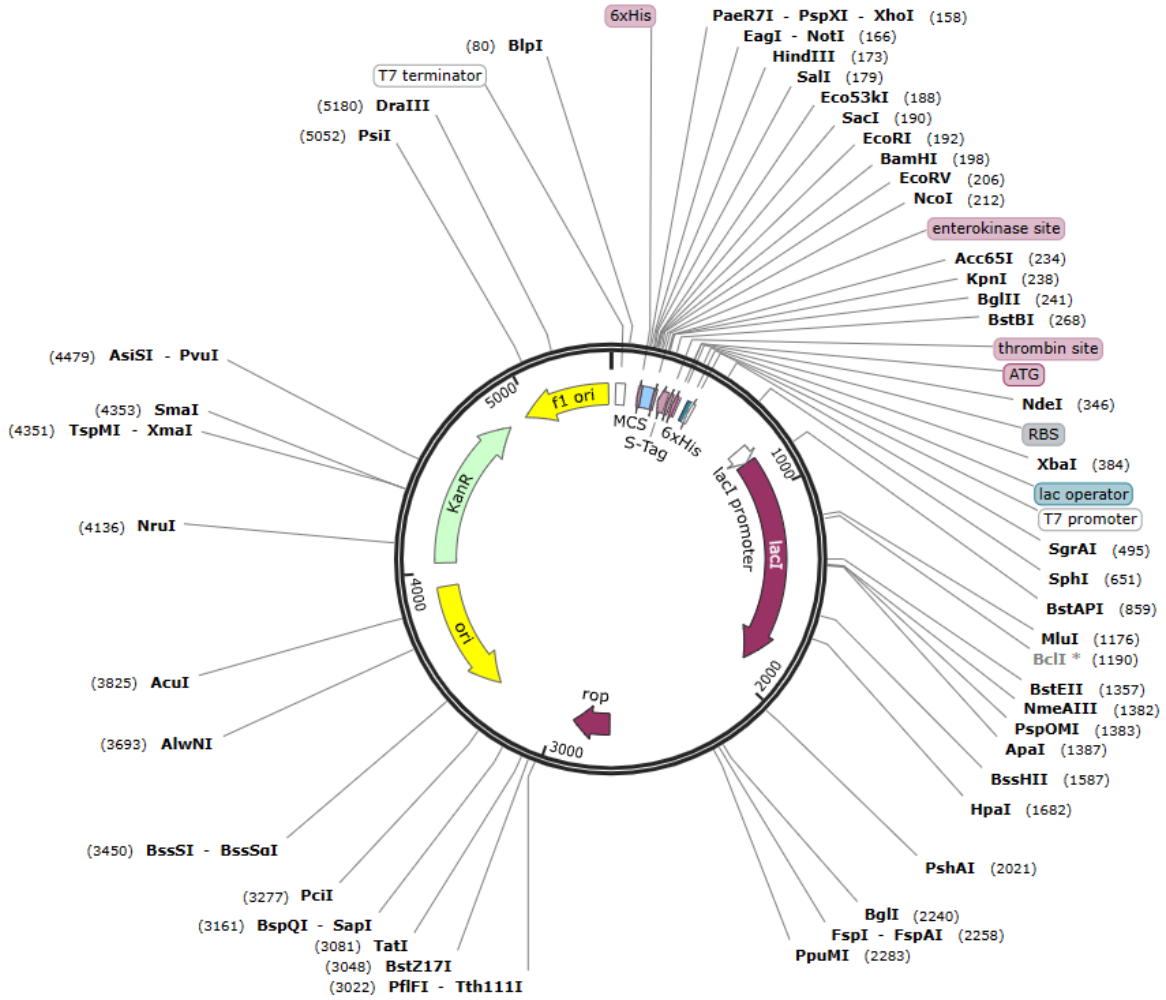

Appendix IV: Plasmid map of pET30a (5422 bp) in which the MurX genes were initially provided from the research group of Prof. S. Van Lanen (taken from: SnapGene).

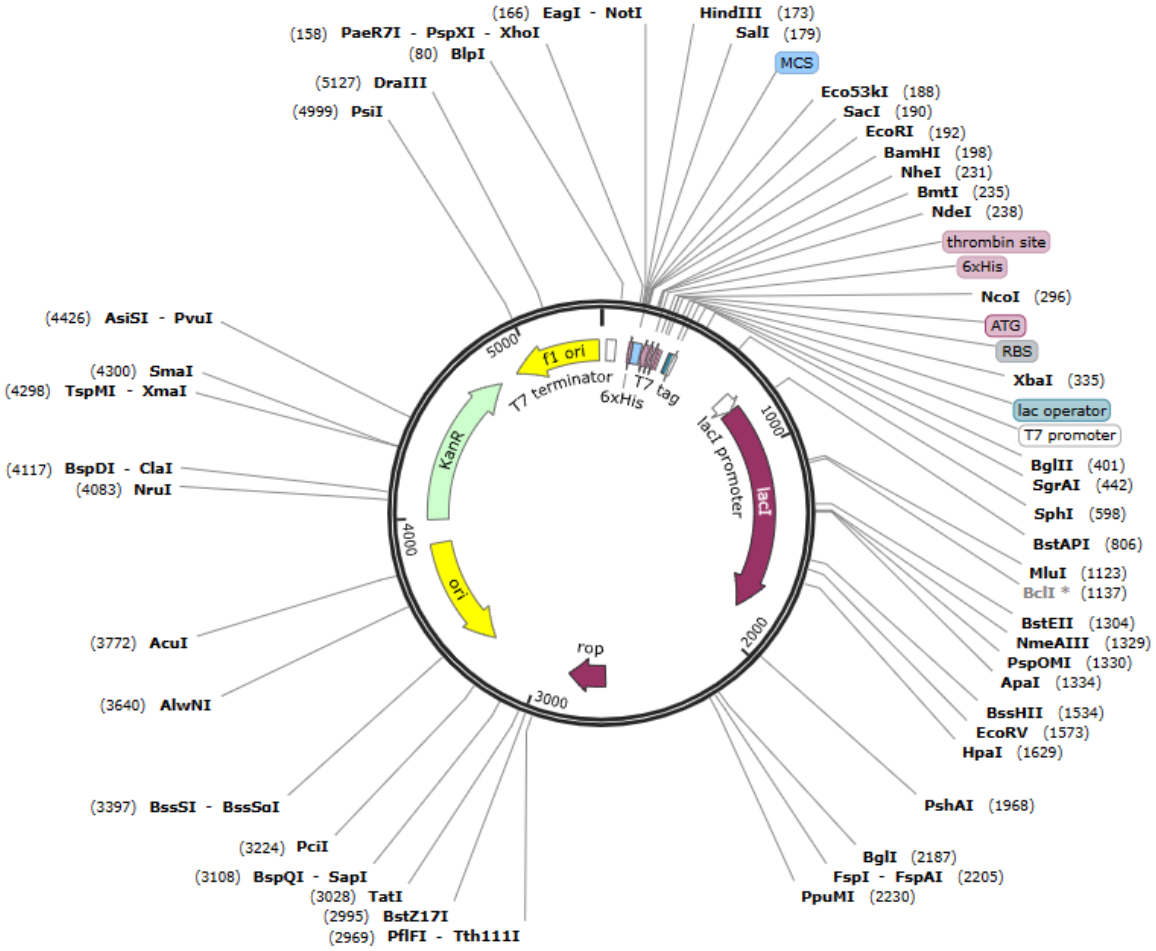

Appendix V: Plasmid map of pET28a (5369 bp) for routinely overexpressed MraY from S. aureus in E. coli as crude membrane preparation (taken from: SnapGene).

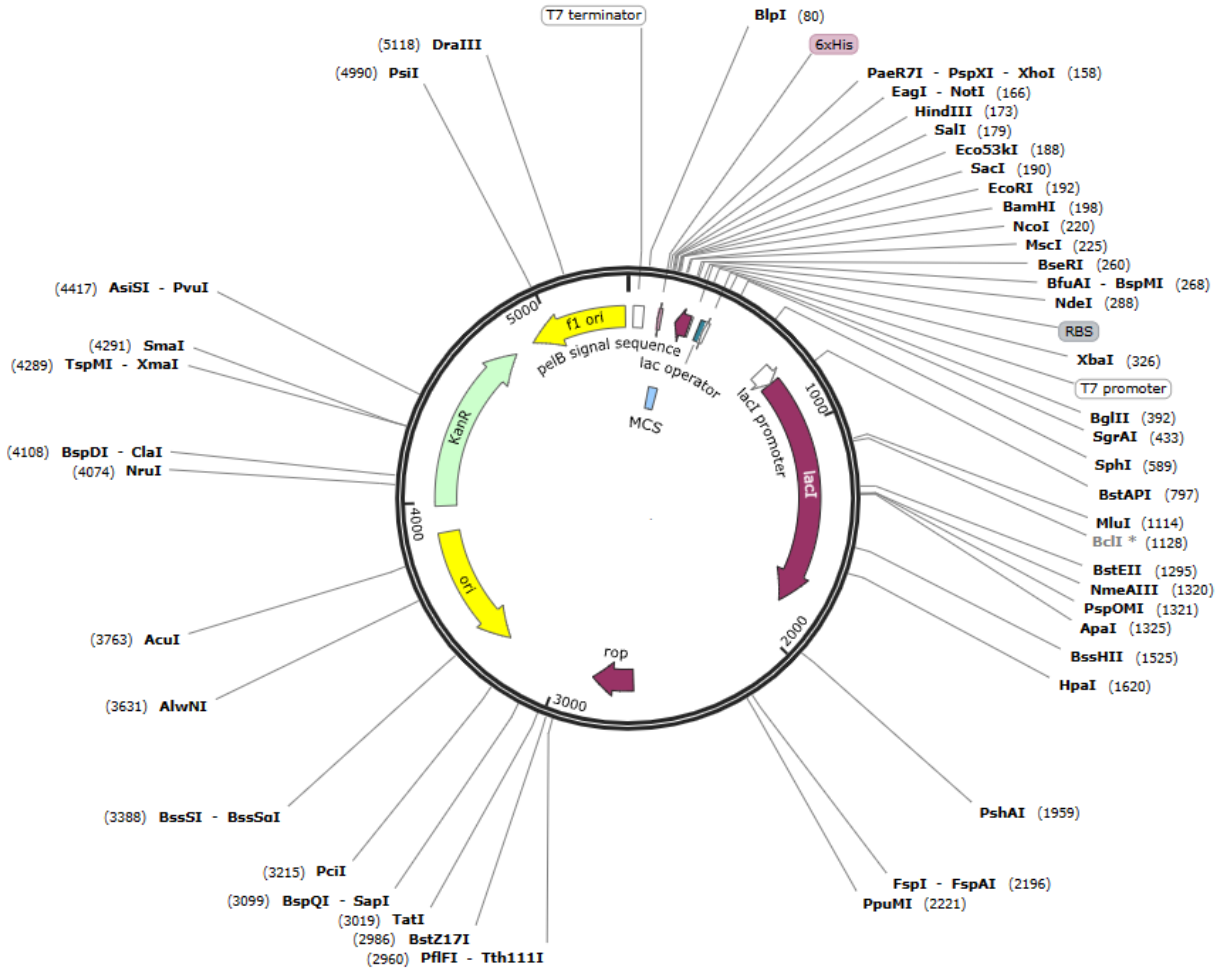

Appendix VI: Plasmid map of pET26a (5360 bp) for MurX expression which was routinely used for expression of purified MraY in detergent micelles (taken from: SnapGene).

Curriculum vitae